frontiers | Research Topics

Regulation of gene expression in enteropathogenic bacteria, volume III

Edited by
Dongsheng Zhou, Shihua Wang and Xihui Shen

Published in
Frontiers in Microbiology

ISSN 1664-8714
ISBN 978-2-8325-2312-4
DOI 10.3389/978-2-8325-2312-4

About Frontiers

Frontiers is more than just an open access publisher of scholarly articles: it is a pioneering approach to the world of academia, radically improving the way scholarly research is managed. The grand vision of Frontiers is a world where all people have an equal opportunity to seek, share and generate knowledge. Frontiers provides immediate and permanent online open access to all its publications, but this alone is not enough to realize our grand goals.

Frontiers journal series

The Frontiers journal series is a multi-tier and interdisciplinary set of open-access, online journals, promising a paradigm shift from the current review, selection and dissemination processes in academic publishing. All Frontiers journals are driven by researchers for researchers; therefore, they constitute a service to the scholarly community. At the same time, the *Frontiers journal series* operates on a revolutionary invention, the tiered publishing system, initially addressing specific communities of scholars, and gradually climbing up to broader public understanding, thus serving the interests of the lay society, too.

Dedication to quality

Each Frontiers article is a landmark of the highest quality, thanks to genuinely collaborative interactions between authors and review editors, who include some of the world's best academicians. Research must be certified by peers before entering a stream of knowledge that may eventually reach the public - and shape society; therefore, Frontiers only applies the most rigorous and unbiased reviews. Frontiers revolutionizes research publishing by freely delivering the most outstanding research, evaluated with no bias from both the academic and social point of view. By applying the most advanced information technologies, Frontiers is catapulting scholarly publishing into a new generation.

What are Frontiers Research Topics?

Frontiers Research Topics are very popular trademarks of the *Frontiers journals series*: they are collections of at least ten articles, all centered on a particular subject. With their unique mix of varied contributions from Original Research to Review Articles, Frontiers Research Topics unify the most influential researchers, the latest key findings and historical advances in a hot research area.

Find out more on how to host your own Frontiers Research Topic or contribute to one as an author by contacting the Frontiers editorial office: frontiersin.org/about/contact

Regulation of gene expression in enteropathogenic bacteria, volume III

Topic editors

Dongsheng Zhou — Beijing Institute of Microbiology and Epidemiology, China
Shihua Wang — Fujian Agriculture and Forestry University, China
Xihui Shen — Northwest A&F University, China

Citation

Zhou, D., Wang, S., Shen, X., eds. (2023). *Regulation of gene expression in enteropathogenic bacteria, volume III*. Lausanne: Frontiers Media SA.
doi: 10.3389/978-2-8325-2312-4

Table of contents

05 cAMP Receptor Protein Positively Regulates the Expression of Genes Involved in the Biosynthesis of *Klebsiella oxytoca* Tilivalline Cytotoxin
Diana Rodríguez-Valverde, Nancy León-Montes, Jorge Soria-Bustos, Jessica Martínez-Cruz, Ricardo González-Ugalde, Sandra Rivera-Gutiérrez, Jorge A. González-y-Merchand, Roberto Rosales-Reyes, Lázaro García-Morales, Hidetada Hirakawa, James G. Fox, Jorge A. Girón, Miguel A. De la Cruz and Miguel A. Ares

19 σ^S-Mediated Stress Response Induced by Outer Membrane Perturbation Dampens Virulence in *Salmonella enterica* serovar Typhimurium
Seul I Kim, Eunsuk Kim and Hyunjin Yoon

33 Polyphosphate Kinase 1 Is a Pathogenesis Determinant in Enterohemorrhagic *Escherichia coli* O157:H7
Yanli Du, Xiangyu Wang, Zongli Han, Ying Hua, Kaina Yan, Bao Zhang, Wei Zhao and Chengsong Wan

49 The Role of the Two-Component System PhoP/PhoQ in Intrinsic Resistance of *Yersinia enterocolitica* to Polymyxin
Haoran Guo, Tong Zhao, Can Huang and Jingyu Chen

61 A Plasmid With Conserved Phage Genes Helps *Klebsiella pneumoniae* Defend Against the Invasion of Transferable DNA Elements at the Cost of Reduced Virulence
Mufeng Cai, Bingchun Pu, Yue Wang, Lin Lv, Chunyu Jiang, Xiaomei Fu, Yan Zhang, Wei Zhao, Ke Dong, Yi Yang, Yangming Liu, Yalu Wei, Zhengyue Zhang, Jianhui Li, Xiaokui Guo, Chang Liu and Jinhong Qin

72 The Small RNA CyaR Activates Translation of the Outer Membrane Haem Receptor *chuA* in Enterohemorrhagic *Escherichia coli*
Brandon M. Sy and Jai J. Tree

84 The Fis Nucleoid Protein Negatively Regulates the Phase Variation *fimS* Switch of the Type 1 Pilus Operon in Enteropathogenic *Escherichia coli*
Zeus Saldaña-Ahuactzi, Jorge Soria-Bustos, Verónica I. Martínez-Santos, Jorge A. Yañez-Santos, Ygnacio Martínez-Laguna, María Lilia Cedillo-Ramirez, José L. Puente and Jorge A. Girón

97 The Global Regulator CcpA of *Listeria monocytogenes* Confers Sensitivity to Antimicrobial Fatty Acids
Rikke S. S. Thomasen, Magnus Ganer Jespersen, Katrine Jørgensen, Patricia T. dos Santos, Eva M. Sternkopf Lillebæk, Marianne N. Skov, Michael Kemp and Birgitte H. Kallipolitis

112 Absence of N-Acetylglucosamine Glycosylation on *Listeria monocytogenes* Wall Teichoic Acids Promotes Fatty Acid Tolerance by Repulsion From the Bacterial Surface
Rikke S. S. Thomasen, Patricia T. dos Santos, Eva M. Sternkopf Lillebæk, Marianne N. Skov, Michael Kemp and Birgitte H. Kallipolitis

124 EspF of Enterohemorrhagic *Escherichia coli* Enhances Apoptosis *via* Endoplasmic Reticulum Stress in Intestinal Epithelial Cells: An Isobaric Tags for Relative and Absolute Quantitation-Based Comparative Proteomic Analysis
Xiangyu Wang, Kaina Yan, Muqing Fu, Song Liang, Haiyi Zhao, Changzhu Fu, Lan Yang, Zhihong Song, Dayong Sun and Chengsong Wan

139 Mr.Vc v2: An updated version of database with increased data of transcriptome and experimental validated interactions
Zhiyuan Zhang, Guozhong Chen, Wajid Hussain, Zixin Qin, Juntong Liu, Yang Su, Hao Zhang and Mingquan Ye

149 Quorum sensing and QsvR tightly control the transcription of *vpa0607* encoding an active RNase II-type protein in *Vibrio parahaemolyticus*
Yiquan Zhang, Xingfan Xue, Fengjun Sun, Xue Li, Miaomiao Zhang, Qimin Wu, Tingting Zhang, Xi Luo and Renfei Lu

161 Serotype conversion gene *rfbT* is directly regulated by histone-like nucleoid structuring protein (H-NS) in *V. cholerae* O1
Yu Han, Jing Li, He Gao, Xiaorui Li, Ran Duan, Qian Cheng, Biao Kan and Weili Liang

171 GrlR, a negative regulator in enteropathogenic *E. coli*, also represses the expression of LEE virulence genes independently of its interaction with its cognate partner GrlA
Cristina Lara-Ochoa, Alejandro Huerta-Saquero, Abraham Medrano-López, Wanyin Deng, B. Brett Finlay, Ygnacio Martínez-Laguna and José L. Puente

frontiers in Microbiology

ORIGINAL RESEARCH
published: 30 September 2021
doi: 10.3389/fmicb.2021.743594

cAMP Receptor Protein Positively Regulates the Expression of Genes Involved in the Biosynthesis of *Klebsiella oxytoca* Tilivalline Cytotoxin

Diana Rodríguez-Valverde[1,2], Nancy León-Montes[1,2], Jorge Soria-Bustos[1], Jessica Martínez-Cruz[1,2], Ricardo González-Ugalde[1,2], Sandra Rivera-Gutiérrez[2], Jorge A. González-y-Merchand[2], Roberto Rosales-Reyes[3], Lázaro García-Morales[4], Hidetada Hirakawa[5], James G. Fox[6], Jorge A. Girón[7], Miguel A. De la Cruz[1] and Miguel A. Ares[1,2]**

[1]Unidad de Investigación Médica en Enfermedades Infecciosas y Parasitarias, Hospital de Pediatría, Centro Médico Nacional Siglo XXI, Instituto Mexicano del Seguro Social, Mexico City, Mexico, [2]Departamento de Microbiología, Escuela Nacional de Ciencias Biológicas, Instituto Politécnico Nacional, Mexico City, Mexico, [3]Unidad de Medicina Experimental, Facultad de Medicina, Universidad Nacional Autónoma de México, Mexico City, Mexico, [4]Departamento de Biomedicina Molecular, Centro de Investigación y de Estudios Avanzados del Instituto Politécnico Nacional, Mexico City, Mexico, [5]Department of Bacteriology, Gunma University Graduate School of Medicine, Maebashi, Japan, [6]Division of Comparative Medicine, Massachusetts Institute of Technology, Cambridge, MA, United States, [7]Centro de Detección Biomolecular, Benemérita Universidad Autónoma de Puebla, Puebla, Mexico

Klebsiella oxytoca is a resident of the human gut. However, certain *K. oxytoca* toxigenic strains exist that secrete the nonribosomal peptide tilivalline (TV) cytotoxin. TV is a pyrrolobenzodiazepine that causes antibiotic-associated hemorrhagic colitis (AAHC). The biosynthesis of TV is driven by enzymes encoded by the *aroX* and NRPS operons. In this study, we determined the effect of environmental signals such as carbon sources, osmolarity, and divalent cations on the transcription of both TV biosynthetic operons. Gene expression was enhanced when bacteria were cultivated in tryptone lactose broth. Glucose, high osmolarity, and depletion of calcium and magnesium diminished gene expression, whereas glycerol increased transcription of both TV biosynthetic operons. The cAMP receptor protein (CRP) is a major transcriptional regulator in bacteria that plays a key role in metabolic regulation. To investigate the role of CRP on the cytotoxicity of *K. oxytoca*, we compared levels of expression of TV biosynthetic operons and synthesis of TV in wild-type strain MIT 09-7231 and a Δ*crp* isogenic mutant. In summary, we found that CRP directly activates the transcription of the *aroX* and NRPS operons and that the absence of CRP reduced cytotoxicity of *K. oxytoca* on HeLa cells, due to a significant reduction in TV production. This study highlights the importance of the CRP protein in the regulation of virulence genes in enteric bacteria and broadens our knowledge on the regulatory mechanisms of the TV cytotoxin.

Keywords: CRP, tilivalline cytotoxin, *aroX*, *npsA*, *Klebsiella oxytoca*

OPEN ACCESS

Edited by:
Dongsheng Zhou,
Beijing Institute of Microbiology and Epidemiology, China

Reviewed by:
Runhua Han,
University of Texas at Austin, United States
Weili Liang,
National Institute for Communicable Disease Control and Prevention (China CDC), China

***Correspondence:**
Miguel A. De la Cruz
miguel_angel_81@live.com
Miguel A. Ares
aresmi26@hotmail.com
maresj@ipn.mx

Specialty section:
This article was submitted to Infectious Diseases, a section of the journal Frontiers in Microbiology

Received: *18 July 2021*
Accepted: *31 August 2021*
Published: *30 September 2021*

Citation:
Rodríguez-Valverde D, León-Montes N, Soria-Bustos J, Martínez-Cruz J, González-Ugalde R, Rivera-Gutiérrez S, González-y-Merchand JA, Rosales-Reyes R, García-Morales L, Hirakawa H, Fox JG, Girón JA, De la Cruz MA and Ares MA (2021) cAMP Receptor Protein Positively Regulates the Expression of Genes Involved in the Biosynthesis of Klebsiella oxytoca Tilivalline Cytotoxin. Front. Microbiol. 12:743594. doi: 10.3389/fmicb.2021.743594

INTRODUCTION

The human gut microbiota is a complex community of microbial species that plays a fundamental role in the health and functioning of the human digestive tract. The homeostasis of this community provides protection against pathogens (Belkaid and Harrison, 2017; Lin et al., 2021). However, the use of antibiotics can break up this ecosystem and cause dysbiosis. Intestinal dysbiosis is defined as a cutback of beneficial commensal bacteria and development of damaging commensal bacteria termed opportunistic pathogens or pathobionts (Nagao-Kitamoto and Kamada, 2017; Kitamoto et al., 2020; Wei et al., 2021). The dysbiotic gut microbiota can trigger the initiation of gastrointestinal diseases including the antibiotic-associated hemorrhagic colitis (AAHC). Hospitalized patients who receive treatment with antibiotics may develop AAHC due to the pathobiont *Klebsiella oxytoca,* a Gram-negative bacterium that resides in the human gut. Toxigenic *K. oxytoca* strains carry a gene cluster that codes for proteins that synthesize a cytotoxin known as tilivalline (TV), which is largely responsible for this disease (Dornisch et al., 2017). Unlike other toxins, TV is not a protein, but a pentacyclic pyrrolobenzodiazepine metabolite. The cytotoxin biosynthetic gene cluster is a part of a pathogenicity island (PAI) and is organized in two operons termed *aroX* and NRPS. The *aroX* operon is a 6.1-kbp region encoding five genes: *aroX*, *dhbX*, *icmX*, *adsX*, and *hmoX*. The NRPS operon is a 6.2-kbp region encoding three genes: *npsA*, *thdA*, and *npsB* (Schneditz et al., 2014; Dornisch et al., 2017; Tse et al., 2017). TV disrupts cell cycle progression due to the enhancement of nucleation and elongation of tubulin polymerization (Unterhauser et al., 2019). Furthermore, TV induces epithelial apoptosis and changes the expression and localization of the tight junction protein claudin-1. Consequently, the intestinal barrier function is impaired (Schneditz et al., 2014; Hering et al., 2019).

The regulation of the expression of the *aroX* and NRPS operons has not been studied. Pathogenic bacteria possess a myriad of transcription factors that control their virulence (Crofts et al., 2018; Huang et al., 2019; King et al., 2020; Lee et al., 2020; Ramamurthy et al., 2020; Wójcicki et al., 2021). The cAMP receptor protein (CRP) is one of the most important global regulators controlling the expression of many genes in bacteria. It has been associated with the regulation of virulence factors, pathogenicity islands, and enzymes involved in the metabolism of various enterobacterial species such as *Klebsiella pneumoniae*, enterotoxigenic *Escherichia coli*, *Salmonella enterica* serovar Typhimurium, and *Pseudomonas aeruginosa* (De la Cruz et al., 2016, 2017; Xue et al., 2016; Berry et al., 2018; El Mouali et al., 2018; Ares et al., 2019). CRP consists of a homodimer, and its function depends on its binding to cAMP. When such interaction occurs, the conformation of CRP changes and this allows it to bind to the promoters on DNA in order to regulate transcriptional expression (Lindemose et al., 2014; Gunasekara et al., 2015; Xu et al., 2021). There are no studies on the role of the global regulator CRP in *K. oxytoca*. Nevertheless, in its close relative *K. pneumoniae,* CRP is a negative regulator of the capsular polysaccharide and a positive regulator of type 3 fimbriae (Ou et al., 2017; Panjaitan et al., 2019). In *E. coli,* CRP has more than 260 binding sites (Salgado, 2004) and controls the transcription of genes that code for proteins involved in a wide range of cellular processes, including its well-known role in the regulation of the *lac* operon, biofilm formation, iron uptake, antibiotic multidrug resistance, quorum sensing, shikimate pathway, and oxidative stress resistance (Jiang and Zhang, 2016; Uppal and Jawali, 2016; Ritzert et al., 2019; Liu et al., 2020b; Kumar et al., 2021). Additionally, CRP is involved in catabolite repression and metabolism of carbon sources. For example, in the absence of some rapidly metabolizable carbon sources such as glucose, CRP activates adenylate cyclase, which leads to an increase in enzyme production involved in the use of alternative carbon sources, such as lactose (Salgado, 2004; Geng and Jiang, 2015; Liu et al., 2020a). Indeed, it was previously reported that culturing a cytotoxin-producing *K. oxytoca* strain in a lactose-containing medium increases the production of TV and consequently the cytopathic effect on epithelial cells (Tse et al., 2017).

In this study, we sought to investigate the role of CRP in the transcriptional control of the enzymes encoded by the *aroX* and NRPS operons in the cytotoxin-producing *K. oxytoca* strain MIT 09-7231 (Darby et al., 2014). In addition, we evaluated the expression of *aroX* and NRPS operons in different environmental growth conditions including utilization of various carbon sources. Furthermore, we investigated the role of CRP protein in the transcriptional regulation of *aroX* and NRPS operons. The regulatory effect of CRP in production of TV cytotoxin was also analyzed by cytotoxicity assays on HeLa cells. To the best of our knowledge, this is the first study addressing the transcriptional regulation of the TV biosynthetic gene cluster, in which CRP acts as an activator.

MATERIALS AND METHODS

Bacterial Strains and Growth Conditions

Klebsiella oxytoca strains and bacterial constructs used in this study are listed in **Table 1**. *K. oxytoca* MIT 09-7231 was used as the prototypic toxigenic strain and for construction of the isogenic Δ*crp* mutant (Darby et al., 2014). To determine gene expression of *aroX* and NRPS operons, different liquid bacteriological media were used: lysogeny broth (LB), tryptone soy broth (TSB), tryptone lactose broth (TLB), and Dulbecco's modified Eagle's medium (DMEM) with high glucose (4.5 g/l). The transcription of *aroX* and *npsA* genes was analyzed under different environmental conditions in TLB medium at 37°C with shaking, and samples were harvested when an OD_{600nm} of 1.6 was reached for RNA extraction. TLB medium was prepared as previously described [17 g/l tryptone, 10 g/l lactose, and 2.5 g/l dipotassium hydrogen phosphate (Tse et al., 2017)]. TLB medium was supplemented with 0.2% glucose, 0.2% glycerol, 0.3 M NaCl, 1.0 mM EDTA, 5.0 mM $CaCl_2$, or 5.0 mM $MgCl_2$. In order to examine the effect of lactose on the transcription of *aroX* and *npsA* genes, tryptone broth (TB) was used and gene expression results were compared with those obtained from cultures

TABLE 1 | Bacterial strains and plasmids used in this study.

Strain or plasmid	Description	References
Strains		
K. oxytoca WT	Wild-type *K. oxytoca* strain MIT 09-7231	Darby et al., 2014
K. oxytoca Δ*crp*	*K. oxytoca* Δ*crp*::FRT	This study
K. oxytoca Δ*npsA*	*K. oxytoca* Δ*npsA*::FRT	This study
E. coli BL21(DE3)	F$^-$*ompT* *hsd*S$_B$ (r$_B^-$, m$_B^-$) *gal* *dcm* (DE3)	Invitrogen
Plasmids		
pTrc99Acrp	*crp* expression plasmid; Ap^R	Kurabayashi et al., 2017
pTrc99K-CRP	*crp* expression plasmid; Km^R	This study
pQE80crp	N-terminal His$_6$-Crp overexpression plasmid; Ap^R	Kurabayashi et al., 2017
pKD119	pINT-ts derivative containing the λ Red recombinase system under an arabinose-inducible promoter, Tc^R	Datsenko and Wanner, 2000
pKD4	pANTsy derivative template plasmid containing the kanamycin cassette for λ Red recombination, Ap^R	Datsenko and Wanner, 2000
pCP20	Plasmid that shows temperature-sensitive replication and thermal induction of FLP synthesis, Ap^R, Cm^R	Datsenko and Wanner, 2000

in TLB medium. Antibiotics [200 μg/ml (ampicillin), 50 μg/ml (kanamycin), or 10 μg/ml (tetracycline)] were added to culture media when necessary.

Construction of Isogenic Mutants

K. oxytoca MIT 09-7231 was targeted for mutagenesis of *crp* and *npsA* genes by using the lambda-Red recombinase system (Datsenko and Wanner, 2000). Briefly, PCR fragments containing *crp* or *npsA* sequences flanking a kanamycin resistance gene were obtained by using gene-specific primer pairs (**Table 2**). Each purified PCR product was electroporated independently into competent *K. oxytoca* carrying the lambda-Red recombinase helper plasmid pKD119, whose expression was induced by the addition of L-(+)-arabinose (Sigma) at a final concentration of 1%. The mutations were confirmed by PCR and sequencing. Subsequently, the FRT-flanked kanamycin cassettes were excised from both Δ*crp* and Δ*npsA* mutant strains after transformation with pCP20 plasmid, as previously described (Datsenko and Wanner, 2000).

Construction of ΔCRP-Box Mutant Probe by Site-Directed Mutagenesis

A fragment with targeted mutations in the putative CRP-Box of intergenic regulatory region of the divergent *aroX* and *npsA* genes was generated using overlapping PCR (Ho et al., 1989) with specific primers (**Table 2**). Two fragments were generated separately in a first round of PCR: one with the 5′ half and other with the 3′ half of the intergenic regulatory region of *aroX* and *npsA* genes including the overlapping mutated region. Subsequently, the two fragments were mixed and amplified in a second round of PCR. DNA sequencing was carried out to verify the introduction of the point mutations.

Construction of pTrc99K-CRP Plasmid

The pTrc99K-CRP plasmid was constructed for complementation experiments by subcloning the *crp* gene from the pTrc99Acrp plasmid (Kurabayashi et al., 2017). The pTrc99Acrp vector was digested with NcoI and BamHI, and the fragment corresponding to the *crp* gene was then purified and ligated into pTrc99K previously digested with the same restriction enzymes. The identity of the insert was confirmed by DNA sequencing.

RNA Extraction and Quantitative RT-PCR

Total RNA was extracted from bacteria grown under different culture conditions using the hot phenol method (Jahn et al., 2008; Ares, 2012), with some modifications. Briefly, after the lysate was obtained, an equal volume of phenol-saturated water was added, mixed, and incubated at 65°C for 5 min. The samples were chilled on ice and centrifuged at 19,000 × *g* for 10 min at 4°C. The aqueous layer was transferred to a microtube, RNA was precipitated with cold ethanol, and it was incubated at −70°C overnight.

The RNA was pelleted by centrifugation at 19,000 x *g* for 10 min at 4°C. Pellets were washed with cold 70% ethanol and centrifuged at 19,000 × *g* for 5 min at 4°C. After careful removal of the ethanol, the pellets were air-dried for 15 min in a Centrifugal Vacuum Concentrator 5,301 (Eppendorf). The pellets were resuspended in DEPC-treated water. Purification of RNA was performed using the TURBO DNA-free kit (Ambion, Inc.). Quality of RNA was assessed using the NanoDrop ONE (Thermo Scientific) and with a bleach denaturing 1.5% agarose gel, as previously described (Aranda et al., 2012). cDNA was synthesized using 1 μg of RNA, 5 pmol/μl of random hexamer primers, and 200 U/μl of RevertAid M-MulV-RT (Reverse transcriptase of Moloney Murine Leukemia Virus; Thermo Scientific).

Quantitative real-time PCR was performed in a LightCycler 480 instrument (Roche) to quantify the gene expression levels. Specific primers (**Table 2**) were designed using the Primer3Plus software[1] (Untergasser et al., 2007). For LightCycler reactions, a master mix of the following components was prepared: 2.0 μl of PCR-grade water, 0.5 μl (10 μM) of forward primer, 0.5 μl (10 μM) of reverse primer, 5 μl of 2x Master Mix, and 2.5 μl of cDNA (~50 ng). A multiwell plate containing all samples was loaded into the LightCycler 480 instrument. Amplification was performed in triplicate wells for each sample analyzed from three independent experiments. In each set of reactions, 16S rRNA (*rrsH*) was used as a reference gene for normalization of the cDNA amount. Real-time PCR analysis was performed using the following optimized assay conditions: (1) denaturation program (95°C for 10 min); amplification and quantification programs were repeated for 45 cycles (95°C for 10 s, 59°C for 10 s, 72°C for 10 s with a single fluorescence measurement), (2) melting curve program (95°C for 10 s, 65°C for 1 min with

[1]http://primer3plus.com/cgi-bin/dev/primer3plus.cgi

TABLE 2 | Primers used in this study.

Primer	Sequence (5"- 3")	Target gene
For Gene Deletion		
crp-H1P1	TATAACAGAGGATAACCGCGCATGGTGCTTGGCAAACCGCAAACATGTAGGCTGGAGCTGCTTCG	*crp*
crp-H2P2	GCAATACGCCGTTTTACCGACTTAACGGGTACCGTAGACGACGATCATATGAATATCCTCCTTAG	
npsA-H1P1	CTAATTCTCCAGGAGAGAGTGATGACGCATTCAGCATATGTCTATTGTAGGCTGGAGCTGCTTCG	*npsA*
npsA-H2P2	GTTGCTCAACGTTGTCCATATTTACACCTGCTCCAGTAAAGAATTCATATGAATATCCTCCTTAG	
For Site-Directed Mutagenesis		
aroX-npsA-CRPBox-F	TGCCGCCAGCTTACCACAGGATGCCCTCGGGCAAACACCGCAAAA	*aroX-npsA*
aroX-npsA-CRPBox-R	TTTTGCGGTGTTTGCCCGAGGGCATCCTGTGGTAAGCTGGCGGCA	
For Mutant Characterization		
crp-MC-F	CGGCACCCGGAGATAGCTTA	*crp*
crp-MC-R	AGGGGAAAACAAAAACGGCG	
npsA-MC-F	TTTGCGGTGTTTTCTTAGAAGCA	*npsA*
npsA-MC-R	CGGGTTAATCGCCTCTGAATG	
FOR qPCR		
aroX-F	TGTTGCCTGCAAGATTGACG	*aroX*
aroX-R	ATGTGTGAACGGCCAAAACG	
dhbX-F	ATGCGGCCAATCTGATGATG	*dhbX*
dhbX-R	AGCCCCAGAGCATAGGTAAATG	
icmx-F	TGATTGTCTGCGGCGTTTAC	*icmX*
icmX-R	GCTAGACGATGCTTTTCTTCGG	
adsX-F	TGCACATTGAACGGCAAGAC	*adsX*
adsX-R	ATCGAAGTGCAGGTTTCGTG	
hmoX-F	TCGCATGCCAAAGATTTCGC	*hmoX*
hmoX-R	ATGAGCTTGACGCGTTCAAC	
npsA-F	AAATACGTGGCTTCCGCATC	*npsA*
npsA-R	TCCTGCGTGACATAACAAGC	
thdA-F	TGGACAACGTTGAGCAACAG	*thdA*
thdA-R	TGCTTACCATTGACGCCAAC	
npsB-F	TGAGCATTTGCAGCTGGTTC	*npsB*
npsB-R	ATGCGTGGCAACTTTGTGTG	
crp-F	TGCTGAACCTGGCAAAACAG	*crp*
crp-R	ATTTTCAGGATGCGGCCAAC	
rrsH-F	CAGGGGTTTGGTCAGACACA	*rrsH*
rrsH-R	GTTAGCCGGTGCTTCTTCTG	
For EMSA		
aroX-npsA-F	TCTCTCACTCGAAATTTAACAGGT	*aroX-npsA*
aroX-npsA-R	TCTCTCCTGGAGAATTAGGAACG	
estA2-F	CCAGAGGCGGTCGAACTC	*estA2*
estA2-R	ATTACCTCCGAAACACGTCGT	
eltA-F	CCAGCGATAAAGTCTGTAAATACGG	*eltA*
eltA-R	TATCATACAAGAAGACAATCCGGA	

The sequence corresponding to the template plasmid pKD4 is underlined.

continuous fluorescence measurement at 97°C), and (3) a cooling step at 40°C for 10 s. The absence of contaminating DNA was tested by the lack of amplification products after 45 qPCR cycles using RNA as template. Control reactions with no RNA template and with no reverse transcriptase enzyme were run in all experiments. The relative gene expression was calculated using the $2^{-\Delta\Delta Ct}$ method (Livak and Schmittgen, 2001; Schmittgen and Livak, 2008). To ensure that 16S rRNA (*rrsH*) was an optimal reference gene for normalization of qPCR, absolute quantification was performed by obtaining a standard curve according to 10-fold dilutions of *K. oxytoca* 09–7231 chromosomal DNA (10^3, 10^4, 10^5, 10^6, and 10^7 theoretical copies). Ct values were interpolated to standard curve to obtain gene expression (gene copies per μg RNA). Expression of 16S rRNA (*rrsH*) gene remained unaffected in all conditions tested (**Supplementary Figure S1**).

Protein Purification

The His_6-CRP expression plasmid pQE80crp (Kurabayashi et al., 2017) was electroporated into competent *E. coli* BL21 (DE3). Bacteria containing recombinant plasmid were grown at 37°C to an OD_{600nm} of 0.5 in LB; 1.0 mM IPTG was then added and cultured for 3 h. Cells were then pelleted by centrifugation and resuspended in urea buffer (8 M urea, 100 mM Na_2HPO_4, and 10 mM Tris-HCl, pH 8.0) and lysed

by sonication. The lysate was centrifuged, and the supernatant was filtered through Ni-NTA agarose column (Qiagen) pre-equilibrated with urea buffer. After washing with buffer containing 50 mM imidazole (200 ml), the protein was eluted with 500 mM imidazole (10 ml). Fractions were analyzed by SDS-PAGE and Coomassie blue staining. Protein concentration was determined by the Bradford procedure. Aliquots of the purified protein were stored at −70°C.

Electrophoretic Mobility Shift Assays

To evaluate CRP binding to the promotor sequence, a 448-bp DNA probe containing the intergenic regulatory region of the divergent *aroX* and *npsA* genes was used. In addition, the probe ΔCRP-Box containing the mutation in the putative CRP-binding site on the intergenic regulatory region of the divergent *aroX* and *npsA* genes was employed. DNA probes from the regulatory region of the enterotoxigenic *E. coli estA2* and *eltA* genes were used as positive and negative controls (Haycocks et al., 2015). The binding reaction was performed with 100 ng of DNA probes and increasing concentrations of purified His_6-CRP with or without 200 μM cAMP (Hirakawa et al., 2020) in a 20 μl reaction mixture containing H/S 10X gel-shift binding buffer (400 mM HEPES, 80 mM $MgCl_2$, 500 mM KCl, 10 mM DTT, 0.5% NP40, and 1 mg/ml BSA, De la Cruz et al., 2007). Samples were incubated for 20 min at room temperature and then separated by electrophoresis in 6% non-denaturing polyacrylamide gels using 0.5X Tris-borate-EDTA buffer at 4°C. The DNA bands were stained with ethidium bromide and visualized under UV light.

Cytotoxicity Assays

HeLa cell line (ATCC CCL-2) was used to determine cytotoxic activity as previously described (Darby et al., 2014). Approximately 1×10^6 cells were suspended in 900 μl of DMEM high glucose (4.5 g/l; Invitrogen) with 10% FBS (Gibco) and seeded into 24-well cell culture plates (Costar). To investigate cytotoxin production in the *K. oxytoca* strains (wild type, Δ*crp*, Δ*crp* pTrc99K-CRP, and Δ*npsA*), 100 μl of bacterial supernatants was filtered through a PVDF 0.22-μm sterile Millex-GV filter (Merck Millipore) and added to the wells containing HeLa cells. After 48 h of incubation at 37°C under a 5% CO_2 atmosphere, the cells were visualized using a Nikon TE300 inverted microscope at 10X magnification. Cytotoxin production was defined as >50% cell rounding and detachment and < 50% confluency, as compared to the negative control samples [(TLB medium only or supernatant of the non-toxigenic *K. oxytoca* Δ*npsA* strain (Schneditz et al., 2014; Dornisch et al., 2017; Tse et al., 2017)]. Negative control samples had a monolayer with minimal cell rounding or detachment and > 80% confluency.

The LDH Cytotoxicity Assay Kit (Invitrogen) was used according to the manufacturer's instructions to measure lactate dehydrogenase (LDH) released from HeLa cells after damage of plasma membrane integrity. 1×10^4 HeLa cells were cultivated in 100 μl DMEM high glucose (4.5 g/l; Invitrogen) with 10% FBS (Gibco), seeded into 96-well flat-bottom culture plates (Costar), and incubated at 37°C under a 5% CO_2 atmosphere for 48 h. Subsequently, the medium was removed, and the cells washed with PBS. Then, 10 μl of negative control (PBS), culture medium control (TLB), positive control (lysis buffer), and filtered bacterial supernatants (wild type, Δ*crp*, Δ*crp* pTrc99K-CRP, and Δ*npsA*) as described before was added to DMEM medium without FBS for 48 h. After treatment, an aliquot of 50 μl each sample medium was transferred to a new 96-well plate, and kit solutions were added into each well. The absorbance was measured at 490 nm and 680 nm with a spectrophotometer (Multiskan Ascent, Thermo Scientific). All samples were tested in triplicate on three independent biological replicates, and the mean results were expressed as LDH cytotoxicity by subtracting the 680 nm absorbance background value from the 490 nm absorbance value.

Statistical Analysis

Statistical analysis was performed using Prism 7.0 (GraphPad Software, Inc., San Diego, CA, United States). Data represent the mean ± standard deviation (SD). The mean differences were determined using one-way ANOVA followed by Tukey's comparison test. Values of $p < 0.05$ were considered statistically significant.

RESULTS

Expression of *aroX* and NRPS Operons Is Enhanced by Growth in TLB Medium

To determine the optimal conditions of expression of the *aroX* and NRPS operons of *K. oxytoca* MIT 09-7231, the bacteria were cultivated in different culture media, such as LB, TSB, TLB, and DMEM transcription analyzed by RT-qPCR. The conventional LB medium was used as a reference to determine the basic levels of expression of genes encoded by the *aroX* and NRPS operons. The lowest levels of transcription of the *aroX* and NRPS operons occurred when the bacteria were cultivated in DMEM; this was rather surprising since expression of most virulence factors of pathogenic *E. coli* strains occurs upon growth in DMEM (Leverton and Kaper, 2005; Platenkamp and Mellies, 2018). In comparison with the growth of MIT 09-7231 in LB, the expression of *aroX* and NRPS operons of MIT 09-7231 cultivated in TSB and TLB media enhanced ~5- and ~150-fold, respectively (**Figure 1A**). Unlike TSB medium, TLB contains lactose instead of soy. The expression levels of TV genes were very similar in the different culture media, supporting the notion that they are genetically organized in operons. Since *aroX* and *npsA* are the first genes of the *aroX* and NRPS operons, respectively, only the expression of these two genes was evaluated throughout the study. When *K. oxytoca* MIT 09-7231 was grown in TLB at 37°C for 12 h, the highest levels of expression of *aroX* and *npsA* genes occurred at 9 h and were maintained for 12 h, which corresponds to stationary growth phase (**Figure 1B**). Our data indicate that growth in TLB medium, which contains lactose, favors the expression of *K. oxytoca aroX* and NRPS operons during stationary growth phase.

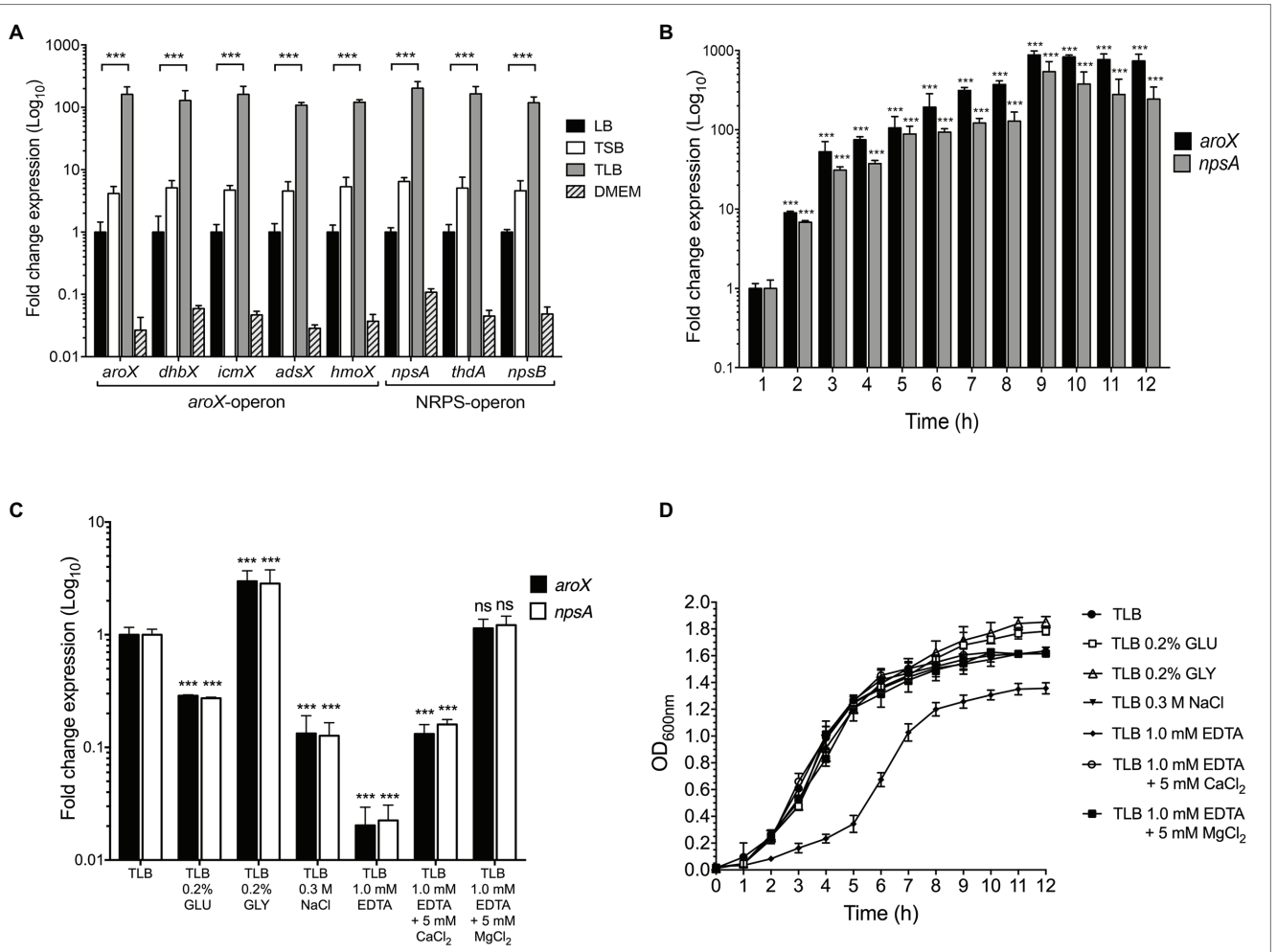

FIGURE 1 | Effect of environmental cues on *aroX* and NRPS operons expression. **(A)** Fold change expression detected by RT-qPCR of *aroX* and NRPS operons of *K. oxytoca* compared to LB. Bacterial cultures were grown at 37°C for 9 h in different culture media: lysogenic broth (LB), tryptone soy broth (TSB), tryptone lactose broth (TLB), and Dulbecco's modified Eagle's medium (DMEM) with high glucose (4.5 g/l). **(B)** Transcription of *aroX* and *npsA* genes during growth phases. **(C)** Transcription of *aroX* and *npsA* genes at stationary phase ($OD_{600nm} = 1.6$) at 37°C under different environmental conditions determined by RT-qPCR. **(D)** Growth curves of wild-type *K. oxytoca* in TLB medium at 37°C for 12 h supplemented with glucose (GLU, 0.2%), glycerol (GLY, 0.2%), sodium chloride (NaCl, 0.3 M), and ethylenediaminetetraacetic acid (EDTA, 1.0 mM, supplemented or not supplemented with 5.0 mM $CaCl_2$/$MgCl_2$). 16S rRNA was used as a reference gene for normalization of expression. These graphs represent the mean of three independent experiments performed in triplicate with standard deviations. Statistically significant with respect to bacteria grown in LB medium (A) or with respect to bacteria grown after 1 h post-inoculation in TLB medium (B) or with respect to bacteria grown in non-supplemented TLB medium (C): $^{**}p < 0.001$. All values of p were calculated using one-way ANOVA and Tukey's comparison test.

Expression of *aroX* and *npsA* Genes Is Differentially Regulated by Nutritional and Environmental Factors

The influence of nutritional factors in the expression of genes involved in TV biosynthesis was quantified by RT-qPCR when *K. oxytoca* was grown in TLB supplemented with 0.2% glucose, 0.2% glycerol, 0.3 M sodium chloride, and 1.0 mM EDTA. The expression of *aroX* and *npsA* genes was repressed (~4-fold) and activated (~3-fold) by glucose and glycerol, respectively (**Figure 1C**). In high osmolarity (0.3 M NaCl), the transcription of *aroX* and *npsA* decreased ~8-fold (**Figure 1C**). Transcription of these genes required divalent cations because the addition of EDTA dramatically diminished their expression (~50-fold), and this effect was partially and fully reverted by the addition of $CaCl_2$ and $MgCl_2$, respectively (**Figure 1C**). Of note, depletion of divalent cations by the addition of EDTA to the culture medium affected negatively bacterial growth (**Figure 1D**). This effect was reversed by the addition of $CaCl_2$ and $MgCl_2$ to TLB containing EDTA (**Figure 1D**). The data indicate that glucose, high osmolarity, and depletion of divalent cations from the growth medium repress *aroX* and *npsA* genes.

CRP Activates the Expression of *aroX* and *npsA* Genes

As described above, carbon sources such as lactose, glucose, and glycerol affect the transcription of *aroX* and *npsA* genes. CRP is a global regulator that senses the fluctuations of

carbon sources and controls the transcription of some enzymes involved in metabolite biosynthesis (Bai et al., 2011; Gao et al., 2012; Soberón-Chávez et al., 2017; Jeong et al., 2021). Hence, we sought to investigate the role of CRP in the regulation of *aroX* and *npsA* genes. Growth rates and expression of these genes in the wild type and its derivative Δ*crp* isogenic mutant were compared after growth in TLB at stationary phase ($OD_{600nm} = 1.6$) by RT-qPCR. In the absence of CRP, growth was significantly attenuated and expression levels of both *aroX* and *npsA* genes were diminished ~10-fold. Both, growth rate and expression were reversed by the complementation of this mutant with the pTrc99K-CRP plasmid (**Figures 2A,B**). These results indicate that CRP positively regulates expression of *aroX* and *npsA* genes.

Effect of Lactose on CRP-Mediated *aroX* and *npsA* Expression

We wanted to know whether the regulation exerted by lactose on TV genes implicated CRP. Thus, we quantified the transcription of *aroX* and *npsA* genes in the wild-type and Δ*crp* mutant strains growing in TLB (medium with lactose) and TB (tryptone broth), which is TLB without lactose. Growth of the wild-type strain in the absence of the lactose decreased TV gene transcription by ~5-fold (**Figure 2C**). This effect was CRP-dependent because transcription of *aroX* and *npsA* was not altered in the Δ*crp* mutant strain (**Figure 2C**). As an expression control of a lactose-regulated gene, we quantified the transcription of *crp* in the wild-type growing in the presence of lactose and found ~2-fold increase in expression. We hypothesized that lactose is involved in the CRP-dependent *aroX* and *npsA* transcription; thus, we analyzed TV-mediated cytotoxicity on HeLa epithelial cells using the supernatants of the wild-type and Δ*crp* mutant cultures grown in the presence and absence of lactose (**Figure 2D**). The supernatant recovered of the wild-type strain grown in TLB (with lactose) presented a higher cytotoxic effect on HeLa cells than the supernatant obtained from the wild-type strain grown in TB (without lactose). The supernatants from the Δ*crp* mutant grown with/without lactose caused a slight cytotoxic effect on HeLa cells (**Figure 2D**). These data support our hypothesis that lactose induces CRP-mediated *aroX* and *npsA* genes transcription and consequently triggers TV-mediated cytotoxicity on HeLa epithelial cells.

CRP Binds to the Intergenic Region of *aroX* and *npsA* Genes

Sequence analysis of the intergenic region of *aroX* and *npsA* genes identified a putative CRP-binding site (**Figure 3A**). This sequence (CGTGA-N_6-TCTAA) shared 7 of 10 bp with the *E. coli* consensus sequence (TGTGA-N_6-TCACA; **Figure 3B**). Electrophoretic mobility shift assays (EMSA) were performed using a recombinant His_6-CRP protein and DNA probes. Indeed, CRP bound to the *aroX-npsA* intergenic region since CRP-DNA complexes were observed using 100 nM of His_6-CRP and this DNA-binding activity was dependent of the presence of cAMP (200 μM; **Figure 3C**). To demonstrate whether the putative CRP-box was required for CRP binding to the *aroX-npsA* intergenic region, site-directed mutagenesis of the CRP-box was performed (**Figure 3B**). CRP did not bind to the *aroX-npsA* intergenic region containing the mutation of CRP-Box (**Figure 3D**). As positive and negative controls, *estA2* and *eltA* regulatory regions were used (**Figures 3E,F**; Haycocks et al., 2015). These results clearly show that CRP binds directly to the *aroX-npsA* intergenic region through recognition of a specific binding site.

CRP Induces TV-Mediated Cytotoxicity on Epithelial Cells

To corroborate the role of CRP on the *aroX* and *npsA* genes transcription, we determined the TV-mediated cytotoxicity on epithelial cells using the supernatants from *K. oxytoca* wild type, Δ*crp* mutant, and complemented Δ*crp* mutant. Cytotoxicity was severely affected in the Δ*crp* mutant as compared to the wild type and the complemented mutant. As expected, the supernatant of the non-toxigenic Δ*npsA* strain did not cause any cytotoxic effect on HeLa cells (**Figure 4A**). Further, the LDH release activity assay showed that wild-type strain supernatant induced death of HeLa cells (~14-fold) as compared to the PBS control. In contrast, the Δ*crp* mutant supernatant significantly reduced the death of HeLa cells by ~6-fold as compared to the wild-type strain supernatant. Levels of released LDH by HeLa cells treated with the supernatant of the complemented Δ*crp* mutant were similar to that of wild-type strain supernatant. Neither the TLB medium nor the non-toxigenic Δ*npsA* supernatant induced death of HeLa cells (**Figure 4B**). These phenotypic data support the role of CRP global regulator as a transcriptional activator of genes involved in the *K. oxytoca* TV biosynthesis.

DISCUSSION

K. oxytoca is a pathobiont of the intestinal microbiota that can produce TV cytotoxin (Beaugerie et al., 2003; Högenauer et al., 2006; Zollner-Schwetz et al., 2015; Glabonjat et al., 2021). After penicillin treatment, alteration of the enteric microbiota occurs, and overgrowth of *K. oxytoca* is originated in the colon causing a severe dysbiosis (Schneditz et al., 2014; Hajishengallis and Lamont, 2016; Dornisch et al., 2017; von Tesmar et al., 2018; Alexander et al., 2020). The imbalance in the gut microbiota and the production of TV cytotoxin result in AAHC (Högenauer et al., 2006; Unterhauser et al., 2019). The *aroX* and NRPS operons encode the proteins involved in the biosynthesis of TV and are clustered in a PAI that is only present in the *K. oxytoca* toxigenic strains (Schneditz et al., 2014; Dornisch et al., 2017). In this study, we analyzed the expression of *aroX* and NRPS operons in strains growing in various culture media since previous work has determined that nutritional components are environmental stimuli that trigger a differential expression of genes related to bacterial virulence (Blair et al., 2013;

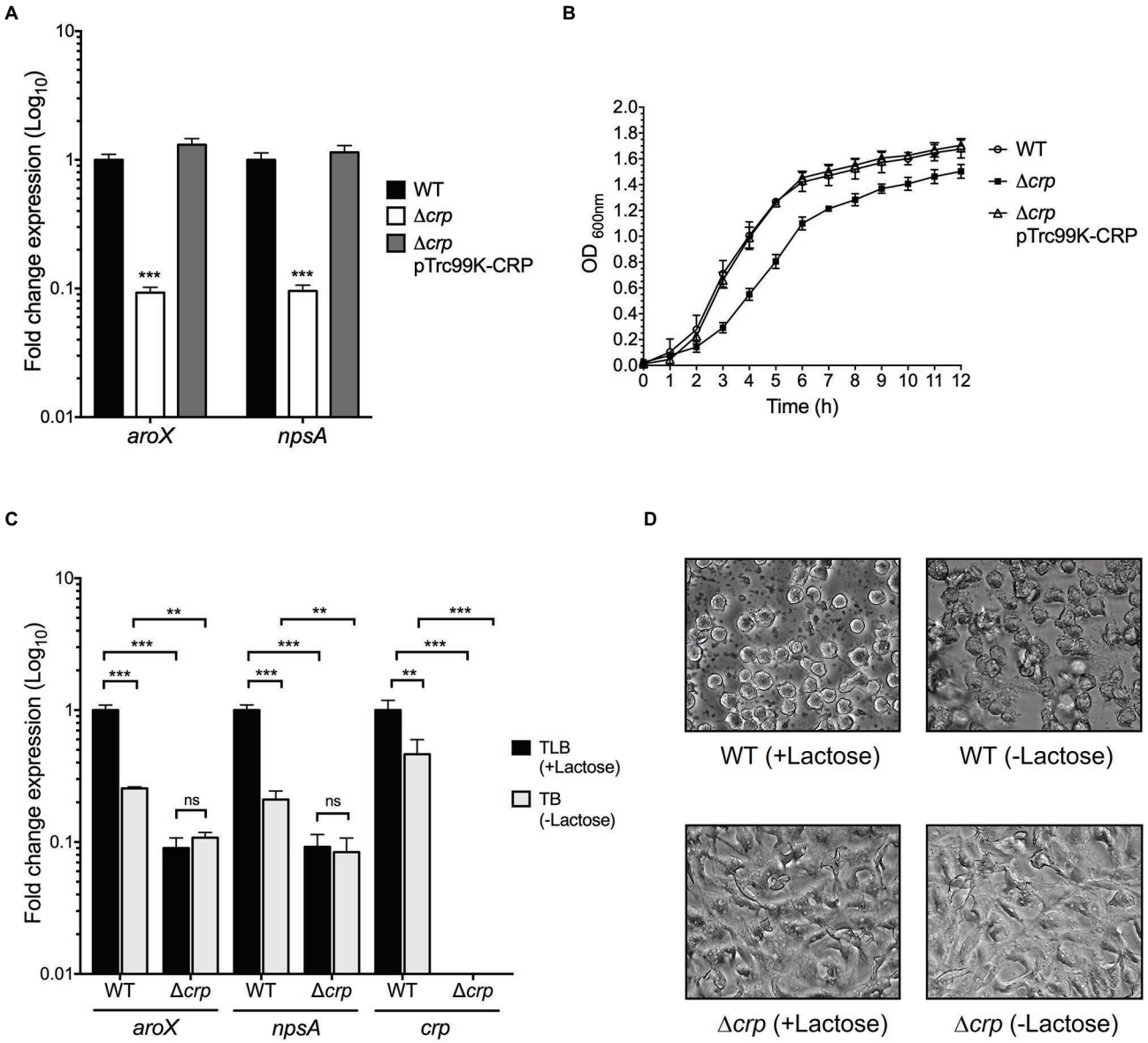

FIGURE 2 | Regulatory activity of CRP in expression of *aroX* and *npsA* genes. **(A)** Determination of transcriptional expression by RT-qPCR of *aroX* and *npsA* genes of wild-type *K. oxytoca*, Δ*crp*, and Δ*crp* pTrc99K-CRP in TLB medium at stationary phase ($OD_{600nm} = 1.6$) at 37°C. **(B)** Growth curves of wild-type *K. oxytoca*, Δ*crp*, and Δ*crp* pTrc99K-CRP, in TLB medium at 37°C. Bacterial cultures were grown for 12 h. **(C)** Transcription of *aroX*, *npsA*, and *crp* genes at stationary phase ($OD_{600nm} = 1.6$) at 37°C determined by RT-qPCR in TLB (medium with lactose), and TB (medium without lactose) at 37°C for 12 h. These graphs represent the mean of three independent experiments performed in triplicate with standard deviations. **(D)** HeLa cell culture inoculated with supernatants recovered from wild-type and Δ*crp* strains grown in TLB (medium with lactose) and TB (medium without lactose). Results represent the mean of three independent experiments performed in triplicate with standard deviations. Statistically significant with respect to wild-type strain (A) or with respect to bacteria grown in TLB medium (B): $^{**}p < 0.01$; $^{***}p < 0.001$. All Values of *p* were calculated using one-way ANOVA and Tukey's comparison test.

De la Cruz et al., 2017; Han et al., 2017; Ares et al., 2019; Soria-Bustos et al., 2020; Jiang et al., 2021). Our results showed that TLB culture medium significantly enhanced the expression of the *aroX* and NRPS operons, in agreement with a previous report in which the production of TV significantly increased in the toxigenic strain *K. oxytoca* MH43-1 when the bacterium was grown in TLB as compared with TSB and LB (Tse et al., 2017). A previous report showed that TV production reaches maximum levels at late exponential and stationary growth phases (Joainig et al., 2010). We determined the expression of *aroX* and *npsA* genes during 12 h of growth in TLB medium and, as expected, transcription attained maximum levels at 9 h and remained as such until 12 h of growth, which corresponds to stationary growth phase. In addition to the effect of nutritional components from different culture media being analyzed,

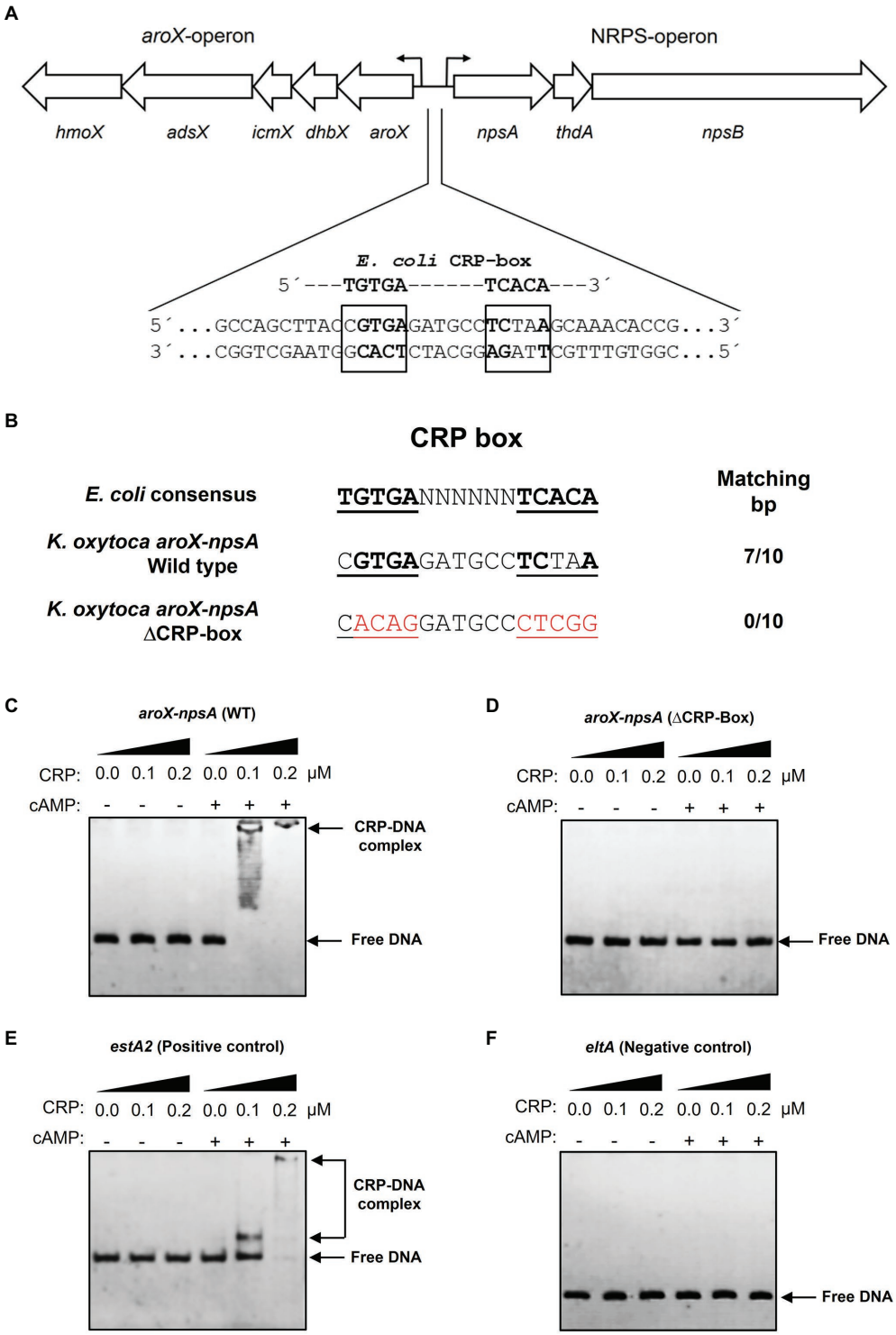

FIGURE 3 | Electrophoretic mobility shift assay showing binding of CRP-cAMP to the intergenic region of *aroX* and *npsA* genes. **(A)** Genetic organization of the *aroX* and NRPS operons and putative CRP-binding sites located in the intergenic regulatory region. The putative CRP-binding site is indicated with bold and boxed letters. **(B)** The intergenic region of *K. oxytoca aroX* and *npsA* genes contains a CRP-Box similar to the CRP-binding consensus sequence found in *E. coli*. An altered CRP-Box was generated to determine CRP binding. Bases matching the consensus sequence are bold, and mutated bases are shown in red. EMSA experiments were conducted to determine the binding of purified recombinant His_6-CRP protein to the corresponding DNA probe from the wild-type intergenic region of *aroX* and *npsA* genes **(C)** and from the intergenic region of *aroX* and *npsA* containing the mutation in the putative CRP-Box **(D).** DNA probes from the *estA2* **(E)** and *eltA* **(F)** regulatory regions were used as positive and negative controls, respectively. 100 ng of DNA probe of each regulatory region was mixed and incubated with increasing concentrations (μM) of purified recombinant His_6-CRP protein (CRP) in the presence or absence of 200 μM of cAMP. Free DNA and CRP-DNA complex stained with ethidium bromide are indicated.

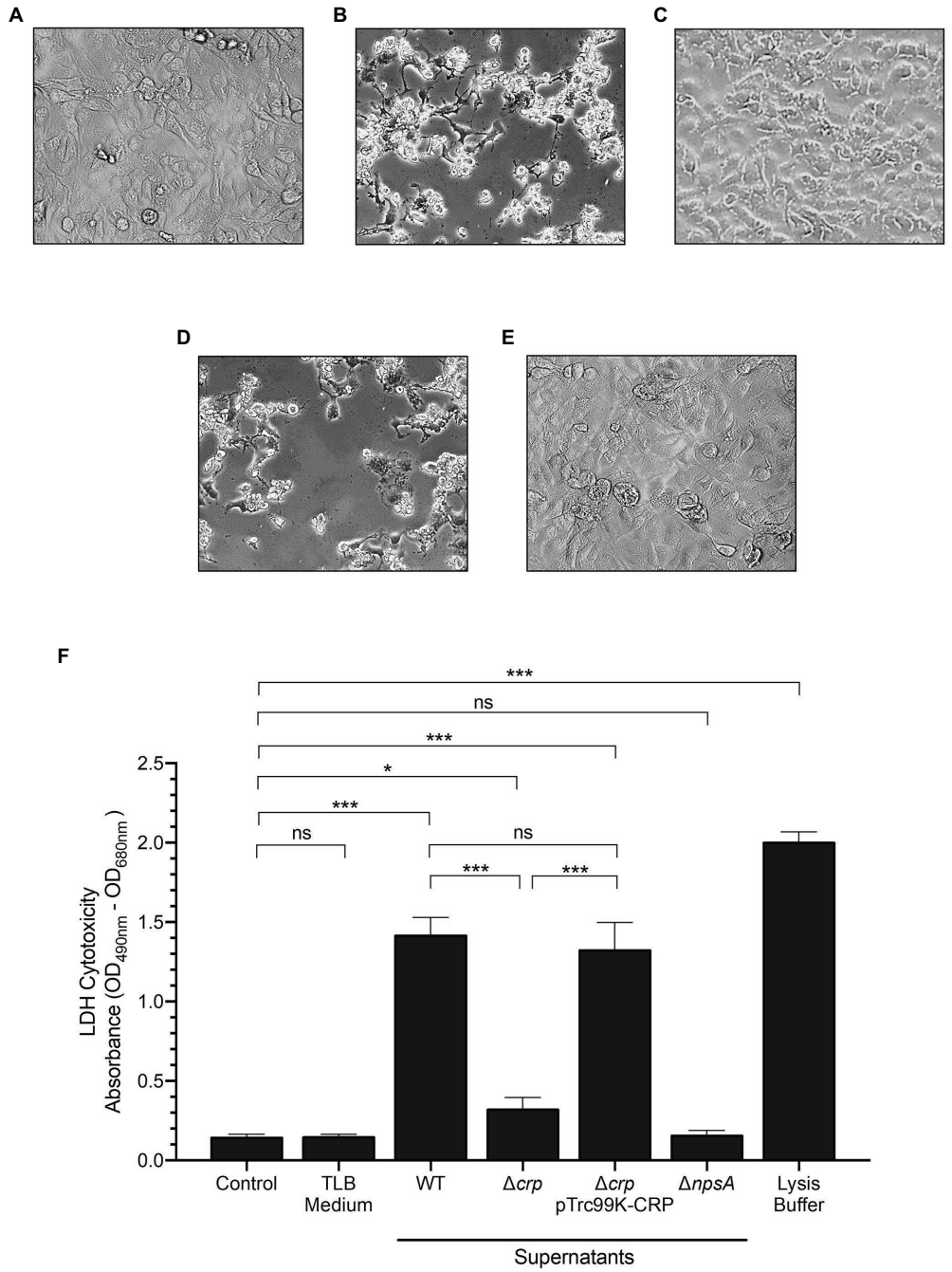

FIGURE 4 | Cytotoxicity of *K. oxytoca* Δ*crp* mutant strain. HeLa cell culture inoculated with: **(A)** TLB medium as control, and **(B)** wild-type **(C)** Δ*crp* **(D)** Δ*crp* pTrc99K-CRP, and **(E)** Δ*npsA K. oxytoca* supernatants. **(F)** HeLa cells were treated with TLB medium, and *K. oxytoca* supernatants (wild-type, Δ*crp*, Δ*crp* pTrc99K-CRP, and Δ*npsA*) for 48 h. Following treatment, aliquots were obtained for measurement of extracellular LDH. Minimal and maximal measurable LDH release was determined by incubating cells with PBS (control), and lysis buffer, respectively. Statistically significant: $*p < 0.05$; $***p < 0.001$; ns: not significant. All values of p were calculated using one-way ANOVA and Tukey's comparison test.

we evaluated the influence of other environmental stimuli such as glucose, glycerol, osmolarity, and divalent cations. Regarding the role of carbon source in transcription, glucose and glycerol repressed and activated the *aroX* and *npsA* gene expression, respectively. It was reported that glucose and glycerol have antagonistic activities in the control of cAMP production, which is necessary for the regulatory activity of the CRP protein (Soberón-Chávez et al., 2017). While glucose inhibits, glycerol induces cAMP synthesis (Deutscher et al., 2006; Fic et al., 2009; Pannuri et al., 2016). Glucose concentration is higher in the small intestine, while glycerol is produced abundantly by enteric microorganisms

residing in the colon (Yuasa et al., 2003; Fujimoto et al., 2006; Ohta et al., 2006; De Weirdt et al., 2010). Our results suggest that the genes involved in TV biosynthesis could be expressed in the glycerol-rich colon environment under regulation of CRP. We found here that sodium chloride repressed *aroX* and *npsA* gene expression. Previously, it was reported that when *Listeria monocytogenes* grows in the presence of high concentrations of sodium chloride, some genes that code for metabolic enzymes and virulence factors are repressed (Bae et al., 2012). In enterotoxigenic *E. coli,* the addition of sodium chloride to culture medium also repressed transcription of the coli surface antigen CS3 (Ares et al., 2019). In contrast, high osmolarity increases the gene expression of the enterotoxigenic *E. coli* Longus pilus (De la Cruz et al., 2017). The ubiquitous divalent cations magnesium and calcium are important nutrients required by bacteria for growth and cell maintenance. The effects of calcium and magnesium can be highlighted in physio-chemical interactions, gene regulation, and bio-macromolecular structural modification (Groisman et al., 2013; Wang et al., 2019). Moreover, it has been reported that divalent cations are involved in transcriptional regulation of virulence factors in pathogenic *E. coli*, *Aeromonas hydrophila*, *P. aeruginosa*, *Vibrio cholerae,* and *Yersinia enterocolitica* (Fälker et al., 2006; Bilecen and Yildiz, 2009; Vilches et al., 2009; Anderson et al., 2010; De la Cruz et al., 2017; Ares et al., 2019; Liu et al., 2020c). In our study, the presence of calcium and magnesium divalent cations was required for *aroX* and *npsA* gene expression.

This work underlines for the first time, the regulatory activity of CRP in the transcription of genes involved in TV biosynthesis. The *K. oxytoca* CRP protein is homologous to other CRP proteins from several enteropathogens such as *K. pneumoniae*, *E. coli*, and *S. enterica*. The absence of CRP exhibited a growth defect in both exponential and stationary phases, as observed in *Vibrio vulnificus* (Kim et al., 2013), *E. coli* (Basak et al., 2014), *K. pneumoniae* (Ou et al., 2017; Lin et al., 2018), and *Haemophilus parasuis* (Jiang et al., 2020). These observations are in accordance with previous reports that explain how growth fitness is affected by the *crp* deletion, which produces fluctuations of metabolic gene expression and alterations of carbon metabolites, α-ketoacids, cAMP, and amino acids that promote proper coordination of protein biosynthesis machinery during metabolism (Klumpp et al., 2009; Berthoumieux et al., 2013; You et al., 2013; Pal et al., 2020). CRP is a central regulator of carbon metabolism and has been implicated as an important facilitator of host colonization and virulence in many bacterial pathogens, including *K. pneumoniae* (Xue et al., 2016; Lin et al., 2018; Panjaitan et al., 2019). In this study, we demonstrated that CRP positively regulates the expression of the *aroX* and NRPS operons and plays a regulatory role in response to lactose as was previously demonstrated in *E. coli* and *K. pneumoniae*, where lactose acts as glycerol inducing the augmentation of cAMP (Deutscher et al., 2006; Panjaitan et al., 2019). We also showed that CRP directly activates the expression of *aroX* and *npsA* genes by binding to their intergenic regulatory region and that cAMP is indispensable for this DNA-binding activity.

Cytotoxic effects of toxigenic *K. oxytoca* strains have been previously reported (Minami et al., 1989, 1994; Higaki et al., 1990; Beaugerie et al., 2003; Darby et al., 2014; Schneditz et al., 2014; Tse et al., 2017; Paveglio et al., 2020). We found that the Δ*crp* mutant strain was remarkably less cytotoxic than the wild-type strain. This was due to downregulation of the TV biosynthetic *aroX* and NRPS operons and reduced TV production in the absence of CRP.

CONCLUSION

This study underscores the role of the CRP-cAMP signaling pathway in the activation of genes involved in TV biosynthesis of toxigenic *K. oxytoca* and provides clues about the intestinal signals that trigger CRP-mediated TV production.

DATA AVAILABILITY STATEMENT

The original contributions presented in the study are included in the article/**Supplementary Material**, and further inquiries can be directed to the corresponding authors.

AUTHOR CONTRIBUTIONS

DR-V, MC, and MA conceived and designed the study. DR-V, NL-M, JS-B, JM-C, RG-U, RR-R, and LG-M performed the experiments. DR-V, SR-G, JG-M, HH, JF, MC, and MA analyzed the data. DR-V, JAG, MC, and MA wrote the manuscript. All authors contributed to the article and approved the submitted version.

ACKNOWLEDGMENTS

DR-V was supported by pre-doctoral fellowships from CONACYT (734002) and IMSS (99097641). This paper constitutes the fulfillment of DR-V's requirement for the PhD Graduate Program in Biomedicine and Molecular Biotechnology, National Polytechnic Institute (IPN), Mexico. The authors thank J. David García for his help with CRP protein purification.

SUPPLEMENTARY MATERIAL

The Supplementary Material for this article can be found online at: https://www.frontiersin.org/articles/10.3389/fmicb.2021.743594/full#supplementary-material

Supplementary Figure S1 | Expression of reference gene (*rrsH*) under the different conditions tested in this study. Panels show the expression of reference gene in different: **(A)** growth conditions, **(B)** growth phases, **(C)** environmental cues, **(D)** *K. oxytoca* strains, and **(E)** growth culture medium with or without lactose. Quantification of expression is showed as *rrsH* (16S rRNA) copies per microgram of RNA.

REFERENCES

Alexander, E. M., Kreitler, D. F., Guidolin, V., Hurben, A. K., Drake, E., Villalta, P. W., et al. (2020). Biosynthesis, mechanism of action, and inhibition of the enterotoxin Tilimycin produced by the opportunistic pathogen *Klebsiella oxytoca*. *ACS Infect. Dis.* 6, 1976–1997. doi: 10.1021/acsinfecdis.0c00326

Anderson, G. G., Yahr, T. L., Lovewell, R. R., and O'Toole, G. A. (2010). The *Pseudomonas aeruginosa* magnesium transporter MgtE inhibits transcription of the type III secretion system. *Infect. Immun.* 78, 1239–1249. doi: 10.1128/IAI.00865-09

Aranda, P. S., LaJoie, D. M., and Jorcyk, C. L. (2012). Bleach gel: A simple agarose gel for analyzing RNA quality. *Electrophoresis* 33, 366–369. doi: 10.1002/elps.201100335

Ares, M. (2012). Bacterial RNA isolation. *Cold Spring Harb. Protoc.* 2012, 1024–1027. doi: 10.1101/pdb.prot071068

Ares, M. A., Abundes-Gallegos, J., Rodríguez-Valverde, D., Panunzi, L. G., Jiménez-Galicia, C., Jarillo-Quijada, M. D., et al. (2019). The coli surface antigen CS3 of Enterotoxigenic *Escherichia coli* is differentially regulated by H-NS, CRP, and CpxRA global regulators. *Front. Microbiol.* 10:1685. doi: 10.3389/fmicb.2019.01685

Bae, D., Liu, C., Zhang, T., Jones, M., Peterson, S. N., and Wang, C. (2012). Global gene expression of *Listeria monocytogenes* to salt stress. *J. Food Prot.* 75, 906–912. doi: 10.4315/0362-028X.JFP-11-282

Bai, G., Schaak, D. D., Smith, E. A., and McDonough, K. A. (2011). Dysregulation of serine biosynthesis contributes to the growth defect of a *Mycobacterium tuberculosis crp* mutant. *Mol. Microbiol.* 82, 180–198. doi: 10.1111/j.1365-2958.2011.07806.x

Basak, S., Geng, H., and Jiang, R. (2014). Rewiring global regulator cAMP receptor protein (CRP) to improve *E. coli* tolerance towards low pH. *J. Biotechnol.* 173, 68–75. doi: 10.1016/j.jbiotec.2014.01.015

Beaugerie, L., Metz, M., Barbut, F., Bellaiche, G., Bouhnik, Y., Raskine, L., et al. (2003). *Klebsiella oxytoca* as an agent of antibiotic-associated hemorrhagic colitis. *Clin. Gastroenterol. Hepatol.* 1, 370–376. doi: 10.1053/S1542-3565(03)00183-6

Belkaid, Y., and Harrison, O. J. (2017). Homeostatic immunity and the microbiota. *Immunity* 46, 562–576. doi: 10.1016/j.immuni.2017.04.008

Berry, A., Han, K., Trouillon, J., Robert-Genthon, M., Ragno, M., Lory, S., et al. (2018). cAMP and Vfr control Exolysin expression and cytotoxicity of *Pseudomonas aeruginosa* taxonomic outliers. *J. Bacteriol.* 200:e00135-18. doi: 10.1128/JB.00135-18

Berthoumieux, S., de Jong, H., Baptist, G., Pinel, C., Ranquet, C., Ropers, D., et al. (2013). Shared control of gene expression in bacteria by transcription factors and global physiology of the cell. *Mol. Syst. Biol.* 9:634. doi: 10.1038/msb.2012.70

Bilecen, K., and Yildiz, F. H. (2009). Identification of a calcium-controlled negative regulatory system affecting *Vibrio cholerae* biofilm formation. *Environ. Microbiol.* 11, 2015–2029. doi: 10.1111/j.1462-2920.2009.01923.x

Blair, J. M. A., Richmond, G. E., Bailey, A. M., Ivens, A., and Piddock, L. J. V. (2013). Choice of bacterial growth medium alters the transcriptome and phenotype of S*almonella enterica* Serovar Typhimurium. *PLoS One* 8:e63912. doi: 10.1371/journal.pone.0063912

Crofts, A. A., Giovanetti, S. M., Rubin, E. J., Poly, F. M., Gutiérrez, R. L., Talaat, K. R., et al. (2018). Enterotoxigenic *E. coli* virulence gene regulation in human infections. *Proc. Natl. Acad. Sci. U. S. A.* 115, E8968–E8976. doi: 10.1073/pnas.1808982115

Darby, A., Lertpiriyapong, K., Sarkar, U., Seneviratne, U., Park, D. S., Gamazon, E. R., et al. (2014). Cytotoxic and pathogenic properties of *Klebsiella oxytoca* isolated from laboratory animals. *PLoS One* 9:e100542. doi: 10.1371/journal.pone.0100542

Datsenko, K. A., and Wanner, B. L. (2000). One-step inactivation of chromosomal genes in *Escherichia coli* K-12 using PCR products. *Proc. Natl. Acad. Sci.* 97, 6640–6645. doi: 10.1073/pnas.120163297

De la Cruz, M. Á., Fernández-Mora, M., Guadarrama, C., Flores-Valdez, M. A., Bustamante, V. H., Vázquez, A., et al. (2007). LeuO antagonizes H-NS and StpA-dependent repression in *Salmonella enterica* ompS1. *Mol. Microbiol.* 66, 727–743. doi: 10.1111/j.1365-2958.2007.05958.x

De la Cruz, M. A., Morgan, J. K., Ares, M. A., Yáñez-Santos, J. A., Riordan, J. T., and Girón, J. A. (2016). The two-component system CpxRA negatively regulates the locus of enterocyte effacement of Enterohemorrhagic *Escherichia coli* involving σ(32) and Lon protease. *Front. Cell. Infect. Microbiol.* 6:11. doi: 10.3389/fcimb.2016.00011

De la Cruz, M. A., Ruiz-Tagle, A., Ares, M. A., Pacheco, S., Yáñez, J. A., Cedillo, L., et al. (2017). The expression of longus type 4 pilus of enterotoxigenic *Escherichia coli* is regulated by LngR and LngS and by H-NS, CpxR and CRP global regulators. *Environ. Microbiol.* 19, 1761–1775. doi: 10.1111/1462-2920.13644

De Weirdt, R., Possemiers, S., Vermeulen, G., Moerdijk-Poortvliet, T. C. W., Boschker, H. T. S., Verstraete, W., et al. (2010). Human faecal microbiota display variable patterns of glycerol metabolism. *FEMS Microbiol. Ecol.* 74, 601–611. doi: 10.1111/j.1574-6941.2010.00974.x

Deutscher, J., Francke, C., and Postma, P. W. (2006). How phosphotransferase system-related protein phosphorylation regulates carbohydrate metabolism in bacteria. *Microbiol. Mol. Biol. Rev.* 70, 939–1031. doi: 10.1128/MMBR.00024-06

Dornisch, E., Pletz, J., Glabonjat, R. A., Martin, F., Lembacher-Fadum, C., Neger, M., et al. (2017). Biosynthesis of the Enterotoxic Pyrrolobenzodiazepine natural product Tilivalline. *Angew. Chem. Int. Ed.* 56, 14753–14757. doi: 10.1002/anie.201707737

El Mouali, Y., Gaviria-Cantin, T., Sánchez-Romero, M. A., Gibert, M., Westermann, A. J., Vogel, J., et al. (2018). CRP-cAMP mediates silencing of *Salmonella* virulence at the post-transcriptional level. *PLoS Genet.* 14:e1007401. doi: 10.1371/journal.pgen.1007401

Fälker, S., Schmidt, M. A., and Heusipp, G. (2006). Altered Ca(2+) regulation of Yop secretion in *Yersinia enterocolitica* after DNA adenine methyltransferase overproduction is mediated by Clp-dependent degradation of LcrG. *J. Bacteriol.* 188, 7072–7081. doi: 10.1128/JB.00583-06

Fic, E., Bonarek, P., Górecki, A., Kedracka-Krok, S., Mikolajczak, J., Polit, A., et al. (2009). cAMP receptor protein from *Escherichia coli* as a model of signal transduction in proteins–a review. *J. Mol. Microbiol. Biotechnol.* 17, 1–11. doi: 10.1159/000178014

Fujimoto, N., Inoue, K., Hayashi, Y., and Yuasa, H. (2006). Glycerol uptake in HCT-15 human colon cancer cell line by Na(+)-dependent carrier-mediated transport. *Biol. Pharm. Bull.* 29, 150–154. doi: 10.1248/bpb.29.150

Gao, C., Hindra, M., Mulde, D., Yin, C., and Elliot, M. A. (2012). Crp is a global regulator of antibiotic production in Streptomyces. *MBio* 3:e00407-12. doi: 10.1128/mBio.00407-12

Geng, H., and Jiang, R. (2015). cAMP receptor protein (CRP)-mediated resistance/tolerance in bacteria: mechanism and utilization in biotechnology. *Appl. Microbiol. Biotechnol.* 99, 4533–4543. doi: 10.1007/s00253-015-6587-0

Glabonjat, R. A., Kitsera, M., Unterhauser, K., Lembacher-Fadum, C., Högenauer, C., Raber, G., et al. (2021). Simultaneous quantification of enterotoxins tilimycin and tilivalline in biological matrices using HPLC high resolution ESMS(2) based on isotopically (15)N-labeled internal standards. *Talanta* 222:121677. doi: 10.1016/j.talanta.2020.121677

Groisman, E. A., Hollands, K., Kriner, M. A., Lee, E.-J., Park, S.-Y., and Pontes, M. H. (2013). Bacterial Mg2+ homeostasis, transport, and virulence. *Annu. Rev. Genet.* 47, 625–646. doi: 10.1146/annurev-genet-051313-051025

Gunasekara, S. M., Hicks, M. N., Park, J., Brooks, C. L., Serate, J., Saunders, C. V., et al. (2015). Directed evolution of the *Escherichia coli* cAMP receptor protein at the cAMP pocket. *J. Biol. Chem.* 290, 26587–26596. doi: 10.1074/jbc.M115.678474

Hajishengallis, G., and Lamont, R. J. (2016). Dancing with the stars: how choreographed bacterial interactions dictate Nososymbiocity and give rise to keystone pathogens, accessory pathogens, and Pathobionts. *Trends Microbiol.* 24, 477–489. doi: 10.1016/j.tim.2016.02.010

Han, R., Xu, L., Wang, T., Liu, B., and Wang, L. (2017). A small regulatory RNA contributes to the preferential colonization of *Escherichia coli* O157:H7 in the large intestine in response to a low DNA concentration. *Front. Microbiol.* 8:274. doi: 10.3389/fmicb.2017.00274

Haycocks, J. R. J., Sharma, P., Stringer, A. M., Wade, J. T., and Grainger, D. C. (2015). The molecular basis for control of ETEC enterotoxin expression in response to environment and host. *PLoS Pathog.* 11:e1004605. doi: 10.1371/journal.ppat.1004605

Hering, F., Bücker, G., Zechner, H., Gorkiewicz, G., Zechner, E., Högenauer, C., et al. (2019). Tilivalline- and Tilimycin-independent effects of *Klebsiella oxytoca* on tight junction-mediated intestinal barrier impairment. *Int. J. Mol. Sci.* 20:5595. doi: 10.3390/ijms20225595

Higaki, M., Chida, T., Takano, H., and Nakaya, R. (1990). Cytotoxic component (s) of Klebsiella oxytoca on HEp-2 cells. *Microbiol. Immunol.* 34, 147–151. doi: 10.1111/j.1348-0421.1990.tb00999.x

Hirakawa, H., Takita, A., Kato, M., Mizumoto, H., and Tomita, H. (2020). Roles of CytR, an anti-activator of cyclic-AMP receptor protein (CRP) on flagellar expression and virulence in uropathogenic *Escherichia coli*. *Biochem. Biophys. Res. Commun.* 521, 555–561. doi: 10.1016/j.bbrc.2019.10.165

Ho, S. N., Hunt, H. D., Horton, R. M., Pullen, J. K., and Pease, L. R. (1989). Site-directed mutagenesis by overlap extension using the polymerase chain reaction. *Gene* 77, 51–59. doi: 10.1016/0378-1119(89)90358-2

Högenauer, C., Langner, C., Beubler, E., Lippe, I. T., Schicho, R., Gorkiewicz, G., et al. (2006). *Klebsiella oxytoca* as a causative organism of antibiotic-associated hemorrhagic colitis. *N. Engl. J. Med.* 355, 2418–2426. doi: 10.1056/NEJMoa054765

Huang, H., Shao, X., Xie, Y., Wang, T., Zhang, Y., Wang, X., et al. (2019). An integrated genomic regulatory network of virulence-related transcriptional factors in *Pseudomonas aeruginosa*. *Nat. Commun.* 10:2931. doi: 10.1038/s41467-019-10778-w

Jahn, C. E., Charkowski, A. O., and Willis, D. K. (2008). Evaluation of isolation methods and RNA integrity for bacterial RNA quantitation. *J. Microbiol. Methods* 75, 318–324. doi: 10.1016/j.mimet.2008.07.004

Jeong, S.-H., Park, J.-B., Wang, Y., Kim, G.-H., Zhang, G., Wei, G., et al. (2021). Regulatory molecule cAMP changes cell fitness of the engineered Escherichia coli for terpenoids production. *Metab. Eng.* 65, 178–184. doi: 10.1016/j.ymben.2020.11.009

Jiang, C., Cheng, Y., Cao, H., Zhang, B., Li, J., Zhu, L., et al. (2020). Effect of cAMP receptor protein gene on growth characteristics and stress resistance of *Haemophilus parasuis* Serovar 5. *Front. Cell. Infect. Microbiol.* 10:19. doi: 10.3389/fcimb.2020.00019

Jiang, L., Wang, P., Song, X., Zhang, H., Ma, S., Wang, J., et al. (2021). *Salmonella* Typhimurium reprograms macrophage metabolism via T3SS effector SopE2 to promote intracellular replication and virulence. *Nat. Commun.* 12:879. doi: 10.1038/s41467-021-21186-4

Jiang, M., and Zhang, H. (2016). Engineering the shikimate pathway for biosynthesis of molecules with pharmaceutical activities in *E. coli*. *Curr. Opin. Biotechnol.* 42, 1–6. doi: 10.1016/j.copbio.2016.01.016

Joainig, M. M., Gorkiewicz, G., Leitner, E., Weberhofer, P., Zollner-Schwetz, I., Lippe, I., et al. (2010). Cytotoxic effects of *Klebsiella oxytoca* strains isolated from patients with antibiotic-associated hemorrhagic colitis or other diseases caused by infections and from healthy subjects. *J. Clin. Microbiol.* 48, 817–824. doi: 10.1128/JCM.01741-09

Kim, Y. R., Lee, S. E., Kim, B., Choy, H., and Rhee, J. H. (2013). A dual regulatory role of cyclic adenosine monophosphate receptor protein in various virulence traits of *Vibrio vulnificus*. *Microbiol. Immunol.* 57, 273–280. doi: 10.1111/1348-0421.12031

King, A. N., de Mets, F., and Brinsmade, S. R. (2020). Who's in control? Regulation of metabolism and pathogenesis in space and time. *Curr. Opin. Microbiol.* 55, 88–96. doi: 10.1016/j.mib.2020.05.009

Kitamoto, S., Nagao-Kitamoto, H., Jiao, Y., Gillilland, M. G. III, Hayashi, A., Imai, J., et al. (2020). The Intermucosal connection between the mouth and gut in commensal Pathobiont-driven colitis. *Cell* 182, 447.e14–462.e14. doi: 10.1016/j.cell.2020.05.048

Klumpp, S., Zhang, Z., and Hwa, T. (2009). Growth rate-dependent global effects on gene expression in bacteria. *Cell* 139, 1366–1375. doi: 10.1016/j.cell.2009.12.001

Kumar, J., Chauhan, A. S., Gupta, J. A., and Rathore, A. S. (2021). Supplementation of critical amino acids improves glycerol and lactose uptake and enhances recombinant protein production in *Escherichia coli*. *Biotechnol. J.* 16:e2100143. doi: 10.1002/biot.202100143

Kurabayashi, K., Tanimoto, K., Tomita, H., and Hirakawa, H. (2017). Cooperative actions of CRP-cAMP and FNR increase the Fosfomycin susceptibility of Enterohaemorrhagic *Escherichia coli* (EHEC) by elevating the expression of glpT and uhpT under anaerobic conditions. *Front. Microbiol.* 8:426. doi: 10.3389/fmicb.2017.00426

Lee, Z.-W., Hwang, S.-H., Choi, G., Jang, K. K., Lee, T. H., Chung, K. M., et al. (2020). A MARTX toxin rtxA gene is controlled by host environmental signals through a CRP-coordinated regulatory network in *Vibrio vulnificus*. *MBio* 11:e00723-20. doi: 10.1128/mBio.00723-20

Leverton, L. Q., and Kaper, J. B. (2005). Temporal expression of enteropathogenic *Escherichia coli* virulence genes in an in vitro model of infection. *Infect. Immun.* 73, 1034–1043. doi: 10.1128/IAI.73.2.1034-1043.2005

Lin, W., Djukovic, A., Mathur, D., and Xavier, J. B. (2021). Listening in on the conversation between the human gut microbiome and its host. *Curr. Opin. Microbiol.* 63, 150–157. doi: 10.1016/j.mib.2021.07.009

Lin, D., Fan, J., Wang, J., Liu, L., Xu, L., Li, F., et al. (2018). The fructose-specific phosphotransferase system of *Klebsiella pneumoniae* is regulated by global regulator CRP and linked to virulence and growth. *Infect. Immun.* 86:e00340-18. doi: 10.1128/IAI.00340-18

Lindemose, S., Nielsen, P. E., Valentin-Hansen, P., and Møllegaard, N. E. (2014). A novel indirect sequence readout component in the E. coli cyclic AMP receptor protein operator. *ACS Chem. Biologicals* 9, 752–760. doi: 10.1021/cb4008309

Liu, Y., Han, R., Wang, J., Yang, P., Wang, F., and Yang, B. (2020c). Magnesium sensing regulates intestinal colonization of Enterohemorrhagic *Escherichia coli* O157:H7. *MBio* 11:e02470-20. doi: 10.1128/mBio.02470-20

Liu, L., Li, F., Xu, L., Wang, J., Li, M., Yuan, J., et al. (2020b). Cyclic AMP-CRP modulates the cell morphology of *Klebsiella pneumoniae* in high-glucose environment. *Front. Microbiol.* 10:2984. doi: 10.3389/fmicb.2019.02984

Liu, C., Sun, D., Zhu, J., Liu, J., and Liu, W. (2020a). The regulation of bacterial biofilm formation by cAMP-CRP: A mini-review. *Front. Microbiol.* 11:802. doi: 10.3389/fmicb.2020.00802

Livak, K. J., and Schmittgen, T. D. (2001). Analysis of relative gene expression data using real-time quantitative PCR and the 2− ΔΔCT method. *Methods* 25, 402–408. doi: 10.1128/mBio.02470-20

Minami, J., Katayama, S., Matsushita, O., Sakamoto, H., and Okabe, A. (1994). Enterotoxic activity of *Klebsiella oxytoca* cytotoxin in rabbit intestinal loops. *Infect. Immun.* 62, 172–177. doi: 10.1128/iai.62.1.172-177.1994

Minami, J., Okabe, A., Shiode, J., and Hayashi, H. (1989). Production of a unique cytotoxin by *Klebsiella oxytoca*. *Microb. Pathog.* 7, 203–211. doi: 10.1016/0882-4010(89)90056-9

Nagao-Kitamoto, H., and Kamada, N. (2017). Host-microbial cross-talk in inflammatory bowel disease. *Immune Netw.* 17, 1–12. doi: 10.4110/in.2017.17.1.1

Ohta, K.-Y., Inoue, K., Hayashi, Y., and Yuasa, H. (2006). Carrier-mediated transport of glycerol in the perfused rat small intestine. *Biol. Pharm. Bull.* 29, 785–789. doi: 10.1248/bpb.29.785

Ou, Q., Fan, J., Duan, D., Xu, L., Wang, J., Zhou, D., et al. (2017). Involvement of cAMP receptor protein in biofilm formation, fimbria production, capsular polysaccharide biosynthesis and lethality in mouse of *Klebsiella pneumoniae* serotype K1 causing pyogenic liver abscess. *J. Med. Microbiol.* 66, 1–7. doi: 10.1099/jmm.0.000391

Pal, A., Iyer, M. S., Srinivasan, S., Seshasayee, A. S., and Venkatesh, K. V. (2020). Global pleiotropic effects in adaptively evolved *Escherichia coli* lacking CRP reveal molecular mechanisms that define growth physiology. bioRxiv [Preprint]. doi:10.1101/2020.06.18.159491.

Panjaitan, N. S. D., Horng, Y.-T., Cheng, S.-W., Chung, W.-T., and Soo, P.-C. (2019). EtcABC, a putative EII complex, regulates type 3 fimbriae via CRP-cAMP signaling in *Klebsiella pneumoniae*. *Front. Microbiol.* 10, 1–15. doi: 10.3389/fmicb.2019.01558

Pannuri, A., Vakulskas, C. A., Zere, T., McGibbon, L. C., Edwards, A. N., Georgellis, D., et al. (2016). Circuitry linking the catabolite repression and Csr global regulatory Systems of *Escherichia coli*. *J. Bacteriol.* 198, 3000–3015. doi: 10.1128/JB.00454-16

Paveglio, S., Ledala, N., Rezaul, K., Lin, Q., Zhou, Y., Provatas, A. A., et al. (2020). Cytotoxin-producing *Klebsiella oxytoca* in the preterm gut and its association with necrotizing enterocolitis. *Emerg. Microbes Infect.* 9, 1321–1329. doi: 10.1080/22221751.2020.1773743

Platenkamp, A., and Mellies, J. L. (2018). Environment controls LEE regulation in Enteropathogenic *Escherichia coli*. *Front. Microbiol.* 9:1694. doi: 10.3389/fmicb.2018.01694

Ramamurthy, T., Nandy, R. K., Mukhopadhyay, A. K., Dutta, S., Mutreja, A., Okamoto, K., et al. (2020). Virulence regulation and innate host response in the pathogenicity of *Vibrio cholerae*. *Front. Cell. Infect. Microbiol.* 10:572096. doi: 10.3389/fcimb.2020.572096

Ritzert, J. T., Minasov, G., Embry, R., Schipma, M. J., and Satchell, K. J. F. (2019). The cyclic AMP receptor protein regulates quorum sensing and global gene expression in *Yersinia pestis* during planktonic growth and growth in biofilms. *MBio* 10:e02613-19. doi: 10.1128/mBio.02613-19

Salgado, H. (2004). RegulonDB (version 4.0): transcriptional regulation, operon organization and growth conditions in *Escherichia coli* K-12. *Nucleic Acids Res.* 32, 303D–306D. doi: 10.1093/nar/gkh140

Schmittgen, T. D., and Livak, K. J. (2008). Analyzing real-time PCR data by the comparative C T method. *Nat. Protoc.* 3:1101. doi: 10.1038/nprot.2008.73

Schneditz, G., Rentner, J., Roier, S., Pletz, J., Herzog, K. A. T., Bucker, R., et al. (2014). Enterotoxicity of a nonribosomal peptide causes antibiotic-associated colitis. *Proc. Natl. Acad. Sci.* 111, 13181–13186. doi: 10.1073/pnas.1403274111

Soberón-Chávez, G., Alcaraz, L. D., Morales, E., Ponce-Soto, G. Y., and Servín-González, L. (2017). The transcriptional regulators of the CRP family regulate different essential bacterial functions and can be inherited vertically and horizontally. *Front. Microbiol.* 8:959. doi: 10.3389/fmicb.2017.00959

Soria-Bustos, J., Ares, M. A., Gómez-Aldapa, C. A., González-Y-Merchand, J. A., Girón, J. A., and De la Cruz, M. A. (2020). Two type VI secretion systems of *Enterobacter cloacae* are required for bacterial competition, cell adherence, and intestinal colonization. *Front. Microbiol.* 11:560488. doi: 10.3389/fmicb.2020.560488

Tse, H., Gu, Q., Sze, K.-H., Chu, I. K., Kao, R. Y. T., Lee, K.-C., et al. (2017). A tricyclic pyrrolobenzodiazepine produced by *Klebsiella oxytoca* is associated with cytotoxicity in antibiotic-associated hemorrhagic colitis. *J. Biol. Chem.* 292, 19503–19520. doi: 10.1074/jbc.M117.791558

Untergasser, A., Nijveen, H., Rao, X., Bisseling, T., Geurts, R., and Leunissen, J. A. M. (2007). Primer3Plus, an enhanced web interface to Primer3. *Nucleic Acids Res.* 35, W71–W714. doi: 10.1093/nar/gkm306

Unterhauser, K., Pöltl, L., Schneditz, G., Kienesberger, S., Glabonjat, R. A., Kitsera, M., et al. (2019). *Klebsiella oxytoca* enterotoxins tilimycin and tilivalline have distinct host DNA-damaging and microtubule-stabilizing activities. *Proc. Natl. Acad. Sci.* 116, 3774–3783. doi: 10.1073/pnas.1819154116

Uppal, S., and Jawali, N. (2016). The cyclic AMP receptor protein (CRP) regulates mqsRA, coding for the bacterial toxin-antitoxin gene pair, in *Escherichia coli*. *Res. Microbiol.* 167, 58–62. doi: 10.1016/j.resmic.2015.09.001

Vilches, S., Jimenez, N., Tomás, J. M., and Merino, S. (2009). *Aeromonas hydrophila* AH-3 type III secretion system expression and regulatory network. *Appl. Environ. Microbiol.* 75, 6382–6392. doi: 10.1128/AEM.00222-09

von Tesmar, A., Hoffmann, M., Abou Fayad, A., Hüttel, S., Schmitt, V., Herrmann, J., et al. (2018). Biosynthesis of the *Klebsiella oxytoca* pathogenicity factor Tilivalline: heterologous expression, in vitro biosynthesis, and inhibitor development. *ACS Chem. Biol.* 13, 812–819. doi: 10.1021/acschembio.7b00990

Wang, T., Flint, S., and Palmer, J. (2019). Magnesium and calcium ions: roles in bacterial cell attachment and biofilm structure maturation. *Biofouling* 35, 959–974. doi: 10.1080/08927014.2019.1674811

Wei, S., Bahl, M. I., Baunwall, S. M. D., Hvas, C. L., and Licht, T. R. (2021). Determining gut microbial Dysbiosis: a review of applied indexes for assessment of intestinal microbiota imbalances. *Appl. Environ. Microbiol.* 87:e00395-21. doi: 10.1128/AEM.00395-21

Wójcicki, M., Świder, O., Daniluk, K. J., Średnicka, P., Akimowicz, M., Roszko, M. Ł., et al. (2021). Transcriptional regulation of the multiple resistance mechanisms in *Salmonella* A review. *PathoGenetics* 10:801. doi: 10.3390/pathogens10070801

Xu, K., Lin, L., Shen, D., Chou, S.-H., and Qian, G. (2021). Clp is a "busy" transcription factor in the bacterial warrior, Lysobacter enzymogenes. *Comput. Struct. Biotechnol. J.* 19, 3564–3572. doi: 10.1016/j.csbj.2021.06.020

Xue, J., Tan, B., Yang, S., Luo, M., Xia, H., Zhang, X., et al. (2016). Influence of cAMP receptor protein (CRP) on bacterial virulence and transcriptional regulation of allS by CRP in *Klebsiella pneumoniae*. *Gene* 593, 28–33. doi: 10.1016/j.gene.2016.08.006

You, C., Okano, H., Hui, S., Zhang, Z., Kim, M., Gunderson, C. W., et al. (2013). Coordination of bacterial proteome with metabolism by cyclic AMP signalling. *Nature* 500, 301–306. doi: 10.1038/nature12446

Yuasa, H., Hamamoto, K., Dogu, S., Marutani, T., Nakajima, A., Kato, T., et al. (2003). Saturable absorption of glycerol in the rat intestine. *Biol. Pharm. Bull.* 26, 1633–1636. doi: 10.1248/bpb.26.1633

Zollner-Schwetz, I., Herzog, K. A. T., Feierl, G., Leitner, E., Schneditz, G., Sprenger, H., et al. (2015). The toxin-producing Pathobiont *Klebsiella oxytoca* is not associated with flares of inflammatory bowel diseases. *Dig. Dis. Sci.* 60, 3393–3398. doi: 10.1007/s10620-015-3765-y

Conflict of Interest: The authors declare that the research was conducted in the absence of any commercial or financial relationships that could be construed as a potential conflict of interest.

Publisher's Note: All claims expressed in this article are solely those of the authors and do not necessarily represent those of their affiliated organizations, or those of the publisher, the editors and the reviewers. Any product that may be evaluated in this article, or claim that may be made by its manufacturer, is not guaranteed or endorsed by the publisher.

frontiers in Microbiology

ORIGINAL RESEARCH
published: 30 September 2021
doi: 10.3389/fmicb.2021.750940

σ^S-Mediated Stress Response Induced by Outer Membrane Perturbation Dampens Virulence in *Salmonella enterica* serovar Typhimurium

*Seul I Kim[1], Eunsuk Kim[1] and Hyunjin Yoon[1,2]**

[1]*Department of Molecular Science and Technology, Ajou University, Suwon, South Korea,* [2]*Department of Applied Chemistry and Biological Engineering, Ajou University, Suwon, South Korea*

OPEN ACCESS

Edited by:
Xihui Shen,
Northwest A&F University, China

Reviewed by:
Sangyong Lim,
Korea Atomic Energy Research Institute (KAERI), South Korea
Aalap Mogre,
Trinity College Dublin, Ireland
Ján Matiašovic,
Veterinary Research Institute (VRI), Czechia

***Correspondence:**
Hyunjin Yoon
yoonh@ajou.ac.kr

Specialty section:
This article was submitted to Infectious Diseases, a section of the journal Frontiers in Microbiology

Received: *31 July 2021*
Accepted: *30 August 2021*
Published: *30 September 2021*

Citation:
Kim S, Kim E and Yoon H (2021) σ^S-Mediated Stress Response Induced by Outer Membrane Perturbation Dampens Virulence in Salmonella enterica serovar Typhimurium. Front. Microbiol. 12:750940. doi: 10.3389/fmicb.2021.750940

Salmonella alters cellular processes as a strategy to improve its intracellular fitness during host infection. Alternative σ factors are known to rewire cellular transcriptional regulation in response to environmental stressors. σ^S factor encoded by the *rpoS* gene is a key regulator required for eliciting the general stress response in many proteobacteria. In this study, *Salmonella* Typhimurium deprived of an outer membrane protein YcfR was attenuated in intracellular survival and exhibited downregulation in *Salmonella* pathogenicity island-2 (SPI-2) genes. This decreased SPI-2 expression caused by the outer membrane perturbation was abolished in the absence of *rpoS*. Interestingly, regardless of the defects in the outer membrane integrity, RpoS overproduction decreased transcription from the common promoter of *ssrA* and *ssrB*, which encode a two-component regulatory system for SPI-2. RpoS was found to compete with RpoD for binding to the P_{ssrA} region, and its binding activity with RNA polymerase (RNAP) to form $E\sigma^S$ holoenzyme was stimulated by the small regulatory protein Crl. This study demonstrates that *Salmonella* undergoing RpoS-associated stress responses due to impaired envelope integrity may reciprocally downregulate the expression of SPI-2 genes to reduce its virulence.

Keywords: *Salmonella* Typhimurium, RpoS (σ^S), *ssrA*, *Salmonella* pathogenicity island-2, virulence

INTRODUCTION

The bacterial RNA polymerase (RNAP) holoenzyme is a provisional complex between a multi-subunit RNAP core enzyme (E, $\alpha_2\beta\beta'\omega$) and an σ factor. The σ factor forming the Eσ complex directs promoter-specific transcription initiation and then dissociates from the core enzyme E after transcription initiation. In many proteobacteria, σ^D (σ^{70}), encoded by *rpoD*, functions as a major σ subunit responsible for the transcription of constitutive promoters. Under unfavorable conditions, bacteria exploit alternative σ factors to redistribute RNAP core enzyme specificity toward discrete subsets of genes whose products help survive and adapt to environmental stressors (Bang et al., 2005). *Salmonella enterica* serovar Typhimurium possesses five alternative σ factors, including extra-cytoplasmic stress-specific σ^E (σ^{24}, RpoE), flagella-chemotaxis-specific

σ^F (σ^{28}, FliA), heat-shock response-specific σ^H (σ^{32}, RpoH), stationary-phase nutrient-starvation-specific σ^S (σ^{38}, RpoS), and nitrogen-starvation-specific σ^N (σ^{54}, RpoN). The abundance of alternative σ factors available for Eσ complex formation is regulated not only by environmental signals (Shimada et al., 2017) but also by the interaction with two types of inhibitory proteins, anti-σ factors, and adaptor proteins (Trevino-Quintanilla et al., 2013). Different σ factors operate discrete regulatory circuits containing cognate genes and operons in response to specific environmental cues, but some transcriptional regulons are coordinated by multiple σ factors that function in a regulatory cascade or by competitive interactions. In response to the diverse stimuli encountered by bacterial pathogens upon host infection, multiple alternative σ factors interact with each other to promote bacterial adaptation in hostile conditions. σ^E can activate one of the *rpoH* promoters (Hiratsu et al., 1995; Vanaporn et al., 2008) and σ^H, in turn, stimulates the transcription of Hfq (Muffler et al., 1996), which is required for efficient translation of *rpoS* mRNA (Bang et al., 2005), indicating sequential activation of multiple regulons by a regulatory cascade of σ^E, σ^H, and σ^S under certain circumstances. Besides, there is a trade-off between self-preservation and nutritional competence and genes required for membrane integrity maintenance and genes associated with metabolism are reciprocally controlled by competitive action between σ factors (Ferenci, 2005; Levi-Meyrueis et al., 2015). In the context of competitive action between σ factors, σ^{70} and σ^S recognize almost identical −35 and −10 promoter elements, especially the −10 region (Hengge-Aronis, 2002b). Therefore, competitive binding of $E\sigma^S$ to the overlapping promoter regions may occlude transcription initiation by $E\sigma^{70}$, inducing the transcription of a repertoire of genes by σ^S under stressful environments (Levi-Meyrueis et al., 2015).

Many genes whose promoters bind to both σ^{70} and σ^S show stronger transcription activities with σ^{70} binding than with σ^S binding, implying a negative role of σ^S in gene expression (Levi-Meyrueis et al., 2015; Grove et al., 2017; Yin et al., 2018). Interestingly, nullifying the negative effects of σ^S is beneficial to bacterial growth in the absence of environmental stressors (Zambrano et al., 1993; Notley-McRobb et al., 2002). The attenuated expression associated with $E\sigma^S$ may confer fitness advantages to bacteria during unfavorable conditions. σ^S is induced under nutrient-depleted stationary phase or in response to various stressors, and its activity in *Salmonella* is known to alter transcription or protein production of more than 20% of its genome (Levi-Meyrueis et al., 2014; Lago et al., 2017). σ^S upregulates or downregulates the expression of a myriad of genes involved in carbohydrate and amino acid metabolism, stress resistance, and membrane integrity directly or indirectly. In contrast to the essential roles of σ^S in bacterial stress resistance, the requirement of σ^S for bacterial virulence varies between bacterial species (Dong and Schellhorn, 2010). *Salmonella* Typhimurium lacking *rpoS* gene showed reduced virulence, and σ^S factor was found to activate the transcription of *spvR* and *spvABCD* virulence plasmid genes (Fang et al., 1992; Kowarz et al., 1994).

In this study, we induced outer membrane perturbation on *S. Typhimurium* by deleting *ycfR* to stimulate σ^S-mediated adaptation responses. YcfR is a putative outer membrane protein that is expressed under stressful conditions in enteric pathogens and is known as a multiple stress resistance protein (Zhang et al., 2007; Salazar et al., 2013). Our previous study demonstrated that the deletion of *ycfR* caused structural alterations in lipopolysaccharide and destabilized *Salmonella* envelope integrity (Kim and Yoon, 2019). *Salmonella* devoid of YcfR tremendously increased *rpoS* transcription and showed an increase in curli fibers, cellulose, and c-di-GMP production and a decrease in motility, implicating comprehensive transcriptional alterations by σ^S in response to stress on the cellular envelope (Kim and Yoon, 2019). Besides the known repertoires of σ^S regulatory circuits, such as biofilm formation, this study revealed that virulence genes of *Salmonella* pathogenicity island-2 (SPI-2) were downregulated by σ^S. SPI-2 is a locus responsible for the type III secretion system (T3SS) injectisome-mediated delivery of virulence factors from *Salmonella* to host cells and is critical for bacterial survival and replication inside host cells (Jennings et al., 2017). The negative role of σ^S in SPI-2 regulation was influenced by a small regulatory protein Crl. Crl is known to be required for σ^S-dependent transcriptional initiation at the promoters of *adrA* and *csgD* genes, whose products activate curli and cellulose production (Robbe-Saule et al., 2006). The role of σ^S in *Salmonella* virulence regulation was elucidated by examining the interaction between σ^S and the *ssrAB* promoter, which encodes the two-component regulatory system SsrAB for SPI-2.

MATERIALS AND METHODS

Bacterial Strains, Plasmids, and Growth Conditions

Salmonella enterica serovar Typhimurium ATCC 14028 was used as the parent strain. *Salmonella* mutants of Δ*ycfR* and Δ*rpoS* were constructed using the phage lambda (λ) Red recombination system as described in previous studies (Yoon et al., 2009; Kim and Yoon, 2019) and a mutant lacking both *ycfR* and *rpoS* was constructed using P22 HT105/1 int-201-mediated transduction (Kwoh and Kemper, 1978). The phage λ Red recombination system was also used for the construction of *Salmonella* strains producing HA-tagged SPI-2 proteins (SseC and SsaN) as described in the previous study (Kim et al., 2018). In brief, the kanamycin resistance (*kan*) cassette of pKD13-2HA was amplified by PCR using primers designed to provide 40-nucleotide sequences homologous to target genes at both termini of the resultant PCR products. The PCR products were introduced into *Salmonella* cells harboring pKD46 to insert the HA-coding sequences with a *kan* cassette prior to the stop codon sequences. The *kan* marker was subsequently removed using pCP20 providing a flip recombinase. Primers used for the construction of HA-tagged SPI-2 genes are listed in **Supplementary Table 1**. *Escherichia coli* DH5α strain was used for plasmid cloning and protein purification.

To express *rpoS* in *trans*, the *rpoS* gene was cloned into pACYC184 (Chang and Cohen, 1978) and pBbA2sk-RFP vectors (Lee et al., 2011). For the construction of pRpoS, the *rpoS*

CDS and its promoter region were amplified by PCR using primers pRpoS-*CF* and pRpoS-CR and inserted into pACYC184 through BamHI and SalI restriction enzyme sites. In cloning pRpoS2, the *rpoS* gene was amplified using PCR with pRpoS-CF2 and pRpoS-CR2 primers, digested with EcoRI and BglII, and ligated with EcoRI/BglII digested pBbA2sk-RFP plasmid. Primer sequences are listed in **Supplementary Table 1**.

To construct transcriptional *lacZ* fusion to the P_{ssrA} and P_{ssrB} regions, the promoter regions of *ssrA* (from −253 to +209) and *ssrB* (from −90 to +303) were amplified by PCR using primers (**Supplementary Table 1**) of pssrA-lacZ-*CF* and pssrA-lacZ-CR for *ssrA* and primers (**Supplementary Table 1**) pssrB-lacZ-*CF* and pssrB-lacZ-CR for *ssrB*, as described by Feng et al. (2003). The amplified promoter regions were cloned into the pRS415 plasmid (Simons et al., 1987) using EcoRI and SalI restriction enzyme sites.

RpoS, RpoD, and Crl proteins were tagged with His_6 at their N-termini by cloning three genes into the pUHE21-lacI^q plasmid (Soncini et al., 1995) *via* EcoRI and HindIII and inducing their expression using IPTG. The primers used for the construction of His_6 tagged proteins are listed in **Supplementary Table 1**. All restriction enzymes and ligases were purchased from Takara Bio, Inc. (CA, United States).

Salmonella cells were cultivated in Luria-Bertani (LB) medium broth or acidic minimal medium (AMM) broth at 220 rpm at 37°C, as described in previous studies (Yoon et al., 2009, 2011). For AMM cultivation, bacterial cells at the stationary growth phase in LB medium broth were washed twice with PBS, diluted in pH 7.0 minimal medium broth at a 1:100 ratio, and cultivated overnight. Pre-cultured *Salmonella* cells in minimal medium broth (pH 7.0) were diluted in minimal medium broth (pH 5.0) at a 1:20 ratio and cultivated for 3 h to mimic intracellular conditions (Yoon et al., 2009). Antibiotics were purchased from Sigma-Aldrich (MO, United States) and used when required: ampicillin (Amp, 50 μg/ml), chloramphenicol (Cm, 35 μg/ml), kanamycin (Kan, 50 μg/ml), and anhydrotetracycline (aTc, 0.2 or 0.5 ng/ml).

Mammalian Cell Infection

To assess bacterial invasiveness, HeLa human epithelial cell line (ATCC CCL-2) was infected as described in the previous study (Kim et al., 2018). HeLa cells were seeded in 24-well plate at 2×10^5 cells/well and incubated in Dulbecco's modified Eagle's medium (DMEM; Corning cellgro, Thermo Scientific Inc., IL, United States) supplemented with 4.5 g/L glucose (Thermo Scientific Inc.) and 10% fetal bovine serum (FBS; Gibco, Thermo Scientific Inc.) at 37°C with 5% CO_2. After overnight incubation, HeLa cells were treated with *Salmonella* cells grown for 2.5 h in LB medium broth at a multiplicity of infection (MOI) of 100 and centrifuged at $500 \times g$ for 5 min. At 30 min post-infection, the infected cells were washed twice with PBS and replenished with fresh DMEM containing 100 μg/ml gentamicin for 1.5 h to remove extracellular *Salmonella* cells. The infected HeLa cells were washed three times with PBS and lysed with 1% Triton X-100. The cell lysates were diluted and plated on LB agar to count intracellular *Salmonella* cells.

Salmonella survival inside macrophages was examined as described elsewhere (Yoon et al., 2009; Kim and Yoon, 2019). Murine macrophage RAW264.7 (ATCC TIB-71) cells were seeded in 24-well plate at 5×10^5 cells/well and incubated in DMEM containing 4.5 g/L glucose and 10% FBS at 37°C with 5% CO_2 overnight. Monolayered-macrophage cells were infected with *Salmonella* cells grown overnight in LB medium broth at MOI 100, as described for HeLa cell infection. After 30 min of infection, the extracellular bacteria were removed by replacing the medium with DMEM containing 100 μg/ml gentamicin for 1.5 h. The infected macrophages were washed with PBS three times and incubated in fresh DMEM containing 20 μg/ml gentamicin for additional 8 h. To enumerate intracellular bacteria, RAW264.7 cells were lysed, and the lysates were spread on LB agar as described above.

qRT-PCR Analysis

Bacterial total RNA was isolated from *Salmonella* cultivated in LB medium and AMM broth or RAW264.7 cells infected with *Salmonella*. Bacterial cells cultivated *in vitro* were treated with RNAprotect Bacteria Reagent (Qiagen, Hilden, Germany) and subjected to total RNA extraction using RNeasy mini kit (Qiagen). For RNA extraction from intracellular bacteria, infected macrophage cells were treated with RNAlater™ Stabilization Solution (Invitrogen, Thermo Scientific Inc.) and processed with RNeasy mini kit according to the manufacturer's recommendations. Isolated total RNA was treated with RNase-free DNase (Ambion, TX, United States) at 37°C for 30 min and used to synthesize cDNA using RNA to cDNA EcoDryTM Premix (Takara Bio United States, Inc.). cDNA corresponding to 10 ng of input RNA was used as a template in each qRT-PCR, and the primer sequences are listed in **Supplementary Table 2**. qRT-PCR was conducted using the StepOnePlus Real-time PCR system (Applied Biosystems, MA, United States) with Power SYBR Green PCR Master Mix (Applied Biosystems), and the levels of amplified PCR products were normalized to those of *gyrB* (Yoon et al., 2009).

β-Galactosidase Assay

The β-galactosidase assay was conducted using the Miller method (Smale, 2010). Bacterial cells were cultivated in LB medium broth, and β-galactosidase activity normalized to the number of input bacteria was represented by Miller units. Miller units were computed as follows: Miller unit = $[1{,}000 \times (OD_{420} - 1.75 \times OD_{550})]/(t \times V \times OD_{600})$, where t is time (min) and V is volume (ml).

Immunoblot Assay

Bacterial cells were pelleted and resuspended in 1× Laemmli sample buffer (Bio-Rad Laboratories, Inc., CA, United States). The aliquots were loaded on 10% SDS-PAGE gels, and the separated proteins were transferred to PVDF membranes (Bio-Rad Laboratories, Inc.). The membrane was blocked with 5% skim milk solution and treated with anti-RpoS antibody (anti-*E. coli* RNA Sigma S antibody, BioLegend, CA, United States) at a 1:2,000 dilution ratio or anti-DnaK antibody (Enzo Life Science, NY, United States) at a 1:10,000 dilution ratio in combination with horseradish peroxidase (HRP)-conjugated secondary antibody (Bio-Rad Laboratories, Inc.) at

a 1:3,000 dilution ratio. SPI-2 proteins tagged with HA were identified using anti-HA antibody (1:10,000 dilution; Sigma, United States) as a primary antibody. Immunoblotting was conducted using ECL™ Western Blotting Detection Reagents kit (GE Healthcare, Thermo Scientific Inc.), and the blot images were visualized using the ChemiDoc™ MP System (Bio-Rad Laboratories, Inc.). The intensity of the blot images was analyzed using ImageJ software.[1]

Chromatin Immunoprecipitation Assay

The Chromatin immunoprecipitation (ChIP) assay was performed as previously described (Gu et al., 2016; Yin et al., 2018) with minor modifications. Briefly, *Salmonella* cells cultivated in the stationary growth phase in LB medium broth were fixed with 1% formaldehyde solution for 10 min and subsequently treated with 100 mM glycine for 5 min. Cells were washed with cold PBS and resuspended in SDS lysis buffer (50 mM Tris–HCl, 10 mM EDTA, 1% SDS, and pH 8.0) containing 1× protease inhibitor. After 10 min of incubation, the cell extract was sonicated to fragment genomic DNA into 200 bp to 1 kb and centrifuged at 12,000 × *g* for 10 min. The supernatant solution was used as input DNA, and the aliquots were further processed for pre-clearing and immunoprecipitation (IP) samples. The lysate solution containing DNA-protein complexes was pre-incubated with Protein A/G Plus-Agarose (Santa Cruz Biotechnology, Inc. TX, United States) at 4°C for 2 h to remove DNA or proteins non-specifically bound to Protein A/G Plus-Agarose and centrifuged at 800 × *g* for 3 min. The resultant pellet fraction was used as a pre-clearing sample, and the supernatant solution was further incubated with the anti-RpoS antibody at 4°C overnight, followed by Protein A/G Plus-Agarose at 4°C for 2 h, and centrifuged at 800 × *g* for 3 min to immunoprecipitate DNA-RpoS complexes bound to the agarose. The pellet fraction was used as an IP sample. The pre-clearing and IP samples were washed with LiCl wash buffer (100 mM Tris–HCl, pH 8.0, 2% Triton X-100, and 250 mM LiCl), twice with high-salt buffer (100 mM Tris–HCl, pH 8.0, 600 mM NaCl, and 2% Triton X-100), twice with low-salt buffer (100 mM Tris–HCl, pH 8.0, 300 mM NaCl, and 2% Triton X-100), and with TE wash buffer (10 mM Tris–HCl, pH 8.0, and 1 mM EDTA). The precipitated DNA-protein complexes were eluted with ChIP elution buffer (50 mM Tris–HCl, pH 8.0, 10 mM EDTA, and 1% SDS) and incubated with 0.2 M NaCl at 65°C overnight to resolve DNA-protein cross-links. All samples were treated with RNase A (10 mg/ml) at 37°C for 30 min and further incubated with a protease solution (1 M Tris–HCl, pH 8.0, 500 mM EDTA, proteinase K, and 5 M NaCl) at 65°C for 4 h. DNA from pre-clearing and IP samples was extracted using phenol: chloroform: isoamyl alcohol (25: 24: 1) solution, precipitated with EtOH and NaOAc (pH 5.2), and resuspended in distilled water.

ChIP-Quantitative PCR Assay

DNA cross-linked to RpoS was analyzed using quantitative PCR (qPCR), as previously described (Hermans et al., 2016). Relative enrichment (RE) of the promoter of interest was computed using differences in Ct values (ΔCt) with *gyrB* gene as an endogenous control as follows: $RE = 2^{-(\Delta Ct_{IP} - \Delta Ct_{Pre\text{-}clearing})}$, where ΔCt_{IP} is $Ct_{promoter\ test} - Ct_{gyrB}$ for the IP samples and $\Delta Ct_{Pre\text{-}clearing}$ is $Ct_{promoter\ test} - Ct_{gyrB}$ for the pre-clearing samples. Aliquots of DNA purified from IP and pre-clearing samples and serial dilutions of input DNA were used as templates in qPCR, and the qPCR primers are listed in **Supplementary Table 3**. Amplified PCR products were analyzed using the StepOnePlus Real-time PCR system with Power SYBR Green reagent.

Purification of His_6-Tagged Protein

Escherichia coli strains producing His_6-tagged RpoS, RpoD, and Crl proteins were cultivated in LB medium broth, and the proteins were induced by adding 0.05 mM (RpoS and RpoD) or 1 mM (Crl) isopropyl β-D-1-thiogalactopyranoside for 7 or 3 h at 30°C. Bacterial cells were centrifuged at 10,000 × *g* for 10 min and resuspended in lysis buffer (50 mM NaH_2PO_4, 300 mM NaCl, 20 mM imidazole, and pH 8.0) containing 1 mg/ml lysozyme. After 30 min incubation on ice, the cells were sonicated and centrifuged at 10,000 × *g* and 4°C for 20 min. The resultant soluble lysate fraction was treated with Ni^{2+}-nitrilotriacetic acid (Ni^{2+}-NTA) agarose beads (Qiagen) at 4°C for 1 h with rotation and loaded onto a Ni^{2+}-NTA agarose affinity column (Qiagen). The column was washed with washing buffer (50 mM NaH_2PO_4, 300 mM NaCl, 40 mM imidazole, and pH 8.0) three times, and the proteins were eluted with elution buffer (50 mM NaH_2PO_4, 300 mM NaCl, 300 mM imidazole, and pH 8.0). The eluted protein fraction was packed into SnakeSkin™ Dialysis tubing with 10 K MWCO (Thermo Scientific Inc.) and subjected to dialysis at 4°C in dialysis buffer (20 mM Tris–HCl, pH 8.0, 150 mM NaCl, 0.1 mM EDTA, 5 mM DTT, and 20% glycerol). Purified proteins were quantified using Bradford assay.

Electrophoretic Mobility Shift Assay

The binding between σ factors and the P_{ssrA} region was investigated using His_6-RpoS or His_6-RpoD in combination with His_6-Crl. The P_{ssrA} region was PCR-amplified using primers ssrA-electrophoretic mobility shift assay (EMSA)-F and ssrA-EMSA-R. The *csgBA* promoter region amplified using primers cgsBA-EMSA-F and cgsBA-EMSA-R was employed as a positive control, whereas the STM14_1978 (putative ABC transporter permease component) CDS region amplified using primers STM14_1978 EMSA-F and STM14_1978 EMSA-R was used as a negative control. The primer sequences used in the EMSA are listed in **Supplementary Table 3**. EMSA was performed as described previously (Bougdour et al., 2004; Storvik and Foster, 2010) with the following modifications. To reconstitute the RNAP holoenzyme, 20 nM RNAP core enzyme (*E. coli* RNAP Core Enzyme; NEB, MA, United States) was incubated with 300 nM His_6-RpoS or His_6-RpoD in a binding buffer (200 mM Tris–HCl, pH 8.0, 30 mM KCl, 10 mM $MgCl_2$, 50 mM NaCl, 1 mM DTT, 1 mM EDTA, and BSA 20 μg/ml) at 30°C for 45 min.

[1]https://imagej.nih.gov/ij/

DNA of 20 ng was incubated with the reconstituted RNAP holoenzyme in a binding buffer (50 mM Tris–HCl, pH 8.0, 200 mM KCl, 3 mM $MgCl_2$, 1 mM DTT, 0.1 mM EDTA, BSA μg/ml, and Poly (di-dc) 12 ng/μl) at 25°C for 30 min. The reactant was analyzed by electrophoresis using 5% native polyacrylamide gel, and DNA fragments were stained with EtBr solution and detected using the ChemiDoc MP System.

In the competitive binding assay between His_6-RpoS and His_6-RpoD, one σ factor was used at a constant concentration of 75 nM and the other competitor σ factor was used at incremental concentrations from 12.5 to 150 nM. After RNAP holoenzyme reconstitution with different concentrations of σ factors, DNA corresponding to the P_{ssrA} region was added to the binding reaction and analyzed as described above. To localize His_6-RpoS after electrophoresis on a native polyacrylamide gel, proteins on the gel were transferred to a PVDF membrane and processed as described in the immunoblot assay above. Anti-*E. coli* RNA sigma S antibody was used as a primary antibody at a 1:2,000 dilution ratio, and HRP-conjugated goat anti-mouse IgG was used as a secondary antibody at a 1:3,000 dilution ratio.

In the competition assay using His_6-RpoS in combination with His_6-Crl, His_6-RpoS (25, 50, and 280 nM) was pre-incubated with 280 nM His_6-Crl at 25°C for 15 min and then used to compete with 50 nM His_6-RpoD in the RNAP holoenzyme reconstitution reaction. After the addition of P_{ssrA} region, the locations of P_{ssrA} DNA and His_6-RpoS were identified using EtBr staining and immunoblotting methods, respectively, as described above.

Statistical Analysis

All assays were repeated at least three times, and the average values were presented with their SDs. To determine the significant differences, Student's *t*-test was applied, and the value of *p* was calculated.

RESULTS

Outer Membrane Perturbation in Δ*ycfR* Decreased SPI-2 Expression

YcfR, which is expressed in response to multiple stress conditions, is a putative outer membrane protein important for stress resistance in enteric pathogens such as *Salmonella* spp. and *E. coli* (Zhang et al., 2007; Salazar et al., 2013). In this study, we observed that *Salmonella* lacking YcfR was significantly attenuated in virulence during host cell infection. The lack of YcfR did not influence bacterial growth *in vitro*, but significantly reduced the ability of bacteria to invade host epithelial cells and survive inside phagocytic cells (**Figure 1**). The transcription of SPI-1 genes, which produce a distinct T3SS (T3SS1) and promote *Salmonella* invasion into host cells (Raffatellu et al., 2005), decreased remarkably in the Δ*ycfR* strain (**Figure 2A**). Besides the attenuated SPI-1 expression, the physiological changes caused by the lack of YcfR, including cellular aggregation and reduced motility (Kim and Yoon, 2019), might impair bacterial invasion ability. Interestingly, the lack of YcfR also decreased the transcription of SPI-2 genes not only inside macrophage cells (**Supplementary Figure 1A**) but also in LB and AMM cells *in vitro* (**Figure 2B**; **Supplementary Figure 1B**, respectively), which partially reproduce the intestinal lumen and intracellular milieux, respectively (Beuzon et al., 1999; Yoon et al., 2011).

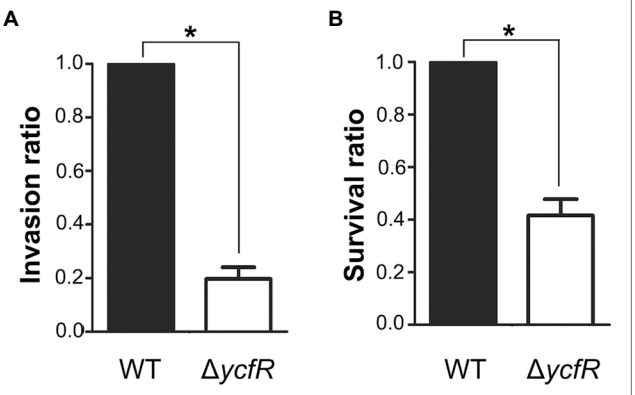

FIGURE 1 | Invasion and survival of a Δ*ycfR* mutant in the host cell. **(A)** Invasive ability of wild-type and Δ*ycfR* mutant strains was assessed by infecting HeLa cells and counting intracellular bacteria 2 h post-infection. The bar indicates relative invasion ability compared to wild-type *Salmonella*. **(B)** Survival inside RAW264.7 macrophages was compared between wild-type and Δ*ycfR* mutant strains 10 h post-infection. The numbers phagocytosed by macrophages were found comparable between two strains (data not shown) and relative survival ratios are depicted. A significant difference (value of $p < 0.05$) is denoted with an asterisk.

Downregulation of SPI-2 in Δ*ycfR* Was Attributable to RpoS

In order to figure out a transcriptional regulator that coordinates bacterial virulence in response to outer membrane perturbation, we assessed the expression of 21 regulators associated with SPI-1 or SPI-2 regulation in the Δ*ycfR* strain (**Supplementary Figure 2**) and found that *rpoS* showed a dramatic increase in its transcription. The levels of RpoS were compared between wild-type and Δ*ycfR* strains in LB and AMM conditions. RpoS increased in the Δ*ycfR* strain grown in both media (1.5-fold in LB; 2.7-fold in AMM; **Figure 3**). To examine whether an increase in RpoS could downregulate virulence genes associated with SPI-2 T3SS (T3SS2), the transcription of *ssrAB* encoding the two-component regulatory system for T3SS2 and its cognate effectors was compared. *Salmonella* deprived of RpoS slightly increased the expression of *ssrAB*, but the introduction of pRpoS expressing *rpoS* under its own promoter significantly decreased the transcription of *ssrAB*, implicating overall downregulation of their cognate T3SS2-associated genes by RpoS (**Figure 4A**). In addition, the decreased transcription of *ssrAB* in the absence of YcfR was nullified by the additional *rpoS* deletion, suggesting the possibility of σ^S-mediated SPI-2 downregulation in the Δ*ycfR* strain (**Figure 4A**). The *ssrA* and *ssrB* genes, located adjacent to each other, encode a sensor kinase and its response regulator, respectively, and are regarded to be transcribed in a polycistronic

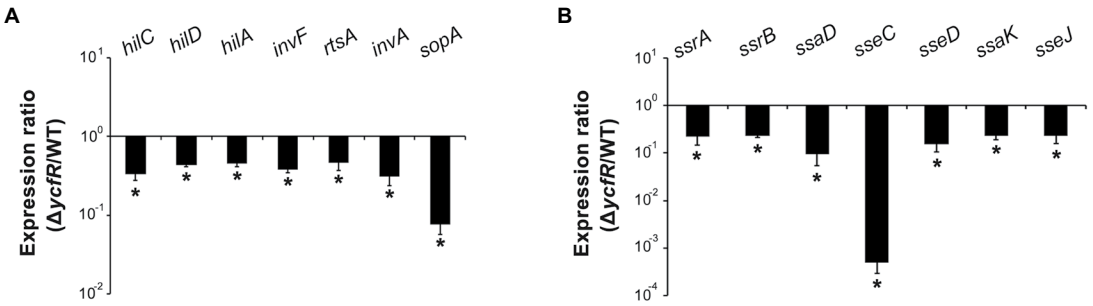

FIGURE 2 | Expression of SPI-1 and *Salmonella* pathogenicity island-2 (SPI-2) genes in Δ*ycfR* mutant. **(A)** Transcription levels of SPI-1 genes were examined using RNA isolated from *Salmonella* strains grown in LB medium broth for 2 h. The Ct values of qRT-PCR were normalized using those of *gyrB* and the fold-change between wild-type and Δ*ycfR* mutant strains was plotted. **(B)** To analyze the expression of SPI-2 genes, *Salmonella* strains were cultivated in LB medium broth for 10 h and subjected to RNA extraction. Ct values of each gene were subtracted from those of *gyrB* for normalization, and the fold-change (Δ*ycfR*/wild-type) was calculated. An asterisk indicates a difference of a value of $p < 0.05$.

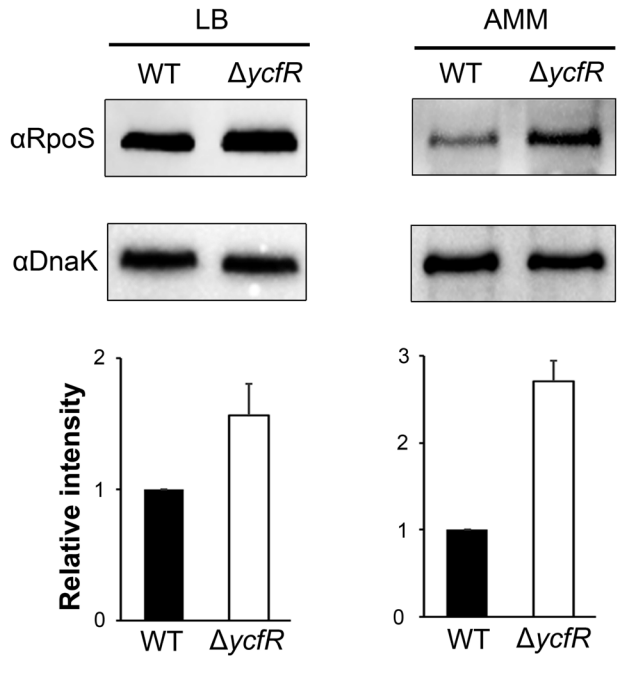

FIGURE 3 | Expression of RpoS in Δ*ycfR* mutant. *Salmonella* wild-type and Δ*ycfR* mutant strains were cultivated in LB medium broth for 10 h or acidic minimal medium (AMM) broth for 3 h, and the expression of RpoS was compared using immunoblot assay with anti-RpoS antibody. The cytosolic protein DnaK was used as a control to standardize the protein amounts between the lanes. The abundance of RpoS was normalized to that of DnaK using ImageJ, and the ratios from three independent assays are depicted below the representative blot images.

mRNA under the same promoter (Bustamante et al., 2008; Fass and Groisman, 2009). However, the identification of a distinct promoter upstream of *ssrB* revealed the possibility that the expression of *ssrA* and *ssrB* could be uncoupled depending on the growth conditions (Feng et al., 2003, 2004). Therefore, the negative role of RpoS was reexamined using *lacZ* transcriptional fusion constructs, where the promoters of *ssrA* and *ssrB* were separately analyzed (**Figure 4B**). The promoter strength of *ssrA* was much stronger than that of *ssrB* in wild-type *Salmonella* harboring intact *rpoS* and *ycfR* genes, and deletion of *rpoS* alone did not alter *ssrA* or *ssrB* transcription. However, *ycfR* deletion, which led to an increase in RpoS, abolished *ssrA* transcription but not *ssrB*, and the additional *rpoS* deletion in Δ*ycfR* mutant derepressed *ssrA* only, indicating differential regulation of *ssrA* and *ssrB* by σ^S (**Figure 4B**). Again, overexpression of RpoS by the introduction of pRpoS2 decreased P_{ssrA}::*lacZ* expression in proportion to aTc concentration. These results suggest that σ^S at high concentrations dampen transcription activity at the promoter region upstream of *ssrAB*.

σ^S Binds Directly to the *ssrA* Promoter Region

To examine whether σ^S directly controls the transcription of *ssrA*, a ChIP assay was performed on *Salmonella* cells in the stationary growth phase using σ^S as a bait. DNA fragments bound to σ^S were co-precipitated using anti-RpoS antibody and used as templates in PCR using primers targeting the promoter regions of *ssrA* and *ssrB* (**Figure 5A**; **Supplementary Figure 2**). DNA fragments containing the P_{ssrA} region were bound to σ^S and amplified by PCR, but the P_{ssrB} region did not co-precipitate with σ^S (**Figure 5B**). When five different primer sets from R1-F/R to R5-F/R were used to dissect the *ssrA* promoter region, only two primer sets, R3-F/R and R4-F/R, resulted in significant PCR amplification (**Figure 5C**), inferring that σ^S binds to DNA sequences covering −61 to +136 bp at least from the transcription start site of *ssrA* (Feng et al., 2003). It is believed that the *ssrA* promoter requires RNAP holoenzyme harnessing σ^{70}, and the consensus −10 and −35 regions for σ^{70} binding were also predicted (Ramachandran et al., 2012; Banda et al., 2019). Our results raised the possibility that the *ssrA* promoter could recruit σ^S as well as σ^{70}. The possibility of σ^S binding to the P_{ssrA} region was also proposed *in silico* in a previous study (Ramachandran et al., 2012). We further investigated transcription initiation at P_{ssrA}, which is controlled by mechanical interaction with σ factors.

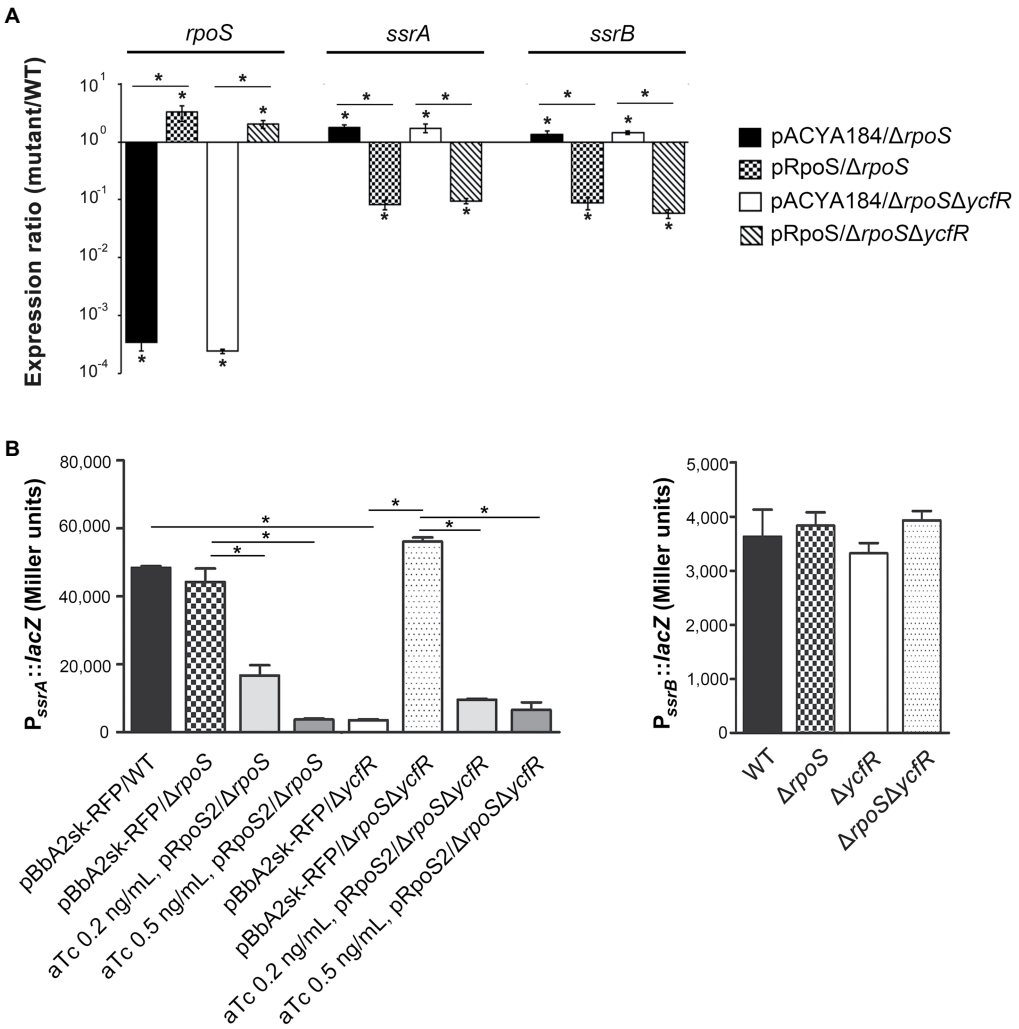

FIGURE 4 | Negative regulation of *ssrA* by RpoS. **(A)** Transcription levels of *rpoS*, *ssrA*, and *ssrB* were measured using qRT-PCR. *Salmonella* strains, including wild-type, Δ*rpoS*, and Δ*rpoS*Δ*ycfR* strains, were transformed with pRpoS or pACYC184 and cultivated to the stationary growth phase in LB medium broth. Ct values of *rpoS*, *ssrA*, and *ssrB* were normalized using those of *gyrB* gene. Expression levels of *rpoS*, *ssrA*, and *ssrB* from each strain were compared with those from wild-type strain harboring pACYC184 and the fold-change (mutant/wild-type) was plotted. Value of p with $p < 0.05$ is denoted with an asterisk. **(B)** Transcription from P_{ssrA} and P_{ssrB} was measured using *lacZ* transcriptional fusions. Plasmids pSsrA::*lacZ* (left) and pSsrB::*lacZ* (right) were introduced into wild-type, Δ*rpoS*, Δ*ycfR*, and Δ*rpoS*Δ*ycfR* strains. To overexpress RpoS, pRpoS2 and its empty plasmid pBbA2sk-RFP were introduced into wild-type and mutant strains, and aTc of 0.2 or 0.5 ng/ml was added in the LB medium broth cultures. β-galactosidase assay was conducted with bacterial cells at the stationary growth phase. An asterisk indicates a value of $p < 0.05$.

σ^S Competes With σ^{70} for Binding to the *ssrA* Promoter Region

The promoter recognition sequences for σ^S and σ^{70} are nearly identical, and a strong functional similarity between σ^S and σ^{70} has been suggested. Many σ^S-regulated genes, such as the *csgBA* operon, can be transcribed by either σ^S or σ^{70} *in vitro* (Arnqvist et al., 1994; Typas et al., 2007b). The possibility of biphasic *ssrA* transcription initiation by σ^S and σ^{70} was examined *in vitro*. A DNA fragment of 172 bp encompassing the P_{ssrA} region targeted by *ssrA* regulators was incubated with each σ factor (His_6-RpoS or His_6-RpoD) in the presence or absence of RNAP core enzyme E. The P_{csgBA} region recognized by either σ^S or σ^{70} was used as a positive control, while a DNA fragment of the STM14_1978 gene devoid of the canonical sequences recognized by σ^S and σ^{70} was used as a negative control. The core enzyme alone could form a complex with DNA fragments of the P_{ssrA} or P_{csgBA} regions in a non-specific manner, as predicted elsewhere, and the addition of either σ factor (σ^S or σ^{70}) retarded the mobility of the DNA-protein complex. This indicated that σ factor was engaged in the complex formation between RNAP holoenzyme (Eσ; $\alpha_2\beta\beta'\sigma\omega$) and the DNA fragments (**Figure 6**). Interestingly, the addition of σ^S produced two bands, presumably a lower one between the core enzyme E and the P_{ssrA} and an upper one between the $E\sigma^S$ and the P_{ssrA}, whereas σ^{70} incorporation produced a single shifted band, representing robust complex formation between

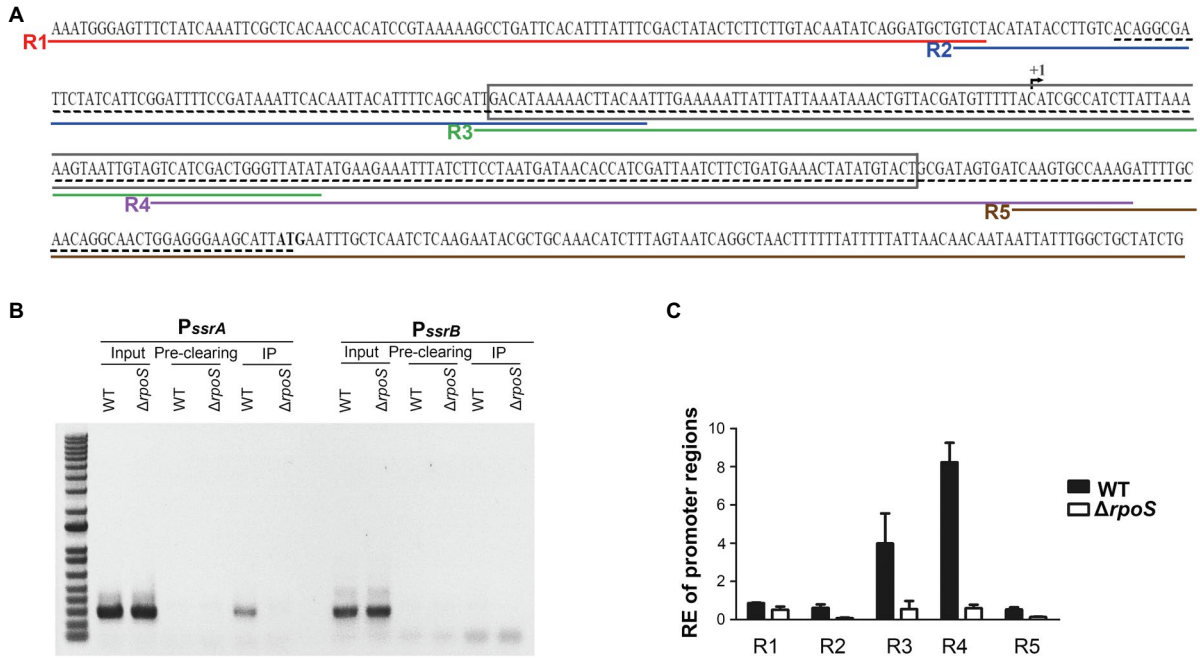

FIGURE 5 | Binding of σ^S to the *ssrA* promoter. **(A)** Scheme for Chromatin immunoprecipitation (ChIP)-PCR and ChIP-quantitative PCR (qPCR). The +1 site of *ssrA* transcription is indicated with a broken arrow and its start codon is in bold. The region amplified by ChIP-PCR is underlined with a black dashed line and that amplified and used in electrophoretic mobility shift assay (EMSA) is boxed. Five regions amplified in ChIP-qPCR are underlined in different colors: R1 in red by primers R1-F and R1-R, R2 in blue by primers R2-F and R2-R, R3 in green by primers R3-F and R3-R, R4 in purple by primers R4-F and R4-R, and R5 in brown by primers R5-F and R5-R. **(B)** DNA-protein cross-links were fixed in *Salmonella* wild-type and Δ*rpoS* mutant strains using formaldehyde. DNA fragments bound to σ^S were immunoprecipitated using anti-RpoS antibody and subjected to PCR using primers specific to the P_{ssrA} (PssrA-ChIP-F/R) and P_{ssrB} (PssrB-ChIP-F/R) regions. Input total DNA and pre-clearing (DNA non-specifically bound to Protein A/G agarose) were analyzed in parallel. The ChIP-PCR products were separated by 1% agarose gel electrophoresis. **(C)** DNA fragments precipitated in IP and pre-clearing were used as templates in ChIP-qPCR using five different primer sets (R1-F/R, R2-F/R, R3-F/R, R4-F/R, and R5-F/R). Enrichment of the P_{ssrA} region with σ^S was relatively computed using the following formula: relative enrichment (RE) = $2^{-(\Delta Ct_{IP} - \Delta Ct_{Pre\text{-}clearing})}$, where ΔCt_{IP} is $Ct_{PssrA} - Ct_{gyrB}$ for the IP samples and $\Delta Ct_{Pre\text{-}clearing}$ is $Ct_{PssrA} - Ct_{gyrB}$ for the pre-clearing samples. *gyrB* was used as an endogenous control.

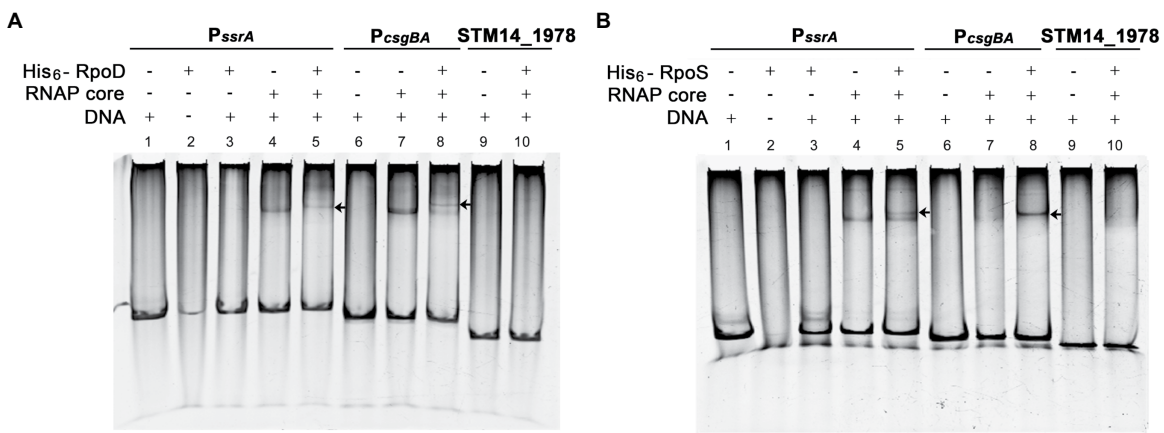

FIGURE 6 | Interaction of P_{ssrA} with either σ^S or σ^{70} *in vitro*. Binding of His_6-RpoD **(A)** and His_6-RpoS **(B)** to the *ssrA* promoter region was tested *in vitro* using EMSA. DNA fragments of the P_{ssrA} region (178 bp), P_{csgBA} region (158 bp; a positive control), and STM14_1978 CDS region (148 bp; a negative control) were incubated with RNA polymerase (RNAP) core enzyme in combination with His_6-RpoD or His_6-RpoS. The DNA-protein complexes were loaded onto a 5% native polyacrylamide gel and stained with EtBr. An arrow indicates a shifted band comprising P_{ssrA} or P_{csgBA} DNA cross-linked with the RNAP holoenzyme.

$E\sigma^{70}$ and P_{ssrA} (compare **Figure 6A**, lane 5 and **Figure 6B**, lane 5). These results stimulated us to compare the binding affinities between $E\sigma^S$ and $E\sigma^{70}$ at the P_{ssrA} region.

The P_{ssrA} DNA fragment was incubated with the core enzyme E and different concentrations of σ factors (His_6-RpoS and His_6-RpoD), and the levels of $E\sigma^S$ associated with the P_{ssrA}

region were determined using an anti-RpoS antibody. When His_6-RpoS was used at a constant concentration of 75 nM, but His_6-RpoD was increased from 0 to 50 nM, the band representing the complex between $E\sigma^S$ and P_{ssrA} gradually diminished and disappeared at 50 nM His_6-RpoD (**Figure 7A**). On the other hand, when His_6-RpoD was maintained at 75 nM but His_6-RpoS was increased from 0 to 150 nM, $E\sigma^S$ failed to bind to the P_{ssrA} region even at a 2-fold higher concentration of His_6-RpoS than His_6-RpoD (**Figure 7B**). This result suggests that the P_{ssrA} region preferentially recruits $E\sigma^{70}$ when $E\sigma^S$ and $E\sigma^{70}$ are present at equivalent concentrations *in vitro*.

Crl Promotes σ^S Competitiveness for Binding to the *ssrA* Promoter Region

For investigating the possibility that σ^S replaces σ^{70} and lowers the *ssrA* transcription, we searched for a co-regulator that could promote σ^S activity under stressful conditions and Crl was chosen as a candidate co-regulator of σ^S-mediated *ssrA* transcriptional regulation. Crl is a small protein known to interact directly with σ^S *in vitro* (Bougdour et al., 2004). The P_{ssrA} fragment was incubated with His_6-tagged σ factors (σ^S and σ^{70}) and Crl individually or in combination, and the σ^S bound to P_{ssrA} was localized using an anti-RpoS antibody. In the absence of competition with σ^{70}, Crl addition enabled σ^S (50 nM) to form a complex between $E\sigma^S$ and the P_{ssrA} region, whereas σ^S alone at 50 nM were insufficient to form the $E\sigma^S$-P_{ssrA} complex (**Figure 8**: compare lanes 4 and 5). In the absence of Crl, His_6-RpoS even at 280 nM was defeated in the competition with 50 nM His_6-RpoD and failed to form the protein-DNA complex (**Figure 8**, lane 8). However, pre-incubation of His_6-RpoS with Crl rendered His_6-RpoS competitive in forming the complex between Eσ and P_{ssrA}, showing a shifted band (**Figure 8**, lane 10). Crl binding to σ^S might facilitate the formation of the RNAP holoenzyme incorporating σ^S instead of σ^{70}, as suggested previously (Gaal et al., 2006; Typas et al., 2007a).

σ^S Abundance Led to a Comprehensive Transcriptional Alteration of SPI-2 in Host Cells

Our results comparing the ability of σ^S and σ^{70} to form the $E\sigma$-P_{ssrA} complex *in vitro* demonstrated that $E\sigma^{70}$ bound to the P_{ssrA} region preferentially than $E\sigma^S$. Given the limited cellular resources of the RNAP core enzyme E, *ssrA* transcription may be dampened when σ^S stimulated by drastic stressors diverts the RNAP core enzyme E to its cognate regulatory circuit, which is critical for surviving the challenging stressors. SPI-2 genes controlled by SsrAB regulators are known to be activated under hostile conditions such as a nutrition-deprived environment and intracellular milieu (Beuzon et al., 1999; Deiwick et al., 1999), which are prone to stimulate σ^S-mediated adaptation responses. We investigated the transcriptional response of SPI-2 genes when σ^S levels surged in response to stress and $E\sigma^S$-mediated transcriptional initiation overwhelmed the transcriptional activity of other Eσ complexes. *Salmonella* wild-type and Δ*rpoS* strains were added to macrophage cells, and the transcription levels of *rpoS*, *rpoD*, and SPI-2 genes were compared at 2, 4, and 10 h after phagocytosis. σ^S was overexpressed by introducing pRpoS into the Δ*rpoS* mutant. The absence of *rpoS* increased *rpoD* transcriptional levels at 4 h post-infection (**Figure 9**). Comparing mRNA levels of SPI-2 genes between wild-type and Δ*rpoS* strains showed that most SPI-2 genes increased their transcription in the absence of σ^S and addition

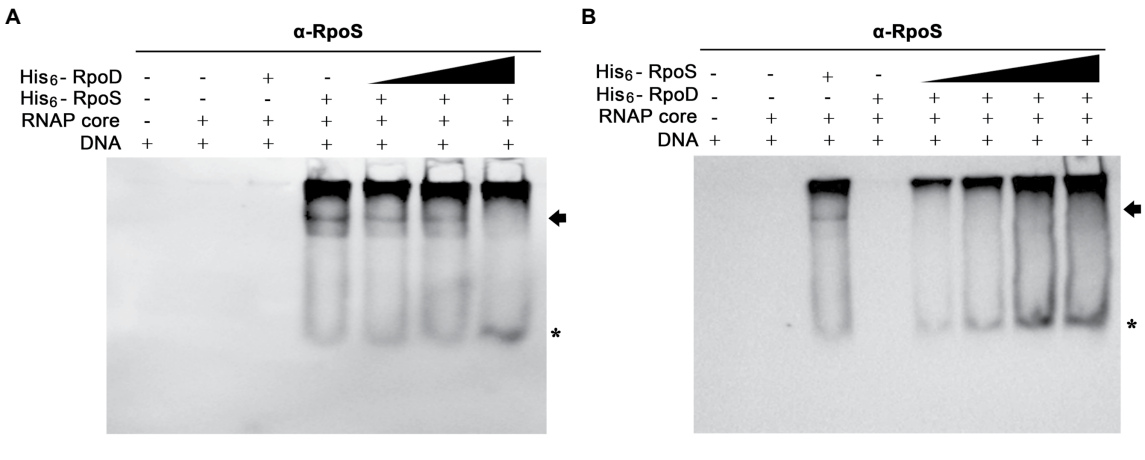

FIGURE 7 | Competitive binding to the P_{ssrA} region between σ^S and σ^{70} *in vitro*. **(A)** Competitive EMSA was conducted with His_6-RpoS at a constant concentration of 75 nM and with increasing concentrations (0, 12.5, 25, and 50 nM) of His_6-RpoD as a competitor. RNAP core enzyme was pre-incubated with different combinations of two σ factors and incubated with DNA containing the P_{ssrA} region. DNA bands were stained using EtBr and shown in **Supplementary Figure 3A**. His_6-RpoS was localized using subsequent immunoblotting with an anti-RpoS antibody. His_6-RpoS comprising $E\sigma^S$ cross-linked with the P_{ssrA} region is indicated with an arrow and free His_6-RpoS is localized with an asterisk. **(B)** Competition EMSA was applied using His_6-RpoD at a constant concentration of 75 nM and with increasing concentrations (0, 25, 50, 100, and 150 nM) of His_6-RpoS as a competitor. After reconstitution of RNAP holoenzyme with different concentrations of σ factors, the interaction between RNAP holoenzyme and P_{ssrA} region was analyzed using native gel electrophoresis followed by DNA staining (**Supplementary Figure 3B**) and immunoblotting with an anti-RpoS antibody. The location of His_6-RpoS comprising $E\sigma^S$-P_{ssrA} complex is indicated with an arrow and free His_6-RpoS not associated with DNA is indicated with an asterisk.

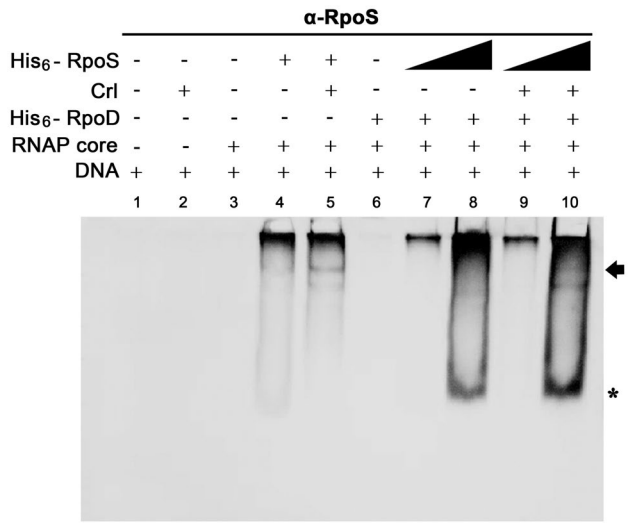

FIGURE 8 | Effect of Crl on the binding affinity of σ^S to the P_{ssrA} region *in vitro*. Competitive binding between His_6-RpoS and His_6-RpoD to the P_{ssrA} region was re-examined in the presence of His_6-Crl. In the absence of His_6-RpoD (lanes 1–5), the RNAP core enzyme was incubated with 50 nM His_6-RpoS, which was pre-incubated with 280 nM His_6-Crl. In the competition between His_6-RpoS and His_6-RpoD (lanes 6–10), His_6-RpoD was maintained at 50 nM, while His_6-RpoS was used at 25 and 280 nM in combination with 280 nM His_6-Crl. RNAP holoenzyme was reconstituted using different combinations of His_6-Crl, His_6-RpoS, and His_6-RpoD and incubated with P_{ssrA} region DNA. After gel electrophoresis, DNA was analyzed by EtBr staining (**Supplementary Figure 4**), and His_6-RpoS was localized using immunoblotting with an anti-RpoS antibody. His_6-RpoS comprising $E\sigma^S$ cross-linked with the P_{ssrA} region is indicated with an arrow, and free His_6-RpoS is indicated by an asterisk.

of pRpoS nullified these alterations (**Figure 9**), indicating a negative role of σ^S in SPI-2 transcription. In accordance with the transcriptional regulation by σ^S, the levels of T3SS2-associated proteins were decreased by the overexpression of σ^S (**Supplementary Figure 6**). However, the transcriptional response to σ^S abundance was different among the SPI-2 genes. Many genes, including *sscB*, *sseFG*, *ssaG*, *sseJ*, and *sspH2*, showed negative transcriptional regulation by σ^S abundance throughout the assay, whereas *sseCD* genes encoding the translocon components of T3SS2 (Chakravortty et al., 2005) showed minimal transcriptional alteration by σ^S abundance (**Figure 9**). Differential requirements among T3SS effectors depending on time and site during infection have been proposed in previous studies (Brawn et al., 2007; Nunez-Hernandez et al., 2014). The differential influence of σ^S between T3SS2-associated genes suggests that SsrA-mediated regulation is not the only mechanism by which σ^S participates in controlling SPI-2 T3SS-associated genes.

DISCUSSION

During host infection, *Salmonella* undergoes various stress conditions, such as gastric acidity, bile salts, oxidative stress, and nutrient starvation. Alternative σ factors are prominent

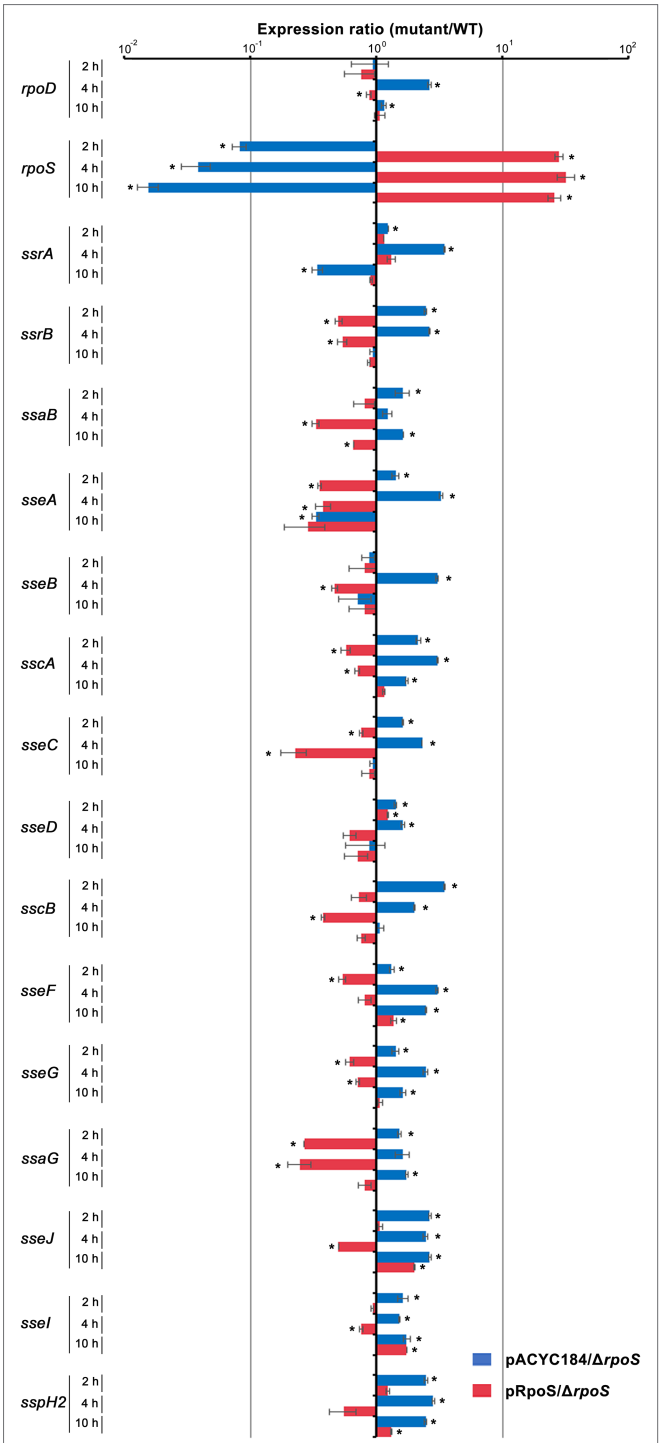

FIGURE 9 | Transcriptional regulation of SPI-2 genes by σ^S. *Salmonella* wild-type and Δ*rpoS* mutant strains containing pRpoS or pACYC184 were added to RAW264.7, and total RNA was isolated at 2, 4, and 10 h post-infection and used to measure the transcription levels of genes, including *rpoD*, *rpoS*, and SPI-2 T3SS-associated genes. The Ct values for each gene were normalized to those of *gyrB*. Expression levels of each gene from Δ*rpoS* mutant strains containing pRpoS or pACYC184 were compared with those from wild-type strain containing pACYC184 and the fold-change (mutant/wild-type) was plotted. An asterisk indicates a value of $p < 0.05$ in comparison with wild-type strain harboring pACYC184.

regulatory proteins that enable bacteria to cope with diverse stresses by redirecting RNAP core enzymes to the transcription of genes required for survival and adaptation in these conditions. RpoS or σ^S, a σ factor comprising the RNAP holoenzyme, is known to activate the transcription of genes associated with general stress resistance (Hengge-Aronis, 2002a). However, the regulatory roles of σ^S are not only restricted to stress-resistance genes. In *Salmonella*, σ^S was found to directly or indirectly control the expression of genes that make up more than 20% of the genome (Levi-Meyrueis et al., 2014; Lago et al., 2017), implying its multifaceted roles ranging from physiological remodeling against cellular damage to metabolic regulation of sugars, amino acids, and fatty acids (Ibanez-Ruiz et al., 2000; Lago et al., 2017). In addition, σ^S is involved in *Salmonella* virulence regulation. Rice et al. (2015) observed genes comprising SPI-1 and SPI-2, which are essential for *Salmonella* invasion into host cells and intracellular survival, were upregulated in the absence of σ^S, indicating a negative role of σ^S in SPI-1 and SPI-2 expression. We found that σ^S could bind to the P_{ssrA} region directly (**Figure 5**), and a surplus of σ^S repressed its transcription. This led to an overall downregulation of SPI-2 T3SS-associated genes (**Figure 9**). Direct negative regulation by σ^S was recently reported in the transcription of *esrB* in *Edwardsiella piscicida* (Yin et al., 2018). *Edwardsiella piscicida*, which is phylogenetically close to *Salmonella enterica*, exploits T3SS and T6SS to translocate virulence factors into host cells, and the expression of these virulence machineries is activated by the two-component regulatory system EsrAB, homologs for SsrAB in *S. enterica* (Wang et al., 2009; Yin et al., 2018). *Edwardsiella piscicida* σ^S was proposed to mediate a trade-off between stress adaptation and virulence by inhibiting *esrB* expression through a direct interaction between σ^S and the P_{esrB} region (Yin et al., 2018). Binding of the Eσ complex to gene promoter regions is typically presumed to activate transcription initiation. Therefore, the negative regulation by σ^S may be attributed to the competition between σ factors for binding to the RNAP core enzyme (Farewell et al., 1998; Hsu, 2002). A surge in σ^S caused by bacterial adaptation to general stresses can exclusively occupy the pool of core enzyme E and impede transcriptional events mediated by other σ factors. However, alternatively to this passive regulation *via* competitive binding between σ factors, adhesion of the $E\sigma^S$ complex to promoter regions may sterically hinder binding of the $E\sigma^{70}$ complex and directly attenuate transcription, as demonstrated in *E. piscicida esrB* gene (Yin et al., 2018) and *S. enterica* serovar Typhimurium *sdh* gene (Levi-Meyrueis et al., 2015).

The promoter region of *ssrA* is occupied by multiple regulators, including HilD, SlyA, OmpR, and H-NS, and its transcription is controlled by the competitive binding of these regulators to the overlapping DNA (Banda et al., 2019). The consensus promoter sequences recognized by σ^{70} are also accessible to H-NS, whose binding blocks the access of $E\sigma^{70}$ and transcriptional activators such as OmpR. Anti-repressors such as HilD and SlyA relieve H-NS-mediated silencing by competitive binding to the P_{ssrA} region (Banda et al., 2019). Considering the similar recognition motifs at −10 and −35 elements between σ^S and σ^{70} and the functional inter-compatibility between two σ factors in some genes, the downregulation of *ssrAB* by binding of σ^S to the P_{ssrA} region can be achievable through several mechanisms. Firstly, binding of $E\sigma^S$ to the P_{ssrA} region may not exert transcriptional initiation, but instead sterically hinder $E\sigma^{70}$-mediated transcription as demonstrated in the *E. piscicida esrB* gene (Yin et al., 2018). A σ factor associated with RNAP core enzyme directs transcription initiation at a specific promoter region but is assumed to dissociate upon transition from transcription initiation to transcription elongation because of a steric clash between the growing RNA product and the σ factor (Hsu, 2002). σ^S that is not released on time may impede promoter escape of the core enzyme E and hinder transcription elongation. Alternatively, the binding of $E\sigma^S$ to P_{ssrA} region may produce incorrect transcripts, as shown in the transcriptional regulation of *crl* gene (Zafar et al., 2014). The *crl* gene with overlapping promoters sensed by two different σ factors of σ^{70} and σ^N may shut down its expression by association with $E\sigma^N$. σ^N increases in response to nitrogen limitation, forming a DNA-$E\sigma^N$ complex at the *crl* promoter region, but its binding results in a long noncoding RNA transcript lacking a ribosome binding site, thereby preventing $E\sigma^{70}$ from binding to the overlapped promoter and producing translatable *crl* mRNA (Zafar et al., 2014). We observed that DNA fragments bound to $E\sigma^S$ *in vivo* covered a long region from the known +1 site of *ssrA* transcript to the start codon for SsrA (**Figure 5**). To differentiate between these two possibilities, it is important to examine whether $E\sigma^S$ bound to the P_{ssrA} region can lead to *ssrA* transcription and whether the resultant transcript can successfully be translated. Another possibility is the competitive $E\sigma^S$ binding among promoters with different binding affinities due to recognition motif preference and topological characteristics. Considering that the cellular σ^S concentration is low even in the stationary phase of growth (Jishage et al., 1996) and its affinity for RNAP core enzyme is the lowest among σ factors *in vitro* (Maeda et al., 2000), the P_{ssrA} region occluded by multiple regulators may be less competent in recruiting $E\sigma^S$ and other promoter sites, which are preferentially responsive to σ^S, may outcompete the *ssrA* promoter.

In order to cope with limited resources, bacteria allocate cellular resources between reproduction and maintenance in response to environmental cues. In the absence of nutrient depletion and hostile stressors, bacteria proliferate and deploy resources for reproduction. Under these favorable conditions, σ^{70} is exclusively used for the transcription initiation of housekeeping genes. On the other hand, bacteria challenged by stressful stimuli divert cellular resources to maintenance and resistance, replacing σ^{70} with alternative σ factors for comprehensive transcription alteration. σ^S orchestrates the expression of a large number of genes under conditions of starvation and general stress caused by pH, temperature, and osmolarity. SPI-2 T3SS and its cognate effectors critical for *Salmonella* intracellular survival and replication are thought to be induced by unfavorable stimuli encountered inside host cells (Lober et al., 2006; Fass and Groisman, 2009), which would also likely promote σ^S-mediated stress adaptation processes. However, we observed that excessive σ^S production rather decreased the transcription of SPI-2 and its associated genes. Virulence effectors translocated *via* SPI-2 T3SS help intracellular *Salmonella* to compromise the host defense systems and facilitate

intracellular proliferation and cell-to-cell spread (Grant et al., 2012; Jennings et al., 2017). However, overgrowth of *Salmonella*, which is less competent to manage hostile stresses, poses a disadvantage to long-term persistence inside hosts because the intense immune responses provoked by the proliferation may eliminate defective bacteria rapidly after all (Nunez-Hernandez et al., 2014). *Salmonella* executing σ^S-mediated stress adaptation may attenuate aggressive virulence ascribed to SPI-2 to achieve a trade-off between stress adaptation and virulence. Notably, the growth rates of intracellular *Salmonella* vary depending on the infected cell types; *Salmonella* proliferated exclusively in CD18-expressing phagocytes *in vivo* (Richter-Dahlfors et al., 1997), while restraining its growth in non-professional phagocytes such as subepithelial fibroblasts (Cano et al., 2001). Therefore, the importance of SPI-2 T3SS for *Salmonella* survival varies depending on infection foci or cell types. For example, SifA, an effector translocated *via* SPI-2 T3SS, is essential for bacterial growth inside macrophages but is dispensable for survival inside fibroblast cells (Nunez-Hernandez et al., 2014). Interestingly, Grant et al. showed that *Salmonella* lacking SPI-2 T3SS remained inside phagocytes at a high replication rate but failed to leave the infected cells, suggesting a new role for SPI-2 T3SS in bacterial dissemination to other sites (Grant et al., 2012). Premature escape from infected host cells may impose unaffordable expenses on *Salmonella* to resist severe host defense systems and constrain its successful host colonization. In this context, it is an energy-effective strategy for *Salmonella* to employ σ^S as a dual-purpose regulator that aids in adaptation and resistance against unfavorable conditions and lowers unnecessary virulence attributable to SPI-2 at the same time.

DATA AVAILABILITY STATEMENT

The original contributions presented in the study are included in the article/**Supplementary Material**, further inquiries can be directed to the corresponding author.

AUTHOR CONTRIBUTIONS

SK designed and conducted the experiment and interpreted the data. EK performed and analyzed the experiment. HY conceived and coordinated the study. SK and HY wrote the manuscript. All authors contributed to the article and approved the submitted version.

FUNDING

This study was supported by a grant (2019R1A6A1A11051471) from the Priority Research Centers Program funded by the National Research Foundation of Korea (NRF) and a grant (2021R1F1A1058498) of the Basic Science Research Program through the NRF funded by the Korean government (MSIT).

SUPPLEMENTARY MATERIAL

The Supplementary Material for this article can be found online at: https://www.frontiersin.org/articles/10.3389/fmicb.2021.750940/full#supplementary-material

REFERENCES

Arnqvist, A., Olsen, A., and Normark, S. (1994). Sigma S-dependent growth-phase induction of the csgBA promoter in *Escherichia coli* can be achieved in vivo by sigma 70 in the absence of the nucleoid-associated protein H-NS. *Mol. Microbiol.* 13, 1021–1032. doi: 10.1111/j.1365-2958.1994.tb00493.x

Banda, M. M., Zavala-Alvarado, C., Perez-Morales, D., and Bustamante, V. H. (2019). SlyA and HilD counteract H-NS-mediated repression on the ssrAB virulence operon of *Salmonella enterica* serovar Typhimurium and thus promote its activation by OmpR. *J. Bacteriol.* 201, e00530–e00618. doi: 10.1128/JB.00530-18

Bang, I. S., Frye, J. G., Mcclelland, M., Velayudhan, J., and Fang, F. C. (2005). Alternative sigma factor interactions in *Salmonella*: sigma and sigma promote antioxidant defences by enhancing sigma levels. *Mol. Microbiol.* 56, 811–823. doi: 10.1111/j.1365-2958.2005.04580.x

Beuzon, C. R., Banks, G., Deiwick, J., Hensel, M., and Holden, D. W. (1999). pH-dependent secretion of SseB, a product of the SPI-2 type III secretion system of *Salmonella* typhimurium. *Mol. Microbiol.* 33, 806–816. doi: 10.1046/j.1365-2958.1999.01527.x

Bougdour, A., Lelong, C., and Geiselmann, J. (2004). Crl, a low temperature-induced protein in *Escherichia coli* that binds directly to the stationary phase sigma subunit of RNA polymerase. *J. Biol. Chem.* 279, 19540–19550. doi: 10.1074/jbc.M314145200

Brawn, L. C., Hayward, R. D., and Koronakis, V. (2007). *Salmonella* SPI1 effector SipA persists after entry and cooperates with a SPI2 effector to regulate phagosome maturation and intracellular replication. *Cell Host Microbe* 1, 63–75. doi: 10.1016/j.chom.2007.02.001

Bustamante, V. H., Martinez, L. C., Santana, F. J., Knodler, L. A., Steele-Mortimer, O., and Puente, J. L. (2008). HilD-mediated transcriptional cross-talk between SPI-1 and SPI-2. *Proc. Natl. Acad. Sci. U. S. A.* 105, 14591–14596. doi: 10.1073/pnas.0801205105

Cano, D. A., Martinez-Moya, M., Pucciarelli, M. G., Groisman, E. A., Casadesus, J., and Garcia-Del Portillo, F. (2001). *Salmonella enterica* serovar Typhimurium response involved in attenuation of pathogen intracellular proliferation. *Infect. Immun.* 69, 6463–6474. doi: 10.1128/IAI.69.10.6463-6474.2001

Chakravortty, D., Rohde, M., Jager, L., Deiwick, J., and Hensel, M. (2005). Formation of a novel surface structure encoded by *Salmonella* pathogenicity island 2. *EMBO J.* 24, 2043–2052. doi: 10.1038/sj.emboj.7600676

Chang, A. C., and Cohen, S. N. (1978). Construction and characterization of amplifiable multicopy DNA cloning vehicles derived from the P15A cryptic miniplasmid. *J. Bacteriol.* 134, 1141–1156. doi: 10.1128/jb.134.3.1141-1156.1978

Deiwick, J., Nikolaus, T., Erdogan, S., and Hensel, M. (1999). Environmental regulation of *Salmonella* pathogenicity island 2 gene expression. *Mol. Microbiol.* 31, 1759–1773. doi: 10.1046/j.1365-2958.1999.01312.x

Dong, T., and Schellhorn, H. E. (2010). Role of RpoS in virulence of pathogens. *Infect. Immun.* 78, 887–897. doi: 10.1128/IAI.00882-09

Fang, F. C., Libby, S. J., Buchmeier, N. A., Loewen, P. C., Switala, J., Harwood, J., et al. (1992). The alternative sigma factor katF (rpoS) regulates *Salmonella* virulence. *Proc. Natl. Acad. Sci. U. S. A.* 89, 11978–11982. doi: 10.1073/pnas.89.24.11978

Farewell, A., Kvint, K., and Nystrom, T. (1998). Negative regulation by RpoS: a case of sigma factor competition. *Mol. Microbiol.* 29, 1039–1051. doi: 10.1046/j.1365-2958.1998.00990.x

Fass, E., and Groisman, E. A. (2009). Control of *Salmonella* pathogenicity island-2 gene expression. *Curr. Opin. Microbiol.* 12, 199–204. doi: 10.1016/j.mib.2009.01.004

Feng, X., Oropeza, R., and Kenney, L. J. (2003). Dual regulation by phospho-OmpR of ssrA/B gene expression in *Salmonella* pathogenicity island 2. *Mol. Microbiol.* 48, 1131–1143. doi: 10.1046/j.1365-2958.2003.03502.x

Feng, X., Walthers, D., Oropeza, R., and Kenney, L. J. (2004). The response regulator SsrB activates transcription and binds to a region overlapping OmpR binding sites at *Salmonella* pathogenicity island 2. *Mol. Microbiol.* 54, 823–835. doi: 10.1111/j.1365-2958.2004.04317.x

Ferenci, T. (2005). Maintaining a healthy SPANC balance through regulatory and mutational adaptation. *Mol. Microbiol.* 57, 1–8. doi: 10.1111/j.1365-2958.2005.04649.x

Gaal, T., Mandel, M. J., Silhavy, T. J., and Gourse, R. L. (2006). Crl facilitates RNA polymerase holoenzyme formation. *J. Bacteriol.* 188, 7966–7970. doi: 10.1128/JB.01266-06

Grant, A. J., Morgan, F. J., Mckinley, T. J., Foster, G. L., Maskell, D. J., and Mastroeni, P. (2012). Attenuated *Salmonella* Typhimurium lacking the pathogenicity island-2 type 3 secretion system grow to high bacterial numbers inside phagocytes in mice. *PLoS Pathog.* 8:e1003070. doi: 10.1371/journal.ppat.1003070

Grove, A. P., Liveris, D., Iyer, R., Petzke, M., Rudman, J., Caimano, M. J., et al. (2017). Two distinct mechanisms govern RpoS-mediated repression of tick-phase genes during mammalian host adaptation by *Borrelia burgdorferi*, the Lyme disease spirochete. *mBio* 8, e01204–e01217. doi: 10.1128/mBio.01204-17

Gu, D., Liu, H., Yang, Z., Zhang, Y., and Wang, Q. (2016). Chromatin immunoprecipitation sequencing technology reveals global regulatory roles of low-cell-density quorum-sensing regulator AphA in the pathogen *vibrio alginolyticus*. *J. Bacteriol.* 198, 2985–2999. doi: 10.1128/JB.00520-16

Hengge-Aronis, R. (2002a). Signal transduction and regulatory mechanisms involved in control of the sigma(S) (RpoS) subunit of RNA polymerase. *Microbiol. Mol. Biol. Rev.* 66, 373–395. doi: 10.1128/MMBR.66.3.373-395.2002

Hengge-Aronis, R. (2002b). Stationary phase gene regulation: what makes an *Escherichia coli* promoter sigmaS-selective? *Curr. Opin. Microbiol.* 5, 591–595. doi: 10.1016/s1369-5274(02)00372-7

Hermans, K., Roberfroid, S., Thijs, I. M., Kint, G., De Coster, D., Marchal, K., et al. (2016). FabR regulates *Salmonella* biofilm formation via its direct target FabB. *BMC Genomics* 17:253. doi: 10.1186/s12864-016-2387-x

Hiratsu, K., Amemura, M., Nashimoto, H., Shinagawa, H., and Makino, K. (1995). The rpoE gene of *Escherichia coli*, which encodes sigma E, is essential for bacterial growth at high temperature. *J. Bacteriol.* 177, 2918–2922. doi: 10.1128/jb.177.10.2918-2922.1995

Hsu, L. M. (2002). Promoter clearance and escape in prokaryotes. *Biochim. Biophys. Acta* 1577, 191–207. doi: 10.1016/s0167-4781(02)00452-9

Ibanez-Ruiz, M., Robbe-Saule, V., Hermant, D., Labrude, S., and Norel, F. (2000). Identification of RpoS (sigma(S))-regulated genes in *Salmonella enterica* serovar typhimurium. *J. Bacteriol.* 182, 5749–5756. doi: 10.1128/JB.182.20.5749-5756.2000

Jennings, E., Thurston, T. L. M., and Holden, D. W. (2017). *Salmonella* SPI-2 type III secretion system effectors: molecular mechanisms and physiological consequences. *Cell Host Microbe* 22, 217–231. doi: 10.1016/j.chom.2017.07.009

Jishage, M., Iwata, A., Ueda, S., and Ishihama, A. (1996). Regulation of RNA polymerase sigma subunit synthesis in *Escherichia coli*: intracellular levels of four species of sigma subunit under various growth conditions. *J. Bacteriol.* 178, 5447–5451. doi: 10.1128/jb.178.18.5447-5451.1996

Kim, S. I., Kim, S., Kim, E., Hwang, S. Y., and Yoon, H. (2018). Secretion of *Salmonella* pathogenicity island 1-encoded type III secretion system effectors by outer membrane vesicles in *Salmonella enterica* serovar typhimurium. *Front. Microbiol.* 9:2810. doi: 10.3389/fmicb.2018.02810

Kim, S. I., and Yoon, H. (2019). Roles of YcfR in biofilm formation in *Salmonella* Typhimurium ATCC 14028. *Mol. Plant-Microbe Interact.* 32, 708–716. doi: 10.1094/MPMI-06-18-0166-R

Kowarz, L., Coynault, C., Robbe-Saule, V., and Norel, F. (1994). The *Salmonella* Typhimurium katF (rpoS) gene: cloning, nucleotide sequence, and regulation of spvR and spvABCD virulence plasmid genes. *J. Bacteriol.* 176, 6852–6860. doi: 10.1128/jb.176.22.6852-6860.1994

Kwoh, D. Y., and Kemper, J. (1978). Bacteriophage P22-mediated specialized transduction in *Salmonella* typhimurium: identification of different types of specialized transducing particles. *J. Virol.* 27, 535–550. doi: 10.1128/jvi.27.3.535-550.1978

Lago, M., Monteil, V., Douche, T., Guglielmini, J., Criscuolo, A., Maufrais, C., et al. (2017). Proteome remodelling by the stress sigma factor RpoS/sigma(S) in *Salmonella*: identification of small proteins and evidence for post-transcriptional regulation. *Sci. Rep.* 7:2127. doi: 10.1038/s41598-017-02362-3

Lee, T. S., Krupa, R. A., Zhang, F., Hajimorad, M., Holtz, W. J., Prasad, N., et al. (2011). BglBrick vectors and datasheets: a synthetic biology platform for gene expression. *J. Biol. Eng.* 5:12. doi: 10.1186/1754-1611-5-12

Levi-Meyrueis, C., Monteil, V., Sismeiro, O., Dillies, M. A., Kolb, A., Monot, M., et al. (2015). Repressor activity of the RpoS/sigmaS-dependent RNA polymerase requires DNA binding. *Nucleic Acids Res.* 43, 1456–1468. doi: 10.1093/nar/gku1379

Levi-Meyrueis, C., Monteil, V., Sismeiro, O., Dillies, M. A., Monot, M., Jagla, B., et al. (2014). Expanding the RpoS/sigmaS-network by RNA sequencing and identification of sigmaS-controlled small RNAs in *Salmonella*. *PLoS One* 9:e96918. doi: 10.1371/journal.pone.0096918

Lober, S., Jackel, D., Kaiser, N., and Hensel, M. (2006). Regulation of *Salmonella* pathogenicity island 2 genes by independent environmental signals. *Int. J. Med. Microbiol.* 296, 435–447. doi: 10.1016/j.ijmm.2006.05.001

Maeda, H., Fujita, N., and Ishihama, A. (2000). Competition among seven *Escherichia coli* sigma subunits: relative binding affinities to the core RNA polymerase. *Nucleic Acids Res.* 28, 3497–3503. doi: 10.1093/nar/28.18.3497

Muffler, A., Fischer, D., and Hengge-Aronis, R. (1996). The RNA-binding protein HF-I, known as a host factor for phage Qbeta RNA replication, is essential for rpoS translation in *Escherichia coli*. *Genes Dev.* 10, 1143–1151. doi: 10.1101/gad.10.9.1143

Notley-McRobb, L., King, T., and Ferenci, T. (2002). rpoS mutations and loss of general stress resistance in *Escherichia coli* populations as a consequence of conflict between competing stress responses. *J. Bacteriol.* 184, 806–811. doi: 10.1128/JB.184.3.806-811.2002

Nunez-Hernandez, C., Alonso, A., Pucciarelli, M. G., Casadesus, J., and Garcia-Del Portillo, F. (2014). Dormant intracellular *Salmonella enterica* serovar Typhimurium discriminates among *Salmonella* pathogenicity island 2 effectors to persist inside fibroblasts. *Infect. Immun.* 82, 221–232. doi: 10.1128/IAI.01304-13

Raffatellu, M., Wilson, R. P., Chessa, D., Andrews-Polymenis, H., Tran, Q. T., Lawhon, S., et al. (2005). SipA, SopA, SopB, SopD, and SopE2 contribute to *Salmonella enterica* serotype Typhimurium invasion of epithelial cells. *Infect. Immun.* 73, 146–154. doi: 10.1128/IAI.73.1.146-154.2005

Ramachandran, V. K., Shearer, N., Jacob, J. J., Sharma, C. M., and Thompson, A. (2012). The architecture and ppGpp-dependent expression of the primary transcriptome of *Salmonella* Typhimurium during invasion gene expression. *BMC Genomics* 13:25. doi: 10.1186/1471-2164-13-25

Rice, C. J., Ramachandran, V. K., Shearer, N., and Thompson, A. (2015). Transcriptional and post-transcriptional modulation of SPI1 and SPI2 expression by ppGpp, RpoS and DksA in *Salmonella enterica* sv typhimurium. *PLoS One* 10:e0127523. doi: 10.1371/journal.pone.0127523

Richter-Dahlfors, A., Buchan, A. M., and Finlay, B. B. (1997). Murine salmonellosis studied by confocal microscopy: *Salmonella* Typhimurium resides intracellularly inside macrophages and exerts a cytotoxic effect on phagocytes in vivo. *J. Exp. Med.* 186, 569–580. doi: 10.1084/jem.186.4.569

Robbe-Saule, V., Jaumouille, V., Prevost, M. C., Guadagnini, S., Talhouarne, C., Mathout, H., et al. (2006). Crl activates transcription initiation of RpoS-regulated genes involved in the multicellular behavior of *Salmonella enterica* serovar typhimurium. *J. Bacteriol.* 188, 3983–3994. doi: 10.1128/JB.00033-06

Salazar, J. K., Deng, K., Tortorello, M. L., Brandl, M. T., Wang, H., and Zhang, W. (2013). Genes ycfR, sirA and yigG contribute to the surface attachment of *Salmonella enterica* Typhimurium and saintpaul to fresh produce. *PLoS One* 8:e57272. doi: 10.1371/journal.pone.0057272

Shimada, T., Tanaka, K., and Ishihama, A. (2017). The whole set of the constitutive promoters recognized by four minor sigma subunits of *Escherichia coli* RNA polymerase. *PLoS One* 12:e0179181. doi: 10.1371/journal.pone.0179181

Simons, R. W., Houman, F., and Kleckner, N. (1987). Improved single and multicopy lac-based cloning vectors for protein and operon fusions. *Gene* 53, 85–96. doi: 10.1016/0378-1119(87)90095-3

Smale, S. T. (2010). Beta-galactosidase assay. *Cold Spring Harb Protoc* 2010:pdb.prot5423. doi: 10.1101/pdb.prot5423

Soncini, F. C., Vescovi, E. G., and Groisman, E. A. (1995). Transcriptional autoregulation of the *Salmonella* Typhimurium phoPQ operon. *J. Bacteriol.* 177, 4364–4371. doi: 10.1128/jb.177.15.4364-4371.1995

Storvik, K. A., and Foster, P. L. (2010). RpoS, the stress response sigma factor, plays a dual role in the regulation of *Escherichia coli's* error-prone DNA polymerase IV. *J. Bacteriol.* 192, 3639–3644. doi: 10.1128/JB.00358-10

Trevino-Quintanilla, L. G., Freyre-Gonzalez, J. A., and Martinez-Flores, I. (2013). Anti-sigma factors in *E. coli*: common regulatory mechanisms controlling

sigma factors availability. *Curr. Genom.* 14, 378–387. doi: 10.2174/1389202911314060007

Typas, A., Barembruch, C., Possling, A., and Hengge, R. (2007a). Stationary phase reorganisation of the *Escherichia coli* transcription machinery by Crl protein, a fine-tuner of sigmas activity and levels. *EMBO J.* 26, 1569–1578. doi: 10.1038/sj.emboj.7601629

Typas, A., Becker, G., and Hengge, R. (2007b). The molecular basis of selective promoter activation by the sigmaS subunit of RNA polymerase. *Mol. Microbiol.* 63, 1296–1306. doi: 10.1111/j.1365-2958.2007.05601.x

Vanaporn, M., Vattanaviboon, P., Thongboonkerd, V., and Korbsrisate, S. (2008). The rpoE operon regulates heat stress response in *Burkholderia pseudomallei*. *FEMS Microbiol. Lett.* 284, 191–196. doi: 10.1111/j.1574-6968.2008.01216.x

Wang, Q., Yang, M., Xiao, J., Wu, H., Wang, X., Lv, Y., et al. (2009). Genome sequence of the versatile fish pathogen *Edwardsiella tarda* provides insights into its adaptation to broad host ranges and intracellular niches. *PLoS One* 4:e7646. doi: 10.1371/journal.pone.0007646

Yin, K., Guan, Y., Ma, R., Wei, L., Liu, B., Liu, X., et al. (2018). Critical role for a promoter discriminator in RpoS control of virulence in *Edwardsiella piscicida*. *PLoS Pathog.* 14:e1007272. doi: 10.1371/journal.ppat.1007272

Yoon, H., Ansong, C., Mcdermott, J. E., Gritsenko, M., Smith, R. D., Heffron, F., et al. (2011). Systems analysis of multiple regulator perturbations allows discovery of virulence factors in *Salmonella*. *BMC Syst. Biol.* 5:100. doi: 10.1186/1752-0509-5-100

Yoon, H., Mcdermott, J. E., Porwollik, S., Mcclelland, M., and Heffron, F. (2009). Coordinated regulation of virulence during systemic infection of *Salmonella enterica* serovar typhimurium. *PLoS Pathog.* 5:e1000306. doi: 10.1371/journal.ppat.1000306

Zafar, M. A., Carabetta, V. J., Mandel, M. J., and Silhavy, T. J. (2014). Transcriptional occlusion caused by overlapping promoters. *Proc. Natl. Acad. Sci. U. S. A.* 111, 1557–1561. doi: 10.1073/pnas.1323413111

Zambrano, M. M., Siegele, D. A., Almiron, M., Tormo, A., and Kolter, R. (1993). Microbial competition: *Escherichia coli* mutants that take over stationary phase cultures. *Science* 259, 1757–1760. doi: 10.1126/science.7681219

Zhang, X. S., Garcia-Contreras, R., and Wood, T. K. (2007). YcfR (BhsA) influences *Escherichia coli* biofilm formation through stress response and surface hydrophobicity. *J. Bacteriol.* 189, 3051–3062. doi: 10.1128/JB.01832-06

Conflict of Interest: The authors declare that the research was conducted in the absence of any commercial or financial relationships that could be construed as a potential conflict of interest.

Publisher's Note: All claims expressed in this article are solely those of the authors and do not necessarily represent those of their affiliated organizations, or those of the publisher, the editors and the reviewers. Any product that may be evaluated in this article, or claim that may be made by its manufacturer, is not guaranteed or endorsed by the publisher.

frontiers in Microbiology

ORIGINAL RESEARCH
published: 27 October 2021
doi: 10.3389/fmicb.2021.762171

Polyphosphate Kinase 1 Is a Pathogenesis Determinant in Enterohemorrhagic *Escherichia coli* O157:H7

Yanli Du[1†], Xiangyu Wang[2,3†], Zongli Han[4], Ying Hua[3], Kaina Yan[3], Bao Zhang[3], Wei Zhao[3] and Chengsong Wan[3,5]*

[1] School of Medical Technology and Nursing, Shenzhen Polytechnic, Shenzhen, China, [2] Department of Gastroenterology, The First Affiliated Hospital of Shenzhen University, Shenzhen Second People's Hospital, Shenzhen, China, [3] Department of Microbiology, School of Public Health, Southern Medical University, Guangzhou, China, [4] Department of Neurosurgery, Peking University Shenzhen Hospital, Shenzhen, China, [5] Key Laboratory of Tropical Disease Research of Guangdong Province, Guangzhou, China

OPEN ACCESS

Edited by:
Dongsheng Zhou, Beijing Institute of Microbiology and Epidemiology, China

Reviewed by:
Runhua Han, University of Texas at Austin, United States
Jincai Ma, Jilin Unversity, China
Ming chun Li, Nankai University, China
James L. Bono, United States Department of Agriculture, United States

***Correspondence:**
Chengsong Wan
gzwcs@smu.edu.cn

[†]These authors have contributed equally to this work and share first authorship

Specialty section:
This article was submitted to Infectious Agents and Disease, a section of the journal Frontiers in Microbiology

Received: *21 August 2021*
Accepted: *08 October 2021*
Published: *27 October 2021*

Citation:
Du Y, Wang X, Han Z, Hua Y, Yan K, Zhang B, Zhao W and Wan C (2021) Polyphosphate Kinase 1 Is a Pathogenesis Determinant in Enterohemorrhagic Escherichia coli O157:H7. Front. Microbiol. 12:762171. doi: 10.3389/fmicb.2021.762171

The *ppk1* gene encodes polyphosphate kinase (PPK1), which is the major catalytic enzyme that *Escherichia coli* utilizes to synthesize inorganic polyphosphate (polyP). The aim of this study was to explore the role of PPK1 in the pathogenesis of Enterohemorrhagic *E. coli* O157:H7 (EHEC O157:H7). An isogenic in-frame *ppk1* deletion mutant (Δ*ppk1*) and *ppk1* complemented mutant (*Cppk1*) were constructed and characterized in comparison to wild-type (WT) EHEC O157:H7 strain EDL933w by microscope observation and growth curve analysis. Survival rates under heat stress and acid tolerance, both of which the bacteria would face during pathogenesis, were compared among the three strains. LoVo cells and a murine model of intestinal colitis were used as the *in vitro* and *in vivo* models, respectively, to evaluate the effect of PPK1 on adhesion and invasion during the process of pathogenesis. Real-time reverse-transcription PCR of regulatory gene *rpoS*, adhesion gene *eae,* and toxin genes *stx1* and *stx2* was carried out to corroborate the results from the *in vitro* and *in vivo* models. The *ppk1* deletion mutant exhibited disrupted polyP levels, but not morphology and growth characteristics. The survival rate of the Δ*ppk1* strain under stringent environmental conditions was lower as compared with WT and *Cppk1.* The *in vitro* assays showed that deletion of the *ppk1* gene reduced the adhesion, formation of attaching and effacing (A/E) lesions, and invasive ability of EHEC O157:H7. Moreover, the virulence of the Δ*ppk1* in BALB/c mice was weaker as compared with the other two strains. Additionally, mRNA expression of *rpoS*, *eae*, *stx1* and *stx2* were consistent with the *in vitro* and *in vivo* results. In conclusion: EHEC O157:H7 requires PPK1 for both survival under harsh environmental conditions and virulence *in vivo*.

Keywords: polyphosphate kinase 1 (PPK1), polyphosphate (polyP), enterohemorrhagic *Escherichia coli* O157:H7, pathogenesis, RpoS

INTRODUCTION

Enterohemorrhagic *Escherichia coli* O157:H7 (EHEC O157:H7) is a gram-negative bacterium that was identified as a human pathogen in 1982 and has continued to be a worldwide threat to public health. EHEC O157:H7 is known to cause hemorrhagic colitis (HC), thrombotic thrombocytopenic purpura (TTP), and hemolytic uremic syndrome (HUS), which results in high mortality

(Riley et al., 1983; Perna et al., 2001; Zhao et al., 2013). The main pathogenic mechanisms of EHEC O157:H7 include the production of Shiga toxin (Stx), which is primarily responsible for the renal complications and neurological sequelae of EHEC infections, as well as a type III secretion system (TTSS) that enables tight adherence of bacteria to host epithelial cells by inducing characteristic actin cytoskeletal rearrangements and loss of microvillus structure (A/E lesions) (Nguyen and Sperandio, 2012; Davis et al., 2014; Melton-Celsa, 2014; Stevens and Frankel, 2014; Pacheco et al., 2018; Menge, 2020). In recent years, progress has been made in understanding the function and mechanism of TTSS effector proteins (Wang et al., 2017; Hua et al., 2020), and factors that have overlapping effects on TTSS and Stx, such as sRNA *Esr055,* which is involved in the regulation of the preferential colonization in the large intestine and inhibition of the *stx2* (Han et al., 2017) as well as targeted loci associated with sphingolipid biosynthesis (Pacheco et al., 2018).

Shiga toxin, including Stx1 and Stx2 produced by bacteria including *Shigella dysenteriae* serotype 1 and EHEC O157:H7 strain 933 (Lee et al., 2016), act as primary virulence factors. Each ribosome-inactivating holotoxin possess an AB_5 molecular configuration consisting of a large monomeric A subunit and small homo-pentameric B subunits (Rangel et al., 2005). Once colonized in intestinal epithelial cells, EHEC induces the delivery of Stx and the production of cytokines and chemokines. Toxins pass through the intestinal mucosa, enter the bloodstream and travel to target organs such as the kidneys and Central Nervous System (CNS). After membrane invasion-mediated endocytosis through the toxin receptor Gb3 on the cell surface, Stxs migrate to the Golgi and endoplasmic reticulum (ER). Stx acts as a multifunctional bacterial protein, promoting ER stress, ribotoxic stress, pro-inflammatory responses, apoptosis, and autophagy in host cells (Lee et al., 2021). In addition to cell death by Stxs, various cells such as neutrophils, induce inflammation in the intestine, which leads to damage.

Adhesion and effacing lesions (A/E lesions) are characterized by intimate bacterial attachment to the surface of intestinal epithelial cells, cytoskeletal rearrangements beneath adherent bacteria, formation of characteristic actin-rich "pedestals" and destruction of proximal microvilli (Stevens and Frankel, 2014).

The EHEC TTSS injects a plethora of effector proteins into host cells that induce alteration or disruption of numerous host cell processes (Pacheco et al., 2018). Tir is the first translocated effector protein inserted into the host cell membrane as a receptor of adhesion intimin. Intimin-Tir interactions are required to cluster Tir, which initiates the process of activating actin assembly and recruiting cytoskeletal proteins, such as clathrin (Hua et al., 2018), at the site of bacterial adherence (Campellone et al., 2004a; Stevens and Frankel, 2014). The main pathway causing actin rearrangement resulting in the formation of actin-rich pedestals eventually in EHEC is the Tir: IRTKS/IRSp53:TccP/EspFu pathway, which triggers Arp2/3-mediated actin polymerization independently of N-WASP (Vingadassalom et al., 2010).

Inorganic polyphosphate (polyP) is abundant in all cells, including bacteria, fungi, parasites, plants, and animals, and plays critical roles (Rao et al., 2009). Polyphosphate kinase 1 (PPK1) reversibly catalases the polymerization of the terminal phosphate of ATP into a polyP chain and is the major catalytic enzyme in *E. coli* that synthesizes polyP. PPK1, encoded by the *ppk1* gene, has been related to stationary phase (SP) survival and pathogenesis in many bacteria species, such as *E. coli, Vibrio cholera, Shigella* and *Salmonella spp.,* via polyP inducing the expression of DNA repair enzymes (Varas et al., 2017) or inducing the expression of *rpoS,* which is the selective σ^S or σ^{38} factor of the RNA polymerase and regulates the expression of survival and other virulence genes in bacteria, such as *E. coli* (Shiba et al., 1997). However, RpoS proteins are not the only regulators of survival and virulence genes during the SP in *E. coli*. A previous study identified a new regulatory gene, *ibeR*, that mediated stress resistance and pathogenesis SP gene expression in *E. coli* K1 RS218, which has a loss-of-function mutation in the *rpoS* gene (Chi et al., 2009). Additionally, Varas et al. (2017) found that the metabolic balance of polyP was necessary for the synthesis of the second messenger (p) ppGpp, which regulated other important cellular and regulatory processes such as the recycling of sigma factors/anti-sigma factors that allowed the bacteria to adapt to a wide range of environmental conditions, including nutritional or stressful conditions (Magnusson et al., 2005; Dalebroux and Swanson, 2012). To investigate the role of PPK1 in the pathogenesis of EHEC O157:H7, an isogenic in-frame *ppk1* deletion mutant of EHEC O157:H7 EDL933w and a *ppk1*-complemented strain, where the *ppk1* open reading frame in the plasmid *pBAD33* was transferred into the *ppk1* deletion mutant, were constructed and characterized. The polyP levels in the *ppk1* deletion mutant (Δ*ppk1*) indicated that the Δ*ppk1* was deficient in polyP synthesis as compared to the wild-type (WT) and *ppk1*-complemented (*Cppk1*) strains. Moreover, the deletion of *ppk1* influenced the survival of EHEC O157:H7 under harsh environmental conditions of 55°C and pH 2.0. PPK1 contributed to the adhesion, formation of A/E lesions, and invasion of LoVo cells *in vitro*. Additionally, deletion of the *ppk1* gene reduced the virulence in BALB/c mice. Moreover, deletion of *ppk1* resulted in decreased expression of *rpoS,* as well as the adhesion gene *eae* and virulence genes *stx1* and *stx2*. Our findings suggest that PPK1 is a determinant in the pathogenesis of EHEC O157:H7.

MATERIALS AND METHODS

Bacterial Strains, Cells, Plasmids and Culture Conditions

Enterohemorrhagic *Escherichia coli* O157:H7 strain EDL933w was obtained from the Chinese Center for Disease Control and Prevention (CDC) (Beijing, China). The nalidixic acid resistant mutant of EHEC O157:H7 strain EDL933w named EHEC O157:H7 EDL933w (Nal^R) was selected as described by published paper by Zhao et al. from our lab (Zhao et al., 2013). Plasmids, pKD46 [containing recombinant enzymes including Gam, Bet, and Exo (Exo is an exonuclease that binds to the ends of double-stranded DNA, degrades the DNA from the 5′ end to the 3′ end, and produces 3′ overhangs. Beta binds to the single-stranded DNA and mediates the complementary single-stranded DNA annealing. Gam protein binds with the RecBCD

enzyme to inhibit its activity of degrading foreign DNA Jeong et al., 2013)] and pKD4 plasmid (containing the kanamycin resistance gene) were obtained from the Institute of Microbiology and Epidemiology (Beijing, China). LoVo colonic carcinoma cells and DH5α cells with the plasmid pBAD33 (ATCC, 87402) were purchased from ATCC. T4 DNA ligase and restriction endonucleases were purchased from TaKaRa Biotechnology Co., Ltd. (Dalian, China). Standard laboratory reagents and chemicals, such as DAPI, were purchased from Sigma-Aldrich (St. Louis, MO, United States) unless otherwise mentioned. Primers used in this study were synthesized by Sangon Biotech Co., Ltd. (Shanghai, China). DNA sequencing was performed by Guangzhou IGE Biotechnology, Ltd. (Guangzhou, China).

All bacterial strains in this study were grown in Luria broth (LB) media (10 g SELECT Peptone 140 (Oxiod, England), 5 g SELECT Yeast Extract (Oxiod, England), and 10 g sodium chloride (Beijing, China) dissolving completely in double-distilled water (ddH_2O) with 5mol/L NaOH for pH = 7.0 and a total volume of 1 L by ddH_2O, autoclave sterilization by 121°C for 20 min) at 37°C at 200 rpm in a constant-temperature, oscillating shaker with nalidixic acid (50 μg/mL) and appropriate antibiotics (WT: no antibiotics; Δ*ppk1*: 100 μg/mL kanamycin; *Cppk1*: 100 μg/mL kanamycin and 10 μg/mL chloramphenicol) if necessary. LoVo cells were cultured in DMEM (Gibco, Waltham, MA, United States) with 10% fetal bovine serum (FBS, Gibco, Waltham, MA, United States) and 1% penicillin/streptomycin (Gibco, Waltham, MA, United States) in 5% CO_2 for routine passage prior to infection.

Female BALB/c (4–5 weeks of age) mice were obtained from the Lab Animal Center of Southern Medical University (Guangzhou, China; Certificate: SCXK (Guangdong Province) 2016-0041, No. 44002100010995]. All mice were housed under specific pathogen-free (SPF) conditions according to the regulations of the animal care committee. This study was conducted in accordance with the recommendations of the Southern Medical University Experimental Animal Ethics Committee (Guangzhou, China).

Construction of an Isogenic In-Frame Deletion Mutant of *ppk1* and *ppk1*-Complemented Strains

A pKD46-mediated λ red homologous recombination system was used to construct EHEC O157:H7 Δ*ppk1*. According to the *ppk1* gene sequence in GenBank (Accession no. NC_002655) and its upstream and downstream DNA sequences, three pairs of primers were designed and synthesized (**Table 1**). H1-K1 and H2-K2 primers contained homologous arms, of which the 5′ end was homologous with the *ppk1* gene and the 3′ end was homologous with the kanamycin resistant gene. PPK-P1, PPK-P2, N1-F, and N2-R were cross-identifying primers specific for the *ppk1* gene in EHEC O157:H7. Kana-F and Kana-R were internal-identifying primers for the kanamycin resistance gene within the pKD4 plasmid. The kanamycin resistance gene was amplified using primers H1-K1 and H2-K2 with the pKD4 plasmid as a template by using overlap extension PCR. The PCR conditions were as follows: 94°C for 3 min, followed by 35 cycles of 94°C for 30 s, 56°C for 30 s, and 72°C for 90 s, and a final extension of 72°C for 10 min. Subsequently, plasmid pKD46 was transformed into EHEC O157:H7 EDL933w and cultured to an OD_{600} = 0.2–0.3. L-arabinose was then added to a final concentration of 10 mmol/L for 40–60 min to induce the full expression of recombinant enzymes Exo, Bet, and Gam of pKD46. Finally, 10 μL of the targeting fragments (34.67 ng/μL) isolated from the gels and the prepared 100 μL EHEC O157:H7 EDL933w competent cells were mixed in a gene pulser cuvette (Bio-Rad Laboratories, Inc., Hercules, CA, United States) and subjected to an electric shock for 10–20 s (25 μF, 200 Ω, 3 KV). Positive strains were screened using LB plates containing 50 μg/mL kanamycin. The recombinant strain was confirmed by PCR and DNA sequencing.

TABLE 1 | Primer sequences used in the construction of the isogenic in-frame deletion mutant of *ppk1* and *ppk1*-complemented strains.

Primers	Sequences (5′-3′)
H1-K1	5′-GCCATAATATCCAGGCAGTGTC CCGTGAATAAAACGGAGTAAAAGT GGTAGTGTAGGCTGGAGCTGCTTC-3′
H2-K2	5′-CCGCAGCAAACTCCTGCGGACGAGGGGATTTATCG TGTATTGGCATAGGGCATATGAATATCCTCCTTAG-3′
PPK-P1	5′-CGAAGAACAAGGCTCCAAC-3′
PPK-P2	5′-AAGGCAGTAACGCAGAATG-3′
Kana-F	5′-CGGTGCCCTGAATGAACTGC-3′
Kana-R	5′-CGGCCACAGTCGATGAATCC-3′
N1-F	5′-TTTGCCGATGGTCGTCTGA-3′
N2-R	5′-TCCAGCCCTGAATACGAAA-3′
PPK1-F	5′-GATTCTAGA***AGGAGG***AAGT GGTAATGGGTCAGGAAAAGCTATACA-3′
PPK1-R	5′-GACAAGCTTTTATTCAGGTTGTTCGAGTGATT-3′
pBAD-F pBAD-R	5′-ATGCCATAGCATTTTTATCC-3′ 5′-GATTTAATCTGTATCAGG-3′
PK1-F	5′-AATGCGCTGGTTGAAGTGTT-3′
P**K**1-R	5′-CAGCACATGCTCAAAGGTGT-3′
16S rRNA-F	5′-AAGCTGGAATCGCTAGTAATC-3′
16s rRNA-R	5′-TGTGTACAAGGCTCGATGAC-3′

The primer of PPK1-F: TCTAGA is the restriction site of Xba I. ***AGGAGG*** *is the Shine-Dalgarno sequence (SD), the synthetic ribosomal binding site. The primer of PPK1-R: AAGCTT is the restriction site of Hind III.*

The complemented strain, *Cppk1,* was constructed using the prokaryotic expression plasmid *pBAD33*. A DNA fragment carrying the complete *ppk1* open reading frame was amplified using the PPK1-F and PPK1-R primers (**Table 1**) with the EDL933w genome as the DNA template. After double-enzyme digestion with *HindIII* and *XbaI*, the DNA fragment and vector *pBAD33* were ligated together with T4 DNA Ligase, and the products were transformed into strain EHEC O157:H7 Δ*ppk1*. Positive strains were screened using LB medium containing 100 μg/mL kanamycin and 10 μg /mL chloramphenicol. PCR and DNA sequencing analyses were conducted to identify the complemented strains. Finally, quantitative real-time PCR using Applied Biosystems (ABI) 7500 FAST Real-Time PCR system (Thermo Fisher, Waltham, MA United States) was performed to verify the transcription of *ppk1* in the complemented strain. Briefly, the WT, Δ*ppk1* and *Cppk1* strains were cultured in liquid LB medium overnight. Total RNA extracted with TRIzol® (Invitrogen, Carlsbad, CA, United States) was reverse transcribed

using the ExScript RT reagent kit (Takara, Japan) according to the manufacturer's instructions. The real-time PCR conditions were: 95°C for 2 min, followed by 40 cycles of 95°C for 15 s and 60°C for 32 s. A 16S rRNA gene fragment (68 bp) was used as an internal control, and the amplification of *ppk1* (255 bp) in the WT strain was used as a reference. Gene expression levels were calculated using the $\mathbf{2}^{-\Delta\Delta CT}$ method (Livak and Schmittgen, 2001).

Gram Staining and Growth Curves

Gram staining was performed with the classical steps (Coico, 2005), and reagents needed for this assay were from Nanjing Jiancheng Technology Co., Ltd., China. The growth curves were determined by measuring the optical density at 600 nm (OD_{600}) of the cultures at different times in LB media at 37°C at 200 rpm in a constant-temperature, oscillating shaker. Antibiotics were added if the strain required them as described above.

Measurement of polyP Levels

Quantification of polyP by DAPI was performed in different fields of view as previously published (Aschar-Sobbi et al., 2008; Diaz and Ingall, 2010; Kulakova et al., 2011; Gomes et al., 2013). Based on these researches, we optimized the procedure in *E. coli*. Briefly, the WT, Δ*ppk1* and *Cppk1* strains were grown in LB media for 12-14 h at 37°C with the appropriate antibiotics. The cells were then diluted to an OD_{600} = 1.0, which equaled approximately 1 × 10^8 CFU/mL, and centrifuged at 10,000 × *g* for 15 min at 4°C. After washing with 20 mM HEPES buffer (pH 7.5) twice, the pellets were resuspended in 1 mL of 20 mM HEPES buffer (pH 7.5). In order to release intracellular polyP from bound state for direct quantification without prior extraction, cells were lysed by a freeze-thaw cycle at − 80°C followed by thawing at 24–26°C. Then, 300 μL of the lysed cells were added to new sterilized microcentrifuge tubes containing 600 μL of 20 mM HEPES buffer (pH 7.5). Next, 100 μL of 100 μM DAPI reagent was added, resulting in a final DAPI concentration of 10 μM. The reaction was allowed to incubate in the dark for 15 min to ensure steady fluorescence. Then 200 μL of each reaction was added to a 96-well plate in triplicate. A polyP standard calibration curve using sodium phosphate glass type 45 (short for polyP45) was constructed on the same 96-well plate. PolyP45 dilutions were prepared in 20 mM HEPES buffer (pH 7.5) for a polyP relative unit (ru) of 0–1 ru, and the concentration of polyP ranged from 0–3 μM Pi. The polyP45 dilutions were mixed with 100 μM DAPI by vortexing for 7.5 min, incubated for 15 min at 24–26°C in the dark, vortexed again, and then 200 μL of each mixture was added to the 96-well plate in triplicate. The fluorescence module of a microplate reader (Infinite M200 Pro, Tecan, Switzerland) was used to measure the fluorescence value in the dark. The excitation wavelength was 415 nm, and the emission wavelength was 550 nm. The polyP quantity of the three strains was extrapolated from the standard curve. For bacteria cultured *in vitro*, we used the polyP concentration in μM Pi/mL, which translates to the amount of polyP in 1 mL of bacteria at an OD600 = 1.0.

Survival Rates Under Different Stringent Environmental Conditions

The WT, Δ*ppk1* and *Cppk1* strains bacteria were grown in LB medium for 12-14 h at 37°C. The bacterial culture was diluted in LB medium without antibiotics until the OD_{600} was 1.0 (approximately 1 × 10^8 CFU/mL). For heat stress, the three strains (prepared as stated above) were incubated at 55°C for 0, 1, 2, 3, 4, 5, 8, 10, and 15 min. Samples collected at these points were serially diluted in LB liquid medium until 10^{-6} and then plated on LB agar plates and cultured for at least for 12 h. The survival rate after heat stress for each culture was calculated by dividing the number of colonies counted after exposure to heat stress by the viable cell number before exposure to stress colonies. For acid tolerance test, the samples (prepared as stated above) were collected by centrifugation. Then they were resuspended in acidified LB (pH 2.0) and incubated at 37°C. Samples were collected at 0, 5, 10, 20, 30, 60, and 120 min. Samples collected at these points were serially diluted in LB liquid medium until 10^{-6} and then plated on LB agar plates and cultured for at least for 12 h. The survival rate after acid tolerance for each culture was calculated by dividing the number of colonies counted after exposure to heat stress by the viable cell number before exposure to stress colonies (Peng et al., 2012).

Preparation of Bacterial Solution for *in vitro* Adhesion and Invasion Assays

The WT, Δ*ppk1* and *Cppk1* strains were grown overnight in LB medium at 37°C. Then the bacteria solution was diluted with LB medium with no antibiotics until the OD_{600} was 1.0 (approximately 1 × 10^8 CFU /mL). The bacteria were collected by centrifugation and resuspended in cell culture medium without antibiotics.

Adherence Quantitation Assay

The adherence assay was carried out according to previous methods (Elsinghorst and Kopecko, 1992; Peng et al., 2012). Briefly, LoVo confluent monolayers in 12-well plates (approximately 1 × 10^6 cells/well) were incubated with the WT, Δ*ppk1* and *Cppk1* strains of EHEC O157:H7 (1 × 10^8 CFU/well) for 2 h in an incubator with 5% CO_2, 95% air [including 78% nitrogen, 21% oxygen, 0.934% rare gases (helium, neon, argon, krypton, xenon, and radon)], 37°C. After incubation, the monolayers were washed at least five times with phosphate buffered saline (PBS). Then the cells were lysed with 0.5% Triton X-100 for 10 min, which had no lethal effect on the bacteria. The lysate was then serially diluted at 1:1000 in PBS, plated on LB plates, and incubated for 12 h. The number of colonies was counted, and the adhesion rate was calculated as follows: ‰ = (number of colonies × 10^3)/1 × 10^8. Each sample was assayed in triplicate.

Adherence Assay by Scanning Electron Microscopy

Nine sterile cell slides for 24-well plates were placed in 9 wells of a 24-well plate. Then 200 μl of LoVo cells (approximately

5×10^5/mL) were added into the 9 wells for cultivation in a 5% CO_2 incubator at 37°C until the cells formed confluent monolayers (approximately 1.0×10^6 cells/well). The WT, Δ*ppk1* and *Cppk1* strains of EHEC O157:H7 with OD_{600} = 1.0 (approximately 1×10^8 CFU/mL of bacteria) were inoculated to those wells at a 1:100 cell:bacteria ratio. The 24-well plate was placed in a 5% CO_2 incubator at 37°C. After washing with PBS five times, the nine wells were placed into wide caliber EP tubers and fixed with 2.5% glutaraldehyde for SEM.

Invasion Assay

LoVo confluent monolayers in 12-well plates (approximately 1×10^6 cells/well) were incubated with bacteria (1×10^8 CFU/well) for 2 h. The monolayers were washed with PBS and incubated with the mixed medium [DMEM with 10% heat-inactivated FBS and gentamicin (100 μg/mL)] for another 2 h at 37°C in order to kill the extracellular bacteria. The monolayers were then washed with PBS and lysed with 0.5% Triton X-100. The released intracellular bacteria were collected, serially diluted, plated on LB plates and cultured for 12 h. The number of bacteria was counted, and the invasion rate is expressed as follows: ‰ = (number of bacteria × 1000)/number of total added bacteria. The assay was performed in triplicate for each strain.

Invasion Assay via Transmission Electron Microscopy

All the procedures were the same as described above (i.e., "Invasion assay" section). After treatment with gentamicin for 2 h at 37°C, the monolayers were washed with warm cell culture medium. The cells were then scraped off the plates and fixed with 2.5% glutaraldehyde for transmission electron microscopy (TEM) imaging.

Intracellular F-Actin Observation in LoVo Cells Infected by Enterohemorrhagic *Escherichia coli* O157:H7 via Confocal Microscopy

LoVo cells were passaged in confocal culture dishes (35 mm in diameter) and cultured into monolayers. The bacterial culture and invasion processes are described above (i.e., "Invasion assay" section). The culture media was removed, and the cells were gently washed once with phosphate buffered saline (PBS) at 37°C. Then cells were fixed in 4% paraformaldehyde for 10 min at 24–26°C, washed with PBS for 30 s, and then permeabilized with 0.15% Triton X-100 for 5 min. The cells were blocked with 1% bovine serum albumin after washing with PBS at 24–26°C for 5 min, and then 100 nM rhodamine phalloidin was added and incubated with the cells for 30 min in the dark at 37°C. After washing three times in PBS, the DNA was counterstained with 100 nM DAPI in PBS for 30 s. The samples were rinsed with PBS, and then confocal images (LSM710, ZEISS, Germany) of intracellular actin were obtained.

Murine Model of Infectious Enterohemorrhagic *Escherichia coli* O157:H7 Colitis

The animal experiments were performed strictly according to the guidelines for animal care at Southern Medical University (Guangzhou, China). The murine model of *E. coli*-induced colitis was performed as described previously (Zhao et al., 2013). In brief, twenty BALB/c mice (4–5 weeks old) were randomly divided into four groups: (1) EHEC WT, (2) Δ*ppk1,* (3) *Cppk1,* and (4) control (uninfected). The mice were provided water containing nalidixic acid (50 μg/mL) for 12 h prior to infection. Mice were then infected twice at an interval of 12 h. Mice were simultaneously administered 300 μL of the bacterial suspension (2×10^{10} CFU/mL total) orally and then intraperitoneally injected with mitomycin C (MMC, 2.5 mg/kg) to improve their infection susceptibility. Mice in the control group were treated with MMC and inoculated equivalently with LB broth under the same conditions. The mice were sacrificed at day 7 post-infection. The distal 5 cm of the colon was harvested. Typical features of the colon, such as the appearance of the colons and solidified feces, were compared among the groups. After cleaning with PBS buffer, the colons were embedded in paraffin and stained with hematoxylin and eosin (H&E) to observe the pathological changes among the groups. Histologic damage scores were performed using previously described methods (Ledwaba et al., 2020) by a pathologist who had no knowledge of this study.

Real-Time Reverse-Transcription PCR

The mRNA expression levels of *rpoS* (encodes RpoS), *eae* (encodes intimin), *stx1A*, *stx1B* (both encode Stx1), *stx2A* and *stx2B* (both encode Stx2) in WT, Δ*ppk1,* and *Cppk1* strains were determined by quantitative real-time PCR. Primers (**Table 2**) were synthesized and used for cDNA amplification of 16S rRNA (68 bp), *rpoS* (225 bp), *eae* (220 bp), *stx1A* (240 bp), *stx1B* (112 bp), *stx2A* (129 bp), and *stx2B* (111 bp). A 16S rRNA gene was used as an internal control. All gene expression was normalized against WT of EHEC O157:H7 using the $\mathbf{2}^{-\Delta\Delta CT}$ method (Livak and Schmittgen, 2001).

Statistical Analysis

Experimental values are expressed as the mean ± standard deviation. A Student's *t*-test was used to analyze values between two groups, while a one-way ANOVA was used to analyze values between three groups. Multiple comparisons were completed by using the Student-Newman-Keuls (S-N-K) and Bonferroni tests. Differences with $p < 0.05$ were regarded as statistically significant.

RESULTS

Construction of Enterohemorrhagic *Escherichia coli* O157:H7 Δ*ppk1* and *Cppk1* Strains

The *ppk1* isogenic in-frame deletion mutant strain of EHEC O157:H7 EDL933w was successfully constructed. As shown in **Figure 1A**, *ppk1* was replaced by a kanamycin resistance cassette,

TABLE 2 | Primers used in qPCR.

Primers	Sequences (5′-3′)
rpoS-F	5′-CAGCTTATGGGACAACTCAC-3′
rpoS-R	5′-GCGTTGCTGGACCTTATC-3′
eae-F	5′-GCATTAAGTGCTGAAGTCAT-3′
eae-R	5′-ACGCCGATACCATTACTTAT-3′
stx1A-F	5′-GCAGGACACTACTCAACCTT-3′
stx1A-R	5′-ATCGCCATTCGTTGACTACT-3′
stx1B-F	5′-AAGCTTCAGCTGTCACAGTA-3′
stx1B-R	5′-CGCCATTCGTTGACTACTTC-3′
stx2A-F	5′-TCTGGCGTTAATGGAGTTCA-3′
stx2A-R	5′-AGTGCCTGACGAAATTCTCT-3′
stx2B-F	5′-TGACGGGAAAGAATACTGGA-3′
stx2B-R	5′-GAGCCTGATTCACAGGTACT-3′
16S rRNA-F	5′-AAGCTGGAATCGCTAGTAATC-3′
16S rRNA-R	5′-TGTGTACAAGGCTCGATGAC-3′

both of which contained the same homologous arm H1 and H2. Deletion of the *ppk1* gene was initially confirmed by colony PCR (**Figure 1B**). All three pairs of primers verified the successful deletion of *ppk1* from the Δ*ppk1* strain, and DNA sequencing further confirmed this deletion.

Similarly, the *Cppk1* strain was constructed based on the Δ*ppk1* and verified by colony PCR (**Figure 1C**) and DNA sequencing. The results of real-time reverse-transcription PCR displayed that the *ppk1* gene in the Δ*ppk1* was minimally expressed as compared with WT ($t = 18.227$, $P < 0.001$), which indicated that the *ppk1* gene was successfully knocked out in Δ*ppk1*. The *ppk1* gene was increased 58-fold in the *Cppk1* strain as compared to WT ($t = -16.869$, $P < 0.001$), demonstrating that 0.2% L-arabinose could induce a high expression of recombinant plasmid in the *Cppk1* strain.

The Influence of the *ppk1* Deletion Mutant in polyP Levels, Morphology and Growth Characteristics

The growth curve of the EHEC O157:H7 strain Δ*ppk1* displayed an identical trend of growth as that of the WT and *Cppk1* strains in LB medium (**Figure 2A**). All three strains entered the exponential phase at 3 h post-inoculation and stationary phase at 12 h post-inoculation. In addition, there were no significant differences in the morphology of the bacteria as revealed by optical microscopy and scanning electron microscopy (data not shown). Yet, based on the results Δ*ppk1* was defective in polyP synthesis. DAPI staining was used to quantify the polyP levels of the three strains. The results demonstrated that polyP levels were significantly different ($F = 38.90$, $P < 0.001$) among the strains. The fluorescence of the Δ*ppk1* strain [304.19 relative fluorescence units (rfu)] was significantly lower than that in the WT (835.38 rfu) and *Cppk1* (899.36 rfu) strains (**Figure 2B**), with no significant differences between WT and *Cppk1*. This indicated that complementation of the Δ*ppk1* with the *ppk1* gene enabled the *Cppk1* strain to produce polyP. All factors above indicated that the deletion of *ppk1* did not change the morphology and growth rate of the Δ*ppk1* in nutritive medium but significantly reduced the polyP level.

Deletion of the *ppk1* Gene Affected the Ability of Enterohemorrhagic *Escherichia coli* O157:H7 to Survive Under Stringent Environmental Conditions

When the Δ*ppk1* strain was incubated at 55°C (EHEC O157:H7 can withstand this temperature) for 3 min, the survival rate was only 6.31% as compared with 58.39% for the WT strain. *Cppk1* (86.96%) was more tolerant to heat than that of WT and Δ*ppk1* strains (**Figure 2C**). When the bacterial strains were suspended and cultured in liquid LB at pH 2 (close to the acidic environment of the human stomach) for 60 min, similar results to the heat shock experiment were obtained. The survival rate of the Δ*ppk1* was only 9.97% as compared with 40.84% of the WT and 43.27% of *Cppk1* (**Figure 2D**). Both the heat shock and strong acid resistance results suggested that *ppk1* played an important role in the stringent response in EHEC O157:H7.

Deletion of the *ppk1* Gene Changed the Adhesion Capacity to Cells, F-Actin Rearrangement in Cells and Adhesion and Effacing Lesion Formation of Enterohemorrhagic *Escherichia coli* O157:H7

Scanning electron microscopy (SEM) results of the adhesion assay demonstrated that the three bacterial strains adhered to LoVo cells, but Δ*ppk1* accumulated on and adhered to LoVo cells at a lower amount as compared to the WT and *Cppk1* strains (**Figure 3A**) under each magnification. These results were verified through an adhesion quantitative assay ($F = 24.680$, $P < 0.001$). The adhesion rate of the Δ*ppk1* was only 4.09‰ as compared with WT (26.02‰) and *Cppk1* (33.88‰) strains (**Figure 3B**).

F-actin was stained with rhodamine phalloidin and observed by confocal microscopy. Results showed that the actin filaments of LoVo cells in the control group were typically present, distributed evenly, and arranged neatly in the cells (**Figure 3C**), whereas the F-actin in the WT and *Cppk1* groups were significantly reduced and rearranged with significant aggregating at the two ends of cells. When the *ppk1* gene was knocked out, the ability to induce actin rearrangement was significantly weaker than that of WT and *Cppk1* strains. These results demonstrated that PPK1 plays an important role in EHEC O157:H7 in the development of A/E lesions.

Deletion of the *ppk1* Gene Affected the Invasive Ability of Enterohemorrhagic *Escherichia coli* O157:H7

Transmission electron microscopy results demonstrated that the three strains all invaded LoVo cells and were wrapped in vacuoles (**Figure 3D**). However, the Δ*ppk1* was less invasive as compared to the WT and *Cppk1* strains. We thus performed gentamicin protection experiments to quantify the invasion rates. The WT reached an invasion rate of 0.56‰, which was not significantly

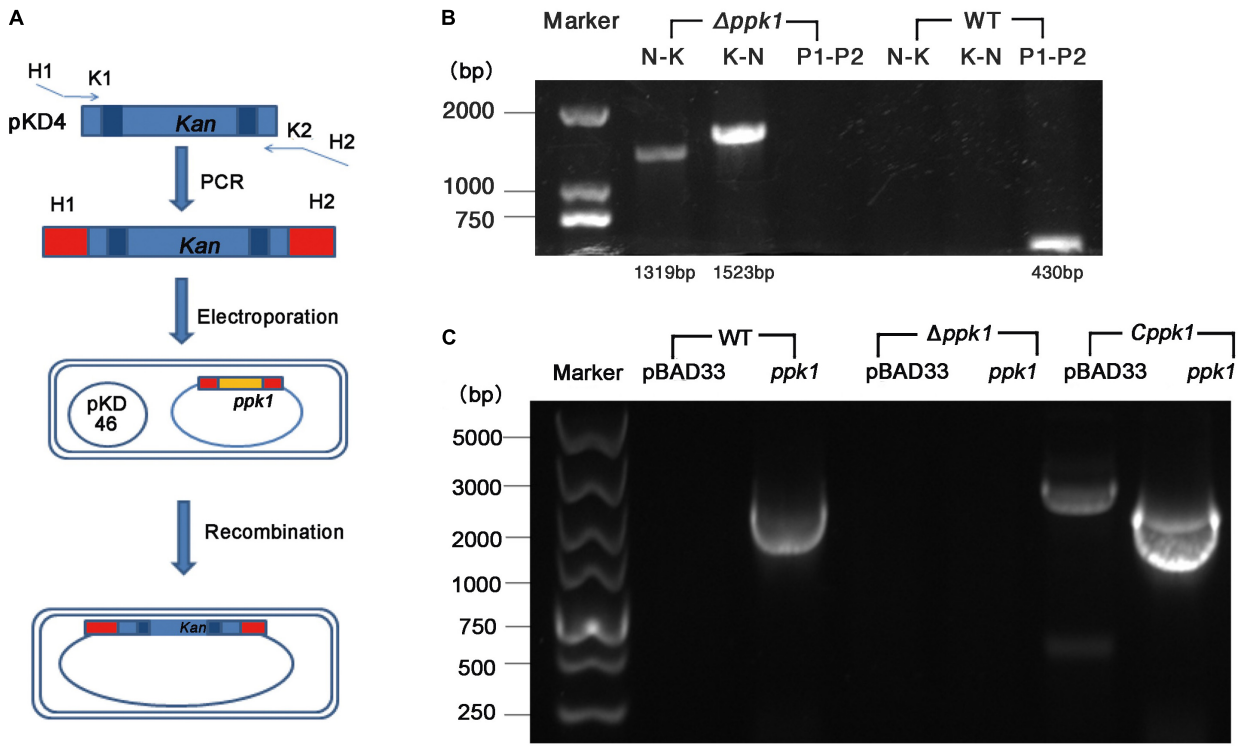

FIGURE 1 | Construction of the *ppk1* deletion mutant (Δ*ppk1*) and complemented strain (*Cppk1*) of EHEC O157:H7. **(A)** Schematic diagram of the λ red system homologous recombination. **(B)** The primers of lane 2 and 5 (N-K) were N1-F and Kana-R. The primers of lane 3 and 6 (K-N) were Kana-F and N2-R. The primers of lane 4 and 7 (P1-P2) were PPK-P1 and PPK-P2. **(C)** Two pairs of primers (*pBAD33-F/R* and *ppk-F/R*) were used to verify the complemented strain, which produced products of 2092 bp and 2268 bp, respectively. The *Cppk1* strain contained both fragments, while WT strain contained only the 2092 bp, and the Δ*ppk1* strain contained neither.

different than the *Cppk1* strain (0.62‰). However, the invasion rate of the Δ*ppk1* was 0.39‰, which confirmed that the *ppk1* gene was also required for bacteria invasion ($F = 5.224$, $P = 0.014$; **Figure 3E**).

The Δ*ppk1* Strain Was Less Pathogenic in BALB/c Mice

Twenty BALB/c mice were divided into four groups and infected with EHEC O157:H7 WT, Δ*ppk1, Cppk1,* or LB (control). Mice infected with the WT strain for 2 days showed some symptoms of illness, such as listlessness, anorexia, slow movements, and diarrhea. These symptoms, including a disheveled coat, became more severe the days following the infection until euthanasia on day 7 post-infection. The symptoms of mice in *the Cppk1* group were similar to the WT group, with one mouse dying 5 days post-infection and others exhibiting bloody diarrhea. Mice infected with the Δ*ppk1*, however, exhibited listlessness, rage, and slow movements without obvious diarrhea 3 days post-infection. All mice began to recover gradually in the following days. The uninfected control group treated only with LB were healthy.

After 7 days of infection, the distal 5-cm of the colon was collected, and the pathological features were compared among the groups (**Figure 4A**). The colon of the control group was normal with solidified stool (**Figure 4A**), while the WT group displayed edematous and congested intestinal colitis with very minimal solidified stool (**Figure 4A**). The colon of the mice infected with the *Cppk1* strain exhibited typical intestinal colitis with severe edema and congestion, without any solidified feces (**Figure 4A**). However, the colon of the mice infected with the Δ*ppk1* group appeared healthier with a small amount of solid stool, although some portions appeared slightly swollen (**Figure 4A**).

Colon paraffin sections were created and stained with H&E to observe the architecture of the intestinal epithelium (**Figure 4B**). In the control group, the colonic epithelium was complete and continuous, with regular, clear, and structural glands without inflammatory cell infiltration. Infection with WT of EHEC resulted in mucosal reactionary hyperplasia, disordered cell arrangement, decreased goblet cells, and inflammatory cell infiltration. The *Cppk1* strain caused mucosal necrosis, and the muscle layer was involved and destructed. The colonic mucosa in mice infected with the Δ*ppk1* strain appeared to have reactive hyperplasia, but the glands were regular with a clear structure. The histopathological scores were consistent with the morphological results observed by H&E staining (**Figure 4C**). The above results demonstrated that the Δ*ppk1* was less pathogenic and induced milder A/E lesions than the WT and *Cppk1* strains. The mild microvilli effacement in the

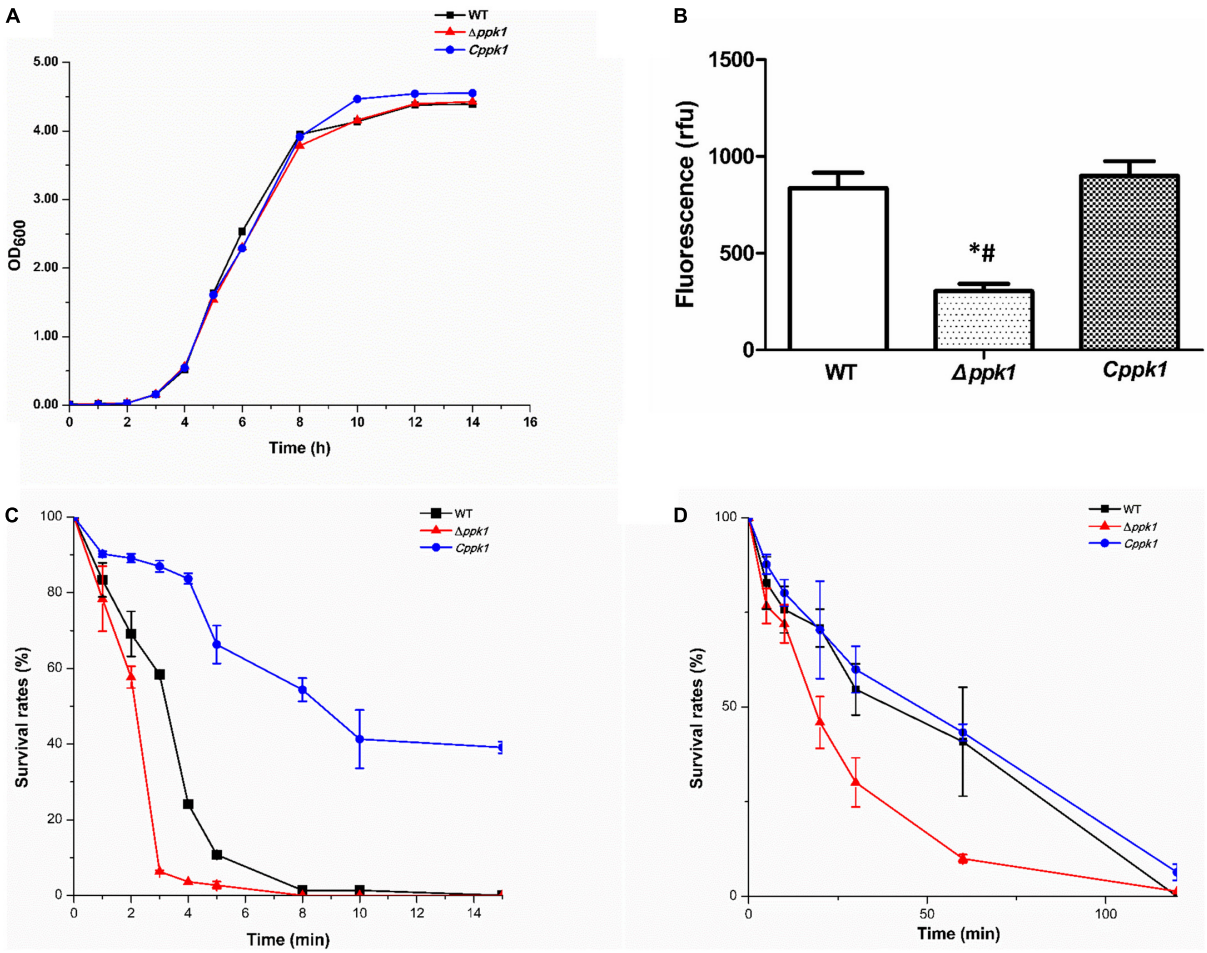

FIGURE 2 | Comparison of the biological characteristics and stringent stress survival assays of the three EHEC O157:H7 strains. **(A)** Growth curve analysis of the WT, Δ*ppk1,* and *Cppk1* strains. OD: Optical density. **(B)** The polyP levels of WT, Δ*ppk1,* and *Cppk1* strains. Error bars indicate standard deviations. *, $p < 0.05$ as compared with the WT strain; #, $p < 0.05$ as compared with the *Cppk1* strain. **(C)** The survival rates of WT, Δ*ppk1,* and *Cppk1* strains after exposure to 55°C at different time points. **(D)** The survival rates of WT, Δ*ppk1,* and *Cppk1* strains under acid stress at pH 2.0 in liquid LB at different time points.

Δ*ppk1* indicated an important role of PPK1 in colonization of the intestinal epithelium.

ppk1 Was Required in Modulating the Expression of *rpoS*, *eae, stx1,* and *stx2*

To determine whether *ppk1* regulated the expression of regulatory gene *rpoS*, adhesion gene *eae,* and virulence genes *stx1* and *stx2,* real-time PCR was conducted. A 16S rRNA gene was used as the internal reference, and WT EHEC was used as the control. The relative level of mRNA in the Δ*ppk1* and *Cppk1* strains was also calculated (**Figure 5**). The relative copies of *rpoS* in the Δ*ppk1* (0.36 ± 0.03) were less than that in the WT strain (1.00 ± 0.13), while there were no differences between *Cppk1* (1.14 ± 0.05) and WT. These results were consistent with the amount of polyP among the three strains. Moreover, the *ppk1* deletion significantly reduced the relative copy numbers of *eae* (0.32 ± 0.02), *stx1A* (0.60 ± 0.02), *stx1B* (0.46 ± 0.06), *stx2A* (0.42 ± 0.02), and *stx2B* (0.86 ± 0.01) as compared to that of WT (1.00 ± 0.02, 1.00 ± 0.08, 1.00 ± 0.04, 1.00 ± 0.06 and 1.00 ± 0.01, respectively). Similarly, these relative expression levels increased to 1.06 ± 0.03, 1.87 ± 0.04, 1.69 ± 0.09, 1.53 ± 0.01, and 1.36 ± 0.03, respectively, in the *Cppk1* strain as compared with WT. These results indicated that *ppk1* plays an important role in regulating the expression of *rpoS*, *eae*, *stx1,* and *stx*2.

DISCUSSION

Polyphosphate is available in living cells and plays an important role in the survival, stress response, and pathogenicity of prokaryotic cells (Rao et al., 2009), which is regulated mainly through the regulation of *rpoS,* a key transcriptional factor. PPK1, encoded by the *ppk1* gene, catalyzes the synthesis of polyP in *E. coli*. At present, the role of PPK1 in the pathogenesis of EHEC O157:H7 has not yet been reported. To determine the role of PPK1 in the pathogenesis of EHEC O157:H7, we successfully

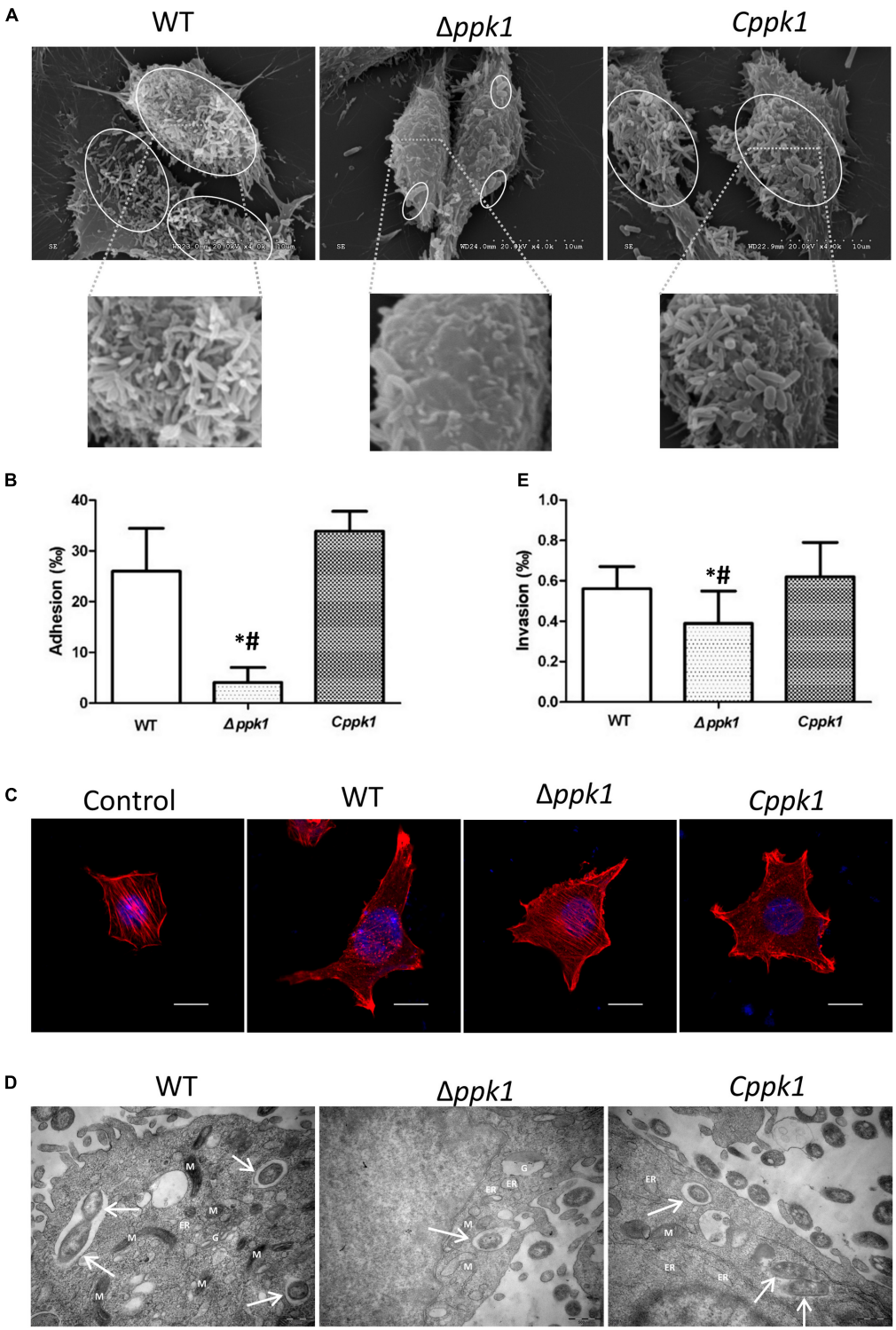

FIGURE 3 | Deletion of the *ppk1* gene reduced the adhesion, A/E lesions, and invasive ability. **(A)** High-resolution SEM images of LoVo cells infected with WT, Δ*ppk1,* or *Cppk1* strains. Scale bar: 10 μm. **(B)** Comparison of adhesion rates between the WT, Δ*ppk*1, or *Cppk*1 strains. **(C)** LoVo cells were stained with rhodamine phalloidin (actin) and DAPI (nuclei) after infection. Scale bar: 10 μm. **(D)** High-resolution TEM images of LoVo cells infected with WT, Δ*ppk1,* or *Cppk1* strains. White arrows point to the bacteria. ER, endoplasmic reticulum; M, mitochondria; G, Golgi apparatus. Scale bar: 500 nm. **(E)** Comparison of invasion rates between the WT, Δ*ppk*1, and *Cppk*1 strains. Error bars in both **(B)** and **(E)** indicate standard deviations. *, $p < 0.05$ as compared with the WT strain; #, $p < 0.05$ as compared with the *Cppk*1 strain. **(E).**

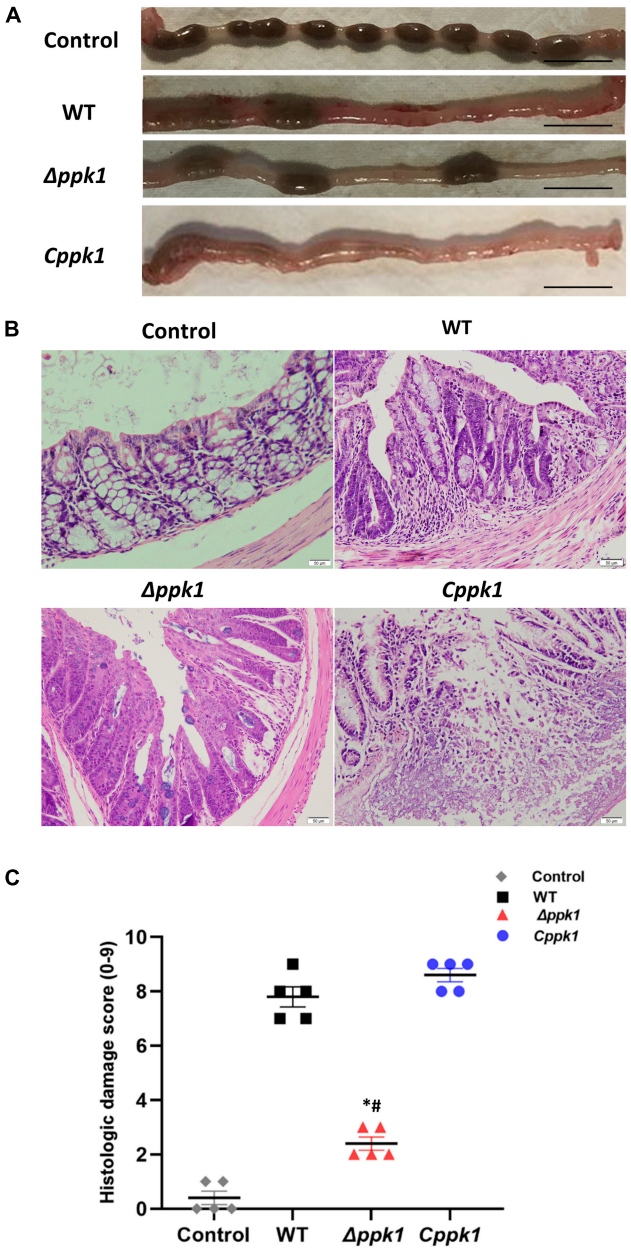

FIGURE 4 | The Δ*ppk*1 strain was less pathogenic in BALB/c mice. **(A)** The colonic morphology of BALB/c mice after the infection. Scale bar: 1 cm. **(B)** Images of colons after infection. Scale bar: 50 μm. **(C)** Histologic damage scores of uninfected (control group), WT, Δ*ppk*1, and *Cppk*1 strains. *, $p < 0.05$ as compared with the WT strain; #, $p < 0.05$ as compared with the *Cppk*1 strain.

constructed a Δ*ppk1* (**Figure 1B**) and a complemented strain *Cppk1* (**Figure 1C**) to test the biological functions of PPK1 via *in vitro* and *in vivo* models.

Evaluation of the growth curve is an important but indirect method to compare the genomic expression of each strain, as the expression of many genes are affected by growth rate (Dong and Schellhorn, 2009). Our results showed that deletion of *ppk1* had little effect on the growth rate or morphology of EHEC in nutritive medium (LB) (**Figure 2A**). The Δ*ppk1* entered the exponential phase and stationary phase (SP) at the same time as the WT and *Cppk1* strains. However, the *ppk1* deletion mutant had reduced polyP levels as compared to the WT and *Cppk1* strains (**Figure 2B**). These results confirmed that at the genetic and protein level, we successfully constructed the Δ*ppk1* and *Cppk1* strains.

According to previous studies, SP is a critical period for bacteria to resist external stress and invade the host during which the function of the bacteria change significantly (Siegele and Kolter, 1992). For *E. coli*, SP is an important stage for the expression of pathogenic invasion-associated virulence genes (Wang and Kim, 2000; Peng et al., 2012). We next verified the role of PPK1 in the survival and pathogenesis of EHEC O157:H7 during SP. EHEC O157:H7 is a fecal-mouth transmitted intestinal pathogen that enters the human stomach from the external environment, passes through the intestine, and finally colonizes the colon to cause diarrhea and hemorrhagic colitis (HC), even hemolytic uremic syndrome (HUS). The premise that bacteria, such as EHEC O157:H7, causes disease was based on the thought that they survive all types of environmental stress, such as high environmental temperatures and low pH values found in the human stomach (Rao and Kornberg, 1996; Ault-Riche et al., 1998; Rao et al., 1998; Kim et al., 2002). The ability to quickly adapt to changing environments is critical for bacteria to successfully transmit and infect hosts (Dong and Schellhorn, 2009). Studies have shown that polyP is involved in the regulation of many microbial stress responses (Magnusson et al., 2005; Rao et al., 2009; Dalebroux and Swanson, 2012; Varas et al., 2017). To determine the effect of *ppk1* deletion on the bacterial stress response of EHEC O157:H7, WT, Δ*ppk1,* and *Cppk1* strains were exposed to 55°C and pH 2.0 during SP. The survival rates were compared at corresponding time points. Our results showed that the survival rates of the Δ*ppk1* strain were significantly lower than that of WT and *Cppk1* (**Figures 2C,D**), which indicated that PPK1 played a key role in stress response during the infection process of EHEC O157:H7.

In certain external environmental stresses, some genes of *E. coli* are induced during SP (Lange and Hengge-Aronis, 1991; Siegele and Kolter, 1992; Hengge-Aronis, 1993), such as *adAXW*, *gadB*, and *yhbO,* but are not induced during the exponential growth phase. A previous study reported that polyP was associated with the expression of RpoS, which plays a central role in SP adaptations (Abramov et al., 2007; Hoac et al., 2013). RpoS is a conserved stress regulator of virulence and pressure adaptation during SP of *E. coli*, *Salmonella typhimurium*, *Shigella*, *Yersinia colitis*, *Vibrio cholerae,* and *Borrelia burgdorferi* (Tzeng and Kornberg, 1998; Hengge-Aronis, 2002; Dong and Schellhorn, 2009). Our results show that loss of *ppk1* decreased the ability of *E. coli* to endure the stress conditions. Furthermore, real-time PCR showed decreased levels of *rpoS* in the Δ*ppk1* as compared to the WT and *Cppk1* strains (**Figure 5A**). This suggested that RpoS might be the stress regulator of EHEC O157:H7 and its expression was induced by polyP.

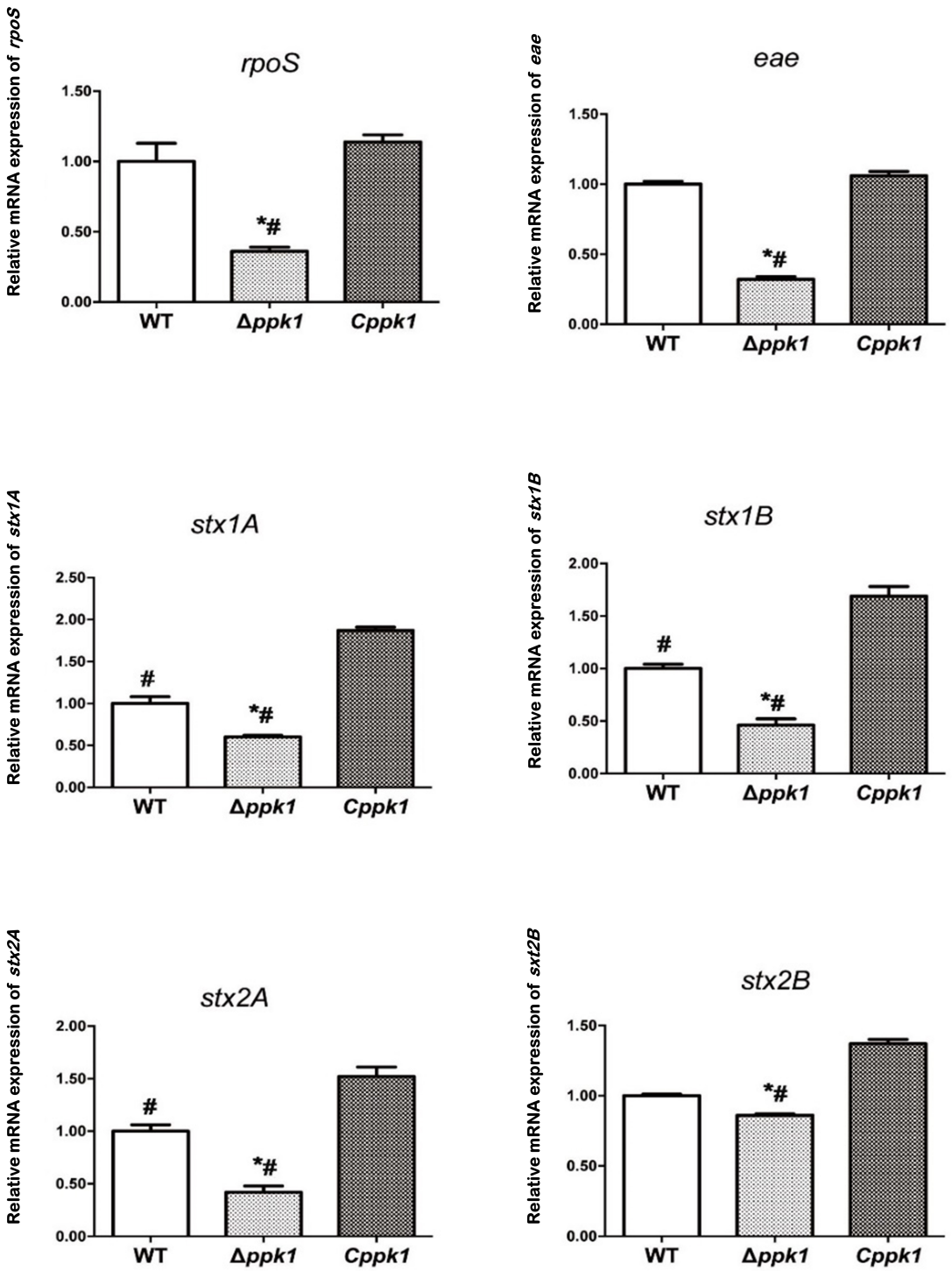

FIGURE 5 | The *ppk1* gene regulated the mRNA expression of *rpoS*, *eae*, *stx1A*, *stx1B*, *stx2A*, and *stx2B*. The relative mRNA expression of *rpoS*, *eae*, *stx1A*, *stx1B*, *stx2A*, and *stx2B* of WT, *ppk1* and *Cppk1* were measured via real-time PCR. Data were normalized to the relative RNA expression of the 16S rRNA. *, $p < 0.05$ as compared with the WT strain; #, $p < 0.05$ as compared with the *Cppk*1 strain.

When *E. coli* is under environmental stress, RpoS initiates a complex regulatory network, inducing and regulating the expression of nearly 600 genes (Dong and Schellhorn, 2009). The expression of RpoS-regulated genes was shown to differ according to the environment. For example, the genes *gadAXW*, *gadB*, and *gadE* were found important for acid resistance

(Ma et al., 2003), and *yhbO* for heat and UV resistance (Weber et al., 2005; Abdallah et al., 2007). The mechanism underlying the influence of polyP on RpoS in EHEC O157:H7 is a current focus of our research. The (p) ppGpp pathway is known to regulate other important cellular and regulatory processes that allow bacteria to adapt to a wide range of environmental conditions, including nutritional or stressful conditions (Magnusson et al., 2005; Dalebroux and Swanson, 2012). Proteomic studies conducted with *E. coli* K12 strains have identified 151 significantly differentially expressed proteins, among which RelA, SpoT, and ArcA protein levels, which influence the metabolic pathways of (p)ppGpp, were significantly decreased in the Δ*ppk1* (Varas et al., 2017). Therefore, the relationships among PPK1/polyP, RpoS and (p)ppGpp are our interest.

PPK1 was shown to be essential not only for the synthesis of polyP and metabolism of ATP, but also for adhesion/invasion and virulence factor expression in bacterial pathogens, such as *E. coli* K1 (RS218) (Peng et al., 2012), *Campylobacter jejuni* (Candon et al., 2007), *Burkholderia pseudomallei* (Srisanga et al., 2019), and *Mycobacterium tuberculosis* (Tiwari et al., 2019). The pathogenesis of EHEC O157:H7 is mainly reflected in the adhesion and effacing lesions (A/E lesions) as well as the secretion of Shiga-like toxin (Stx) (Nguyen and Sperandio, 2012).

Adhesion and effacing lesions were characterized by EHEC O157:H7 adhesion to host epithelium and then induction of extensive F-actin cytoskeletal rearrangements within cells, formation of pedestal-like structures underneath the bacteria and loss of microvillus structure (Caprioli et al., 2005). Successful adhesion and colonization of EHEC O157:H7 in the large intestine is dependent upon the type TTSS (Pacheco et al., 2018; Liu et al., 2020) by which Tir was the first translocated effector protein to the epithelial cells. Tir is inserted into the membrane of cells, where it then binds to the bacterial adhesion receptor intimin (encoded by *eae*) to mediate the adhesion between bacteria and host cells (Yi et al., 2010). Interactions between intimin and Tir were also required for recruitment and rearrangement of actin and other cytoskeletal proteins underneath adherent bacteria, which results in characteristic actin-rich "pedestals" through triggering host signal events (Ritchie et al., 2003; Golan et al., 2011).

To gain insight into the effect of *ppk1* deficiency in EHEC O157:H7 on the interaction with host cells, we elucidated whether the Δ*ppk1* mutant possessed a defect in adhesion and A/E lesion formation into host cells. Our results showed that the deletion of the *ppk1* gene reduced the adhesion as compared with WT (4.09‰ vs. 26.02‰, respectively) (**Figures 3A,B**). Moreover, the F-actin filaments of cells infected with the WT or *Cppk1* strains were significantly reduced and aggregated to the edge, showing a typical rearrangement phenomenon, whereas the Δ*ppk1* strain was weaker in actin filament rearrangement (**Figure 3C**). Accordingly, real-time PCR was carried out to test expression levels of the intimin gene *eae* in the three strains. The *ppk1* deletion significantly reduced the relative copy number of *eae* (0.32), as compared with WT (1.00) and *Cppk1* (1.06) (**Figure 5**), which was consistent with these results at the cellular level. In animal models, deletions of *eae* (the intimin locus) and mutations that render the TTSS inactive markedly reduced the pathogen's capacity to colonize the intestine (Ritchie et al., 2003), which was similar to our results above.

When colonizing the human intestine, EHEC O157:H7 forms A/E lesions on the colonic epithelial cells. The genes required for A/E lesions were encoded within the chromosomal pathogenicity island known as the locus for enterocyte effacement (LEE) (Elliott et al., 1998; Muller et al., 2009; Nguyen and Sperandio, 2012). The secreted effector proteins by the type III secretion system within LEE were directly injected into the cells through a "molecular injector". One of the important secreted proteins injected into the host was the translocated intimin receptor (Tir) (Nguyen and Sperandio, 2012). Once released into the host cytoplasm, Tir localizes to the host cytoplasmic membrane and binds to the LEE-encoded surface protein intimin (encoded by *eae*) to intimately attach the bacteria to the cell (Kenny et al., 1997; Deibel et al., 1998; Nguyen and Sperandio, 2012). Together, with other effector proteins secreted into the cell, F-actin was aggregated, leading to rearrangement of the cytoskeleton of the colonic epithelial cell (Campellone et al., 2004b; Weiss et al., 2009). Actin rearrangement was followed by the appearance of characteristic pathological manifestation of A/E lesions, including intestinal epithelial cytoskeletal (F-actin) rearrangement, destruction of tight junctions, intestinal microvilli actin dimerization, microvilli loss (Rao and Kornberg, 1996), and a pedestal-like structure formation, which cup the individual bacteria (Nataro and Kaper, 1998; Nguyen and Sperandio, 2012). Our results indicated that *ppk1* deletion mutant downregulated the *eae* gene and then reduced the expression of intimin. As a result, Tir could not bind to sufficient intimin, leading to the decrease in adhesion of Δ*ppk1* to LoVo cells. Adhesion is an important step of A/E lesions, which directly affects the rearrangement of F-actin and formation of the pedestal. Therefore, the rearrangement of F-actin in Δ*ppk1* was not obvious, resulting in weak A/E lesions. Thus, PPK1 played an important role in the adhesion and formation of A/E lesions which was verified in other bacteria (Candon et al., 2007; Peng et al., 2012; Tiwari et al., 2019).

Aside from A/E lesions, another main pathogenic factor of EHEC O157:H7 causing severe diarrhea and HUS is the secretion of Shiga-like toxins (Stx1 and Stx2) (Leotta et al., 2008). The Stx molecule consists of one A subunit and five B subunits through covalent bonding via an AB5 structure, and its toxic effect on host cells has already been widely recognized (Laing et al., 2012; Page and Liles, 2013; Perera et al., 2015). Briefly, after adhesion and colonization in the colon, STEC, such as EHEC O157:H7, induced the delivery of Stx, which passes through the intestinal mucosa. Then toxins entered the bloodstream and traveled to target organs such as kidneys with toxin receptor Gb3 on the cell surface. Once bounded to Gb3, Stxs were internalized and delivered from early endosome to the trans-Golgi network, through the Golgi apparatus, to the endoplasmic reticulum (ER), leading to inhibition of protein synthesis, ER stress, ribotoxic stress, pro-inflammatory responses, and

autophagy in host cells (Leyva-Illades et al., 2012; Lee et al., 2016, 2021). Therefore, Stx causes severe inflammation and extensive histological damage, resulting in bloody dysentery or bloody diarrhea and acute renal failure. In addition, Stx also causes programmed cell death or apoptosis (Jones et al., 2000; Suzuki et al., 2000).

Moreover, Stx maybe a virulence factor to affect intestinal tissue damage alone (Lee et al., 2021). Gigliucci et al. (2018) detected *stx2a* (encoding Stx2a) and *eae* (encoding intimin) in the feces of STEC-infected patients, which suggested that Stx not only works by migrating to the lamina propria but can also act in the intestinal lumen. Robinson et al. (2006) found that Stx2 was involved in increasing the colonization capacity of EHEC by increasing the expression of nucleolin in HEp-2 cells, which implied that Stxs affected the EHEC colonization of the intestine (Lee et al., 2021).

To determine the influence of the deletion of the *ppk1* gene on the Stx virulence of EHEC O157:H7, real-time reverse-transcription PCR was performed. Our results showed that the *ppk1* deletion significantly reduced the relative copy number of *stx1A*, *stx1B*, *stx2A*, and *stx2B* as compared to the WT and *Cppk1* strains (**Figure 5**). This suggested that *ppk1* affected the virulence of EHEC O157:H7 at a molecular level. Moreover, to identify the effect of *ppk1* deletion on the bacterial invasion of cells, an invasion assay was performed via TEM and gentamicin protection experiments. Our results demonstrated that the invasion rate of Δ*ppk1* was reduced to 0.39‰ as compared with WT (0.56‰) and *Cppk1* (0.62‰) (**Figures 3B,D**).

Enterohemorrhagic *Escherichia coli* invasions is sometimes associated with recurrent infection and persistent diarrhea. It attained some degree of coexistence with the infected cell and survived in the intracellular milieu for a long time. That strategy seemed appropriate to assure the persistence of the micro-organism in the animal reservoir, as well as to sustain its continuous shedding to the environment (Cordeiro et al., 2013). On the other hand, host cell cytoskeletal rearrangement and phosphorylation-mediated signal transduction are also involved in cell invasion by pathogens, which leads to the intestinal injury (Cossart and Sansonetti, 2004). Based on the adhesion, A/E lesions and invasion results, we concluded that the Δ*ppk1* was less adherent and invasive in LoVo cells. We further confirmed the effect of *ppk1* deletion on intestinal injury through animal experiments.

Three commonly used species (pigs, rabbits, and mice) as animal models have been developed to facilitate study of EHEC pathogenesis *in vivo*. The piglet intestine is permissive for EHEC replication and shows typical signs of central nervous system (CNS) as human beings (Ritchie, 2014). But their breeding and maintenance require considerable veterinary skill, space, and financial support (Mohawk and O'Brien, 2011). Rabbits have been used both to study the toxic effects of Stx and the intestinal biology of the organism. Despite being sensitive to the intestinal manifestations of EHEC infection, suckling rabbits do not develop HUS or any other evidence of renal failure. Mouse is another small animal model systems are preferable for general use. Mice are naturally resistant to colonization by EHEC and fail to develop signs of intestinal disease following oral infection. Thus, we tried to use mitomycin C (MMC) (an alkylating agent regarded as an important chemotherapeutic drug and is widely used in the treatment of several malignant human tumors) as an agent to induce toxin expression and form animal model of EHEC O157:H7 infection (Fujii et al., 1994; Shimizu et al., 2003).

Our experimental results showed that the diarrhea symptoms of WT and *Cppk1* mice were obvious, but the diarrhea symptoms of Δ*ppk1* were not, which could be seen on fecal formation (**Figure 4A**). Moreover, colonic HE staining and histologic damage scores showed that Δ*ppk1* was less destructive to the colon, which was also an evidence of mild symptoms of enteritis, as shown in **Figure 4B**.

All these results indicated that PPK1 was a key factor in the pathogenesis of EHEC O157:H7. The *ppk1*-deficient strain exhibited defects in adhesion and invasion in human colonic epithelial cells, which was consistent with the results of others (Dong and Schellhorn, 2009; Peng et al., 2012; Srisanga et al., 2019).

In summary, we demonstrated that *ppk1* was involved in the pathogenesis of EHEC O157:H7. PPK1 improved the stress response by regulating the expression of the stable phase regulatory gene *rpoS*, promoted A/E lesions, and increased the expression of virulence genes *stx1 and stx2,* which enhanced the pathogenicity of the bacteria. However, further research regarding the mechanism of PPK1-mediated regulation will improve our understanding of the pathogenesis and aid in the prevention of EHEC O157:H7 infection. PPK1 is not present in humans, and as such, the unique ATP-binding pocket in its structure is an important target for the development of PPK1 inhibitors, especially for new antibiotics. This study identified PPK1 as a potential target for the development of novel treatments for EHEC O157:H7 infection.

DATA AVAILABILITY STATEMENT

The original contributions presented in the study are included in the article/supplementary material, further inquiries can be directed to the corresponding author/s.

ETHICS STATEMENT

The animal study was reviewed and approved by Southern Medical University Experimental Animal Ethics Committee.

AUTHOR CONTRIBUTIONS

YD and XW did the conception and design of the work and drafted the article. YD, YH and KY collected the data. ZH, BZ, and WZ did the data analysis and interpretation. CW did the critical revision of the article. WZ and CW did the final approval of the version to be published. All authors contributed to the article and approved the submitted version.

FUNDING

This work were supported by the National Natural Science Foundation of China (No. 81902022), the Natural Science Foundation of Guangdong Province (Nos: 2018B030311063 and 2014A030313312), and the Shenzhen Polytechnic Fund (6021310006K).

ACKNOWLEDGMENTS

We would like to thank Ruifu Yang (Institute of Microbiology and Epidemiology, Beijing, China) for providing pKD46 and pKD4. We also thank LetPub (www.letpub.com) for linguistic assistance and pre-submission expert review.

REFERENCES

Abdallah, J., Caldas, T., Kthiri, F., Kern, R., and Richarme, G. (2007). YhbO protects cells against multiple stresses. *J. Bacteriol.* 189, 9140–9144. doi: 10.1128/JB.01208-07

Abramov, A. Y., Fraley, C., Diao, C. T., Winkfein, R., Colicos, M. A., Duchen, M. R., et al. (2007). Targeted polyphosphatase expression alters mitochondrial metabolism and inhibits calcium-dependent cell death. *Proc. Natl. Acad. Sci. U.S.A.* 104, 18091–18096. doi: 10.1073/pnas.0708959104

Aschar-Sobbi, R., Abramov, A. Y., Diao, C., Kargacin, M. E., Kargacin, G. J., French, R. J., et al. (2008). High sensitivity, quantitative measurements of polyphosphate using a new DAPI-based approach. *J. Fluoresc.* 18, 859–866. doi: 10.1007/s10895-008-0315-4

Ault-Riche, D., Fraley, C. D., Tzeng, C. M., and Kornberg, A. (1998). Novel assay reveals multiple pathways regulating stress-induced accumulations of inorganic polyphosphate in *Escherichia coli*. *J. Bacteriol.* 180, 1841–1847. doi: 10.1128/JB.180.7.1841-1847.1998

Campellone, K. G., Rankin, S., Pawson, T., Kirschner, M. W., Tipper, D. J., and Leong, J. M. (2004a). Clustering of Nck by a 12-residue Tir phosphopeptide is sufficient to trigger localized actin assembly. *J. Cell Biol.* 164, 407–416. doi: 10.1083/jcb.200306032

Campellone, K. G., Robbins, D., and Leong, J. M. (2004b). EspFU is a translocated EHEC effector that interacts with Tir and N-WASP and promotes Nck-independent actin assembly. *Dev. Cell* 7, 217–228. doi: 10.1016/j.devcel.2004.07.004

Candon, H. L., Allan, B. J., Fraley, C. D., and Gaynor, E. C. (2007). Polyphosphate kinase 1 is a pathogenesis determinant in *Campylobacter jejuni*. *J. Bacteriol.* 189, 8099–8108. doi: 10.1128/JB.01037-07

Caprioli, A., Morabito, S., Brugere, H., and Oswald, E. (2005). Enterohaemorrhagic *Escherichia coli*: emerging issues on virulence and modes of transmission. *Vet. Res.* 36, 289–311. doi: 10.1051/vetres:2005002

Chi, F., Wang, Y., Gallaher, T. K., Wu, C. H., Jong, A., and Huang, S. H. (2009). Identification of IbeR as a stationary-phase regulator in meningitic *Escherichia coli* K1 that carries a loss-of-function mutation in rpoS. *J. Biomed. Biotechnol.* 2009:520283. doi: 10.1155/2009/520283

Coico, R. (2005). Gram staining. *Curr. Protoc. Microbiol.* Appendix 3:Aendix3C. doi: 10.1002/9780471729259.mca03cs00

Cordeiro, F., da Silva, R. I. K., Vargas-Stampe, T. L. Z., Cerqueira, A. M. F., and Andrade, J. R. C. (2013). Cell invasion and survival of Shiga toxin-producing *Escherichia coli* within cultured human intestinal epithelial cells. *Microbiology (Reading)* 159(Pt 8), 1683–1694. doi: 10.1099/mic.0.064204-0

Cossart, P., and Sansonetti, P. J. (2004). Bacterial invasion: the paradigms of enteroinvasive pathogens. *Science* 304, 242–248. doi: 10.1126/science.1090124

Dalebroux, Z. D., and Swanson, M. S. (2012). ppGpp: magic beyond RNA polymerase. *Nat. Rev. Microbiol.* 10, 203–212. doi: 10.1038/nrmicro2720

Davis, T. K., Van De Kar, N., and Tarr, P. I. (2014). Shiga toxin/verocytotoxin-producing *Escherichia coli* Infections: practical clinical perspectives. *Microbiol. Spectr.* 2:EHEC–0025–2014. doi: 10.1128/microbiolspec.EHEC-0025-2014

Deibel, C., Kramer, S., Chakraborty, T., and Ebel, F. (1998). EspE, a novel secreted protein of attaching and effacing bacteria, is directly translocated into infected host cells, where it appears as a tyrosine-phosphorylated 90 kDa protein. *Mol. Microbiol.* 28, 463–474. doi: 10.1046/j.1365-2958.1998.00798.x

Diaz, J. M., and Ingall, E. D. (2010). Fluorometric quantification of natural inorganic polyphosphate. *Environ. Sci. Technol.* 44, 4665–4671. doi: 10.1021/es100191h

Dong, T., and Schellhorn, H. E. (2009). Global effect of RpoS on gene expression in pathogenic *Escherichia coli* O157:H7 strain EDL933. *BMC Genomics* 10:349. doi: 10.1186/1471-2164-10-349

Elliott, S. J., Wainwright, L. A., McDaniel, T. K., Jarvis, K. G., Deng, Y. K., Lai, L. C., et al. (1998). The complete sequence of the locus of enterocyte effacement (LEE) from enteropathogenic *Escherichia coli* E2348/69. *Mol. Microbiol.* 28, 1–4. doi: 10.1046/j.1365-2958.1998.00783.x

Elsinghorst, E. A., and Kopecko, D. J. (1992). Molecular cloning of epithelial cell invasion determinants from enterotoxigenic *Escherichia coli*. *Infect. Immun.* 60, 2409–2417. doi: 10.1128/iai.60.6.2409-2417.1992

Fujii, J., Kita, T., Yoshida, S., Takeda, T., Kobayashi, H., Tanaka, N., et al. (1994). Direct evidence of neuron impairment by oral infection with verotoxin-producing *Escherichia coli* O157:H- in mitomycin-treated mice. *Infect. Immun.* 62, 3447–3453. doi: 10.1128/iai.62.8.3447-3453.1994

Gigliucci, F., von Meijenfeldt, F. A. B., Knijn, A., Michelacci, V., Scavia, G., Minelli, F., et al. (2018). Metagenomic characterization of the human intestinal microbiota in fecal samples from STEC-infected patients. *Front. Cell Infect. Microbiol.* 8:25. doi: 10.3389/fcimb.2018.00025

Golan, L., Gonen, E., Yagel, S., Rosenshine, I., and Shpigel, N. Y. (2011). Enterohemorrhagic *Escherichia coli* induce attaching and effacing lesions and hemorrhagic colitis in human and bovine intestinal xenograft models. *Dis. Model. Mech.* 4, 86–94. doi: 10.1242/dmm.005777

Gomes, F. M., Ramos, I. B., Wendt, C., Girard-Dias, W., De Souza, W., Machado, E. A., et al. (2013). New insights into the in situ microscopic visualization and quantification of inorganic polyphosphate stores by 4',6-diamidino-2-phenylindole (DAPI)-staining. *Eur. J. Histochem.* 57:e34. doi: 10.4081/ejh.2013.e34

Han, R., Xu, L., Wang, T., Liu, B., and Wang, L. (2017). A small regulatory RNA contributes to the preferential colonization of *Escherichia coli* O157:H7 in the large intestine in response to a low DNA concentration. *Front. Microbiol.* 8:274. doi: 10.3389/fmicb.2017.00274

Hengge-Aronis, R. (1993). Survival of hunger and stress: the role of rpoS in early stationary phase gene regulation in *E. coli*. *Cell* 72, 165–168. doi: 10.1016/0092-8674(93)90655-a

Hengge-Aronis, R. (2002). Signal transduction and regulatory mechanisms involved in control of the sigma(S) (RpoS) subunit of RNA polymerase. *Microbiol. Mol. Biol. Rev.* 66, 373–395. doi: 10.1128/MMBR.66.3.373-395.2002

Hoac, B., Kiffer-Moreira, T., Millan, J. L., and McKee, M. D. (2013). Polyphosphates inhibit extracellular matrix mineralization in MC3T3-E1 osteoblast cultures. *Bone* 53, 478–486. doi: 10.1016/j.bone.2013.01.020

Hua, Y., Wu, J., Fu, M., Liu, J., Li, X., Zhang, B., et al. (2020). Enterohemorrhagic *Escherichia coli* effector protein EspF interacts with host protein ANXA6 and triggers myosin light chain kinase (MLCK)-dependent tight junction dysregulation. *Front. Cell Dev. Biol.* 8:613061. doi: 10.3389/fcell.2020.613061

Hua, Y., Yan, K., and Wan, C. (2018). Clever cooperation: interactions between EspF and Host proteins. *Front. Microbiol.* 9:2831. doi: 10.3389/fmicb.2018.02831

Jeong, J., Cho, N., Jung, D., and Bang, D. (2013). Genome-scale genetic engineering in *Escherichia coli*. *Biotechnol. Adv.* 31:804–810. doi: 10.1016/j.biotechadv.2013.04.003

Jones, N. L., Islur, A., Haq, R., Mascarenhas, M., Karmali, M. A., Perdue, M. H., et al. (2000). *Escherichia coli* Shiga toxins induce apoptosis in epithelial cells that is regulated by the Bcl-2 family. *Am. J. Physiol. Gastrointest. Liver Physiol.* 278, G811–G819. doi: 10.1152/ajpgi.2000.278.5.G811

Kenny, B., DeVinney, R., Stein, M., Reinscheid, D. J., Frey, E. A., and Finlay, B. B. (1997). Enteropathogenic *E. coli* (EPEC) transfers its receptor for intimate adherence into mammalian cells. *Cell* 91, 511–520. doi: 10.1016/s0092-8674(00)80437-7

Kim, K. S., Rao, N. N., Fraley, C. D., and Kornberg, A. (2002). Inorganic polyphosphate is essential for long-term survival and virulence factors in *Shigella* and *Salmonella* spp. *Proc. Natl. Acad. Sci. U.S.A.* 99, 7675–7680. doi: 10.1073/pnas.112210499

Kulakova, A. N., Hobbs, D., Smithen, M., Pavlov, E., Gilbert, J. A., Quinn, J. P., et al. (2011). Direct quantification of inorganic polyphosphate in microbial cells using 4'-6-diamidino-2-phenylindole (DAPI). *Environ. Sci. Technol.* 45, 7799–7803. doi: 10.1021/es201123r

Laing, C. R., Zhang, Y., Gilmour, M. W., Allen, V., Johnson, R., Thomas, J. E., et al. (2012). A comparison of Shiga-toxin 2 bacteriophage from classical enterohemorrhagic *Escherichia coli* serotypes and the German *E. coli* O104:H4 outbreak strain. *PLoS One* 7:e37362. doi: 10.1371/journal.pone.0037362

Lange, R., and Hengge-Aronis, R. (1991). Growth phase-regulated expression of bolA and morphology of stationary-phase *Escherichia coli* cells are controlled by the novel sigma factor sigma S. *J. Bacteriol.* 173, 4474–4481. doi: 10.1128/jb.173.14.4474-4481.1991

Ledwaba, S. E., Costa, D. V. S., Bolick, D. T., Giallourou, N., Medeiros, P., Swann, J. R., et al. (2020). Enteropathogenic *Escherichia coli* infection induces diarrhea, intestinal damage, metabolic alterations, and increased intestinal permeability in a murine model. *Front. Cell Infect. Microbiol.* 10:595266. doi: 10.3389/fcimb.2020.595266

Lee, K. S., Jeong, Y. J., and Lee, M. S. (2021). *Escherichia coli* Shiga Toxins and gut microbiota interactions. *Toxins (Basel)* 13:416. doi: 10.3390/toxins13060416

Lee, M. S., Koo, S., Jeong, D. G., and Tesh, V. L. (2016). Shiga Toxins as multi-functional proteins: induction of host cellular stress responses, role in pathogenesis and therapeutic applications. *Toxins (Basel)* 8:77. doi: 10.3390/toxins8030077

Leotta, G. A., Miliwebsky, E. S., Chinen, I., Espinosa, E. M., Azzopardi, K., Tennant, S. M., et al. (2008). Characterisation of Shiga toxin-producing *Escherichia coli* O157 strains isolated from humans in Argentina, Australia and New Zealand. *BMC Microbiol.* 8:46. doi: 10.1186/1471-2180-8-46

Leyva-Illades, D., Cherla, R. P., Lee, M. S., and Tesh, V. L. (2012). Regulation of cytokine and chemokine expression by the ribotoxic stress response elicited by Shiga toxin type 1 in human macrophage-like THP-1 cells. *Infect. Immun.* 80, 2109–2120. doi: 10.1128/IAI.06025-11

Liu, Y., Han, R., Wang, J., Yang, P., Wang, F., and Yang, B. (2020). Magnesium sensing regulates Intestinal colonization of enterohemorrhagic *Escherichia coli* O157:H7. *mBio* 11, 1–17. doi: 10.1128/mBio.02470-20

Livak, K. J., and Schmittgen, T. D. (2001). Analysis of relative gene expression data using real-time quantitative PCR and the 2(-Delta Delta C(T)) Method. *Methods* 25, 402–408. doi: 10.1006/meth.2001.1262

Ma, Z., Gong, S., Richard, H., Tucker, D. L., Conway, T., and Foster, J. W. (2003). GadE (YhiE) activates glutamate decarboxylase-dependent acid resistance in *Escherichia coli* K-12. *Mol. Microbiol.* 49, 1309–1320. doi: 10.1046/j.1365-2958.2003.03633.x

Magnusson, L. U., Farewell, A., and Nystrom, T. (2005). ppGpp: a global regulator in *Escherichia coli*. *Trends Microbiol.* 13, 236–242. doi: 10.1016/j.tim.2005.03.008

Melton-Celsa, A. R. (2014). Shiga Toxin (Stx) classification, structure, and function. *Microbiol. Spectr.* 2:EHEC–0024–2013. doi: 10.1128/microbiolspec.EHEC-0024-2013

Menge, C. (2020). Molecular biology of *Escherichia Coli* Shiga Toxins' effects on mammalian cells. *Toxins (Basel)* 12:345. doi: 10.3390/toxins12050345

Mohawk, K. L., and O'Brien, A. D. (2011). Mouse models of *Escherichia coli* O157:H7 infection and shiga toxin injection. *J. Biomed. Biotechnol.* 2011:258185. doi: 10.1155/2011/258185

Muller, D., Benz, I., Liebchen, A., Gallitz, I., Karch, H., and Schmidt, M. A. (2009). Comparative analysis of the locus of enterocyte effacement and its flanking regions. *Infect. Immun.* 77, 3501–3513. doi: 10.1128/IAI.00090-09

Nataro, J. P., and Kaper, J. B. (1998). Diarrheagenic *Escherichia coli*. *Clin. Microbiol. Rev.* 11, 142–201. doi: 10.1128/CMR.11.1.142

Nguyen, Y., and Sperandio, V. (2012). Enterohemorrhagic *E. coli* (EHEC) pathogenesis. *Front. Cell Infect. Microbiol.* 2:90. doi: 10.3389/fcimb.2012.00090

Pacheco, A. R., Lazarus, J. E., Sit, B., Schmieder, S., Lencer, W. I., Blondel, C. J., et al. (2018). CRISPR screen reveals that EHEC's T3SS and Shiga toxin rely on shared host factors for infection. *mBio* 9:e01003–18. doi: 10.1128/mBio.01003-18

Page, A. V., and Liles, W. C. (2013). Enterohemorrhagic *Escherichia coli* infections and the hemolytic-uremic syndrome. *Med. Clin. North Am.* 97, 681–695. doi: 10.1016/j.mcna.2013.04.001

Peng, L., Luo, W. Y., Zhao, T., Wan, C. S., Jiang, Y., Chi, F., et al. (2012). Polyphosphate kinase 1 is required for the pathogenesis process of meningitic *Escherichia coli* K1 (RS218). *Future Microbiol.* 7, 411–423. doi: 10.2217/fmb.12.3

Perera, A., Clarke, C. M., Dykes, G. A., and Fegan, N. (2015). Characterization of Shiga Toxigenic *Escherichia coli* O157 and Non-O157 isolates from ruminant feces in Malaysia. *Biomed. Res. Int.* 2015:382403. doi: 10.1155/2015/382403

Perna, N. T., Plunkett, G. III, Burland, V., Mau, B., Glasner, J. D., Rose, D. J., et al. (2001). Genome sequence of enterohaemorrhagic *Escherichia coli* O157:H7. *Nature* 409, 529–533. doi: 10.1038/35054089

Rangel, J. M., Sparling, P. H., Crowe, C., Griffin, P. M., and Swerdlow, D. L. (2005). Epidemiology of *Escherichia coli* O157:H7 outbreaks, United States, 1982-2002. *Emerg. Infect. Dis.* 11, 603–609. doi: 10.3201/eid1104.040739

Rao, N. N., and Kornberg, A. (1996). Inorganic polyphosphate supports resistance and survival of stationary-phase *Escherichia coli*. *J. Bacteriol.* 178, 1394–1400. doi: 10.1128/jb.178.5.1394-1400.1996

Rao, N. N., Gomez-Garcia, M. R., and Kornberg, A. (2009). Inorganic polyphosphate: essential for growth and survival. *Annu. Rev. Biochem.* 78, 605–647.

Rao, N. N., Liu, S., and Kornberg, A. (1998). Inorganic polyphosphate in *Escherichia coli*: the phosphate regulon and the stringent response. *J. Bacteriol.* 180, 2186–2193. doi: 10.1128/JB.180.8.2186-2193.1998

Riley, L. W., Remis, R. S., Helgerson, S. D., McGee, H. B., Wells, J. G., Davis, B. R., et al. (1983). Hemorrhagic colitis associated with a rare *Escherichia coli* serotype. *N. Engl. J. Med.* 308, 681–685. doi: 10.1056/NEJM198303243081203

Ritchie, J. M. (2014). Animal models of enterohemorrhagic *Escherichia coli* infection. *Microbiol. Spectr.* 2:EHEC–0022–2013. doi: 10.1128/microbiolspec.EHEC-0022-2013

Ritchie, J. M., Thorpe, C. M., Rogers, A. B., and Waldor, M. K. (2003). Critical roles for stx2, eae, and tir in enterohemorrhagic *Escherichia coli*-induced diarrhea and intestinal inflammation in infant rabbits. *Infect. Immun.* 71, 7129–7139. doi: 10.1128/IAI.71.12.7129-7139.2003

Robinson, C. M., Sinclair, J. F., Smith, M. J., and O'Brien, A. D. (2006). Shiga toxin of enterohemorrhagic *Escherichia coli* type O157:H7 promotes intestinal colonization. *Proc. Natl. Acad. Sci. U.S.A.* 103, 9667–9672. doi: 10.1073/pnas.0602359103

Shiba, T., Tsutsumi, K., Yano, H., Ihara, Y., Kameda, A., Tanaka, K., et al. (1997). Inorganic polyphosphate and the induction of rpoS expression. *Proc. Natl. Acad. Sci. U.S.A.* 94, 11210–11215. doi: 10.1073/pnas.94.21.11210

Shimizu, K., Asahara, T., Nomoto, K., Tanaka, R., Hamabata, T., Ozawa, A., et al. (2003). Development of a lethal Shiga toxin-producing *Escherichia coli*-infection mouse model using multiple mitomycin C treatment. *Microb. Pathog.* 35, 1–9. doi: 10.1016/s0882-4010(03)00065-2

Siegele, D. A., and Kolter, R. (1992). Life after log. *J. Bacteriol.* 174, 345–348. doi: 10.1128/jb.174.2.345-348.1992

Srisanga, K., Suthapot, P., Permsirivisarn, P., Govitrapong, P., Tungpradabkul, S., and Wongtrakoongate, P. (2019). Polyphosphate kinase 1 of *Burkholderia pseudomallei* controls quorum sensing, RpoS and host cell invasion. *J. Proteomics* 194, 14–24. doi: 10.1016/j.jprot.2018.12.024

Stevens, M. P., and Frankel, G. M. (2014). The locus of enterocyte effacement and associated virulence factors of enterohemorrhagic *Escherichia coli*. *Microbiol. Spectr.* 2:EHEC–0007–2013. doi: 10.1128/microbiolspec.EHEC-0007-2013

Suzuki, A., Doi, H., Matsuzawa, F., Aikawa, S., Takiguchi, K., Kawano, H., et al. (2000). Bcl-2 antiapoptotic protein mediates verotoxin II-induced cell death: possible association between bcl-2 and tissue failure by *E. coli* O157:H7. *Genes Dev.* 14, 1734–1740.

Tiwari, P., Gosain, T. P., Singh, M., Sankhe, G. D., Arora, G., Kidwai, S., et al. (2019). Inorganic polyphosphate accumulation suppresses the dormancy response and virulence in *Mycobacterium tuberculosis*. *J. Biol. Chem.* 294, 10819–10832. doi: 10.1074/jbc.RA119.008370

Tzeng, C. M., and Kornberg, A. (1998). Polyphosphate kinase is highly conserved in many bacterial pathogens. *Mol. Microbiol.* 29, 381–382. doi: 10.1046/j.1365-2958.1998.00887.x

Varas, M., Valdivieso, C., Mauriaca, C., Ortiz-Severin, J., Paradela, A., Poblete-Castro, I., et al. (2017). Multi-level evaluation of *Escherichia coli* polyphosphate related mutants using global transcriptomic, proteomic and phenomic analyses. *Biochim. Biophys. Acta Gen. Subj.* 1861, 871–883. doi: 10.1016/j.bbagen.2017.01.007

Vingadassalom, D., Campellone, K. G., Brady, M. J., Skehan, B., Battle, S. E., Robbins, D., et al. (2010). Enterohemorrhagic *E. coli* requires N-WASP for efficient type III translocation but not for EspFU-mediated actin pedestal formation. *PLoS Pathog.* 6:e1001056. doi: 10.1371/journal.ppat.1001056

Wang, X., Du, Y., Hua, Y., Fu, M., Niu, C., Zhang, B., et al. (2017). The EspF N-terminal of enterohemorrhagic *Escherichia coli* O157:H7 EDL933w imparts stronger toxicity effects on HT-29 cells than the C-Terminal. *Front. Cell Infect. Microbiol.* 7:410. doi: 10.3389/fcimb.2017.00410

Wang, Y., and Kim, K. S. (2000). Effect of rpoS mutations on stress-resistance and invasion of brain microvascular endothelial cells in *Escherichia coli* K1. *FEMS Microbiol. Lett.* 182, 241–247. doi: 10.1111/j.1574-6968.2000.tb08902.x

Weber, H., Polen, T., Heuveling, J., Wendisch, V. F., and Hengge, R. (2005). Genome-wide analysis of the general stress response network in *Escherichia coli*: sigmaS-dependent genes, promoters, and sigma factor selectivity. *J. Bacteriol.* 187, 1591–1603. doi: 10.1128/JB.187.5.1591-1603.2005

Weiss, S. M., Ladwein, M., Schmidt, D., Ehinger, J., Lommel, S., Stading, K., et al. (2009). IRSp53 links the enterohemorrhagic *E. coli* effectors Tir and EspFU for actin pedestal formation. *Cell Host Microbe* 5, 244–258. doi: 10.1016/j.chom.2009.02.003

Yi, Y., Ma, Y., Gao, F., Mao, X., Peng, H., Feng, Y., et al. (2010). Crystal structure of EHEC intimin: insights into the complementarity between EPEC and EHEC. *PLoS One* 5:e15285. doi: 10.1371/journal.pone.0015285

Zhao, S., Zhou, Y., Wang, C., Yang, Y., Wu, X., Wei, Y., et al. (2013). The N-terminal domain of EspF induces host cell apoptosis after infection with enterohaemorrhagic *Escherichia coli* O157:H7. *PLoS One* 8:e55164. doi: 10.1371/journal.pone.0055164

Conflict of Interest: The authors declare that the research was conducted in the absence of any commercial or financial relationships that could be construed as a potential conflict of interest.

Publisher's Note: All claims expressed in this article are solely those of the authors and do not necessarily represent those of their affiliated organizations, or those of the publisher, the editors and the reviewers. Any product that may be evaluated in this article, or claim that may be made by its manufacturer, is not guaranteed or endorsed by the publisher.

frontiers in Microbiology

ORIGINAL RESEARCH
published: 10 February 2022
doi: 10.3389/fmicb.2022.758571

The Role of the Two-Component System PhoP/PhoQ in Intrinsic Resistance of *Yersinia enterocolitica* to Polymyxin

Haoran Guo, Tong Zhao, Can Huang and Jingyu Chen*

Beijing Laboratory for Food Quality and Safety, College of Food Science and Nutritional Engineering, China Agricultural University, Beijing, China

Polymyxin is the "last resort" of antibiotics. The self-induced resistance to polymyxin in Gram-negative bacteria could be mediated by lipopolysaccharide (LPS) modification, which is regulated by the two-component system, PhoP/PhoQ. *Yersinia enterocolitica* is a common foodborne pathogen. However, PhoP/PhoQ has not been thoroughly studied in *Y. enterocolitica*. In this study, the functions of PhoP/PhoQ in *Y. enterocolitica* intrinsic resistance were investigated. The resistance of *Y. enterocolitica* was found to decrease with the deletion of PhoP/PhoQ. Further, PhoP/PhoQ was found to play an important role in maintaining membrane permeability, intercellular metabolism, and reducing membrane depolarization. Based on subsequent studies, the binding ability of polymyxin to *Y. enterocolitica* was decreased by the modification of LPS with structures, such as L-Ara4N and palmitate. Analysis of the gene transcription levels revealed that the LPS modification genes, *pagP* and *arn* operon, were downregulated with the deletion of PhoP/PhoQ in *Y. enterocolitica* during exposure to polymyxin. In addition, *pmrA*, *pmrB*, and *eptA* were downregulated in the mutants compared with the wild-type strain. Such findings demonstrate that PhoP/PhoQ contributes to the intrinsic resistance of *Y. enterocolitica* toward polymyxins. LPS modification with L-Ara4N or palmitate is mainly responsible for the resistance of *Y. enterocolitica* to polymyxins. The transcription of genes related to LPS modification and PmrA/PmrB can be both affected by PhoP/PhoQ in *Y. enterocolitica*. This study adds to current knowledge regarding the role of PhoP/PhoQ in intrinsic resistance of *Y. enterocolitica* to polymyxin.

Keywords: *Yersinia enterocolitica*, PhoP/PhoQ, LPS modification, polymyxin, intrinsic resistance

OPEN ACCESS

Edited by:
Dongsheng Zhou, Beijing Institute of Microbiology and Epidemiology, China

Reviewed by:
Paola Sperandeo, University of Milan, Italy
Alberto Sola, Instituto de Biotecnología de León, Spain

***Correspondence:**
Jingyu Chen
chenjy@cau.edu.cn

Specialty section:
This article was submitted to Infectious Agents and Disease, a section of the journal Frontiers in Microbiology

Received: *14 August 2021*
Accepted: *06 January 2022*
Published: *10 February 2022*

Citation:
Guo H, Zhao T, Huang C and Chen J (2022) The Role of the Two-Component System PhoP/PhoQ in Intrinsic Resistance of Yersinia enterocolitica to Polymyxin. Front. Microbiol. 13:758571. doi: 10.3389/fmicb.2022.758571

INTRODUCTION

Yersinia enterocolitica is a common foodborne pathogen that causes a broad range of gastrointestinal syndromes in humans (yersiniosis; Shoaib et al., 2019). *Yersinia enterocolitica* is widely distributed in various environments and food production (Shoaib et al., 2019). To infect humans, *Y. enterocolitica* must survive in the host environment by escaping cationic antibiotic peptides (AMPs), which mediate parts of the innate immune system against infections (Rahnamaeian, 2011).

In bacteria, two-component systems (TCSs) are employed to sense and respond to various environmental stresses (West and Stock, 2001). Typical TCSs consist of a membrane-embedded sensor kinase and a cytosolic response regulator. These systems can sense extracellular signals and perform cascade phosphorylation in response. The activated response regulator then regulates the expression of specific genes directly or indirectly, thereby initiating cellular responses to environmental changes (Hoch, 2000; West and Stock, 2001).

PhoP/PhoQ is a prototypical TCS present in many bacteria. PhoQ, the dimeric sensor kinase of this system, contains cytoplasmic, transmembrane, and periplasmic domains (Véscovi et al., 1997; Bader et al., 2005; Prost et al., 2007). The patch of acidic residues close to the membrane surface in the periplasmic sensing domain of PhoQ is crucial for sensing cationic AMPs (Bader et al., 2005). Divalent cation concentrations, low pH conditions, and high osmolarity have been reported to activate PhoQ (Véscovi et al., 1997; Bader et al., 2005; Prost et al., 2007). And PhoP is a phosphorylated response regulator which is controlled by activated PhoQ (Simpson and Trent, 2019). PhoP directly regulates a set of genes that vary among different bacteria (Winfield et al., 2005; Hong et al., 2018; Chen et al., 2021). However, some Gram-negative bacteria have conserved ancestral genes, such as *mgtA* in *Escherichia coli* acting as magnesium transporter and *mgrB* as the direct negative regulator of PhoP/PhoQ (Minagawa et al., 2003; Zwir et al., 2012). The protein, PmrD, which is also directly regulated by PhoP, could combine PhoP/PhoQ and PmrA/PmrB. Thus, PhoP/PhoQ is indirectly involved in PmrA/PmrB regulation of genes (**Figures 1A,B**; Rubin et al., 2015; Hong et al., 2018).

Polymyxins are AMPs that target Gram-negative outer membranes (Mitchell and Silhavy, 2019). Lipid A of Gram-negative bacterial outer membrane is the target binding site for AMPs, which mediates the interaction with negatively charged LPS. A hydrophobic domain is known to insert itself into membranes, forming pores, which results in cell lysis and death (Brogden, 2005). The resistance of Gram-negative bacteria to polymyxins primarily relies on chemical modifications of the lipopolysaccharide (LPS) structure and leads to major changes in the physicochemical properties of the outer membrane (Trimble et al., 2016). In most resistant strains, LPS modified with 4-amino-4-deoxy-L-arabinose (L-Ara4N), phosphoethanolamine (pEtN), as well as other modification substituents, showed polymyxin resistance (Santos et al., 2017). Expression of most of the genes in the LPS modification pathway is controlled by several TCSs, including PhoP/PhoQ and PmrA/PmrB (Rubin et al., 2015; Trimble et al., 2016; Duperthuy, 2020).

Although PhoP/PhoQ has been best studied in *Salmonella* typhimurium, it has not been thoroughly studied in *Y. enterocolitica*. Further, some proteins such as PmrD in PhoP/PhoQ regulatory pathway in *Salmonella* have not been found in *Y. enterocolitica*. Therefore, whether the resistance of *Y. enterocolitica* to polymyxins could be affected by the deletion of PhoP/PhoQ needs to be determined. Further, the role of PhoP/PhoQ in the intrinsic resistance mechanism of *Y. enterocolitica* to AMP is unclear. In this study, the role of PhoP/PhoQ in the polymyxin resistance of *Y. enterocolitica* as well as the growth, membrane damage, and intracellular metabolism of *Y. enterocolitica* was identified. The difference in the ability of polymyxins to bind to resistant or sensitive membranes regulated by PhoP/PhoQ was assessed. In addition, *Y. enterocolitica* lipid A modifications implicated in polymyxin resistance were characterized. By analyzing gene expression, PhoP/PhoQ was found to affect polymyxin resistance by regulating various genes related to LPS modification. These findings reveal some of the roles of PhoP/PhoQ in *Y. enterocolitica* polymyxin resistance.

MATERIALS AND METHODS

Bacterial Strains, Plasmids, and Culture Conditions

The bacterial strains and plasmids used in this study are listed in **Table 1**. *Escherichia coli* S17-λpir was used as the host bacteria in plasmid construction and was cultured at 37°C in lysogeny broth (LB) containing 5 g/L yeast extract, 10 g/L tryptone, and 5 g/L NaCl. *Yersinia enterocolitica* ATCC23715 (biotype 1 B and serotype O:8) was used as the parent strain for the construction of *Y. enterocolitica* mutants, which were cultured at 26°C in LB broth and LBNS (LB without salts). Ampicillin (100 μg/ml), chloramphenicol (16 μg/ml), cefsulodin (15 μg/ml), irgasan (4 μg/ml), and novobiocin (2.5 μg/ml) were added as required.

Construction of Plasmids and Strains

To construct pDS132-Δ*phoP*, fragments upstream and downstream of the *phoP* gene were amplified from the *Y. enterocolitica* genome using the primers, *phoP-up-F/phoP-up-R* and *phoP-down-F/phoP-down-R*. The upstream and downstream fragments were fused and amplified by fusion PCR with primers *phoP-up-F/phoP-down-R*. The resultant long fragment was then digested with *Sac*I and *Sal*I and ligated into pDS132 digested with the same enzymes to yield pDS132-Δ*phoP*. The same approach was used to construct pDS132-Δ*phoQ* with the corresponding primers. To construct the *phoP* knockout strain, the suicide plasmid, pDS132-Δ*phoP*, was introduced into *E. coli* S17-1 λpir by electroporation and then mobilized into *Y. enterocolitica* by conjugation. The strategy used for gene deletion in the *Y. enterocolitica* chromosome was based on the two-step homologous recombination with plasmid pDS132 containing the *sacB* counter-selectable marker and a chloramphenicol resistant marker, as described previously (Schäfer et al., 1994). Similarly, the plasmid pDS132-Δ*phoQ* was used to construct the Δ*phoQ* mutants.

To construct pBAD24-*phoP*, the *phoP* fragment was amplified from the *Y. enterocolitica* genome using primers *p-phoP-F*/*p-phoP-R*, digested with *Xbal*I and *Hin*dIII, and inserted into pBAD24 digested with the same enzymes. The resultant pBAD24-*phoP* plasmid contained the *phoP* gene, which was controlled by the *araBAD* promoter (P*BADphoP*). The plasmid, pBAD24-*phoP*, was used to transform the Δ*phoP* mutant by electroporation to construct the Δ*phoP-phoP* complemented strain. The same method was also used to construct Δ*phoQ-phoQ* complemented

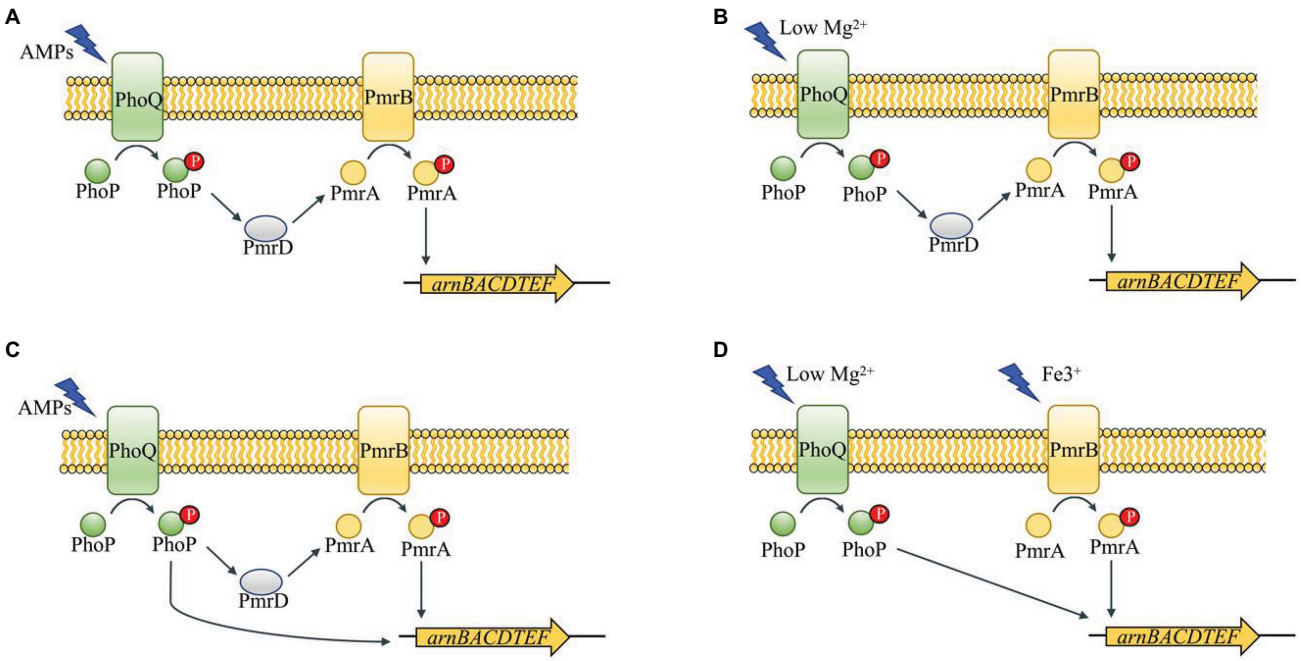

FIGURE 1 | Schematic of PhoP/PhoQ and PmrA/PmrB regulation network in different genera of Enterobacteriaceae (Winfield et al., 2005; Rubin et al., 2015; Hong et al., 2018; Chen et al., 2021). PmrD functions as a connector between PhoP/PhoQ and PmrA/PmrB in *Salmonella enterica* **(A)**. The connector function of PmrD is activated under low Mg^{2+} in *Escherichia coli* **(B)**. PhoP can regulate *arn* operon directly and indirectly in *Klebsiella pneumoniae* **(C)**. PhoP/PhoQ and PmrA/PmrB perform a cross-regulation of *arn* operon under different environments in *Yersinia pestis* **(D)**.

TABLE 1 | Strains and plasmids used in this study.

Strains and plasmids	Relevant characteristics	Sources
Yersinia enterocolitica		
ATCC23715	WT, serotype O:8, Biotype 1B, pYV⁻	Lab stock
Δ*phoP*	Δ*phoP*	This study
Δ*phoP-phoP*	Δ*phoP*, P_{BAD}*phoP*; Amp^r	This study
Δ*phoQ*	Δ*phoQ*	This study
Δ*phoQ-phoQ*	Δ*phoQ*, P_{BAD}*phoQ*; Amp^r	This study
Escherichia coli		
S17-1 λpir	*recA1*, *thi*, *pro*, *hsdR*-M⁺, RP4:2-Tc:Mu⁻Kan:Tn7, λpir	Lab stock
Plasmids		
pDS132	Conditional replication vector; R6K origin, mobRK4 transfer origin, sucrose-inducible-*sacB*; Cm^r	Lab stock
pDS132-Δ*phoP*	Upstream and downstream *phoP* fragments were cloned into pDS132; Cm^r	This study
pDS132-Δ*phoQ*	Upstream and downstream *phoQ* fragments were cloned into pDS132; Cm^r	This study
pBAD24	*AraC*, promoter P_{BAD}; Amp^r	Lab stock
pBAD24-*phoP*	*AraC*, P_{BAD}*phoP*; Amp^r	This study
pBAD24-*phoQ*	*AraC*, P_{BAD}*phoQ*; Amp^r	This study

Amp^r, ampicillin resistance and Cm^r, chloramphenicol resistance.

strains. All primers used in this study are listed in **Supplementary Table 1**. Ampicillin (100 μg/ml) and L-arabinose (0.6 g/L) were added to maintain plasmid and induce the expression of *phoP* or *phoQ*, respectively.

Growth Curves Measurement

Growth curves of the strains were determined by measuring the OD_{600} at 60 min intervals over a period of 24 h. Overnight cultures of bacterial strains were inoculated into LB medium supplemented 0.5 μg/ml PMB or PME (at 1:50 dilution) and incubated at 26°C with shaking at 180 rpm. Growth curves under no PMB or PME were also measured for the control group. L-arabinose (0.6 g/L) was added to induce the expression of *phoP* or *phoQ* of complemented strains. The experiments were performed with three biological replicates.

Minimal Inhibitory Concentration and Minimal Bactericidal Concentration

The minimal inhibitory concentration (MIC) of PMB and PME were assessed according to the CLSI guidelines with some modifications (CLSI, 2017). Briefly, overnight cultures of WT, *phoP*, and *phoQ* mutants were diluted in cation-adjusted Mueller–Hinton broth (CaMHB) with approximately10^6 colony forming units (CFU)/ml in tubes. Then, the suspended bacteria were exposed to PMB or PME at 0.5, 1.0, 2.0, 4.0, 8.0, and 16.0 μg/ml. All tubes were incubated for 18–24 h at 26°C with shaking. The MIC was determined as the minimal concentration at which turbidity was not visible in comparison with the blank and minimal bactericidal concentration (MBC) was the minimal concentration which had no growth. And it was performed with three biological replicates.

Laser Scanning Confocal Microscope

The overnight cultures were inoculated to LBNS broth and grown at 26°C and 180 rpm to mid-log phase. The bacterial cells were collected and washed with PBS buffer for three times and then resuspended at a final optical density of $OD_{600} = 1.0$. The equal volume of bacterial suspension was mixed with PMB or PME solution (10 μg/ml) and incubated at 26°C for 2 h. Then, the solutions were centrifuged at 5,000 × *g* for 5 min and resuspended at the same volume with PBS. And cell viability after PMB or PME treatment was assessed using fluorescently labeled propidium iodide (PI) and 4′,6-diamidino-2-phenylindole (DAPI) and analyzed with a laser scanning confocal microscope (LSCM). DAPI is a blue, fluorescent stain that labels both live and dead cells while PI is a red fluorescent nucleic acid stain that only penetrates cells with damaged cell membranes (dead cells). All images were captured by LSCM (Leica TCS SP8, Mannheim, Germany) and quantified using ImageJ.

Cell Membrane Permeabilization and Potential

N-phenyl-1-naphthylamine (NPN) uptake assays were performed to evaluate the outer membrane permeability of *Y. enterocolitica* strains, as previously described (Lee and Je, 2013). Briefly, cells were harvested in the log phase of growth and centrifuged at 5,000 rpm for 10 min at 4°C. Thereafter, the cells were washed three times with PBS and resuspended to an OD_{600} of 0.5. An aliquot of bacterial suspension and polymyxin solutions were fully mixed with NPN at a final concentration of 10 μM. The fluorescence value was then measured immediately using a spectrofluorometer FS5 (Edinburgh Instruments, United Kingdom). Excitation and emission wavelengths for NPN were set at 350 and 420 nm, respectively, with a slit width of 0.5 nm. The inner membrane permeability was tested with O-nitrophenyl-β-D-galactoside (ONPG) according to the method previously mentioned (Lee and Je, 2013). Logarithmic-phase bacteria were washed with PBS and resuspended to OD_{600} at 0.5. Then, 100 μl of bacterial suspension was added to 100 μl polymyxin solutions and 10 μl ONPG (30 mM) in each well. And the absorbance at 410 nm was used to evaluate o-nitrophenol over time using a spectrophotometer.

Overnight cultures were inoculated to LBNS and grown at 180 rpm, 26°C to mid-log phase. And bacteria were washed with 20 mM HEPES buffer for three times at 4°C and adjust to $OD_{600} = 0.5$. Then, bacteria were exposed under 0.5 μg/ml PMB or PME for 2 h at 26°C. Changes in membrane polarity were detected using the bis-oxonol dye, $DiBAC_4(3)$ (AAT Bioquest, Inc., CA, United States). The assay was performed according to a previously described method with some modifications (Clementi et al., 2014).

Measurement of Intracellular Adenosine Triphosphate Concentration

Overnight cultures were inoculated to LBNS and grown at 180 rpm, 26°C to mid-log phase. Then, bacteria were washed with 20 mM HEPES buffer for three times at 4°C and adjust to $OD_{600} = 0.5$. Then, equal volume of bacteria suspension and 1 μg/ml PMB or PME solutions were incubate for 2 h at 26°C. The adenosine triphosphate (ATP) concentration of *Y. enterocolitica* after PMB or PME treatment was assayed using an ATP assay kit (Beyotime Biotechnology, Jiangsu, China). ATP remain rate was used which was calculated by dividing the ATP content of *Y. enterocolitica* treated with PMB or PME by the corresponding ATP content without PMB or PME treated.

Dansyl-Polymyxin Binding Experiments

Dansyl-PMB and dansyl-PME were prepared according to the modified method of Schindler and Teuber (Schindler and Teuber, 1975). The synthesized Dansyl-PMB and Dansyl-PME were dissolved in 3 ml of 1× PBS buffer (pH 7.0), purified using a Sephadex G-25 column, and quantitated using the dinitrophenylation assay (Bader and Teuber, 1973). The concentrations of dansyl-PMB and dansyl-PME were 0.519 and 0.409 mg/ml, respectively, relative to a triplicate standard curve derived from a 1 mg/ml stock solution of PMB and PME.

The fluorescence of dansyl-polymyxin bound to bacteria was measured using a spectrofluorometer FS5 (Edinburgh Instruments, United Kingdom), set at an excitation wavelength of 330 nm and an emission wavelength of 565 nm. To quantify Dansyl-PMB and Dansyl-PME binding, previous methods were used as reference, with some modifications (Cullen et al., 2011; Akhoundsadegh et al., 2019). All strains were grown to an OD_{600} of 0.8 to 1.0, and the cells were washed three times with PBS. Thereafter, the same volume of Dansyl-PMB or Dansyl-PME was applied to washed cells and incubated for 2 min. Following incubation, the cells were washed with PBS and resuspended in PBS. The fluorescence was determined by spectrofluorometer FS5 and A_{600} was determined using a microplate reader (Thermo Scientific, Waltham, MA, United States). Each experiment was repeated in triplicate, and data are reported as the ratio of fluorescence intensity to A_{600}.

Lipid A Extraction and Analysis by MALDI-TOF

Yersinia enterocolitica cultures (200 ml) were grown to an A_{600} of 0.5 and then exposed to 1.0 μg/ml PMB or PME for 3 h. The cells were then harvested by centrifugation. Lipid A was purified from bacteria as described previously (Hankins et al., 2013; Henderson et al., 2013) and stored frozen at −20°C. The lipid A species were analyzed using a Bruker Atuoflex III MALDI-TOF mass spectrometer (Bruker Daltonics, Germany) according to a previous method (Hankins et al., 2013; Henderson et al., 2013; Han et al., 2018b).

RNA Extraction and Real-Time Quantitative PCR

Overnight cultures were inoculated to LBNS and grown at 180 rpm, 26°C for 3 h, and then exposed to 1.0 μg/ml PMB or PME for 3 h until OD_{600} was approximately at 0.5. Total RNA was extracted from *Y. enterocolitica* strains using the TransZol Up Plus RNA Kit (TransGen, Beijing, China). The

extracted RNA was then tested for concentration and quality using a Nanodrop 2000c (Thermo Scientific, Waltham, United States). Real-time quantitative PCR (RT-qPCR) was conducted using SYBR Green and specific primers (**Supplementary Table 2**) in a Light Cycler 480 II (Roche, Basel, Switzerland). Reactions were performed in triplicate. Relative transcription of the target genes was analyzed by the $2^{-\Delta\Delta Ct}$ method described previously, and the 16S rRNA gene was used as a reference for normalization (Meng et al., 2020).

Statistical Analysis

Statistical analysis was performed using GraphPad Prism 8 (GraphPad Software, San Diego, CA, United States). One-way ANOVA analysis was performed, and the levels of significance are indicated in the figure legends.

RESULTS

Deletion of PhoP/PhoQ Decreases the Resistance of *Yersinia enterocolitica* to Polymyxins

Studies have shown that the PhoP/PhoQ system can respond to the presence of antimicrobial peptides and increase resistance (Shprung et al., 2012; Lin et al., 2018). To explore the role of the PhoP/PhoQ system in *Y. enterocolitica* exposed to polymyxins, MIC and MBC of wild-type and mutants were evaluated (**Table 2**). MIC to PMB and PME of wild type were both 2 μg/ml, while *phoP* or *phoQ* mutants was 1 μg/ml. And MBC were also decreased when PhoP/PhoQ was deleted in *Y. enterocolitica*. Then, the growth curves of wild-type, mutants, and complemented strains were also measured. The growth of *Y. enterocolitica* was not affected by the deletion of PhoP/PhoQ (**Supplementary Figure 1**). However, the lag phase of the growth curves was prolonged in *phoP* and *phoQ* mutants compared to the wild-type and complemented strains under 0.5 μg/ml PMB or PME (**Figure 2**). Both wild-type and mutant strains were stained with PI and DAPI after treatment with 5 μg/ml of PMB or PME and observed using LCSM (**Supplementary Figure 2**). The live-to-dead bacterial ratio was quantitatively analyzed, and the ratios of the mutants were lower than those of the wild type. Combined with the above evidence, the deletion of the PhoP/PhoQ system was found to decrease the resistance of *Y. enterocolitica* to PMB and PME and affected the growth of *Y. enterocolitica* under PMB or PME at sub-inhibitory concentration.

TABLE 2 | Minimal inhibitory concentration (MIC) and minimal bactericidal concentration (MBC) of wild type, *phoP* and *phoQ* mutants to PMB and PME.

	MIC (μg/ml)		MBC (μg/ml)	
	PMB	PME	PMB	PME
WT	2	2	16	16
Δ*phoP*	1	1	8	8
Δ*phoQ*	1	1	4	8

Deletion of PhoP/PhoQ Increases Membrane Sensitivity and Decreases Intracellular Metabolism When Exposed to Polymyxin

According to several reports, polymyxin can cause membrane damage, thereby interfering with the normal physiological functions of bacteria (Santos et al., 2017). Therefore, the changes in cell membrane potential and cell membrane permeability of the wild-type and mutant strains under sub-inhibitory concentrations of PMB or PME were explored. When PME and PMB were stimulated with 0.5 μg/ml, the permeability of the outer membrane and the changes in the membrane potential were measured, the results of which are displayed in **Figures 3A,B**. The NPN uptake method was used to evaluate the permeability of the outer membrane. NPN is a hydrophobic fluorescent probe that can be embedded in the cell membrane (Lee and Je, 2013). As its fluorescence intensity increases in a hydrophobic environment, it is often used to reflect the permeability of the cell membrane (Lee and Je, 2013; Akhoundsadegh et al., 2019). The fluorescence of the *phoP* and *phoQ* mutants was significantly higher than that of the wild type. In addition, the absorbance at 410 nm of the mutants was higher than that of the wild type under PMB or PME (**Supplementary Figure 3**). Thus, PMB or PME can be concluded to cause severe damage to the membrane permeability of mutants compared to the wild type. The membrane potential dye, $DiBAC_4(3)$, was used to measure the cellular membrane potential of *Y. enterocolitica*. At 0.5 μg/ml of PMB or PME, the membrane depolarization of the mutants was significantly enhanced compared with that of the wild type (**Figures 3C,D**).

Treatment with AMP can reduce cytoplasmic ATP concentration and inhibit respiration (Brogden, 2005). Bacterial resistance to PMB has also been reported to be strongly related to energy metabolism (Yu et al., 2019). To further explore whether the PhoP/PhoQ system influences the intracellular metabolism of *Y. enterocolitica* under stimulation with the same sub-inhibitory concentration, the intracellular ATP contents of mutants and wild type were determined at 0.5 μg/ml PMB or PME, and the results are shown in **Figures 3E,F**. The intracellular ATP content of wild type and mutants were reduced after PMB or PME treatment, but the mutants showed a significantly higher degree of reduction when compared with the wild type. Therefore, the resistance of *Y. enterocolitica* to PMB or PME after the deletion of the PhoP/PhoQ system was observed, which was demonstrated by more severe changes in cell membrane permeability, membrane depolarization, and intracellular metabolism.

PhoP/PhoQ Is Responsible for the Increased Resistance of Cell Membrane to Polymyxin Binding

Polymyxin binding to membrane promote cation displacement and structural changes in membrane curvature. And this binding

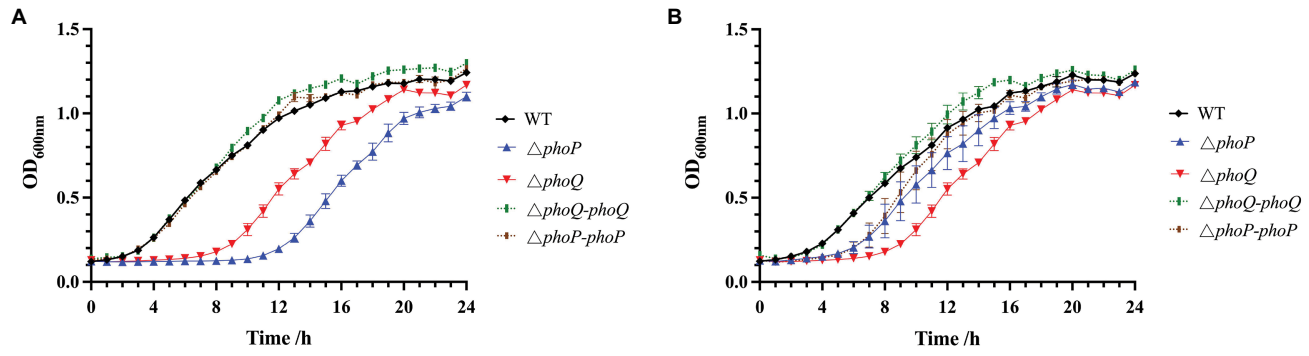

FIGURE 2 | Effect of PhoP/PhoQ on the growth of *Y. enterocolitica* under PMB or PME. Growth curves of wild type, mutants and complemented strains under 0.5 μg/ml PMB **(A)**. Growth curves of wild type, mutants and complemented strains under 0.5 μg/ml PME **(B)**.

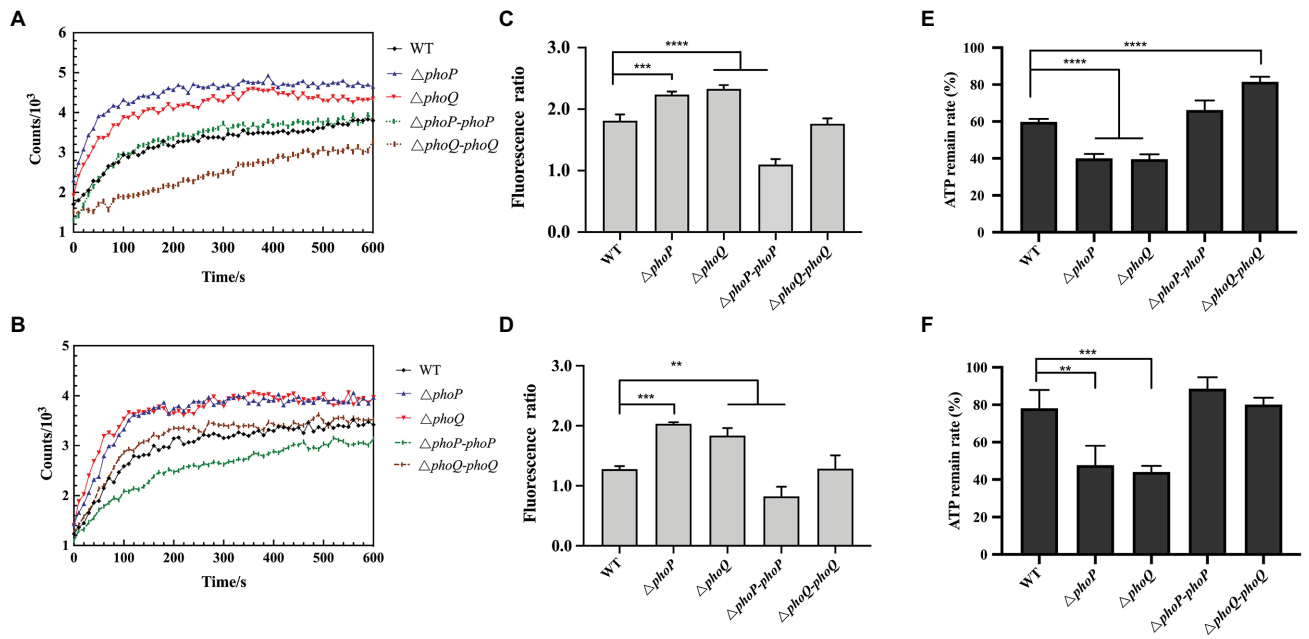

FIGURE 3 | PhoP/PhoQ is essential for *Y. enterocolitica* to maintain membrane stability and intercellular metabolism when treated with 0.5 μg/ml PMB or PME. Outer membrane permeability evaluated by the N-phenyl-1-naphthylamine (NPN) uptake of wild type, mutants and complemented strains treated with 0.5 μg/ml PMB **(A)** and PME **(B)**. Membrane depolarization of wild type, mutants and complemented strains treated with 0.5 μg/ml PMB **(C)** and PME **(D)** and measured using $DiBAC_4(3)$. The ordinate is the fluorescence ratio between the treatment group and the blank (untreated with PMB or PME). The intercellular ATP remain rate following treatment with 0.5 μg/ml PMB **(E)** and PME **(F)**. Asterisks indicate a significant difference. ****, $p < 0.0001$; ***, $p < 0.001$; and **, $p < 0.01$.

is selectively which determines the sensitivity or resistance of bacteria to AMPs (Santos et al., 2017). The interactions between polymyxins and the Gram-negative outer membrane play an important role in polymyxin resistance (Brogden, 2005). Thus, the following hypothesis was proposed: the existence of the PhoP/PhoQ system can increase the resistance to polymyxins by reducing the binding and/or entry ability of polymyxin to *Y. enterocolitica*. To prove this hypothesis, PMB or PME binding assays were performed using the fluorescently labeled polymyxin compounds, Dansyl-PMB and Dansyl-PME. The quantification results of the binding or entry ability of Dansyl-PMB and Dansyl-PME with *Y. enterocolitica* are presented in **Figure 4**. First, the fluorescence intensity increased with increasing concentrations of Dansyl-PMB or Dansyl-PME, indicating increased surface-bound or entry of Dansyl-PMB or Dansyl-PME. No significant difference in fluorescence was found between the wild type and mutants when dansyl-PMB and dansyl-PME concentrations of 5 and 4 μg/ml were, respectively, employed. However, *phoP* and *phoQ* mutants showed significantly increased fluorescence compared to the wild type when the concentrations of dansyl-PMB and dansyl-PME were 50, 500, 40, and 400 μg/ml, respectively, confirming the protective effect of PhoP/PhoQ against polymyxin attack on the bacterial surface of *Y. enterocolitica*. Therefore, these results proved our hypothesis

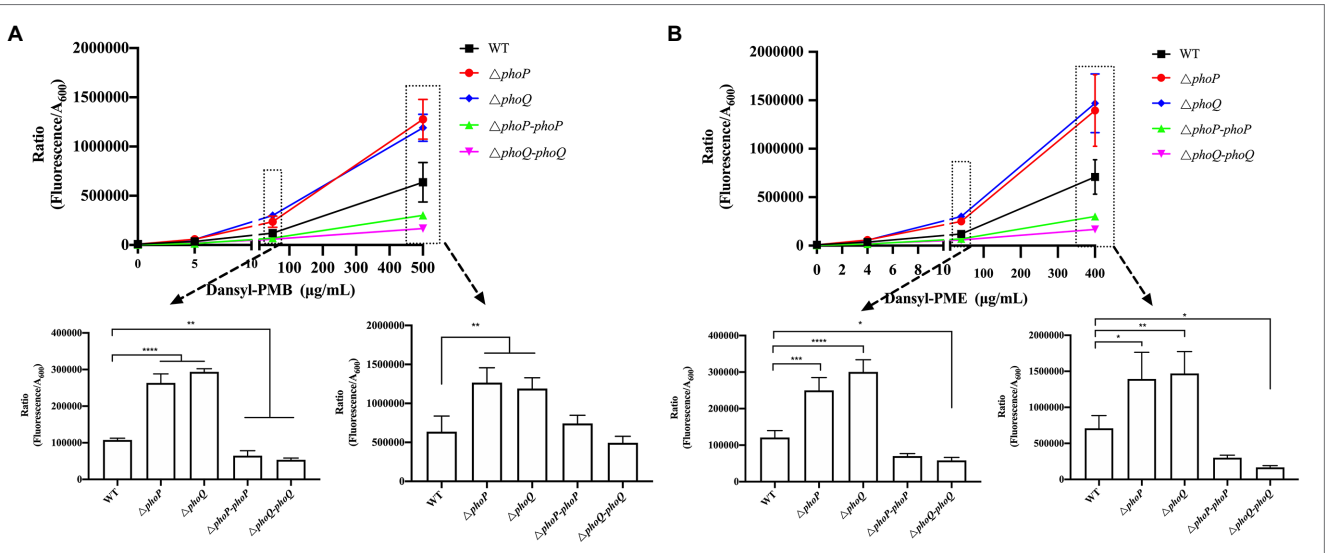

FIGURE 4 | PhoP/PhoQ created a more resistant *Y. enterocolitica* membrane for the binding of polymyxin. The binding ability of different concentrations of Dansyl-PMB **(A)** and Dansyl-PME **(B)** to wild type, mutants and complemented strains. Asterisks indicate a significant difference. ****, $p<0.0001$; ***, $p<0.001$; **, $p<0.01$; and *, $p<0.05$.

that the existence of PhoP/PhoQ provides more resistance to polymyxin binding in the cell membrane of *Y. enterocolitica*.

LPS Structure, Which Is Associated With AMP Resistance, Depends on the Regulation of PhoP/PhoQ

The interaction of AMPs with the anionic bacterial surface is necessary for the exertion of their microbicidal action (Brogden, 2005). LPS modifications that reduce the negative charge or alter the acyl chains of lipid A provide resistance against AMP binding through charge repulsion or decrease the fluidity of the outer membrane (Simpson and Trent, 2019). To further explore the relationship between the binding ability of AMPs to the outer membrane of *Y. enterocolitica* and LPS modification, MALDI-TOF mass spectrometry was used to characterize the lipid A structure. **Figure 5Aa** shows that lipid A from *Y. enterocolitica* exposed to PMB contained a predominant peak at *m*/*z* 1,224. And three peaks were also found at *m*/*z* 1,864, *m*/*z* 1,708, and *m*/*z* 1,724 which contained two glucosamines, one or two phosphates, 2-OH-C12, and aminoarabinose (**Figure 5B**; Reinés et al., 2012a,b; Han et al., 2018a). The wild type grown under the PME showed a predominant peak at *m*/*z* 1,823 for a lipid A species that predominantly contained hexa-acylated species that correspond to two glucosamines, two phosphates, four 3-OH-C14, one C12, and one C16:1 (**Figure 5B**; Reinés et al., 2012b). The presence of polymyxins caused *Y. enterocolitica* to induce palmitate and aminoarabinose lipid A modification, which increased the resistance to polymyxins. Lipid A from wild type and mutants also did not undergo pEtN modification under PMB and PME stimulation, which may be related to the absence of PmrD in *Y. enterocolitica* (Reinés et al., 2012b). In the presence of PMB or PME, modifications to lipid A by aminoarabinose or palmitate could be detected in *Y. enterocolitica* under the regulation of PhoP/PhoQ, which led to resistance in polymyxin binding to the membrane and higher resistance. It was showed that lipid A from *phoP* and *phoQ* mutants under PME lacked multiple modifications, which could explain the higher fluorescence of the polymyxin binding mutants. Similarly, the *phoQ* mutants treated with PMB also lacked multiple modifications. However, for *phoP* mutants under PMB, result was also shown that peak at *m*/*z* 1,686 which was closely to *m*/*z* 1,684 has also been detected. This reveals that other pathways may involve in the regulation of lipid A modifications. Although PmrD is absent in *Y. enterocolitica*, but whether the cross-regulation between PhoP/PhoQ and PmrA/PmrB is existence has not been proved, so the quantification of the transcription level of PmrA/PmrB was performed which may give some explanation.

Activated PhoP/PhoQ Upregulates Genes Related to LPS Modification in *Yersinia enterocolitica*

The above data confirmed that the presence of the PhoP/PhoQ system can increase the viability of *Y. enterocolitica* when exposed to PMB or PME. The increased resistance was achieved by reducing the binding ability of PMB or PME to *Y. enterocolitica*. The chemical characteristics of lipid A were characterized by MALDI-TOF, which revealed that wild-type *Y. enterocolitica* had a variety of structures related to AMP resistance compared to the mutants. Studies have shown that PhoP/PhoQ regulates *pagP* directly to maintain the asymmetry of the outer membrane (Simpson and Trent, 2019). Moreover, *arnBCADTEF* is required for the synthesis and addition of aminoarabinose to lipid A (Reinés et al., 2012a). *Salmonella enterica* subspp. and *E. coli* encode the protein, PmrD, which mediates coupling between PhoP/PhoQ and PmrA/PmrB (Rubin et al., 2015; Hong et al., 2018). Although PmrD was not found in *Y. enterocolitica* (Reinés et al., 2012b), the connections between PhoP/PhoQ and PmrA/

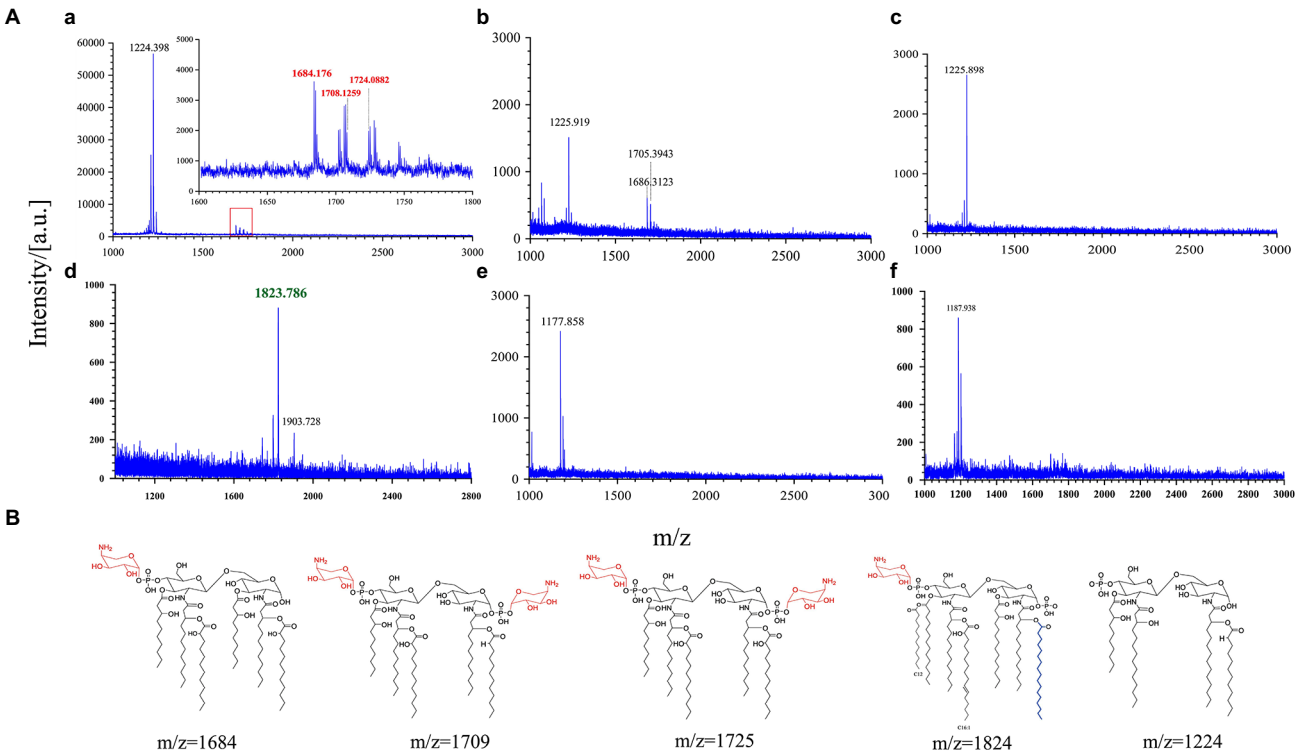

FIGURE 5 | PhoP/PhoQ regulates *Y. enterocolitica* to form different lipopolysaccharide (LPS) modifications. MALDI-TOF analysis of wild type and mutants treated with PMB or PME **(A)**. **(a–c)** Display the results of wild type, *phoP* mutants, and *phoQ* mutants treated with PMB and **(d–f)** display the results of wild type, *phoP* mutants, and *phoQ* mutants treated with PME. Possible structures of lipid A at different *m/z* **(B)**.

PmrB can also be revealed using small RNAs, which remain unclear in *Y. enterocolitica*. In this study, the transcription levels of lipid A modification genes were analyzed to determine the regulatory effects of PhoP/PhoQ on lipid A modification (**Figure 6**). When exposed to PMB or PME at the MIC, the transcription levels of the genes, *pagP* and *arnC*, in the mutant strains were both reduced compared to those in the wild type. When exposed to PMB, *pagP* was downregulated by an average of 71 and 83% in the *phoP* and *phoQ* mutants, respectively, whereas *arnC* was downregulated by an average of 67 and 78%, respectively. The transcription levels of these genes in the Δ*phoP-phoP* and Δ*phoQ-phoQ* strains were restored. Exposed to PME, *arnC* was downregulated by an average of 32.4 and 30.8% in the *phoP* and *phoQ* mutants, respectively. And *pagP* was downregulated by an average of 42.5 and 36%, respectively, in *phoP* and *phoQ* mutants. There are differences of genes transcription between PMB and PME treatment. It may be caused by the differences of these two AMPs, as LPS modifications formed by *Y. enterocolitica* were also various under PMB and PME.

Since the absent of PmrD, we speculated that PmrA/PmrB and PhoP/PhoQ independently regulated LPS modification pathways and without interaction. But the transcription levels of *pmrA*, *pmrB*, and *eptA* in the mutants were reduced to varying degrees compared with the wild type, indicating that the deletion of PhoP/PhoQ in *Y. enterocolitica* can also affect the transcription of the PmrA/PmrB system.

DISCUSSION

Polymyxins have been employed as "last resort" antimicrobials (Han et al., 2018a). Gaining a better understanding of the mechanism of resistance to polymyxin is of critical importance. Currently, there are two main mechanisms to explain bacterial resistance to polymyxin: intrinsic resistance (adaptive resistance), which relies on LPS modifications, such as L-Ara4N and pEtN; and *mcr* genes induced resistance, which are encoded on plasmids and phages (Trimble et al., 2016; MacNair et al., 2018; Simpson and Trent, 2019). In this study, PhoP/PhoQ was demonstrated to be essential for the resistance of *Y. enterocolitica* to polymyxins (**Figure 2**). This was mainly because PhoP/PhoQ conferred a more resistant membrane for the binding of polymyxin by regulating LPS modification related to AMP resistance (**Figures 4, 5**). However, the LPS modification of *Y. enterocolitica* under PMB and PME was found to be different (**Figure 5**). In the presence of PMB, a variety of lipid-modified structures containing L-Ara4N were detected. However, when exposed to PME, in addition to containing L-Ara4N, the structures of palmitate and C16:1 were also observed (*m/z* at 1,823). Thus, when *Y. enterocolitica* was exposed to different AMPs, the LPS modification was not totally the same. And L-Ara4N was the main structure for *Y. enterocolitica* to set the adaptive resistance to polymyxin. Deletion of *phoP* and *phoQ*

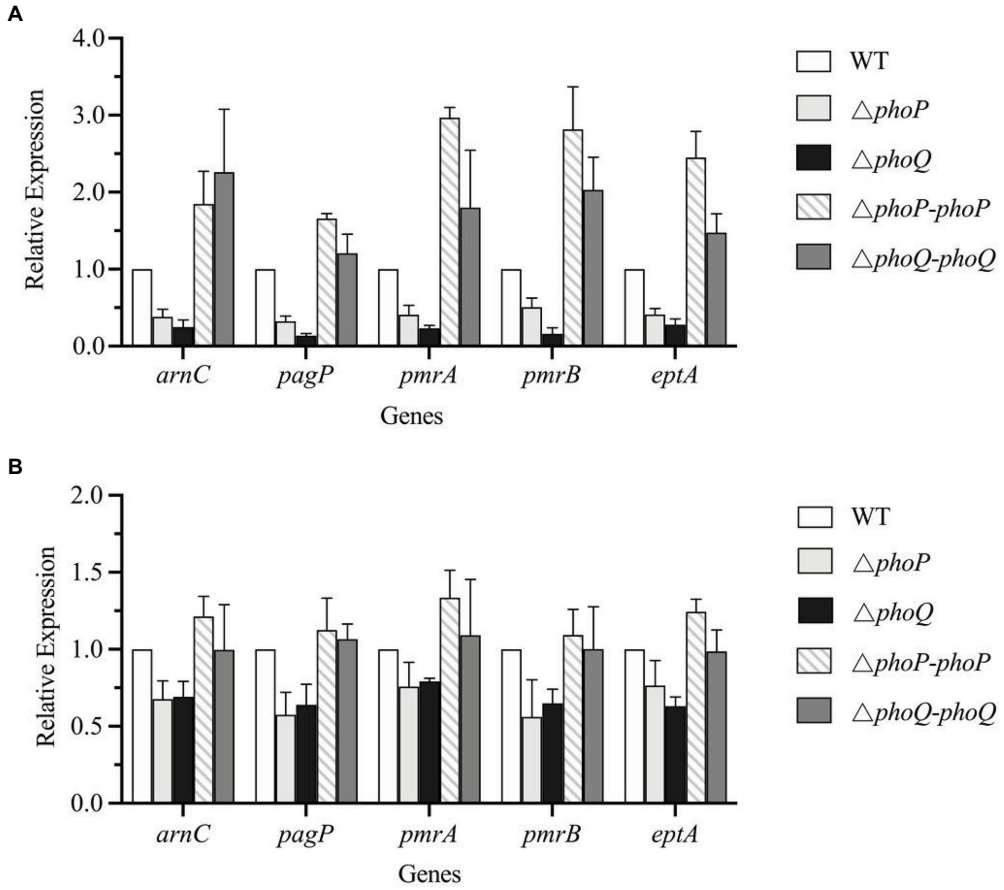

FIGURE 6 | PhoP/PhoQ is involved in the regulation of genes related to LPS modification. Transcriptional changes of wild type, mutants and complemented strains treated with PMB **(A)** and PME **(B)**.

in *Y. enterocolitica* resulted the downregulation of the *arnBCADTEF* and *papP* which encode enzymes that responsible for L-Ara4N and palmitate (**Figure 6**). These results emphasized the role of PhoP/PhoQ in response to polymyxin in *Y. enterocolitica*. LPS modification also reduced the binding ability of polymyxin to *Y. enterocolitica* (**Figure 4**). This decrease may be due to a reduction in the negative charge and resistance to polymyxin induced by charge repulsion (Simpson and Trent, 2019). In addition, steric hindrance and lipid A tail packing produced by LPS modification could decrease the fluidity of the outer membrane, which may also prevent polymyxin from binding to *Y. enterocolitica* (Khondker et al., 2019; Simpson and Trent, 2019). Studies have shown that polymyxin exerts antimicrobial activity by targeting the bacterial cell membrane and gradually destroys the outer and inner membranes (Brogden, 2005). The destruction of the inner and outer membranes also increased when PhoP/PhoQ was absent (**Figure 3**; **Supplementary Figure 2**). Besides, study has reported that polymyxin B causes malfunction of respiration and severe consumption of ATP, leading to cell death and carbon starvation. And maintaining ATP level benefits the polymyxin resistance (Yu et al., 2019). Similarly, in **Figures 3E,F**, it is showed that the mutants of *phoP* and *phoQ* were sensitive to polymyxins and maintained lower intercellular ATP content compared to wild type.

In most Gram-negative bacteria, the TCSs, PhoP/PhoQ and PmrA/PmrB, mediate polymyxin resistance by governing the LPS modification pathway (Trimble et al., 2016; Simpson and Trent, 2019). However, there are some differences in the LPS modification mechanisms among different Gram-negative bacteria, as shown in **Figure 1**. For example, PhoP phosphorylated in *Salmonella* can activate PmrA/PmrB through the protein, PmrD (Hong et al., 2018). Although PmrD in *E. coli* cannot function in the same manner as *Salmonella*, it is required for the modification of lipid A in *E. coli* under low Mg^{2+} growth conditions (Rubin et al., 2015). In *Klebsiella pneumoniae*, the *arn* operon can not only be regulated directly by PhoP/PhoQ, but also indirectly through PmrD (Chen et al., 2021). In *Yersinia pestis*, despite the lack of PmrD, protein lipid A with L-Ara4N can be promoted by PhoP dependently and independently through different inducing signals (Winfield et al., 2005). Based on our results, the role of PhoP/PhoQ in intrinsic resistance mechanism of *Y. enterocolitica* to polymyxins summarized

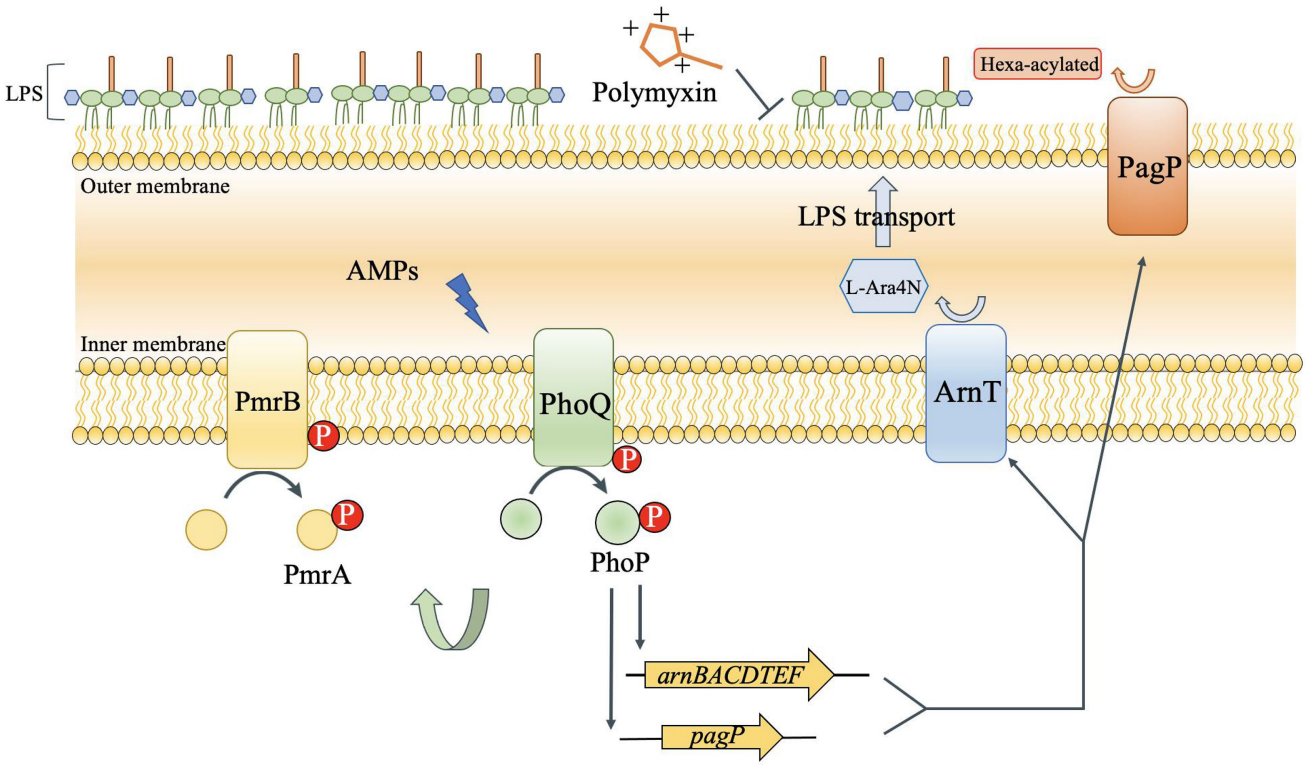

FIGURE 7 | Regulation of LPS modification by the PhoP/PhoQ pathway of *Y. enterocolitica* to increase self-induced resistance to polymyxin. PhoP/PhoQ regulates genes that encode enzymes that alter acylation (*PagP*) and modify phosphates with aminoarabinose (*arnT*). The activity of PhoP can also affect the transcription of *pmrA* and *pmrB*. The increased modification of lipid A by *ArnT* and *PagP* alters the charge of the outer membrane and accumulates lipid tail packing to decrease the fluidity, which caused the resistance of *Y. enterocolitica* to AMP.

as shown in **Figure 7**. The modification of LPS with L-Ara4N and palmitate regulated by PhoP/PhoQ increase the resistance of *Y. enterocolitica*. It reduces the binding ability of polymyxin to cell membrane. For the cross-regulation between PhoP/PhoQ and PmrA/PmrB, although PmrD was absent in *Y. enterocolitica*, and such pEtN structure was not observed under PMB and PME (**Figure 5**), the connection between PhoP/PhoQ and PmrA/PmrB was also observed. By comparing the results of gene expression analysis, the transcription of *pmrA*, *pmrB*, and *eptA* in the *phoP* and *phoQ* mutants was downregulated (**Figure 6**). Besides, for *Y. enterocolitica*, the intrinsic resistance mechanism induced by PhoP/PhoQ showed difference compared with *Salmonella*, not only the absent of PmrD, but also other genes such as *lpxT* lacking a PhoP binding site (Hong et al., 2018). And lipid A containing L-Ara4N has still been detected in *phoP* mutants (**Figure 5**), these all indicates that the response to polymyxin is not independently regulated by PhoP/PhoQ. Some non-coding small RNAs may play an important role in regulation pathways in *Y. enterocolitica* (Simpson and Trent, 2019). But, detail mechanism of the intrinsic resistance needs further study.

Although the regulation pathway of PhoP/PhoQ in the presence of polymyxin in *Y. enterocolitica* is not completely understood, we demonstrated the role of PhoP/PhoQ to increase the resistance of *Y. enterocolitica* to polymyxins. And we also raised some new tasks to find out the mechanism of the intrinsic resistance in *Y. enterocolitica*. Firstly, finding out the other potential regulatory factors involved in the connection between PhoP/PhoQ and PmrA/PmrB. Secondly, screening other regulatory factors involved in lipid A modifications which enhance the intrinsic resistance to polymyxins.

CONCLUSION

All in all, it is important to gain a better understanding of the intrinsic resistance toward polymyxin in Gram-negative bacteria. In this study, the role of PhoP/PhoQ in *Y. enterocolitica* intrinsic resistance to polymyxins was demonstrated. The existence of PhoP/PhoQ in *Y. enterocolitica* showed a higher resistance to polymyxins, which was mainly caused by the modification of LPS with palmitate and L-Ara4N, and regulated by PhoP/PhoQ, conferring a more resistant membrane for the binding of polymyxin. According to the transcription analysis, the PhoP/PhoQ of *Y. enterocolitica* not only regulated LPS modification genes, but also affected the transcription of PmrA/PmrB. These findings expand our understanding of the intrinsic resistance to polymyxin in

Y. enterocolitica and expand current knowledge regarding the role of PhoP/PhoQ in Enterobacteriaceae.

DATA AVAILABILITY STATEMENT

All datasets generated for this study are included in the article/**Supplementary Material**.

AUTHOR CONTRIBUTIONS

HG performed the experiments under the guidance of JC, analyzed the experimental data, and drafted the manuscript. JC and HG developed the idea for the study and designed the research. TZ and CH made substantial contributions to conception, interpretation of data and revised the manuscript. All authors have read and approved the final manuscript.

FUNDING

This work was supported by the Beijing Natural Science Foundation (6202016) and the National Natural Science Foundation of China (31671830).

SUPPLEMENTARY MATERIAL

The Supplementary Material for this article can be found online at: https://www.frontiersin.org/articles/10.3389/fmicb.2022.758571/full#supplementary-material

REFERENCES

Akhoundsadegh, N., Belanger, C. R., and Hancock, R. E. W. (2019). Outer membrane interaction kinetics of new polymyxin B analogs in Gram-negative bacilli. *Antimicrob. Agents Chemother.* 63, 1–13. doi: 10.1128/AAC.00935-19

Bader, M. W., Sanowar, S., Daley, M. E., Schneider, A. R., Cho, U., Xu, W., et al. (2005). Recognition of antimicrobial peptides by a bacterial sensor kinase. *Cell* 122, 461–472. doi: 10.1016/j.cell.2005.05.030

Bader, J., and Teuber, M. (1973). Binding to the O-antigenic lipopolysaccharide of *Salmonella* typhimurium. *Z. Naturforsch.* 28, 422–430.

Brogden, K. A. (2005). Antimicrobial peptides: pore formers or metabolic inhibitors in bacteria? *Nat. Rev. Microbiol.* 3, 238–250. doi: 10.1038/nrmicro1098

Chen, A. I., Albicoro, F. J., Zhu, J., and Goulian, M. (2021). Effects of regulatory network organization and environment on PmrD connector activity and polymyxin resistance in *Klebsiella pneumoniae* and *Escherichia coli*. *Antimicrob. Agents Chemother.* 65, e00889–20. doi: 10.1128/AAC.00889-20

Clementi, E. A., Marks, L. R., Roche-Håkansson, H., and Håkansson, A. P. (2014). Monitoring changes in membrane polarity, membrane integrity, and intracellular ion concentrations in *Streptococcus pneumoniae* using fluorescent dyes. *J. Vis. Exp.* 84, 1–8. doi: 10.3791/51008

CLSI (2017). *M100 Performance Standards for Antimicrobial Susceptibility Testing. 27th Edn*. Clinical and Laboratory Standards Institute.

Cullen, T. W., Giles, D. K., Wolf, L. N., Ecobichon, C., Boneca, I. G., and Trent, M. S. (2011). Helicobacter pylori versus the host: remodeling of the bacterial outer membrane is required for survival in the gastric mucosa. *PLoS Pathog.* 7:e1002454. doi: 10.1371/journal.ppat.1002454

Duperthuy, M. (2020). Antimicrobial peptides: virulence and resistance modulation in Gram-negative bacteria. *Microorganisms* 8:280. doi: 10.3390/microorganisms8020280

Han, M. L., Velkov, T., Zhu, Y., Roberts, K. D., Le Brun, A. P., Chow, S. H., et al. (2018a). Polymyxin-induced lipid A deacylation in *Pseudomonas aeruginosa* perturbs polymyxin penetration and confers high-level resistance. *ACS Chem. Biol.* 13, 121–130. doi: 10.1021/acschembio.7b00836

Han, M. L., Zhu, Y., Creek, D. J., Lin, Y. W., Anderson, D., Shen, H. H., et al. (2018b). Alterations of metabolic and lipid profiles in polymyxin-resistant *Pseudomonas aeruginosa*. *Antimicrob. Agents Chemother.* 62, 1–14. doi: 10.1128/AAC.02656-17

Hankins, J. V., Madsen, J. A., Needham, B. D., Brodbelt, J. S., and Trent, M. S. (2013). The outer membrane of Gram-negative bacteria: lipid A isolation and characterization. *Methods Mol. Biol.* 966, 239–258. doi: 10.1007/978-1-62703-245-2_15

Henderson, J. C., O'Brien, J. P., Brodbelt, J. S., and Trent, M. S. (2013). Isolation and chemical characterization of lipid A from Gram-negative bacteria. *J. Vis. Exp.* 79, 1–11. doi: 10.3791/50623

Hoch, J. A. (2000). Two-component and phosphorelay signal transduction. *Curr. Opin. Microbiol.* 3, 165–170. doi: 10.1016/S1369-5274(00)00070-9

Hong, X., Chen, H. D., and Groisman, E. A. (2018). Gene expression kinetics governs stimulus-specific decoration of the *Salmonella* outer membrane. *Sci. Signal.* 11, 1–12. doi: 10.1126/scisignal.aar7921

Khondker, A., Dhaliwal, A. K., Saem, S., Mahmood, A., Fradin, C., Moran-Mirabal, J., et al. (2019). Membrane charge and lipid packing determine polymyxin-induced membrane damage. *Commun. Biol.* 2, 1–11. doi: 10.1038/s42003-019-0297-6

Lee, D. S., and Je, J. Y. (2013). Gallic acid- grafted -chitosan inhibits foodborne pathogens by a membrane damage mechanism. *J. Agric. Food Chem.* 61, 6574–6579. doi: 10.1021/jf401254g

Lin, Z., Cai, X., Chen, M., Ye, L., Wu, Y., Wang, X., et al. (2018). Virulence and stress responses of *Shigella flexneri* regulated by PhoP/PhoQ. *Front. Microbiol.* 8:2689. doi: 10.3389/fmicb.2017.02689

MacNair, C. R., Stokes, J. M., Carfrae, L. A., Fiebig-Comyn, A. A., Coombes, B. K., Mulvey, M. R., et al. (2018). Overcoming mcr-1 mediated colistin resistance with colistin in combination with other antibiotics. *Nat. Commun.* 9:458. doi: 10.1038/s41467-018-02875-z

Meng, J., Huang, C., Huang, X., Liu, D., Han, B., and Chen, J. (2020). Osmoregulated periplasmic glucans transmit external signals through Rcs phosphorelay pathway in *Yersinia enterocolitica*. *Front. Microbiol.* 11:122. doi: 10.3389/fmicb.2020.00122

Minagawa, S., Ogasawara, H., Kato, A., Yamamoto, K., Eguchi, Y., Oshima, T., et al. (2003). Identification and molecular characterization of the Mg^{2+} stimulon of *Escherichia coli*. *J. Bacteriol.* 185, 3696–3702. doi: 10.1128/JB.185.13.3696-3702.2003

Mitchell, A. M., and Silhavy, T. J. (2019). Envelope stress responses: balancing damage repair and toxicity. *Nat. Rev. Microbiol.* 17, 417–428. doi: 10.1038/s41579-019-0199-0

Prost, L. R., Daley, M. E., Le Sage, V., Bader, M. W., Le Moual, H., Klevit, R. E., et al. (2007). Activation of the bacterial sensor kinase PhoQ by acidic pH. *Mol. Cell* 26, 165–174. doi: 10.1016/j.molcel.2007.03.008

Rahnamaeian, M. (2011). Antimicrobial peptides: modes of mechanism, modulation of defense responses. *Plant Signal. Behav.* 6, 1325–1332. doi: 10.4161/psb.6.9.16319

Reinés, M., Llobet, E., Dahlström, K. M., Pérez-Gutiérrez, C., Llompart, C. M., Torrecabota, N., et al. (2012a). Deciphering the acylation pattern of *Yersinia enterocolitica* lipid A. *PLoS Pathog.* 8:e1002978. doi: 10.1371/journal.ppat.1002978

Reinés, M., Llobet, E., Llompart, C. M., Moranta, D., Pérez-Gutiérrez, C., and Bengoechea, J. A. (2012b). Molecular basis of *Yersinia enterocolitica* temperature-dependent resistance to antimicrobial peptides. *J. Bacteriol.* 194, 3173–3188. doi: 10.1128/JB.00308-12

Rubin, E. J., Herrera, C. M., Crofts, A. A., and Trent, M. S. (2015). PmrD is required for modifications to *Escherichia coli* endotoxin that promote antimicrobial resistance. *Antimicrob. Agents Chemother.* 59, 2051–2061. doi: 10.1128/AAC.05052-14

Santos, D. E. S., Pol-Fachin, L., Lins, R. D., and Soares, T. A. (2017). Polymyxin binding to the bacterial outer membrane reveals cation displacement and increasing membrane curvature in susceptible but not in resistant lipopolysaccharide chemotypes. *J. Chem. Inf. Model.* 57, 2181–2193. doi: 10.1021/acs.jcim.7b00271

Schäfer, A., Tauch, A., Jäger, W., Kalinowski, J., Thierbach, G., and Pühler, A. (1994). Small mobilizable multi-purpose cloning vectors derived from the Escherichia coli plasmids pK18 and pK19: selection of defined deletions in the chromosome of *Corynebacterium glutamicum*. *Gene* 145, 69–73. doi: 10.1016/0378-1119(94)90324-7

Schindler, P. R. G., and Teuber, M. (1975). Action of polymyxin B on bacterial membranes: morphological changes in the cytoplasm and in the outer membrane of *Salmonella* typhimurium and *Escherichia coli* B. *Antimicrob. Agents Chemother.* 8, 95–104. doi: 10.1128/AAC.8.1.95

Shoaib, M., Shehzad, A., Raza, H., Niazi, S., Khan, I. M., Akhtar, W., et al. (2019). A comprehensive review on the prevalence, pathogenesis and detection of *Yersinia enterocolitica*. *RSC Adv.* 9, 41010–41021. doi: 10.1039/c9ra06988g

Shprung, T., Peleg, A., Rosenfeld, Y., Trieu-Cuot, P., and Shai, Y. (2012). Effect of PhoP-PhoQ activation by broad repertoire of antimicrobial peptides on bacterial resistance. *J. Biol. Chem.* 287, 4544–4551. doi: 10.1074/jbc.M111.278523

Simpson, B. W., and Trent, M. S. (2019). Pushing the envelope: LPS modifications and their consequences. *Nat. Rev. Microbiol.* 17, 403–416. doi: 10.1038/s41579-019-0201-x

Trimble, M. J., Mlynárčik, P., Kolář, M., and Hancock, R. E. W. (2016). Polymyxin: alternative mechanisms of action and resistance. *Cold Spring Harb. Perspect. Med.* 6:a025288. doi: 10.1101/cshperspect.a025288

Véscovi, E. G., Ayala, Y. M., Di Cera, E., and Groisman, E. A. (1997). Characterization of the bacterial sensor protein PhoQ: evidence for distinct binding sites for Mg^{2+} and Ca^{2+}. *J. Biol. Chem.* 272, 1440–1443. doi: 10.1074/jbc.272.3.1440

West, A. H., and Stock, A. M. (2001). Histidine kinases and response regulator proteins in two-component signaling systems. *Trends Biochem. Sci.* 26, 369–376. doi: 10.1016/S0968-0004(01)01852-7

Winfield, M. D., Latifi, T., and Groisman, E. A. (2005). Transcriptional regulation of the 4-amino-4-deoxy-L-arabinose biosynthetic genes in *Yersinia pestis*. *J. Biol. Chem.* 280, 14765–14772. doi: 10.1074/jbc.M413900200

Yu, W., Yu, W., Pan, Q., and Ye, B. (2019). Glucose-induced cyclic lipopeptides resistance in bacteria via ATP maintenance through enhanced glycolysis glucose-induced cyclic lipopeptides resistance in bacteria via ATP maintenance through enhanced glycolysis. *iScience* 21, 135–144. doi: 10.1016/j.isci.2019.10.009

Zwir, I., Latifi, T., Perez, J. C., Huang, H., and Groisman, E. A. (2012). The promoter architectural landscape of the *Salmonella* PhoP regulon. *Mol. Microbiol.* 84, 463–485. doi: 10.1111/j.1365-2958.2012.08036.x

Conflict of Interest: The authors declare that the research was conducted in the absence of any commercial or financial relationships that could be construed as a potential conflict of interest.

Publisher's Note: All claims expressed in this article are solely those of the authors and do not necessarily represent those of their affiliated organizations, or those of the publisher, the editors and the reviewers. Any product that may be evaluated in this article, or claim that may be made by its manufacturer, is not guaranteed or endorsed by the publisher.

frontiers in Microbiology

ORIGINAL RESEARCH
published: 17 March 2022
doi: 10.3389/fmicb.2022.827545

A Plasmid With Conserved Phage Genes Helps *Klebsiella pneumoniae* Defend Against the Invasion of Transferable DNA Elements at the Cost of Reduced Virulence

Mufeng Cai[1†], Bingchun Pu[1†], Yue Wang[1], Lin Lv[2], Chunyu Jiang[1], Xiaomei Fu[1], Yan Zhang[3,4], Wei Zhao[5], Ke Dong[3,4], Yi Yang[1], Yangming Liu[1], Yalu Wei[1], Zhengyue Zhang[1], Jianhui Li[6], Xiaokui Guo[3,4], Chang Liu[1,3,4] and Jinhong Qin[1,6,7]**

[1] Department of Microbiology and Immunology, Shanghai Jiao Tong University School of Medicine, Shanghai, China, [2] Shanghai Institute of Immunology, Shanghai Jiao Tong University School of Medicine, Shanghai, China, [3] Chinese Center for Tropical Diseases Research, School of Global Health, Shanghai Jiao Tong University School of Medicine, Shanghai, China, [4] One Health Center, Shanghai Jiao Tong University-The University of Edinburgh, Shanghai, China, [5] Experiment Teaching Center of Basic Medicine, Shanghai Jiao Tong University School of Medicine, Shanghai, China, [6] Shanghai Public Health Clinical Center, Shanghai Institute of Phage, Fudan University, Shanghai, China, [7] NHC Key Laboratory of Parasite and Vector Biology (National Institute of Parasitic Diseases, Chinese Center for Disease Control and Prevention), Shanghai, China

OPEN ACCESS

Edited by:
Dongsheng Zhou,
Beijing Institute of Microbiology and Epidemiology, China

Reviewed by:
Jason Gill,
Texas A&M University, United States
Andrew Spiers,
Abertay University, United Kingdom

***Correspondence:**
Chang Liu
tiantianlc@sjtu.edu.cn
Jinhong Qin
jinhongqin@sjtu.edu.cn

[†] These authors have contributed equally to this work

Specialty section:
This article was submitted to Infectious Agents and Disease, a section of the journal Frontiers in Microbiology

Received: 02 December 2021
Accepted: 17 February 2022
Published: 17 March 2022

Citation:
Cai M, Pu B, Wang Y, Lv L, Jiang C, Fu X, Zhang Y, Zhao W, Dong K, Yang Y, Liu Y, Wei Y, Zhang Z, Li J, Guo X, Liu C and Qin J (2022) A Plasmid With Conserved Phage Genes Helps Klebsiella pneumoniae Defend Against the Invasion of Transferable DNA Elements at the Cost of Reduced Virulence. Front. Microbiol. 13:827545. doi: 10.3389/fmicb.2022.827545

Klebsiella pneumoniae exhibits extensive phenotypic and genetic diversity. Higher plasmid loads in the cell were supposed to play an key role in its genome diversity. Although some plasmids are widely distributed in *Kp* populations, they are poorly recognized. A plasmid named p2 in strain *Kp1604* was predicted to be an intact prophage like *Salmonella* phage SSU5. However, our study showed that p2 was specifically packaged into membrane vesicles (MVs) rather than phage particles triggered by mitomycin C and subinhibitory concentrations of antibiotics. p2-minus mutant *Kp1604*Δ*p2* did not affect MV production. Compared with *Kp1604*, the capacity of plasmid uptake and the amount of phage burst of *Kp1604*Δ*p2* were improved. Moreover, virulence of *Kp1604*Δ*p2* also increased. Our results indicated that p2 could contribute to the host defense against the invasion of transferable DNA elements at the cost of reduced virulence. Further study on the mechanism will help us understand how it provides adaptive phenotypes to host evolution.

Keywords: transferable element, *Klebsiella pneumonia*, plasmid, membrane vesicles (MVs), virulence

INTRODUCTION

Klebsiella pneumoniae (*Kp*) is a gram-negative bacterium belonging to *Enterobacteriaceae*, in which there are also the well-known genera *Salmonella* and *Escherichia* (Wyres et al., 2020). *Kp* can survive in a wide range of host-associated and environmental niches. It can cause a variety of serious hospital-acquired infections, especially in patients with a compromised immune system. Hypervirulent *Kp* (hvKp) infections could cause lethal infections, such as liver abscesses, pneumoniae, meningitis, etc., and have therefore worsened public health worldwide since the early 1980s (Liu et al., 1986). HvKp is an evolving pathotype from classical *Kp* (cKp) due to its acquisition of a cluster of virulence factors encoded on a virulence plasmid and other mobile

chromosomally integrated genetic elements (Marr and Russo, 2018; Russo and Marr, 2019). HvKp was rarely resistant to commonly used antimicrobial agents except for being intrinsically resistant to ampicillin for a long period of time after discovery.

In 1996, carbapenem-resistant *Kp* (CRKp) was originally identified in regional outbreaks in the United States (Yigit et al., 2001; Tzouvelekis et al., 2012; Munoz-Price et al., 2013). From then on, multidrug-resistant (MDR) and extremely drug-resistant (XDR) strains continued to emerge as acquisition of plasmids or other transferable genetic elements carrying different antibiotic resistance genes (Munoz-Price et al., 2013; Chen et al., 2014; Wyres and Holt, 2016; Lam et al., 2019). Nowadays, carbapenem-resistant hvKp isolates have emerged (Lam et al., 2019). The emergence of such strains is supposed to be the dissemination of mobile plasmids encoding carbapenemases among HvKp strains or the acquisition of a virulence plasmid by carbapenem-resistant Kp (Wyres et al., 2020). For example, a conjugative plasmid p15 WZ-82_Vir simultaneously encoding antimicrobial resistance (AMR) and virulence determinants was reported, which formed because of the integration of a 100-kb fragment of the hypervirulence plasmid pLVPK into a conjugative IncFIB carbapenem-resistant plasmid (Yang et al., 2019). Such an hv-AMR plasmid could rapidly spread and cause serious infections with extremely limited treatment options, further exacerbating the public health threat posed by Kp (Gao et al., 2020).

Kp population has exhibited extensive phenotypic and genetic diversity (Wyres and Holt, 2016; Wyres et al., 2020). However, if only the genes encoded by the core genome were compared, the *Kp* genomics were conserved (Wyres and Holt, 2016; Wyres et al., 2020). The diversity of pan-genome in *Kp* is primarily due to mobile elements that can move frequently by horizontal transfer, including plasmids, phages, integrative and conjugative elements (ICEs), and insertion elements (ISs) (Wyres and Holt, 2016; Wyres et al., 2020). Among the sequenced *Kp* isolates, some strains carried up to 10 different plasmids (Conlan et al., 2016; Wyres et al., 2020). It seems that *Kp* may be particularly permissive for plasmid uptake and/or maintenance, resulting in plasmid loads that are typically greater than those reported for other *Enterobacteriaceae*. Although plasmids are key contributors to the spread of virulence and antibiotic resistance genes, some plasmids that do not encode any known function beyond those may still provide a fitness advantage to their hosts. We sequenced a strain named *Kp1604,* which contained a 5.2 Mb chromosome and 2 plasmids. p1 encoded virulence-related genes, while p2 encoded several conserved phage genes. In this study, we investigated the function and role of plasmid p2 in *Kp1604.*

MATERIALS AND METHODS

Bacterial Strains and Culture Conditions

Klebsiella pneumoniae strains, phage and plasmids used in this study are listed in **Supplementary Table 1** with their genome accession number if available. The *Kp* strains was sampled from patients as part of routine work in hospital treatment. Competent *Escherichia coli* DH5α was purchased from Takara Biomedical Technology (Beijing) Co., Ltd, Beijing, China. When needed, 50 mg/mL apramycin or spectinomycin was added to the LB broth (1% tryptone, 0.5% yeast extract, 1% NaCl; Sigma-Aldrich, St. Louis, WI, United States).

Genome Sequencing and Analysis of *Kp1604*

Strain *Kp1604* was grown in LB broth at 37°C with shaking until an OD_{600} of 0.5∼1. DNA from *Kp1604* was extracted and genome sequencing was performed with the PacBio Sequel and Illumina NovaSeq platforms at Shanghai Personal Biotechnology Co., Ltd. The assembly of the whole-genome sequence was carried out by HGAP (Chin et al., 2016) and CANU (Koren et al., 2017). Gene prediction was carried out by GeneMarkS (Besemer et al., 2001).

For further sequence analysis of strain *Kp1604*, the predicted genes were blasted with the VFDB[1] and CARD[2] to identify virulence factors and antibiotic resistance genes. Multilocus sequence typing (MLST) and capsular typing by the wzi allele was performed online.[3] The CRISPR-Cas systems, genomics islands, insertion sequences, prophages and replicons were analyzed online by CRISPRCas Finder,[4] islandviewer,[5] ISfinder,[6] Phaster[7] and PlasmidFinder 2.1 (Carattoli and Hasman, 2020).

Bioinformatics Analysis of Plasmid p1 and p2

A comparative plasmid map of p1 (CP085479) in strain *Kp1604* with three known virulence plasmids of phvKp060 (CP034776.1), pK2044 (AP006726.1), and pLVPK (Y378100) was drawn with BLAST Ring Image Generator (BRIG) using pLVPK as a reference sequence (Alikhan et al., 2011).

For comparative analysis of plasmid p2 in strain *Kp1604*, BLASTn search of p2 (CP085480) with the *Kp* strains (**Supplementary Table 1**) sequenced in this study showed sequence similarity with plasmids of pKp1 (CP086286) and pAF41-1 (JAJGSV000000000). Further, the sequences of *Enterobacteriaceae* plasmids publicly available (2,423 in total) were downloaded from BACTERIAL BIOINFORMATICS RESOURCE CENTER, PATRIC.[8] The PlasmidFinder 2.1 tools was used to identify replicons in the plasmid sequences (Carattoli and Hasman, 2020). For plasmid cluster analysis, annotation for each plasmid sequence was generated using Prokka (Seemann, 2014) with default parameters. After annotation, 2,426 plasmids were clustered by gene overlap method as following. General Feature Format Version 3 (Gff3) files generated by Prokka were analyzed for gene presence/absence matrix by Roary (Page et al., 2015) with default parameters. To build a plasmid gene presence/absence, matrix in which each entry was 1 if

[1]http://www.mgc.ac.cn/VFs/

[2]https://card.mcmaster.ca/

[3]https://bigsdb.pasteur.fr

[4]http://crispr.i2bc.paris-saclay.fr/Server/

[5]https://www.pathogenomics.sfu.ca/islandviewer/

[6]https://www-is.biotoul.fr/

[7]http://phaster.ca/

[8]https://www.patricbrc.org/

plasmid contained a homolog found in gene cluster or 0 if plasmid did not contain a homolog found in gene cluster. With the matrix, the percentage of gene overlap was calculated by dividing the overlapping gene cluster by all gene clusters of any two plasmid sequences. Then, plasmids were clustered by the Markov cluster algorithm based on gene overlap (van Dongen and Abreu-Goodger, 2012). Network construction Adjacency matrices and network edge lists were created in R. The map of the sequence comparison across plasmid clusters was drawn by Easyfig (Sullivan et al., 2011).

Antimicrobial Susceptibility Testing and Isolation of Membrane Vesicles

Frozen stock *Kp1604* was grown in LB broth at 37°C overnight. The MICs of chloramphenicol (CHL), tetracycline (TET), ciprofloxacin (CIP) and kanamycin (KAN) were determined by microdilution methods according to the Clinical Laboratory Standards Institute (CLSI), and 1/2 MICs of them used in this study were 4, 4, 2, and 16 μg/mL, respectively. For isolation of membrane vesicles (MVs) from *Kp1604*, overnight cultures were adjusted to a starting OD_{600} of 0.1. Cells were grown until an OD_{600} of 0.6 at 37°C with shaking and then supplemented with 5 μg/mL mitomycin C, 1/2 MIC CHL (4 μg/mL), TET (4 μg/mL), CIP (2 μg/mL), or KAN (16 μg/mL) and cultured for 8 h. Cells cultured without any antibiotics was grown at same conditions as control. Cultured bacterial cells were removed from the supernatant by centrifugation at 8,000 g for 15 min at 4°C. The supernatant was filtered through 0.22 μm pore size filters to remove intact cells and debris. The collected supernatant was further dialyzed against phosphate-buffered saline (PBS) buffer three times for 4 h each time. The MVs were then pelleted through ultracentrifugation at 100,000 g for 1 h at 4°C. The pellets were resuspended in PBS buffer for further experiments. To verify the absence of intact cells in the filtered supernatant, 0.2 mL was plated on LB agar and grown at 37°C for 24 h. The purified MVs was stored at 4°C for further analysis.

Membrane Vesicles Size and Distribution Determination

The purified MVs from 30 mL cultures of *Kp1604* were dissolved in 0.5 mL PBS. The size (diameter) and size distribution profile of MVs was determined by Zetasizer Nano S equipped with 4.0 mW He-Ne laser (633 nm) (Malvern Instruments Ltd., Worcestershire, United Kingdom).

TABLE 1 | General features of the *Kp1604* chromosomes.

Features	Chromosome	Plasmid	
		p1	p2
Size (bp)	5,205,350	144,892	109,308
GC content	57.58%	49.69%	48.93%
No. of ORFs	4,855	172	118
Coding percentage	86.46%	81.40%	86.56%
Number of rRNAs	25	0	0
Number of tRNAs	86	0	1
Predicted intact prophage	0	0	1
Genomic islands	21	–	–
Insertion sequence	41	82	0
Replicon	–	IncFIB	IncFIB

Electron Microscopy

The purified MVs was negatively stained with 2% phosphotungstic acid and the morphology was examined by transmission electron microscopy (Tecnai G2 Spirit Biotwin, FEI COMPANY, Hillsboro, QR, United States).

DNA and Proteome Analysis of Membrane Vesicles

The purified MVs was treated with DNase I Takara Biomedical Technology (Beijing) Co., Ltd, Beijing, China at 37°C for 30 min. To test whether the DNA outside the vesicles was completely removed, 2 μl treated MVs was heated at 100°C for 10 min and 16S rRNA sequence was amplified with primers of 27F and 1492R (**Supplementary Table 2**). DNA from the treated MVs was extracted using the QIAamp DNA Mini Kit (Qiagen, Venlo Netherlands), following manufacturer's instructions. Sequencing was performed with the Illumina NovaSeq platform at the Chinese National Human Genome Center at Shanghai. The sequence result of *Kp1604-MV* was deposited in GenBank with accession number OK644452. For PCR verification of DNA contained in MVs, two pairs of primers (p1-1-F and p1-1-R, p1-2-F, and p1-2-R) were designed to amplify p1-1 and p1-2 sequence fragment in p1 (**Supplementary Table 2**). Two pairs of primers (p2-1-F and p2-1-R, p2-2-F and p2-2-R) were designed to amplify p2-1 and p2-2 sequence fragment in p2 (**Supplementary Table 2**). 16S rRNA sequences was amplified with primers 27F and 1492R.

For proteome analysis of MVs, the purified MV sample was analyzed on a Thermo Fusion Lumos mass spectrometer connected to an Easy-nLC 1200 *via* an Easy Spray (Thermo Fisher, Waltham, MA, United States) according to the protocol. All MS/MS ion spectra were analyzed using PEAKS 10.0 (Bioinformatics Solutions, Waterloo, ON, Canada) for processing, *de novo* sequencing and database searching. Subcellular localization of the proteins identified in MVs was predicted by Psort (Nakai and Horton, 1999).

Construction of p2-Minus Strain

To delete p2 from strain *Kp1604*, a two-plasmid CRISPR-Cas system was used as previously described (Wang et al., 2018). Preparation of competent *Kp1604* cells and electroporation were carried out as previously described (Wang et al., 2018). Briefly, temperature-sensitive pCasKP-apr was electroporated into *Kp1604*. The CRISPR–Cas9 spacer plasmid was constructed by cloning the *rep* gene sequence (5′-GAGCAAACCTGAGAAGCCAG-3′) of p2 into pSGKP-spe. The resulting plasmid was electroporated into the pCasKP-apr-harboring strain *Kp1604*. The two-plasmid CRISPR-Cas system was cured as described (Wang et al., 2018). The successful p2-minus mutant *Kp1604△p2* was verified by PCR with primers (p2-1-F and p2-1-R, p2-2-F, and p2-2-R) to amplify p2-1 and p2-2 sequence fragment in p2.

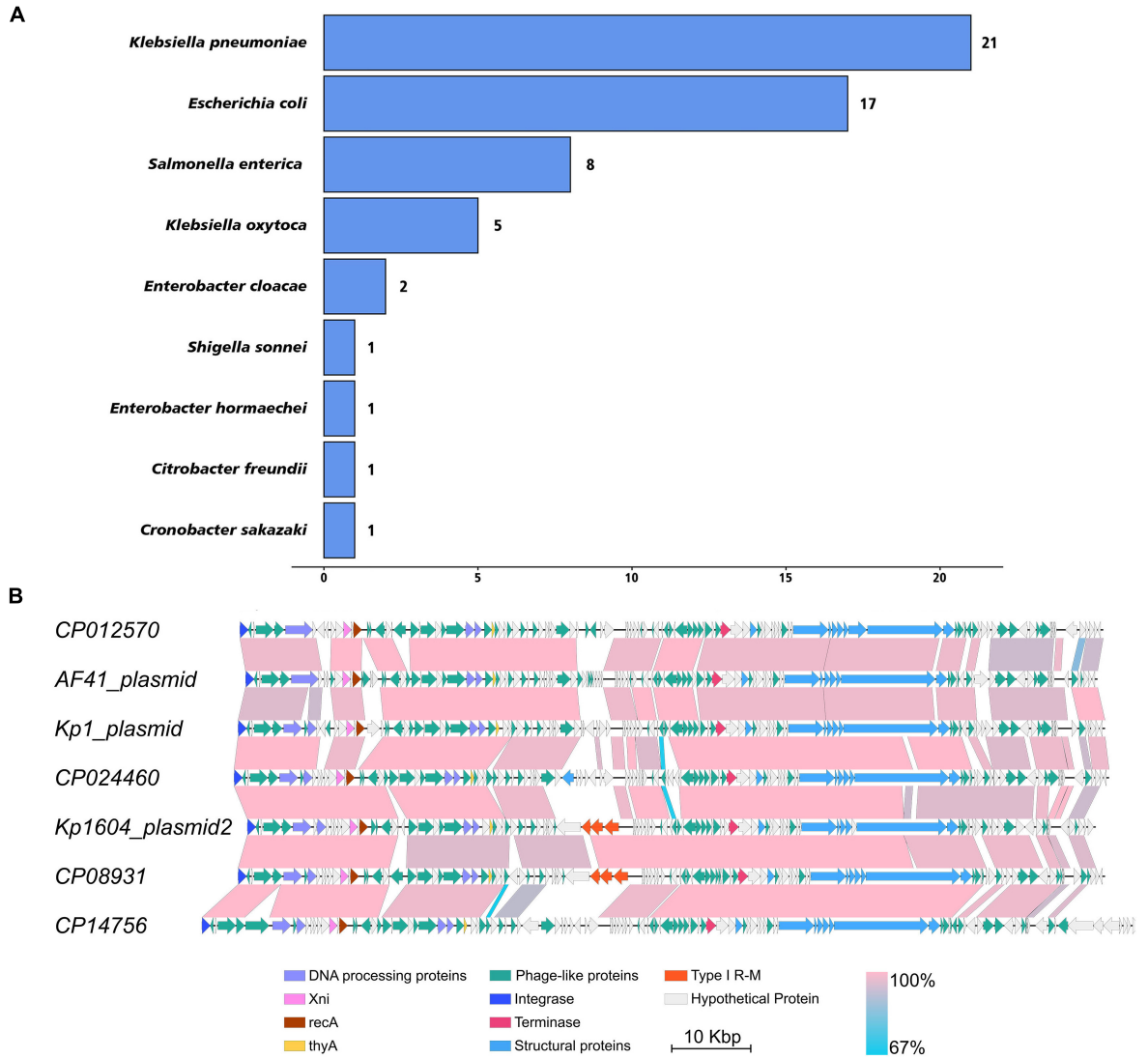

FIGURE 1 | The distribution of p2-like plasmids in *Enterobacteriaceae* and sequence alignment of p2-like plasmids. **(A)** The distribution of p2-like plasmids in *Enterobacteriaceae*. A total of 2,426 plasmid sequences were downloaded and clustered. 57 of them were clustered as p2-like plasmids, which were mainly distributed in *Klebsiella pneumoniae, Escherichia coli, Salmonella enterica, and Klebsiella oxytoca.* **(B)** Sequence alignment of the complete genome of selected p2-like plasmids. The nucleotide identity of the homologous regions (percentage) is indicated in color; the scale is shown below. Known functional homologous genes are shown below.

Efficiency of Plasmid Transformation and Phage Infection

To test the efficiency of plasmid transformation, pSGKP-spe was electroporated into competent *Kp1604* and *Kp1604p2* (Wang et al., 2018). *Kp1604* and *Kp1604*△*p2* were electroporated without plasmid as controls. Transformation frequency is defined as the number of pSGKP-spe-containing transformants divided by the number of control cells that survived electroporation. We evaluated the efficiency of phage infecting *Kp1604* and *Kp1604*△*p2* by phage spot plaque tittering method as following. 2 μl aliquots of 10-fold serial dilutions of bacteriophage Φ1209, Φ168R, and Φ 9226R were spotted on bacterial *Kp1604* and *Kp1604*△*p2* lawns to examine plaque formation. The plaque morphology of bacteriophages Φ1209, Φ168R, and Φ 9226R was observed by the soft-agar overlay method (Luong et al., 2020), 10 μl of serially diluted bacteriophage Φ1209, Φ168R, and Φ 9226R was used to infect 100 μl culture of *Kp1604* and *Kp1604*△*p2* in a 4 mL overlay of LB containing 0.7% agar. Infection plates were incubated at 37℃ for 4∼8 h to observe the phage plaque formation.

Mouse Infection Studies of *Kp1604* and *Kp1604*△*p2*

Female 6∼8 weeks old BALB/c mice were purchased from the Shanghai SLAC Laboratory Animal Co., Ltd. All animal

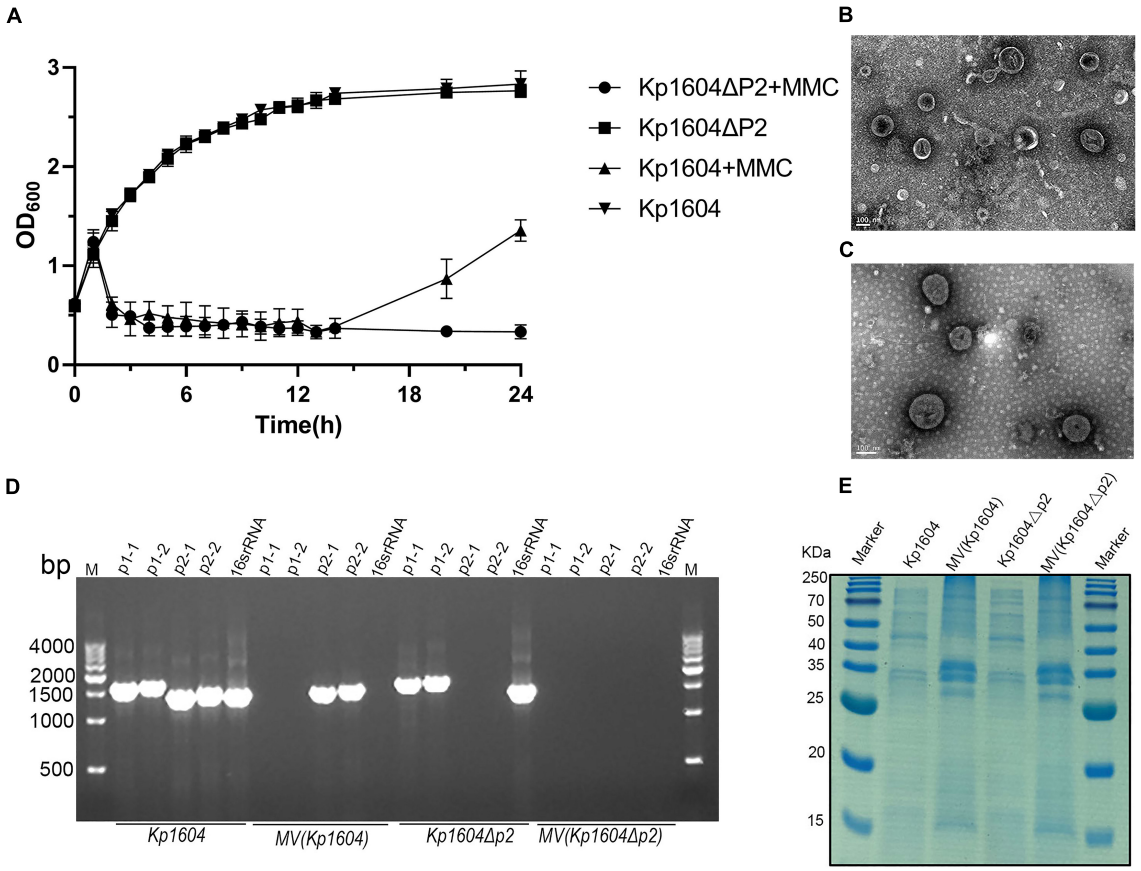

FIGURE 2 | MVs analysis from *Kp1604* and *Kp1604*Δ*p2*. **(A)** The growth of *Kp1604* and *Kp1604*Δ*p2* with or without mitomycin C. Transmission electron microscopy photograph of MV products from *Kp1604* **(B)** and *Kp1604*Δ*p2* **(C)** with mitomycin C induction. Scale bar of 100 nm is shown in the images. **(D)** PCR amplification of sequence fragment of p1, p2 and 16S rRNA. As indicated below, *Kp1604* and *Kp1604*Δ*p2* represent DNA extracted from whole cell lysates; MV(*Kp1604*) and MV(*Kp1604*Δ*p2)* represent DNA extracted from purified supernatants treated with DNase I. As indicated above, p1-1 and p1-2 represent specific sequence fragment in p1 plasmid amplified with primers p1-1-F and p1-1-R, p1-2-F and p1-2-R; p2-1 and p2-2 represent specific sequence fragment in p2 plasmid amplified with primers p2-1-F and p2-1-R, p2-2-F and p2-2-R; 16S rRNA was amplified with primers 27F and 1492R. **(E)** SDS–PAGE analysis of protein content in MVs and whole cell lysates of *Kp1604* and *Kp1604*Δ*p2*. *Kp1604* and *Kp1604*Δ*p2* represent whole cell lysates, and MV(*Kp1604*) and MV(*Kp1604*Δ*p2)* represent purified supernatants from *Kp1604* and *Kp1604*Δ*p2* triggered with mitomycin C.

protocols were approved by the Animal Ethics Committee in accordance with the guidelines for the use of laboratory animals in China. 13 mice per group were infected intraperitoneally with 100 μl PBS buffer, or doses of 5.0×10^6, 5.0×10^7 CFU of overnight culture of *Kp1604* or *Kp1604*△*p2* in 100 μl PBS buffer. Three mice each group were euthanized at 24 h after challenge to determine the bacterial loads in organs. Serially diluted homogenates of blood, livers, lungs were plated on LB agar and incubated at 37°C overnight for quantification of CFU. The mortality rate of ten mice each group was recorded for 96 h after challenge.

Statistical Analyses

Survival curves of mice were generated using GraphPad Prism 9. Statistical analyses of the efficiency of plasmid transformation and bacterial loads in various organs of mice were performed by the Mann–Whitney *U*-test ($^*p < 0.05$, $^{**}p < 0.01$, $^{***}p < 0.001$).

RESULTS

Genome Analysis of *Kp1604*

Klebsiella pneumoniae strain *Kp1604* was isolated from a patient's blood sample. The genome sequence showed that *Kp1604* contained a circular chromosome of 5,205,350 bp with a GC content of 57.58% and two plasmids (p1 and p2) of 144,892 bp and 109,308 bp with GC contents of 49.69 and 48.93%, respectively (**Table 1** and **Supplementary Figure 1**). *Kp1604* belonged to ST412 based on multilocus sequence typing (MLST) and the K57 serotype based on capsular typing by the wzi allele.

The genome sequence of plasmid p1 encoded five virulence-related genes, including *rmpA, iroB, iroC, iroD* and *iroN*. Genome sequence alignment of p1 with pLVPK, a well-known virulence plasmid, showed that they shared regions of homology (**Supplementary Figure 2**). These results suggested that p1 may be a virulence-related plasmid. The DNA sequence of p2 encoded 118 putative genes, 103 of which were predicted to phage-related

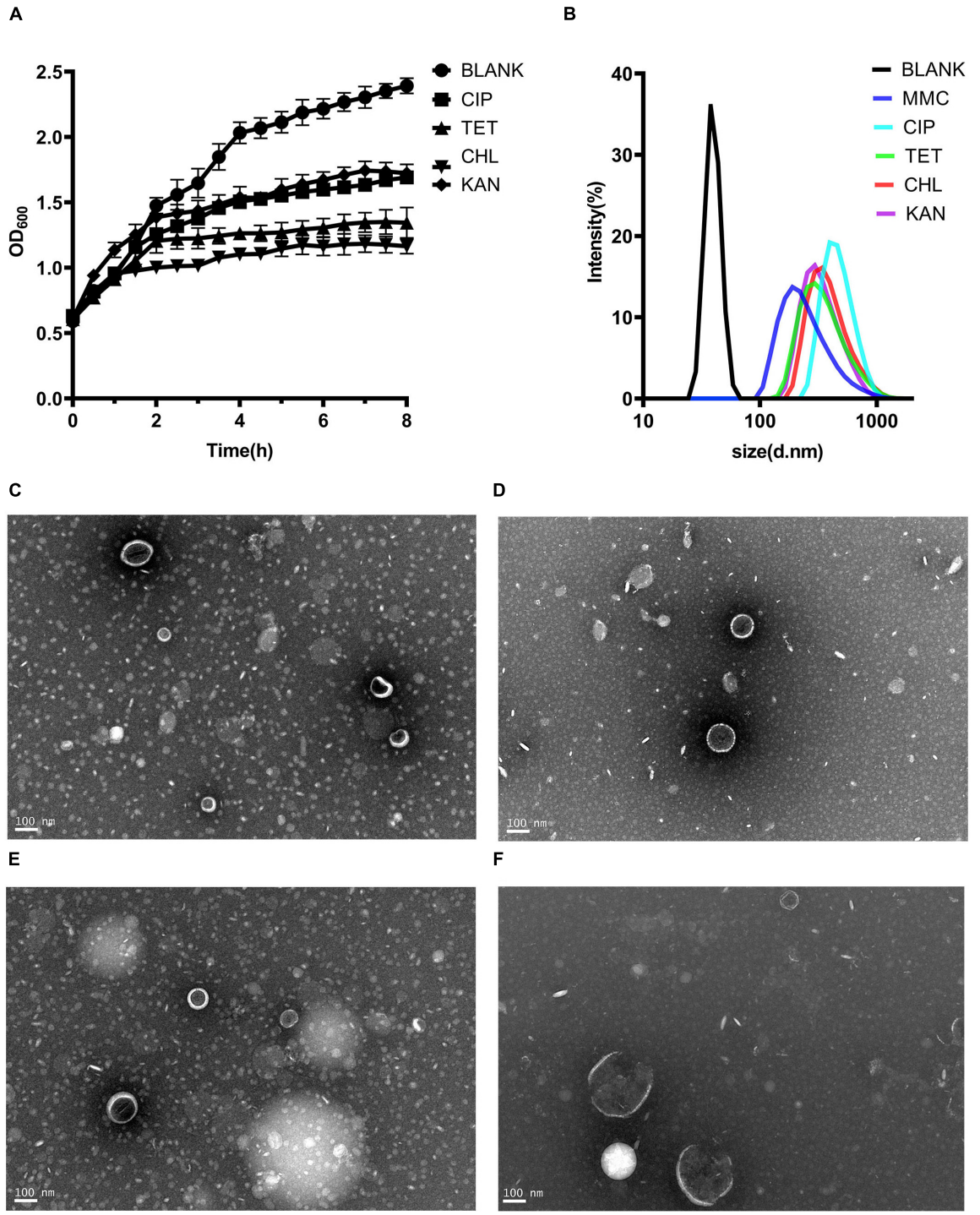

FIGURE 3 | Production of MVs from *Kp1604* cultured under antibiotic stress conditions. **(A)** Bacterial growth of *Kp1604* cultured with 1/2 MIC of ciprofloxacin (CIP), tetracycline (TET), chloramphenicol (CHL) and kanamycin (KAN). **(B)** Size and distribution of MVs. Single particle tracking analysis of MVs isolated from *Kp1604* after treatment with 1/2 MIC of CHL **(C)**, TET **(D)**, CIP **(E)**, and KAN **(F)**, as compared to non-treated (BLANK). Transmission electron microscopy photograph of MVs produced by *Kp1604* cultured with 1/2 MIC of CHL **(B)**, TET **(C)**, CIP **(D)**, and KAN **(E)**. Scale bars of 100 nm are shown in the images.

genes by Phaster, including phage structure genes, integrase, terminase, etc. (**Supplementary Table 3**). p2 was predicted to be an intact prophage by Phaster, similar to *Salmonella* phage SSU5 in *Salmonella enterica* serovar Typhimurium rough strain (Kim et al., 2012). Whole-genome sequence analysis of *Kp1604* identified 21 genomic islands but none of the phage-related

sequences except p2 (**Supplementary Table 4**). A BLAST search of the p2 sequence against the CARD and VFDB databases showed that p2 did not carry any virulence-related or AMR-related genes.

Widely Distribution of p2-Like Plasmid in *Enterobacteriaceae*

To investigate the distribution of this kind of plasmid, we downloaded 2,423 plasmid sequences of *Enterobacteriaceae* deposited in the Patricbrc database and three plasmid sequences of *Kp* deposited in GenBank. Plasmid cluster analysis showed that cluster 1 was an MDR plasmid cluster, including pSWU01 and pKP048 (**Supplementary Figure 3**); cluster 11 was virulent plasmid cluster, including pLVPK and pNTUH-K2044 (**Supplementary Figure 3**). p2 clustered to cluster 13, which contained 57 plasmids (**Supplementary Figure 3** and **Figure 1A**). The PlasmidFinder analysis of cluster 13 showed they all belonged to same replicon of IncFIB. Of them, 21, 17, 8, and 5 plasmids were distributed in *Klebsiella pneumoniae, Escherichia coli, Salmonella enterica* and *Klebsiella oxytoca,* respectively (**Figure 1A**). Notably, all p2-like plasmid-harboring strains were isolated from human samples where information about isolation was available. Further alignment of selected p2-like plasmids showed that they all encoded several phage-related proteins, integrase, terminase, recA, Xni and thyA (**Figure 1B**).

p2 DNA Specifically Packaged Into Membrane Vesicles in Response to Mitomycin C and Subinhibitory Concentrations of Antibiotics

Stresses such as UV light and mitomycin C are known to stimulate the SOS response and induce prophage particles (Du Toit, 2019). We therefore evaluated the impact of mitomycin C exposure on strain *Kp1604* to investigate whether plasmid p2 could be induced as a phage. After supplementation of mitomycin C, the growth of bacteria began to decline after 2 h (**Figure 2A**). TEM analysis of the purified supernatant revealed round particles sized from 50 to 300 nm (**Figure 2B**). p2 DNA was confirmed to specifically package into particles, as identified by both DNA sequence (accession number OK644452) and PCR amplification (**Figure 2D**). However, when the collected particles were spotted on 14 different *Kp* strains, no phage plaque was observed. SDS–PAGE analysis showed that the protein profiles of purified particles were different from those of bacterial lysates (**Figure 2E**). A proteomic analysis showed that a total of 221 proteins were identified, and OmpC and OmpA were the major components, accounting for 1.86 and 1.55%, respectively, which is consistent with the band pattern of SDS–PAGE (**Supplementary Table 5**). There were 81, 86, 40, and 14 identified proteins predicted to be located in the cytoplasm, inner membrane, outer membrane and periplasmic space, respectively (**Supplementary Table 5**). Combined with the identified proteins, this structure was more similar to MVs than phages. Therefore, it suggested that *Kp1604* secreted p2 DNA-containing MVs after induction by mitomycin C.

MVs are thought to be produced when bacteria are under environmental stress (Toyofuku et al., 2019). Four kinds of sub-inhibitory concentration antibiotics, chloramphenicol, ciprofloxacin, tetracycline and kanamycin were selected. Although the growth of bacteria did not decline significantly under antibiotic stress, it was inhibited (**Figure 3A**). Single particle tracking (SPT) analysis revealed that major particles in the induced supernatant were 100∼300 nm in size (**Figure 3B**). TEM analysis further confirmed there were round vesicles of the same size (**Figures 3C–F**).

Deletion of p2 Improved the Acquisition of Transferable Elements in *Kp1604Δp2*

To demonstrate that MV production was not p2-related, we deleted p2 from *Kp1604* and obtained the plasmid-minus mutant strain *Kp1604Δp2*. Deletion of p2 did not affect the growth of *Kp1604Δp2* compared with *Kp1604* (**Figure 2A**). MVs were produced by *Kp1604Δp2* with mitomycin C induction, similar to *Kp1604* (**Figure 2C**). Further protein analysis by SDS–PAGE showed negligible differences in the protein composition between MVs from *Kp1604* and the plasmid-minus mutant *Kp1604Δp2* (**Figure 2E**). This experiment further demonstrated that *Kp1604* produced MVs rather than phages triggered by mitomycin C.

To determine whether p2 could inhibit other phage infections against *Kp1604,* the efficiencies of plating (EOP) of three lytic phages of Φ1209, Φ168R, and Φ9226R were spotted on *Kp1604* and *Kp1604Δp2* lawn with serial dilutions. We observed the same pattern with three lytic phages: their EOP on *Kp1604* was reduced by 1∼2 orders of magnitude compared to the mutant *Kp1604Δp2* (**Figure 4A**). In addition, the phage plaques on *Kp1604Δp2* were significantly larger in diameter than those on *Kp1604* (**Figure 4B**). These results suggest that p2 could mediate host defense against phage infection. Plasmid acquisition was also investigated using plasmid pSGKP-spe transformation into strains *Kp1604* and *Kp1604Δp2*. The plasmid acquisition efficiency of *Kp1604Δp2* was significantly higher than that of *Kp1604* (**Figure 4C**). Thus, the presence of p2 could help host defend against foreign DNA invasion.

Deletion of p2 Increased Bacterial Virulence of *Kp1604Δp2*

The virulence potentials of strains *Kp1604* and *Kp1604Δp2* were determined in mouse infection models with intraperitoneal injection. To our surprise, the virulence of *Kp1604Δp2* increased significantly with an inoculum of $5 \times 10^{7^{\circ}}$ CFU, resulting in 100% mortality at 24 h, whereas only 70% mortality was observed for *Kp1604* (**Figure 5A**). There was no significant difference in bacterial load in various tissues of the mice when challenged with *Kp1604* and *Kp1604Δp2* at a dose of 5×10^7 CFU (**Figure 5B**). When challenged with the lower dose of 5×10^6 CFU, 10% mortality was observed for *Kp1604* and *Kp1604Δp2* at 48 h, and 10 and 25% mortality was observed for *Kp1604* and *Kp1604Δp2,* respectively, at 60 h (**Figure 5C**). However, the bacterial

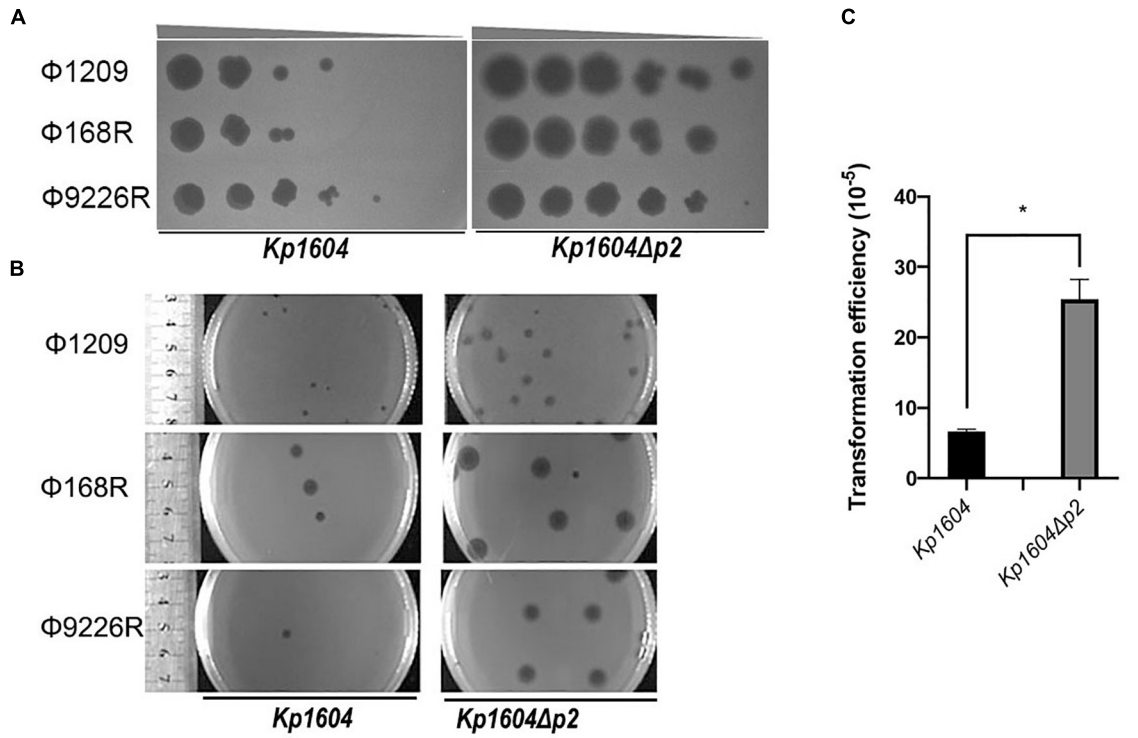

FIGURE 4 | Deletion of p2 from *Kp1604* affected the acquisition of transferable elements. **(A)** The efficiencies of phage propagation assays. Ten-fold serial dilutions of phages Φ1209, Φ168R, and Φ9226R were spotted on lawns of *Kp1604* and *Kp1604*Δ*p2*, respectively, from 10^{-3} to 10^{-8} serial dilutions as indicated. **(B)** Phage plaque diameter of Φ1209, Φ168R, and Φ9226R infecting *Kp1604* and *Kp1604*Δ*p2*. **(C)** Transformation efficiencies of strains *Kp1604* and *Kp1604*Δ*p2* by electroporation with plasmid pSGKP-spe. Transformation efficiency was defined as the number of pSGKP-spe-containing transformants divided by the number of control cells that survived electroporation, $^*p < 0.05$.

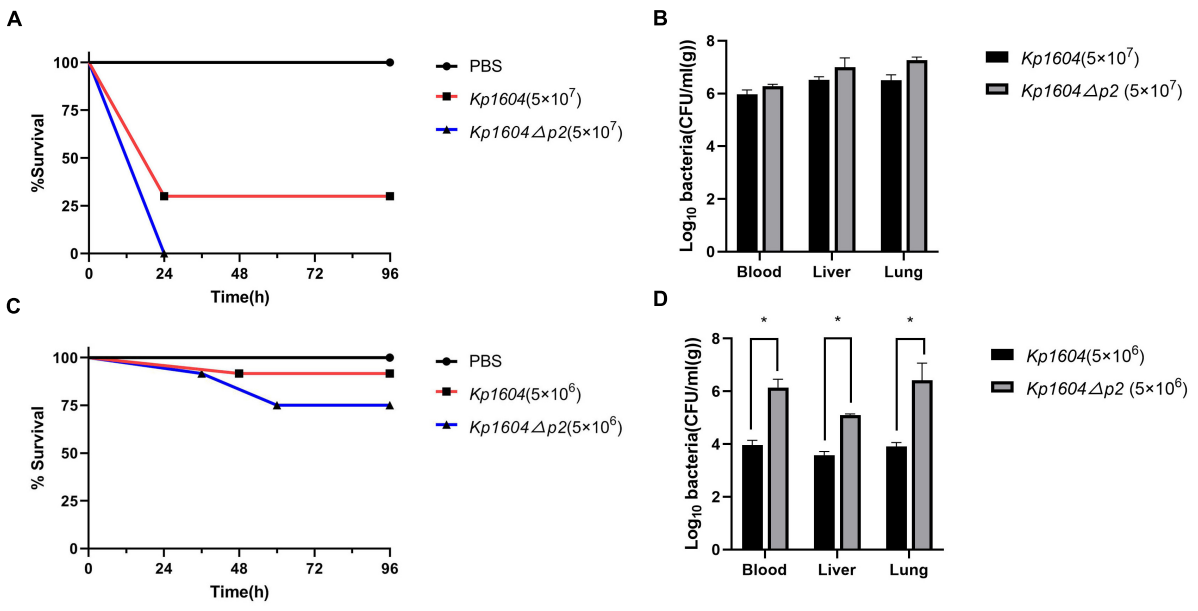

FIGURE 5 | Virulence potential of *Kp1604* and *Kp1604*Δ*p2*. Percent survival of mice with an inoculum of 5×10^7 CFU **(A)** and 5×10^6 CFU **(C)**. Strains of *Kp1604* and *Kp1604*Δ*p2* were monitored with intraperitoneal injection in 10 mice per group. Bacterial loads in blood, liver, and lung with an inoculum of 5×10^7 CFU **(B)** and 5×10^6 CFU **(D)**. Three mice each group were euthanized at 24 h after challenge. Blood, livers, and lungs were aseptically homogenized. For the bacterial load analysis, serially diluted homogenates were cultured overnight for counting. $^*p < 0.05$.

loads in the liver, lung and blood of mice at 24 h after challenge at the lower dose of 5×10^6 CFU showed that the bacterial load of the *Kp1604*Δ*p2* strain was significantly higher than that of the *Kp1604* strain (**Figure 5D**). These data implied that plasmid p2 decreased the virulence of *Kp1604* in mice.

DISCUSSION

Plasmids have an important role in bacterial evolution by transferring beneficial traits within and between species of bacteria, potentially contributing to host advantage fitness (Rodriguez-Beltran et al., 2021). Many diverse plasmids have been sequenced from *Kp*, among which virulence plasmids and AMR plasmids have been widely studied (Ernst et al., 2020; Wyres et al., 2020; Yang et al., 2020). Although some plasmids are widely distributed in *Kp* populations, their beneficial contribution to host was far from studied.

In this study, we isolated a virulent *Kp* strain harboring two plasmids inside the cell. p2 was predicted to be an intact prophage. Typically, phages integrate into bacterial chromosomes to be prophages. However, numerous phage plasmids have also been reported as extrachromosomal plasmids based on their encoding proteins homologous to both phage-related and plasmid-related proteins (Ikeda and Tomizawa, 1968; Zhang et al., 2017; Gilcrease and Casjens, 2018; Galetti et al., 2019; Pfeifer et al., 2021). Although plasmid prophages such as P1 and P6 of *Escherichia coli* can be both maintained as plasmids and converted to viral particles for release, most of the others cannot be released as viral particles (Ikeda and Tomizawa, 1968; Gilcrease and Casjens, 2018). The conversion controls between plasmid replication and bacteriophage lytic cycle is highly sophisticated, and the absence of any of the key regulators may lead to conversion failure (Sternberg and Austin, 1981). Although a total of 103 genes in p2 was predicted to encode conserved phage proteins, p2 still could not be induced as phage. Therefore, it suggested that p2 was still a plasmid that carried many phage-like elements. Membrane vesicles are nanoparticles sized from 20 to 400 nm in diameter originating from blebbing of the outer membrane of bacteria (Toyofuku et al., 2019). The structure and composition of MVs secreted by different bacteria are different. It was reported that proteins, nucleic acids, toxins could be packaged into MVs (Schwechheimer and Kuehn, 2015; Gilmore et al., 2021). MVs play a significant role in biological processes including virulence, horizontal gene transfer (Chatterjee et al., 2017; Bielaszewska et al., 2020), export of cellular metabolites (Orench-Rivera and Kuehn, 2016), phage infection and cell-to-cell communication (Zingl et al., 2020). In our study, mitomycin C and sub-inhibitory concentration of antibiotics could trigger p2-DNA contained MVs secretion in strain *Kp1604*. The function of P2 specifically packaged into MVs should be further investigated.

This study confirmed that p2 could contribute to defense against phage infections and affect uptake of plasmids. Bacteria have evolved numerous defense mechanisms against mobile genetic elements (MGEs) invasion, including restriction modification (RM) systems, CRISPR-Cas systems, abortive infection (Abi) systems and others (Samson et al., 2013). The RM system is one of the innate immune systems which limits incorporation of MGEs. RM system encoded by p2 was inferred to defense MGEs uptake in *Kp1604*. On the other hand, plasmid encodes genes to ensure itself replication, maintenance, and transmission, which are often considered disadvantageous to the host (Rodriguez-Beltran et al., 2021). Our results showed that the mortality of *Kp1604* was decreased compared with that of *Kp1604*Δ*p2* when challenged in a mouse model. It seemed that *Kp1604* reduced virulence at cost to maintenance of p2. Plasmids are widely distributed and highly diverse in the *Kp* population (Wyres et al., 2020; Yang et al., 2020). Further study on the mechanism of providing adaptive phenotypes to bacterial hosts will help us understand new contributions of plasmids to host evolution.

DATA AVAILABILITY STATEMENT

The datasets presented in this study can be found in online repositories. The names of the repository/repositories and accession number(s) can be found in the article/**Supplementary Material**.

ETHICS STATEMENT

The animal study was reviewed and approved by the Shanghai Jiao Tong University School of Medicine.

AUTHOR CONTRIBUTIONS

MC, BP, CL, and JQ contributed to the study design and wrote the manuscript. MC, BP, YW, LL, CJ, YZ, WZ, KD, YY, YL, YLW, ZZ, JL, XG, CL, and JQ contributed to experiment and data collection. JQ, CL, BP, and CJ did the data analyses. All authors contributed to data interpretation, provided critical revision of the manuscript, approved the final manuscript, and agreed to submit for publication.

FUNDING

This work was supported by the grants from the National Natural Science Foundation of China under (32170141).

SUPPLEMENTARY MATERIAL

The Supplementary Material for this article can be found online at: https://www.frontiersin.org/articles/10.3389/fmicb.2022.827545/full#supplementary-material

REFERENCES

Alikhan, N. F., Petty, N. K., Ben Zakour, N. L., and Beatson, S. A. (2011). BLAST Ring Image Generator (BRIG): simple prokaryote genome comparisons. *BMC Genomics* 12:402. doi: 10.1186/1471-2164-12-402

Besemer, J., Lomsadze, A., and Borodovsky, M. (2001). GeneMarkS: a self-training method for prediction of gene starts in microbial genomes. *Implications for finding sequence motifs in regulatory regions. Nucleic Acids Res.* 29, 2607–2618.

Bielaszewska, M., Daniel, O., Karch, H., and Mellmann, A. (2020). Dissemination of the blaCTX-M-15 gene among *Enterobacteriaceae via* outer membrane vesicles. *J. Antimicrob. Chemother.* 75, 2442–2451. doi: 10.1093/jac/dkaa214

Carattoli, A., and Hasman, H. (2020). PlasmidFinder and *In Silico* pMLST: identification and Typing of Plasmid Replicons in Whole-Genome Sequencing (WGS). *Methods Mol. Biol.* 2075, 285–294. doi: 10.1007/978-1-4939-9877-7_20

Chatterjee, S., Mondal, A., Mitra, S., and Basu, S. (2017). *Acinetobacter baumannii* transfers the blaNDM-1 gene *via* outer membrane vesicles. *J. Antimicrob. Chemother.* 72, 2201–2207. doi: 10.1093/jac/dkx131

Chen, L., Mathema, B., Chavda, K. D., DeLeo, F. R., Bonomo, R. A., and Kreiswirth, B. N. (2014). Carbapenemase-producing *Klebsiella pneumoniae*: molecular and genetic decoding. *Trends Microbiol.* 22, 686–696. doi: 10.1016/j.tim.2014.09.003

Chin, C. S., Peluso, P., Sedlazeck, F. J., Nattestad, M., Concepcion, G. T., Clum, A., et al. (2016). Phased diploid genome assembly with single-molecule real-time sequencing. *Nat. Methods* 13, 1050–1054. doi: 10.1038/nmeth.4035

Conlan, S., Park, M., Deming, C., Thomas, P. J., Young, A. C., Coleman, H., et al. (2016). Plasmid Dynamics in KPC-Positive *Klebsiella pneumoniae* during Long-Term Patient Colonization. *mBio* 7, e742–e716. doi: 10.1128/mBio.00742-16

Du Toit, A. (2019). Phage induction in different contexts. *Nat. Rev. Microbiol.* 17, 126–127. doi: 10.1038/s41579-019-0150-4

Ernst, C. M., Braxton, J. R., Rodriguez-Osorio, C. A., Zagieboylo, A. P., Li, L., Pironti, A., et al. (2020). Adaptive evolution of virulence and persistence in carbapenem-resistant *Klebsiella pneumoniae*. *Nat. Med.* 26, 705–711.

Galetti, R., Andrade, L. N., Varani, A. M., and Darini, A. L. C. (2019). A Phage-Like Plasmid Carrying bla KPC-2 Gene in Carbapenem-Resistant *Pseudomonas aeruginosa*. *Front. Microbiol.* 10:572. doi: 10.3389/fmicb.2019.00572

Gao, H., Liu, Y., Wang, R., Wang, Q., Jin, L., and Wang, H. (2020). The transferability and evolution of NDM-1 and KPC-2 co-producing *Klebsiella pneumoniae* from clinical settings. *EBioMedicine* 51:102599. doi: 10.1016/j.ebiom.2019.102599

Gilcrease, E. B., and Casjens, S. R. (2018). The genome sequence of *Escherichia coli* tailed phage D6 and the diversity of *Enterobacteriales* circular plasmid prophages. *Virology* 515, 203–214. doi: 10.1016/j.virol.2017.12.019

Gilmore, W. J., Bitto, N. J., and Kaparakis-Liaskos, M. (2021). Pathogenesis Mediated by Bacterial Membrane Vesicles. *Subcell. Biochem.* 97, 101–150.

Ikeda, H., and Tomizawa, J. (1968). Prophage P1, and extrachromosomal replication unit. *Biol. Cold Spring Harb. Symp. Quant.* 33, 791–798. doi: 10.1101/sqb.1968.033.01.091

Kim, M., Kim, S., and Ryu, S. (2012). Complete genome sequence of bacteriophage SSU5 specific for *Salmonella enterica* serovar Typhimurium rough strains. *J. Virol.* 86:10894. doi: 10.1128/JVI.01796-12

Koren, S., Walenz, B. P., Berlin, K., Miller, J. R., Bergman, N. H., and Phillippy, A. M. (2017). Canu: scalable and accurate long-read assembly *via* adaptive k-mer weighting and repeat separation. *Genome Res.* 27, 722–736. doi: 10.1101/gr.215087.116

Lam, M. M. C., Wyres, K. L., Wick, R. R., Judd, L. M., Fostervold, A., Holt, K. E., et al. (2019). Convergence of virulence and MDR in a single plasmid vector in MDR *Klebsiella pneumoniae* ST15. *J. Antimicrob. Chemother.* 74, 1218–1222. doi: 10.1093/jac/dkz028

Liu, Y. C., Cheng, D. L., and Lin, C. L. (1986). *Klebsiella pneumoniae* liver abscess associated with septic endophthalmitis. *Arch. Intern. Med.* 146, 1913–1916.

Luong, T., Salabarria, A. C., Edwards, R. A., and Roach, D. R. (2020). Standardized bacteriophage purification for personalized phage therapy. *Nat. Protoc.* 15, 2867–2890. doi: 10.1038/s41596-020-0346-0

Marr, C. M., and Russo, T. A. (2018). Hypervirulent *Klebsiella pneumoniae*: a new public health threat. *Expert Rev. Anti Infect. Ther.* 17, 71–73.

Munoz-Price, L. S., Poirel, L., Bonomo, R. A., Schwaber, M. J., Daikos, G. L., Cormican, M., et al. (2013). Clinical epidemiology of the global expansion of *Klebsiella pneumoniae* carbapenemases. *Lancet Infect. Dis.* 13, 785–796. doi: 10.1016/s1473-3099(13)70190-7

Nakai, K., and Horton, P. (1999). PSORT: a program for detecting sorting signals in proteins and predicting their subcellular localization. *Trends Biochem. Sci.* 24, 34–36. doi: 10.1016/s0968-0004(98)01336-x

Orench-Rivera, N., and Kuehn, M. J. (2016). Environmentally controlled bacterial vesicle-mediated export. *Cell Microbiol.* 18, 1525–1536. doi: 10.1111/cmi.12676

Page, A. J., Cummins, C. A., Hunt, M., Wong, V. K., Reuter, S., Holden, M. T., et al. (2015). Roary: rapid large-scale prokaryote pan genome analysis. *Bioinformatics* 31, 3691–3693. doi: 10.1093/bioinformatics/btv421

Pfeifer, E., Moura, de Sousa, J. A., Touchon, M., and Rocha, E. P. C. (2021). Bacteria have numerous distinctive groups of phage-plasmids with conserved phage and variable plasmid gene repertoires. *Nucleic Acids Res.* 49, 2655–2673. doi: 10.1093/nar/gkab064

Rodriguez-Beltran, J., DelaFuente, J., Leon-Sampedro, R., MacLean, R. C., and San Millan, A. (2021). Beyond horizontal gene transfer: the role of plasmids in bacterial evolution. *Nat. Rev. Microbiol.* 19, 347–359. doi: 10.1038/s41579-020-00497-1

Russo, T. A., and Marr, C. M. (2019). Hypervirulent *Klebsiella pneumoniae*. *Clin. Microbiol. Rev.* 32:e00001.

Samson, J. E., Magadan, A. H., Sabri, M., and Moineau, S. (2013). Revenge of the phages: defeating bacterial defences. *Nat. Rev. Microbiol.* 11, 675–687. doi: 10.1038/nrmicro3096

Schwechheimer, C., and Kuehn, M. J. (2015). Outer-membrane vesicles from Gram-negative bacteria: biogenesis and functions. *Nat. Rev. Microbiol.* 13, 605–619. doi: 10.1038/nrmicro3525

Seemann, T. (2014). Prokka: rapid prokaryotic genome annotation. *Bioinformatics* 30, 2068–2069. doi: 10.1093/bioinformatics/btu153

Sternberg, N., and Austin, S. (1981). The maintenance of the P1 plasmid prophage. *Plasmid* 5, 20–31. doi: 10.1016/0147-619x(81)90075-5

Sullivan, M. J., Petty, N. K., and Beatson, S. A. (2011). Easyfig: a genome comparison visualizer. *Bioinformatics* 27, 1009–1010. doi: 10.1093/bioinformatics/btr039

Toyofuku, M., Nomura, N., and Eberl, L. (2019). Types and origins of bacterial membrane vesicles. *Nat. Rev. Microbiol.* 17, 13–24. doi: 10.1038/s41579-018-0112-2

Tzouvelekis, L. S., Markogiannakis, A., Psichogiou, M., Tassios, P. T., and Daikos, G. L. (2012). Carbapenemases in *Klebsiella pneumoniae* and other *Enterobacteriaceae*: an evolving crisis of global dimensions. *Clin. Microbiol. Rev.* 25, 682–707. doi: 10.1128/CMR.05035-11

van Dongen, S., and Abreu-Goodger, C. (2012). Using MCL to extract clusters from networks. *Methods Mol. Biol.* 804, 281–295. doi: 10.1007/978-1-61779-361-5_15

Wang, Y., Wang, S., Chen, W., Song, L., Zhang, Y., Shen, Z., et al. (2018). CRISPR-Cas9 and CRISPR-Assisted Cytidine Deaminase Enable Precise and Efficient Genome Editing in *Klebsiella pneumoniae*. *Appl. Environ. Microbiol.* 84:e01834-18 doi: 10.1128/AEM.01834-18

Wyres, K. L., and Holt, K. E. (2016). *Klebsiella pneumoniae* Population Genomics and Antimicrobial-Resistant Clones. *Trends Microbiol.* 24, 944–956. doi: 10.1016/j.tim.2016.09.007

Wyres, K. L., Lam, M. M. C., and Holt, K. E. (2020). Population genomics of *Klebsiella pneumoniae*. *Nat. Rev. Microbiol.* 18, 344–359.

Yang, X., Dong, N., Chan, E. W., Zhang, R., and Chen, S. (2020). Carbapenem Resistance-Encoding and Virulence-Encoding Conjugative Plasmids in *Klebsiella pneumoniae*. *Trends Microbiol.* 29, 65–83. doi: 10.1016/j.tim.2020.04.012

Yang, X., Wai-Chi Chan, E., Zhang, R., and Chen, S. (2019). A conjugative plasmid that augments virulence in *Klebsiella pneumoniae*. *Nat. Microbiol.* 4, 2039–2043. doi: 10.1038/s41564-019-0566-7

Yigit, H., Queenan, A. M., Anderson, G. J., Domenech-Sanchez, A., Biddle, J. W., Steward, C. D., et al. (2001). Novel carbapenem-hydrolyzing beta-lactamase. *KPC-1, from a carbapenem-resistant strain of Klebsiella pneumoniae. Antimicrob. Agents Chemother.* 45, 1151–1161. doi: 10.1128/AAC.45.4.1151-1161.2001

Zhang, C., Feng, Y., Liu, F., Jiang, H., Qu, Z., Lei, M., et al. (2017). A Phage-Like IncY Plasmid Carrying the mcr-1 Gene in *Escherichia coli* from a Pig Farm in China. *Antimicrob. Agents Chemother.* 61, e2035–e2016. doi: 10.1128/AAC.02035-16

Zingl, F. G., Kohl, P., Cakar, F., Leitner, D. R., Mitterer, F., Bonnington, K. E., et al. (2020). Outer Membrane Vesiculation Facilitates Surface Exchange and In Vivo Adaptation of *Vibrio cholerae*. *Cell Host Microbe* 27, 225-237.e8. doi: 10.1016/j.chom.2019.12.002

Conflict of Interest: The authors declare that the research was conducted in the absence of any commercial or financial relationships that could be construed as a potential conflict of interest.

Publisher's Note: All claims expressed in this article are solely those of the authors and do not necessarily represent those of their affiliated organizations, or those of the publisher, the editors and the reviewers. Any product that may be evaluated in this article, or claim that may be made by its manufacturer, is not guaranteed or endorsed by the publisher.

frontiers in Microbiology

ORIGINAL RESEARCH
published: 29 March 2022
doi: 10.3389/fmicb.2022.821196

The Small RNA CyaR Activates Translation of the Outer Membrane Haem Receptor *chuA* in Enterohemorrhagic *Escherichia coli*

*Brandon M. Sy and Jai J. Tree**

School of Biotechnology and Biomolecular Sciences, University of New South Wales, Sydney, NSW, Australia

To sense the transition from environment to host, bacteria use a range of environmental cues to control expression of virulence genes. Iron is tightly sequestered in host tissues and in the human pathogen enterohemorrhagic *Escherichia coli* (EHEC) iron-limitation induces transcription of the outer membrane haem transporter encoded by *chuAS*. ChuA expression is post-transcriptionally activated at 37°C by a FourU RNA thermometer ensuring that the haem receptor is only expressed under low iron, high temperature conditions that indicate the host. Here we demonstrate that expression of *chuA* is also independently regulated by the cAMP-responsive small RNA (sRNA) CyaR and transcriptional terminator Rho. These results indicate that *chuAS* expression is regulated at the transcription initiation, transcript elongation, and translational level. We speculate that additional sensing of the gluconeogenic environment allows further precision in determining when EHEC is at the gastrointestinal epithelium of the host. With previous studies, it appears that the *chuAS* transcript is controlled by eight regulatory inputs that control expression through six different transcriptional and post-transcriptional mechanisms. The results highlight the ability of regulatory sRNAs to integrate multiple environmental signals into a layered hierarchy of signal input.

Keywords: small RNA, Hfq, heme, iron, post-transcriptional, non-coding RNA, EHEC

OPEN ACCESS

Edited by:
Dongsheng Zhou,
Beijing Institute of Microbiology and Epidemiology, China

Reviewed by:
Runhua Han,
University of Texas at Austin, United States
Toru Tobe,
Osaka University, Japan

***Correspondence:**
Jai J. Tree
j.tree@unsw.edu.au

Specialty section:
This article was submitted to Infectious Agents and Disease, a section of the journal Frontiers in Microbiology

Received: *24 November 2021*
Accepted: *10 February 2022*
Published: *29 March 2022*

Citation:
Sy BM and Tree JJ (2022) The Small RNA CyaR Activates Translation of the Outer Membrane Haem Receptor chuA in Enterohemorrhagic Escherichia coli. Front. Microbiol. 13:821196. doi: 10.3389/fmicb.2022.821196

INTRODUCTION

During infection, nutrients required by pathogenic bacteria are withheld by the host in a process known as nutritional immunity (Weinberg, 1975; Hood and Skaar, 2012). An example can be found in iron, a transition metal that is essential for pathogenic bacteria due to its role in essential physiological processes, such as respiration (Skaar, 2010; Evstatiev and Gasche, 2012). To deprive pathogens of this vital nutrient, the host sequesters iron in the high affinity iron binding molecules haem, ferritin and transferrin (Barber and Elde, 2014; Cornelissen, 2018). These ensure that the concentration of extracellular free iron in the host is too low to support bacterial growth and infection. To overcome this nutritional deficit, pathogens such as

Haemophilus influenzae, Campylobacter jejuni, Pseudomonas aeruginosa, and uropathogenic *Escherichia coli* have evolved multiple systems that allow for the scavenging of iron, these include siderophores and haem uptake systems (Rossi et al., 2001; Torres et al., 2001; Ong et al., 2006; Ridley et al., 2006; Hagan and Mobley, 2009; Skaar, 2010; Fournier et al., 2011; Garcia et al., 2011; Morgenthau et al., 2013; Zambolin et al., 2016).

Enterohemorrhagic *E. coli* (EHEC) is an enteric pathogen that causes haemorrhagic colitis which can progress into potentially fatal hemolytic uremic syndrome. The primary reservoir of this pathogen are ruminants and transmission mainly occurs *via* the consumption of contaminated foodstuffs (Kaper et al., 2004; Gyles, 2007; Karpman and Ståhl, 2014). EHEC can express an outer membrane haem receptor from the iron regulated *chu* haem uptake operon (Torres and Payne, 1997). The *chu* locus is homologous to the *shu* locus found in *Shigella,* and contains genes that allow for haem uptake, transport, utilization and degradation. The locus consists of a bicistronic operon (*chuAS)* as well as two polycistronic operons (*chuTWXY* and *chuUV*). ChuA is a TonB-dependent outer membrane haem receptor that imports haem into the periplasm (Celia et al., 2016). The periplasmic binding protein ChuT binds to haem, and *via* the ABC transporter ChuUV, is shuttled into the cytoplasm. Haem is processed by the haem oxygenase ChuS that converts haem into biliverdin, carbon monoxide and free iron. This breakdown also prevents haem toxicity (Anzaldi and Skaar, 2010). Under anaerobic conditions, this role is taken up by the SAM-methyltransferase ChuW and the anaerobilin reductase ChuY (LaMattina et al., 2016, 2017).

The haem uptake operon is part of a larger regulatory network that allows EHEC to achieve iron homeostasis. Transcription of *chuA* is repressed by the iron-dependent transcriptional regulator Fur. In iron-rich conditions, Fur binds to iron which increases the affinity of Fur for its DNA-binding site ∼1000-fold (Bags and Neilands, 1987). Fur also regulates a Hfq-dependent small RNA (sRNA) RyhB that is central to maintaining iron homeostasis (Massé and Gottesman, 2002; Massé et al., 2007; Waters and Storz, 2009; Wagner and Romby, 2015). RyhB prevents the expression of non-essential proteins that require Fe as a cofactor such as the TCA cycle and respiration genes *sdhC* and *fumAC*, and iron storage genes such as bacterioferritin. Genes that contribute to iron uptake, such as the shikimate permease *shiA* and the colicin I receptor *cirA,* are positively regulated by this sRNA (Massé and Gottesman, 2002; Oglesby-Sherrouse and Murphy, 2013; Chareyre and Mandin, 2018).

Enterohemorrhagic *Escherichia coli* utilizes the Chu system when it is in an iron-poor, haem-rich host. For that reason, as well as the toxicity that accompanies haem and iron over-accumulation, it is necessary to precisely control expression of this operon. FourU RNA-thermometers are used in different bacterial pathogens, such as *Shigella dysenteriae, Yersinia pseudotuberculosis, Vibrio cholerae*, and *Salmonella typhimurium*, to regulate expression of their virulence factors in a temperature-dependent manner (Waldminghaus et al., 2007; Kouse et al., 2013; Weber et al., 2014; Righetti et al., 2016). A FourU RNA-thermometer was found in the *chuA* 5′UTR that blocks the ribosomal binding site (RBS) and is formed at temperatures below 37°C, indicating that the pathogen is outside of the host (Kouse et al., 2013). This limits *chuA* expression outside of the host where haem is unlikely to be available.

Identification of binding sites for the small RNA chaperone Hfq in EHEC identified the phage-encoded sRNA AsxR that positively regulates the haem oxygenase *chuS* by sponging interactions with the negatively regulating sRNA, FnrS (Tree et al., 2014). Further, analysis of the EHEC sRNA interactome revealed that the outer membrane haem receptor *chuA* was also negatively regulated by the EHEC-specific Hfq-binding sRNA Esr41 (Waters et al., 2017). Here, we show that translation of *chuA* is activated by the Crp-cAMP regulated sRNA CyaR in a temperature- and Rho-termination-independent manner. Our results suggest that EHEC employs an AND-OR logic gate that integrates information on iron availability, temperature and carbon availability to sense its location within the host for appropriate expression of *chuA*.

RESULTS

The Outer Membrane Haem Receptor *chuA* Is Regulated by CyaR and ChiX

In previous work the binding sites of the small RNA chaperone Hfq were mapped using UV-crosslinking, denaturing purification and sequencing of Hfq-crosslinked RNA (termed CRAC) (Tree et al., 2014). Deletions introduced at the site of protein-RNA crosslinking during reverse transcription of UV-crosslinked RNAs can be used to identify the site of direct Hfq-RNA contact. Analysis of our previous Hfq-CRAC dataset reveals that Hfq binds strongly to the 5′UTR of the outer membrane haem receptor *chuA* (**Figures 1A,B**). Canonically, gene regulation through sRNAs occurs through direct base-pairing of the sRNA to the RBS within the 5′UTR of mRNA targets. Hfq-CRAC sequencing reads and contact-dependent deletions peaked at the RBS consistent with RyhB and Esr41 negative regulation at this site (Waters et al., 2017; Banerjee et al., 2020). A further Hfq-binding peak was located at position +160 to +200 suggesting that *chuA* may be subject to additional regulatory inputs within the 5′UTR (**Figures 1A,B**).

The *chuA* transcription start site is predicted to be ∼300 nt upstream of the *chuA* start codon (Nagy et al., 2001). To precisely map the transcription start site of *chuA* in EHEC str. Sakai, we analyzed our previously published differential RNA-seq (dRNA-seq) data, which enriches for primary transcripts using terminator exonuclease (TEX) (Sharma et al., 2010; Sy et al., 2020). This showed that the +1 site for *chuA* is at position 4,391,862, and that the 5′UTR is 291 nucleotides long, which concurs with previous predictions (**Figure 1B**; Nagy et al., 2001).

In previous analyses we found that sRNA-mRNA seed sites are often positioned within Hfq-bound reads recovered by Hfq-CRAC, and that the Hfq binding site can be used to restrict the sequence space for predicting sRNA–mRNA interactions (Tree et al., 2014; Wang et al., 2018). To identify sRNAs that may regulate *chuA*, IntaRNA (Busch et al., 2008; Mann et al., 2017) was used to predict interactions between the *chuA* 5′UTR and

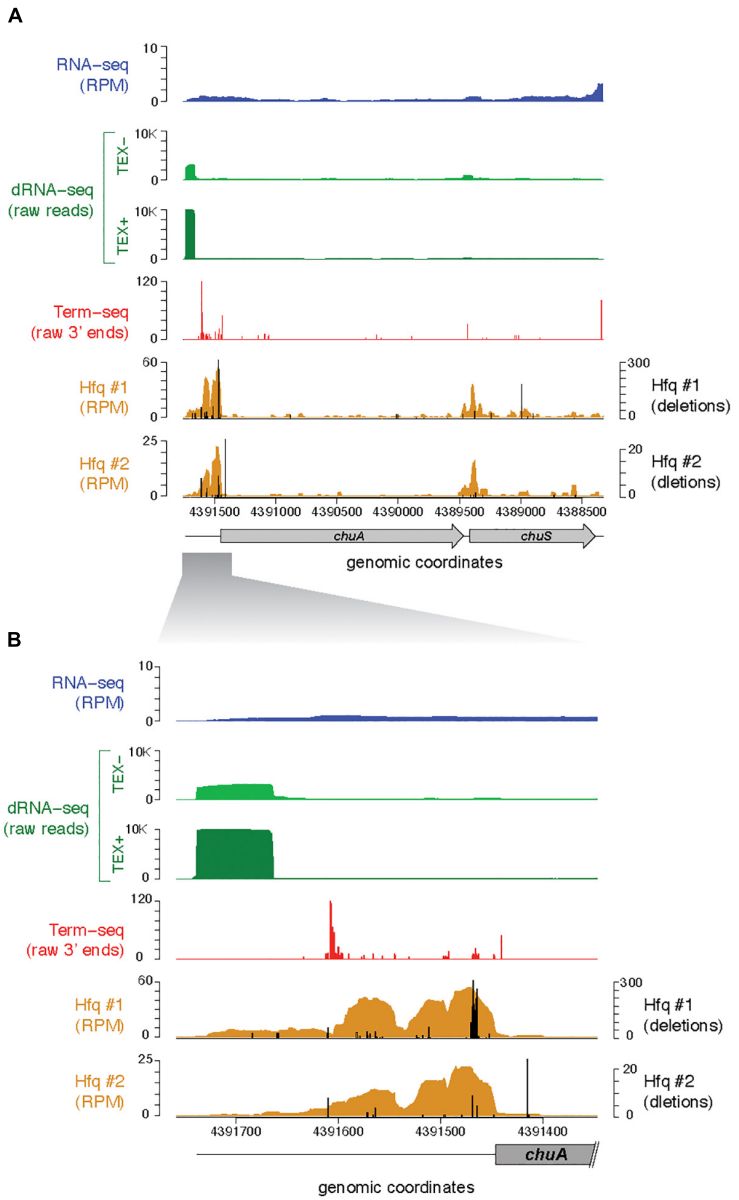

FIGURE 1 | The *chuA* 5′UTR is regulated by Hfq-dependent small RNAs. **(A)** RNA-sequencing data mapping to the *chuAS* operon. From top to bottom: total RNA-seq (dark blue; RPM), differential RNA-seq in samples untreated (light green) and treated (dark green) with TEX, Term-seq (red; raw 3′ end reads) (BioProject PRJNA601151), Hfq-binding sites from UV-crosslinking datasets (BioProject PRJNA197291). Sequencing deletions which indicate direct contact with Hfq are indicated in black. **(B)** Same as **(A)**, but focusing on the 5′UTR of *chuA*. **(C)** Fluorescence measurements of the EHEC *chuA*-sfGFP fusion in the presence of predicted binding sRNAs. **(D)** Fluorescence measurements of the UPEC *chuA*-sfGFP fusion in the presence of CyaR or ChiX (***$p < 0.001$, **$p < 0.01$).

44 known Hfq-dependent sRNAs (Li et al., 2013). Small RNAs that were predicted to interact within Hfq read peaks were retained. Through this analysis, we predicted that the sRNAs CyaR, SgrS, SdsR, ChiX, FnrS, RyhB, DicF, SroC, and MicC may have regulatory effects on *chuA*.

To confirm these predicted interactions the 5′UTR of *chuA*, starting from the +1 site up until the 15th codon of the coding sequence was fused to sfGFP by cloning into the plasmid pXG10SF (Corcoran et al., 2012). The fluorescence of this translational fusion was monitored in *E. coli* strain DH5α in the presence and absence of the candidate sRNAs expressed from constitutive expression plasmids (**Figure 1C**). This revealed that the Hfq-dependent sRNAs CyaR and ChiX have an activating and repressive effect on *chuA*, respectively.

CyaR Regulation of *chuA* Is Conserved in Uropathogenic *Escherichia coli*

Earlier work from the Murphy Lab indicated that *chuA* 5′UTR from EHEC and *Shigella* are more closely related than

the 5′UTR from EHEC and uropathogenic *E. coli* (UPEC) (Kouse et al., 2013). We next examined whether CyaR and ChiX regulation are conserved in the divergent EHEC and UPEC 5′UTRs. In UPEC, haem acquisition using *chuA* is required for maximal colonization of the kidneys (Hagan and Mobley, 2009). The 5′UTRs of EHEC and UPEC ($chuA_{EHEC}$ and $chuA_{UPEC}$) *chuA* share 83.4% identity (Nagy et al., 2001). The UPEC 5′UTR sequence has only 67.4% identity within the Hfq-binding site suggesting that $chuA_{UPEC}$ may not be regulated by Hfq-dependent sRNAs. To test whether $chuA_{UPEC}$ is post-transcriptionally regulated by CyaR and ChiX we constructed a translational fusion of $chuA_{UPEC}$ with sfGFP and monitored fluorescence in the presence or absence of CyaR and ChiX overexpression plasmids. The $chuA_{UPEC}$ fusion was activated by CyaR consistent with our results for $chuA_{EHEC}$ but was not significantly repressed by ChiX (**Figure 1D**). Notably, the $chuA_{UPEC}$ fusion was 55% more fluorescent than the $chuA_{EHEC}$ fusion. This suggests that while *chuA* in both pathotypes is subject to regulation by CyaR, the divergent 5′UTR sequence has de-repressed *chuA* expression in UPEC.

CyaR Activates *chuA* Translation Through Direct Base-Pairing

Both CyaR and ChiX are class II sRNAs that are known to modulate sRNA regulation by displacing sRNAs from Hfq when overexpressed (Moon and Gottesman, 2011; Santiago-Frangos et al., 2016). To determine whether CyaR and ChiX control *chuA* through direct RNA–RNA interactions with the *chuA* 5′UTR or indirectly through titration of Hfq, point mutations were made in both *chuA* and the sRNAs CyaR and ChiX to disrupt the predicted interaction sites. A predicted 3 nt compensatory mutation was made in the top scoring *chuA*–ChiX interaction as predicted by IntaRNA. The M1 mutation made in ChiX resulted in the de-repression of *chuA*-GFP expression. However, this effect was not observed when the compensatory *chuA* M1 mutation was introduced. This suggested that while the nucleotides mutated in ChiX contributed to *chuA* regulation, they did not interact with the predicted *chuA* interaction site. A second set of compensatory point mutants (M2) were made for the next highest scoring interaction that used the same ChiX seed region that was previously tested. Mutations in either *chuA* or ChiX alone resulted in the disruption of the *chuA*–ChiX interaction, but testing the mutants together did not restore the repression of *chuA* (**Supplementary Figure 1**). These results indicated that while ChiX affects translation of *chuA*, it is not due to a direct interaction with the *chuA* M1 or M2 site and may occur indirectly.

CyaR is predicted to bind approximately 15 nt upstream of the *chuA* Shine–Dalgarno sequence. The interaction between CyaR and *chuA* results in a 1.3-fold activation of translation. Mutating CyaR at the M1 site reduced CyaR activation by a modest 8.1%, while the *chuA* point mutant completely abolished the interaction (**Figure 2**). Providing the CyaR-M1 mutant partially restore translational activation of *chuA*-M1, supporting a direct interaction between CyaR and the 5′UTR of *chuA* that activates translation.

CyaR Activates ChuA Translation Independently of Temperature

Regulation of *chuA* occurs on both the transcriptional and translational level. Transcription of *chuA* is inhibited by Fur when cells are grown in iron-rich conditions (Torres and Payne, 1997), while the level of translation is dependent on the environmental temperature. At 25°C, translation is inhibited by the formation of a FourU RNA thermometer that occludes the RBS (Kouse et al., 2013). This inhibitory structure lies 15 nt downstream of the CyaR binding site. To determine whether CyaR-mediated activation of *chuA* translation occurs by inhibiting the formation of this RNA-thermometer, a U273A point mutation known to disrupt the formation of the FourU hairpin loop was made in the 5′UTR of the *chuA*-GFP translational fusion (**Figure 3A**; Kouse et al., 2013). Expression of wild-type and mutant *chuA*-sfGFP translational fusions were monitored in the presence and absence of CyaR overexpression plasmids at 25°C. Disruption of the RNA thermometer *via* the U273A point mutation resulted in a 2.6-fold increase in fluorescence compared to the wild-type, confirming the FourU temperature-dependent regulation of *chuA* translation. Disruption of this secondary structure however did not affect CyaR-mediated activation of *chuA,* as a 1.6-fold increase in fluorescence was observed when CyaR was provided with the U273A mutation in *chuA* (**Figure 3B**). This demonstrated that CyaR-mediated activation of *chuA* acts independently of post-transcriptional inhibition through the FourU RNA thermometer structure.

The *chuA* 5′UTR Contains a Sequence That Inhibits Its Expression

While the activation of *chuA* translation by CyaR is not due to disruption of the RNA thermometer, *in silico* folding predictions on the 5′UTR of *chuA* indicated potential secondary structure throughout the 5′UTR, including some that occluded sequences downstream of the RBS (**Supplementary Figure 2**). To understand whether the activating *chuA*–CyaR interaction requires structured sequences within the *chuA* 5′UTR, we progressively removed sequence from the 5’ end in four truncations of the *chuA*-sfGFP translational fusion (**Figure 4A**). Predicted secondary structure and the presence of Hfq distal face binding motifs [$(ARN)_x$] were used as guides in making truncates of the *chuA* 5′UTR (Soper and Woodson, 2008; Zhang et al., 2013; Schu et al., 2015). A search through the 5′UTR of *chuA* identified 10 $(ARN)_4$ sites with one mismatch tolerated (ARN_4m_1). The first truncate (T1) begins at +57 nt and removes a section that forms two hairpins as well as 9 out of 10 ARN_4m_1 sites. The second (T2) and third (T3) begin at +116 and +177, respectively, and each one removes another hairpin from the overall predicted secondary structure while maintaining the RNA-thermometer. The second truncate T2 also removes the last ARN_4m_1 motif. The fourth truncate (T4) begins at +217 and leaves only the CyaR binding site, the RNA-thermometer, RBS and the start codon. In the absence of the CyaR overexpression plasmid, the *chuA* 5′UTR T1-T4 truncates caused 2.1-, 1.9-, 2.9-, and 9.2-fold increases in *chuA* translation, respectively. CyaR was able to activate

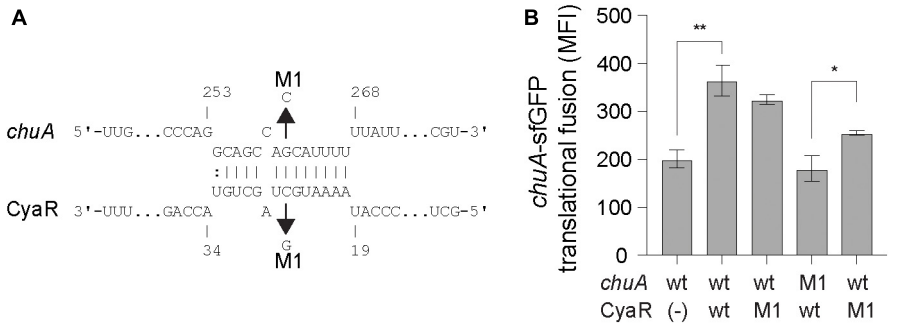

FIGURE 2 | CyaR activates *chuA* translation through direct base-pairing. **(A)** IntaRNA prediction of the *chuA*–CyaR interaction. Compensatory point mutations predicted to disrupt the interaction are indicated by the arrows. **(B)** Fluorescence measurements of wild-type or mutant *chuA*-sfGFP translational fusions in the presence and absence of wild-type or mutant CyaR overexpression plasmid. Measurements are the mean median fluorescence intensity of three biological replicates (**$p < 0.01$, *$p < 0.05$).

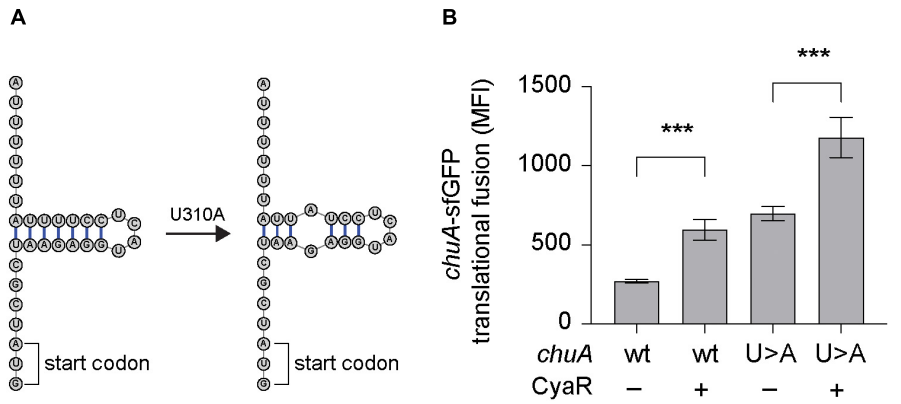

FIGURE 3 | CyaR activates *chuA* translation independently of a FourU RNA-thermometer. **(A)** Diagram indicating the point mutation made to disrupt the formation of the *chuA* FourU RNA thermometer. **(B)** Fluorescence measurements of wild-type and RNA-thermometer disrupted *chuA*-sfGFP translational fusions in the presence and absence of CyaR overexpression plasmid. Measurements are the mean median fluorescence intensity of three biological replicates (***$p < 0.001$).

truncates T1, T2, and T4 between 20 and 40% consistent with CyaR activation of the wild-type construct (**Figure 4B**). These results indicate that CyaR does not act through alleviation of an inhibitory secondary structure or a regulatory sequence in the upstream +1 to +217 nt region of the 5′UTR. Notably, removing the region between +177 and +217 nt (T3–T4) of the *chuA* 5′UTR resulted in a dramatic increase in *chuA*-GFP expression (9.2-fold) indicating that the T3–T4 region of the 5′UTR contains sequences or RNA structures that strongly repress expression.

chuA Is Subject to Premature Transcription Termination by Rho

In *E. coli,* the average 5′UTR is approximately 25–35 nucleotides in length (Kim et al., 2012; Evfratov et al., 2017). The 5′UTR of *chuA* is 291 nucleotides, making it an unusually long UTR (Wyckoff et al., 1998; Kouse et al., 2013). In commensal *E. coli*, over half of all annotated genes with long 5′UTRs (defined as >80 nt) are prematurely terminated by the transcription termination factor Rho (Sedlyarova et al., 2016). Further, horizontally transferred genes have been shown to be more susceptible to regulation by Rho-dependent termination (Cardinale et al., 2008; Peters et al., 2012). By analyzing our previously published Term-seq data, we noticed that there were termination sites at positions +129, +271, and +297 within the *chuA* mRNA (**Figure 5A**). We did not identify Rho-independent (intrinsic) terminators within the *chuA* 5′UTR using ARNold (**Figure 5A**; Naville et al., 2011; Sy et al., 2020). Collectively, this suggested that transcription of the pathogenicity island encoded *chuA* may be prematurely terminated by Rho.

To identify Rho-termination sites in EHEC, we sequenced total RNA extracted from cells treated with the Rho-inhibiting antibiotic bicyclomycin (BCM) (Zwiefka et al., 1993). Rho-termination sites were identified by using the approach adopted by Adams et al. (2021) that previously identified termination sites in BCM-treated *E. coli* cells. Consistent with earlier studies we found that horizontally acquired regions and antisense RNAs are enriched among genes that are up-regulated by BCM treatment (**Figure 5B**; Cardinale et al., 2008; Peters et al., 2009). Read-through scores were calculated to assess Rho-dependent termination using previously published scripts (Adams et al., 2021). Read-through scores were maximal for all

three replicates (±BCM) at positions +267–273 nt correlating well with the termination site at +271 nt identified by Term-seq. Read-through transcription at this site was up-regulated between 1.33- and 1.47-fold by BCM treatment indicating that Rho prematurely terminates transcription of *chuA* at position +271 (**Figure 5A**). To verify that *chuA* was subject to premature transcription termination by Rho, we measured the fluorescence of inducible full-length and truncated *chuA*-GFP translational fusions in the presence or absence of BCM (**Figure 5A**). Treatment with BCM resulted in a ∼1.4-fold increase in fluorescence for the full-length and T1–T3 *chuA*-GFP constructs. No significant change was observed for *chuA* truncate T4 (**Figure 5C**). Rho-dependent termination requires recruitment of the Rho at upstream Rho utilization sites (*rut*) and we speculate that the *rut* site for Rho-dependent termination at +271 is removed in the T4 truncate. Taken together, these results indicate that *chuA* is negatively regulated by Rho-dependent termination at position +271 and this repression requires the 30 nt between +177 and +217 nt of the *chuA* 5′UTR.

Small RNAs can regulate Rho-dependent termination by altering the accessibility of Rho utilization sites, either as a by-product of translation inhibition, or by directly binding to the *rut* site itself (Bossi et al., 2012; Sedlyarova et al., 2016; Chen et al., 2019; Silva et al., 2019). We hypothesized that CyaR may activate *chuA* translation by preventing premature Rho termination within the 5′UTR. To test this, we measured the fluorescence of our *chuA*-GFP translational fusion in the presence or absence of BCM and CyaR. CyaR was able to activate translation of *chuA* in the presence of BCM, indicating that CyaR activates *chuA* independently of Rho termination (**Figure 5D**). Collectively our data demonstrate that *chuA* expression is independently regulated by CyaR sRNA, Rho terminator, and the FourU RNA thermometer.

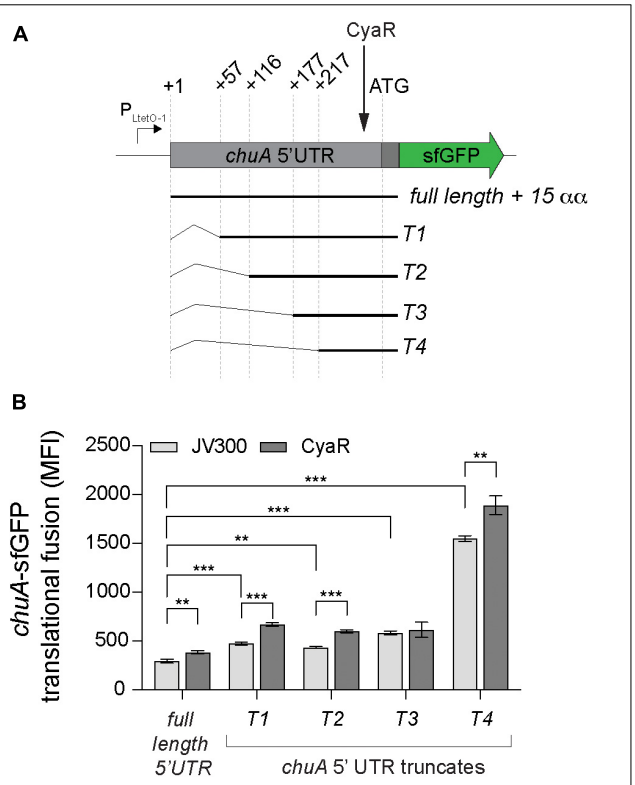

FIGURE 4 | The *chuA* 5′UTR contains a sequence that disrupts its translation independently of CyaR. **(A)** Diagram indicating the positions of the different *chuA*-sfGFP truncates used. **(B)** Fluorescence measurements of full-length and truncated *chuA*-sfGFP constructs in the presence and absence of CyaR overexpression plasmid. The position of the CyaR binding site is indicated. Measurements are the mean median fluorescence intensity of three biological replicates (***$p < 0.001$, **$p < 0.01$).

Expression of CyaR Is Correlated With *chuA* Expression *in vivo*

In order to obtain a more biologically relevant representation of the relationship between CyaR and *chuA* expression, we analyzed previously published RNA sequencing data of EHEC str. EDL933 obtained during colonization of a bovine rectum, intestine and rumen (Segura et al., 2018, 2021). Previously, these datasets have been used to show that genes relating to iron acquisition are differentially regulated in each of the gastrointestinal niches when compared to minimal M9 media. We compared the expression of both *chuA* and CyaR between each of the gastrointestinal niches and we find that *chuA* is most highly expressed in the rectum, followed by the rumen, then the intestine (**Figure 6**). These findings are consistent with induction of *chuA* by environmental signals at this site, including iron-limitation, temperature and a gluconeogenic environment (Snider et al., 2009; Bertin et al., 2013). We also observe this trend with CyaR expression, with the sRNA being maximally expressed in the rectum. This suggests that CyaR contributes to the maximal expression of *chuA* in the rectum, allowing for better colonization of this environmental niche.

DISCUSSION

To successfully grow and colonize a host, pathogens utilize systems that allow them to retrieve trace minerals required for growth that are normally sequestered. Various pathotypes of *E. coli*, including EHEC and UPEC, utilize the ChuA outer membrane haem receptor to transport host derived haem. Transcription of *chuA* is repressed in the presence of iron by Fur (Torres and Payne, 1997), while translation is regulated by temperature through a FourU RNA-thermometer that occludes the RBS (Kouse et al., 2013). The combination of these two modes of regulation allows the pathogen to sense two signals associated with the host environment (low iron and high temperature) and activate expression of the haem receptor inside the host. Notably, each signal in isolation would generate many false positives when deciding on whether the cell had entered a mammalian host.

The natural order imposed by transcription and post-transcriptional regulation creates an AND-logic gate, where low iron levels AND high temperature are required for expression of *chuA* in the host. Here we have shown that *chuA* is controlled by two additional post-transcriptional signals: repression through Rho termination and activation through

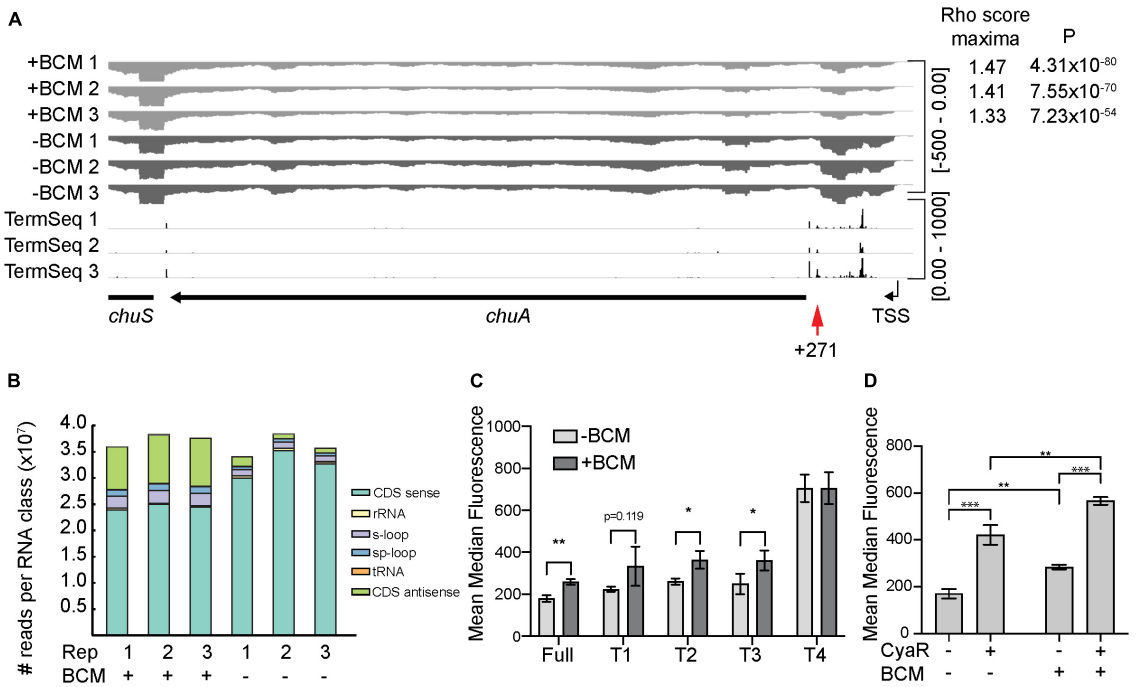

FIGURE 5 | The *chuA* 5′UTR is subject to termination by Rho. **(A)** RNA-seq coverage of *chuA* in EHEC O157:H7 strain Sakai treated and untreated with bicyclomycin. Rho scores for each replicate is shown. TSS is derived from differential RNA-seq data and is indicated by an arrow. Term-seq reads indicating *chuA* 3′ ends are also included. **(B)** Classification and number of reads per RNA class upon treatment of EHEC O157:H7 strain Sakai with bicyclomycin. **(C)** Fluorescence measurements of full-length and truncated *chuA*-sfGFP fusions in the presence and absence of induction with bicyclomycin. **(D)** Fluorescence measurements of *chuA*-sfGFP translational fusion in the presence and absence of CyaR overexpression plasmid and treatment with bicyclomycin. Measurements are the mean median fluorescence intensity of three biological replicates (***$p < 0.001$, **$p < 0.01$, *$p < 0.05$).

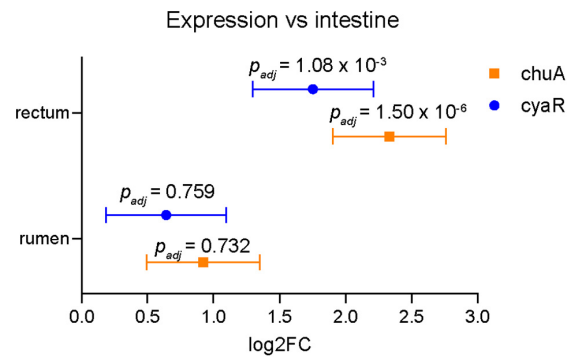

FIGURE 6 | Expression of chuA and CyaR in bovine gastrointestinal niches. Log2FC expression of chuA (orange squares) and CyaR (blue circles) in rectum and rumen compared to intestine. Data from SRA accession SRP136076. Error values are standard errors calculated from DEseq2. Adjusted *p*-values are calculated from DEseq2.

CyaR. CyaR acts independently of both Rho and the FourU thermometer potentially creating a post-transcriptional OR-logic gate. The effect of the FourU thermometer and CyaR are additive, and either regulator can activate independently of the other. In Boolean terms it appears that *chuA* uses an AND-OR logic gate where expression requires low iron AND (high temperature OR CyaR) (**Figure 7**).

Transcription of CyaR is activated by the global regulator Crp when cyclic-AMP levels are high, such as in the absence of glucose (De Lay and Gottesman, 2009). EHEC colonizes the colon where the primary source of carbon is mucins. *Bacteroides thetaiotaomicron (Bt)* can cleave mucins to release sugars that are utilized by EHEC (Xu et al., 2003; Fischbach and Sonnenburg, 2011). During colonization of the gastrointestinal mucus layer and epithelium, EHEC is likely to encounter varying niches that include both glycolytic and gluconeogenic environments (Miranda et al., 2004). Sensing variation in the availability of sugars and oxygen availability have been suggested to be key regulatory signals that allow EHEC to determine location in the gastrointestinal tract and proximity to the epithelium (Carlson-Banning and Sperandio, 2016). Close to the intestinal epithelium, the relative absence of microorganisms that metabolize and release sugars from mucins creates at gluconeogenic environment (Conway and Cohen, 2015). Lower levels of fucose, and higher levels of succinate reduces the level of the fucose-sensing two-component system FusKR that induces expression of Cra. In gluconeogenic environments, Cra can enhance binding of the cAMP receptor protein Crp to its targets (Ryu et al., 1995). Activation of Cra can induce expression of genes required for T3SS and adhesion to the epithelium (Njoroge et al., 2012; Curtis et al., 2014; Carlson-Banning and Sperandio, 2016). Expression of Crp can also be activated in the presence of Cra (Zhang et al., 2014). We propose that the gluconeogenic environment

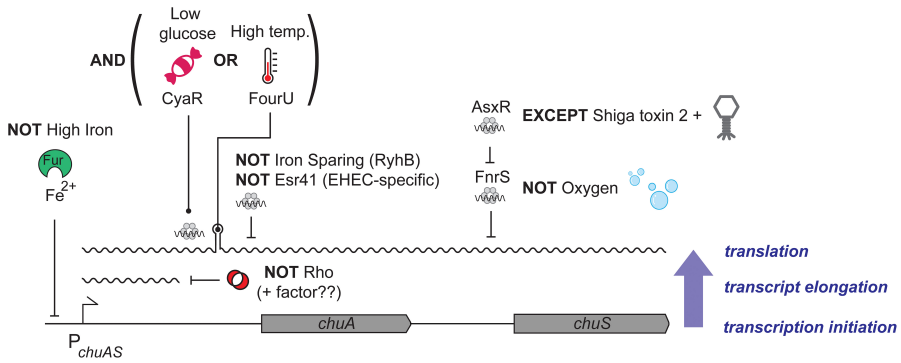

FIGURE 7 | Model of *chuAS* regulation. Regulation of *chuAS* expression occurs at the transcriptional, transcript elongation, and translational levels (indicated blue, right). The dependence of each layer on the previous creates regulatory AND gates. (*Bottom layer*) Repression of *chuAS* transcription by Fe-loaded Fur is relieved under iron-limited conditions allowing transcription initiation. (*Middle layer*) Elongating RNAP is prematurely terminated by Rho within the 5′UTR of *chuA*. An additional factor (potentially another sRNA) is likely to modulate Rho termination and allow read-through transcription. (*Top layer*) Translation of the *chuAS* transcript is activated by the cAMP-responsive sRNA CyaR or temperatures ł37°C that melt the FourU thermometer. Melting of the *chuAS* mRNA FourU element can be overridden under iron-sparing conditions by the sRNA RyhB or the EHEC-specific sRNA Esr41 that repress translation from the exposed RBS. The downstream haem oxygenase encoded by *chuS* is repressed under aerobic conditions by the sRNA FnrS, except in EHEC where repression is relieved by the sRNA sponge AsxR carried by the Shiga toxin 2-encoding bacteriophage.

encountered at the gastrointestinal tract provides an activating signal for CyaR that has been incorporated into *chuA* regulation as an additional signal that indicates host colonization and haem availability. Consistent with this hypothesis, we find that both CyaR and *chuA* transcription is activated in bovine rectal samples (**Figure 6**).

The mechanism of CyaR activation of *chuA* expression remains unclear although we have ruled out three probable mechanisms: CyaR acts through direct base-pairing with the *chuA* 5′UTR rather than general titration of Hfq, CyaR does not disrupt the FourU RNA thermometer to override temperature-dependence, and CyaR does not inhibit premature Rho termination of *chuA*. While these results have uncovered two additional post-transcriptional regulators of *chuA* (CyaR and Rho) they also suggest that there exists an additional repressive element in the *chuA* 5′UTR that is overcome by CyaR binding. We note that our *chuA*-GFP translational fusion reports on multiple post-transcriptional processes including translation efficiency and mRNA stability, and that CyaR may be modulating either of these to affect *chuA* expression.

Our Term-seq data indicates that the *chuA* 5′UTR is terminated at positions +129, +271, and +297 with position +271 nt maximally sensitive to treatment with BCM. Using truncates of the *chuA* 5′UTR we have also found that the sequence between +177 and +217 nt (T3 and T4) represses *chuA* expression almost 10-fold. We suggest that Rho associates with the nascent *chuA* transcript between +177 and +217 nt to terminate transcription at +271 nt. Small RNAs can promote or occlude *rut* sites to control Rho termination in response to regulatory signals (Sedlyarova et al., 2016; Silva et al., 2019) and it remains plausible that Rho termination is modulated by yet another regulatory signal.

The *chuA* encoded haem receptor is transcribed as a bicistronic transcript with the haem oxygenase *chuS*. In previous work we showed that *chuS* expression is repressed by the sRNA FnrS that is induced under anaerobic conditions, consistent with ChuS requiring oxygen for activity. FnrS repression is over-ridden by the sRNA sponge AsxR transcribed from the Shiga toxin 2 encoding bacteriophage Sp5 (Tree et al., 2014). Collectively, expression of *chuAS* is subject to an impressive level of post-transcriptional regulation that provides complex integration of environmental signals beyond low iron (transcriptional regulation by Fur). These post-transcriptional signals appear to provide a much more accurate interpretation of the environment to indicate whether haem transport is required (i.e., whether EHEC is at the gastrointestinal epithelium). The logic of the regulatory circuit that controls *chuAS* expression is outlined in **Figure 7**.

Post-transcriptional regulation appears ideally suited to this layering of logic gates because the natural order (dependence) imposed by transcriptional and post-transcriptional signals creates AND gates. There are at least three ordered layers of AND gates in the *chuA* transcript that need to be satisfied before the next layer of signals are incorporated. Fur-dependent transcription, Rho-dependent termination, and post-transcriptional control through sRNAs or the FourU thermometer. Together these form an elegant set of AND, OR, and NOT gates that interpret the environment and genetic background of the host (the later through the EHEC-specific sRNAs AsxR and Esr41) (**Figure 7**). The extensive post-transcriptional logic of the *chuAS* operon suggests that layered post-transcriptional regulation can create complex regulatory logic gates to integrate and interpret environmental signals.

MATERIALS AND METHODS

Bacterial Strains and Growth Conditions

Bacterial strains, oligonucleotides and plasmids used for this study are listed in **Supplementary Table 1**. *E. coli* was routinely

grown at 37°C in liquid Luria-Bertani (LB) broth or on solid LB-agar plates. Bacterial media was supplemented with ampicillin (100 μg/mL) or chloramphenicol (34 μg/mL) where appropriate. For inhibition of Rho termination, bicyclomycin (BioAustralis, 50 μg/mL) was added to exponential phase (OD_{600} = 0.6) cultures for 30 min before being assayed.

In silico Prediction of Interacting sRNAs

A list of published sRNAs present in enterohemorrhagic *E. coli* was taken from the Bacterial Small Regulatory RNA Database (Li et al., 2013). sRNAs listed as not being Hfq-binding were filtered out, and the sequences of the remaining sRNAs were input into IntaRNA (Busch et al., 2008; Wright et al., 2014; Mann et al., 2017) to search for interactions with the 5′UTR of *chuA*. sRNAs that were predicted to bind to regions of the *chuA* 5′UTR that were not Hfq-binding were removed from consideration.

Construction of GFP-Translational Fusions and sRNA Expression Vectors for Testing sRNA–mRNA Interactions

Plasmids pXG10SF containing the full-length and truncated *chuA*-GFP translational fusion and pZE12 carrying candidate sRNAs were cloned according to method described in Urban and Vogel (2007). Briefly, the 5′UTR of *chuA* and candidate sRNAs were amplified from genomic DNA using primers identified in **Supplementary Table 1**. The *chuA*-GFP translational fusion was inserted using *Nhe*I-*Nsi*I restriction cloning. Candidate sRNAs were inserted by first linearizing pZE12-*luc* using primers pLlac_O-B and pLlac_O-D. The linearized amplicon, as well as the candidate sRNA amplicon were digested using *Xba*I and ligated together using T4 DNA ligase.

Mutations were made in the *chuA* or sRNA sequences by using the Quikchange XL mutagenesis kit (Agilent) according to the manufacturer's instructions. Primers for mutagenesis were designed using the Quikchange primer design program.[1]

Confirmation of sRNA–*chuA* Interactions Using the sfGFP 2-Plasmid System

The expression of sfGFP was monitored and quantified with and without candidate sRNAs using a BD FACSCanto II or a BD LSRFortessa™ Special Order Research Product cell analyzer. Fluorescence was measured using a 530/30 nm bandpass filter. Forward scatter (FSC) and side scatter (SSC) were also measured to gate the bacterial population. For each sample, at least 100,000 events were recorded. Data was analyzed using FlowJo software (BD) and statistics were calculated using Prism 8 (GraphPad) to obtain each sample's mean median fluorescence intensity (mean MFI). *p*-Values were calculated using a standard two-tailed Student's *t*-test.

Plasmids expressing the wild-type or mutant *chuA*-GFP translational fusion and those expressing candidate sRNAs were co-transformed into *E. coli* DH5α or TOP10F′. Three colonies from each transformation were purified and grown overnight in LB broth. Overnight cultures are subcultured 1/100 in 0.22 μm filtered LB broth and grown to exponential phase (OD_{600} = 0.6). Expression of the *chuA*-GFP translational fusions were induced in TOP10F′ using 200 nM of anhydrotetracycline. These are diluted fivefold in 0.22 μm-filtered PBS, then read on the flow cytometer as described above. Plasmid pJV300 expressing a scrambled sRNA, and pXG1 and pXG0 plasmids expressing GFP and Lux, respectively, were used as controls.

RNA Secondary Structure Prediction

The secondary structure for the 5′UTR of *chuA* was predicted using the mfold[2] and RNAfold webservers (Zuker, 2003; Lorenz et al., 2011). Figures were drawn on RNAStructure version 6.0.1 (Reuter and Mathews, 2010). ARN motifs were detected using custom scripts previously used in Tree et al. (2014).

RNA Sequencing of Bicyclomycin-Treated Cells

Three single colonies of *E. coli* O157:H7 str. Sakai *stx*- were grown for 16 h in LB broth. The following day, these subcultured 1/100 in MEM-HEPES supplemented with 0.1% glucose and 250 nM $Fe(NO_3)_3$. At an OD_{600} of 0.75, cultures were split into two (treated and untreated), and 50 μg/mL of bicyclomycin was added to the treated sample. Cultures were incubated for a further 15 min, followed by addition of RNA stop solution (5% water-saturated phenol in ethanol). RNA was extracted using guanidinium thiocyanate-phenol as previously described in Tollervey and Mattaj (1987). Genomic DNA was digested using RQ1 DNase (Promega) and RNA was cleaned using another phenol-chloroform extraction. Total RNA was ribodepleted using the Zymo-Seq RiboFree Total RNA library kit and libraries were prepared using the Illumina NextSeq 500/550 Mid-Output Kit. Samples were 2 × 75 bp paired-end sequenced on an Illumina NextSeq 500 platform. Library preparation and sequencing were performed by the Ramaciotti Centre for Genomics in the University of New South Wales, Sydney, NSW, Australia.

RNA Sequencing Analysis and Identification of Rho-Dependent Transcripts

RNA sequencing data for *in vivo* analysis was taken from SRA accession number SRP136076. Alignment and DEseq analysis of RNA sequencing output was done using the "align," "coverage," "gene-quanti," and "deseq" modules of READemption v1.0 (Förstner et al., 2014) using default settings.

To identify Rho-terminated transcripts, fastq files were re-aligned to the *E. coli* O157:H7 str. Sakai genome (accession number: NC_002695.2) using BWA-MEM (v0.7.17) (Li and Durbin, 2010). BAM files were generated using samtools (v.1.10) (Li et al., 2009) and 3′ end read counts were calculated using the genomecov tool from bedtools (v2.27.1) (Quinlan and Hall, 2010). Rho readthrough scores were calculate using the program RhoTerm-Peaks using a window size of 250 nt (Adams et al., 2021).

[1] https://www.agilent.com/store/primerDesignProgram.jsp

[2] https://unafold.rna.albany.edu/?q=mfold

DATA AVAILABILITY STATEMENT

RNA sequencing datasets are deposited at the NCBI Gene Expression Omnibus (GEO) under accession numbers GSE143631, GSE46118, and GSE197379.

AUTHOR CONTRIBUTIONS

BS and JT conceived and designed the experimental work, analyzed the data, and wrote the manuscript. BS performed the experimental work. Both authors contributed to the article and approved the submitted version.

FUNDING

BS was supported by a Research Training Program Scholarship from the Australian Government. JT and BS were supported by funding from the National Health and Medical Research Council (GNT1161161). Flow cytometry in this work was performed at the Mark Wainwright Analytical Centre of the University of New South Wales (UNSW) Sydney, which is part funded by the Research Infrastructure Programme of UNSW Sydney.

SUPPLEMENTARY MATERIAL

The Supplementary Material for this article can be found online at: https://www.frontiersin.org/articles/10.3389/fmicb.2022.821196/full#supplementary-material

Supplementary Figure 1 | ChiX indirectly represses *chuA* translation. **(A,B)** (*Left*) IntaRNA prediction of the *chuA*–ChiX interaction. Compensatory point mutations predicted to disrupt the interaction are indicated by the arrows. (*Right*) Fluorescence measurements of wild-type or mutant *chuA*-sfGFP translational fusions in the presence and absence of wild-type or mutant ChiX overexpression plasmid. Measurements are the mean median fluorescence intensity of three biological replicates.

Supplementary Figure 2 | Secondary structure of the *chuA* 5′UTR as predicted by RNAfold. The +1 site, CyaR binding site, FourU RNA thermometer and sites where truncations were made are indicated.

Supplementary Table 1 | Primers, bacterial strains, and plasmids used in this work.

REFERENCES

Adams, P. P., Baniulyte, G., Esnault, C., Chegireddy, K., Singh, N., Monge, M., et al. (2021). Regulatory roles of *Escherichia coli* 5' UTR and ORF-internal RNAs detected by 3' end mapping. *eLife* 10:e62438. doi: 10.7554/eLife.62438

Anzaldi, L. L., and Skaar, E. P. (2010). Overcoming the heme paradox: Heme toxicity and tolerance in bacterial pathogens. *Infect. Immun.* 78, 4977–4989. doi: 10.1128/IAI.00613-10

Bags, A., and Neilands, J. B. (1987). Ferric uptake regulation protein acts as a repressor, employing iron(II) as a cofactor to bind the operator of an iron transport operon in *Escherichia coli*. *Biochemistry* 26, 5471–5477. doi: 10.1021/bi00391a039

Banerjee, R., Weisenhorn, E., Schwartz, K. J., Myers, K. S., Glasner, J. D., Perna, N. T., et al. (2020). Tailoring a global iron regulon to a uropathogen. *mBio* 11:e00351-20. doi: 10.1128/mBio.00351-20

Barber, M. F., and Elde, N. C. (2014). Escape from bacterial iron piracy through rapid evolution of transferrin. *Science* 346, 1362–1366. doi: 10.1126/science.1259329

Bertin, Y., Chaucheyras-Durand, F., Robbe-Masselot, C., Durand, A., de la Foye, A., Harel, J., et al. (2013). Carbohydrate utilization by enterohaemorrhagic *Escherichia coli* O157: H7 in bovine intestinal content. *Environ. Microbiol.* 15, 610–622. doi: 10.1111/1462-2920.12019

Bossi, L., Schwartz, A., Guillemardet, B., Boudvillain, M., and Figueroa-Bossi, N. (2012). A role for Rho-dependent polarity in gene regulation by a noncoding small RNA. *Genes Dev.* 26, 1864–1873. doi: 10.1101/gad.195412.112

Busch, A., Richter, A. S., and Backofen, R. (2008). IntaRNA: efficient prediction of bacterial sRNA targets incorporating target site accessibility and seed regions. *Bioinformatics* 24, 2849–2856. doi: 10.1093/bioinformatics/btn544

Cardinale, C. J., Washburn, R. S., Tadigotla, V. R., Brown, L. M., Gottesman, M. E., and Nudler, E. (2008). Termination factor Rho and its cofactors NusA and NusG silence foreign DNA in *E. coli*. *Science* 320, 935–938. doi: 10.1126/science.1152763

Carlson-Banning, K. M., and Sperandio, V. (2016). Catabolite and oxygen regulation of enterohemorrhagic *Escherichia coli* virulence. *mBio* 7:e01852-16. doi: 10.1128/mBio.01852-16

Celia, H., Noinaj, N., Zakharov, S. D., Bordignon, E., Botos, I., Santamaria, M., et al. (2016). Structural insight into the role of the Ton complex in energy transduction. *Nature* 538, 60–65. doi: 10.1038/nature19757

Chareyre, S., and Mandin, P. (2018). Bacterial iron homeostasis regulation by sRNAs. *Microbiol. Spectr.* 6, 1–15. doi: 10.1128/microbiolspec.RWR-0010-2017

Chen, J., Morita, T., and Gottesman, S. (2019). Regulation of transcription termination of small RNAs and by small RNAs: molecular mechanisms and biological functions. *Front. Cell. Infect. Microbiol.* 9:201. doi: 10.3389/fcimb.2019.00201

Conway, T., and Cohen, P. S. (2015). Commensal and pathogenic *Escherichia coli* metabolism in the gut. *Microbiol Spectr.* 3:10.1128/microbiolspec.MBP-0006-2014. doi: 10.1128/9781555818883.ch16

Corcoran, C. P., Podkaminski, D., Papenfort, K., Urban, J. H., Hinton, J. C. D., and Vogel, J. (2012). Superfolder GFP reporters validate diverse new mRNA targets of the classic porin regulator, MicF RNA. *Mol. Microbiol.* 84, 428–445. doi: 10.1111/j.1365-2958.2012.08031.x

Cornelissen, C. N. (2018). Subversion of nutritional immunity by the pathogenic *Neisseriae*. *Pathog. Dis.* 76:ftx112. doi: 10.1093/femspd/ftx112

Curtis, M. M., Hu, Z., Klimko, C., Narayanan, S., Deberardinis, R., and Sperandio, V. (2014). The gut commensal *Bacteroides thetaiotaomicron* exacerbates enteric infection through modification of the metabolic landscape. *Cell Host Microbe* 16, 759–769. doi: 10.1016/j.chom.2014.11.005

De Lay, N., and Gottesman, S. (2009). The crp-activated small noncoding regulatory RNA CyaR (RyeE) links nutritional status to group behavior. *J. Bacteriol.* 191, 461–476. doi: 10.1128/JB.01157-08

Evfratov, S. A., Osterman, I. A., Komarova, E. S., Pogorelskaya, A. M., Rubtsova, M. P., Zatsepin, T. S., et al. (2017). Application of sorting and next generation sequencing to study 5'-UTR influence on translation efficiency in *Escherichia coli*. *Nucleic Acids Res.* 45, 3487–3502. doi: 10.1093/nar/gkw1141

Evstatiev, R., and Gasche, C. (2012). Iron sensing and signalling. *Gut* 61, 933–952. doi: 10.1136/gut.2010.214312

Fischbach, M. A., and Sonnenburg, J. L. (2011). Eating for two: how metabolism establishes interspecies interactions in the gut. *Cell Host Microbe* 10, 336–347. doi: 10.1016/j.chom.2011.10.002

Förstner, K. U., Vogel, J., and Sharma, C. M. (2014). READemption-a tool for the computational analysis of deep-sequencing-based transcriptome data. *Bioinformatics* 30, 3421–3423. doi: 10.1093/bioinformatics/btu533

Fournier, C., Smith, A., and Delepelaire, P. (2011). Haem release from haemopexin by HxuA allows *Haemophilus influenzae* to escape host nutritional immunity. *Mol. Microbiol.* 80, 133–148. doi: 10.1111/j.1365-2958.2011.07562.x

Garcia, E. C., Brumbaugh, A. R., and Mobley, H. L. T. (2011). Redundancy and specificity of *Escherichia coli* iron acquisition systems during urinary tract infection. *Infect. Immun.* 79, 1225–1235. doi: 10.1128/iai.01222-10

Gyles, C. L. (2007). Shiga toxin-producing *Escherichia coli*: an overview. *J. Anim. Sci.* 85, E45–E62. doi: 10.2527/jas.2006-508

Hagan, E. C., and Mobley, H. L. T. (2009). Haem acquisition is facilitated by a novel receptor Hma and required by uropathogenic *Escherichia coli* for kidney infection. *Mol. Microbiol.* 71, 79–91. doi: 10.1111/j.1365-2958.2008.06509.x

Hood, M. I., and Skaar, E. P. (2012). Nutritional immunity: transition metals at the pathogen-host interface. *Nat. Rev. Microbiol.* 10, 525–537. doi: 10.1038/nrmicro2836

Kaper, J. B., Nataro, J. P., and Mobley, H. L. (2004). Pathogenic *Escherichia coli*. *Nat. Rev. Microbiol.* 2, 123–140. doi: 10.1038/nrmicro818

Karpman, D., and Ståhl, A.-L. (2014). Enterohemorrhagic *Escherichia coli* pathogenesis and the host response. *Microbiol. Spectr.* 2, 1–15. doi: 10.1128/microbiolspec.EHEC-0009-2013

Kim, D., Hong, J. S. J., Qiu, Y., Nagarajan, H., Seo, J. H., Cho, B. K., et al. (2012). Comparative analysis of regulatory elements between *Escherichia coli* and *Klebsiella pneumoniae* by genome-wide transcription start site profiling. *PLoS Genet.* 8:e1002867. doi: 10.1371/journal.pgen.1002867

Kouse, A. B., Righetti, F., Kortmann, J., Narberhaus, F., and Murphy, E. R. (2013). RNA-mediated thermoregulation of iron-acquisition genes in *Shigella dysenteriae* and pathogenic *Escherichia coli*. *PLoS One* 8:e63781. doi: 10.1371/journal.pone.0063781

LaMattina, J. W., Delrossi, M., Uy, K. G., Keul, N. D., Nix, D. B., Neelam, A. R., et al. (2017). Anaerobic heme degradation: ChuY is an anaerobilin reductase that exhibits kinetic cooperativity. *Biochemistry* 56, 845–855. doi: 10.1021/acs.biochem.6b01099

LaMattina, J. W., Nix, D. B., and Lanzilotta, W. N. (2016). Radical new paradigm for heme degradation in *Escherichia coli* O157:H7. *Proc. Natl. Acad. Sci. U.S.A.* 113, 12138–12143. doi: 10.1073/pnas.1603209113

Li, H., and Durbin, R. (2010). Fast and accurate long-read alignment with Burrows-Wheeler transform. *Bioinformatics* 26, 589–595. doi: 10.1093/bioinformatics/btp698

Li, H., Handsaker, B., Wysoker, A., Fennell, T., Ruan, J., Homer, N., et al. (2009). The Sequence Alignment/Map format and SAMtools. *Bioinformatics* 25, 2078–2079. doi: 10.1093/bioinformatics/btp352

Li, L., Huang, D., Cheung, M. K., Nong, W., Huang, Q., and Kwan, H. S. (2013). BSRD: a repository for bacterial small regulatory RNA. *Nucleic Acids Res.* 41, 233–238. doi: 10.1093/nar/gks1264

Lorenz, R., Bernhart, S. H., Höner zu Siederdissen, C., Tafer, H., Flamm, C., Stadler, P. F., et al. (2011). ViennaRNA Package 2.0. *Algorithms Mol. Biol.* 6, 122–128. doi: 10.1186/1748-7188-6-26

Mann, M., Wright, P. R., and Backofen, R. (2017). IntaRNA 2.0: enhanced and customizable prediction of RNA-RNA interactions. *Nucleic Acids Res.* 45, W435–W439. doi: 10.1093/nar/gkx279

Massé, E., and Gottesman, S. (2002). A small RNA regulates the expression of genes involved in iron metabolism in *Escherichia coli*. *Proc. Natl. Acad. Sci. U.S.A.* 99, 4620–4625. doi: 10.1073/pnas.032066599

Massé, E., Salvail, H., Desnoyers, G., and Arguin, M. (2007). Small RNAs controlling iron metabolism. *Curr. Opin. Microbiol.* 10, 140–145. doi: 10.1016/j.mib.2007.03.013

Miranda, R. L., Conway, T., Leatham, M. P., Chang, D. E., Norris, W. E., Allen, J. H., et al. (2004). Glycolytic and gluconeogenic growth of *Escherichia coli* O157:H7 (EDL933) and *E. coli* K-12 (MG1655) in the mouse intestine. *Infect. Immun.* 72, 1666–1676. doi: 10.1128/IAI.72.3.1666-1676.2004

Moon, K., and Gottesman, S. (2011). Competition among Hfq-binding small RNAs in *Escherichia coli*. *Mol. Microbiol.* 82, 1545–1562. doi: 10.1111/j.1365-2958.2011.07907.x

Morgenthau, A., Pogoutse, A., Adamiak, P., Moraes, T. F., and Schryvers, A. B. (2013). Bacterial receptors for host transferrin and lactoferrin: molecular mechanisms and role in host-microbe interactions. *Future Microbiol.* 8, 1575–1585. doi: 10.2217/fmb.13.125

Nagy, G., Dobrindt, U., Kupfer, M., Emody, L., Karch, H., and Hacker, J. (2001). Expression of hemin receptor molecule *chuA* is influenced by rfaH in uropathogenic *E. coli* strain 356. *Infect. Immun.* 69, 1924–1928. doi: 10.1128/IAI.69.3.1924

Naville, M., Ghuillot-Gaudeffroy, A., Marchais, A., and Gautheret, D. (2011). ARNold: a web tool for the prediction of rho-independent transcription terminators. *RNA Biol.* 8, 10–13. doi: 10.4161/rna.8.1.13346

Njoroge, J. W., Nguyen, Y., Curtis, M. M., Moreira, C. G., and Sperandio, V. (2012). Virulence meets metabolism: Cra and KdpE gene regulation in enterohemorrhagic *Escherichia coli*. *mBio* 3:e00280-12. doi: 10.1128/mBio.00280-12

Oglesby-Sherrouse, A. G., and Murphy, E. R. (2013). Iron-responsive bacterial small RNAs: variations on a theme. *Metallomics* 5, 276–286. doi: 10.1039/c3mt20224k

Ong, S. T., Shan Ho, J. Z., Ho, B., and Ding, J. L. (2006). Iron-withholding strategy in innate immunity. *Immunobiology* 211, 295–314. doi: 10.1016/j.imbio.2006.02.004

Peters, J. M., Mooney, R. A., Grass, J. A., Jessen, Tran, F., and Landick, R. (2012). Rho and NusG suppress pervasive antisense transcription in *E. coli*. *Genes Dev.* 26, 2621–2633. doi: 10.1101/gad.196741.112.The

Peters, J. M., Mooney, R. A., Kuan, P. F., Rowland, J. L., Keles, S., and Landick, R. (2009). Rho directs widespread termination of intragenic and stable RNA transcription. *Proc. Natl. Acad. Sci. U.S.A.* 106, 15406–15411. doi: 10.1073/pnas.0903846106

Quinlan, A. R., and Hall, I. M. (2010). BEDTools: a flexible suite of utilities for comparing genomic features. *Bioinformatics* 26, 841–842. doi: 10.1093/bioinformatics/btq033

Reuter, J. S., and Mathews, D. H. (2010). RNAstructure: software for RNA secondary structure prediction and analysis. *BMC Bioinformatics* 11:129. doi: 10.1186/1471-2105-11-129

Ridley, K. A., Rock, J. D., Li, Y., and Ketley, J. M. (2006). Heme utilization in *Campylobacter jejuni*. *J. Bacteriol.* 188, 7862–7875. doi: 10.1128/JB.00994-06

Righetti, F., Nuss, A. M., Twittenhoff, C., Beele, S., Urban, K., Will, S., et al. (2016). Temperature-responsive in vitro RNA structurome of *Yersinia pseudotuberculosis*. *Proc. Natl. Acad. Sci. U.S.A.* 113, 7237–7242. doi: 10.1073/pnas.1523004113

Rossi, M. S., Fetherston, J. D., Létoffé, S., Carniel, E., Perry, R. D., and Ghigo, J. M. (2001). Identification and characterization of the hemophore-dependent heme acquisition system of *Yersinia pestis*. *Infect. Immun.* 69, 6707–6717. doi: 10.1128/IAI.69.11.6707-6717.2001

Ryu, S., Ramseier, T. M., Michotey, V., Saier, M. H., and Garges, S. (1995). Effect of the FruR regulator on transcription of the *pts* operon in *Escherichia coli*. *J. Biol. Chem.* 270, 2489–2496. doi: 10.1074/jbc.270.6.2489

Santiago-Frangos, A., Kavita, K., Schu, D. J., Gottesman, S., and Woodson, S. A. (2016). C-terminal domain of the RNA chaperone Hfq drives sRNA competition and release of target RNA. *Proc. Natl. Acad. Sci. U.S.A.* 113, E6089–E6096. doi: 10.1073/pnas.1613053113

Schu, D. J., Zhang, A., Gottesman, S., and Storz, G. (2015). Alternative Hfq-sRNA interaction modes dictate alternative mRNA recognition. *EMBO J.* 34, 2557–2573. doi: 10.15252/embj.201591569

Sedlyarova, N., Shamovsky, I., Bharati, B. K., Epshtein, V., Chen, J., Gottesman, S., et al. (2016). sRNA-mediated control of transcription termination in *E. coli*. *Cell* 167, 111–121.e13. doi: 10.1016/j.cell.2016.09.004

Segura, A., Bertin, Y., Durand, A., Benbakkar, M., and Forano, E. (2021). Transcriptional analysis reveals specific niche factors and response to environmental stresses of enterohemorrhagic *Escherichia coli* O157:H7 in bovine digestive contents. *BMC Microbiol.* 21:284. doi: 10.1186/s12866-021-02343-7

Segura, A., Bertoni, M., Auffret, P., Klopp, C., Bouchez, O., Genthon, C., et al. (2018). Transcriptomic analysis reveals specific metabolic pathways of enterohemorrhagic *Escherichia coli* O157:H7 in bovine digestive contents. *BMC Genomics* 19:766. doi: 10.1186/s12864-018-5167-y

Sharma, C. M., Hoffmann, S., Darfeuille, F., Reignier, J., Findeiß, S., Sittka, A., et al. (2010). The primary transcriptome of the major human pathogen *Helicobacter pylori*. *Nature* 464, 250–255. doi: 10.1038/nature08756

Silva, I. J., Barahona, S., Eyraud, A., Lalaouna, D., Figueroa-Bossi, N., Massé, E., et al. (2019). SraL sRNA interaction regulates the terminator by preventing premature transcription termination of rho mRNA. *Proc. Natl. Acad. Sci. U.S.A.* 116, 3042–3051. doi: 10.1073/pnas.1811589116

Skaar, E. P. (2010). The battle for iron between bacterial pathogens and their vertebrate hosts. *PLoS Pathog.* 6:e1000949. doi: 10.1371/journal.ppat.1000949

Snider, T. A., Fabich, A. J., Conway, T., and Clinkenbeard, K. D. (2009). *E. coli* O157:H7 catabolism of intestinal mucin-derived carbohydrates and colonization. *Vet. Microbiol.* 136, 150–154. doi: 10.1016/j.vetmic.2008.10.033

Soper, T. J., and Woodson, S. (2008). The rpoS mRNA leader recruits Hfq to facilitate annealing with DsrA sRNA. *RNA* 14, 1907–1917. doi: 10.1261/rna.1110608

Sy, B. M., Lan, R., and Tree, J. J. (2020). Early termination of the Shiga toxin transcript generates a regulatory small RNA. *Proc .Natl. Acad. Sci. U.S.A.* 117, 25055–25065. doi: 10.1073/pnas.2006730117

Tollervey, D., and Mattaj, I. W. (1987). Fungal small nuclear ribonucleoproteins share properties with plant and vertebrate U-snRNPs. *EMBO J.* 6, 469–476. doi: 10.1002/j.1460-2075.1987.tb04777.x

Torres, A. G., and Payne, S. M. (1997). Haem iron-transport system in enterohaemorrhagic *Escherichia coli* O157:H7. *Mol. Microbiol.* 23, 825–833. doi: 10.1046/j.1365-2958.1997.2641628.x

Torres, A. G., Redford, P., Welch, R. A., and Payne, S. M. (2001). TonB-dependent systems of uropathogenic *Escherichia coli*: Aerobactin and heme transport and TonB are required for virulence in the mouse. *Infect. Immun.* 69, 6179–6185. doi: 10.1128/IAI.69.10.6179-6185.2001

Tree, J. J., Granneman, S., McAteer, S. P., Tollervey, D., and Gally, D. L. (2014). Identification of bacteriophage-encoded anti-sRNAs in pathogenic *Escherichia coli*. *Mol. Cell* 55, 199–213. doi: 10.1016/j.molcel.2014.05.006

Urban, J. H., and Vogel, J. (2007). Translational control and target recognition by *Escherichia coli* small RNAs *in vivo*. *Nucleic Acids Res.* 35, 1018–1037. doi: 10.1093/nar/gkl1040

Wagner, E. G. H., and Romby, P. (2015). "Small RNAs in bacteria and archaea: Who they are, what they do, and how they do it," in *Advances in Genetics*, eds T. Friedmann, J. C. Dunlap and S. F. Goodwin (Waltham, MA: Academic Press). doi: 10.1016/bs.adgen.2015.05.001

Waldminghaus, T., Heidrich, N., Brantl, S., and Narberhaus, F. (2007). FourU: a novel type of RNA thermometer in *Salmonella*. *Mol. Microbiol.* 65, 413–424. doi: 10.1111/j.1365-2958.2007.05794.x

Wang, D., McAteer, S. P., Wawszczyk, A. B., Russell, C. D., Tahoun, A., Elmi, A., et al. (2018). An RNA-dependent mechanism for transient expression of bacterial translocation filaments. *Nucleic Acids Res.* 46, 3366–3381. doi: 10.1093/nar/gky096

Waters, L. S., and Storz, G. (2009). Regulatory RNAs in bacteria. *Cell* 136, 615–628. doi: 10.1016/j.cell.2009.01.043

Waters, S. A., McAteer, S. P., Kudla, G., Pang, I., Deshpande, N. P., Amos, T. G., et al. (2017). Small RNA interactome of pathogenic *E. coli* revealed through crosslinking of RNase E. *EMBO J.* 36, 374–387. doi: 10.15252/embj.201694639

Weber, G. G., Kortmann, J., Narberhaus, F., and Klose, K. E. (2014). RNA thermometer controls temperature-dependent virulence factor expression in *Vibrio cholerae*. *Proc. Natl. Acad. Sci. U.S.A.* 111, 14241–14246. doi: 10.1073/pnas.1411570111

Weinberg, E. D. (1975). Nutritional Immunity: host's attempt to withhold iron from microbial invaders. *J. Am. Med. Assoc.* 231, 39–41. doi: 10.1093/ajcn/30.9.1485

Wright, P. R., Georg, J., Mann, M., Sorescu, D. A., Richter, A. S., Lott, S., et al. (2014). CopraRNA and IntaRNA: predicting small RNA targets, networks and interaction domains. *Nucleic Acids Res.* 42, 119–123. doi: 10.1093/nar/gku359

Wyckoff, E. E., Duncan, D., Torres, A. G., Mills, M., Maase, K., and Payne, S. M. (1998). Structure of the *Shigella dysenteriae* haem transport locus and its phylogenetic distribution in enteric bacteria. *Mol. Microbiol.* 28, 1139–1152. doi: 10.1046/j.1365-2958.1998.00873.x

Xu, J., Bjursell, M. K., Himron, J., Deng, S., Carmichael, L. K., Chaing, H. C., et al. (2003). A genomic view of the human-*Bacteroides thetaiotaomicron* symbiosis. *Science* 299, 2074–2076. doi: 10.1126/science.1080029

Zambolin, S., Clantin, B., Chami, M., Hoos, S., Haouz, A., Villeret, V., et al. (2016). Structural basis for haem piracy from host haemopexin by *Haemophilus influenzae*. *Nat. Commun.* 7:11590. doi: 10.1038/ncomms11590

Zhang, A., Schu, D. J., Tjaden, B. C., Storz, G., and Gottesman, S. (2013). Mutations in interaction surfaces differentially impact *E. coli* Hfq association with small RNAs and their mRNA targets. *J. Mol. Biol.* 425, 3678–3697. doi: 10.1016/j.jmb.2013.01.006

Zhang, Z., Aboulwafa, M., and Saier, M. H. (2014). Regulation of crp gene expression by the catabolite repressor/activator, Cra, in *Escherichia coli*. *J. Mol. Microbiol. Biotechnol.* 24, 135–141. doi: 10.1159/000362722

Zuker, M. (2003). Mfold web server for nucleic acid folding and hybridization prediction. *Nucleic Acids Res.* 31, 3406–3415. doi: 10.1093/nar/gkg595

Zwiefka, A., Kohn, H., and Widger, W. R. (1993). Transcription termination factor rho: the site of bicyclomycin inhibition in *Escherichia coli*. *Biochemistry* 32, 3564–3570. doi: 10.1021/bi00065a007

Conflict of Interest: The authors declare that the research was conducted in the absence of any commercial or financial relationships that could be construed as a potential conflict of interest.

Publisher's Note: All claims expressed in this article are solely those of the authors and do not necessarily represent those of their affiliated organizations, or those of the publisher, the editors and the reviewers. Any product that may be evaluated in this article, or claim that may be made by its manufacturer, is not guaranteed or endorsed by the publisher.

frontiers | Frontiers in Microbiology

ORIGINAL RESEARCH
published: 28 April 2022
doi: 10.3389/fmicb.2022.882563

The Fis Nucleoid Protein Negatively Regulates the Phase Variation *fimS* Switch of the Type 1 Pilus Operon in Enteropathogenic *Escherichia coli*

*Zeus Saldaña-Ahuactzi[1], Jorge Soria-Bustos[2], Verónica I. Martínez-Santos[3], Jorge A. Yañez-Santos[4], Ygnacio Martínez-Laguna[5], María Lilia Cedillo-Ramirez[6], José L. Puente[7] and Jorge A. Girón[6]**

[1]Paul G. Allen School for Global Health, College of Veterinary Medicine, Washington State University, Pullman, WA, United States, [2]Instituto de Ciencias de la Salud, Universidad Autónoma del Estado de Hidalgo, Pachuca, Mexico, [3]CONACyt Facultad de Ciencias Químico-Biológicas, Universidad Autónoma de Guerrero, Chilpancingo, Mexico, [4]Facultad de Estomatología, Benemérita Universidad Autónoma de Puebla, Puebla, Mexico, [5]Centro de Investigaciones en Ciencias Microbiológicas, Benemérita Universidad Autónoma de Puebla, Puebla, Mexico, [6]Centro de Detección Biomolecular, Benemérita Universidad Autónoma de Puebla, Puebla, Mexico, [7]Instituto de Biotecnología, Universidad Nacional Autónoma de México, Cuernavaca, Mexico

OPEN ACCESS

Edited by:
Dongsheng Zhou,
Beijing Institute of Microbiology and Epidemiology, China

Reviewed by:
William R. Schwan,
University of Wisconsin–La Crosse, United States
Runhua Han,
University of Manitoba, Canada
Aaron White,
University of Saskatchewan, Canada

***Correspondence:**
Jorge A. Girón
jagiron@gmail.com

Specialty section:
This article was submitted to Infectious Agents and Disease, a section of the journal Frontiers in Microbiology

Received: *24 February 2022*
Accepted: *23 March 2022*
Published: *28 April 2022*

Citation:
Saldaña-Ahuactzi Z, Soria-Bustos J, Martínez-Santos VI, Yañez-Santos JA, Martínez-Laguna Y, Cedillo-Ramirez ML, Puente JL and Girón JA (2022) The Fis Nucleoid Protein Negatively Regulates the Phase Variation fimS Switch of the Type 1 Pilus Operon in Enteropathogenic Escherichia coli. Front. Microbiol. 13:882563. doi: 10.3389/fmicb.2022.882563

In *Escherichia coli* the expression of type 1 pili (T1P) is determined by the site-specific inversion of the *fimS* ON–OFF switch located immediately upstream of major fimbrial subunit gene *fimA*. Here we investigated the role of virulence (Ler, GrlR, and GrlA) and global regulators (H-NS, IHF, and Fis) in the regulation of the *fimS* switch in the human enteropathogenic *E. coli* (EPEC) O127:H6 strain E2348/69. This strain does not produce detectable T1P and PCR analysis of the *fimS* switch confirmed that it is locked in the OFF orientation. Among the regulator mutants analyzed, only the Δ*fis* mutant produced significantly high levels of T1P on its surface and yielded high titers of agglutination of guinea pig erythrocytes. Expression analysis of the *fimA*, *fimB*, and *fimE* promoters using *lacZ* transcriptional fusions indicated that only P*fimA* activity is enhanced in the absence of Fis. Collectively, these data demonstrate that Fis is a negative regulator of T1P expression in EPEC and suggest that it is required for the FimE-dependent inversion of the *fimS* switch from the ON-to-OFF direction. It is possible that a similar mechanism of T1P regulation exists in other intestinal and extra-intestinal pathogenic classes of *E. coli*.

Keywords: Fis, phase variation, *fimS* switch, type 1 pilus, EPEC

INTRODUCTION

Type 1 pili (T1P) are hair-like structures produced by *Escherichia coli* strains and other members of the *Enterobacteriaceae* (Werneburg and Thanassi, 2018). The clinical importance of T1P has been clearly demonstrated in the pathogenesis of uropathogenic *E. coli* (UPEC) strains that colonize and cause disease in the urinary tract (Welch et al., 2002; Flores-Mireles et al., 2015). In the bladder, T1P mediate bacterial attachment of UPEC to mannose-containing receptors present on epithelial cells. T1P are also important colonization factors of avian

pathogenic *E. coli* strains that cause respiratory disease and adherent-invasive *E. coli* (AIEC) strains that cause inflammation of the colon (La Ragione et al., 2000; La Ragione and Woodward, 2002; Kaper et al., 2004; Martinez-Medina and Garcia-Gil, 2014; Yang et al., 2020). The role of T1P in the pathogenesis of enteropathogenic *E. coli* (EPEC), a cause of childhood diarrhea in the developing world, remains unclear. An early study in human volunteers fed with EPEC strain E2348/69 showed that antibodies against T1P are developed during infection suggesting that these pili are produced *in vivo* (Levine et al., 1978). However, the contribution of T1P to the adherence and colonization of the small bowel has not been studied. In contrast, T1P appear to play an important role in the interaction of BFP-negative atypical EPEC strains with abiotic surfaces favoring biofilm formation (Hernandes et al., 2013; Nascimento et al., 2014).

T1P cause mannose-sensitive agglutination of guinea pig and fowl erythrocytes (Abraham et al., 1985; Klemm, 1986; Spaulding et al., 2018). These pili are composed of a major repeating FimA 17 kDa-subunit that form a helical structure of about 0.5 to 2.0 μm in length and a diameter of 7 nm (Hahn et al., 2002; Puorger et al., 2011). At the tip of the filament sits the FimH adhesin protein, which forms a fibrillum structure responsible for the receptor mannose-binding specificity (Puorger et al., 2011). Regulation of fimbrial expression in *E. coli* is determined in general by regulatory genetic elements as well as by environmental signals (Roesch and Blomfield, 1998; Hung et al., 2001; Blomfield and van der Woude, 2007; Müller et al., 2009; De la Cruz et al., 2017; Matter et al., 2018; Ares et al., 2019). Determining what fimbriae are expressed at particular sites in the host is crucial for the microorganism for tissue colonization and survival against the immune system and to adapt to different hosts and environments. The chromosomal *fimAICDFGH* gene cluster encode the machinery for T1P assembly (Klemm, 1986; Remaut et al., 2006). *fimA* is transcriptionally regulated by a phase variation mechanism involving the inversion of a 314-bp chromosomal DNA segment (*fimS*) located immediately upstream of *fimA* (Abraham et al., 1985; Klemm, 1986). The *fimA* promoter is believed to reside within this invertible *fimS* element and directs transcription of the *fimAICDFGH* gene cluster when *fimS* is in the ON orientation promoting production of pili. In the alternate OFF orientation, no pili are produced (Freitag et al., 1985; Blomfield et al., 1991). Further, T1P phase variation is controlled by two recombinases encoded by *fimB* and *fimE*, located upstream of *fimA* (Klemm, 1986; Dorman and Higgins, 1987). Both recombinases bind to specific half-sites that flank, and overlap with, the left and right inverted repeats (IRL and IRR, respectively; Gally et al., 1996). FimE and FimB act in opposite ways such that FimE shows a strong preference for the *fimS* switch in the OFF orientation whereas FimB facilitates switching in both directions (Klemm, 1986; McClain et al., 1991, 1993; McCusker et al., 2008). In wild-type cells, FimE activity predominates over FimB and hence, most bacteria are non-piliated. *fimB* mutants retain FimE thus they are locked in the OFF orientation (Klemm, 1986; McClain et al., 1993; Gally et al., 1996).

Several other regulatory DNA-binding proteins also bind to and affect the inversion of the *fimS* switch including the integration host factor (IHF), the histone-like protein (H-NS), and the leucine-responsive global regulatory protein (Lrp; Schmid, 1990; Blomfield et al., 1993; Finkel and Johnson, 1993; Roesch and Blomfield, 1998; Bessaiah et al., 2022). In wild-type strains, normal expression of *fimA* requires IHF, whereas IHF mutants have expression of *fimA* locked either in the ON or OFF phase. IHF plays a dual role in controlling *fimA* expression as it is required both for inversion of the *fimA* control region and efficient expression from the *fimA* promoter and this protein was shown to bind with high affinity to two sites within the *fimS* invertible element (Dorman and Higgins, 1987; Blomfield et al., 1997). The DNA-binding protein Lrp is involved in transcriptional activation and repression of metabolic genes in *E. coli* and it binds to the *fimS* switch promoting phase variation (Blomfield et al., 1993; Gally et al., 1993; Calvo and Matthews, 1994). Lrp binds to two sites in or near the *fimS* switch, where it acts positively on DNA inversion. This protein alters the trajectory of the invertible element to enhance the formation of a synaptic complex for recombination. Interestingly, both binding sites for Lrp and for IHF are overlapped, suggesting a possible interaction between these two regulators (Blomfield et al., 1993; Gally et al., 1994; Kelly et al., 2006).

Fis, the factor for inversion stimulation, is an *E. coli* host factor required for *in vitro* DNA inversion (Johnson et al., 1986; Koch et al., 1988; Finkel and Johnson, 1993). Fis affects the expression of multiple genes by binding to promoters containing the degenerate sequence 5'GNNC/TA/TNNA/TNNT/CG/ANNC3', where N can be any base (Finkel and Johnson, 1993; Hengen et al., 1997; Schneider et al., 2001; Feldman et al., 2006). Fis alters the conformation of DNA through bending as well as through contact with the a-subunit of RNA polymerase (Thompson et al., 1988; Bokal et al., 1997; Dorman and Deighan, 2003). Fis participates in site-specific recombination events, such as in the excision of the lambda phage, and acts as an enhancer of site-specific DNA inversion (Gille et al., 1991). Fis is a key activator of exponential phase genes and a repressor of stationary phase genes (Ross et al., 1990; Ball et al., 1992; Xu and Jhonson, 1995; González-Gil et al., 1996; Kelly et al., 2004; Mallik et al., 2004; Lenz and Bassler, 2007; Duprey et al., 2014).

In EPEC, Fis activates transcription of *E. coli* type three secreted proteins genes (*espA, espB*, and *espD*), and the virulence regulator gene *ler*, and represses expression of the bundle-forming pilus gene (*bfpA*; Goldberg et al., 2001). Fis also acts as a negative regulator of curli in EPEC and Enterohemorrhagic *E. coli* (EHEC) O157:H7 (Saldaña et al., 2009). The present study was initiated to investigate the role of global and virulence factors on the expression of T1P in EPEC and to further understand how the ON–OFF phase variation switch works in this organism. The data support a role for Fis as a negative regulator in the *fimS* phase variation switch of the *fim* operon. This study advances our knowledge on the regulation of a pilus structure that is widely distributed among the *Enterobacteriaceae*.

RESULTS

Comparative Analysis of the *fim* Operon of Different *E. coli* Pathotypes

The nucleotide sequence of the *fim* operon of representative prototypic strains of EPEC, UPEC, NMEC, AIEC, EHEC, EAEC, and ETEC was analyzed using the NCBI Multiple Sequence Alignment Viewer, version 1.21.0. This analysis shows that the *fim* operon is highly conserved among the *E. coli* pathotypes, ranking from 97% to 98% identity (**Supplementary Figure 1**). We then sought to determine the homology of the *fimS* invertible element if these *E. coli* pathotypes. The T-Coffee software was used to align the sequences. (**Supplementary Figure 2**). The analysis shows that the *fimS* switch is highly conserved among the *E. coli*.

Fis is a Negative Regulator of T1P

Ultrastructural analysis of EPEC E2348/69 by electron microscopy has revealed that this strain does not produce detectable amounts of T1P when growing in Luria-Bertani (LB) broth at 37°C, suggesting that expression of T1P is under the influence of a strict regulatory control. A PCR-based analysis of the *fimS* switch of EPEC E2348/69 showed that this *fim* switch is locked in the OFF orientation. We set out to investigate the reason(s) for the lack of T1P in EPEC and so we began by studying the effect of mutations in virulence (*perABC, ler, grlA*, and *grlR*) and global (*hns, ihf, rpoS*, and *fis*) regulator genes in the production of T1P. These virulence and global regulators regulate the expression of EPEC chromosome- and plasmid-encoded virulence factors. Among all of the mutants analyzed, only the Δ*fis* mutant showed a dramatic effect on *fimA* expression. Namely, a significant increase of FimA synthesis was detected with anti-T1P antibodies by immunoblotting, a 50-fold increase in T1P production was recorded employing flow cytometry, and *fimA* expression by RT-PCR when compared to the wild-type strain and the other mutants (**Figures 1A–C**). Transmission electron microscopy analysis of the E2348/69Δ*fis* mutant (**Figure 2C**) confirmed these results, which showed an increased production of fimbriae on the surface of the bacteria as compared to E2348/69 (**Figure 2A**). Immunogold labeling with anti-T1P antibody confirmed the presence of T1P on the surface of E2348/69Δ*fis* (**Figure 2D**). No gold labeling was observed on E2348/69 (**Figure 2B**). To further confirm the identity of the pili structures produced by the Δ*fis* mutant, we purified the pili as described in Experimental Procedures. The pili purified from the E2348/69Δ*fis* mutant dissociated into 17 kDa protein subunits after HCl treatment in SDS-PAGE gels (**Supplementary Figure 3**) and the peptides generated after trypsin digestion were analyzed by mass spectrometry. The amino acid sequence of these peptides corresponded to the FimA amino acid (AATTVNGGTV) sequence of *E. coli* K-12 (data not shown). Given that T1P mediate mannose-sensitive hemagglutination (HA) of guinea pig red blood cells, we tested the ability of E2348/69Δ*fis* and the wild-type strain to hemagglutinate guinea pig erythrocytes in the presence and absence of 1% D-mannose. While the wild-type strain showed no HA reaction, the E2348/69Δ*fis* showed a high HA titer of 1:1,024 (**Figure 2E**). This result correlates with the electron microscopy and immunoassays described above.

Role of Temperature in Regulation of *fimA*

In most laboratory *E. coli* strains the production of T1P is favored by growth in static liquid cultures at 26°C. We wanted to know if temperature had a role in the regulation of T1P in EPEC. Thus, we compared T1P production and transcription levels of *fimA* in the E2348/69 wild-type strain, the Δ*fis* mutant, and the Δ*fis* mutant complemented with *fis* on a plasmid. The data show that T1P production in the Δ*fis* mutant is increased 68-fold and 16-fold at 37°C and 26°C, respectively, with respect to the wild-type strain. E2348/69 produced extremely low levels of T1P at either temperature. Complementation of the Δ*fis* mutant with *fis* on pUC19 (**Figure 3A**) or low-copy plasmid pBR322 (data not shown) resulted in the absence of T1P as shown for the wild-type strain at both temperatures. These results are in line with the *fimA* expression data obtained by RT-PCR (**Figure 3B**).

The Orientation of the *fimS* Switch Correlates With the Strain Phenotype

The *fimS* switch contains a promoter that directs transcription of the *fimA* subunit gene in one orientation (ON), but not in the other (OFF) orientation (McClain et al., 1991). To learn about the orientation of the *fimS* switch in E2348/69 and the Δ*fis* mutant we used PCR with different sets of forward and reverse primers derived from different regions of the *fimS* switch. Amplicons of the expected sizes were obtained in all but two of the combinations of primers in E2348/69; no amplicons were obtained with F1F2 and R1R2 primers confirming that the *fimS* switch in the wild-type strain E2348/69 is locked in the OFF orientation. In contrast, the *fis* mutant showed a mixed population of variants containing the *fimS* invertible element in the ON and OFF orientations as determined by the size of the PCR products that were obtained with all the combinations of primers tested (**Figures 4A–C**).

Role of Fis in the Transcriptional Expression of the *fimA, fimB,* and *fimE* Promoters

We wanted to elucidate if the negative effect on the expression of T1P by Fis was at the level of transcription of the fimbrial subunit gene *fimA* or the recombinases *fimB* and *fimE*. For this purpose, transcriptional fusions containing the promoter regions of *fimA*, *fimB*, and *fim*E were fused to the promoter-less *β*-galactosidase reporter gene in plasmid pMBL1034. The resulting fusions were sequenced for confirmation and the plasmids mobilized into EPEC E2348/69 and the Δ*fis* mutant. Transcriptional analysis of these fusions was performed with the strains growing at 25°C and 37°C in LB broth. E2348/69 carrying the *β*-galactosidase reporter gene alone in plasmid pMLB1034 was used as negative control. While a 4.7-fold (**Figure 5A**) and 10-fold increase in transcription activity of the *fimA* promoter (P*fimA*) was obtained in E2348/69Δ*fis* at

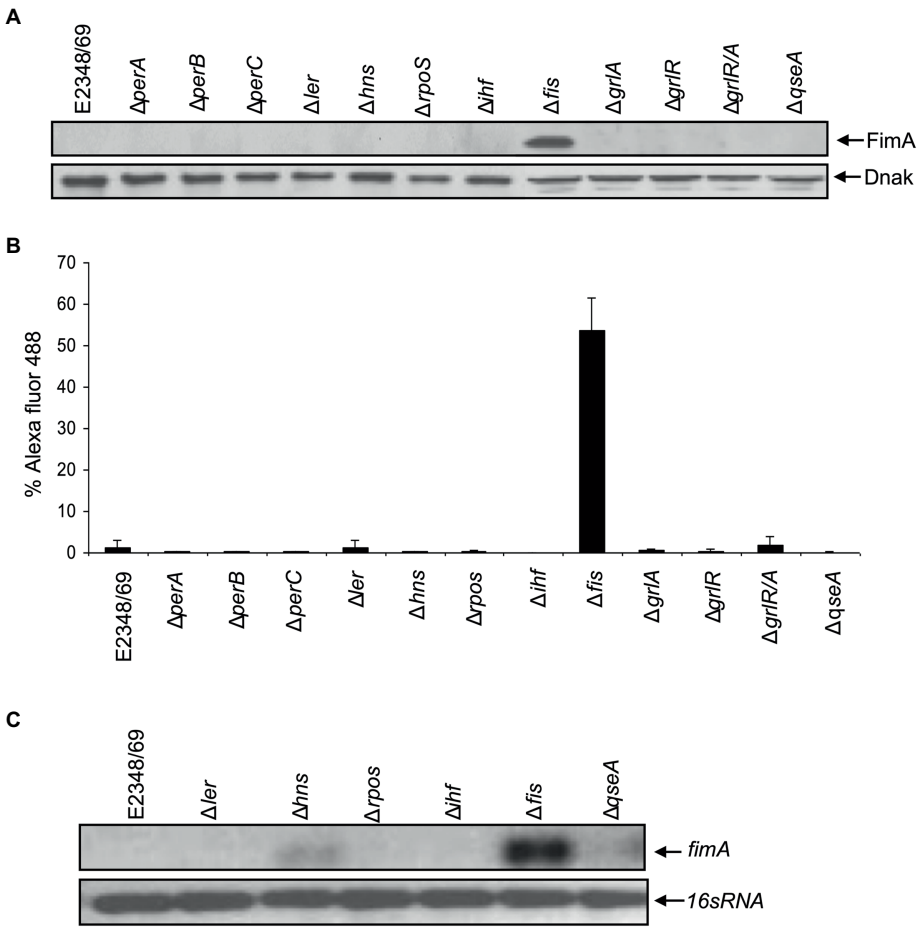

FIGURE 1 | Fis is a negative regulator of T1P. **(A)** Western blot and **(B)** flow cytometry, using antibodies raised against T1P revealed that E2348/69 does not produce detectable amounts of T1P compared to the Δ*fis* mutant. **(C)** RT-PCR using primers for *fimA* gene.

37°C and 25°C, respectively, with respect to the wild-type strain carrying the pMLB1034, no significant transcriptional activity was seen in the strains carrying the P*fimB* or P*fimE* fusions (**Figure 5B**). It is clear from these experiments that in the absence of Fis, particularly at 25°C, the inversion of the *fimS* switch is favored to the ON orientation allowing transcription from the P*fimA* only and yielding increased production of T1P. This result suggests that the negative effect of Fis is not at the level of transcription of any of the recombinases but most likely due to the binding of Fis to P*fimA* region, cooperating with FimE in locking the *fimS* switch to the OFF position.

FimE Recombinase Requires Fis to Efficiently Invert the *fimS* Switch to the OFF State

Next, we wanted to determine if the mechanism of inversion of the *fimS* switch required Fis. Our hypothesis was that the FimE recombinase requires Fis to efficiently invert the *fimS* switch to the OFF state. The data obtained so far indicated that in the absence of Fis, high levels of *fimA* expression are displayed. We inquired if this result was caused by a shift of the *fimS* switch as a consequence of the absence of Fis. Thus, we constructed a set of double and triple mutants of *fimE, fimB*, and *fis* containing the *fimS* switch locked in the ON or OFF orientation. The mutants were then complemented with *fimE* on a plasmid. The strains generated were grown overnight in LB medium at 37°C and processed for flow cytometry using anti-T1P antibodies (**Figure 6**). Similar levels of T1P production were found in the Δ*fis* mutant, the double Δ*fimBE*, and triple Δ*fisfimBE* mutants in which the *fimS* switch is locked in the ON orientation (**Figure 6**). Interestingly, when the Δ*fimBE*-ON strain was complemented with pFimE, the production of T1P returned to wild-type levels. However, the Δ*fisfimBfimE* strain in the same orientation complemented with pFimE showed 2-fold reduction in T1P production with respect to the triple mutant, but yet, expressed 5 times more T1P than the wild-type strain, suggesting that FimE-mediated inversion of the *fimS* switch to the OFF state requires Fis.

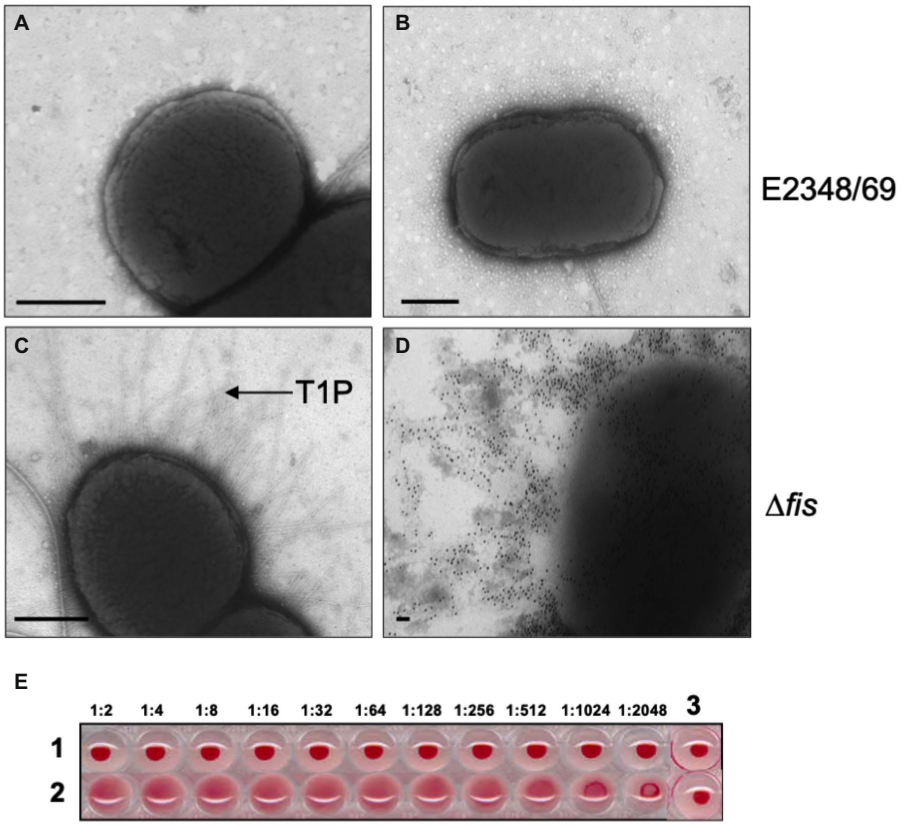

FIGURE 2 | Transmission electron microscopy and hemagglutination. **(A,B)** Negative staining and immuno-staining of E2348/69 showing no production of T1P. **(C,D)** Negative staining and immuno-gold labeling of E2348/69Δ*fis* producing abundant T1P. Magnification bars, 0.5 μm. **(E)** Hemagglutinations (HA) showing (1) E2348/69, which does not produce T1P and consequently does not produce HA; (2) E2348/69Δ*fis* produces T1P and shows strong HA titer. (3) RBCs alone as negative control. The HA assay was done with 1% guinea pig red blood cells (RBCs) with the bacteria in the dilutions noted above.

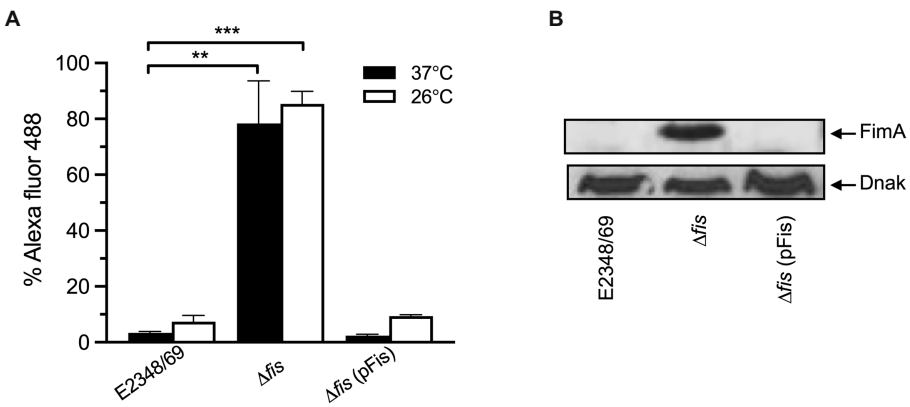

FIGURE 3 | Complementation of E2348/69Δ*fis* with *fis* on a plasmid restores negative regulation. **(A)** Flow cytometry and **(B)** Western blot to determine production of T1P by wild-type E2348/69, E2348/69Δ*fis* mutant, and E2348/69Δ*fis* complemented with *fis* on pUC19. These data are the mean of at least three experiments performed in triplicate on different days. $^{**}p < 0.01$; $^{***}p < 0.001$.

DISCUSSION

T1P are the most common and best-characterized fimbrial adhesins in the *Enterobacteriaceae* family. While T1P is well-recognized as a virulence factor in the pathogenesis scheme of UPEC and APEC, the role of T1P in the colonization of the human gut mucosa by EPEC is uncertain. Production of T1P is transcriptionally regulated by phase variation, a

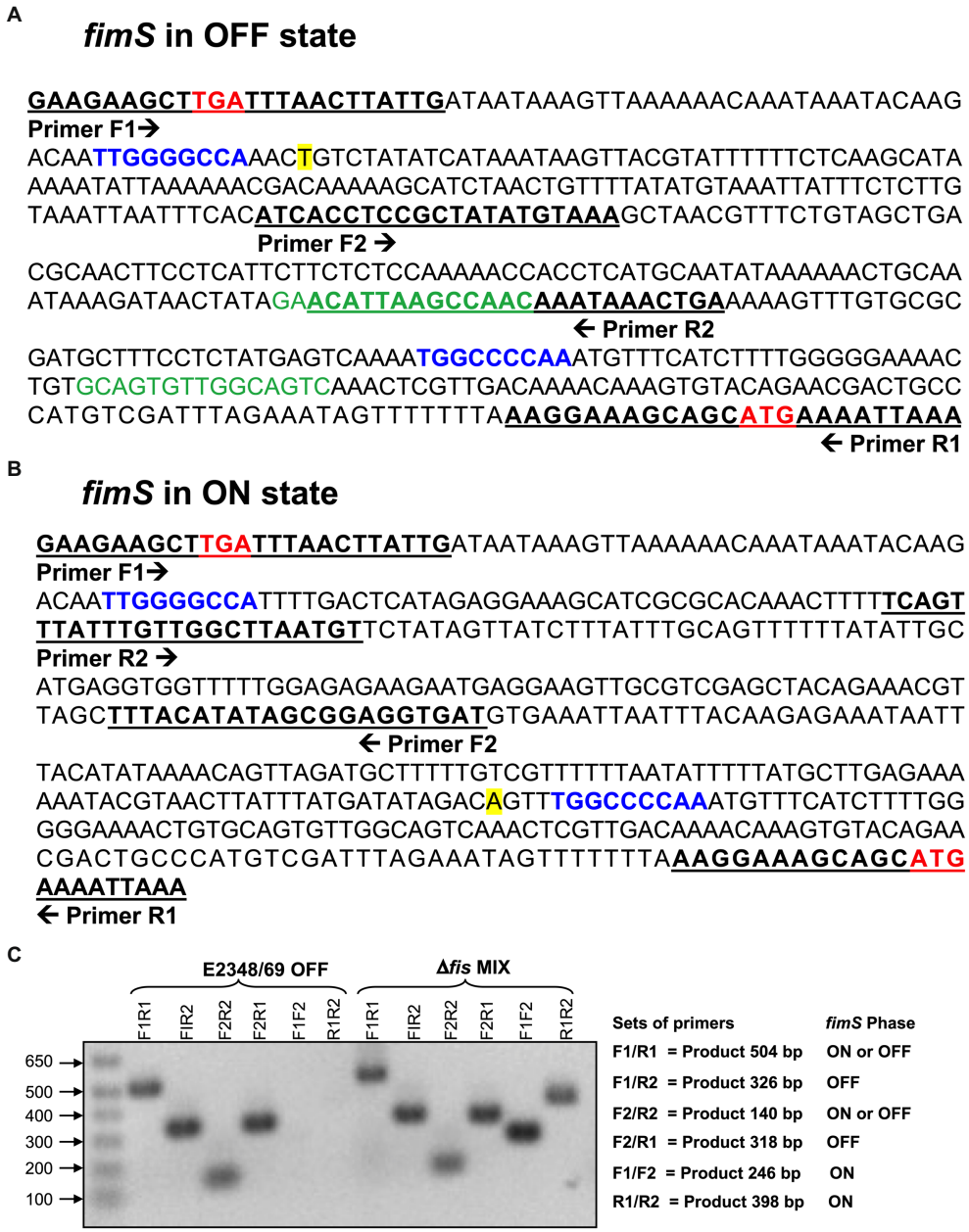

FIGURE 4 | Orientation of the *fimS* invertible element in EPEC strains. **(A)** The nucleotide sequence of the region upstream of the *fimA* structural gene in E2348/69 (Abraham et al., 1985; Klemm, 1986) contains the *fimS* invertible element locked in the OFF orientation. Putative Fis-binding sites are denoted in green. **(B)** Sequence of the *fimS* switch oriented in the ON position. The stop codon (TGA) of *fimE* and the start codon (ATG) of *fimA* are denoted in bold red. The inverted repeat (IR) sequences, IRL (left) and IRR (right), are indicated in blue. The transcription start [A] of *the fimA* promoter is highlighted in yellow. The underlined nucleotide sequences show the binding sites of the primers used in the PCR reaction and the arrows indicate the direction of each primer. **(C)** PCR with different sets of primers show that the Δ*fis* mutant is a mixture of cells containing the *fimS* invertible element oriented in either ON or OFF position. In contrast, the *fimS* switch in the E2348/69 is oriented in the OFF position. The set of primers used, products expected, and the *fimS* phase for each set of primers used are shown on the right.

mechanism that involves the inversion of the *fimS* switch located immediately upstream of *fimA* (Abraham et al., 1985; Klemm, 1986) allowing for two different orientations (ON and OFF). The phase variation of T1P allows a population of bacteria to generate a number of phenotypic variants, some of which may be better suited to colonize certain host niches, for example UPEC expresses T1P in the bladder where it can bind the mannose-rich uroplakin receptors (Thumbikat et al., 2009). As the bacteria ascend to the kidneys the pH drops and the osmolarity increases, which

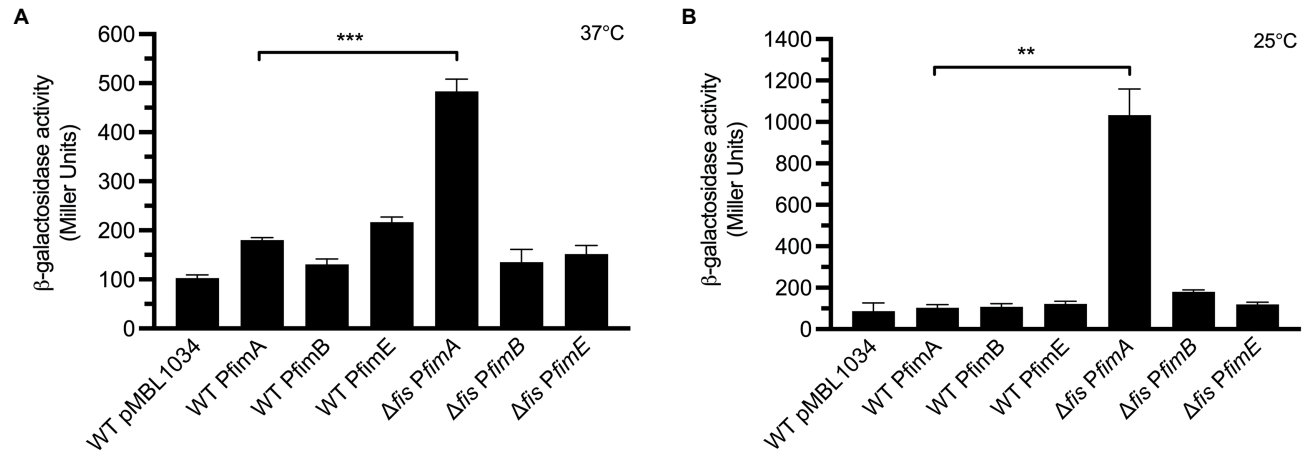

FIGURE 5 | Analysis of transcriptional expression. Fusion constructs consisting of *fimA*, *fimB*, and *fimE* promoters fused to the promoter-less *β*-galactosidase reporter gene were employed to quantitatively determine the expression of *fim* promoters. **(A,B)** A 3-fold and 10-fold increased activity of the P*fimA* promoter in the E2348/69Δ*fis* was recorded at 37°C and 25°C, respectively, in comparison with the wild-type strain. No transcriptional activity was seen in the rest of the fusions. E2348/69 and E2348/69Δ*fis* carrying pMLB1034 were used as negative controls. These data are the mean of at least three experiments performed in triplicate on different days. $^{**}p < 0.01$; $^{***}p < 0.001$.

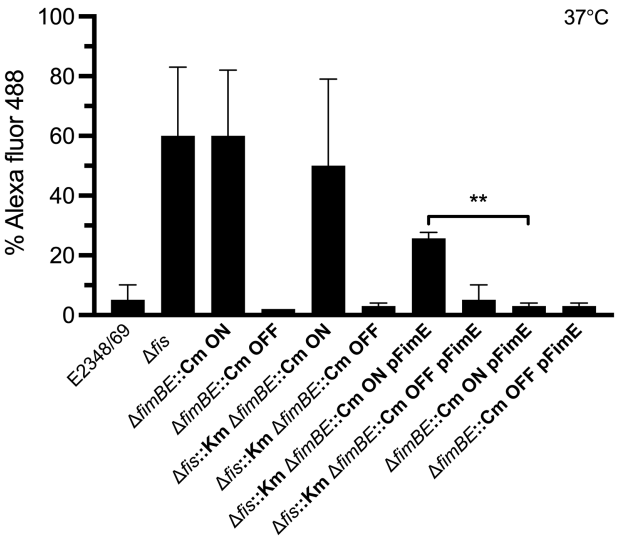

FIGURE 6 | FimE recombinase requires Fis to efficiently switch the *fimS* to the OFF state. T1P expression analysis using double and triple mutants in *fimB*, *fimE*, and *fis* with the *fimS* switch locked in either ON or OFF orientation and complemented with pFimE to evaluate T1P production. T1P was detected by flow cytometry using specific rabbit antibodies anti-T1P and goat anti-rabbit IgG Alexa Fluor conjugate. The Δ*fis*, Δ*fimBE* ON, and Δ*fis* Δ*fimBE* ON strains with the *fimS* locked in the ON orientation produce high levels of T1P pili. Although the E2348/69 Δ*fis* strain has a mix of the *fimS* orientations. No T1P expression was detected in the Δ*fimBE*::Cm and Δ*fis*::Km Δ*fimBE*::Cm strains with the *fimS* locked in the OFF orientation. Interestingly, a 20-fold expression of T1P was displayed in the Δ*fis*::Km Δ*fimBE*::Cm ON strain (*fimS* locked in the ON orientation) complemented with pFimE plasmid as compared to the Δ*fimBE*::Cm ON pFimE strain (*fimS* locked in the ON orientation), which was able to switch the *fimS* element to the OFF state completely. These data are the mean of at least three experiments performed in triplicate on different days. $^{**}p < 0.01$.

trigger H-NS, RpoS, and OmpR regulators to directly or indirectly shut down *fimB* and *fimE* expression and to lock the *fimS* element in the phase-OFF position (Schwan, 2011). Therefore, the expression of *fim* genes is most optimal during stationary growth phase, in liquid broth, at temperatures below 37°C, and under low osmolarity. It is clear then that expression of T1P is tightly controlled by regulatory genes that determine whether the bacteria will produce or not T1P during interaction with the host or under *in vitro* conditions. Many global regulators, such as H-NS, integration host factor (IHF), RpoS, leucine-responsive regulatory protein (Lrp), CRP-cAMP, known to be involved in regulation of metabolism, stress response, or production of virulence factors, have also been shown to affect T1P expression in response to growth conditions (Martínez-Antonio et al., 2008; Bessaiah et al., 2022). In AIEC, Fis represses expression of *fimE*, and consequently, the *fimS* switch is oriented in the OFF position (Miquel et al., 2010). The role of Fis in the regulation of T1P in EPEC is so far unknown.

In the present study, we inquired about the reasons why E2348/69 lacks T1P although it contains an intact T1P operon. We began by asking if any of the best-known global and virulence regulators described in EPEC played a role in the negative regulation of T1P. E2348/69 isogenic mutants in *perABC, ler, grlA*, and *grlR* (virulence regulators) as well as in *hns, ihf, rpoS, qseA*, and *fis* (global regulators) were tested for the production of T1P. To our surprise, only the Δ*fis* mutant showed a significant increase of FimA synthesis and T1P production, strongly suggesting that Fis acts as a negative regulator of *fimA* expression.

This led us to hypothesize that in wild-type conditions Fis is involved in maintaining the phase variation *fimS* switch oriented in the OFF position and probably is acting in concert with the FimE recombinase to repress *fimA* expression.

This is confirmed by the high levels of *fimA* expression found in the Δ*fis* mutant Interestingly, we did not find downregulation of *fimE* occurring in the *fis*-negative mutant. This is in contrast to a published report on AIEC strain LF82 that showed that a LF82Δ*fis* mutant exhibited upregulation of *fimE* indicating that Fis promotes orientation of the *fimS* switch in the OFF state by downregulating the expression of the FimE recombinase (Miquel et al., 2010). These data suggest that the regulation exerted over the *fim* operon by the Fis-FimE couple occurs in various ways in different pathogenic *E. coli* strains.

The *fimS* switch contains a promoter that directs the transcription of the *fimA* subunit gene in the ON orientation but not in the other (McClain et al., 1991). An important question to address was to determine the orientation of the *fimS* switch in E2348/69 to explain why T1P production is on the OFF state and to inquire about the role of Fis in this event. Thus, using different set of primers derived from different regions of the *fimS* switch we compared amplificons obtained in the wild-type and the Δ*fis* mutant. The analysis of the amplicons confirmed that the *fimS* switch in the wild-type strain E2348/69 is locked in the OFF orientation while the *fis* mutant displayed a mixed population of variants containing the *fimS* invertible element in the ON and OFF orientations. It is tempting to speculate that having a mix population of bacterial cells in the ON and OFF states would be of benefit for attachment to intestinal mannose receptors or for detachment from the gut to exit and colonize other hosts, respectively. The data indicate that the presence of Fis ensures the OFF orientation of the *fimS* switch and therefore we hypothesized that perhaps Fis does this by regulating the expression of *fimA* or the *fimB* and *fimE* recombinase genes (**Figure 7**). Using promoterless β-galactosidase transcriptional fusions containing the promoter regions of *fimA*, *fimB*, and *fim*E we determined transcription levels of these genes in E2348/69 and the Δ*fis* mutant growing at 25°C and 37°C in LB broth. Except for the P*fimA* whose expression increased in the Δ*fis* mutant at both temperatures, no significant transcriptional activity was seen in the strains carrying the P*fimB* or P*fimE* fusions. Thus, in the absence of Fis, particularly at 25°C, the *fimS* switch is oriented in the ON position yielding increased *fimA* expression and production of T1P. In contrast, when Fis is present, T1P expression is repressed likely due to the binding of Fis to the *fimS* element and together with FimE, they lock the *fimS* switch on the OFF orientation. To confirm this, we constructed double and triple mutants *fimE*, *fimB*, and *fis* containing the *fimS* locked in the ON or OFF orientation and complemented the mutants with *fimE* on a plasmid (pFimE). T1P production was similar in the Δ*fis*, the double Δ*fimBE* and triple Δ*fisfimBE* mutants with the *fimS* switch locked in the ON orientation. Notably, the Δ*fimBE*-ON(pFimE) strain displayed wild-type levels of T1P while the Δ*fisfimBE*-ON(pFimE) strain expressed 5 times more T1P than the wild-type strain. In all, these data strongly suggest that the FimE-mediated inversion of the *fimS* switch to the OFF state requires Fis. It is possible that Fis stimulates site-specific DNA recombination in conjunction with FimE.

The *E. coli* Fis protein regulates a diverse set of reactions including recombination, transcription, and replication (Finkel and Johnson, 1993) and it does this by binding to specific promoter DNA sequences whose base composition varies enormously. In this study, we sought to investigate

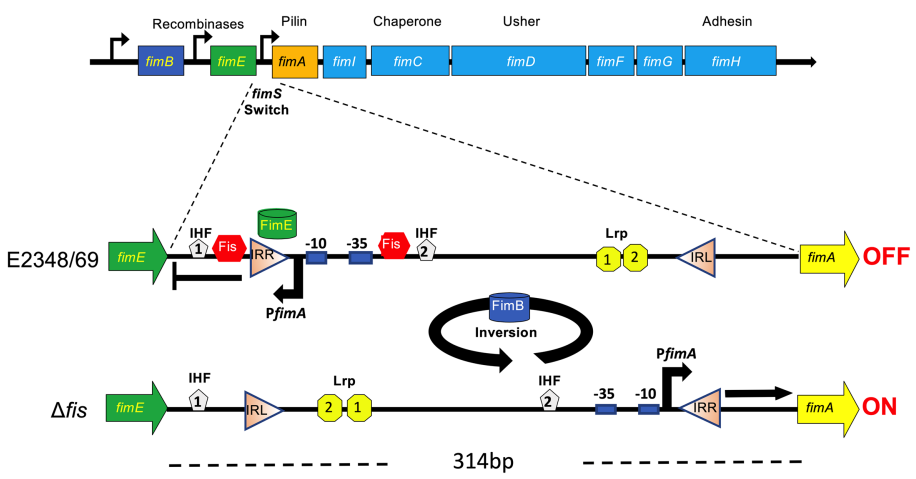

FIGURE 7 | Model for the role of Fis in the site-specific inversion of the *fimS* switch in EPEC. The orientation of the *fimS* invertible segment (314 bp long) located between *fimE* and *fimA*, is controlled by two recombinases, FimB and FimE. FimE locks the *fimS* switch in the OFF orientation while FimB inverts the *fimS* switch in both directions. The *fimS* switch is flanked by the left and right inverted repeats (IRL and IRR, respectively). In EPEC E2348/69, the inversion of the *fimS* to the OFF position is mediated by FimE and Fis. Based on the data obtained, we postulate that in the absence of Fis (e.g., Δ*fis* mutant), high levels of *fimA* expression are displayed and that FimE-mediated inversion of the *fimS* switch to the OFF state requires Fis. The putative binding sites of IHF, Lrp and Fis shown are based on the nucleotide sequence homology of the *fimS* switch between different *Escherichia coli* pathotypes.

the presence of Fis-binding sites within the *fimS* invertible element. Analysis of the promoter of *fimA* in OFF orientation shows two predicted Fis-binding sites (**Figure 5A**), which correlate with the consensus Fis-binding sequence previously reported (Finkel and Johnson, 1993; Hengen et al., 1997; Schneider et al., 2001; Feldman et al., 2006). Future protein–DNA binding will help to understand the interaction of Fis with nucleotide sequences within the *fimS* switch in EPEC. Fis levels in *E. coli* vary greatly during the course of growth being elevated in early exponential phase and undetectable after stationary phase upon a nutrient up-shift and in response to changing nutritional conditions and this variation may be important for its physiological roles in the cell (Ball et al., 1992; Nilsson et al., 1992; Ali Azam et al., 1999). The fact that T1P are mainly produced during stationary growth phase when Fis levels are low, is in line with our finding that Fis acts as a negative regulator of T1P expression in EPEC. In contrast to Fis, intracellular levels of H-NS are generally high and quite constant, (Ball et al., 1992; Dillon and Dorman, 2010). Published data show that many promoters regulated by Fis are also regulated by H-NS (Dorman, 2007), from which we could speculate that during early exponential growth, Fis and H-NS repress the expression of the *fim* operon. However, here we found that in contrast to the Δ*fis* mutant that expressed high levels of *fimA* and abundant T1P, the Δ*hns* mutant expressed low levels of *fimA* but showed no detectable T1P. It is possible that the lack of Fis has an indirect effect on the expression or function of other transcriptional factors, such as *ihf* or *rpoS* or virulence regulators. Nevertheless, in contrast to what has been reported in UPEC (Bessaiah et al., 2022), the EPEC Δ*ihf* and Δ*rpoS* mutants did not show *fimA* expression, FimA synthesis, or T1P production. Likewise, the mutants in virulence regulators showed no-to-negligible amounts of T1P. From these experiments, we conclude that Fis is required for the FimE-mediated ON-to-OFF switching. In all, this study reveals that the regulation of T1P in different *E. coli* pathotypes depends of a complex network of regulatory elements that work in concert to facilitate tropism and colonization of the appropriate niches in the host.

EXPERIMENTAL PROCEDURES

Strains and Culture Conditions

Bacterial strains used in this study are listed in **Supplementary Table 1** and were grown on Luria-Bertani (LB) at 37°C, unless otherwise noted. When necessary, kanamycin or ampicillin was added at a concentration of 50 or 100 μg/ml, respectively.

Construction of Isogenic Mutants

Non-polar deletion mutants in *fis*, *fimB*, and *fimE* genes were generated by the lambda Red recombinase method previously described (Datsenko and Wanner, 2000). The primers employed for DNA amplification are listed in **Supplementary Table 2**. Primers *fis*/H1P1 and *fis*/H2P2 were employed to mutate *fis* in EPEC E2348/69. Primers G356 and G357 and primers G360 and G361 were employed to mutate *fimB* and *fimE*, respectively, in EPEC E2348/69. Primers flanking the *fis*, *fimB*, and *fimE* genes as well as primers inside the kanamycin and chloramphenicol resistance gene were used to confirm the required gene replacement by PCR (**Supplementary Table 2**). To complement the *fis* mutation, the pFis vector carrying the *fis* gene was used (Saldaña et al., 2009). To generate the deletion of both recombinase genes (*fimB and fimE*) we used primers G356 and G361.

SDS-PAGE and Immunoblotting

The bacterial suspensions were adjusted to an absorbance of 0.7 at the optical density (OD) at 600 nm (OD_{600}). Equal numbers of bacteria were used to prepare whole cell extracts. To dissociate T1P from the bacteria, the cultures were treated with acidified water (pH 1.8), boiled for 10 min in denaturation sample buffer, neutralized to pH 7.2, and then resolved by SDS-PAGE and transferred to PVDF membranes. The membranes were incubated with rabbit anti-T1P (1:3,000) in PBS-Tween 80 for 1 h followed by anti-rabbit IgG-peroxidase conjugate (Sigma; 1:5,000) and the reaction was visualized by addition of a chemiluminescent substrate (Amersham). Anti-DnaK antibody was used to control for the amount of protein loaded in the gels.

Flow Cytometry

Flow cytometry was used to quantitate the production of T1P by the EPEC strains. These strains were grown overnight in LB media at 37°C or 26°C and the optical density adjusted to an OD_{600} of 1.1. Forty-five μl aliquots were incubated for 1 h on ice with 25 μl of anti-T1P antibodies at a dilution of 1:500. After three gentle washes with PBS, the bacteria were resuspended in 25 μl of a 1:500 dilution of goat anti-rabbit IgG (H + L) Alexa Fluor conjugate (Invitrogen, Carlsbad, CA). After 1 h incubation at 4°C, the bacteria were gently washed three times with PBS and resuspended in 800-μl final volume of PBS. For the analysis, the bacteria were labeled with 3 μl of a propidium iodide solution (Sigma, St. Louis, MO). Propidium iodide (red) was visualized through a 42 nm band pass centered at 585. These experiments were repeated in triplicate. The FITC (green) fluorescence emission was collected through a 30 nm band pass filter centered at 530 in which 50,000 events were measured. The samples were analyzed at the ARL Biotechnology/ACCC Cytometry Core Facility at the University of Arizona, by using a FACScan (Becton Dickinson, Franklin Lakes, NJ).

RT-PCR

Total RNA was extracted from LB-grown bacterial cultures using TRIzol Reagent (Invitrogen) following the manufacturer's

guidelines. Prior to RT-PCR, 2 µg of total RNA were treated with RQ1 RNAse-free DNase, according to the manufacturer's protocol. Specific transcripts were amplified using the one-step RT-PCR kit (Qiagen) and 0.1 mg/ml of total RNA as template. 16S RNA (*rrsB*) was used as a loading control.

Ultrastructural Studies

The pili on the bacterial surface were visualized by negative staining with 1% phosphotungstic acid followed by transmission electron microscopy (TEM). For immunogold labeling, samples were incubated with 1:10 dilution of rabbit anti-T1P antibody in normal horse serum for 1 h followed by incubation with anti-rabbit IgG conjugated to 10 nm gold particles (1:10) for 1 h. After washing the grids were stained as before (Girón et al., 2002).

Purification of Pili

Pili produced by E2348/69Δ*fis* were purified from the bacteria cultivated in 40 plates (150 × 15 mm) of LB agar and resuspended in 100 ml of distilled water. The suspension was vigorously shaken for 5 min to shear the pili from the bacterial cells. The supernatant was obtained by centrifugation at 10,408 x *g* for 20 min in a Sorval GSA rotor. A second centrifugation step at 17,210 x *g* for 20 min in a Sorval SS34 rotor was performed to remove bacterial debris. The clear supernatant was spun at 148,230 x *g* for 3 h in a Beckman 70 Ti rotor to concentrate the pili. The pili was resuspended in 0.1 mM Tris–HCl and centrifuged 18 h at 256,136 x *g* in a Beckman SW 40 Ti rotor in a Beckman L-100 K ultracentrifuge using a cesium chloride/1% sarkosyl gradient to obtain purified fimbriae (Tacket et al., 1987).

Production of Rabbit Polyclonal Antiserum against T1P

The purified T1P was used to custom-order polyclonal antibodies at Lampire Laboratories in a New Zealand rabbit by intramuscular injection with Freund's complete adjuvant at day 0 followed by a second immunization at day 15 in incomplete Freund's adjuvant. The final bleed was obtained at day 50 and the serum stored at −70°C.

Hemagglutination Assays

Guinea pig red blood cells (RBC; Lampire, PA) were assayed for agglutination by EPEC and isogenic mutant strains as previously described (Erdem et al., 2007). Hemagglutination (HA) assays were performed with 96-well, round-bottom microtiter plates. Bacteria were adjusted to 10^8 cells per ml in PBS. Two-fold serial dilutions of the bacteria in 100 ml were incubated with 100 ml 1% RBC suspensions and incubated on ice for 2 h. HA titers were recorded when a pellet of RBC was observed in the well containing only RBC in PBS (Erdem et al., 2007).

Construction of *fimA::lacZ, fimB::lacZ,* and *fimE::lacZ* Transcriptional Fusions

Transcriptional fusions consisting of the EPEC *fimA, fimB*, and *fimE* promoters linked to promoter-less *lacZ* reporter gene were constructed to monitor the expression of *fimA, fimB*, and *fimE*, respectively. The *fimA* promoter was amplified from E2348/69 using the primers G307 and G135 and cloned into the *EcoRI* and *BamHI* sites in pMLB1034 vector, yielding p*fimA*. To clone the *fimB* promoter (located 610 bp upstream of the start codon) we used primers G310 and G311; primers G308 and G311 were used to clone the *fimE* promoter into the *EcoRI* and *BamHI* sites in pMLB1034 vector, yielding p*fimB* and p*fimE*, respectively. These plasmids were transformed into E2348/69 and E2348/69Δ*fis*, and transcriptional activity of *fimA*, *fimB*, and *fimE* was monitored by measuring *β*-galactosidase activity as previously described (Miller, 1972). As negative control, E2348/69 carrying pMLB1034 was employed.

β-Galactosidase Assays

Transcriptional expression analysis using several fusion constructs (promoters from *fimA*, *fimB*, and *fimE* fused to the *β*-galactosidase reporter gene) were grown with shaking for 21 h at 37°C. We chose this time point to measure *fimA, fimB*, and *fimE* expression because *fim* genes are expressed at stationary phase and Fis is a repressor of stationary phase genes. The cultures were diluted 1:50 in fresh LB and cultivated at 37°C to an OD_{600} of 0.65–0.70. When required the cultures were grown at 37°C or 25°C. The cultures were then diluted 1:5 in Z buffer (0.06 M Na_2HPO_4, 0.04 M Na_2HPO_4, 0.01 M KCl, 0.001 M $MgSO_4$, and 0.05 M *β*-mercaptoethanol) and the *β*-galactosidase activity was assayed using ONPG as a substrate. The color was read in a spectrophotometer (Miller, 1972). The *β*-galactosidase experiments were repeated at least four times in quadruplicate.

Amplification of the *fimS* Invertible Element in EPEC Strains

Cultures of E2348/69 and the Δ*fis* mutant were analyzed by PCR utilizing sets of different primers (**Supplementary Table 2**) expanding different regions of the *fimS* switch to determine the orientation of the *fimS* switch in each strain. The absence of amplicons in the E2348/69 strain utilizing sets of primers F1F2 and R1R2 confirm the OFF orientation of the *fimS* switch in this strain. In contrast, the presence of amplicons in the Δ*fis* mutant with these sets of primers confirmed the ON position of the *fimS* switch.

Statistical Analysis

All data were the averages of at least three independent experiments performed by triplicate. GraphPad Prism 9 software (GraphPad, San Diego, CA, United States) was used for statistical differences. One way ANOVA followed by Tukey's multiple comparison test and unpaired Student's *t* test were performed. A *value of* $p \leq 0.05$ was considered statistically significant.

DATA AVAILABILITY STATEMENT

The original contributions presented in the study are included in the article/**Supplementary Material**, further inquiries can be directed to the corresponding author.

AUTHOR CONTRIBUTIONS

ZS-A and JG conceived and designed the experiments. ZS-A and VM-S performed the experiments. ZS-A, JS-B, JY-S, YM-L, MC-R, JP, and JG analyzed the data. ZS-A, JS-B, and JG wrote the manuscript. All authors contributed to the article and approved the submitted version.

SUPPLEMENTARY MATERIAL

The Supplementary Material for this article can be found online at: https://www.frontiersin.org/articles/10.3389/fmicb.2022.882563/full#supplementary-material

REFERENCES

Abraham, J. M., Freitag, C. S., Clements, J. R., and Eisenstein, B. I. (1985). An invertible element of DNA controls phase variation of type 1 fimbriae of Escherichia coli. *Proc. Natl. Acad. Sci. U. S. A.* 82, 5724–5727. doi: 10.1073/pnas.82.17.5724

Ali Azam, T., Iwata, A., Nishimura, A., Ueda, S., and Ishihama, A. (1999). Growth phase-dependent variation in protein composition of the Escherichia coli nucleoid. *J. Bacteriol.* 181, 6361–6370. doi: 10.1128/JB.181.20.6361-6370.1999

Ares, M. A., Abundes-Gallegos, J., Rodríguez-Valverde, D., Panunzi, L. G., Jiménez-Galicia, C., Jarillo-Quijada, M. D., et al. (2019). The coli surface antigen CS3 of enterotoxigenic Escherichia coli is differentially regulated by H-NS, CRP, and Cpx RA global regulators. *Front. Microbiol.* 10:1685. doi: 10.3389/fmicb.2019.01685

Ball, C. A., Osuna, R., Ferguson, K. C., and Johnson, R. C. (1992). Dramatic changes in Fis levels upon nutrient upshift in Escherichia coli. *J. Bacteriol.* 174, 8043–8056. doi: 10.1128/jb.174.24.8043-8056.1992

Bessaiah, H., Anamalé, C., Sung, J., and Dozois, C. M. (2022). What flips the switch? Signals and stress regulating extraintestinal pathogenic Escherichia coli type 1 fimbriae (pili). *Microorganisms* 10:5. doi: 10.3390/microorganisms10010005

Blomfield, I. C., Calie, P. J., Eberhardt, K. J., McClain, M. S., and Eisenstein, B. I. (1993). Lrp stimulates phase variation of type 1 fimbriation in Escherichia coli K-12. *J. Bacteriol.* 175, 27–36. doi: 10.1128/jb.175.1.27-36.1993

Blomfield, I. C., Kulasekara, D. H., and Eisenstein, B. I. (1997). Integration host factor stimulates both FimB- and FimE-mediated site-specific DNA inversion that controls phase variation of type 1 fimbriae expression in Escherichia coli. *Mol. Microbiol.* 23, 705–707. doi: 10.1046/j.1365-2958.1997.2241615.x

Blomfield, I. C., McClain, M. S., Princ, J. A., Calie, P. J., and Eisenstein, B. I. (1991). Type 1 fimbriation and fim E mutants of Escherichia coli K-12. *J. Bacteriol.* 173, 5298–5307. doi: 10.1128/jb.173.17.5298-5307.1991

Blomfield, I., and van der Woude, M. (2007). Regulation of fimbrial expression. *EcoSal Plus* 2. doi: 10.1128/ecosal.2.4.2.2

Bokal, A. J., Ross, W., Gaal, T., Johnson, R. C., and Gourse, R. L. (1997). Molecular anatomy of a transcription activation patch: FIS-RNA polymerase interactions at the Escherichia coli rrnB P1 promoter. *EMBO J.* 16, 154–162. doi: 10.1093/emboj/16.1.154

Calvo, J. M., and Matthews, R. G. (1994). The leucine-responsive regulatory protein, a global regulator of metabolism in Escherichia coli. *Microbiol. Rev.* 58, 466–490. doi: 10.1128/mr.58.3.466-490.1994

Datsenko, K. A., and Wanner, B. L. (2000). One-step inactivation of chromosomal genes in Escherichia coli K-12 using PCR products. *Proc. Natl. Acad. Sci. U. S. A.* 97, 6640–6645. doi: 10.1073/pnas.120163297

De la Cruz, M. A., Ruiz-Tagle, A., Ares, M. A., Pacheco, S., Yáñez, J. A., Cedillo, L., et al. (2017). The expression of Longus type 4 pilus of enterotoxigenic Escherichia coli is regulated by LngR and LngS and by H-NS, CpxR and CRP global regulators. *Environ. Microbiol.* 19, 1761–1775. doi: 10.1111/1462-2920.13644

Dillon, S. C., and Dorman, C. J. (2010). Bacterial nucleoid-associated proteins, nucleoid structure and gene expression. *Nat. Rev. Microbiol.* 8, 185–195. doi: 10.1038/nrmicro2261

Dorman, C. J. (2007). H-NS, the genome sentinel. *Nat. Rev. Microbiol.* 5, 157–161. doi: 10.1038/nrmicro1598

Dorman, C. J., and Deighan, P. (2003). Regulation of gene expression by histone-like proteins in bacteria. *Curr. Opin. Genet. Dev.* 13, 179–184. doi: 10.1016/s0959-437x(03)00025-x

Dorman, C. J., and Higgins, C. F. (1987). Fimbrial phase variation in Escherichia coli: dependence on integration host factor and homologies with other site-specific recombinases. *J. Bacteriol.* 169, 3840–3843. doi: 10.1128/jb.169.8.3840-3843.1987

Duprey, A., Reverchon, S., and Nasser, W. (2014). Bacterial virulence and Fis: adapting regulatory networks to the host environment. *Trends Microbiol.* 22, 92–99. doi: 10.1016/j.tim.2013.11.008

Erdem, A. L., Avelino, F., Xicohtencatl-Cortes, J., and Girón, J. A. (2007). Host protein binding and adhesive properties of H6 and H7 flagella of attaching and effacing Escherichia coli. *J. Bacteriol.* 189, 7426–7435. doi: 10.1128/JB.00464-07

Feldman, L. S., Shao, Y. P., Meinhold, D., Miller, C., Colon, W., and Osuna, R. (2006). Common and variable contributions of Fis residues to high-affinity binding at different DNA sequences. *J. Bacteriol.* 188, 2081–2095. doi: 10.1128/JB.188.6.2081-2095.2006

Finkel, S. E., and Johnson, R. C. (1993). The Fis protein: it's not just for DNA inversion anymore. *Mol. Microbiol.* 7:1023. doi: 10.1111/j.1365-2958.1993.tb01193.x

Flores-Mireles, A. L., Walker, J. N., Caparon, M. G., and Hultgren, S. J. (2015). Urinary tract infections: epidemiology, mechanisms of infection and treatment options. *Nat. Rev. Microbiol.* 13, 269–284. doi: 10.1038/nrmicro3432

Freitag, C. S., Abraham, J. M., Clements, J. R., and Eisenstein, B. I. (1985). Genetic analysis of the phase variation control of expression of type 1 fimbriae in Escherichia coli. *J. Bacteriol.* 162, 668–675. doi: 10.1128/jb.162.2.668-675.1985

Gally, D. L., Bogan, J. A., Eisenstein, B. I., and Blomfield, I. C. (1993). Environmental regulation of the fim switch controlling type 1 fimbrial phase variation in Escherichia coli K-12: effects of temperature and media. *J. Bacteriol.* 175, 6186–6193. doi: 10.1128/jb.175.19.6186-6193.1993

Gally, D. L., Leathart, J., and Blomfield, I. C. (1996). Interaction of FimB and FimE with the fim switch that controls the phase variation of type 1 fimbriae in Escherichia coli K-12. *Mol. Microbiol.* 21, 725–738. doi: 10.1046/j.1365-2958.1996.311388.x

Gally, D. L., Rucker, T. J., and Blomfield, I. C. (1994). The leucine-responsive regulatory protein binds to the fim switch to control phase variation of type 1 fimbrial expression in Escherichia coli K-12. *J. Bacteriol.* 176, 5665–5672. doi: 10.1128/jb.176.18.5665-5672.1994

Gille, H., Egan, J. B., Roth, A., and Messer, W. (1991). The FIS protein binds and bends the origin of chromosomal DNA replication, oriC, of Escherichia coli. *Nucleic Acids Res.* 19, 4167–4172. doi: 10.1093/nar/19.15.4167

Girón, J. A., Torres, A. G., Freer, E., and Kaper, J. B. (2002). The flagella of enteropathogenic Escherichia coli mediate adherence to epithelial cells. *Mol. Microbiol.* 44, 361–379. doi: 10.1046/j.1365-2958.2002.02899.x

Goldberg, M. D., Johnson, M., Hinton, J. C. D., and Williams, P. H. (2001). Role of the nucleoid-associated protein Fis in the regulation of virulence properties of enteropathogenic Escherichia coli. *Mol. Microbiol.* 41, 549–559. doi: 10.1046/j.1365-2958.2001.02526.x

González-Gil, G., Bringmann, P., and Kahmann, R. (1996). FIS is a regulator of metabolism in Escherichia coli. *Mol. Microbiol.* 22, 21–29. doi: 10.1111/j.1365-2958.1996.tb02652.x

Hahn, E., Wild, P., Hermanns, U., Sebbel, P., Glockshuber, R., Häner, M., et al. (2002). Exploring the 3D molecular architecture of Escherichia coli type 1 pili. *J. Mol. Biol.* 323, 845–857. doi: 10.1016/s0022-2836(02)01005-7

Hengen, P. N., Bartram, S. L., Stewart, L. E., and Schneider, T. D. (1997). Information analysis of Fis binding sites. *Nucleic Acids Res.* 25, 4994–5002. doi: 10.1093/nar/25.24.4994

Hernandes, R. T., De la Cruz, M. A., Yamamoto, D., Girón, J. A., and Gomes, T. A. T. (2013). Dissection of the role of pili and type 2 and 3 secretion systems in adherence and biofilm formation of an atypical enteropathogenic Escherichia coli strain. *Infect. Immun.* 81, 3793–3802. doi: 10.1128/IAI.00620-13

Hung, D. L., Raivio, T., Jones, C., Silhavy, T., and Hultgren, S. J. (2001). Cpx signaling pathway monitors biogenesis and affects assembly and expression of P pili. *EMBO J.* 20, 1508–1518. doi: 10.1093/emboj/20.7.1508

Johnson, R. C., Bruist, M. F., and Simon, M. I. (1986). Host protein requirements for in vitro site-specific DNA inversion. *Cell* 46, 531–539. doi: 10.1016/0092-8674(86)90878-0

Kaper, J. B., Nataro, J. P., and Mobley, H. L. (2004). Pathogenic Escherichia coli. *Nat. Rev. Microbiol.* 2, 123–140. doi: 10.1038/nrmicro818

Kelly, A., Conway, C. O., Cróinín, T., Smith, S. G., and Dorman, C. J. (2006). DNA supercoiling and the Lrp protein determine the directionality of fim switch DNA inversion in Escherichia coli K-12. *J. Bacteriol.* 188, 5356–5363. doi: 10.1128/JB.00344-06

Kelly, A., Goldberg, M. D., Carroll, R. K., Danino, V., Hinton, J. C. D., and Dorman, C. J. (2004). A global role for Fis in the transcriptional control of metabolism and type III secretion in salmonella enterica serovar Typhimurium. *Microbiology* 150, 2037–2053. doi: 10.1099/mic.0.27209-0

Klemm, P. (1986). Two regulatory fim genes, fimB, and fimE, control the phase variation of type 1 fimbriae in Escherichia coli. *EMBO J.* 5, 1389–1393. doi: 10.1002/j.1460-2075.1986.tb04372.x

Koch, C., Vandekerckhove, J., and Kahmann, R. (1988). Escherichia coli host factor for site-specific DNA inversion: cloning and characterization of the fis gene. *Proc. Natl. Acad. Sci. U. S. A.* 85, 4237–4241. doi: 10.1073/pnas.85.12.4237

La Ragione, R. M., Sayers, A. R., and Woodward, M. J. (2000). The role of fimbriae and flagella in the colonization, invasion and persistence of Escherichia coli O78:K80 in the day-old-chick model. *Epidemiol. Infect.* 124, 351–363. doi: 10.1017/s0950268899004045

La Ragione, R. M., and Woodward, M. J. (2002). Virulence factors of Escherichia coli serotypes associated with avian colisepticaemia. *Res. Vet. Sci.* 73, 27–35. doi: 10.1016/s0034-5288(02)00075-9

Lenz, D. H., and Bassler, B. L. (2007). The small nucleoid protein Fis is involved in Vibrio cholerae quorum sensing. *Mol. Microbiol.* 63, 859–871. doi: 10.1111/j.1365-2958.2006.05545.x

Levine, M. M., Bergquist, E. J., Nalin, D. R., Waterman, D. H., Hornick, R. B., Young, C. R., et al. (1978). Escherichia coli strains that cause diarrhoea but do not produce heat-labile or heat-stable enterotoxins and are non-invasive. *Lancet* 311, 1119–1122. doi: 10.1016/s0140-6736(78)90299-4

Mallik, P., Pratt, T. S., Beach, M. B., Bradley, M. D., Undamatla, J., and Osuna, R. (2004). Growth phase-dependent regulation and stringent control of fis are conserved processes in enteric bacteria and involve a single promoter (fis P) in Escherichia coli. *J. Bacteriol.* 186, 122–135. doi: 10.1128/JB.186.1.122-135.2004

Martínez-Antonio, A., Janga, S. C., and Thieffry, D. (2008). Functional organisation of Escherichia coli transcriptional regulatory network. *J. Mol. Biol.* 381, 238–247. doi: 10.1016/j.jmb.2008.05.054

Martinez-Medina, M., and Garcia-Gil, L. J. (2014). Escherichia coli in chronic inflammatory bowel diseases: an update on adherent invasive Escherichia coli pathogenicity. *World J. Gastrointest. Pathophysiol.* 5, 213–227. doi: 10.4291/wjgp.v5.i3.213

Matter, L. B., Ares, M. A., Abundes-Gallegos, J., Cedillo, M. L., Yáñez, J. A., Martínez-Laguna, Y., et al. (2018). The CpxRA stress response system regulates virulence features of avian pathogenic Escherichia coli. *Environ. Microbiol.* 20, 3363–3377. doi: 10.1111/1462-2920.14368

McClain, M. S., Blomfield, I. C., Eberhardt, K. J., and Eisenstein, B. I. (1993). Inversion-independent phase variation of type 1 fimbriae in Escherichia coli. *J. Bacteriol.* 175, 4335–4344. doi: 10.1128/jb.175.14.4335-4344.1993

McClain, M. S., Blomfield, I. C., and Eisenstein, B. I. (1991). Roles of fimB and fimE in site-specific DNA inversion associated with phase variation of type 1 fimbriae in Escherichia coli. *J. Bacteriol.* 173, 5308–5314. doi: 10.1128/jb.173.17.5308-5314.1991

McCusker, M. P., Turner, E. C., and Dorman, C. J. (2008). DNA sequence heterogeneity in Fim tyrosine-integrase recombinase-binding elements and functional motif asymmetries determine the directionality of the fim genetic switch in Escherichia coli K-12. *Mol. Microbiol.* 67, 171–187. doi: 10.1111/j.1365-2958.2007.06037.x

Miller, J. H. (1972). *Experiments in Molecular Genetics*. Cold Spring Harbor, NY: Cold Spring Harbor Laboratory.

Miquel, S., Claret, L., Bonnet, R., Dorboz, I., Barnich, N., and Darfeuille-Michaud, A. (2010). Role of decreased levels of Fis histone-like protein in Crohn's disease-associated adherent invasive Escherichia coli LF82 bacteria interacting with intestinal epithelial cells. *J. Bacteriol.* 192, 1832–1843. doi: 10.1128/JB.01679-09

Müller, C. M., Åberg, A., Straseviçiene, J., and Em˝ody, L., Uhlin, B. E., Balsalobre, C., (2009). Type 1 fimbriae, a colonization factor of uropathogenic Escherichia coli, are controlled by the metabolic sensor CRP-cAMP. *PLoS Pathog.* 5:e1000303. doi: 10.1371/journal.ppat.1000303

Nascimento, H. H., Silva, L. E., Souza, R. T., Silva, N. P., and Scaletsky, I. C. (2014). Phenotypic and genotypic characteristics associated with biofilm formation in clinical isolates of atypical enteropathogenic Escherichia coli (aEPEC) strains. *BMC Microbiol.* 14:184. doi: 10.1186/1471-218014-184

Nilsson, L., Verbeek, H., Vijgenboom, E., van Drunen, C., Vanet, A., and Bosch, L. (1992). FIS-dependent trans activation of stable RNA operons of Escherichia coli under various growth conditions. *J. Bacteriol.* 174, 921–929. doi: 10.1128/jb.174.3.921-929.1992

Puorger, C., Vetsch, M., Wider, G., and Glockshuber, R. (2011). Structure, folding and stability of fim A, the main structural subunit of type 1 pili from uropathogenic Escherichia coli strains. *J. Mol. Biol.* 412, 520–535. doi: 10.1016/j.jmb.2011.07.044

Remaut, H., Rose, R. J., Hannan, T. J., Hultgren, S. J., Radford, S. E., Ashcroft, A. E., et al. (2006). Donor-strand exchange in chaperone-assisted pilus assembly proceeds through a concerted beta strand displacement mechanism. *Mol. Cell* 22, 831–842. doi: 10.1016/j.molcel.2006.05.033

Roesch, P. L., and Blomfield, I. C. (1998). Leucine alters the interaction of the leucine-responsive regulatory protein (Lrp) with the fim switch to stimulate site-specific recombination in Escherichia coli. *Mol. Microbiol.* 27, 751–761. doi: 10.1046/j.1365-2958.1998.00720.x

Ross, W., Thompson, J. F., Newlands, J. T., and Gourse, R. L. (1990). E. coli Fis protein activates ribosomal RNA transcription in vitro and in vivo. *EMBO J.* 9, 3733–3742. doi: 10.1002/j.1460-2075.1990.tb07586.x

Saldaña, Z., Xicohtencatl-Cortes, J., Avelino, F., Phillips, A. D., Kaper, J. B., Puente, J. L., et al. (2009). Synergistic role of curli and cellulose in cell adherence and biofilm formation of attaching and effacing Escherichia coli and identification of Fis as a negative regulator of curli. *Environ. Microbiol.* 11, 992–1006. doi: 10.1111/j.1462-2920.2008.01824.x

Schmid, M. B. (1990). More than just "histone-like" proteins. *Cell* 63, 451–453. doi: 10.1016/0092-8674(90)90438-k

Schneider, R., Lurz, R., Lüder, G., Tolksdorf, C., Travers, A., and Muskhelishvili, G. (2001). An architectural role of the Escherichia coli chromatin protein FIS in organising DNA. *Nucleic Acids Res.* 29, 5107–5114. doi: 10.1093/nar/29.24.5107

Schwan, W. R. (2011). Regulation of fim genes in uropathogenic Escherichia coli. *World J. Clin. Infect. Dis.* 1, 17–25. doi: 10.5495/wjcid.v1.i1.17

Spaulding, C. N., Schreiber, H. L., Zheng, W., Dodson, K. W., Hazen, J. E., Conover, M. S., et al. (2018). Functional role of the type 1 pilus rod structure in mediating host-pathogen interactions. *eLife* 7:e31662. doi: 10.7554/eLife.31662

Tacket, C. O., Maneval, D. R., and Levine, M. M. (1987). Purification, morphology, and genetics of a new fimbrial putative colonization factor of enterotoxigenic Escherichia coli O159: H4. *Infect. Immun.* 55, 1063–1069. doi: 10.1128/iai.55.5.1063-1069.1987

Thompson, J. F., Snyder, U. K., and Landy, A. (1988). Helical-repeat dependence of integrative recombination of bacteriophage lambda: role of the P1 and H1 protein binding sites. *Proc. Natl. Acad. Sci. U. S. A.* 85, 6323–6327. doi: 10.1073/pnas.85.17.6323

Thumbikat, P., Berry, R. E., Zhou, G., Billips, B. K., Yaggie, R. E., Zaichuk, T., et al. (2009). Bacteria-induced uroplakin signaling mediates bladder response to infection. *PLoS Pathog.* 5:e1000415. doi: 10.1371/journal.ppat.1000415

Welch, R. A., Burland, V., Plunkett, G., Redford, P., Roesch, P., Rasko, D., et al. (2002). Extensive mosaic structure revealed by the complete genome sequence of uropathogenic Escherichia coli. *Proc. Natl. Acad. Sci. U. S. A.* 99, 17020–17024. doi: 10.1073/pnas.252529799

Werneburg, G. T., and Thanassi, D. G. (2018). Pili assembled by the chaperone/usher pathway in Escherichia coli and salmonella. *EcoSal Plus* 8. doi: 10.1128/ecosalplus.ESP-0007-2017

Xu, J., and Johnson, R. C. (1995). Fis activates the Rpo S-dependent stationary-phase expression of pro P in Escherichia coli. *J. Bacteriol.* 177, 5222–5231. doi: 10.1128/jb.177.18.5222-5231.1995

Yang, H., Mirsepasi-Lauridsen, H. C., Struve, C., Allaire, J. M., Sivignon, A., Vogl, W., et al. (2020). Ulcerative colitis-associated E. coli pathobionts potentiate colitis in susceptible hosts. *Gut Microbes* 12:1847976. doi: 10.1080/19490976.2020.1847976

Conflict of Interest: The authors declare that the research was conducted in the absence of any commercial or financial relationships that could be construed as a potential conflict of interest.

frontiers | Frontiers in Microbiology

ORIGINAL RESEARCH
published: 03 May 2022
doi: 10.3389/fmicb.2022.895942

The Global Regulator CcpA of *Listeria monocytogenes* Confers Sensitivity to Antimicrobial Fatty Acids

*Rikke S. S. Thomasen[1], Magnus Ganer Jespersen[1,2], Katrine Jørgensen[1], Patricia T. dos Santos[1,3], Eva M. Sternkopf Lillebæk[1], Marianne N. Skov[4], Michael Kemp[4,5] and Birgitte H. Kallipolitis[1]**

[1]Department of Biochemistry and Molecular Biology, University of Southern Denmark, Odense, Denmark, [2]Department of Microbiology and Immunology, The Peter Doherty Institute for Infection and Immunity, University of Melbourne, Melbourne, VIC, Australia, [3]National Food Institute, Technical University of Denmark, Kgs. Lyngby, Denmark, [4]Department of Clinical Microbiology, Odense University Hospital and Research Unit of Clinical Microbiology, University of Southern Denmark, Odense, Denmark, [5]The Regional Department of Clinical Microbiology, Region Zealand, Zealand University Hospital, Koege, Denmark

OPEN ACCESS

Edited by:
Dongsheng Zhou,
Beijing Institute of Microbiology and Epidemiology, China

Reviewed by:
Xiaohui Zhou,
University of Connecticut, United States
Veronica Guariglia-Oropeza,
Cornell University, United States
Ilya Borovok,
Tel Aviv University, Israel
Hossam Abdelhamed,
Mississippi State University, United States
Séamus Fanning,
University College Dublin, Ireland

***Correspondence:**
Birgitte H. Kallipolitis
bhk@bmb.sdu.dk

Specialty section:
This article was submitted to Infectious Agents and Disease, a section of the journal Frontiers in Microbiology

Received: 14 March 2022
Accepted: 15 April 2022
Published: 03 May 2022

Citation:
Thomasen RSS, Jespersen MG, Jørgensen K, dos Santos PT, Sternkopf Lillebæk EM, Skov MN, Kemp M and Kallipolitis BH (2022) The Global Regulator CcpA of Listeria monocytogenes Confers Sensitivity to Antimicrobial Fatty Acids. Front. Microbiol. 13:895942. doi: 10.3389/fmicb.2022.895942

Free fatty acids (FFAs) are known to exhibit antimicrobial and anti-virulent properties against bacterial pathogens. Specific FFAs, such as lauric acid (LA; C12:0), exert both effects against the foodborne pathogen *Listeria monocytogenes*: at low levels, LA acts to inhibit the activity of the virulence regulator PrfA, whereas at higher levels, LA inhibits bacterial growth. Deletion of *prfA* is known to promote tolerance toward antimicrobial FFAs, suggesting that the response of *L. monocytogenes* to anti-virulent and antimicrobial FFAs could be linked. In this study, we explored the response of *L. monocytogenes* toward antimicrobial FFAs holding an anti-virulence activity by isolating strains that can grow at high concentrations of LA. We found that LA-tolerant isolates carry mutations in the gene encoding the global regulator CcpA. Importantly, we discovered that mutation or deletion of *ccpA* protect *L. monocytogenes* against the antimicrobial activity of FFAs, whereas the *ccpA* mutants remain sensitive toward FFA's PrfA inhibitory effect. A regulatory link involving CcpA, connecting the response toward the antimicrobial and anti-virulence activities of FFAs, is therefore unlikely. To further study how deletion of *ccpA* promotes FFA tolerance, we performed a transcriptomic analysis of the response to LA. Our data indicated that the FFA-tolerant phenotype of the Δ*ccpA* strain is not induced upon LA exposure but appears to be an inherent phenotypic trait of the *ccpA* deletion mutation. Interestingly, we found that the bacterial surface of *L. monocytogenes* becomes more hydrophilic upon deletion of *ccpA*, and we demonstrate that CcpA plays a role in the response of *L. monocytogenes* to other stress conditions, including low pH and antibiotics. Altogether, our study revealed that regulatory activities of CcpA lead to an increased hydrophobicity of the bacterial surface, which may confer sensitivity of *L. monocytogenes* against the antimicrobial activity of FFAs. Notably, CcpA is not involved in responding to the PrfA inhibitory effect of FFAs, showing that FFA-tolerant strains can still be targeted by the anti-virulent activity of FFAs.

Keywords: Ccpa, *Listeria monocytogenes*, antimicrobial fatty acids, anti-virulence activity, tolerance

INTRODUCTION

Listeria monocytogenes is a Gram-positive foodborne bacterium causing life-threatening infections in humans and animals. During infection of susceptible individuals, *L. monocytogenes* gains access to the cytoplasm of host cells; here, the bacterium multiplies and spreads from cell-to-cell through a mechanism that involves host actin polymerization (Freitag et al., 2009). Several virulence factors are known to contribute to the intracellular lifestyle of *L. monocytogenes*, including the internalins InlA and InlB, which allow bacterial invasion of non-phagocytic cells; the pore-forming toxin LLO, which is required for escape from host cell vacuoles, and the surface protein ActA, which promotes actin polymerization and cell-to-cell movement (Freitag et al., 2009). Inside the intracellular environment, the virulence regulator, PrfA, responds to bacterial- and host-derived glutathione (GSH) and activates transcription of PrfA-regulated virulence genes encoding LLO, ActA, and other virulence factors required for intracellular infection (Scortti et al., 2007; de las Heras et al., 2011; Reniere et al., 2015; Hall et al., 2016). In the extracellular environment, PrfA is generally not active, but constitutively active mutant variants of PrfA, named PrfA*, are known to bypass the need of GSH for PrfA activation of virulence gene expression (Ripio et al., 1997b; Eiting et al., 2005; Xayarath and Freitag, 2012; Johansson and Freitag, 2019). PrfA* proteins are locked in an active conformation that promotes optimal binding to specific DNA sequences (PrfA boxes) located in the promoter regions of PrfA-regulated virulence genes (Eiting et al., 2005; Johansson and Freitag, 2019).

Upon ingestion of contaminated food, *L. monocytogenes* enters the gastrointestinal tract. Here, the pathogen encounters dietary components, the gut microbiota, and host immune parameters. Together, these conditions strongly influence the ability of *L. monocytogenes* to cause disease (Tiensuu et al., 2019). We previously found that specific dietary free fatty acids (FFAs) act as signaling molecules to reduce virulence factor expression in *L. monocytogenes* by a mechanism that involves direct inhibition of PrfA (Kallipolitis, 2017; Sternkopf Lillebæk et al., 2017; Dos Santos et al., 2020). Interestingly, exposure to specific FFAs prevented the constitutively active variant PrfA* from binding to the PrfA box in the promoter region of *hly*, encoding LLO (Dos Santos et al., 2020). Notably, some PrfA inhibitory FFAs also exert an antimicrobial effect on *L. monocytogenes* (Sternkopf Lillebæk et al., 2017; Dos Santos et al., 2020). The mechanism underlying the antimicrobial activity of FFAs is presently unknown, but they most likely target and interfere with vital functions of the bacterial membrane (Desbois and Smith, 2010).

The saturated medium-chain fatty acid lauric acid (LA; C12:0) is commonly found in nuts, seeds, plants, and milk and is generally known as a potent antimicrobial agent (Petrone et al., 1998; Desbois and Smith, 2010). Growth of *L. monocytogenes* is efficiently inhibited in the presence of 50 μg/ml LA in rich medium, whereas at subinhibitory concentrations (≤10 μg/ml), LA acts to inhibit PrfA-dependent activities (Sternkopf Lillebæk et al., 2017). Thus, LA belongs to the category of dietary FFAs that act as an antimicrobial agent as well as a virulence inhibitory signaling compound in *L. monocytogenes*. We previously observed that the general stress sigma factor, Sigma B, is dispensable for the tolerance of *L. monocytogenes* against FFAs, suggesting that the response of *L. monocytogenes* to antimicrobial FFAs relies on other stress regulatory pathways (Sternkopf Lillebæk et al., 2017). Curiously, a Δ*prfA* mutant strain grows well in the presence of >75 μg/ml LA, suggesting that PrfA somehow acts to increase the sensitivity of *L. monocytogenes* to the antimicrobial activity of LA (Sternkopf Lillebæk et al., 2017). This means that PrfA could play several roles in the response to LA: at subinhibitory concentrations, LA targets PrfA directly to inhibit its DNA binding activity, resulting in repression of key virulence genes, whereas at higher concentrations, LA relies on PrfA for its antimicrobial activity (Sternkopf Lillebæk et al., 2017; Dos Santos et al., 2020). These findings prompted us to investigate in more detail the molecular mechanisms underlying the response of *L. monocytogenes* to LA.

In the present study, we aimed to reveal if the anti-virulence activity of LA can be linked to its antimicrobial action. To address this question, we isolated LA-tolerant *L. monocytogenes* mutant strains and analyzed their response to the PrfA inhibitory signaling effect of LA. Curiously, the LA-tolerant strains expressed a mutant version of the catabolite control protein A, CcpA, containing an extended C-terminal tail. CcpA is known as the major global transcription regulator of carbon catabolite repression (CCR) in *L. monocytogenes* and other Gram-positive bacteria; a complex regulatory mechanism that allows bacteria to use available carbon sources in an optimal manner (Jones et al., 1997; Herro et al., 2005; Deutscher, 2008). Accordingly, CcpA acts to repress multiple genes encoding proteins involved in transport and metabolism of various carbohydrates (Mertins et al., 2007) Here, we present the results of our investigations on the role of CcpA in the response of *L. monocytogenes* to the antimicrobial and PrfA inhibitory FFA, LA.

MATERIALS AND METHODS

Bacterial Strains and Growth Conditions

In this study, we used a wild-type *L. monocytogenes* EGD serotype 1/2a strain and its isogenic mutant derivative Δ*prfA* (Böckmann et al., 1996) obtained from W. Goebel (Biozentrum). Furthermore, we used the isogenic mutant strain EGD-*prfA** expressing the constitutively active PrfA mutant derivative G155S; this strain was constructed in a previous study (Sternkopf Lillebæk et al., 2017). As part of the present study, the EGD-*prfA** strain (from here, *prfA**) was genome sequenced and compared to the genomes of the EGD and EGD-e strains sequenced by Bécavin et al. (2014). A single nucleotide polymorphism (SNP) search revealed 20101 SNPs between *prfA** and the EGD strain studied by Bécavin et al. (2014), whereas only 10 SNPs were found when comparing *prfA** and EGD-e. These findings showed that the EGD derivatives used in the present study are more closely related to EGD-e than the EGD strain sequenced by Bécavin et al. (2014). We therefore used EGD-e as reference

genome for the whole-genome sequencing and RNA-sequencing analyses (described below).

For construction of the *ccpA*-mut1 1 bp deletion ($A_{8\rightarrow7}$ at location 1,642,875), in-frame deletion of 981 bp in *ccpA* (Δ*ccpA*); 1955 bp in *lmo0109-0110* (Δ*lmo0109-0110*); 792 bp in *lmo0517* (Δ*lmo0517*); 744 bp in *lmo2175* (Δ*lmo2175*); and 1830 bp in *lmo2772* (Δ*lmo2772*), the corresponding primers P1, P2, P3 and P4 (**Supplementary Table S7**) were used, respectively, for a 2-step PCR amplification of the fragments. CcpA complementation mutant (*prfA**-Δ*ccpA*::compl.) was constructed using P1 and P4 for Δ*ccpA* and the fragment was produced by a 1-step PCR reaction. The fragments were inserted into the temperature sensitive shuttle vector pAUL-A (Schäferkordt and Chakraborty, 1995) and transformed into *L. monocytogenes* as earlier described (Mollerup et al., 2016). Homologous recombination was carried out as described previously (Christiansen et al., 2004). The resulting deletion mutants were validated by PCR using primers P5 and P6. The plasmids p*hly-lacZ*, with a transcriptional fusion between the *hly* promoter and the *lacZ* gene, and p*lhrA-36-lacZ*, containing a transcriptional fusion between the *lhrA* core promoter and *lacZ*, were constructed previously (Larsen et al., 2006; Nielsen et al., 2011). *L. monocytogenes* was routinely grown in brain heart infusion broth (BHI, Oxoid) at 37°C with aeration. When appropriate, cultures were supplemented with either kanamycin (50 μg/ml) or erythromycin (5 μg/ml). During cloning in pAUL-A, *Escherichia coli* TOP10 (Invitrogen) was grown in Luria-Bertani broth (LB, Sigma) supplemented with 150 μg/ml erythromycin at 37°C with aeration.

Fatty Acid-Tolerant Strains

Fatty acids used in this study were lauric acid (LA; C12:0; Sigma-Aldrich, purity ≥98%), palmitoleic acid (PA; C16:1; Sigma-Aldrich, purity ≥98.5%), and palmitic acid (PAL; C16:0; Sigma-Aldrich, purity ≥99%). 96% ethanol was used as vehicle to dissolve the FFAs.

Three independent ON cultures of *prfA** were diluted to OD_{600} = 0.0002 and stressed with increasing concentrations of LA (10 μg/ml, 20 μg/ml, 40 μg/ml, 80 μg/ml, 160 μg/ml, 320 μg/ml, and 500 μg/ml) for 7 days; the concentration of vehicle was kept constant at 0.25% during the selection process. Glycerol stocks were made, and single mutants were isolated from the three biological replicates. Bacterial identification was performed by PCR using primers for *hly* (**Supplementary Table S7**).

Growth Experiments

For growth experiments in culture flasks, ON cultures were diluted to OD_{600} = 0.002. Growth was monitored until cultures reached stationary phase by OD_{600} measurements.

In growth experiments, where strains were screened for FFA tolerance, ON cultures were diluted to OD_{600} = 0.0002 and 4 ml was transferred to glass tubes with various concentrations of LA, PA, or PAL. As controls, cultures were left untreated or stressed with vehicle corresponding to the highest concentration used in FFA-treated samples. OD_{600} was measured after 20 h of incubation.

Growth experiments with other stress conditions than FFAs were performed in a plate reader (Synergy™ H1 multi-mode microplate reader, BioTek) using 96-well plates (standard, F, SARSTEDT). ON cultures were diluted to a final OD_{600} = 0.005 in the 96-well plate with the different stress conditions. The plate was incubated at 37°C with 15 s. of orbitally shaking every 30 min for 24 h.

β-Galactosidase Assays

ON cultures of the strains containing the plasmids p*hly-lacZ* or p*lhrA-36-lacZ* were diluted to OD_{600} = 0.02. At OD_{600} = 0.3 the cultures were split and FFA was added to the following final concentrations: 10 μg/ml LA, 2 μg/ml PA, or 150 μg/ml PAL. As control, vehicle was added corresponding to the final concentration in FFA-treated cultures. Samples (1 ml) were harvested after 20 h of growth. β-galactosidase assay was conducted as previously described (Christiansen et al., 2004).

Whole-Genome Sequencing

Sequencing libraries of *prfA** and the nine isolated LA-tolerant strains were prepared using Nextera XT DNA kit. Libraries were sequenced using Illumina Miseq platform in pair-end mode, read length of 150 bp. The quality of the reads was tested using FastQC standard settings. Before SNP analysis, the reads were trimmed using seqTK. The trimmed reads were mapped and polymorphisms called relative to the reference genome of *L. monocytogenes* EGD-e (NCBI ASM19603v1) using Breseq standard settings (Deatherage and Barrick, 2014). SNPs common for both read directions were found using gdtools and are listed in **Table 1**.

Total RNA Extraction and Purification

ON cultures of *prfA** and *prfA**-Δ*ccpA* were diluted in BHI medium to OD_{600} = 0.02. At OD_{600} = 0.35 cultures were split and left untreated or treated with a final concentration of 10 μg/ml LA. After 1 h, 5 ml samples were mixed with 10 ml RNAprotect bacteria reagent (Qiagen) and incubated at RT for 5 min. The samples were centrifuged at 8,000 rpm for 3 min at 4°C, and pellet was snap-cooled in liquid nitrogen.

Cells were disrupted by the Fastprep instrument (Bio101, Thermo Scientific Corporation). Total RNA was extracted by Tri reagent (Molecular Research Center, Inc.), as previously reported (Nielsen et al., 2010). RNA purity and concentration were determined by agarose gel electrophoresis and DeNovix DS-11 Fx.

Northern Blot Analysis

Agarose northern blot analysis was performed as described previously (Dos Santos et al., 2020). The membrane was hybridized with ^{32}P-labeled single-stranded probes (**Supplementary Table S7**). Visualization of bands was performed using Typhoon FLA9000 (GE Healthcare) and quantified using IQTL 8.0 quantification software (GE Healthcare).

rRNA Removal

To remove rRNA, RiboMinus™ Transcriptome Isolation Kit (Yeast and Bacteria; Invitrogen) was used. Briefly, magnetic

TABLE 1 | Mutations found in LA-tolerant strains by WGS.

LA-tolerant strains	Location	Gene	Codon	Mutation	Description
[1]LA-1A, LA-1D, LA-2A, LA-2B LA-3A, LA-3B, LA-3C	1,642,875	*ccpA*	333	$A_{8\rightarrow7}$	1 bp is deleted resulting in a frameshift that removes the STOP codon. The new STOP codon is therefore placed 26 codons downstream *ccpA*.
LA-1B	1,642,965	*ccpA*	303	G→T	Nucleotide substitution, which results in a missense mutation. Arginine is substituted by leucine (R303L).
LA-1C	1,033,670	*lmo1003*	161	$(TTG)_{3\rightarrow4}$	In-frame mutation, where an extra codon is inserted after codon 160, which extends the repeat sequence $(TTG)_{3\rightarrow4}$, and results in addition of an extra leucine amino acid into the protein sequence.

[1]*The strains ccpA-mut1 and prfA*-ccpA-mut1 were constructed by site-directed mutagenesis to contain the frameshift mutation observed in these LA-tolerant strains.*

beads were washed twice in RNase-free water, once in hybridization buffer, and then resuspended in hybridization buffer and kept at 37°C until use. A total of 8 µg RNA were incubated with RiboMinus probe and hybridization buffer at 37°C for 5 min to denature RNA, and samples were incubated on ice for 30 s. Cooled hybridized samples were mixed with the magnetic beads and incubated for 15 min at 37°C. The supernatant was isolated, and mRNA was precipitated by ethanol precipitation. 1 µl glycogen (20 µg/µL), 0.1X sample volume of 3 M sodium acetate and 2.5X sample volume of 96% ethanol was added to the supernatant. Samples were incubated at −20°C for 50 min. Precipitated mRNA was washed twice in 70% cold ethanol and resuspended in RNase-free water after the pellet was air-dried.

Library Preparation, RNA-Sequencing, and Analysis

Libraries were constructed utilizing the NEBNext Ultra RNA Library Prep Kit for Illumina according to the manufacture's protocol (NEB) and paired-end sequenced on the NovaSeq 6,000 platform (Illumina). The quality of the sequenced reads was checked by FastQC. Reads were mapped to the reference genome of EGD-e (NCBI ASM19603v1) using Bowtie 2 version 2.3.5.1 with standard settings and local alignment (Langmead and Salzberg, 2012). SAM files were converted to BAM files, sorted, and indexed by samtools version 1.7. Sorted BAM files were loaded as input in SeqMonk mapped sequence data analyzer version 1.45.3 with following settings: Duplicate reads were not removed, the minimum mapping quality was set to 28, primary alignments only, and paired-end RNA-seq data. Raw counts were generated by RNA quantification pipeline. Differentially expressed (DE) genes were found by DESeq2 analysis using R version 4.0.3 and were reported as $\log_2$ fold changes. Fold changes were calculated in this study by comparing expression levels for LA vs. control condition for *prfA**, and *prfA**-Δ*ccpA* (**Supplementary Tables S2, S3**, respectively). Additionally, expression level of *prfA**-Δ*ccpA* vs. *prfA** upon control and LA conditions were compared (**Supplementary Tables S4, S5**, respectively). Genes that were found to have a $\log_2 \geq 1$ or ≤ -1 (at least a 2-fold change) and a *value of p* below 0.05 were determined to be DE genes. Genes with less than 10 raw reads in all six biological replicates included in the comparison were excluded.

Hydrophobicity Assay

Bacteria were harvested from ON cultures by centrifugation for 5 min at 4,000 rpm and supernatant was removed. Bacteria were washed three times in 5 ml 1 × PBS and diluted in 1 x PBS to $OD_{600} = 0.3$ (OD_{600}_1). 300 µl n-hexadecane (Sigma-Aldrich) was added to 3 ml of the diluted cultures in culture tubes and samples were vortexed for 2 min followed by 15 min incubation at RT for phase separation. Afterward, OD_{600} was measured again for the water phase (OD_{600}_2). Percentage of cells staying in the hydrophilic phase was calculated by OD_{600}_2/OD_{600}_1 × 100%. Data were analyzed using two-tailed t-test. Only differences with at least 95% confidence were reported as statistically significant.

RESULTS

Selection of LA-Tolerant Strains

To generate FFA-tolerant strains, *L. monocytogenes prfA** was grown in BHI medium containing increasing concentrations of the antimicrobial and PrfA inhibitory FFA, LA. LA-tolerant strains were selected in a *prfA** background to allow further studies on the PrfA inhibitory activity of FFAs in BHI medium (Sternkopf Lillebæk et al., 2017; Dos Santos et al., 2020). A total of nine single strains were isolated from three independent biological replicates grown with 500 µg/ml LA. To test if these isolates had obtained tolerance toward LA, they were grown in the presence of increasing concentrations of LA (**Figure 1A**; **Supplementary Figure S1**). In addition to the parental strain, a PrfA-deficient strain, Δ*prfA*, was included as control since deletion of *prfA* is known to increase the tolerance of *L. monocytogenes* to antimicrobial FFAs (Sternkopf Lillebæk et al., 2017). All nine isolates and Δ*prfA* could grow at 6-fold higher concentrations of LA relative to the parental strain, *prfA**, demonstrating that the selected strains were indeed tolerant toward LA (**Figure 1A**; **Supplementary Figure S1**). To investigate if the strains selected were tolerant to other FFAs, growth experiments were performed with the antimicrobial and PrfA inhibitory FFA palmitoleic acid (PA; C16:1). As control, we included its saturated counterpart palmitic acid (PAL; C16:0), which is known to leave *L. monocytogenes* unaffected (Sternkopf Lillebæk et al., 2017). Interestingly, the nine selected strains showed an increased tolerance toward PA as well, whereas their response to PAL was comparable

to the parental strain (**Figure 1A**; **Supplementary Figure S1**). Thus, although the strains were selected for their LA-tolerant phenotype, they were clearly tolerant to the antimicrobial FFA PA as well.

The Inhibitory Effect of FFAs on PrfA Is Unaffected by FFA Tolerance

We previously showed that LA and PA act to inhibit PrfA-dependent activation of virulence genes in *L. monocytogenes prfA** (Sternkopf Lillebæk et al., 2017). Importantly, the PrfA inhibitory activities were observed at subinhibitory concentrations of LA and PA. To study how the FFA-tolerant strains respond to the PrfA inhibitory activity of LA and PA, a β-galactosidase assay was performed. Briefly, the nine selected strains were transformed with a p*hly-lacZ* fusion plasmid, which contains the PrfA-activated *hly* promoter fused to the reporter gene *lacZ* in the vector pTCV-lac (Larsen et al., 2006). Furthermore, the strains were transformed with the control reporter plasmid p*lhrA*-36-*lacZ*, which contains a PrfA-independent promoter fused to *lacZ*. Again, *prfA** and Δ*prfA* were included as controls. The resulting strains were exposed to subinhibitory levels of LA, PA, PAL, or vehicle, and cells were harvested after 20 h of growth. Under control conditions, all strains (except from Δ*prfA*) produced high levels of β-galactosidase activity, showing that the nine selected strains encode functional PrfA* protein (**Figure 1B** and **Supplementary Figure S2**). Exposure to the non-inhibitory PAL did not affect the promoter activity of *hly* in any of the strains tested (**Figure 1B**; **Supplementary Figure S2**A). In contrast, the activity was clearly repressed in *prfA** and the nine tolerant strains upon exposure to LA or PA (**Figure 1B, Supplementary Figure S2**A). Notably, all strains containing the PrfA-independent reporter plasmid p*lhrA-36-lacZ* were largely unaffected by the FFAs (**Supplementary Figure S2**B). These results demonstrate that LA and PA act to inhibit PrfA-dependent activation of *hly* in the nine selected strains, even at FFA levels much lower (approx. 50-fold) than required for exerting a growth inhibitory response.

Altogether, these results suggest that all nine LA-tolerant strains encode functional PrfA protein, implying that the FFA-tolerant phenotype is likely due to mutations in genes other than *prfA*. Furthermore, the PrfA inhibitory effect of LA and PA appears to be unaffected by the FFA-tolerant phenotype of the selected strains.

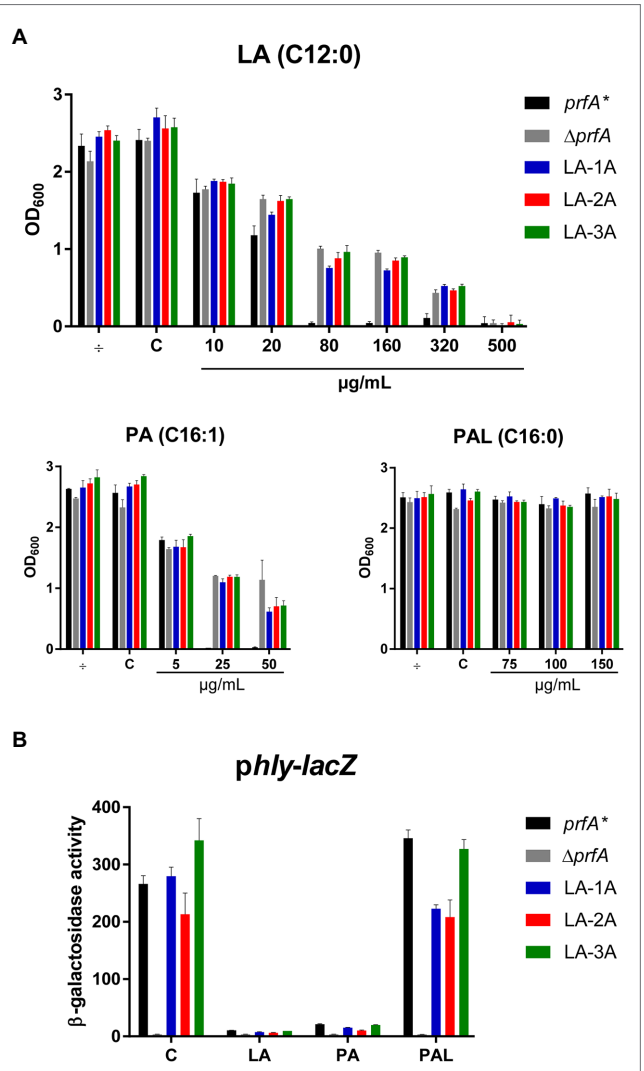

FIGURE 1 | The response of selected LA-tolerant strains toward antimicrobial and anti-virulent FFAs. **(A)** Growth of isolated LA-tolerant strains ON. The *prfA**, Δ*prfA* and one isolate from each biological replicate of the selected LA-tolerant strains (LA-1A, LA-2A, and LA-3A) were diluted to OD_{600} = 0.0002 and exposed to various concentrations of LA, PA, or PAL. As controls, cultures were left untreated (÷) or exposed to a corresponding concentration of vehicle (C). Growth was measured after 20 h. Results are the average of at least three independent experiments. **(B)** β-galactosidase assay for LA-tolerant strains. The pTCV-*lacZ*-derivative containing the *hly* promoter fused to *lacZ* was transformed into *prfA**, Δ*prfA*, and selected LA-tolerant strains (LA-1A, LA-2A, and LA-3A). The resulting strains were grown to OD_{600} = 0.3 and exposed to 10 µg/ml LA, 2 µg/ml PA, or 150 µg/ml PAL. As control, strains were incubated with a corresponding concentration of vehicle (C). Bacteria were harvested after 20 h of growth. Results are the average of three independent experiments, each performed in technical duplicates.

A Frameshift Mutation or Deletion of *ccpA* Result in FFA Tolerance

The nine LA-tolerant strains were characterized through whole-genome sequencing. Three mutations were found in the nine selected strains: a frameshift mutation in *ccpA*, a missense mutation in *ccpA* or an in-frame mutation in *lmo1003* (**Table 1**). The frameshift mutation in *ccpA* was consistently found in seven out of nine strains; notably, this mutation was represented in strains selected from all three biological replicates (**Table 1**). The genomic organization of the region encoding *ccpA* is illustrated in **Figure 2A**. In *L. monocytogenes*, CcpA is known as a major transcriptional regulator of carbon metabolism (Behari and Youngman, 1998; Mertins et al., 2007). The activity of CcpA is modulated by different cofactors, and it controls the expression of many genes, most importantly those involved in the uptake and metabolism of carbohydrates (Galinier et al., 1997). CcpA consists of a N-terminal DNA binding domain and a C-terminal core domain involved in cofactor binding

(Chaptal et al., 2006). Most likely, the 1 bp deletion in codon 333 (of 336) results in a CcpA protein, from now on referred to as CcpA-mut1, with an extended C-terminus (**Figure 2B**).

Since the *ccpA*-mut1 frameshift mutation is highly prevalent among the LA-tolerant strains, we decided to specifically examine the effect of *ccpA*-mut1 on FFA tolerance. Thus, the *ccpA*-mut1 frameshift mutation was introduced in the parental strain, *prfA**, and the wild-type strain. Furthermore, since the expected extension of the CcpA protein in *ccpA*-mut1 could affect the protein's functionality, we constructed *ccpA* knock-out strains, corresponding to an in-frame deletion of the entire *ccpA* gene in the *prfA** and wild-type strains, allowing a direct comparison of *ccpA* phenotypes. First, the effect of *ccpA*-mut1 and Δ*ccpA* on bacterial growth was compared under standard growth conditions (**Figure 2C**). For *prfA** and wild-type, we observed that *ccpA*-mut1 had a minor effect on growth in BHI medium (2–8% increase in doubling time, **Supplementary Table S1**). Furthermore, comparable doubling times were determined for *prfA*-ccpA*-mut1 and one of the selected strains harboring the *ccpA*-mut1 mutation (LA-1A). Notably, deletion of *ccpA* had a clear effect on the bacterial growth (**Figure 2C**); the doubling time of the Δ*ccpA* mutant strains increased by 22–36% compared to the parental strains (**Supplementary Table S1**). The growth phenotype of Δ*ccpA* was restored to that of the parental strains by complementation with wild-type *ccpA* (**Supplementary Figure S3**A). Similar growth phenotypes were obtained in a previous study, using a *ccpA* insertion mutant (Mertins et al., 2007). Collectively, our data show that deletion of *ccpA* had a more negative impact on bacterial fitness relative to the *ccpA*-mut1 mutation, suggesting that *ccpA*-mut1 frameshift mutation might not lead to complete loss of CcpA functionality.

Next, the effect of *ccpA*-mut1 and Δ*ccpA* on FFA tolerance was tested by comparing the growth of mutants and parental strains in increasing concentrations of LA or PA (**Figure 3A**). The *ccpA*-mut1 and Δ*ccpA* mutant strains were equally tolerant toward LA and PA, and much more tolerant compared to the corresponding parental strains (**Figure 3A**). Complementation with wild-type *ccpA* restored the phenotype to that of the parental strain, confirming that CcpA confers sensitivity toward antimicrobial FFAs (**Supplementary Figure S3B**). Altogether, these data revealed that the frameshift mutation *ccpA*-mut1, present in seven out of nine selected mutants, confer FFA tolerance. Notably, Δ*ccpA* mutants were clearly tolerant to LA and PA as well, confirming that regulatory activities of CcpA confer increased sensitivity of *L. monocytogenes* to antimicrobial FFAs. Furthermore, we observed that mutation of *ccpA* confers FFA tolerance independently of PrfA activity, since an increased tolerance to LA and PA was observed in both the wild-type and the *prfA** background (**Figure 3A**).

To examine if *ccpA*-mut1 or deletion of *ccpA* interfere with the PrfA inhibitory activity of FFAs, we performed a β-galactosidase assay. The *prfA** mutant series, containing p*hly-lacZ* or p*lhrA-36-lacZ* fusion plasmids, were exposed to subinhibitory levels of LA, PA, or PAL (**Figure 3B** and **Supplementary Figure S4**). Under control conditions, *ccpA*-mut1 and Δ*ccpA* mutant cells produced high levels of β-galactosidase activity, indicating that the *ccpA* mutations *per se* do not interfere with PrfA-dependent activation of *hly*. Importantly, *ccpA*-mut1 and Δ*ccpA* mutant cells were still sensitive toward the PrfA inhibitory effect of LA and PA, since the promoter activity of *hly* was strongly reduced upon LA and PA exposure (**Figure 3B**). As expected, PAL had no major effect on any of the strains tested (**Figure 3B**). These results show that the *ccpA* mutations do not affect the activity of PrfA*; furthermore, they do not interfere with the PrfA inhibitory effect of LA and PA.

Altogether, these data clearly demonstrate that CcpA confers sensitivity toward the antimicrobial activity of the FFAs. Importantly, the PrfA inhibitory activity of the FFAs does not rely on a functional CcpA.

Exploring How Lack of CcpA Confers FFA Tolerance

Since the *ccpA*-mut1 and Δ*ccpA* strains were equally tolerant toward FFAs (**Figure 3A**), we reasoned that the mechanism conferring FFA tolerance is related to the absence of CcpA's regulatory activities. To investigate in more detail how lack of CcpA functionality confers FFA tolerance, transcriptome analysis was performed for *prfA** and *prfA**-Δ*ccpA* under control conditions and upon exposure to a subinhibitory level LA for 1 h. Again, a *prfA** background was chosen to reveal any effect of LA and/or CcpA on PrfA-dependent regulatory activities in BHI medium.

After RNA-sequencing, we first analyzed the response of each of the two strains to LA exposure. In general, LA seemed to have a very limited effect on global gene expression; for each strain, less than 15 genes were significantly induced or repressed by at least 2-fold in response to LA (**Supplementary Tables S2, S3**). The two strains do not share any of the upregulated genes (**Figure 4A**). For the downregulated genes, a more common tendency was observed; most importantly, the PrfA-regulated genes *hly, plcA*, and *actA* were significantly downregulated in both strains upon LA exposure (**Figure 4A**; **Supplementary Tables S2, S3**). In addition, *plcB, mpl*, and *uhpT*, which are controlled by PrfA as well, were significantly downregulated upon LA exposure in Δ*ccpA* (**Figure 4A**; **Supplementary Tables S2, S3**). To summarize, the results of the transcriptome study confirmed that LA exposure leads to downregulation of PrfA-dependent virulence gene expression in a strain encoding the constitutively active variant of PrfA, PrfA-G155S. In general, LA exposure affected only a limited set of genes in *L. monocytogenes prfA**, suggesting that at subinhibitory concentrations, LA primarily acts as a signal to downregulate PrfA-dependent virulence gene expression. Additionally, we note that CcpA does not seem to be required for LA-mediated inhibition of PrfA-regulated genes.

As a very low number of genes were affected by LA exposure, we speculated that the FFA-tolerant phenotype observed for Δ*ccpA* might result from transcriptional changes caused by lack of CcpA functionality in general. Therefore, to find genes potentially important for the FFA-tolerant phenotype, we compared the transcriptomes of *prfA** and *prfA**-Δ*ccpA* cells. Deletion of *ccpA* resulted in up- or

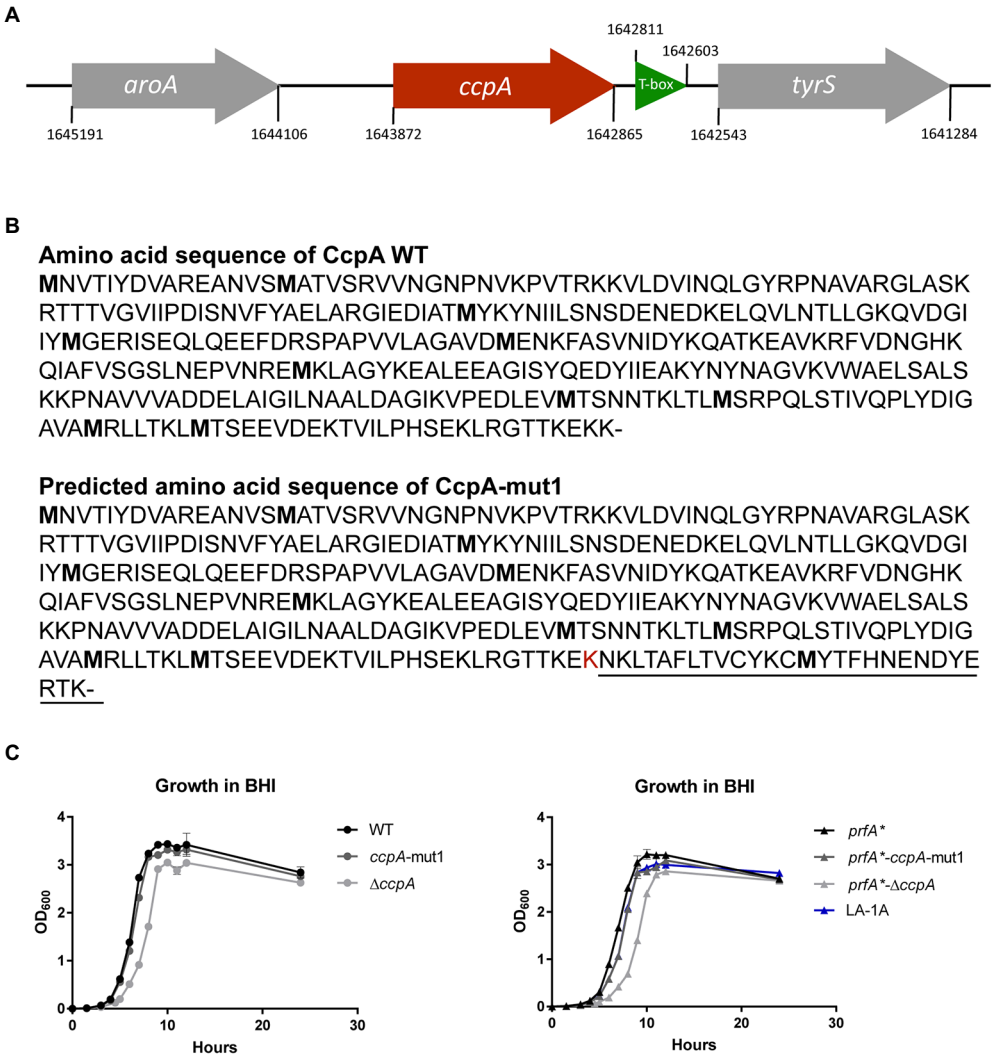

FIGURE 2 | LA-tolerant strains carry mutations in the *ccpA* gene **(A)** Schematic illustration of the genomic region encoding CcpA. The *aroA* gene (gray) is located upstream from *ccpA* (red), whereas *tyrS* (gray) is situated downstream from *ccpA*. Potentially, mutations in *ccpA* could have polar effects on the expression of *tyrS*, which is regulated *via* an upstream located T-box leader, shown in green. However, in our RNA-seq analyses, we did not observe any significant differences in *tyrS* expression when comparing strains *prfA** and *prfA**-Δ*ccpA* (this study) or strains *prfA** and *prfA**-*ccpA*-mut1 (our unpublished observations). **(B)** The annotated amino acid sequence of wild-type CcpA protein and the predicted CcpA-mut1 amino acid sequence. The estimated amino acid sequence of CcpA-mut1 is based on the frameshift mutation detected by whole-genome sequencing and terminator predictions using the web tool ARNold finding terminators. **(C)** Growth of CcpA mutants in BHI medium. Cultures of wild-type, *ccpA*-mut1, Δ*ccpA*, *prfA**, *prfA**-*ccpA*-mut1, *prfA**-Δ*ccpA*, and LA-1A were diluted to OD_{600} = 0.002. Growth was measured every hour for the first 12 h with an additional 24 h point. Results are the average of three independent experiments.

downregulation of 312 and 143 genes, respectively, by ≥2-fold under regular growth conditions (**Supplementary Table S4**). As expected, more genes were up- than downregulated, because the majority of genes belonging to the CcpA regulon in *L. monocytogenes* are repressed by CcpA (Mertins et al., 2007). In accordance with CcpA's role in CCR control, 20% of the genes upregulated in the Δ*ccpA* mutant strain are related to carbohydrate transport and metabolism (**Figure 4B**). The largest group of genes downregulated in *prfA**-Δ*ccpA*, relative to *prfA**, are involved in amino acid transport and metabolism (18%). In the presence of LA, 218 and 66 genes were significantly up- or downregulated, respectively, by ≥2-fold in the Δ*ccpA* mutant relative to the parental strain (**Supplementary Table S5**). The largest groups of up- and downregulated genes are still involved in carbohydrate transport and metabolism (26%) and amino acid transport and metabolism (24%), respectively (**Figure 4B**). The transcriptome analysis was validated by northern blot analysis of four selected genes (**Supplementary Figure S5**). Altogether, these results confirm that CcpA is a major gene regulator of metabolic pathways in *L. monocytogenes*, as shown previously by others (Mertins et al., 2007). Notably, although CcpA promotes sensitivity to antimicrobial FFAs, its regulatory activities appear to be largely unaffected by FFA exposure.

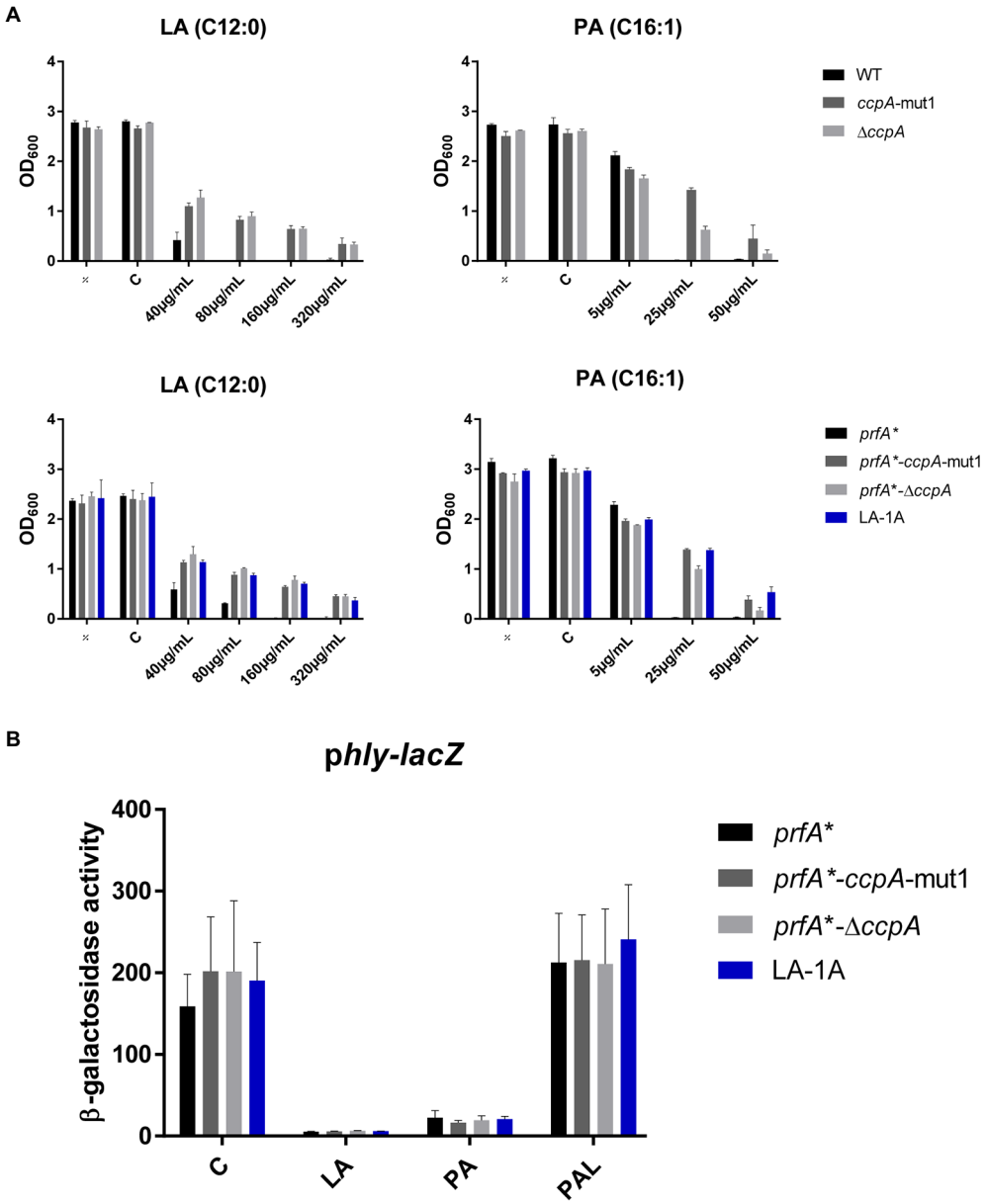

FIGURE 3 | The response of CcpA mutants to antimicrobial and anti-virulent FFAs. **(A)** Growth of CcpA mutants upon LA exposure. Wild-type, *ccpA*-mut1, Δ*ccpA*, *prfA**, *prfA*-ccpA*-mut1, *prfA**-Δ*ccpA* and LA-1A were diluted to OD_{600} = 0.0002 and exposed to different concentrations of LA and PA. As controls, cultures were left untreated (÷) or exposed to a corresponding concentration of vehicle (C). After 20 h of incubation growth was measured. The results represent the average of three independent experiments. **(B)** β-galactosidase assay for CcpA mutants. Strains *prfA**, *prfA*-ccpA*-mut1, *prfA**-Δ*ccpA*, and LA-1A were transformed with p*hly-lacZ*, containing a transcriptional fusion of the *hly* promoter to the *lacZ* gene. Resulting strains were grown to OD_{600} = 0.3 and exposed to 10 μg/ml LA, 2 μg/ml PA, or 150 μg/ml PAL. As control, cultures were exposed to a corresponding concentration of vehicle (C). Results are the average of three independent experiments each performed in technical duplicates.

To investigate in more detail if some of the CcpA-regulated genes contribute to FFA tolerance, we focused on genes significantly upregulated by at least 4-fold in Δ*ccpA* relative to the parental strain, both under regular growth conditions and upon LA exposure (**Supplementary Table S6**). Two of the three most upregulated genes, chosen for mutational analysis, encode a PTS system component (*lmo2772*) and a hypothetical protein (*lmo0517*), respectively. Strikingly, these genes were upregulated more than 100-fold in the absence of CcpA (**Supplementary Table S6**). When going through the list of genes highly upregulated in the absence of CcpA, we furthermore noticed that the *lmo0109-lmo0110* operon is predicted to encode a transcriptional regulator and a protein with esterase/lipase function, respectively, suggesting

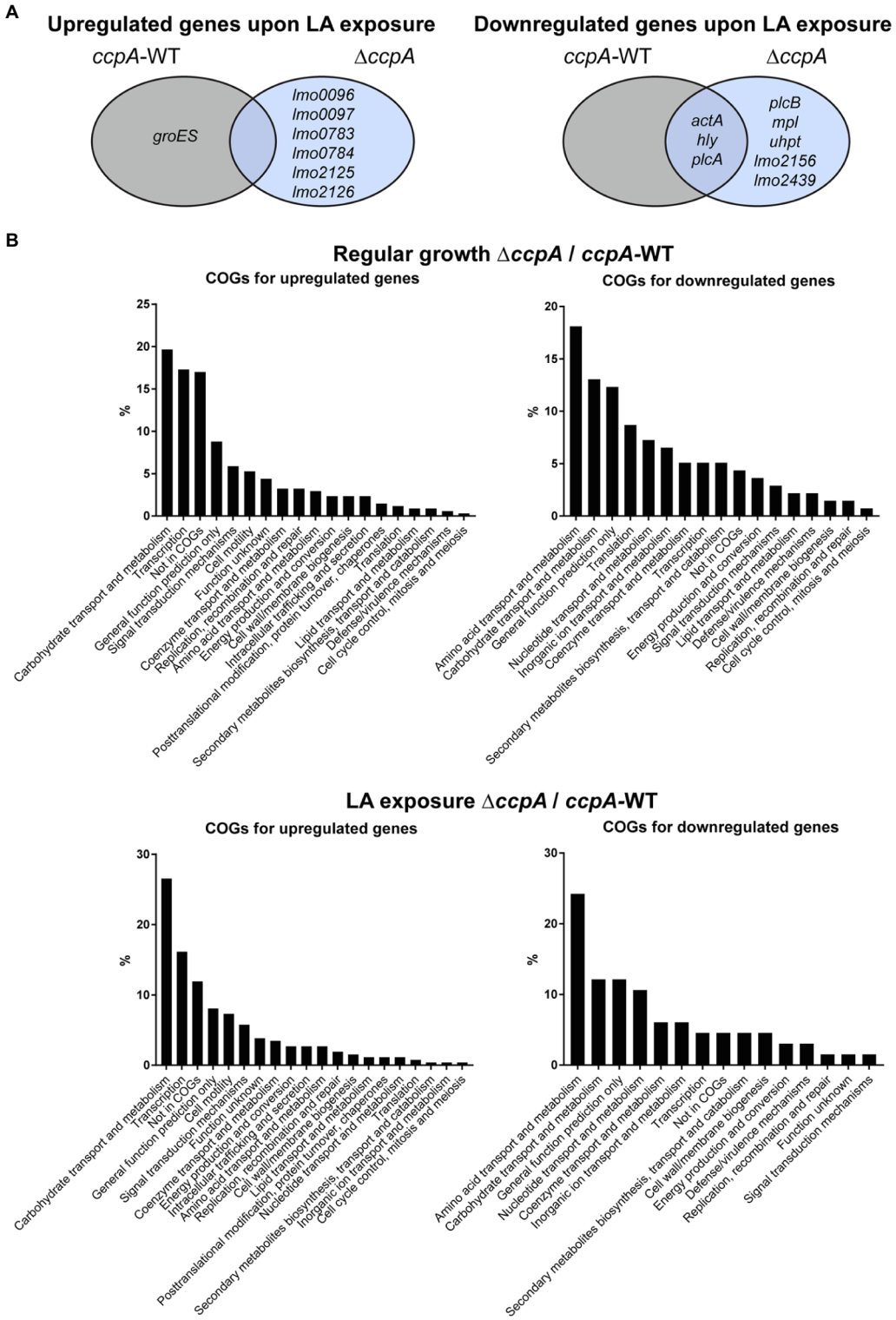

FIGURE 4 | Transcriptomic profiles for *prfA** and *prfA**-Δ*ccpA* cells upon regular growth and exposure to LA. **(A)** Venn diagram for genes significantly regulated upon exposure to LA in *prfA** and *prfA**-Δ*ccpA*. Genes up- or downregulated by at least 2-fold upon exposure to LA relative to control conditions are gathered in a Veen diagram for *prfA** and *prfA**-Δ*ccpA*. **(B)** Clusters of Orthologous Genes (COGs) distribution of significantly regulated genes in the Δ*ccpA* strain compared to the parental strain. The transcriptome profile of *prfA**-Δ*ccpA* and *prfA** strains were compared both upon control conditions and upon exposure to LA. Genes significantly up- or downregulated by more than 2-fold were determined as differentially expressed. The distribution of regulated genes according to their corresponding COGs is presented in the graphs.

that this operon could play a role in the response of *L. monocytogenes* to FFAs (**Supplementary Table S6**). Additionally, we observed that *lmo2175* (*fabG*) encodes a 3-ketoacyl-(acyl carrier protein) reductase, which catalyzes the first of two reduction steps in the elongation cycle of fatty acid synthesis (**Supplementary Table S6**). Knock-out mutants of *lmo2772*, *lmo0517*, the *lmo0109-lmo0110* operon, and *lmo2175* were therefore constructed in the FFA-tolerant Δ*ccpA* background, to examine if deletion of any of these genes would restore FFA sensitivity. Growth upon exposure to increasing concentrations of LA was studied for the various mutants (**Figure 5A**). The data revealed that deletion of the selected genes and operon, individually, does not restore FFA sensitivity in the *prfA**-Δ*ccpA* strain, indicating that upregulation of these CcpA-regulated genes does not confer FFA tolerance on its own. Instead, FFA tolerance might be due to altered CcpA regulation of other genes, which have not been tested in this study.

Deletion of *ccpA* Results in a More Hydrophilic Bacterial Surface

It is well known that CcpA regulates multiple PTS systems located in the bacterial cell envelope (Schumacher et al., 2004). We therefore speculated if deletion of *ccpA* could affect the polarity of the bacterial surface. To test this idea, we compared the surface hydrophobicity of the Δ*ccpA* mutant and its parental strain by studying the microbial adhesion to *n*-hexadecane using the hydrocarbon test (**Figure 5B**). The Δ*ccpA* strain has an increased percentage of cells staying in the hydrophilic phase compared to its parental strain, indicating that deletion of *ccpA* confers a more hydrophilic bacterial surface. The change in surface polarity upon deletion of *ccpA* could very well be related to its FFA-tolerant phenotype. Indeed, lack of CcpA most likely increases FFA tolerance by promoting repulsion of antimicrobial FFAs, due to a more hydrophilic bacterial surface.

CcpA Plays a Role in the Response to Acid Stress, Ampicillin, and Gentamicin

The experiments presented in **Figure 3A** clearly showed that CcpA confers sensitivity to the antimicrobial activity of LA and PA, which are known to target the bacterial membrane (Desbois and Smith, 2010). In line with this, we found that FFA tolerance of the Δ*ccpA* strain is most likely caused by changes in surface polarity (**Figure 5B**). These findings prompted us to investigate if CcpA plays a role in the response of *L. monocytogenes* to other stress conditions. The *prfA**-Δ*ccpA* and *prfA** strains were subjected to growth in the presence of 2% ethanol, osmotic stress (0.25 M NaCl), acid stress (pH = 5), or antibiotics (bacitracin, ampicillin, vancomycin, gentamicin; **Figure 6**). Curiously, the *ccpA* deletion mutant was clearly more tolerant to low pH and ampicillin, but more sensitive to gentamicin, compared to the parental strain (**Figure 6**). These findings suggest that CcpA plays a role in the response of *L. monocytogenes* to acid stress conditions, as well as antibiotics used for treating listeriosis: ampicillin and gentamicin (Temple and Nahata, 2000).

DISCUSSION

The PrfA regulator plays a key role in the pathogenicity of *L. monocytogenes* and is essential for production of virulence factors promoting the intracellular lifestyle of this pathogen. Various signals from the environment affect the level or activity of PrfA (Scortti et al., 2007; Johansson and Freitag, 2019). The transcription of *prfA* is positively controlled by the general stress sigma factor Sigma B and the global metabolic regulator CodY, whereas translation of *prfA* mRNA is affected by temperature and two *trans*-acting S-adenosyl methionine responsive riboswitches, SreA and SreB (Johansson and Freitag, 2019; Tiensuu et al., 2019). At the post-translational level, PrfA is positively controlled by GSH which binds directly to PrfA, whereas inhibitory peptides prevent binding of GSH to PrfA (Reniere et al., 2015; Hall et al., 2016; Krypotou et al., 2019). Readily utilizable carbohydrates, such as glucose, fructose, and cellobiose, have long been known to inhibit the activity of PrfA, but the exact mechanism remains to be revealed (Milenbachs et al., 1997). Although the PrfA inhibitory carbohydrates are taken up by PTS systems, CcpA is not required for carbon source regulation of virulence genes in *L. monocytogenes* (Behari and Youngman, 1998; Deutscher et al., 2005; Herro et al., 2005; Mertins et al., 2007).

We used a *prfA** strain to investigate the response of *L. monocytogenes* to antimicrobial and PrfA inhibitory FFAs. PrfA* variants are locked in a constitutively active conformation and stimulate transcription of virulence genes in BHI broth culture, where wild-type PrfA is not active (Ermolaeva et al., 2004). Importantly, PrfA* does not respond to inhibition by readily metabolizable carbohydrates (Ripio et al., 1997a) or inhibitory peptides (Krypotou et al., 2019). However, specific FFAs inhibit PrfA-dependent transcription of virulence genes in *prfA** by preventing PrfA* from binding to DNA (Dos Santos et al., 2020). The transcriptome analysis of *prfA** confirmed that PrfA-regulated virulence genes were indeed repressed following exposure to subinhibitory concentrations of LA (**Figure 4A**). Notably, less than 5 genes were differentially expressed in LA-treated cells relative to untreated cells, demonstrating that repression of virulence genes is the most prominent outcome following exposure of *prfA** to LA.

At higher concentrations, LA inhibits the growth of *L. monocytogenes*, and PrfA is known to affect the sensitivity against the antimicrobial activity of LA (Sternkopf Lillebæk et al., 2017). These findings prompted us to investigate if the antimicrobial activity of LA could be linked to its PrfA inhibitory activity. We found that a frameshift mutation in *ccpA* promoted tolerance of *L. monocytogenes* to LA as well as PA, and deletion of *ccpA* generated a similar phenotype. As expected, CcpA was dispensable for PrfA-dependent activation of virulence genes in *L. monocytogenes prfA** under normal growth conditions (**Figure 3B**). Importantly, all FFA-tolerant mutants responded well to FFA-mediated inhibition of virulence gene expression, indicating that virulence inhibitory signaling by FFAs is not linked to its antimicrobial actions. These results are well in line with recent data demonstrating that two non-antimicrobial FFAs, myristic acid (C14:0) and oleic acid (C18:1), were capable of downregulating PrfA-dependent activities, showing that antimicrobial activity is not compulsory for the PrfA inhibitory

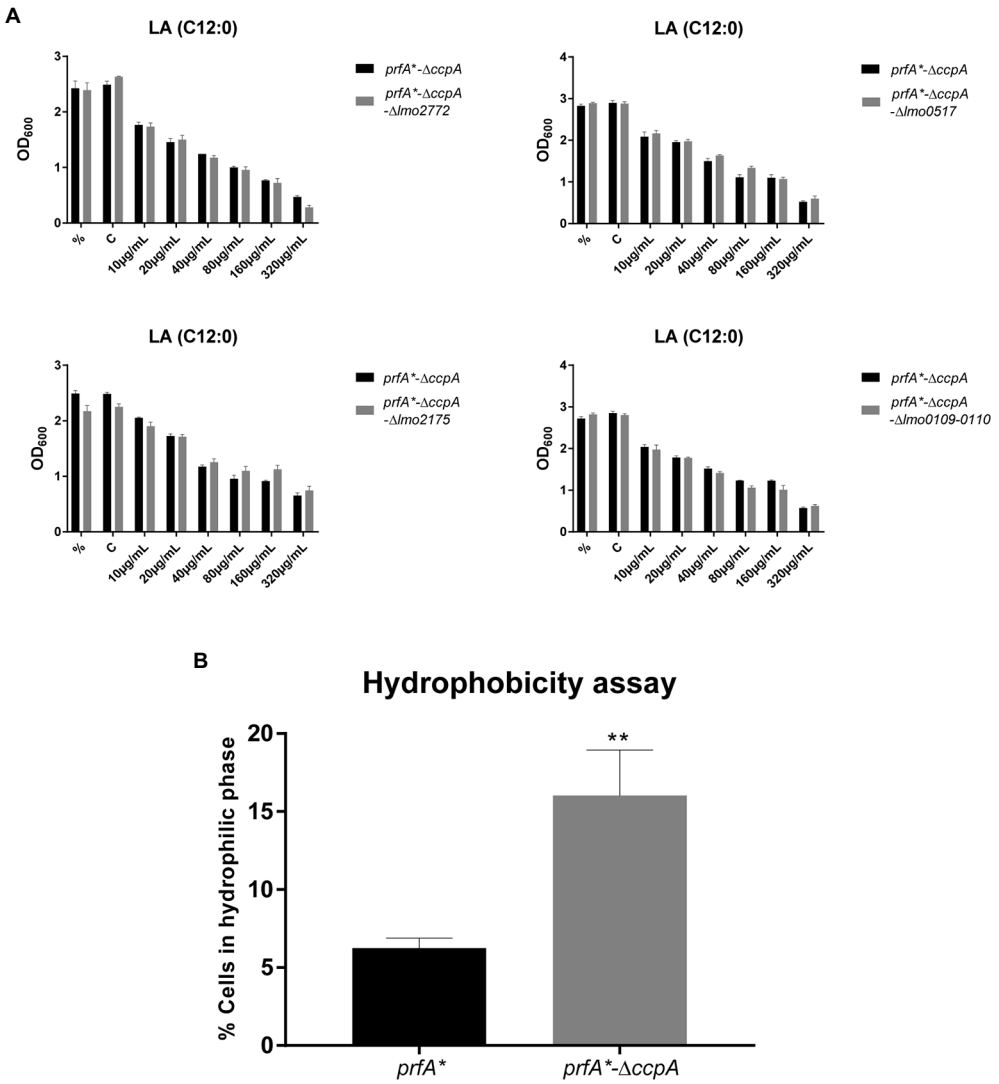

FIGURE 5 | Deletion of *ccpA* results in a more hydrophilic surface. **(A)** Growth experiments for knock-out mutants with increasing concentrations of LA. ON cultures were diluted and stressed with various increasing concentrations of LA. As controls, one sample was left untreated (%) and another was stressed with a corresponding concentration of vehicle (C). Growth was measured after 20 h of growth. Results are the average of three independent experiments. **(B)** Hydrophobicity assay for *prfA** and *prfA**-Δ*ccpA*. Bacteria were washed and diluted in 1x PBS, followed by incubation with *n*-hexadecane to measure the bacterial adhesion. OD_{600} was measured for the water phase before and after incubation with *n*-hexadecane. Data are presented as percentage of cells that stayed in the water phase, based on the OD_{600} measurements. Results are the average of three independent experiments. Statistical analysis was performed using two-tailed t-test. Only differences with at least 95% confidence were reported as statistically significant (**$p < 0.01$).

ability of an FFA (Dos Santos et al., 2020). Altogether, these findings support that exposure of *L. monocytogenes* to LA generates two separate responses: one relating to the antimicrobial activity of the FFA, and another leading to inhibition of PrfA activity. Notably, inhibition of PrfA activity may be expected to further sensitize *L. monocytogenes* to the antimicrobial actions of FFAs (Sternkopf Lillebæk et al., 2017). Future studies should aim to uncover the specific role of PrfA in mediating sensitivity to antimicrobial FFAs.

Our data clearly demonstrate that CcpA confers sensitivity toward the antimicrobial response of the FFAs, as deletion of *ccpA* caused FFA tolerance (**Figure 3A**). Our transcriptome analysis revealed that the FFA-tolerant phenotype, which is observed for Δ*ccpA*, does not seem to be induced upon LA exposure, but appears to be an inherent phenotype of the Δ*ccpA* mutant. Based on these observations, we hypothesized that genes underlying the FFA-tolerant phenotype are regulated by CcpA both during regular growth and upon LA exposure. To analyze this further, we deleted two genes, that are highly upregulated in the absence of CcpA (*lmo2772* and *lmo0517*), and three genes of specific interest based on their predicted protein function (*lmo2175* and *lmo0109-0110*). However, deletion of these genes did not restore FFA sensitivity in a Δ*ccpA* background (**Figure 5A**), suggesting that the FFA-tolerant

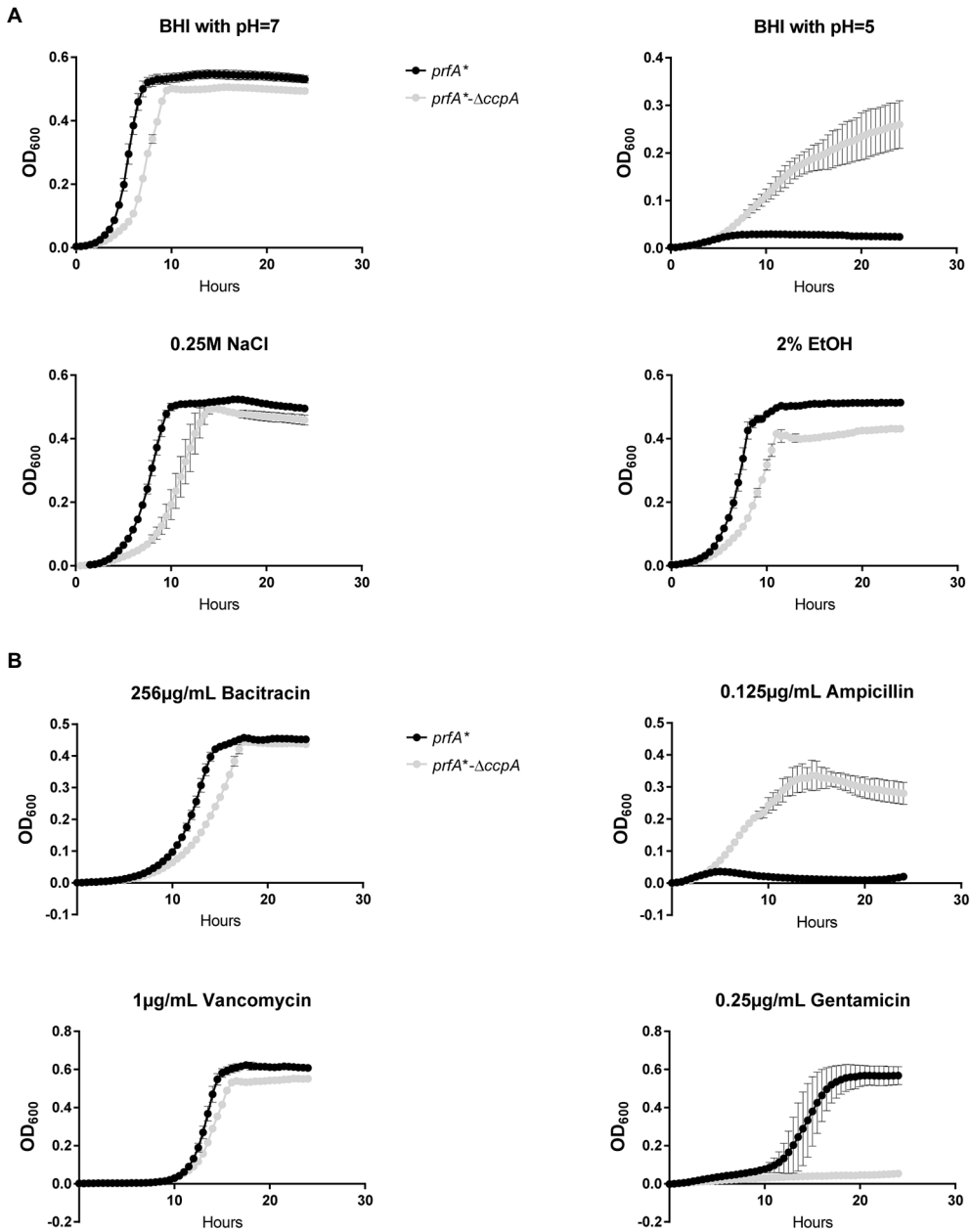

FIGURE 6 | Growth of the Δ*ccpA* mutant and parental strains upon different stress conditions. **(A)** Growth upon exposure to acid, salt, or ethanol stress. ON cultures were diluted to OD_{600} = 0.005 in 96 well plates with corresponding stress conditions. Plates were incubated for 24 h at 37°C and orbitally shaken for 15 s every 30 min. Growth was measured regularly. Results are the average of three independent experiments. **(B)** Growth upon addition of different antibiotics. ON cultures were diluted to OD_{600} = 0.005 in 96-well plates with corresponding stress conditions. Plates were incubated for 24 h at 37°C and orbitally shaken for 15 s every 30 min. Growth was measured regularly. The results are the average of three independent experiments.

phenotype must be based on other regulatory activities of CcpA. In Gram-positive bacteria, several mechanisms have been suggested to confer resistance to antimicrobial FFAs. In *Staphylococcus aureus*, mutant variants selected for their ability to grow in the presence of the antimicrobial FFA linoleic acid (LNA, C18:2), resulted in the identification of the fatty acid efflux pump FarE (Alnaseri et al., 2015). The LNA-tolerant mutant carried a substitution in the transcription regulator FarR, which is divergently transcribed from *farE*. The expression of *farE* is highly induced in the presence of LNA and arachidonic acid (AA, C20:4), and accordingly, FarE mediates resistance to LNA and AA, but not PA (Alnaseri et al., 2015). Notably, another efflux pump, encoded by the PA-inducible *tet38* gene, has been reported to promote resistance to PA in *S. aureus* (Truong-Bolduc et al., 2013). These studies demonstrate that FFA-tolerant phenotypes may be attributable to FFA detoxification

with efflux pumps. In addition, alterations of the bacterial surface may shield the bacterium against antimicrobial FFAs. For instance, the surface protein IsdA increases the surface hydrophilicity of *S. aureus*, thereby precluding the binding of antimicrobial FFAs to the bacterium (Clarke et al., 2007). Furthermore, wall teichoic acids are known to protect *S. aureus* against antimicrobial FFAs, by repulsing FFAs from the bacterial surface (Kohler et al., 2009). Since CcpA regulates multiple genes encoding transport proteins located in the cell envelope of *L. monocytogenes*, we investigated if lack of CcpA affects the surface polarity. Our data revealed that deletion of *ccpA* results in a more hydrophilic surface of *L. monocytogenes* (**Figure 5B**), as observed for IsdA and wall teichoic acids in *S. aureus* (Clarke et al., 2007; Kohler et al., 2009). Based on these findings, we propose that the regulatory changes occurring by deletion of *ccpA* lead to a decrease in surface hydrophobicity, which results in a more FFA-tolerant phenotype. The specific CcpA-regulated gene(s) conferring the FFA-tolerant phenotype waits to be identified. Notably, deletion of *ccpA* not only resulted in tolerance toward antimicrobial FFAs, but also acid stress and the cell wall acting antibiotic ampicillin (**Figure 6**). Additionally, sensitivity was obtained toward gentamicin upon deletion of *ccpA*; an antibiotic acting to inhibit bacterial translation, which has commonly been used together with ampicillin to treat listeriosis. Together these data show that CcpA not only is involved in the response to antimicrobial FFAs; apparently, this regulator plays a broader role in the response toward multiple stress conditions encountered by *L. monocytogenes* as both a saprophyte and pathogen. Future studies should aim to reveal the regulatory role of CcpA, as well as PrfA, in responding to such conditions.

We previously suggested that FFAs acting to inhibit PrfA-dependent expression of virulence genes could be future candidates for novel anti-virulence therapies against *L. monocytogenes* (Kallipolitis, 2017; Sternkopf Lillebæk et al., 2017; Dos Santos et al., 2020). In addition to their PrfA inhibitory effect, a subset of FFAs seem particularly attractive, because they exert a dual inhibitory effect on *L. monocytogenes*: at lower concentrations, they act as signaling compounds to inhibit virulence gene expression, whereas at higher concentrations, they prevent bacterial growth. However, as for most growth inhibitory compounds, bacteria are likely to develop resistance against antimicrobial FFAs. Indeed, LA-tolerant mutant variants were readily isolated in the present study, but most importantly, the LA-tolerant strains were still susceptible to the PrfA inhibitory activity of LA. Altogether, these findings support that FFAs having a dual inhibitory effect in this pathogen may be useful candidates in future therapies against *L. monocytogenes*.

DATA AVAILABILITY STATEMENT

The datasets presented in this study can be found in online repositories. The names of the repository/repositories and accession number(s) can be found at: https://www.ncbi.nlm.nih.gov/, PRJNA815746 and PRJNA815751.

AUTHOR CONTRIBUTIONS

RT and BK contributed to conception and design of the study. RT, KJ, PS, and EL contributed to the experimental work. RT, MJ, MS, and MK contributed to the sequencing analysis. RT and BK wrote the first draft of the manuscript. All authors contributed to manuscript revision, read, and approved the submitted version.

FUNDING

This work was supported by the Novo Nordisk Foundation (grant number NNF17OC0028528).

ACKNOWLEDGMENTS

RNA-sequencing was carried out at the Center for Functional Genomics and Tissue Plasticity, Functional Genomics & Metabolism Research Unit, University of Southern Denmark. The authors thank Tenna P. Mortensen, Maibrith Wishoff, and Ronni Nielsen for sequencing assistance.

SUPPLEMENTARY MATERIAL

The Supplementary Material for this article can be found online at: https://www.frontiersin.org/articles/10.3389/fmicb.2022.895942/full#supplementary-material

REFERENCES

Alnaseri, H., Arsic, B., Schneider, J. E., Kaiser, J. C., Scinocca, Z. C., Heinrichs, D. E., et al. (2015). Inducible expression of a resistance-nodulation-division-type efflux pump in *Staphylococcus aureus* provides resistance to linoleic and arachidonic acids. *J. Bacteriol.* 197, 1893–1905. doi: 10.1128/JB.02607-14

Bécavin, C., Bouchier, C., Lechat, P., Archambaud, C., Creno, S., Gouin, E., et al. (2014). Comparison of widely used *Listeria monocytogenes* strains EGD, 10403S, and EGD-e highlights genomic variations underlying differences in pathogenicity. *mBio* 5, e00969–e00914.

Behari, J., and Youngman, P. (1998). A homolog of CcpA mediates catabolite control in *listeria monocytogenes* but not carbon source regulation of virulence genes. *J. Bacteriol.* 180, 6316–6324. doi: 10.1128/JB.180.23.6316-6324.1998

Böckmann, R., Dickneite, C., Middendorf, B., Goebel, W., and Sokolovic, Z. (1996). Specific binding of the *Listeria monocytogenes* transcriptional regulator PrfA to target sequences requires additional factor(s) and is influenced by iron. *Mol. Microbiol.* 22, 643–653. doi: 10.1046/j.1365-2958.1996.d01-1722.x

Chaptal, V., Gueguen-Chaignon, V., Poncet, S., Lecampion, C., Meyer, P., Deutscher, J., et al. (2006). Structural analysis of *B. subtilis* CcpA effector binding site. *Proteins* 64, 814–816. doi: 10.1002/prot.21001

Christiansen, J. K., Larsen, M. H., Ingmer, H., Søgaard-Andersen, L., and Kallipolitis, B. H. (2004). The RNA-binding protein Hfq of *Listeria monocytogenes*: role in stress tolerance and virulence. *J. Bacteriol.* 186, 3355–3362. doi: 10.1128/JB.186.11.3355-3362.2004

Clarke, S. R., Mohamed, R., Bian, L., Routh, A. F., Kokai-Kun, J. F., Mond, J. J., et al. (2007). The *Staphylococcus aureus* surface protein IsdA mediates

resistance to innate defenses of human skin. *Cell Host Microbe* 1, 199–212. doi: 10.1016/j.chom.2007.04.005

de las Heras, A., Cain, R. J., Bielecka, M. K., and Vázquez-Boland, J. A. (2011). Regulation of *listeria* virulence: PrfA master and commander. *Curr. Opin. Microbiol.* 14, 118–127. doi: 10.1016/j.mib.2011.01.005

Deatherage, D. E., and Barrick, J. E. (2014). Identification of mutations in laboratory-evolved microbes from next-generation sequencing data using breseq. *Methods Mol. Biol.* 1151, 165–188. doi: 10.1007/978-1-4939-0554-6_12

Desbois, A. P., and Smith, V. J. (2010). Antibacterial free fatty acids: activities, mechanisms of action and biotechnological potential. *Appl. Microbiol. Biotechnol.* 85, 1629–1642. doi: 10.1007/s00253-009-2355-3

Deutscher, J. (2008). The mechanisms of carbon catabolite repression in bacteria. *Curr. Opin. Microbiol.* 11, 87–93. doi: 10.1016/j.mib.2008.02.007

Deutscher, J., Herro, R., Bourand, A., Mijakovic, I., and Poncet, S. (2005). P-Ser-HPr: A link between carbon metabolism and the virulence of some pathogenic bacteria. *Biochim. Biophys. Acta* 1754, 118–125. doi: 10.1016/j.bbapap.2005.07.029

Dos Santos, P. T., Thomasen, R. S. S., Green, M. S., Færgeman, N. J., and Kallipolitis, B. H. (2020). Free fatty acids interfere with the DNA binding activity of the virulence regulator PrfA of *Listeria monocytogenes*. *J. Bacteriol.* 202, e00156–e00120. doi: 10.1128/JB.00156-20

Eiting, M., Hageluken, G., Schubert, W. D., and Heinz, D. W. (2005). The mutation G145S in PrfA, a key virulence regulator of *Listeria monocytogenes*, increases DNA-binding affinity by stabilizing the HTH motif. *Mol. Microbiol.* 56, 433–446. doi: 10.1111/j.1365-2958.2005.04561.x

Ermolaeva, S., Novella, S., Vega, Y., Ripio, M. T., Scortti, M., and Vázquez-Boland, J. A. (2004). Negative control of *Listeria monocytogenes* virulence genes by a diffusible autorepressor. *Mol. Microbiol.* 52, 601–611. doi: 10.1111/j.1365-2958.2004.04003.x

Freitag, N. E., Port, G. C., and Miner, M. D. (2009). *Listeria monocytogenes* – from saprophyte to intracellular pathogen. *Nat. Rev. Microbiol.* 7, 623–628. doi: 10.1038/nrmicro2171

Galinier, A., Haiech, J., Kilhoffer, M. C., Jaquinod, M., Stülke, J., Deutscher, J., et al. (1997). The *Bacillus subtilis* crh gene encodes a HPr-like protein involved in carbon catabolite repression. *Proc. Natl. Acad. Sci. U. S. A.* 94, 8439–8444. doi: 10.1073/pnas.94.16.8439

Hall, M., Grundstrom, C., Begum, A., Lindberg, M. J., Sauer, U. H., Almqvist, F., et al. (2016). Structural basis for glutathione-mediated activation of the virulence regulatory protein PrfA in *Listeria*. *Proc. Natl. Acad. Sci. U. S. A.* 113, 14733–14738. doi: 10.1073/pnas.1614028114

Herro, R., Poncet, S., Cossart, P., Buchrieser, C., Gouin, E., Glaser, P., et al. (2005). How seryl-phosphorylated HPr inhibits PrfA, a transcription activator of *Listeria monocytogenes* virulence genes. *J. Mol. Microbiol. Biotechnol.* 9, 224–234. doi: 10.1159/000089650

Johansson, J., and Freitag, N. E. (2019). Regulation of *Listeria monocytogenes* virulence. *Microbiol. Spectr.* 7, 1–20. doi: 10.1128/microbiolspec.GPP3-0064-2019

Jones, B. E., Dossonnet, V., Küster, E., Hillen, W., Deutscher, J., and Klevit, R. E. (1997). Binding of the catabolite repressor protein CcpA to its DNA target is regulated by phosphorylation of its corepressor HPr. *J. Biol. Chem.* 272, 26530–26535. doi: 10.1074/jbc.272.42.26530

Kallipolitis, B. H. (2017). How can naturally occurring fatty acids neutralize *Listeria*? *Future Microbiol.* 12, 1239–1241. doi: 10.2217/fmb-2017-0176

Kohler, T., Weidenmaier, C., and Peschel, A. (2009). Wall teichoic acid protects *Staphylococcus aureus* against antimicrobial fatty acids from human skin. *J. Bacteriol.* 191, 4482–4484. doi: 10.1128/JB.00221-09

Krypotou, E., Scortti, M., Grundström, C., Oelker, M., Luisi, B. F., Sauer-Eriksson, A. E., et al. (2019). Control of bacterial virulence through the peptide signature of the habitat. *Cell Rep.* 26, 1815.e5–1827.e5. doi: 10.1016/j.celrep.2019.01.073

Langmead, B., and Salzberg, S. L. (2012). Fast gapped-read alignment with bowtie 2. *Nat. Methods* 9, 357–359. doi: 10.1038/nmeth.1923

Larsen, M. H., Kallipolitis, B. H., Christiansen, J. K., Olsen, J. E., and Ingmer, H. (2006). The response regulator ResD modulates virulence gene expression in response to carbohydrates in *Listeria monocytogenes*. *Mol. Microbiol.* 61, 1622–1635. doi: 10.1111/j.1365-2958.2006.05328.x

Mertins, S., Joseph, B., Goetz, M., Ecke, R., Seidel, G., Sprehe, M., et al. (2007). Interference of components of the phosphoenolpyruvate phosphotransferase system with the central virulence gene regulator PrfA of *Listeria monocytogenes*. *J. Bacteriol.* 189, 473–490. doi: 10.1128/JB.00972-06

Milenbachs, A. A., Brown, D. P., Moors, M., and Youngman, P. (1997). Carbon-source regulation of virulence gene expression in *Listeria monocytogenes*. *Mol. Microbiol.* 23, 1075–1085. doi: 10.1046/j.1365-2958.1997.2711634.x

Mollerup, M. S., Ross, J. A., Helfer, A. C., Meistrup, K., Romby, P., and Kallipolitis, B. H. (2016). Two novel members of the LhrC family of small RNAs in *Listeria monocytogenes* with overlapping regulatory functions but distinctive expression profiles. *RNA Biol.* 13, 895–915. doi: 10.1080/15476286.2016.1208332

Nielsen, J. S., Larsen, M. H., Lillebæk, E. M., Bergholz, T. M., Christiansen, M. H., Boor, K. J., et al. (2011). A small RNA controls expression of the chitinase ChiA in *Listeria monocytogenes*. *PLoS One* 6:e19019. doi: 10.1371/journal.pone.0019019

Nielsen, J. S., Lei, L. K., Ebersbach, T., Olsen, A. S., Klitgaard, J. K., Valentin-Hansen, P., et al. (2010). Defining a role for Hfq in gram-positive bacteria: evidence for Hfq-dependent antisense regulation in *Listeria monocytogenes*. *Nucleic Acids Res.* 38, 907–919. doi: 10.1093/nar/gkp1081

Petrone, G., Conte, M. P., Longhi, C., di Santo, S., Superti, F., Ammendolia, M. G., et al. (1998). Natural milk fatty acids affect survival and invasiveness of *listeria monocytogenes*. *Lett. Appl. Microbiol.* 27, 362–368. doi: 10.1046/j.1472-765X.1998.00441.x

Reniere, M. L., Whiteley, A. T., Hamilton, K. L., John, S. M., Lauer, P., Brennan, R. G., et al. (2015). Glutathione activates virulence gene expression of an intracellular pathogen. *Nature* 517, 170–173. doi: 10.1038/nature14029

Ripio, M. T., Brehm, K., Lara, M., Suarez, M., and Vázquez-Boland, J. A. (1997a). Glucose-1-phosphate utilization by *Listeria monocytogenes* is PrfA dependent and coordinately expressed with virulence factors. *J. Bacteriol.* 179, 7174–7180. doi: 10.1128/jb.179.22.7174-7180.1997

Ripio, M. T., Dominguez-Bernal, G., Lara, M., Suarez, M., and Vázquez-Boland, J. A. (1997b). A Gly145Ser substitution in the transcriptional activator PrfA causes constitutive overexpression of virulence factors in *listeria monocytogenes*. *J. Bacteriol.* 179, 1533–1540. doi: 10.1128/jb.179.5.1533-1540.1997

Schäferkordt, S., and Chakraborty, T. (1995). Vector plasmid for insertional mutagenesis and directional cloning in *Listeria* spp. *BioTechniques* 19, 720–725.

Schumacher, M. A., Allen, G. S., Diel, M., Seidel, G., Hillen, W., and Brennan, R. G. (2004). Structural basis for allosteric control of the transcription regulator CcpA by the phosphoprotein HPr-Ser46-P. *Cell* 118, 731–741. doi: 10.1016/j.cell.2004.08.027

Scortti, M., Monzó, H. J., Lacharme-Lora, L., Lewis, D. A., and Vázquez-Boland, J. A. (2007). The PrfA virulence regulon. *Microbes Infect.* 9, 1196–1207. doi: 10.1016/j.micinf.2007.05.007

Sternkopf Lillebæk, E. M., Lambert Nielsen, S., Scheel Thomasen, R., Færgeman, N. J., and Kallipolitis, B. H. (2017). Antimicrobial medium- and long-chain free fatty acids prevent PrfA-dependent activation of virulence genes in *Listeria monocytogenes*. *Res. Microbiol.* 168, 547–557. doi: 10.1016/j.resmic.2017.03.002

Temple, M. E., and Nahata, M. C. (2000). Treatment of listeriosis. *Ann. Pharmacother.* 34, 656–661. doi: 10.1345/aph.19315

Tiensuu, T., Guerreiro, D. N., Oliveira, A. H., O'Byrne, C., and Johansson, J. (2019). Flick of a switch: regulatory mechanisms allowing *Listeria monocytogenes* to transition from a saprophyte to a killer. *Microbiology* 165, 819–833. doi: 10.1099/mic.0.000808

Truong-Bolduc, Q. C., Villet, R. A., Estabrooks, Z. A., and Hooper, D. C. (2013). Native efflux pumps contribute resistance to antimicrobials of skin and the ability of *Staphylococcus aureus* to colonize skin. *J. Infect. Dis.* 209, 1485–1493. doi: 10.1093/infdis/jit660

Xayarath, B., and Freitag, N. E. (2012). Optimizing the balance between host and environmental survival skills: lessons learned from *Listeria monocytogenes*. *Future Microbiol.* 7, 839–852. doi: 10.2217/fmb.12.57

Conflict of Interest: The authors declare that the research was conducted in the absence of any commercial or financial relationships that could be construed as a potential conflict of interest.

Publisher's Note: All claims expressed in this article are solely those of the authors and do not necessarily represent those of their affiliated organizations, or those of the publisher, the editors and the reviewers. Any product that may

be evaluated in this article, or claim that may be made by its manufacturer, is not guaranteed or endorsed by the publisher.

frontiers | Frontiers in Microbiology

ORIGINAL RESEARCH
published: 12 May 2022
doi: 10.3389/fmicb.2022.897682

Absence of N-Acetylglucosamine Glycosylation on *Listeria monocytogenes* Wall Teichoic Acids Promotes Fatty Acid Tolerance by Repulsion From the Bacterial Surface

*Rikke S. S. Thomasen[1], Patricia T. dos Santos[1,2], Eva M. Sternkopf Lillebæk[1], Marianne N. Skov[3], Michael Kemp[3,4] and Birgitte H. Kallipolitis[1]**

[1]Department of Biochemistry and Molecular Biology, University of Southern Denmark, Odense, Denmark, [2]National Food Institute, Technical University of Denmark, Kgs. Lyngby, Denmark, [3]Department of Clinical Microbiology, Odense University Hospital and Research Unit of Clinical Microbiology, University of Southern Denmark, Odense, Denmark, [4]The Regional Department of Clinical Microbiology, Zealand University Hospital, Koege, Denmark

OPEN ACCESS

Edited by:
Shihua Wang,
Fujian Agriculture and Forestry University, China

Reviewed by:
Thomas Denes,
The University of Tennessee, Knoxville, United States
Filipe Carvalho,
INRAE Centre Jouy-en-Josas, France

***Correspondence:**
Birgitte H. Kallipolitis
bhk@bmb.sdu.dk

Specialty section:
This article was submitted to Infectious Agents and Disease, a section of the journal Frontiers in Microbiology

Received: 16 March 2022
Accepted: 27 April 2022
Published: 12 May 2022

Citation:
Thomasen RSS, dos Santos PT, Sternkopf Lillebæk EM, Skov MN, Kemp M and Kallipolitis BH (2022) Absence of N-Acetylglucosamine Glycosylation on Listeria monocytogenes Wall Teichoic Acids Promotes Fatty Acid Tolerance by Repulsion From the Bacterial Surface. Front. Microbiol. 13:897682. doi: 10.3389/fmicb.2022.897682

Free fatty acids (FFAs) have strong antimicrobial properties against pathogenic bacteria and are known as natural protective agents against bacterial infections. Growth of the foodborne pathogen *Listeria monocytogenes* is highly affected by the presence of antimicrobial FFAs, however, the response of *L. monocytogenes* toward FFAs is not fully understood. Here, we explore how *L. monocytogenes* gains tolerance toward FFAs and present a novel mechanism conferring bacterial protection against FFA toxicity. Strains tolerant against the antimicrobial FFA palmitoleic acid were isolated and whole genome sequenced, and mutations were found in genes involved in wall teichoic acid (WTA) glycosylations. We show that mutation or deletion of *lmo1079*, which is essential for N-acetylglucosamine (GlcNAc) glycosylation of WTAs, confer tolerance against several antimicrobial FFAs. The FFA tolerant strains are lacking GlcNAc on their WTAs, which result in a more hydrophilic surface. In line with this, we observed a reduced binding of FFAs to the surface of the FFA tolerant strains. Additionally, lack of GlcNAc on WTAs confers tolerance toward acid stress. Altogether, these findings support that GlcNAc modification of WTA plays an important role in the response of *L. monocytogenes* toward stress conditions encountered during growth as a saprophyte and pathogen, including FFA-rich environments. Most importantly, our data revealed that *L. monocytogenes* strains lacking GlcNAc on their WTAs are protected against FFA toxicity, because the FFAs are repulsed from the bacterial surface of GlcNAc-deficient strains.

Keywords: *Listeria monocytogenes*, wall teichoic acid, antimicrobial fatty acids, anti-virulence activity, N-acetylglucosamine glycosylation

INTRODUCTION

Production of free fatty acids (FFAs) are known as a natural protection strategy against bacterial infections in humans, animals, and plants (Kengmo Tchoupa et al., 2021). In humans, FFAs are present in multiple areas, such as the skin and the gastrointestinal tract, where their antimicrobial properties protect the host against bacterial infections (Chatterjee et al., 2007; Kohler et al., 2009). Although FFAs are known to inhibit bacterial growth, the mechanism underlying their antimicrobial activity is not fully understood. In general, FFAs are thought to interfere with biological processes in the membrane, causing reduced nutrient uptake, cell lysis, leakage of cell metabolites, or disruption of the electron transport chain (Desbois and Smith, 2010). To cope with antimicrobial FFAs in FFA-rich environments, bacteria have evolved various strategies to avoid FFA toxicity (Kengmo Tchoupa et al., 2021). Those strategies primarily involve repulsion of FFAs from the bacterial surface, detoxification of the FFAs, or efflux of FFAs from the cytosol to the extracellular environment (Kengmo Tchoupa et al., 2021). For some pathogens, the presence of wall teichoic acids (WTAs) on the bacterial surface is essential to retain tolerance toward FFAs, e.g., those found on the skin (Kohler et al., 2009). Additionally, some bacteria can induce the expression of specific surface proteins in stressful environments, which then decrease surface hydrophobicity and cause repulsion of the FFAs (Clarke et al., 2007). By using such mechanisms, bacteria manage to protect themselves against FFAs in the environment.

Listeria monocytogenes is a facultative intracellular pathogen causing life-threatening foodborne diseases in susceptible individuals. During growth as a saprophyte and pathogen, *L. monocytogenes* is exposed to FFAs in various environments, including food products such as salmon and milk, and in the gastrointestinal tract of a host (Petrone et al., 1998; Chatterjee et al., 2007; Cascant et al., 2018). Upon ingestion of contaminated food, *L. monocytogenes* adapts to the gastrointestinal conditions and initiates internalization into intestinal epithelial cells through the surface protein Internalin A (InlA). When inside the phagosome, the bacterium gains access to the cytoplasm of the host cell by secretion of the pore forming virulence factor Listeriolysin O (LLO). *Listeria monocytogenes* then proliferates inside the cytosol and spreads to neighboring host cells using an actin comet tail generated by the help of Actin assembly-inducing protein (ActA; Freitag et al., 2009). The expression of virulence factors required for *L. monocytogenes*' intracellular lifestyle is controlled by the virulence regulator PrfA (Scortti et al., 2007). We recently discovered that at low doses, specific FFAs act to repress transcription of PrfA-dependent virulence genes by inhibiting the DNA-binding activity of PrfA (Sternkopf Lillebæk et al., 2017; Dos Santos et al., 2020). At high doses, some FFAs act to prevent the growth of *L. monocytogenes*, but the response of this pathogen to the antimicrobial activity of FFAs is presently unclear.

In this study, we aimed to explore how *L. monocytogenes* responds to and copes with the antimicrobial activity of FFAs. More specifically, we studied the molecular mechanism underlying the response of *L. monocytogenes* to the antimicrobial monounsaturated FFA palmitoleic acid (PA, C16:1). PA is found in different oils from both macadamia nuts and sea buckthorn and was chosen for this study because it has a dual effect on *L. monocytogenes*: at high doses, PA acts to inhibit growth of *L. monocytogenes*, whereas at low doses, PA inhibits the activity of a PrfA mutant variant, PrfA*, that is known to be locked in a constitutively active conformation (Sternkopf Lillebæk et al., 2017; Dos Santos et al., 2020). Curiously, a mutant variant deleted for *prfA* is tolerant to PA, suggesting that PrfA also plays a role in the response to the antimicrobial activity of PA. To improve our understanding of how *L. monocytogenes* reacts to FFAs, we isolated mutant strains that are tolerant toward the antimicrobial activity of PA. Interestingly, when the PA tolerant strains were whole genome sequenced, we found a nonsense mutation in *lmo1079* in four out of six PA tolerant mutants. The *lmo1079* gene encodes for an YfhO homolog, which is essential for the N-acetylglucosamine (GlcNAc) glycosylation of the WTAs (Rismondo et al., 2018). Notably, the *L. monocytogenes* strain used in this work belongs to serotype 1/2a, which contains two substitutions on their WTAs: GlcNAc and rhamnose (Rha; Kamisango et al., 1983). Here, we present our investigations on how the lack of GlcNAc glycosylation of WTAs contributes to FFA tolerance in *L. monocytogenes*.

MATERIALS AND METHODS

Bacterial Strains and Growth Conditions

The wild-type *Listeria monocytogenes* EGD 1/2a strain (obtained from W. Goebel, University of Wurzburg, Wurzburg, Germany) was used in the study, together with its two isogenic derivates Δ*prfA* (Böckmann et al., 1996) and *prfA** (expressing a constitutive active PrfA mutant, G155S; Sternkopf Lillebæk et al., 2017). For construction of *lmo1079*-sub1, *lmo1079*-sub2, *lmo1083*-sub, and in-frame deletion mutants Δ*lmo1079* and Δ*lmo1083*, the corresponding primers (P1, P2, P3, and P4) were used (**Supplementary Table S1**). The fragments were amplified using a two-step PCR procedure and inserted into the temperature sensitive shuttle vector pAUL-A (Schäferkordt and Chakraborty, 1995). For *lmo1079*-sub1 complementation mutants (*lmo1079*-sub1::*lmo1079*-sub1-c and *lmo1079*-sub1-*lmo1083*-sub::*lmo1079*-sub1-c), P1 and P4 for *lmo1079*-sub1 were used for PCR amplification followed by integration into pAUL-A. The resulting pAUL-A plasmid constructs were transformed into competent *L. monocytogenes* as previously described by (Mollerup et al., 2016). Integration and disintegration of the plasmids into the bacterial genome occurred based on homolog recombination as described in (Christiansen et al., 2004). The double mutant, *lmo1079*-sub1-*lmo1083*-sub, was constructed in a two-step process, where the mutations were introduced into the bacterial genome consecutively. The resulting mutants were validated by PCR and sequencing using primers P5 and P6 flanking the mutated regions (**Supplementary Table S1**). p*hly-lacZ*, containing the promotor region of *hly* transcriptionally fused to *lacZ*, and p*lhrA36-lacZ*, containing the promotor region of the *lhrA* core promotor transcriptionally fused to *lacZ*, were previously constructed (Larsen

et al., 2006; Nielsen et al., 2011). *Listeria monocytogenes* was routinely grown at 37°C with aeration in Brain Heart Infusion medium (BHI, Oxoid) and supplemented with 50 μg/ml kanamycin (Kan) or 5 μg/ml erythromycin (Erm) when appropriate. During cloning in pAULA, *Escherichia coli* TOP10 (Invitrogen) was used and grown at 37°C with aeration in Luria Bertani broth (LB, Sigma-Aldrich) supplemented with 150 μg/ml Erm.

Free Fatty Acids

The following FFAs were included in this study: palmitoleic acid (PA; C16:1; Sigma-Aldrich, purity ≥98.5%), palmitic acid (PAL; C16:0; Sigma-Aldrich, purity ≥99%), lauric acid (LA; C12:0; Sigma-Aldrich, purity ≥98%), and eicosapentaenoic acid (EPA, C20:5; Sigma-Aldrich, purity ≥99%). Ninety-six percent ethanol was used as vehicle to dissolve the FFAs.

Promotion of PA Tolerant Strains

Overnight (ON) cultures of *prfA** were diluted to OD_{600} = 0.0002 in BHI and stressed with increasing concentrations of PA (2, 4, 8, 16, 32, 64, and 125 μg/ml) for 7 days. The concentration of vehicle was kept constant at 0.25% during the selection process. Glycerol stocks were made at 125 μg/ml PA, and a total of six single mutants were isolated from three biological replicates for further studies.

Growth Experiment With FFAs

Overnight (ON) cultures were diluted to OD_{600} = 0.0002; 4 ml of the diluted cultures were transferred to culture tubes and stressed with increasing concentrations of FFAs. As controls, one culture was left untreated, and another only exposed to the vehicle. Cultures were incubated for 20 h, followed by OD_{600} measurements.

Growth Experiments in 96-Well Plates

Overnight (ON) cultures were diluted to OD_{600} = 0.2 and 5 μl of the diluted cultures were added to their corresponding wells in the TC 96-well plate (standard, F, SARSTEDT). A final volume of 200 μl was obtained in each well by adding 195 μl BHI ± stress agents to the corresponding wells. An initial OD_{600} of 0.005 was thereby obtained. The 96-well plate was incubated in the plate reader (Synergy™ H1 multi-mode microplate reader, BioTek) for 24 h at 37°C with orbital shaking for 15 s every 30 min.

β-Galactosidase Assay

ON cultures of the strains containing either p*hly-lacZ* or p*lhrA36-lacZ* were diluted to OD_{600} = 0.02. At OD_{600} = 0.3 the cultures were split and treated with either 2 μg/ml PA or 150 μg/ml PAL. As controls, a culture was left untreated, or treated with only vehicle corresponding to the final concentration of vehicle in FFA treated samples. After 20 h of growth OD_{600} was measured and 1 ml samples were harvested. The β-galactosidase assay was performed as previously described (Christiansen et al., 2004).

Cell Harvest, RNA Extraction, and Northern Blot Analysis

Overnight (ON) cultures of *prfA**, PA-1A, PA-2A and PA-3A were diluted to OD_{600} = 0.02 and incubated. At OD_{600} = 0.3 the cultures were split and treated with either vehicle or 2 μg/ml PA for 1 h. Next, cultures were snap cooled in liquid nitrogen followed by centrifugation at 8,000 rpm for 3 min at 4°C. The supernatant was removed, and pellet was snap cooled in liquid nitrogen before samples were stored at −80°C. Total RNA was extracted using Tri reagent (Molecular Research Center, Inc.), as previously reported (Nielsen et al., 2010). RNA purity and concentration were determined by agarose gel electrophoresis and DeNovix DS-11 Fx, respectively. Agarose northern blot analysis was performed as early described (Dos Santos et al., 2020). Membranes were hybridized with ^{32}P-labeled single stranded probes (**Supplementary Table S1**). Visualization of bands was done using Typhoon FLA9000 (GE Healthcare).

Whole Genome Sequencing

Sequencing libraries were prepared for *prfA**, PA-1A, PA-1B, PA-2A, PA-2B, PA-3A and PA-3B using Nextera XT DNA kit. Libraries were sequenced using Illumina Miseq platform in pair-end mode, read length of 150 bp. Quality of the reads was checked using FastQC version 0.11.8, standard settings. Reads were mapped to the reference genome of *L. monocytogenes* EGD-e (ASM19603v1, NCBI) using Breseq version 0.33.0 pipeline, standard settings (Deatherage and Barrick, 2014). SNPs were found using gdtools, and Single nucleotide polymorphisms (SNPs) present in both read directions for the isolates are listed in **Table 1**.

Fluorescent Microscopy With Wheat Germ Agglutinin, Alexa Fluor™ 594 Conjugate

One milliliter of ON culture was centrifuged at 3,500 rpm for 3 min, and the supernatant was removed and resuspended in 100 μl 1x PBST (1x PBS + 0.1% Tween 20; Sigma-Aldrich). The resuspended cells were incubated for 5 min at room temperature (RT) in darkness with 50 μl 0.1 mg/ml Wheat Germ Agglutinin, Alexa Fluor™ 594 Conjugate (Invitrogen; resuspended in 1x PBS). The samples were centrifuged again and washed two times in 500 μl 1x PBST. The bacteria were resuspended in 1x PBST and spotted on poly-lysin [poly-lysin solution 0.1% (w/v); Sigma-Aldrich] coated microscopy slides. Bacteria were visualized by phase contrast (PH) and Texas-Red using an inverted fluorescence Olympus IX83 microscope. Images were analyzed using FIJI ImageJ (Schindelin et al., 2012).

Hydrophobicity Assay

Overnight (ON) cultures (5 ml) were centrifuged for 5 min at 4,000 rpm, the supernatant was removed, and pellet was washed three times in 5 ml 1x PBS. Pellet was resuspended in 1x PBS and diluted to OD_{600} = 0.3 (OD_{600}_1). Three milliiliter of the diluted cultures was transferred to culture tubes and 300 μl n-hexadecane (Sigma-Aldrich) was added. Samples were vortexed for 2 min followed by incubation for 15 min at RT for phase separation. OD_{600} was measured again for the water phase (OD_{600}_2), and the percentage of cells staying in the hydrophilic

TABLE 1 | Mutations found in PA tolerant strains based on whole genome sequencing.

PA tolerant strain	Location	Gene	Codon	Mutation	Mutation ID	Description
PA-1A PA-1B	1,111,021	*lmo1079*	85	Q➔STOP (CAA➔TAA)	*lmo1079*-sub1	A nonsense mutation, which results in the introduction of a STOP codon at codon 85 in *lmo1079*.
PA-2A PA-2B	1,113,036	*lmo1079*	756	Y➔STOP (TAC➔TAA)	*lmo1079*-sub2	A nonsense mutation, which results in the introduction of a STOP codon at codon 756 in *lmo1079*.
PA-1A PA-1B	1,117,421	*lmo1083*	110	Δ1 bp (AAT➔ATG)	*lmo1083*-sub	A 1 bp deletion, which results in a frameshift mutation in *lmo1083*. The frameshift introduces a STOP codon at codon 115.
PA-3A PA-3B	1,928,124	*lmo1851*	101	G➔D (GGT➔GAT)	*lmo1851*-sub	A missense mutation, which results in amino acid substitution of codon 101, from glycine to aspartic acid, in *lmo1851*.

phase was calculated by OD_{600}_2/OD_{600}_1 x 100%. Data were analyzed by one-way ANOVA with Bonferroni's multiple-comparison test. Only differences with at least 95% CI were reported as statistically significant.

Membrane Potential

Membrane potential was measured using BacLight Bacterial Membrane Potential Kit (Invitrogen). ON cultures were diluted to $OD_{600} = 0.003$ in 1 x PBS and split into falcon tubes (1 ml in each). Ten microliter of a proton ionophore carbonyl cyanide 3-chlorophenylhydrazone (CCCP) 500 μM was added to the depolarization control and incubated for 5 min. Ten microliter of the fluorescent membrane-potential indicator dye 3,3′-diethyloxacarbocyanine iodide ($DiOC_2$) was then added to the samples and the samples were incubated in darkness for 15–30 min followed by fluorescence-activated cell sorting using FACSAria II. One hundred thousand events were measured for each sample.

BODIPY-C12 Binding Assay

Overnight (ON) cultures (5 ml) were centrifuged at 3,500 rpm for 5 min. The supernatant was removed, and pellet was washed twice in 5 ml 1x PBS. After the washing step, bacteria were resuspended in 1x PBS and OD_{600} was measured. Samples were diluted in 1x PBS to $OD_{600} = 0.3$. Each sample was split into two falcon tubes (1 ml in each), one was incubated with 5 μl of vehicle (nonfluorescent) and the other with 5 μl of 0.5 mg/ml BODIPY™ 558/568 C_{12} (Invitrogen; diluted in 96% ethanol) for 5 min at 4°C. The fluorescence of the samples was measured using FACSAria II, with the following parameters: 100,000 events per sample, neutral density filter size 0.5 and a flow rate of 1. The mean background fluorescence of each sample (vehicle) was subtracted from the mean fluorescence of the BODIPY treated samples, before ratios were calculated. Data were analyzed by one-way ANOVA with Bonferroni's multiple-comparison test. Only differences with at least 95% CI were reported as statistically significant.

RESULTS

Selection of PA Tolerant Mutants

FFA tolerant strains were isolated in a *prfA** background to allow further investigation of whether the mutations obtained confer tolerance toward the antimicrobial activity as well as the PrfA-inhibitory effect of PA (Sternkopf Lillebæk et al., 2017; Dos Santos et al., 2020). To select for PA tolerance, the *prfA** strain was diluted in BHI and incubated overnight (ON) with PA; the concentration of PA was increased by 2-fold each day. A total of six PA tolerant candidates were isolated from three independent cultures after growth in BHI with 125 μg/ml PA. To investigate their PA tolerance, the six isolates were cultured ON with increasing concentrations of PA (**Figure 1A**). As controls, the parental strain (*prfA**) and a PrfA-deficient strain (Δ*prfA*) were included; Δ*prfA* is known to exert increased tolerance toward FFAs (Sternkopf Lillebæk et al., 2017; Dos Santos et al., 2020). As shown in **Figure 1A**, growth of *prfA** was restricted at 25 μg/ml of PA, whereas growth of the six isolates and Δ*prfA* was prevented at 125 μg/ml of PA, demonstrating that the isolated strains are 5-fold more tolerant against PA compared to the parental strain. Additionally, growth in presence of PA's saturated counter partner, the non-antimicrobial FFA palmitic acid (PAL, C16:0), was evaluated (**Figure 1A**). This growth experiment revealed that all six isolates, as well as the two control strains, could grow in presence of PAL. Altogether, the six isolated strains exhibit tolerance toward PA, whereas their growth is unaffected by PAL.

PA Tolerant Strains Are Still Sensitive Toward the PrfA Inhibitory Effect of FFAs

Since PA is also known to inhibit the activity of PrfA (Sternkopf Lillebæk et al., 2017), we performed a β-galactosidase assay to investigate if the six PA tolerant strains had become insensitive toward the PrfA inhibitory effect of FFAs. The six strains were transformed with the p*hly-lacZ* fusion plasmid, which contains the PrfA-dependent promotor region of *hly* fused to *lacZ*. The *prfA** and Δ*prfA* strains were again included as controls. The resulting eight strains were grown to mid-exponential phase; then, the cultures were split and treated with sub-inhibitory levels of PA or PAL. Untreated and vehicle treated cultures were included as controls. After 20 h of growth, cells were harvested; the results from the β-galactosidase assay are presented in **Figure 1B**. Except for Δ*prfA*, the β-galactosidase activity ranged from 80 to 300 units for all strains tested during regular growth and after exposure to the vehicle or the non-inhibitory FFA PAL. These results demonstrate that all six PA tolerant

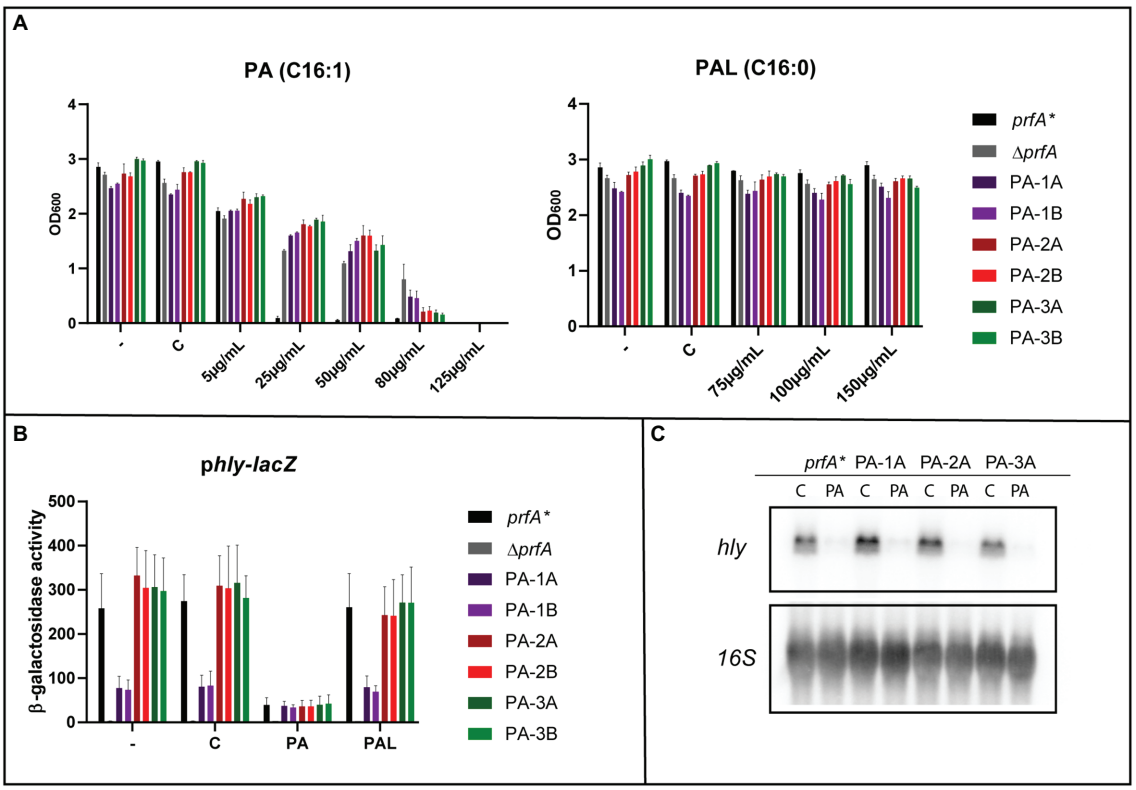

FIGURE 1 | The response of selected palmitoleic acid (PA) tolerant isolates toward free fatty acid (FFA) exposure. **(A)** Growth of *prfA**, Δ*prfA* and the six selected PA tolerant strains upon exposure to different concentrations of PA or palmitic acid (PAL). As controls, cultures were left untreated (–) or exposed to vehicle (C). OD_{600} values were measured after 20 h of growth. Results are the average of three independent experiments. **(B)** Expression of the PrfA-dependent virulence gene *hly* upon exposure to PA or PAL. The promotor region of *hly* cloned into the reporter plasmid pTCV-*lacZ* was transformed into *prfA**, Δ*prfA* and the six selected PA mutants. The resulting strains were grown to OD_{600} = 0.3 and exposed to 2 µg/ml PA or 150 µg/ml PAL. As controls cells were left untreated (–) or incubated with a concentration of vehicle (C) corresponding to the one used for FFA conditions. Samples were harvested after 20 h and used for β-galactosidase assays. Results are the average of three independent experiments, each performed in technical duplicates. **(C)** Northern blot analysis of *hly* mRNA levels upon exposure to PA. The *prfA** strain and three selected PA mutants were grown to OD_{600} = 0.3 and exposed to 2 µg/ml PA or as control a corresponding concentration of vehicle (C). Cells were harvested after 1 h. Northern blots were probed for *hly* mRNA and 16S rRNA (loading control). The experiment was performed in three biological replicates.

mutants encode a functional PrfA protein. Upon exposure to sub-inhibitory levels of PA, the β-galactosidase activity was remarkably reduced for *prfA** and the six isolated mutants. These data show that the PA tolerant isolates are still sensitive toward the PrfA inhibitory activity of PA. Notably, high levels of β-galactosidase activity were observed for all strains containing the PrfA independent p*lhrA36-lacZ* fusion plasmid under all growth conditions tested (**Supplementary Figure S1**).

In addition to the β-galactosidase assays, northern blotting was performed to evaluate the effect of PA on the expression of *hly*. Three PA tolerant strains and *prfA** were grown to mid-exponential phase and exposed to a sub-inhibitory level of PA for 1 h. Results from the northern blot are shown in **Figure 1C**. The mRNA level of *hly* was strongly reduced in all four strains upon exposure to PA, indicating that PA acts to inhibit PrfA dependent virulence gene expression in the PA tolerant strains. When comparing the results of the β-galactosidase assay and the northern blot analysis under control conditions, we note that *hly-lacZ* expression in isolates PA-1A and PA-1B is lower relative to the other strains, whereas *hly* mRNA levels are comparable for all strains tested (**Figures 1B,C**). Most likely, these isolates are slightly more resistant to the conditions used for cell lysis in β-galactosidase assays versus northern blotting. In line with this, the PA dependent increase in *lhrA36-lacZ* expression could be due to an increased susceptibility of PA-1A/1B to cell lysis after PA exposure (**Supplementary Figure S1**).

Altogether, the results from the β-galactosidase assay and the northern blot experiment confirm that any kind of mutations, which might have occurred in the PA tolerant strains, are only relevant to studies of the antimicrobial activity of FFAs.

GlcNAc Glycosylation on the WTAs Contributes to PA Sensitivity in *Listeria monocytogenes*

To reveal the type of mutations that led to PA tolerance, the six isolates and the parental strain *prfA** were whole genome sequenced (WGS). As shown in **Tables 1**, a total of four mutations were found in the PA tolerant strains. Isolates from

the first biological replicate carry two mutations: a frameshift mutation in *lmo1083* and a nonsense mutation in *lmo1079*. The two isolates from the second biological replicate carry a nonsense mutation in *lmo1079* as well, whereas isolates from the third biological replicate carry a missense mutation in *lmo1851*. The latter gene (*lmo1851*) encodes for a carboxyl-terminal protease, whereas both *lmo1079* and *lmo1083* encode enzymes involved in modification of WTAs in *L. monocytogenes* serovar 1/2a. More specifically, *lmo1079* encodes an YfhO homolog that is essential for the GlcNAc glycosylation of WTAs (Rismondo et al., 2018), whereas *lmo1083* (*rmlB*) is a part of the *rmlACBD* locus encoding the RmlABCD proteins that are essential for rhamnosylation of WTAs (Carvalho et al., 2015). We assume that the two different nonsense mutations found in *lmo1079* will result in truncated Lmo1079 protein variants, due to premature termination of translation. The frameshift mutation found in *lmo1083* leads to the formation of a STOP codon at codon 115 out of 329, which is expected to cause loss of function and result in lack of rhamnosylation, as seen for similar mutations studied previously (Denes et al., 2015; Eugster et al., 2015) Since three of the four detected mutations are present in genes encoding for WTA glycosylation enzymes, we decided to focus on the role of *lmo1079* and *lmo1083* in the response toward antimicrobial FFAs.

To investigate if mutations in *lmo1079* and *lmo1083* contribute to PA tolerance, the three single mutations *lmo1079* [Q85 (STOP)), *lmo1079* (Y756 (STOP)] and *lmo1083* (position 329 nt, Δ1 bp), from now on referred to as *lmo1079*-sub1, *lmo1079*-sub2 and *lmo1083*-sub, respectively, were introduced into the wild-type strain. Additionally, we constructed a double mutant harboring both *lmo1079*-sub1 and *lmo1083*-sub. Furthermore, since all three mutations are expected to affect the functionality of the resulting proteins, deletion mutants for *lmo1079* and *lmo1083* were constructed as controls. Initially, the mutants and wild-type were cultured in BHI medium (**Supplementary Figure S2**), which showed that none of the mutations affect bacterial growth. To examine if the mutations lead to PA tolerance, growth was studied upon exposure to increasing concentrations of PA (**Figure 2A**). Growth of the wild-type, *lmo1083*-sub and Δ*lmo1083* mutant strains was prevented at 15 μg/ml PA, whereas growth of the *lmo1079* mutants was restricted at higher concentrations of PA (50 or 80 μg/ml). Thus, mutations in *lmo1079* confer tolerance toward PA by 3–5-fold compared to the wild-type strain. To confirm that the *lmo1079* mutations are causing PA tolerance, growth experiments with increasing concentrations of PA were performed for complementation mutants as well (**Supplementary Figure S3A**). The *lmo1079*-sub1 mutation was complemented on the chromosome of the single and double mutant, referred to as *lmo1079*-sub1::*lmo1079*-c and *lmo1079*-sub1-*lmo1083*-sub::*lmo1079*-c, respectively. In both cases, complementation of the *lmo1079*-sub1 mutation restores the phenotype back to wild-type, which confirms that mutation of *lmo1079* confers PA tolerance.

To address if the PA tolerance can be linked to GlcNAc glycosylation of WTAs, we studied the presence of GlcNAc on the WTAs of wild-type and various *lmo1079* and *lmo1083* mutant strains, using fluorescence microscopy to detect fluorescently labeled Wheat Germ Agglutinin (WGA) selective for GlcNAc (**Figure 2B**). Wild-type and *lmo1083* single mutants fluoresce, confirming that they have GlcNAc expressed on the WTAs, whereas no signal was seen for all *lmo1079* mutants tested. Based on these observations, we conclude that the mutants, which had acquired tolerance toward PA, are lacking the GlcNAc glycosylation on their WTAs.

Lack of GlcNAc on WTAs Induces Tolerance Toward Multiple Antimicrobial FFAs

Since multiple FFAs have shown antimicrobial properties against *L. monocytogenes* (Sternkopf Lillebæk et al., 2017; Dos Santos et al., 2020), we wanted to study if the absence of GlcNAc on WTAs results in increased tolerance toward other antimicrobial FFAs than PA. Strains were grown in increasing concentrations of the long-chain polyunsaturated FFA eicosapentaenoic acid (EPA, C20:5) and the medium-chain saturated FFA lauric acid (LA, C12:0). The results from the growth experiments are presented in **Figure 3A**. In presence of EPA, *lmo1079* mutants show increased tolerance compared to the wild-type and *lmo1083* mutants. The *lmo1079* mutants are, however, still quite sensitive toward the presence of EPA. For LA, the same tendency is observed as for PA in **Figure 2A**, since the growth of EGD and *lmo1083* mutants is inhibited at 80 μg/ml of LA, while all *lmo1079* mutants are still capable of growing at 160 μg/ml of LA. Lack of GlcNAc clearly induces tolerance toward LA and, to a lesser extent, EPA. Based on these findings, we conclude that if GlcNAc is absent on the WTAs, *L. monocytogenes* becomes more tolerant toward different types of antimicrobial FFAs.

Changes in WTA Glycosylation Result in a More Hydrophilic Bacterial Surface

In *Staphylococcus aureus*, it is known that WTAs are important for maintaining tolerance toward antimicrobial FFAs. More specifically, in the absence of WTAs the bacterial surface becomes more hydrophobic and increases the sensitivity of *S. aureus* toward antimicrobial FFAs (Kohler et al., 2009). Our data show that lack of the GlcNAc glycosylation on WTAs in *L. monocytogenes* causes FFA tolerance. Therefore, we investigated if changes in WTA decorations affect the hydrophobicity of the bacterial surface in *L. monocytogenes* by studying the microbial adhesion to *n*-hexadecane using the hydrocarbon test (Rosenberg et al., 1980; Kohler et al., 2009). The percentage of bacteria that stayed in the hydrophilic phase is presented in **Figure 3B**. For all *lmo1079* mutants, a higher percentage of the cells stayed in the hydrophilic phase, relative to the wild-type, whereas *lmo1083* mutants were only slightly (*lmo1083*-sub) or not significantly different (Δ*lmo1083*) from wild-type. The increased FFA tolerance, which was observed for the *lmo1079* mutants, thereby correlates with a more hydrophilic surface. Furthermore, by complementing *lmo1079*-sub1 the hydrophobicity of the bacterial surface was restored to the level of the parental strain (**Supplementary Figure S3B**). Finally, we examined if *lmo1079*-sub1 and/or *lmo1083*-sub affect the membrane potential of *L. monocytogenes* compared to the

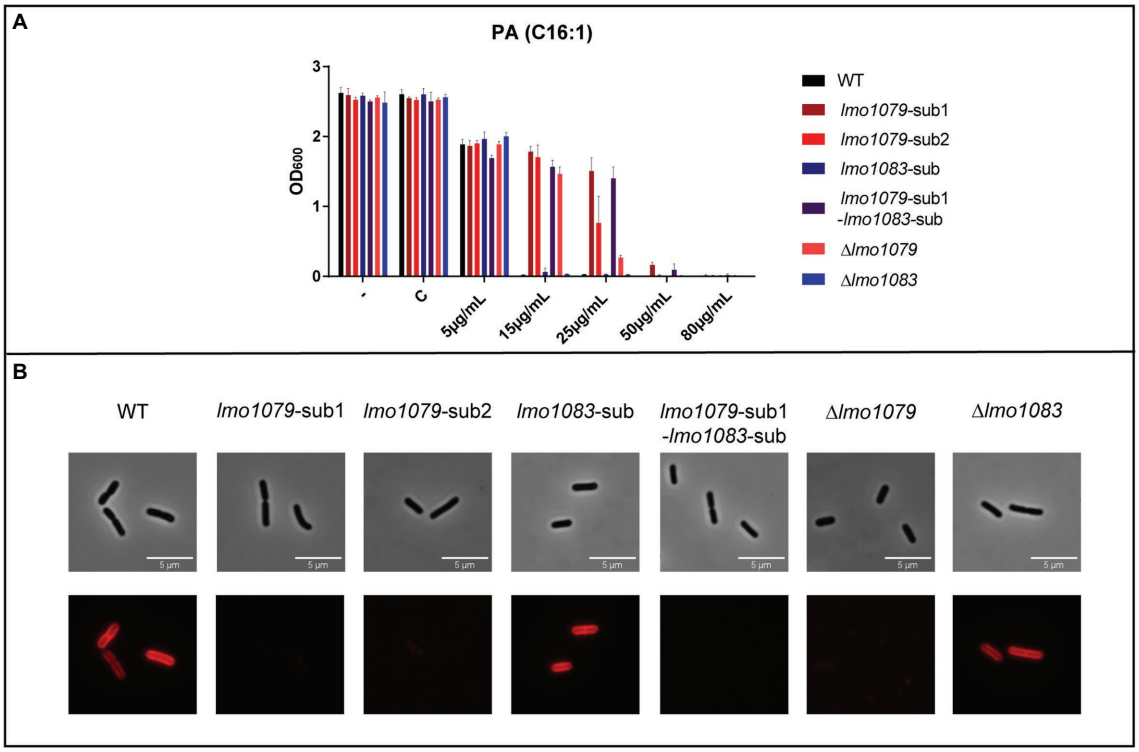

FIGURE 2 | The impact of *lmo1079* and *lmo1083* mutations on PA tolerance and GlcNAc glycosylation of wall teichoic acid (WTA). **(A)** Growth of wild-type and *lmo1079* and *lmo1083* mutant strains upon PA exposure. Strains were diluted to $OD_{600} = 0.0002$ and exposed to various concentrations of PA. As controls cultures were left untreated (–) or exposed to the vehicle (C). Results are the average of three independent experiments. **(B)** Detection of GlcNAc on WTAs. Wild-type, *lmo1079* and *lmo1083* mutant cells were harvested and resuspended in 1x PBST. Alexa Fluor™ 594 conjugated WGA was added to a final concentration of 33 µg/ml. Samples were washed and resuspended in 1 x PBST and cells were visualized on poly-lysin coated slides by fluorescence microscopy. The experiment was performed in triplicates; one representative example is shown.

parental strain. The results obtained confirmed that none of the mutations had a detectable effect on the membrane potential (**Supplementary Figure S4**). Based on these observations, we conclude that lack of GlcNAc entails a more hydrophilic bacterial surface in *L. monocytogenes* resulting in an increased tolerance to FFA.

Antimicrobial FFAs Are Repulsed From the Surface of *Listeria monocytogenes* in Absence of GlcNAc on the WTAs

Since *lmo1079* mutants have a more hydrophilic surface, it could be speculated that FFAs are repulsed from the cell surface when GlcNAc is lacking. This hypothesis was tested by measuring the interaction between fluorescent-labeled LA (BODIPY FFA C12) and the bacterial surface by fluorescence-activated cell sorting (FACS). The mean fluorescence of single and double mutants relative to the parental strain is presented in **Figure 3C**. The mean fluorescence of the *lmo1083* single mutant is comparable to the parental strain, indicating that the FFA interacts with the bacterial surface to the same extent regardless of the mutation in the rhamnosylation gene. However, a significant decrease in the mean fluorescence was observed when *lmo1079* is mutated, showing that the FFA cannot efficiently interact with the bacterial surface, when GlcNAc modification of WTA is absent. FFAs are therefore most likely repulsed from the bacterial surface when GlcNAc is missing on the WTAs of *L. monocytogenes*.

GlcNAc Modification of WTA Mediates Sensitivity Toward Acid Stress

WTA decorations have previously been shown to be essential for *L. monocytogenes*' ability to invade host cells (Sumrall et al., 2020), anchoring membrane proteins (Sumrall et al., 2020) and maintaining resistance toward antimicrobial peptides and sensitivity toward antibiotics (Carvalho et al., 2015; Meireles et al., 2020). Therefore, we examined if the PA tolerant mutants were affected in their tolerance toward other environmental stress conditions, which *L. monocytogenes* may encounter upon disinfection, host infection, food production and preservation. The *lmo1079* and *lmo1083* mutants were, together with the parental strain, grown in 96-well plates under different stress conditions, e.g., salt, ethanol, and acid. The results from the growth experiments are presented in **Figure 4**. All strains grew equally well in BHI medium. In the presence of salt or ethanol, growth of the double mutant was slightly impaired relative to the single mutants and wild-type. Upon exposure to acidic conditions, a clear growth phenotype was observed for the *lmo1079* mutants; they were all able to grow at pH = 5, whereas

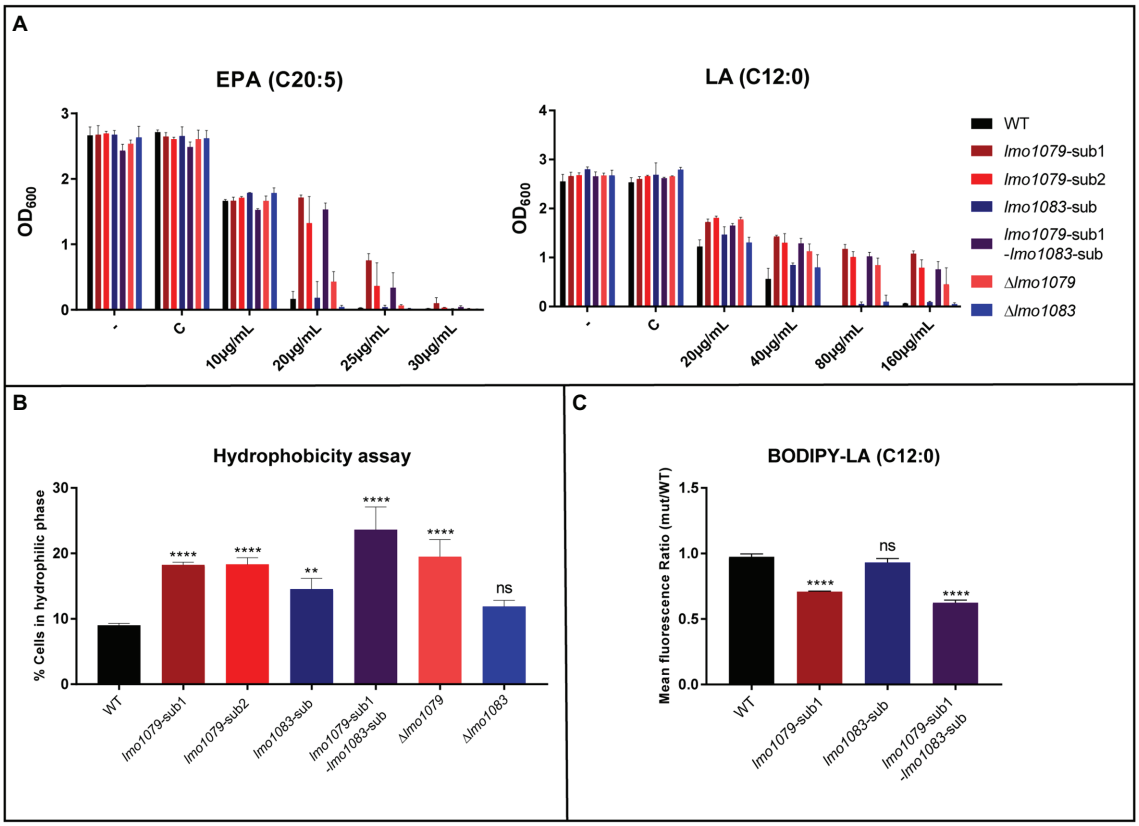

FIGURE 3 | The role of WTA modifications in FFA tolerance. **(A)** Wild-type, *lmo1079* and *lmo1083* mutant strains were diluted to $OD_{600} = 0.0002$ and exposed to different concentrations of eicosapentaenoic acid (EPA) or LA. As controls, cultures were left untreated (–) or exposed to the vehicle (C). Growth was measured after 20 h. Results are the average of three independent experiments. **(B)** Hydrophobicity of the bacterial surface. Bacteria from overnight (ON) cultures were harvested and washed in 1x PBS. Cells were resuspended in 1x PBS to $OD_{600} = 0.3$ and vortexed together with *n*-hexadecane. OD_{600} was measured again for the hydrophilic phase after phase separation. Percentage of cells in hydrophilic phase was determined. Results are the average of three independent experiments. Statistical analysis was performed by one-way ANOVA with Bonferroni's multiple-comparison test, (ns) = not significant, (**) = $p < 0.01$, (****) = $p < 0.0001$. **(C)** LA binding assay. Bacteria were harvested and washed in 1x PBS. Cells were diluted in 1x PBS to $OD_{600} = 0.3$ and incubated with 2.5 µg/ml BODIPY-C12 or a corresponding concentration of vehicle as control. Bacterial fluorescence was determined by fluorescence-activated cell sorting (FACS). Results are mean fluorescence relative to wild-type and the average of three independent experiments. Statistical analysis was performed by one-way ANOVA with Bonferroni's multiple-comparison test, (ns) = not significant, (****) = $p < 0.0001$.

growth of wild-type and the *lmo1083* single mutants was restricted. The acid tolerant phenotype was confirmed to be strictly dependent on the lack of GlcNAc, as complementation of *lmo1079*-sub1 restores wild-type sensitivity (**Supplementary Figure S5**). Altogether, mutations of both WTA substitution genes caused a slight growth deficiency upon exposure to salt and ethanol. Notably, lack of GlcNAc on WTAs not only resulted in FFA tolerance, but also tolerance toward acid stress. Altogether, our findings demonstrate that GlcNAc modification of WTA plays a role in the response toward stress conditions encountered by *L. monocytogenes* during life as a saprophyte and a pathogen.

DISCUSSION

Microbial development of resistance toward traditional antibiotics is expanding worldwide much faster than new antibiotics are discovered (Ventola, 2015). Due to the rapid increase in antibiotic resistance, alternative treatment options and combination therapies are attracting more attention (Brown, 2015). Natural compounds like FFAs are known to have antimicrobial properties against pathogens, however, the specific mechanism of action is not fully understood (Desbois and Smith, 2010). In fact, multiple organisms (plants, mice, humans, etc.) use antimicrobial FFAs as a natural protection mechanism to avoid bacterial infection (Kengmo Tchoupa et al., 2021). Pathogenic bacteria therefore use different strategies to avoid FFA toxicity, so they can adapt to the host environment and cause infections despite the presence of host delivered antimicrobial FFAs. These bacterial defense strategies may involve changes in surface polarity, export of FFAs or detoxification of antimicrobial FFAs (Kengmo Tchoupa et al., 2021). In *S. aureus*, the FFAs are repulsed from the bacterial surface by different mechanisms. *Staphylococcus aureus* induces the expression of capsule biosynthesis genes upon exposure to FFAs, as the polysaccharides in the capsule

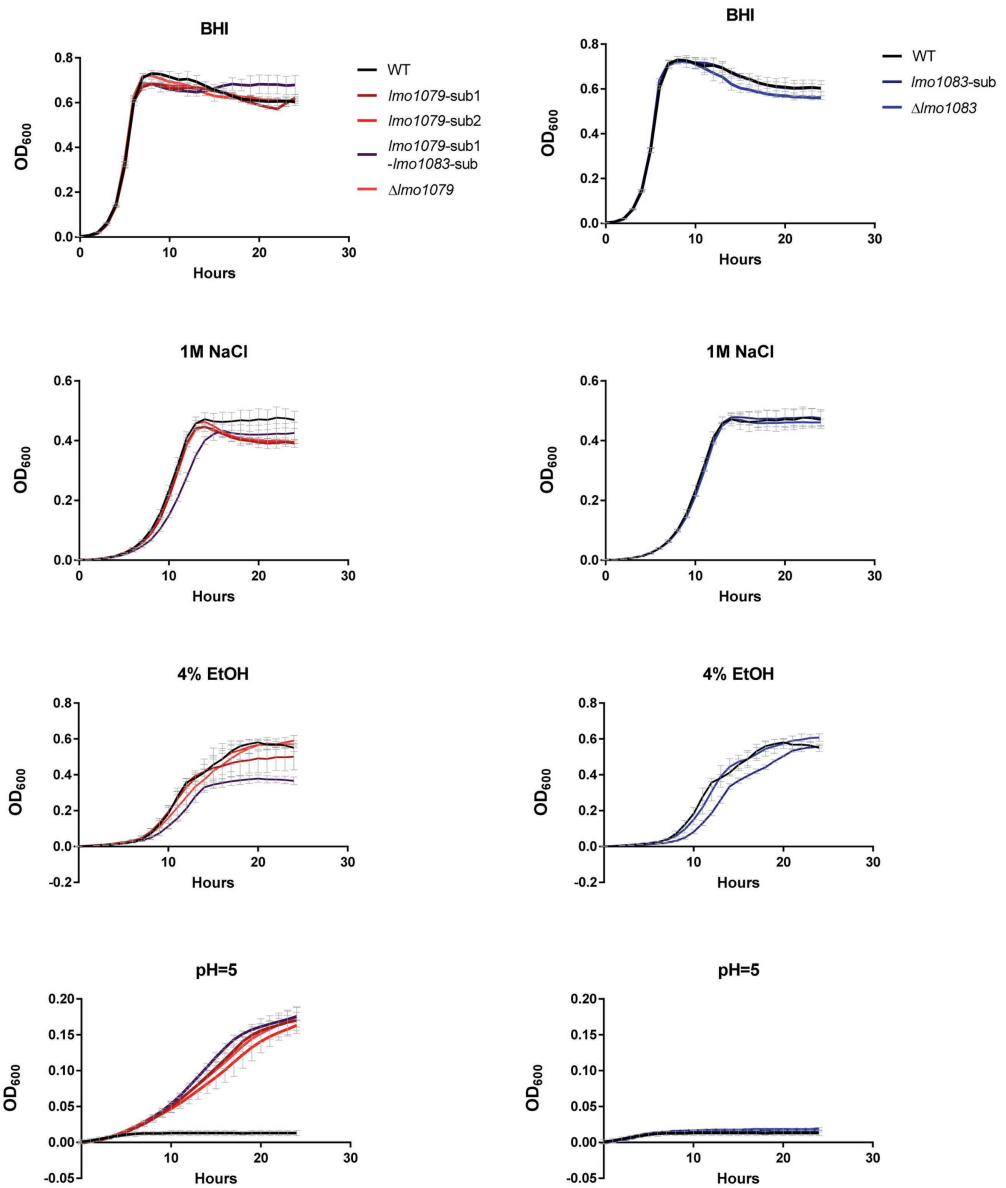

FIGURE 4 | Growth of WTA modification mutants upon exposure to different stress conditions. Strains were diluted to $OD_{600} = 0.005$ in 200 µl growth medium in 96-well plates. The growth medium employed was either untreated BHI medium (BHI), BHI supplemented with 4% ethanol (4% EtOH), 1 M NaCl, or adjusted to pH = 5. Cultures were incubated for 24 h and growth was measured regularly by a microplate reader. Results are the average of three independent experiments.

make the bacterial surface more hydrophilic (Mortensen and Kapral, 1992; Kenny et al., 2009; Moran et al., 2017). Furthermore, WTAs on the surface of *S. aureus* are known to be hydrophilic and hinder the interaction between the FFAs and bacterial membrane (Kohler et al., 2009). Additionally, *S. aureus* expresses the cell-wall anchored protein iron-regulated surface determinant A (IsdA), which decreases the surface hydrophobicity and hamper binding of the FFAs to the bacterium (Clarke et al., 2007). All these hydrophilic factors will naturally increase tolerance toward antimicrobial FFAs in *S. aureus* by repulsing the host delivered FFAs from the bacterial surface. If the intracellular concentration of antimicrobial FFAs in the bacterial cytosol exceed the inhibitory threshold, detoxification can occur by efflux systems, such as the resistance-nodulation-cell division (RND) superfamily (Kengmo Tchoupa et al., 2021). The FFAs are then exported out of the bacterium into the extracellular environment to reduce the intracellular concentration and promote bacterial growth (Alnaseri et al., 2015; Kengmo Tchoupa et al., 2021). Alternatively, FFAs can be detoxified by either oleate dehydratases or fatty-acid-modifying enzyme (FAME) after uptake to prevent intracellular accumulation (Long et al., 1992; Mortensen and Kapral, 1992; Volkov et al., 2010; Subramanian et al., 2019). The antimicrobial FFAs are metabolized into hydroxy-FFAs or esterified FFAs, which are less toxic and

will promote cell survival (Long et al., 1992; Subramanian et al., 2019). Pathogens thereby possess multiple natural protection strategies against antimicrobial FFAs.

To examine how *L. monocytogenes* responds to antimicrobial FFAs, we studied mutations occurring in selected PA tolerant strains. Most of the isolated PA tolerant strains carry mutations in genes encoding for enzymes essential for WTA substitutions; *lmo1079* and *lmo1083* (*rmlB*; **Table 1**). The glycosyltransferase (Lmo1079) is responsible for transferring GlcNAc from a lipid carrier molecule in the outer leaflet of the bacterial membrane onto the growing ribitol backbone of Type I WTAs (Eugster et al., 2015; Rismondo et al., 2018). RmlB on the other hand is involved in the dTDP-L-Rha biosynthetic pathway, which is essential for construction of dTDP-L-Rha for the Type I WTA rhamnosylation (Carvalho et al., 2015). Since both genes are involved in WTA glycosylations, it could be speculated that the mutations in these two genes contribute to PA tolerance. However, our studies confirmed that only mutations in *lmo1079* induced PA tolerance, whereas the effect of mutating *lmo1083* was insignificant. This also might explain why no single *lmo1083* mutants were identified among the PA tolerant isolates. Notably, there seems to be a competition between Rhamnose and GlcNAc modification of WTA at 30 and 37°C (Tokman et al., 2016). In the present study, the PA tolerant strains were selected and analyzed at 37°C. Future studies should focus on testing the putative role of WTA decorations in FFA tolerance at lower temperatures.

Mutation of *lmo1079* induced tolerance toward different types of antimicrobial FFAs (saturated, mono- and poly-unsaturated), demonstrating that *lmo1079* plays an important role in the response of *L. monocytogenes* to antimicrobial FFAs in general. The acquired FFA tolerance of the *lmo1079* mutant strains correlated with a common absence of GlcNAc on their WTAs (**Figure 2B**), suggesting that lack of GlcNAc on Type I WTAs of *L. monocytogenes* confers FFA tolerance. As mentioned above, the presence of WTAs on *S. aureus* is necessary to sustain tolerance toward exogenous FFAs (Kohler et al., 2009). Thus, WTAs in general repulse FFAs from the bacterial surface and induce tolerance, whereas the GlcNAc modification seems to cause sensitivity, as lack of GlcNAc contribute to FFA tolerance. In *L. monocytogenes*, the GlcNAc modification thereby plays a separate role in relation to the response to antimicrobial FFAs, which is opposite to the role shown for WTAs in general in *S. aureus*.

The absence of WTAs in *S. aureus* causes a more hydrophobic bacterial surface; the FFAs are then more efficiently drawn to the surface, which increases sensitivity to FFAs (Kohler et al., 2009). These observations made us to speculate if WTA glycosylations in *L. monocytogenes* affect surface polarity as well. Our data show that lack of GlcNAc on the WTAs, through mutation or deletion of *lmo1079*, led to a more hydrophilic surface compared to *lmo1083* mutants and the parental strain (**Figure 3B**). These observations are further supported by data from (Brauge et al., 2018), where deletion of the two other genes involved in GlcNAc glycosylation (*lmo2549* and *lmo2550*) results in decreased hydrophobicity of the bacterial surface. The FFA tolerance caused by the absence of GlcNAc is therefore most likely due to a more hydrophilic surface. In support of this theory, we found that lack of GlcNAc resulted in reduced interaction between the antimicrobial FFA, LA, and the bacterial surface (**Figure 3C**). Thus, the FFAs are repulsed from the bacterial surface when GlcNAc is lacking, due to a more hydrophilic surface. Altogether, our observations support that the WTA decoration GlcNAc interferes with the surface polarity and thereby the ability of FFAs to interact with the bacterial surface.

WTA glycosylations of *L. monocytogenes* serovar 1/2a have shown to be crucial for sustaining tolerance toward other antimicrobial compounds. For example, absence of GlcNAc slightly increases the sensitivity toward the antimicrobial peptide CRAMP (Meireles et al., 2020). Notably, the sensitivity is amplified if both GlcNAc and Rha are lacking on the WTAs, indicating that the two types of WTA decorations cooperate to confer resistance toward antimicrobial peptides (Meireles et al., 2020). In addition, both WTA glycosylations confer decreased susceptibility of *L. monocytogenes* serovar 1/2a toward the antibiotics, gentamicin and ampicillin, which are commonly used for treatment of Listeriosis (Meireles et al., 2020). In our study, we furthermore found that lack of GlcNAc alone increases the tolerance of *L. monocytogenes* toward acid stress, and mutations of both *lmo1079* and *lmo1083* led to a slight increase in bacterial susceptibility toward ethanol and salt stress. Importantly, WTA glycosylations are known to serve as binding targets for bacteriophages in the environment and changes in these structures therefore prevent phage adsorption to WTAs (Denes et al., 2015; Eugster et al., 2015). Bacteriophage resistance for Type I WTA serovars is caused by point mutations in genes belonging to the *rmlACBD* operon (responsible for Rha modifications), or genes encoding for the GlcNAc glycosylation enzymes (i.e., *lmo1079*, *lmo2549* or *lmo2550*; Denes et al., 2015; Eugster et al., 2015). Altogether, these findings substantiate an important role for GlcNAc glycosylation of WTA, alone or together with Rha modifications, in the response of *L. monocytogenes* toward various antimicrobial agents, environmental stress conditions, and bacteriophages.

As mentioned above, the WTA glycosylation GlcNAc contributes to sensitivity toward antimicrobial agents, such as FFAs and bacteriophages, so why does *L. monocytogenes* retain the GlcNAc decorations? As previously described, GlcNAc contributes to tolerance toward antimicrobial peptides (Meireles et al., 2020). Additionally, the GlcNAc WTA substitution has been shown to be important for adhesion and biofilm formation (Brauge et al., 2018). The lack of GlcNAc results in decreased attachment of *L. monocytogenes* to surfaces and the biofilm architecture that arises is different compared to wild-type. The difference in biofilm structure is expected to be caused by a more hydrophilic bacterial surface (Brauge et al., 2018). Lack of GlcNAc results in a less efficient biofilm structure, which reduce adherence and increase sensitivity toward cleaning procedures (Brauge et al., 2018). Clearly, this outcome of lacking GlcNAc is therefore not beneficial for bacterial survival under these conditions. Additionally, it is known that the most glycosylated serovars of *L. monocytogenes* (serovar 1/2a, 1/2b, and 4b) represent the majority of outbreak strains worldwide (Maury et al., 2016; Braga et al., 2017; Datta and Burall, 2018;

Smith et al., 2019), indicating that WTA decorations contribute to virulence. In line with this, change in serovar, caused by phage resistance, leads to virulence attenuation (Sumrall et al., 2020). To summarize, although GlcNAc decoration of WTA increases the sensitivity of *L. monocytogenes* toward some antimicrobial agents, the pathogen may retain GlcNAc on WTA to promote important functions related to biofilm formation, tolerance toward cleaning products and antimicrobial peptides, and possibly, to sustain virulence.

In conclusion, this work demonstrated for the first time, that the lack of GlcNAc on WTA protects *L. monocytogenes* against the antimicrobial activity of FFAs. We also showed that in the absence of GlcNAc, the FFAs are repulsed from the bacterium due to a more hydrophilic surface. Notably, the FFA PA efficiently inhibited the expression of PrfA-dependent virulence genes, irrespectively of the absence or presence of WTA decorations (**Figures 1B,C**). Thus, strains deficient of WTA decorations can still be targeted by the anti-virulence activity of FFAs.

DATA AVAILABILITY STATEMENT

The datasets presented in this study can be found in online repositories. The names of the repository/repositories and accession number(s) can be found at: https://www.ncbi.nlm.nih.gov/, PRJNA815746.

AUTHOR CONTRIBUTIONS

RT and BK contributed to the conception and design of the study and wrote the first draft of the manuscript. RT, PS, and ES contributed to the experimental work. RT, MS, and MK contributed to the sequencing analysis. All authors contributed to the article and approved the submitted version.

FUNDING

This work was supported by the Novo Nordisk Foundation (grant number NNF17OC0028528).

SUPPLEMENTARY MATERIAL

The Supplementary Material for this article can be found online at: https://www.frontiersin.org/articles/10.3389/fmicb.2022.897682/full#supplementary-material

REFERENCES

Alnaseri, H., Arsic, B., Schneider, J. E., Kaiser, J. C., Scinocca, Z. C., Heinrichs, D. E., et al. (2015). Inducible expression of a resistance-nodulation-division-type efflux pump in *Staphylococcus aureus* provides resistance to linoleic and arachidonic acids. *J. Bacteriol.* 197, 1893–1905. doi: 10.1128/JB.02607-14

Böckmann, R., Dickneite, C., Middendorf, B., Goebel, W., and Sokolovic, Z. (1996). Specific binding of the *Listeria monocytogenes* transcriptional regulator PrfA to target sequences requires additional factor(s) and is influenced by iron. *Mol. Microbiol.* 22, 643–653. doi: 10.1046/j.1365-2958.1996.d01-1722.x

Braga, V., Vázquez, S., Vico, V., Pastorino, V., Mota, M. I., Legnani, M., et al. (2017). Prevalence and serotype distribution of *listeria monocytogenes* isolated from foods in Montevideo-Uruguay. *Braz. J. Microbiol.* 48, 689–694. doi: 10.1016/j.bjm.2017.01.010

Brauge, T., Faille, C., Sadovskaya, I., Charbit, A., Benezech, T., Shen, Y., et al. (2018). The absence of N-acetylglucosamine in wall teichoic acids of *listeria monocytogenes* modifies biofilm architecture and tolerance to rinsing and cleaning procedures. *PLoS One* 13:e0190879. doi: 10.1371/journal.pone.0190879

Brown, D. (2015). Antibiotic resistance breakers: can repurposed drugs fill the antibiotic discovery void? *Nat. Rev. Drug Discov.* 14, 821–832. doi: 10.1038/nrd4675

Carvalho, F., Atilano, M. L., Pombinho, R., Covas, G., Gallo, R. L., Filipe, S. R., et al. (2015). L-Rhamnosylation of *listeria monocytogenes* wall teichoic acids promotes resistance to antimicrobial peptides by delaying interaction with the membrane. *PLoS Pathog.* 11:e1004919. doi: 10.1371/journal.ppat.1004919

Cascant, M. M., Breil, C., Fabiano-Tixier, A. S., Chemat, F., Garrigues, S., and de la Guardia, M. (2018). Determination of fatty acids and lipid classes in salmon oil by near infrared spectroscopy. *Food Chem.* 239, 865–871. doi: 10.1016/j.foodchem.2017.06.158

Chatterjee, A., Dutta, P. K., and Chowdhury, R. (2007). Effect of fatty acids and cholesterol present in bile on expression of virulence factors and motility of *vibrio cholerae*. *Infect. Immun.* 75, 1946–1953. doi: 10.1128/IAI.01435-06

Christiansen, J. K., Larsen, M. H., Ingmer, H., Søgaard-Andersen, L., and Kallipolitis, B. H. (2004). The RNA-binding protein Hfq of *Listeria monocytogenes*: role in stress tolerance and virulence. *J. Bacteriol.* 186, 3355–3362. doi: 10.1128/JB.186.11.3355-3362.2004

Clarke, S. R., Mohamed, R., Bian, L., Routh, A. F., Kokai-Kun, J. F., Mond, J. J., et al. (2007). The *Staphylococcus aureus* surface protein IsdA mediates resistance to innate defenses of human skin. *Cell Host Microbe* 1, 199–212. doi: 10.1016/j.chom.2007.04.005

Datta, A. R., and Burall, L. S. (2018). Serotype to genotype: the changing landscape of listeriosis outbreak investigations. *Food Microbiol.* 75, 18–27. doi: 10.1016/j.fm.2017.06.013

Deatherage, D. E., and Barrick, J. E. (2014). Identification of mutations in laboratory-evolved microbes from next-generation sequencing data using breseq. *Methods Mol. Biol.* 1151, 165–188. doi: 10.1007/978-1-4939-0554-6_12

Denes, T., den Bakker, H. C., Tokman, J. I., Guldimann, C., and Wiedmann, M. (2015). Selection and characterization of phage-resistant mutant strains of *listeria monocytogenes* reveal host genes linked to phage adsorption. *Appl. Environ. Microbiol.* 81, 4295–4305. doi: 10.1128/AEM.00087-15

Desbois, A. P., and Smith, V. J. (2010). Antibacterial free fatty acids: activities, mechanisms of action and biotechnological potential. *Appl. Microbiol. Biotechnol.* 85, 1629–1642. doi: 10.1007/s00253-009-2355-3

Dos Santos, P. T., Thomasen, R. S. S., Green, M. S., Færgeman, N. J., and Kallipolitis, B. H. (2020). Free fatty acids interfere with the DNA binding activity of the virulence regulator PrfA of *Listeria monocytogenes*. *J. Bacteriol.* 202, e00156–e001520. doi: 10.1128/JB.00156-20

Eugster, M. R., Morax, L. S., Hüls, V. J., Huwiler, S. G., Leclercq, A., Lecuit, M., et al. (2015). Bacteriophage predation promotes serovar diversification in *listeria monocytogenes*. *Mol. Microbiol.* 97, 33–46. doi: 10.1111/mmi.13009

Freitag, N. E., Port, G. C., and Miner, M. D. (2009). *Listeria monocytogenes* - from saprophyte to intracellular pathogen. *Nat. Rev. Microbiol.* 7, 623–628. doi: 10.1038/nrmicro2171

Kamisango, K., Fujii, H., Okumura, H., Saiki, I., Araki, Y., Yamamura, Y., et al. (1983). Structural and immunochemical studies of teichoic acid of *Listeria monocytogenes*. *J. Biochem.* 93, 1401–1409. doi: 10.1093/oxfordjournals.jbchem.a134275

Kengmo Tchoupa, A., Eijkelkamp, B. A., and Peschel, A. (2021). Bacterial adaptation strategies to host-derived fatty acids. *Trends Microbiol.* 30, 241–253. doi: 10.1016/j.tim.2021.06.002

Kenny, J. G., Ward, D., Josefsson, E., Jonsson, I. M., Hinds, J., Rees, H. H., et al. (2009). The *Staphylococcus aureus* response to unsaturated long chain free fatty acids: survival mechanisms and virulence implications. *PLoS One* 4:e4344. doi: 10.1371/journal.pone.0004344

Kohler, T., Weidenmaier, C., and Peschel, A. (2009). Wall teichoic acid protects *Staphylococcus aureus* against antimicrobial fatty acids from human skin. *J. Bacteriol.* 191, 4482–4484. doi: 10.1128/JB.00221-09

Larsen, M. H., Kallipolitis, B. H., Christiansen, J. K., Olsen, J. E., and Ingmer, H. (2006). The response regulator ResD modulates virulence gene expression in response to carbohydrates in *Listeria monocytogenes*. *Mol. Microbiol.* 61, 1622–1635. doi: 10.1111/j.1365-2958.2006.05328.x

Long, J. P., Hart, J., Albers, W., and Kapral, F. A. (1992). The production of fatty acid modifying enzyme (FAME) and lipase by various staphylococcal species. *J. Med. Microbiol.* 37, 232–234. doi: 10.1099/00222615-37-4-232

Maury, M. M., Tsai, Y. H., Charlier, C., Touchon, M., Chenal-Francisque, V., Leclercq, A., et al. (2016). Uncovering *Listeria monocytogenes* hypervirulence by harnessing its biodiversity. *Nat. Genet.* 48, 308–313. doi: 10.1038/ng.3501

Meireles, D., Pombinho, R., Carvalho, F., Sousa, S., and Cabanes, D. (2020). Listeria monocytogenes wall Teichoic acid glycosylation promotes surface anchoring of virulence factors, resistance to antimicrobial peptides, and decreased susceptibility to antibiotics. *Pathogens* 9:290. doi: 10.3390/pathogens9040290

Mollerup, M. S., Ross, J. A., Helfer, A. C., Meistrup, K., Romby, P., and Kallipolitis, B. H. (2016). Two novel members of the LhrC family of small RNAs in *listeria monocytogenes* with overlapping regulatory functions but distinctive expression profiles. *RNA Biol.* 13, 895–915. doi: 10.1080/15476286.2016.1208332

Moran, J. C., Alorabi, J. A., and Horsburgh, M. J. (2017). Comparative transcriptomics reveals discrete survival responses of *S. aureus* and *S. epidermidis* to sapienic acid. *Front. Microbiol.* 8:33. doi: 10.3389/fmicb.2017.00033

Mortensen, J. E., and Kapral, F. A. (1992). Effect of capsulation on the resistance of *Staphylococcus aureus* to the bactericidal lipids produced in abscesses. *J. Med. Microbiol.* 36, 337–340. doi: 10.1099/00222615-36-5-337

Nielsen, J. S., Larsen, M. H., Lillebæk, E. M., Bergholz, T. M., Christiansen, M. H., Boor, K. J., et al. (2011). A small RNA controls expression of the chitinase ChiA in *Listeria monocytogenes*. *PLoS One* 6:e19019. doi: 10.1371/journal.pone.0019019

Nielsen, J. S., Lei, L. K., Ebersbach, T., Olsen, A. S., Klitgaard, J. K., Valentin-Hansen, P., et al. (2010). Defining a role for Hfq in gram-positive bacteria: evidence for Hfq-dependent antisense regulation in *listeria monocytogenes*. *Nucleic Acids Res.* 38, 907–919. doi: 10.1093/nar/gkp1081

Petrone, G., Conte, M. P., Longhi, C., di Santo, S., Superti, F., Ammendolia, M. G., et al. (1998). Natural milk fatty acids affect survival and invasiveness of *Listeria monocytogenes*. *Lett. Appl. Microbiol.* 27, 362–368. doi: 10.1046/j.1472-765X.1998.00441.x

Rismondo, J., Percy, M. G., and Gründling, A. (2018). Discovery of genes required for lipoteichoic acid glycosylation predicts two distinct mechanisms for wall teichoic acid glycosylation. *J. Biol. Chem.* 293, 3293–3306. doi: 10.1074/jbc.RA117.001614

Rosenberg, M., Gutnick, D., and Rosenberg, E. (1980). Adherence of bacteria to hydrocarbons: A simple method for measuring cell-surface hydrophobicity. *FEMS Microbiol. Lett.* 9, 29–33. doi: 10.1111/j.1574-6968.1980.tb05599.x

Schäferkordt, S., and Chakraborty, T. (1995). Vector plasmid for insertional mutagenesis and directional cloning in listeria spp. *BioTechniques* 19, 24–25.

Schindelin, J., Arganda-Carreras, I., Frise, E., Kaynig, V., Longair, M., Pietzsch, T., et al. (2012). Fiji: an open-source platform for biological-image analysis. *Nat. Methods* 9, 676–682. doi: 10.1038/nmeth.2019

Scortti, M., Monzó, H. J., Lacharme-Lora, L., Lewis, D. A., and Vázquez-Boland, J. A. (2007). The PrfA virulence regulon. *Microbes Infect.* 9, 1196–1207. doi: 10.1016/j.micinf.2007.05.007

Smith, A. M., Tau, N. P., Smouse, S. L., Allam, M., Ismail, A., Ramalwa, N. R., et al. (2019). Outbreak of *Listeria monocytogenes* in South Africa, 2017-2018: laboratory activities and experiences associated with whole-genome sequencing analysis of isolates. *Foodborne Pathog. Dis.* 16, 524–530. doi: 10.1089/fpd.2018.2586

Sternkopf Lillebæk, E. M., Lambert Nielsen, S., Scheel Thomasen, R., Færgeman, N. J., and Kallipolitis, B. H. (2017). Antimicrobial medium- and long-chain free fatty acids prevent PrfA-dependent activation of virulence genes in *Listeria monocytogenes*. *Res. Microbiol.* 168, 547–557. doi: 10.1016/j.resmic.2017.03.002

Subramanian, C., Frank, M. W., Batte, J. L., Whaley, S. G., and Rock, C. O. (2019). Oleate hydratase from *Staphylococcus aureus* protects against palmitoleic acid, the major antimicrobial fatty acid produced by mammalian skin. *J. Biol. Chem.* 294, 9285–9294. doi: 10.1074/jbc.RA119.008439

Sumrall, E. T., Schefer, C. R. E., Rismondo, J., Schneider, S. R., Boulos, S., Gründling, A., et al. (2020). Galactosylated wall teichoic acid, but not lipoteichoic acid, retains InlB on the surface of serovar 4b *Listeria monocytogenes*. *Mol. Microbiol.* 113, 638–649. doi: 10.1111/mmi.14455

Tokman, J. I., Kent, D. J., Wiedmann, M., and Denes, T. (2016). Temperature significantly affects the plaquing and adsorption efficiencies of listeria phages. *Front. Microbiol.* 7:631. doi: 10.3389/fmicb.2016.00631

Ventola, C. L. (2015). The antibiotic resistance crisis: part 1: causes and threats. *P T* 40, 277–283.

Volkov, A., Liavonchanka, A., Kamneva, O., Fiedler, T., Goebel, C., Kreikemeyer, B., et al. (2010). Myosin cross-reactive antigen of *streptococcus pyogenes* M49 encodes a fatty acid double bond hydratase that plays a role in oleic acid detoxification and bacterial virulence. *J. Biol. Chem.* 285, 10353–10361. doi: 10.1074/jbc.M109.081851

Conflict of Interest: The authors declare that the research was conducted in the absence of any commercial or financial relationships that could be construed as a potential conflict of interest.

Publisher's Note: All claims expressed in this article are solely those of the authors and do not necessarily represent those of their affiliated organizations, or those of the publisher, the editors and the reviewers. Any product that may be evaluated in this article, or claim that may be made by its manufacturer, is not guaranteed or endorsed by the publisher.

frontiers | Frontiers in Microbiology

ORIGINAL RESEARCH
published: 30 June 2022
doi: 10.3389/fmicb.2022.900919

EspF of Enterohemorrhagic *Escherichia coli* Enhances Apoptosis *via* Endoplasmic Reticulum Stress in Intestinal Epithelial Cells: An Isobaric Tags for Relative and Absolute Quantitation-Based Comparative Proteomic Analysis

Xiangyu Wang[1†], Kaina Yan[2,3†], Muqing Fu[2], Song Liang[2], Haiyi Zhao[4], Changzhu Fu[5], Lan Yang[1], Zhihong Song[1], Dayong Sun[1] and Chengsong Wan[2*]*

[1] Department of Gastroenterology, The First Affiliated Hospital of Shenzhen University, Shenzhen Second People's Hospital, Shenzhen, China, [2] BSL-3 Laboratory (Guangdong), Guangdong Provincial Key Laboratory of Tropical Disease Research, School of Public Health, Southern Medical University, Guangzhou, China, [3] Center for Novel Target and Therapeutic Intervention, Institute of Life Sciences, Chongqing Medical University, Chongqing, China, [4] Genecreate Biological Engineering Co., Ltd., National Bio-industry Base, Wuhan, China, [5] MRC Toxicology Unit, School of Biological Sciences, University of Cambridge, Cambridge, United Kingdom

OPEN ACCESS

Edited by:
Xihui Shen,
Northwest A&F University, China

Reviewed by:
Bin Yang,
Nankai University, China
Carlos J. Blondel,
Andrés Bello National University, Chile

***Correspondence:**
Dayong Sun
dayongsunsz@163.com
Chengsong Wan
gzwcs@smu.edu.cn

[†] These authors have contributed equally to this work

Specialty section:
This article was submitted to Infectious Agents and Disease, a section of the journal Frontiers in Microbiology

Received: 21 March 2022
Accepted: 07 June 2022
Published: 30 June 2022

Citation:
Wang X, Yan K, Fu M, Liang S, Zhao H, Fu C, Yang L, Song Z, Sun D and Wan C (2022) EspF of Enterohemorrhagic Escherichia coli Enhances Apoptosis via Endoplasmic Reticulum Stress in Intestinal Epithelial Cells: An Isobaric Tags for Relative and Absolute Quantitation-Based Comparative Proteomic Analysis. Front. Microbiol. 13:900919. doi: 10.3389/fmicb.2022.900919

There have been large foodborne outbreaks related to Enterohemorrhagic *Escherichia coli* (EHEC) around the world. Among its virulence proteins, the EspF encoded by locus of enterocyte effacement is one of the most known functional effector proteins. In this research, we infected the HT-29 cells with the EHEC wild type strain and EspF-deficient EHEC strain. Via the emerging technique isobaric tags for relative and absolute quantitation (iTRAQ), we explored the pathogenic characteristics of EspF within host cells. Our data showed that the differences regarding cellular responses mainly contained immune regulation, protein synthesis, signal transduction, cellular assembly and organization, endoplasmic reticulum (ER) stress, and apoptosis. Notably, compared with the EspF-deficient strain, the protein processing in the ER and ribosome were upregulated during wild type (WT) infection. Our findings proved that the EspF of Enterohemorrhagic *Escherichia coli* induced ER stress in intestinal epithelial cells; the ER stress-dependent apoptosis pathway was also activated within the host cells. This study provides insight into the virulence mechanism of protein EspF, which will deepen our general understanding of A/E pathogens and their interaction with host proteins.

Keywords: Enterohemorrhagic *Escherichia coli*, EspF, endoplasmic reticulum stress, apoptosis, iTRAQ

INTRODUCTION

Enterohemorrhagic *Escherichia coli* (EHEC) is a pathogen of foodborne zoonotic intestinal infectious diseases that spreads through the fecal-oral route (Qadri and Kayali, 1998). EHEC has a variety of serotypes, but only a few of them are related to human diseases. Among these, the serotype O157: H7, first discovered in 1982, has produced outbreaks and epidemics in many countries, especially Northern Europe, Canada (Honish et al., 2017), the United States

(Heiman et al., 2015), Argentina, Japan (Kanayama et al., 2015), and China. Symptoms caused by EHEC include abdominal cramps and non-bloody watery diarrhea, which sometimes can develop into bloody diarrhea. The aged people and young children may develop life-threatening diseases, for instance, thrombotic thrombocytopenic purpura and hemolytic uremic syndrome. Currently, there is no effective treatment for EHEC infections. It has strong pathogenicity and lethality, and antibiotic treatment can cause exacerbations. EHEC infection has become a global concern for safety and health issues (Li et al., 2020).

Enterohemorrhagic *Escherichia coli* was classified into attaching and effacing (A/E) pathogens, targeting the mammalian intestines and causing pathological lesions on the apical surface of the host enterocytes (Spears et al., 2006). A/E pathogens consist of EHEC, *Citrobacter rodentium* (CR), and enteropathogenic *Escherichia coli* (EPEC). They all contain the locus of enterocyte effacement (LEE), which carries many toxic genes, including the bacterium's type III secreted system (T3SS) and effector proteins: EspG, Tir, Map, EspZ, EspH, and EspF (Gaytan et al., 2016). These effector proteins cause significant damage to the host cell, eventually leading to diseases such as diarrhea and inflammation. Through the T3SS, A/E pathogens directly inject the effector proteins into the host cell. These proteins work together to produce characteristic intestinal pathological changes, such as loss of bacterial intestinal microvilli, regulation of actin aggregation, destruction of tight junction barrier, and rearrangement of cell cytoskeleton, ultimately leading to diarrhea diseases (Holmes et al., 2010).

The EspF is one of the most important functional effector proteins encoded by LEE. This protein displays emerging characteristics and becomes a model bacterial effector of multifunctionality. The EspF protein consists of the N-terminal and C-terminal domains. The N-terminus (1–73 aa) is composed of the host cell mitochondrial targeting signal (MTS), the secretion signal and the nucleolar targeting part (NTD); the C-terminus (73–248 aa) contains four proline-rich repeats (PRR) (Mayer, 2001). The EspF protein can inhibit the phagocytosis of macrophages (Tapia et al., 2017), lead to the effacement of host microvilli, remodel the host membrane, and regulate its cytoskeleton (McNamara et al., 2001). EspF can block ribosome synthesis and protein translation by targeting the nucleoli (Dean et al., 2010), regulate DNA mismatch repair (Maddocks et al., 2009), destroy the host cell intermediate fibers, and inhibit sodium-glucose cotransporters, aquaporins, and Na^+/H^+ exchanger (Hodges et al., 2008). Our earlier findings showed that the N-terminal portion of the EspF targeted the mitochondria and disrupted its transmembrane potential, destroyed the tight junctions of the epithelial barrier, led to host cell apoptosis (Wang et al., 2017; Xia et al., 2019). Though EspF is multifunctional, the pathogenic pathways and specific regulatory mechanisms that mediate its interaction with the intracellular proteins of host cells are still unclear.

A quantitative proteomic assay combining isobaric tags for relative and absolute quantitation (iTRAQ) and liquid chromatography-tandem mass spectrometry (LC-MS/MS) is developing into a powerful technique to unravel the overall protein changes within host cells (Wiese et al., 2007). At present, the iTRAQ has a wide range of applications in the proteomics (Mertins et al., 2012). At the MS/MS level, it could identify the proteins immediately and conduct relative quantification from peptide fragments and low mass reporter ions.

The superiorities of iTRAQ are the high throughput, high quality, high stability, and little sample limitations compared with other quantitative methods.

In this research, we infected host cells with the EHEC (WT) and EspF-deficient (Δ*espF*) strains. Via iTRAQ, we captured the differentially expressed proteins from HT-29 cells after infecting WT and Δ*espF* strains. These differential proteins were annotated by bioinformatics tools. They were involved in many KEGG pathways. Furthermore, we constructed protein-protein interaction networks after the EHEC WT and Δ*espF* infection. In general, this work compared complete cellular protein alterations induced by EHEC WT and Δ*espF* strain through iTRAQ based proteomic analysis. It will deepen our understanding of the EspF and contribute to the prevention and control of EHEC O157:H7 infection.

MATERIALS AND METHODS

Cell Culture and Bacterial Strains

The EHEC O157:H7 EDL 933 (WT) and its isogenic strains lacking the *espF* gene (Δ*espF*, with kanamycin resistance), complemented strain (Δ*espF*/*pespF*, with kanamycin and chloramphenicol resistance) were constructed in the previous work (Wang et al., 2017). The *espF* gene expression of the complemented strain was induced by L-arabinose. The bacterial strains were grown in Luria Bertani media (Oxiod #LP0137, Basingstoke, United Kingdom) at 37°C at 200 rpm in a constant-temperature, oscillating shaker with appropriate antibiotics: 100 μg/ml kanamycin (Solarbio #K8020, Beijing, China) for Δ*espF* and Δ*espF*/*pespF*; 10 μg/ml chloramphenicol (Solarbio #C8050, Beijing, China) and 2 mg/ml L-arabinose (Solarbio #L8060, Beijing, China) for Δ*espF*/*pespF* strain.

HT-29, Vero, Hela and Caco-2 cells were preserved in our laboratory. Briefly, they were grown in RPMI-1640 (Gibco #C11875500BT, New York, NY, United States) or DMEM medium (Gibco # C11995500BT, New York, NY, United States) containing 10% fetal bovine serum (Gibco #10270-106, New York, NY, United States) and 1% penicillin/streptomycin (Gibco #15140122, New York, NY, United States). The cells were cultured in tissue culture plates at 37°C under humidified 5% CO_2 prior to infection.

The Isobaric Tags for Relative and Absolute Quantitation and Liquid Chromatography-Tandem Mass Spectrometry Process

The HT-29 cells were infected with WT, Δ*espF* strains at MOI (multiplicity of infection) of 100:1 for 6 h at 37°C and 5% CO_2. Then the WT-, Δ*espF*- and mock-infected cell samples were collected via the cell scraper, centrifuged, and washed with PBS (Gibco #10010023, New York, NY, United States) twice. The cell samples were dissolved with 200 μl TEAB dissolution buffer and cracked by the ultrasonic. Then they were centrifuged at 12000

r/min for 20 min. The clear supernatant was transferred into a new tube and added cold acetone containing 10 mM DTT (Thermo #20290, MA, United States) for about 2 h, followed by centrifugation. The precipitate was collected and mixed with 800 μl cold acetone at 56°C. The samples were centrifuged at 12000 r/min for 20 min at 4°C again and dried. Total protein concentration was measured by the BCA protein assay kit (Beyotime # P0012S, Shanghai, China).

Samples were labeled with iTRAQ multiplex kit (AB Sciex, United Kingdom) as follows: iTRAQ 113 and 114 for mock-infected samples; iTRAQ 115 and 116 for WT strain infected samples; iTRAQ 117 and 118 for Δ*espF* strain infected samples. We mixed all the labeled samples in equal quantities. Next, the high-performance liquid chromatography (HPLC) system (DINOEX Ultimate 3000 BioRS, Thermo, United States) was employed to fractionate the labeled samples. The LC-MS/MS analysis was conducted on the Triple TOF 5600 plus system (AB SCIEX, United States).

TABLE 1 | Sequences of the primers used in this study.

Primers	Sequences (5′→3′)
Bip-F	CTGGGTACATTTGATCTGACTGG
Bip-R	GCATCCTGGTGGCTTTCCAGCCATTC
Atf-F	TCCTCGGTCAGTGGACTCTTA
Atf-R	CTTGGGCTGAATTGAAGGTTTTG
Chop-F	CAGAACCAGCAGAGGTCACA
Chop-R	ACCATTCGGTCAATCAGAGC
Caspase12-F	ACCGTAACTGCCAGAGTCTGAA
Caspase12-R	ACCTTGCAAGAGCCGACCAT
Caspase9-F	GATCAGATCGGGAATTGCAA
Caspase9-R	AGGTGAGGAATTGGCTCCTT
Caspase3-F	AACGATATCGCGGGCCCGAA
Caspase3-R	GGAGGTGCCTTGAGCTAATT
GAPDH-F	AGCTCACTGGCATGGCCTTC
GAPDH-R	CGCCTGCTTCACCACCTTCT

Bioinformatics Analysis

The identified protein sequences were annotated by the Gene Ontology Terms (Gene Ontology Consortium, 2021) (GO[1]), Clusters of Orthologous Genes (Galperin et al., 2021) (COG[2]) and Kyoto Encyclopedia of Genes and Genomes (Kanehisa, 1997) (KEGG[3]) to predict the possible function and classify them functionally. We applied hypergeometric tests to perform GO and KEGG enrichment to discover differentially expressed biomarkers in each group. The R language was applied to draw all other figures in the research.

RNA Extraction and Real-Time PCR Analysis

The HT-29 cells were grown in tissue culture plates (approximately 10^6 cells per well) overnight. The cells were infected with WT, Δ*espF* or Δ*espF/pespF* strains (at MOI of 100:1) for 6 h. The total RNA of the treated cells was extracted using TRIzol Reagent (Invitrogen #15596026, CA, United States). We used the primescript RT reagent kit (Takara # RR036A, Dalian, China) to remove genomic DNA and perform pre-cDNA synthesis in RT-PCR.

We detected the amplification of PCR products via the TB GreenTM premix Ex (Takara #RR820B, Dalian, China). The primers Bip-F/R, Atf6-F/R, Chop-F/R, Caspase12-F/R, Caspase 9-F/R, Caspase3-F/R, GAPDH-F/R, RT-PCR were designed and synthesized to detect changes in mRNA expression (**Table 1**). The RT-PCR process was as follows: 95°C 30 s; followed by 40 cycles of 95°C for 5 s, 60°C for 30 s, and 95°C for 5 s, 60°C 1 min; then a final extension step of 72°C for 30 s.

Western Blot Analysis

The HT-29 cells were seeded in 10 cm diameter tissue culture dishes (approximately 1×10^7 cells per dish) overnight. Then the cells were infected with WT, Δ*espF*, and Δ*espF/pespF* strains (at MOI of 100:1) for 6 h. Cells were washed with ice-cold PBS and then lysed in RIPA lysate (Beyotime #P0013B, Shanghai, China), and added PMSF protease inhibitor (Beyotime #ST506-2, Shanghai, China) to collect protein. The cell lysates were centrifugated at 13,000 rpm for 10 min at 4°C and the protein concentration was measured via the BCA protein assay kit (Beyotime #P0012S, Shanghai, China). Equivalent amounts of protein from each sample were separated by SDS-PAGE and electro-transferred to PVDF membrane (Millpore #IPVH00010/ISEQ00010, MA, United States).

The membrane was blocked with 3% bovine serum albumin (Beyotime #ST023, Shanghai, China) and incubated in primary antibody at 4°C overnight. The primary antibody included: Phospho-eIF2α (CST #Ser51, 1:1000) Rabbit mAb (CST #3398S, 1:1000, Boston, MA, United States), eIF2α Rabbit mAb (CST #5324S, 1:1000, Boston, MA, United States), Phospho-JNK (CST #Thr183/Tyr185, 1:1000, Boston, MA, United States) Rabbit mAb (CST #4668S, 1:1000), JNK Antibody (CST #9252S, 1:1000, Boston, MA, United States), Cleaved Caspase-3 (Asp175) (5A1E) Rabbit mAb (CST #9664S, 1:1000, Boston, MA, United States), BiP Antibody (CST #3183S, 1:1000, Boston, MA, United States), Bax Antibody (CST #2772S, 1:1000, Boston, MA, United States), CHOP (CST #L63F7, 1:1000, Boston, MA, United States) Mouse mAb (CST #2895S, 1:1000), IRE1α (CST #14C10, 1:1000, Boston, MA, United States) Rabbit mAb (CST #3294S, 1:1000) from Cell Signaling Technology (United States); ATF6 Rabbit polyclonal Antibody (Abcam #ab37149, 1:1000, Cambridge, United Kingdom), DDIT3 Mouse monoclonal Antibody (Abcam #ab11419, 1:1000, Cambridge, United Kingdom), Caspase-12 Rabbit polyclonal Antibody (Abcam #ab62484, 1:1000, Cambridge, United Kingdom), Cleaved Caspase-9 Rabbit monoclonal Antibody (Abcam #ab2324, 1:1000, Cambridge, United Kingdom) from Abcam (United Kingdom); GAPDH Rabbit polyclonal Antibody (Proteintech #10494-1-AP, 1:10000, Chicago, IL, United States), β-actin Rabbit polyclonal Antibody (Proteintech #20536-1-AP, 1:10000, Chicago, IL, United States), α-tubulin Rabbit polyclonal Antibody (Proteintech #11224-1-AP, 1:10000, Chicago, IL, United States) from Proteintech (United States). The membranes were washed with TBST and

[1]http://geneontology.org/

[2]http://www.ncbi.nlm.nih.gov/COG/

[3]https://www.kegg.jp/

then incubated with horseradish peroxidase (HRP) conjugated rabbit (Bioss #bs-0295G, Beijing, China) or mouse (Bioss #bs-0296G, Beijing, China) secondary antibody. The signals were collected via the hypersensitive chemiluminescence (ECL) reagent (Bioworld #BLH01S100CN, MI, United States). Then the target band was photographed by the Tanon MP software.

The Ca^{2+} Release Experiments

The HT-29 cells were grown in tissue culture dishes (approximately 1×10^6 cells per dish) overnight. Then the cells were infected with WT, Δ*espF* and Δ*espF/pespF* strains (at MOI of 100:1) for 6 h. A Fluo-4 AM kit (Yeasen #HB180709, Shanghai, China) was used to measure the cytosolic Ca^{2+} concentration within host cells. After washing, the Fluo-4 AM working solution was added to each well, followed by incubation at 5% CO^2 and 37°C for 30 min. Then, cells were gently washed three times by HBSS and stained with Hoechst33342 at room temperature for 10 min. The fluorescent signals were visualized on the laser confocal microscope FV1000 (Olympus, Japan) with the excitation wavelength of 494 nm and emission wavelength of 516 nm.

Cell Apoptosis Detection

The HT-29 cells were grown in tissue culture dishes (approximately 1×10^7 cells per dish) overnight. Then the cells were infected with WT, Δ*espF,* and Δ*espF/pespF* strains (at MOI of 100:1) for 6 h. The cells were trypsinized, collected, and resuspended in PBS (approximately 1×10^6 cells per tube). We used the annexin V-FITC kit (Keygen Biotech #KGA107-50T, Nanjing, China) to stain apoptotic cells in the dark. The apoptotic cells were detected immediately using the flow cytometry (BD FACScan, United States).

Immunofluorescence Assay

Vero cells were grown in tissue culture plates (approximately 10^6 cells per well) overnight. The cells were infected with WT, Δ*espF* or Δ*espF/pespF* strains (at MOI of 100:1) for 6 h. Cells were washed with PBS, fixed with 4% PFA (Leagene #DF0135, Beijing, China), added with 0.1% TritonX-100 (Sigma-Aldrich #T9284, St Louis, MO, United States) and blocked with 10% goat serum (Boster #AR1009, Wuhan, China). Each well was incubated with Bip Rabbit Polyclonal antibody (Proteintech #11587-1-AP, 1: 300, Chicago, IL, United States) overnight at 4°C, then incubated with goat anti-rabbit IgG Alexa 488 (Proteintech #SA00013-2, 1:500, Chicago, IL, United States) for 1 h. The samples were washed with PBS (Gibco, United States) and stained for nucleus using DAPI (Solarbio #C0065, Beijing, China). The fluorescent signals were visualized on the laser confocal microscope FV1000 (Olympus, Japan).

The *espF* gene of EHEC O157: H7 EDL933 was cloned into the eukaryotic expression vector pEGFP-N1 to construct the pEGFP-DH5α-EspF plasmid. Hela cells have good cell morphology and are commonly used in organelle localization experiments. Hela cells were grown in tissue culture plates (approximately 10^6 cells per well) overnight.

Hela cells were transfected via the pEGFP-DH5α and the pEGFP-DH5α-EspF plasmids. After 24 h, actinomycin (15 μg/ml) was added. After 48 h, the endoplasmic reticulum, nucleoli were stained by ER-tracker red (Beyotime #C1041, Shanghai, China), Hochest33258 (AAT Bioquest #17525, CA, United States). The localization of plasmids within host cells were traced via the FV1000 (Olympus, Japan).

Transmission Electron Microscopy Analysis

The Caco-2 cells were cultured in tissue culture plates (approximately 10^6 cells per well) overnight. The cells were infected with WT, Δ*espF,* or Δ*espF/pespF* strains (at MOI of 100:1) for 6 h. Then the infected cells were washed and fixed by 2.5% glutaraldehyde solution (Servicebio #G1102, Wuhan, China) at 4°C for 4 h. Then, the cells were harvested with centrifugation at low-speed centrifugation and coated with 1% agarose. Subsequently, cells were fixed by 1% acetic acid 0.1M phosphate buffer at room temperature for 2 h. The samples were rinsed again, dehydrated with a graded alcohol, and embedded in plates containing pure 812 embedding agent (SPI #90529-77-4, United States). An ultra-thin slicer (Leica UC7, Germany) was used to cut 60–80 nm ultrathin slice. The ultrathin slices were double stained with uranium and lead and visualized on the HT7700 transmission electron microscope (Hitachi, Japan).

Data Analyses

We applied Protein Pilot Software v4.5 to analyze the original MS/MS file data. The Paragon algorithm (Shilov et al., 2007) was integrated into Protein Pilot to search in the Uniprot Homo sapiens (154724 items) database. The qualified proteins (unique peptide $\geq$ 1, unused value $\geq$ 1.3) were considered for further analysis. The results were presented as the mean ± SD of at least three independent experiments performed. Statistical analyses were performed via the SPSS 19.0 software (SPSS, United States). We applied the student's *t*-test, one-way ANOVA and then performed Bonferroni *post hoc* test for multiple comparisons to compare the values in different groups. The p-value < 0.05 was considered significant.

RESULTS

Differentially Expressed Proteins Identified in the Study

In this study, 3175 distinct proteins (unused value $\geq$ 1.3, confidence $\geq$ 95%) were identified via the iTRAQ (Smith et al., 2015). In total, using a strict cutoff value of 1.5-fold for expressed variation (Deutsch et al., 2014), we detected 145, 230, and 229 proteins differentially expressed in the sample pairs Δ*espF* versus uninfected, Δ*espF* versus WT, and WT versus uninfected ($p < 0.05$), respectively. **Supplementary Material** reported more details of protein identification (see **Supplementary Figures 1a–c**).

According to the criteria for defining differentially expressed proteins (fold change ratio $\geq$ 1.5 and $p \leq 0.05$), the number of downregulated and upregulated proteins are shown in **Table 2**. The detailed identification and quantification of each regulated protein was showed in **Supplementary Table 1**. The COG, KEGG function analysis of differentially expressed proteins within host

TABLE 2 | Differentially expressed proteins identified in the study.

Sample pairs	Δ*espF*/Control	WT/ Control	Δ*espF*/ WT
Quantified	3,125	3,128	3,126
Upregulated	80	214	22
Downregulated	65	15	208
Total difference	145	229	230

cells after infection were displayed in the **Supplementary Table 2**. In our study, two biological replicates among WT-infected, Δ*espF*-infected, and uninfected groups were well-mixed during sampling. And we performed three technical replicates to improve the reliability of our data. The coefficient of variation (CV) analysis was performed to verify the repeatability of technical replicates (see **Supplementary Figure 1d**).

Bioinformatics Analysis of the Host Cell Proteome

We adopted several function annotation analyses for identified proteins and function enrichment analyses for differentially expressed proteins to explore more essential proteins and pathways.

Gene Ontology Annotation

Gene Ontology annotation comparison was applied to clarify the features of total altered proteins in HT-29 cells treated by Δ*espF* or WT infection, which might associate with pathogenicity and virulence. The corresponding GO function of each protein is shown in **Supplementary Table 3**. To analyze the function of differential proteins more clearly, we performed an independent functional annotation analysis of differentially up- and downregulated proteins and compared the altered proteins within WT vs. control, Δ*espF* vs. control and Δ*espF* vs. WT groups respectively. The comparison of the GO term annotations for the differentially expressed proteins in HT-29 cells infected with the WT strain or control group is shown in **Figure 1A** (Δ*espF* or control group is shown in **Figure 1B**, and Δ*espF*, or WT group is shown in **Figure 1C**). GO annotation comparison was conducted to clarify the features of total altered proteins in HT-29 cells induced by WT or Δ*espF* infection (see in **Figure 1C**), which might be associated with virulence and pathogenicity.

From the **Figure 1C**, these 229 differentially expressed proteins were categorized into biological processes, cellular components, and molecular functions according to their annotation. The most prevalent biological processes were cellular process, metabolic process, regulation of biological process, cellular component organization or biogenesis and response to stimulus. The most prevalent cellular components were located in the cell, cell part, organelle and organelle part. The most predominant molecular function was binding, catalytic activity, structural molecule activity, enzyme regulator activity.

Kyoto Encyclopedia of Genes and Genomes Pathways Analysis

All proteins were sub-categorized into 243 KEGG classifications. **Figure 2A** shows a pie chart of the top 10 functions of KEGG pathways from the analysis of up- and downregulated proteins

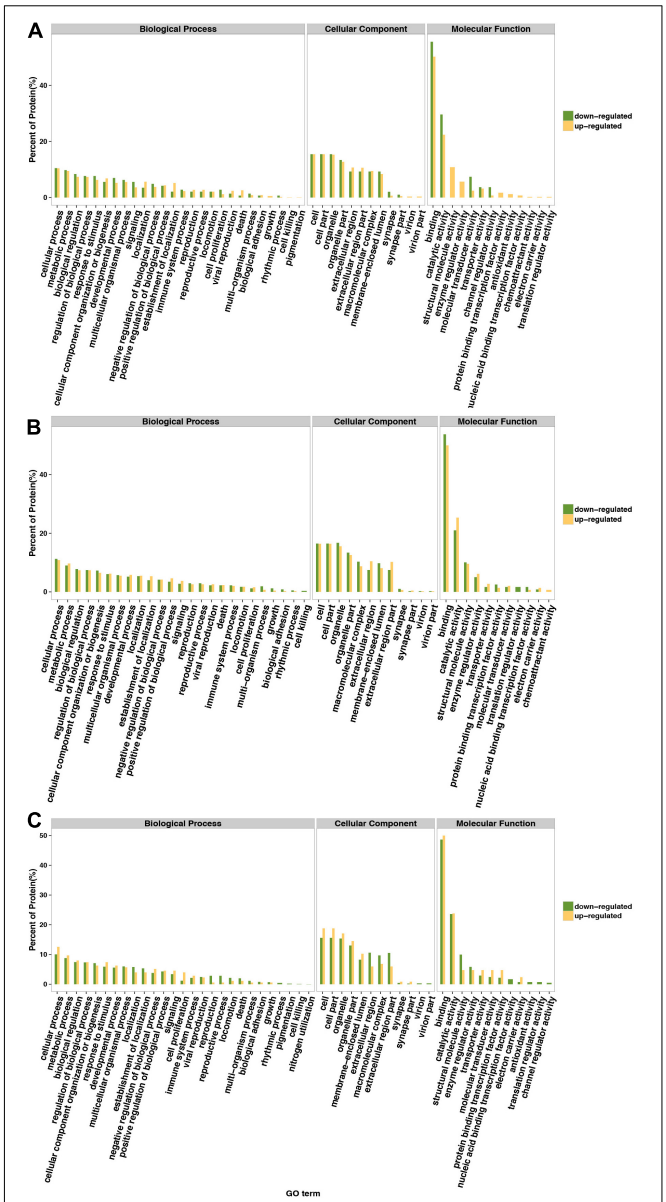

FIGURE 1 | Gene Ontology classification of upregulated and downregulated differentially expressed proteins. The green bar indicates downregulated differentially expressed proteins; the yellow bar indicates upregulated differentially expressed proteins. **(A)** Compared to the control group, the differentially expressed proteins within host cell after WT infection. **(B)** Compared to the control group, the differentially expressed proteins within host cell after Δ*espF* infection. **(C)** Compared to the WT infection, the differentially expressed proteins within host cell after Δ*espF* infection.

in cells infected with Δ*espF* respect to cells infected with WT strains. The three pathway's metabolic function types (metabolic pathways, regulation of actin cytoskeleton, Huntington's disease) were in all the up and down differential proteins from **Figure 2A**. It is worth noting that the biological processes involved in endocytosis, T cell receptor signaling pathway, and Fc gamma R-mediated phagocytosis were underscored in Δ*espF* infection, while protein processing in the ER and ribosome were highlighted during WT infection. In order to

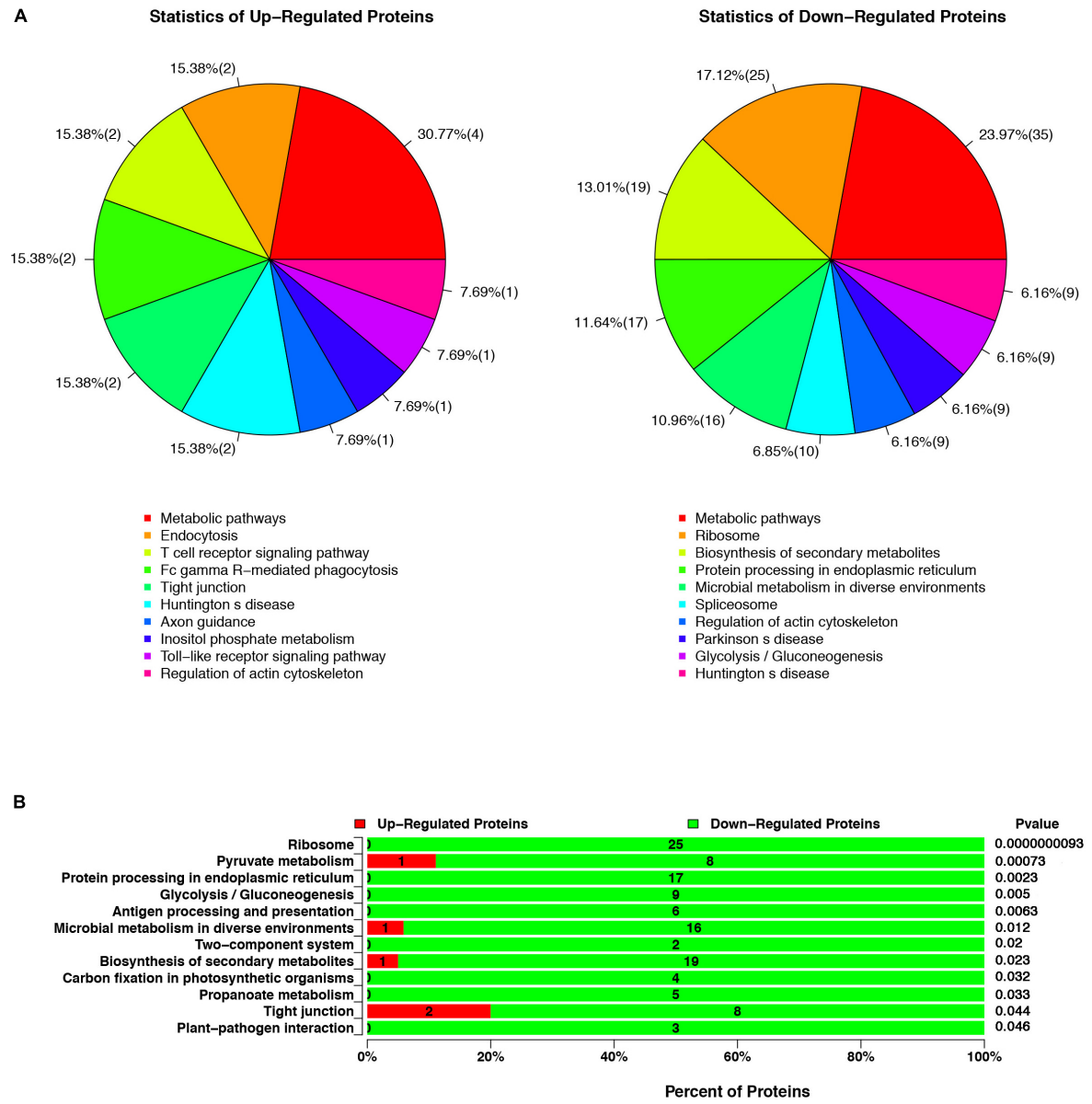

FIGURE 2 | The KEGG pathway analysis of up- or downregulated proteins in cells infected with Δ*espF* respect to cells infected with WT strains. **(A)** Compared with the WT infection, the top ten functions of KEGG pathways from the analysis of up- and downregulated proteins after the Δ*espF* infection. **(B)** Compared with the WT infection, KEGG pathway enrichment analysis after Δ*espF* infection. The green bar indicates downregulated expressed proteins; the red bar indicates upregulated expressed proteins.

figure out the function related to altered proteins, we applied KEGG pathway enrichment analysis to reveal the enriched pathways of the considerably altered proteins (Yang et al., 2019). A hypergeometric distribution based on *p*-value was performed to determine the significantly enriched pathways. The KEGG pathway enrichment analysis of up- and downregulated proteins in cells infected with Δ*espF* respect to cells infected with WT strains are shown in **Figure 2B**. Compared with the Δ*espF* infection, several pathways were more up-regulated after WT infection, such as Ribosome (p-value = 9.3×10^{-9}), Protein processing in the ER (p-value = 2.3×10^{-3}), Antigen processing and presentation (p-value = 6.3×10^{-3}), Biosynthesis of secondary metabolites (p-value = 2.3×10^{-2}), and tight junction (p-value = 4.4×10^{-2}).

The Protein–Protein Interaction Analysis

The protein–protein interaction (PPI) analysis is uniformly evaluated based on credibility scores via STRING database (Szklarczyk et al., 2019). This project used the medium credibility of 0.4 (including 0.4) as the threshold to screen the interaction relationship. **Supplementary Table 4** shows the detailed results. Cytoscape 3.4 was applied to visualize the

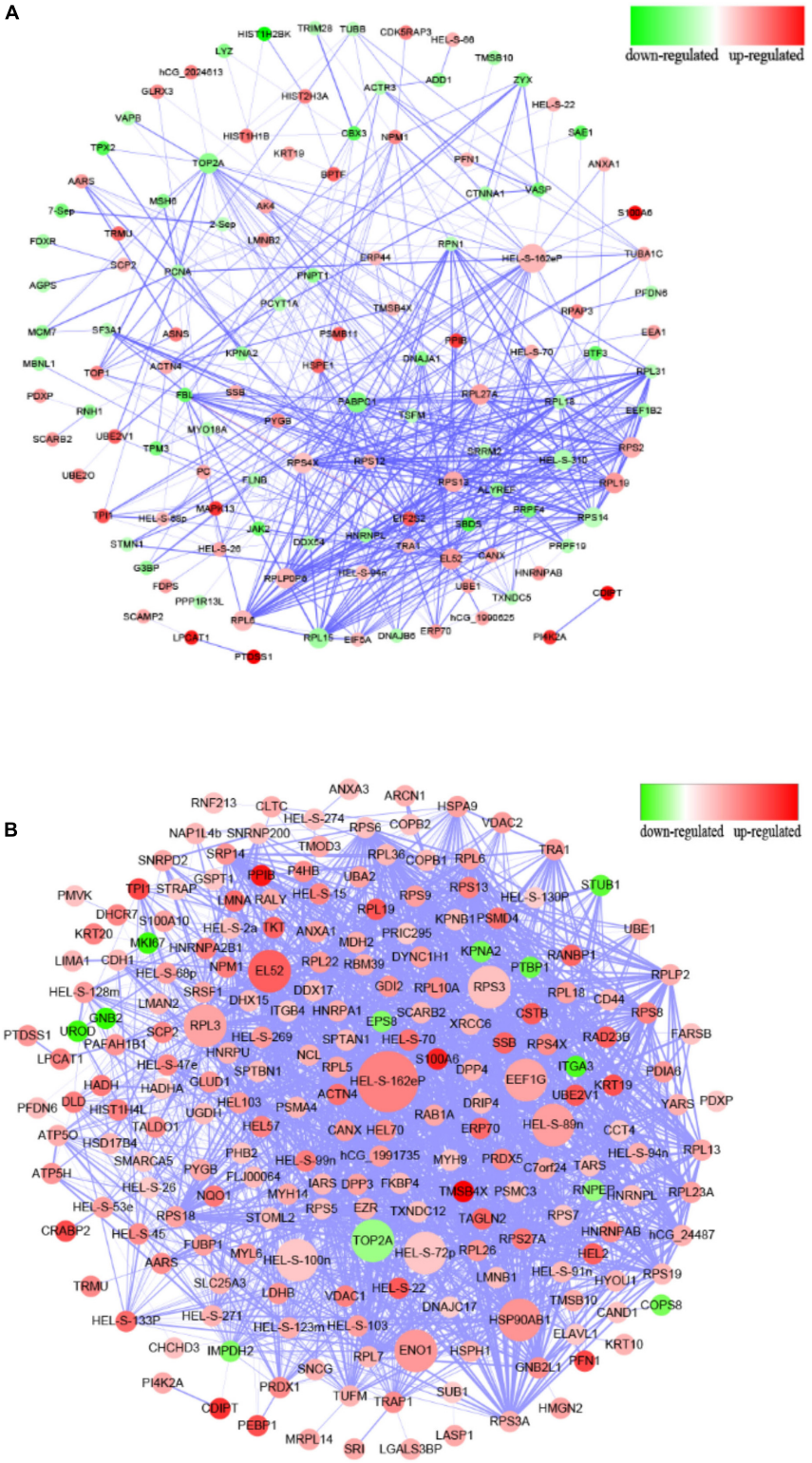

FIGURE 3 | Protein–protein interaction analysis of differentially expressed proteins. **(A)** PPI interaction from the analysis of up- and downregulated proteins comparing the Δ*espF* infected cells against the control cells. **(B)** PPI interaction from the analysis of up- and downregulated proteins comparing the WT infected cells against the control cells. Circular nodes represent the differentially expressed proteins. The red node indicates the upregulation of proteins, while the green node indicates the downregulation. The size of node is proportional to the interaction degree. The interacting proteins are connected by edges. The higher the credibility of the interaction between proteins, the thicker the connection between the nodes.

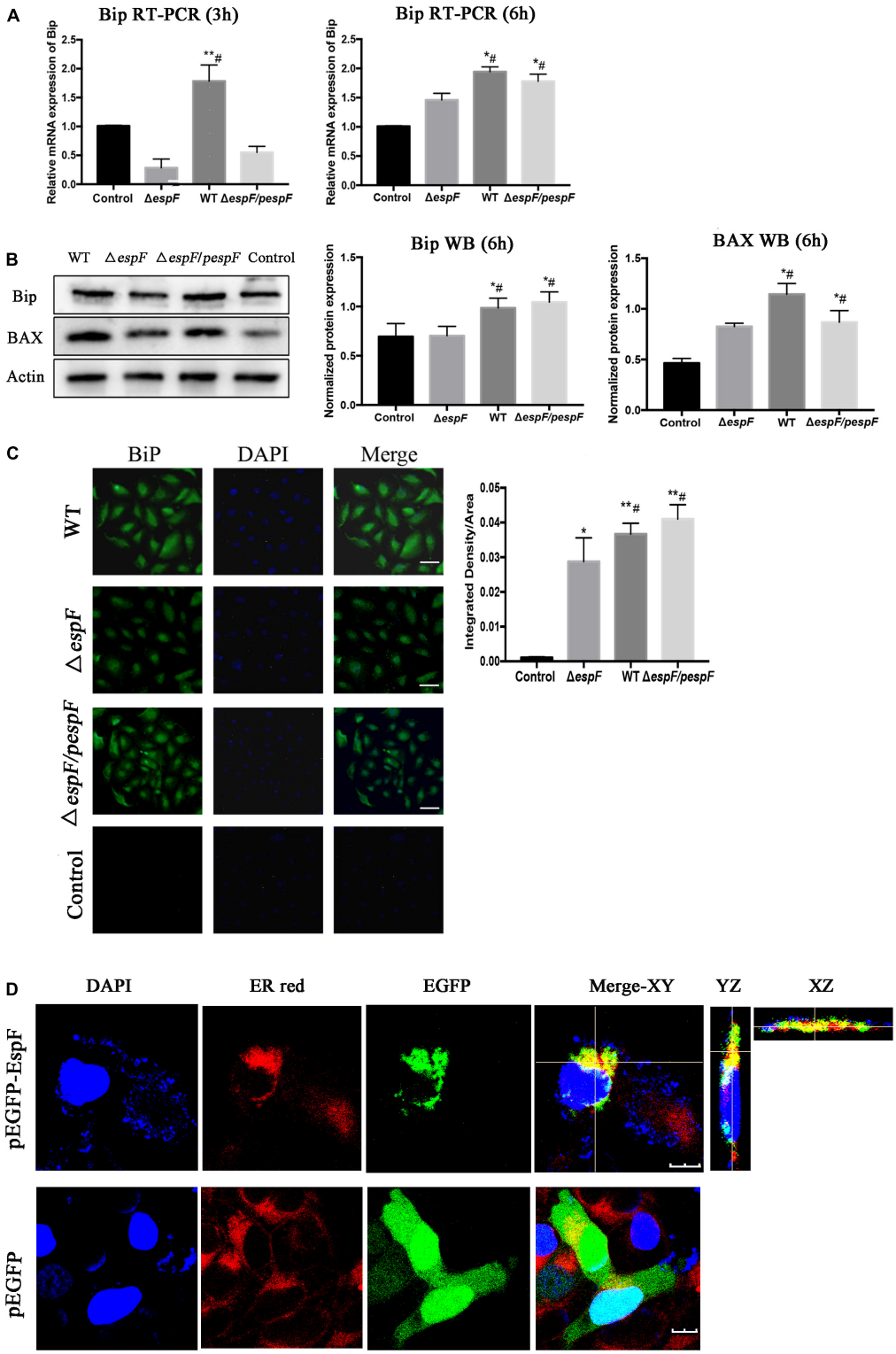

FIGURE 4 | EspF co-localizes with endoplasmic reticulum and upregulates the expression of Bip. **(A,B)** After 6 h of WT, Δ*espF*, and Δ*espF/pespF* infection, the relative RNA expression and protein expression of Bip in HT-29 cells was measured via qPCR and western blot assay. Data were normalized to relative RNA expression, and protein expression is presented as means ± SD from three biological replicates. One-way ANOVA test the *p*-value. $^{*}p < 0.05$, $^{**}p < 0.01$ as compared with the control group. #$p < 0.05$ as compared with the Δ*espF* group. **(C)** Immunofluorescent staining assay to visualize the level of Bip expression after the infection of WT, Δ*espF*, and Δ*espF/pespF*. Host cells infected by each group were stained with Bip rabbit polyclonal antibody and goat anti-rabbit IgG Alexa 488

(Continued)

FIGURE 4 | to visualize Bip (green) and DAPI to stain DNA (blue). Representative images from a single experiment are shown. Scale bar, 50 μm. The integrated density of Bip fluorescence signal per field was counted for five randomly selected fields. One-way ANOVA test the *p*-value. $^{*}p < 0.05$, $^{**}p < 0.01$ as compared with the control group. $\#p < 0.05$ as compared with the Δ*espF* group. **(D)** Immunofluorescent staining assay to visualize the location of EspF and ER after the transfection of plasmids pEGFP-DH5α and pEGFP-DH5α-EspF. Host cells transfected by each group were stained with ER-tracker red to visualize the ER (red) and DAPI to stain DNA (blue). Representative z-stack images were shown. The fluorescence signal in host cells was observed by the confocal microscope FV1000. The Pearson's correlation was calculated by the NIS-viewer software. Scale bar, 10 μm.

network. The node means the protein, and the edge means the interaction relationship between the two nodes. Proteins with higher connectivity than others in the network are called "hubs," which might play a vital role in the network regulation. The connectivity of each node is evaluated by Degree (Deg), which means the total number of edges connected to this node. The greater the value of Deg, the greater the importance of this node in the network.

Compared to the control group, the PPI network diagram was drawn to clarify the features of total altered proteins in HT-29 cells induced by Δ*espF* infection (**Figure 3A**) and WT infection (**Figure 3B**). There are 123 nodes in **Figure 3A**, which form 478 interaction relationships via Δ*espF* infection. PPI analysis revealed the following molecular hubs: Glyceraldehyde-3-phosphate dehydrogenase (Deg:33), ribosomal protein S2 (Deg:27), Epididymis luminal secretory protein 52 (Deg:26), DNA topoisomerase 2-alpha (Deg:26), acidic ribosomal protein P0 (Deg:25), ribosomal protein S14 (Deg:25), ribosomal protein S13 (Deg:24), Polyadenylate-binding protein (Deg:23), ribosomal protein L27a (Deg:22), and ribosomal protein S4 (Deg:22).

There are 213 nodes (**Figure 3B**), which form 1,882 interaction relationships via WT infection. PPI analysis revealed the following molecular hubs: Glyceraldehyde-3-phosphate dehydrogenase (Deg:77), Epididymis luminal secretory protein 52 (Deg:69), Epididymis luminal protein 33 (Deg:67), Epididymis secretory sperm binding protein Li 89n (Deg:64), Heat shock protein-α (Deg:61), DNA topoisomerase 2-α (Deg:59), Chaperonin containing TCP1 (Deg:55), Enolase 1 (Deg:53), ribosomal protein L3 (Deg:53), and ribosomal protein S3 (Deg:52). As illustrated in **Figure 3**, the nodes of the WT infection are darker; the Deg value is greater, and the interaction relationship between genes is highly reliable and more complex than the network associated with the Δ*espF* infection.

EspF Upregulates the Expression of Bip

From the ER pathway results of KEGG analysis (**Supplementary Figure 1e**), several proteins associated with ER stress were significantly upregulated after the WT infection compared with the Δ*espF* infection ($p < 0.05$). Among these, immunoglobulin-binding protein (Bip; Alao known as Grp78) stands out as an ER chaperone that plays a crucial role in protein folding and quality control in the ER lumen (Dana et al., 1990; Evensen et al., 2013; Oka et al., 2013; Cuevas et al., 2017). From the original iTRAQ results, compared with the Δ*espF* infection, the expression of Bip in host cells was significantly upregulated after WT infection with a fold change of 2.845 and p-value < 0.001. QPCR and Western blot tests were applied to verify the above results. Compared with Δ*espF* infection, the relative RNA expression (**Figure 4A**) and protein expression (**Figure 4B**) of Bip in host cells were significantly upregulated 6 h after WT infection ($p < 0.05$). Immunofluorescent staining assay was applied to visualize the level of Bip expression after the infection of WT versus Δ*espF* in **Figure 4C** ($p < 0.05$). The integrated density of the Bip fluorescence signal per area was elevated after the WT infection. Furthermore, an expression vector pEGFP-DH5α-EspF was constructed to trace the EspF. The Pearson's correlation of ER-red and EGFP-green signals were 0.662 (pEGFP-DH5α-EspF) and 0.029 (pEGFP-DH5α group) respectively. By merging the fluorescence signal in host cells after transfection, we demonstrated that EspF localized to the ER (**Figure 4D**).

EspF Induces Endoplasmic Reticulum Stress in Host Cells

Since Bip ensures the proper folding of proteins and is involved in the degradation of misfolded proteins, it acts as a key repressor of the ERS. The expression of Bip was upregulated within host cells. To further clarify whether ER stress was induced in our cell model, we performed transmission electron microscopy (TEM) to observe the ultrastructure of the infected Caco-2 cells. The rough ER in Caco-2 cells of the Control group did not expand significantly; ribosomes were attaching on the surface (**Figure 5A**). After Δ*espF* infection, the RER in the cells were abundant, slightly expanded, and some of the surface ribosomes fell off. In the WT infection group, most of the RER expanded, a dilatation change appeared, and the ribosomes on the surface fell off. When ER stress occurs, the Ca^{2+} within the ER will leak into the cytoplasm. We traced the concentration of Ca^{2+} via the Fluo-4 probe (**Figure 5B**). The cytosolic Ca^{2+} combined the probe and emitted green fluorescence. The fluorescence intensity of the WT-infected group was significantly higher than that of the Δ*espF* infected group and the uninfected group. The Δ*espF*/*pespF*-infected group regained a high fluorescence intensity.

EspF Induces the Endoplasmic Reticulum Stress-Dependent Apoptosis Within Host Cells

Evidence in KEGG pathway showed that the protein processing pathway in the ER was highlighted after WT strain infection compared with the Δ*espF* infection. Several ER stress related proteins were significantly upregulated, which indicated that EspF might induce ER stress. Thus, we explored the expression of downstream signaling molecules. To assess the alternation of ERS after EspF infection, the expression and phosphorylation profiles of IRE1*a*, JNK, NF-κB, eIF2*a*, ATF-6, CHOP, and Caspase3/9/12 were detected by western blot analysis. As shown

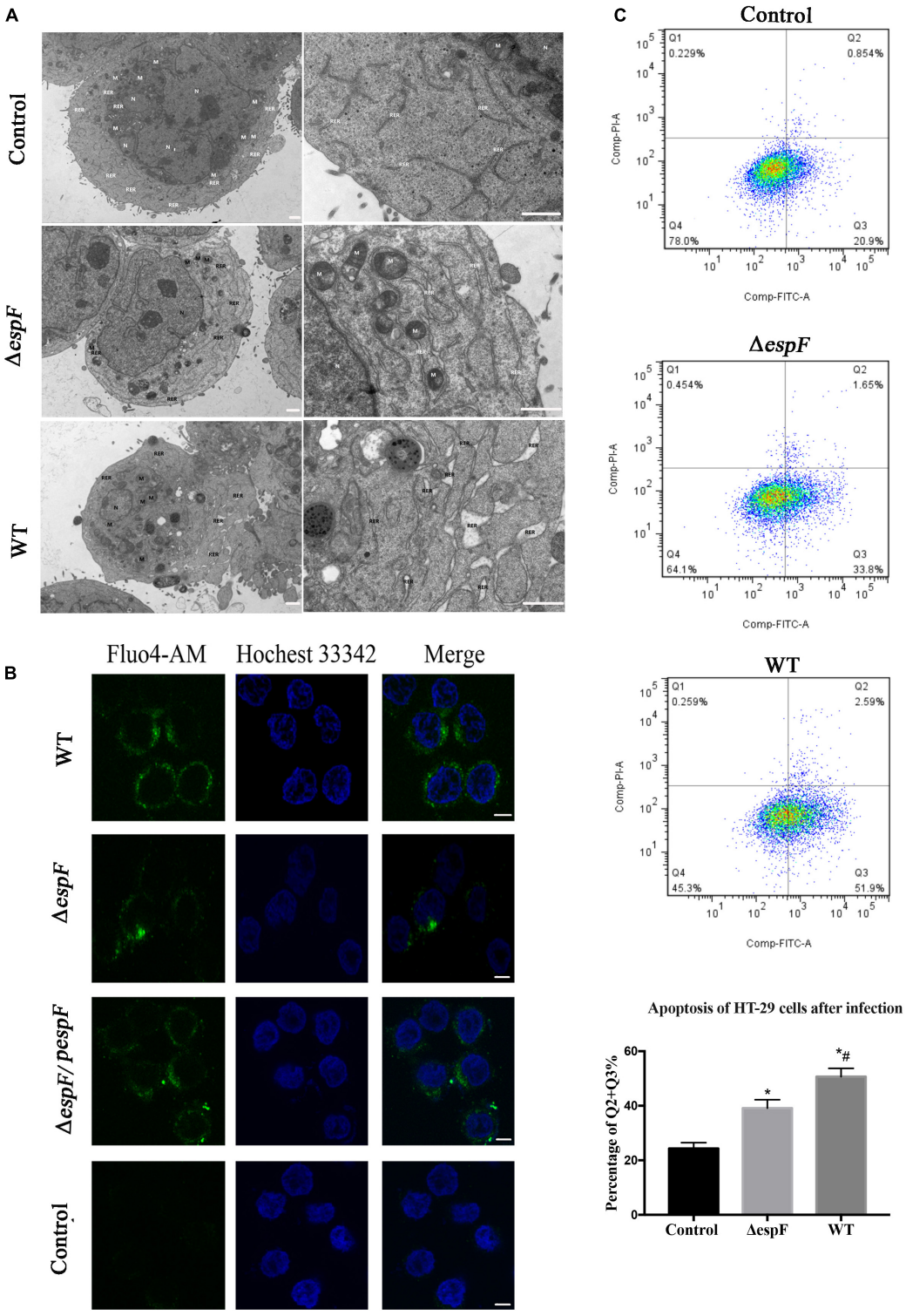

FIGURE 5 | EspF induces ER stress and apoptosis in host cells. **(A)** High-resolution TEM images of Caco-2 cells infected with WT or Δ*espF* for 6 h. Compared to the untreated cells, the TEM images showed the dilatation of the ER after the WT and Δ*espF* infection. RER, rough ER; M, mitochondria; N, nucleus. Scale bar, 1 μm. **(B)** The cytosolic Ca^{2+} concentration within host cells. The HT-29 cells transfected by each group were stained with Fluo-4 probe to visualize Ca^{2+} (green) and Hochest 33342 to stain DNA (blue). Scale bar, 10 μm. **(C)** The effect of WT and Δ*espF* on the viability of HT-29 cells. Detecting HT-29 apoptotic cells after infection via the PI and Annexin V-FITC double-staining. The ratio of late and early apoptotic cells in every group was shown as Q2 + Q3%. Data were expressed as the mean ± SD from three biological replicates. One-way ANOVA test the p value. *$p < 0.05$ as compared with the control group. #$p < 0.05$ as compared with the Δ*espF* group.

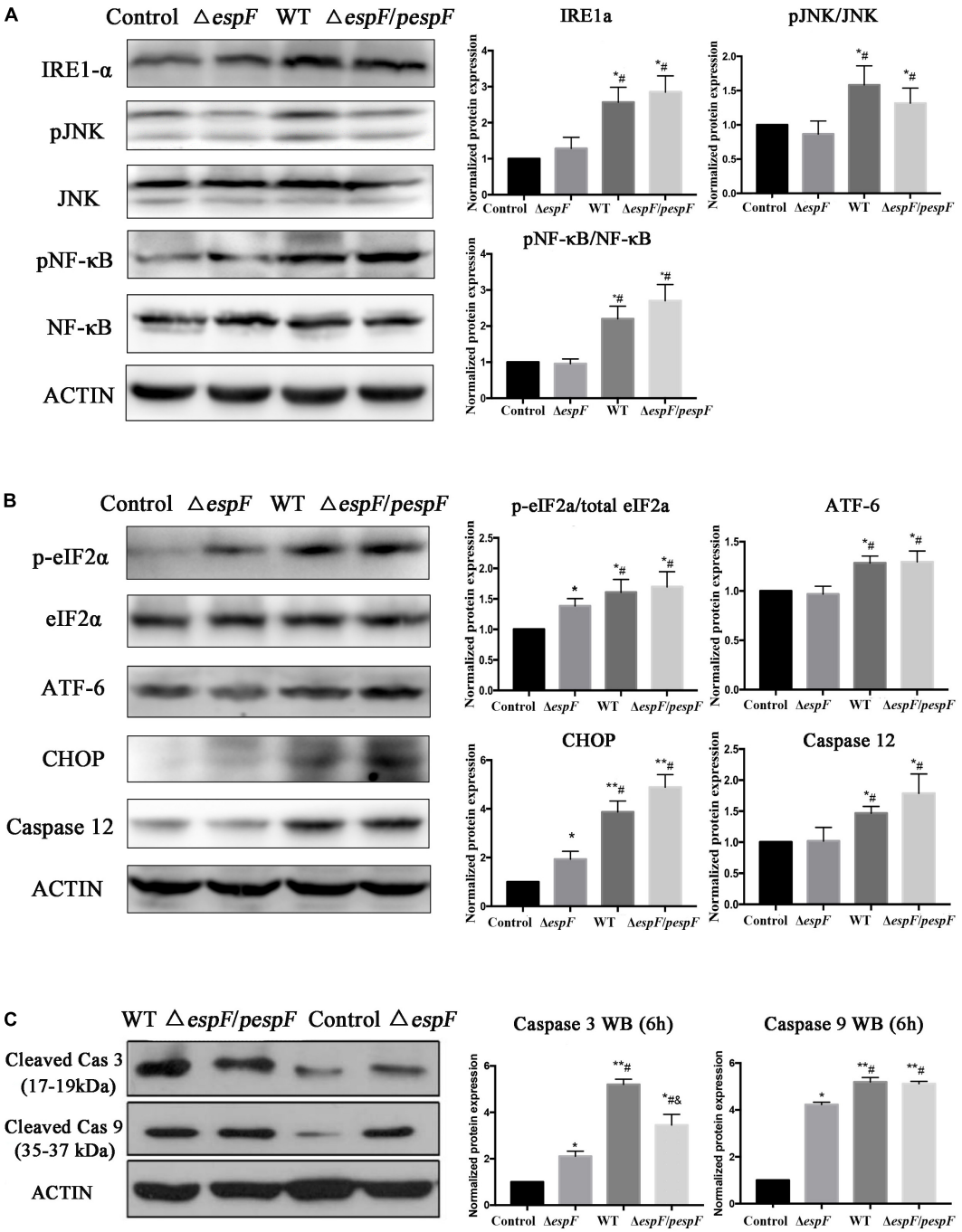

FIGURE 6 | EspF upregulates the proteins associated with ER stress in host cells. After 6 h of WT, Δ*espF*, and Δ*espF/pespF* infection, the expression of proteins associated with ER stress in HT-29 cells was measured via western blot assay. **(A,B)** Protein and phosphor-protein levels of IRE1*a*, JNK, NF-κB, eIF2*a*, ATF-6, CHOP, and Caspase12 in HT-29 cells were assessed by Western blot and quantified. **(C)** Cleaved Caspase 3/9 in HT-29 cells were assessed by Western blot and quantified. Data normalized to protein expression are presented as means ± SD from three biological replicates. One-way ANOVA test the *p*-value. $^{*}p < 0.05$, $^{**}p < 0.01$ as compared with the control group. #$p < 0.05$ as compared with the Δ*espF* group. &$p < 0.05$ as compared with the WT group.

in **Figure 6A**, the expression level of IRE1*a* was elevated, followed by increased expression of phosphorylated JNK and NF-κB mediated by WT and Δ*espF/pespF* infection but not by Δ*espF* ($p < 0.05$).

As shown in **Figures 6B,C**, the phosphorylation levels of eIF2*a* and ATF-6 were elevated, followed by increased expression of CHOP, pro-apoptotic protein Bax (**Figure 4B**), and activated caspase3/9/12 mediated by WT or Δ*espF/pespF*

infection compared with Δ*espF* ($p < 0.05$). To further explore the apoptotic effect of EspF, we also detected the activities of three intrinsic apoptosis markers, caspase-3/caspase-9/caspase-12.

The results were consistent with the proteomic data obtained via the iTRAQ labeled LC-MS/MS method. These protein expression changes were accompanied by significant induction of apoptosis in WT and Δ*espF/pespF*-infected HT-29 cells. The results suggested that the EspF promoted cell death via induction of ERS, which subsequently led to massive DNA strand breaks and the activation of the intrinsic apoptotic pathway. Furthermore, we assessed the apoptosis level of infected HT-29 cells via PI and Annexin V-FITC double staining united with flow cytometry (**Figure 5C**). The average apoptosis percentage (including late and early apoptosis) of the uninfected, WT, and Δ*espF* infected groups was 24.34, 50.68, and 39.11%, respectively. Compared to the uninfected group (13.1%), the number of apoptotic cells (including late and early apoptosis) significantly increased in the Δ*espF* and WT groups ($p < 0.05$). Compared to the Δ*espF* group, the WT group showed fewer living cells, but apoptotic cells increased significantly ($p < 0.05$).

DISCUSSION

So far, although proteomic techniques have been widely utilized for bacteria–host interaction research, little information is available on intracellular protein regulation within host cells after EHEC infection.

Here, we applied iTRAQ united with LC-MS/MS for the comparative proteomic analysis of host cells infected with WT and Δ*espF* strains of EHEC, owing to its superior capability in the simultaneous comparison of multi-samples with a vast dynamic protein abundance (Zhao et al., 2016). In this research, based on a fold change > 1.5 or <0.67 and a *p*-value < 0.05229, 145 and 229 differentially regulated proteins were identified in HT-29 cells treated by EHEC WT and Δ*espF*, respectively. Compared with Δ*espF*-infected cells, a total of 230 proteins have been identified in WT-infected group, including 208 up-regulated proteins and 22 down-regulated proteins. The differences in cellular responses mainly included immune regulation, cellular assembly and organization, protein synthesis, signal transduction, ER stress, and apoptosis.

From GO analysis, it indicated that EspF regulated the host metabolic and biological process for its colonization and infection. As for the cellular components part, it demonstrated EspF altered proteins were mostly located in the organelle and organelle part, which was consistent with our previous research that EspF targeted to the mitochondria and nucleus (Zhao et al., 2013; Fu et al., 2021). The most predominant molecular function of EspF infection was binding. As EspF could disrupt the tight junction, degrade the intermediate filament and induce actin polymerization (Holmes et al., 2010).

Several host proteins were once screened and verified to interact with EspF (Holmes et al., 2010; Hua et al., 2018).

From our proteomic analysis, we found three EspF-binding proteins were up-regulated after WT infection (compared with Δ*espF*): profilin (0.2997, $p = 0.00016$), Arp2/3 (0.3679, $p = 0.02157$) and 14-3-3ζ (0.4835, $p = 0.0089$). It meant that the interaction of EspF to these proteins upregulated their expression within host cells significantly. Other proteins were not found to be significantly up- or down- regulated, perhaps because of iTRAQ methodological limitations, insufficient replicates, or inappropriate incubation time.

Using KEGG pathway analysis, several pathways were more up-regulated after WT infection such as Ribosome, Protein processing in the ER, Antigen processing and presentation and tight junction. The ER is a vital membrane organelle for protein synthesis, folding, and secretion in eukaryotic cells. It can also participate in metabolic processes such as Ca^{2+} storage, gluconeogenesis, lipid and cholesterol synthesis, and the formation of autophagic vacuolization (Cao, 2015). When the intracellular oxidation-reduction homeostasis is disturbed, lots of misfolded or unfolded proteins will accumulate in the ER cavity, a phenomenon called ER stress (Cao and Kaufman, 2014). To eliminate the harmful consequences of ER stress, cells have developed the unfolded protein response (UPR) (Hua et al., 2018). Under the ER stress condition, Bip dissociates from sensors and binds to misfolded proteins in the ER, which then activates downstream signals of inositol inositol-requiring protein-1 (IRE1*a*), transcription factor-6 (ATF6), and protein kinase RNA-like ER kinase (PERK) (Kimata et al., 2003).

On the IRE1*a* pathway, the phosphorylated IRE1 interacts with the TRAF2 (tumor necrosis factor receptor-associated factor-2), ultimately activating Jun amino-terminal kinase (JNK) (Urano et al., 2000). Given the connection between sustained JNK activity and cell death, activating JNK may link IRE1-mediated ER stress to cell death (Xia et al., 1995; Ventura et al., 2006). On the PERK pathway, PERK phosphorylates the eIF2 (eukaryotic translation initiation factor 2), which leads to the translation of the ATF4 (activating transcription factor 4). Therefore, the expression of ATF4's key downstream target, CHOP (C/EBP-homologous protein), is increased when eIF2α is phosphorylated by PERK (Ron and Walter, 2007). Studies involving depleted or overexpressed CHOP have proved that CHOP is involved in ER stress-induced apoptosis (Guo et al., 2012; Shen et al., 2014). CHOP can lead to the activation of NF-κB. The activated NF-κB enhances the production of interleukin-8 (IL-8) and then leads to intestinal dysfunction. In addition, CHOP can promote the macrophage infiltration and induce the production of reactive oxygen species (ROS) and interleukin-1β (IL-1β) (Tabas and Ron, 2011). Furthermore, CHOP can enhance the apoptosis of epithelial cells, goblet cells, Paneth cells and impair their secretion ability. These cells are more sensitive to inflammatory transmitters and bacterial products, which leads to the development of colitis (Ma et al., 2017).

In our following study, we verified that the total expression of Bip, IRE1*a*, ATF-6, CHOP, BAX, caspase 12, cleaved caspase3/9, and cytosolic Ca^{2+} concentration within host cells were elevated after WT and Δ*espF/pespF* infection but not after Δ*espF* infection. The phosphorylation profiles of pJNK/JNK, p-eIF2*a*/eIF2*a*, and pNF-κB/NF-κB were elevated after WT and Δ*espF/pespF* infection. Earlier studies demonstrated that EspF initiated the induction of the intrinsic apoptotic pathway by disrupting the mitochondrial membrane potential (MMP), which

released cytochrome *c* into the cytoplasm, thereby leading to caspase 9 cleavage (Nougayrede and Donnenberg, 2004). In the ER stress-induced apoptosis pathway, the excessive accumulation of misfolded proteins in the ER and disturbance in Ca^{2+} homeostasis induced caspase 12-mediated apoptosis, in which activated caspase 12 translocated from the ER into the cytosol to directly cleave caspase 9 and then activate caspase 3 (Chen et al., 2018). Our study proved that caspase 12, cleaved caspase 9, and cleaved caspase 3 levels were elevated in the presence of EspF, which indicated that the ER stress-dependent apoptosis pathway could also be activated within host cells.

Furthermore, we identified that the IRE1*a* pathway was activated after EspF infection.

Prolonged IRE1-mediated activation may promote apoptosis by degrading mRNAs encoding essential cell-survival proteins, including XBP-1. XBP-1 plays a crucial role in the highly secretory cells such as hepatocytes (Reimold et al., 2000), plasma cells (Iwakoshi et al., 2003), plasmacytoid dendritic cells (Lee et al., 2005), and pancreatic acinar cells (Iwakoshi et al., 2007). In addition, ER stress can cause a subsequent series of physiological changes within host cells, including autophagy and autophagic cell death. Hence, ER stress has been increasingly recognized to be both a secondary consequence of inflammation and neoplasia (Zhang and Kaufman, 2008) as well as a primary factor in causing inflammation and potentially cancer (Kaser et al., 2008). Whether the EspF protein participates in these subsequent reactions still needs further experiments to be clarified.

In summary, these results provided novel evidence that EspF activates the ER stress response and enhances cell death of HT-29 cells.

This study shows that the regulation of the UPR signal by EspF protein can promote endoplasmic reticulum stress-related death and enhance cell apoptosis. EHEC has the characteristics of poor prognosis for antibiotic treatment. The findings of this study may be an effective strategy that can be combined with current treatment options to improve the treatment effect of EHEC.

CONCLUSION

Based on the iTRAQ results and experiments described herein, we conclude that the EspF of Enterohemorrhagic *Escherichia coli* induced ER stress in intestinal epithelial cells, and the ER stress-dependent apoptosis pathway is activated within host cells.

DATA AVAILABILITY STATEMENT

The datasets presented in this study can be found in online repositories. The names of the repository/repositories and accession number(s) can be found below: Figshare – doi: 10.6084/m9.figshare.14933373.v1.

AUTHOR CONTRIBUTIONS

XW and CW designed the study. KY, MF, SL, and CF engaged in the acquisition and analysis of the data. HZ, LY, ZS, and DS participated in bioinformatics interpretation and following analysis. XW and DS drafted the manuscript. All authors had final approval of the version to be submitted.

FUNDING

This work was supported by the National Natural Science Foundation of China [Nos. 81902022 and 81972202]; Natural Science Foundation of Guangdong Province [No. 2018B030311063]; and Science and Technology Foundation of Shenzhen City [No. JCYJ20210324102814038].

ACKNOWLEDGMENTS

We would like to thank LetPub (www.letpub.com) for its linguistic assistance during the preparation of this manuscript.

SUPPLEMENTARY MATERIAL

The Supplementary Material for this article can be found online at: https://www.frontiersin.org/articles/10.3389/fmicb.2022.900919/full#supplementary-material

REFERENCES

Cao, S. S. (2015). Endoplasmic reticulum stress and unfolded protein response in inflammatory bowel disease. *Inflamm. Bowel Dis.* 21, 636–644.

Cao, S. S., and Kaufman, R. J. (2014). Endoplasmic reticulum stress and oxidative stress in cell fate decision and human disease. *Antioxidants Redox Signal.* 21, 396–413. doi: 10.1089/ars.2014.5851

Chen, Q., Kang, J., and Fu, C. (2018). The independence of and associations among apoptosis, autophagy, and necrosis. *Signal. Transduct. Target Ther.* 3:18. doi: 10.1038/s41392-018-0018-5

Cuevas, E. P., Eraso, P., Mazón, M. J., Santos, V., Moreno-Bueno, G., Cano, A., et al. (2017). LOXL2 drives epithelial-mesenchymal transition via activation of IRE1-XBP1 signalling pathway. *Sci. Rep.* 7:44988. doi: 10.1038/srep44988

Dana, R. C., Welch, W. J., and Deftos, L. J. (1990). Heat shock proteins bind calcitonin. *Endocrinology* 126, 672–674. doi: 10.1210/endo-126-1-672

Dean, P., Scott, J. A., Knox, A. A., Quitard, S., Watkins, N. J., and Kenny, B. (2010). The enteropathogenic *E. coli* effector EspF targets and disrupts the nucleolus by a process regulated by mitochondrial dysfunction. *PLoS Pathogens.* 6:e1000961. doi: 10.1371/journal.ppat.1000961

Deutsch, D. R., Fröhlich, T., Otte, K. A., Beck, A., Habermann, F. A., Wolf, E., et al. (2014). Stage-specific proteome signatures in early bovine embryo development. *J. Prot. Res.* 13, 4363–4376. doi: 10.1021/pr500550t

Evensen, N. A., Kuscu, C., Nguyen, H. L., Zarrabi, K., Dufour, A., Kadam, P., et al. (2013). Unraveling the role of KIAA1199, a novel endoplasmic reticulum protein, in cancer cell migration. *J. Natl. Cancer Inst.* 105, 1402–1416. doi: 10.1093/jnci/djt224

Fu, M., Liang, S., Wu, J., Hua, Y., Chen, H., Zhang, Z., et al. (2021). An *Escherichia coli* Effector Protein EspF May Induce Host DNA Damage via Interaction With SMC1. *Front. Microbiol.* 12:682064. doi: 10.3389/fmicb.2021.682064

Galperin, M. Y., Wolf, Y. I., Makarova, K. S., Vera Alvarez, R., Landsman, D., and Koonin, E. V. (2021). COG database update: focus on microbial diversity, model

organisms, and widespread pathogens. *Nucleic Acids Res.* 49, D274–D281. doi: 10.1093/nar/gkaa1018

Gaytan, M. O., Martinez-Santos, V. I., Soto, E., and Gonzalez-Pedrajo, B. (2016). Type Three Secretion System in Attaching and Effacing Pathogens. *Front. Cell. Infect. Microbiol.* 6:129. doi: 10.3389/fcimb.2016.00129

Gene Ontology Consortium (2021). The Gene Ontology resource: enriching a GOld mine. *Nucleic Acids Res.* 49, D325–D334. doi: 10.1093/nar/gkaa1113

Guo, F. J., Liu, Y., Zhou, J., Luo, S., Zhao, W., Li, X., et al. (2012). XBP1S protects cells from ER stress-induced apoptosis through Erk1/2 signaling pathway involving CHOP. *Histochem. Cell. Biol.* 138, 447–460.

Heiman, K. E., Mody, R. K., Johnson, S. D., Griffin, P. M., and Gould, L. H. (2015). *Escherichia coli* O157 Outbreaks in the United States, 2003-2012. *Emerg. Infect. Dis.* 21, 1293–1301.

Hodges, K., Alto, N. M., Ramaswamy, K., Dudeja, P. K., and Hecht, G. (2008). The enteropathogenic *Escherichia coli* effector protein EspF decreases sodium hydrogen exchanger 3 activity. *Cell. Microbiol.* 10, 1735–1745. doi: 10.1111/j.1462-5822.2008.01163.x

Holmes, A., Muhlen, S., Roe, A. J., and Dean, P. (2010). The EspF effector, a bacterial pathogen's Swiss army knife. *Infect. Immun.* 78, 4445–4453. doi: 10.1128/IAI.00635-10

Honish, L., Punja, N., Nunn, S., Nelson, D., Hislop, N., Gosselin, G., et al. (2017). *Escherichia coli* O157:H7 Infections Associated with Contaminated Pork Products - Alberta, Canada, July-October 2014. *Can. Commun. Dis. Rep.* 65, 1477–1481. doi: 10.14745/ccdr.v43i01a04

Hua, Y., Yan, K., and Wan, C. (2018). Clever Cooperation: Interactions Between EspF and Host Proteins. *Front. Microbiol.* 9:2831. doi: 10.3389/fmicb.2018.02831

Iwakoshi, N. N., Lee, A. H., Vallabhajosyula, P., Otipoby, K. L., Rajewsky, K., and Glimcher, L. H. (2003). Plasma cell differentiation and the unfolded protein response intersect at the transcription factor XBP-1. *Nat. Immunol.* 4, 321–329. doi: 10.1038/ni907

Iwakoshi, N. N., Pypaert, M., and Glimcher, L. H. (2007). The transcription factor XBP-1 is essential for the development and survival of dendritic cells. *J. Exp. Med.* 204, 2267–2275. doi: 10.1084/jem.20070525

Kanayama, A., Yahata, Y., Arima, Y., Takahashi, T., Saitoh, T., Kanou, K., et al. (2015). Enterohemorrhagic *Escherichia coli* outbreaks related to childcare facilities in Japan, 2010-2013. *BMC Infect. Dis.* 15:539. doi: 10.1186/s12879-015-1259-3

Kanehisa, M. (1997). A database for post-genome analysis. *Trends Gene.* 13, 375–376. doi: 10.1016/s0168-9525(97)01223-7

Kaser, A., Lee, A. H., Franke, A., Glickman, J. N., Zeissig, S., Tilg, H., et al. (2008). XBP1 links ER stress to intestinal inflammation and confers genetic risk for human inflammatory bowel disease. *Cell* 134, 743–756. doi: 10.1016/j.cell.2008.07.021

Kimata, Y., Kimata, Y. I., Shimizu, Y., Abe, H., Farcasanu, I. C., Takeuchi, M., et al. (2003). Genetic evidence for a role of BiP/Kar2 that regulates Ire1 in response to accumulation of unfolded proteins. *Mol. Biol. Cell.* 14, 2559–2569. doi: 10.1091/mbc.e02-11-0708

Lee, A. H., Chu, G. C., Iwakoshi, N. N., and Glimcher, L. H. (2005). XBP-1 is required for biogenesis of cellular secretory machinery of exocrine glands. *EMBO J.* 24, 4368–4380. doi: 10.1038/sj.emboj.7600903

Li, Y., Huang, T. Y., Ye, C., Chen, L., Liang, Y., Wang, K., et al. (2020). Formation and Control of the Viable but Non-culturable State of Foodborne Pathogen *Escherichia coli* O157:H7. *Front. Microbiol.* 11:1202. doi: 10.3389/fmicb.2020.01202

Ma, X., Dai, Z., Sun, K., Zhang, Y., Chen, J., Yang, Y., et al. (2017). Intestinal Epithelial Cell Endoplasmic Reticulum Stress and Inflammatory Bowel Disease Pathogenesis: An Update Review. *Front. Immunol.* 8:1271. doi: 10.3389/fimmu.2017.01271

Maddocks, O. D., Short, A. J., Donnenberg, M. S., Bader, S., and Harrison, D. J. (2009). Attaching and effacing *Escherichia coli* downregulate DNA mismatch repair protein *in vitro* and are associated with colorectal adenocarcinomas in humans. *PLoS One* 4:e5517. doi: 10.1371/journal.pone.0005517

Mayer, B. J. (2001). SH3 domains: complexity in moderation. *J. Cell Sci.* 114, 1253–1263. doi: 10.1242/jcs.114.7.1253

McNamara, B. P., Koutsouris, A., O'Connell, C. B., Nougayrede, J. P., Donnenberg, M. S., and Hecht, G. (2001). Translocated EspF protein from enteropathogenic *Escherichia coli* disrupts host intestinal barrier function. *J. Clin. Invest.* 107, 621–629. doi: 10.1172/JCI11138

Mertins, P., Udeshi, N. D., Clauser, K. R., Mani, D. R., Patel, J., Ong, S. E., et al. (2012). iTRAQ labeling is superior to mTRAQ for quantitative global proteomics and phosphoproteomics. *Mol. Cell Proteomics* 11:M111014423. doi: 10.1074/mcp.M111.014423

Nougayrede, J. P., and Donnenberg, M. S. (2004). Enteropathogenic *Escherichia coli* EspF is targeted to mitochondria and is required to initiate the mitochondrial death pathway. *Cell. Microbiol.* 6, 1097–1111. doi: 10.1111/j.1462-5822.2004.00421.x

Oka, O. B., Pringle, M. A., Schopp, I. M., Braakman, I., and Bulleid, N. J. (2013). ERdj5 is the ER reductase that catalyzes the removal of non-native disulfides and correct folding of the LDL receptor. *Mol. Cell.* 50, 793–804. doi: 10.1016/j.molcel.2013.05.014

Qadri, S. M., and Kayali, S. (1998). Enterohemorrhagic *Escherichia coli*. A dangerous food-borne pathogen. *Postgrad. Med.* 103, 179–180.

Reimold, A. M., Etkin, A., Clauss, I., Perkins, A., Friend, D. S., Zhang, J., et al. (2000). An essential role in liver development for transcription factor XBP-1. *Genes Dev.* 14, 152–157.

Ron, D., and Walter, P. (2007). Signal integration in the endoplasmic reticulum unfolded protein response. *Nat. Rev. Mol. Cell Biol.* 8, 519–529.

Shen, M., Wang, L., Yang, G., Gao, L., Wang, B., Guo, X., et al. (2014). Baicalin protects the cardiomyocytes from ER stress-induced apoptosis: inhibition of CHOP through induction of endothelial nitric oxide synthase. *PLoS One* 9:e88389. doi: 10.1371/journal.pone.0088389

Shilov, I. V., Seymour, S. L., Patel, A. A., Loboda, A., Tang, W. H., Keating, S. P., et al. (2007). The Paragon Algorithm, a next generation search engine that uses sequence temperature values and feature probabilities to identify peptides from tandem mass spectra. *Mol. Cell. Prot.* 6, 1638–1655. doi: 10.1074/mcp.T600050-MCP200

Smith, S. J., Kroon, J. T., Simon, W. J., Slabas, A. R., and Chivasa, S. A. (2015). Novel Function for Arabidopsis CYCLASE1 in Programmed Cell Death Revealed by Isobaric Tags for Relative and Absolute Quantitation (iTRAQ) Analysis of Extracellular Matrix Proteins. *Mol. Cell Prot.* 14, 1556–1568. doi: 10.1074/mcp.M114.045054

Spears, K. J., Roe, A. J., and Gally, D. L. (2006). A comparison of enteropathogenic and enterohaemorrhagic *Escherichia coli* pathogenesis. *FEMS Microbiol. Lett.* 255, 187–202. doi: 10.1111/j.1574-6968.2006.00119.x

Szklarczyk, D., Gable, A. L., Lyon, D., Junge, A., Wyder, S., Huerta-Cepas, J., et al. (2019). STRING v11: protein-protein association networks with increased coverage, supporting functional discovery in genome-wide experimental datasets. *Nucleic Acids Res.* 47, D607–D613. doi: 10.1093/nar/gky1131

Tabas, I., and Ron, D. (2011). Integrating the mechanisms of apoptosis induced by endoplasmic reticulum stress. *Nat. Cell Biol.* 13, 184–190. doi: 10.1038/ncb0311-184

Tapia, R., Kralicek, S. E., and Hecht, G. A. (2017). EPEC effector EspF promotes Crumbs3 endocytosis and disrupts epithelial cell polarity. *Cell. Microbiol.* 19:10.1111/cmi.12757. doi: 10.1111/cmi.12757

Urano, F., Wang, X., Bertolotti, A., Zhang, Y., Chung, P., Harding, H. P., et al. (2000). Coupling of stress in the ER to activation of JNK protein kinases by transmembrane protein kinase IRE1. *Science (New York, NY).* 287, 664–666. doi: 10.1126/science.287.5453.664

Ventura, J. J., Hübner, A., Zhang, C., Flavell, R. A., Shokat, K. M., and Davis, R. J. (2006). Chemical genetic analysis of the time course of signal transduction by JNK. *Mol Cell.* 21, 701–710. doi: 10.1016/j.molcel.2006.01.018

Wang, X., Du, Y., Hua, Y., Fu, M., Niu, C., Zhang, B., et al. (2017). The EspF N-Terminal of Enterohemorrhagic *Escherichia coli* O157:H7 EDL933w Imparts Stronger Toxicity Effects on HT-29 Cells than the C-Terminal. *Front. Cell. Infect. Microbiol.* 7:410. doi: 10.3389/fcimb.2017.00410

Wiese, S., Reidegeld, K. A., Meyer, H. E., and Warscheid, B. (2007). Protein labeling by iTRAQ: a new tool for quantitative mass spectrometry in proteome research. *Proteomics* 7, 340–350. doi: 10.1002/pmic.200600422

Xia, X., Liu, Y., Hodgson, A., Xu, D., Guo, W., Yu, H., et al. (2019). EspF is crucial for Citrobacter rodentium-induced tight junction disruption and

lethality in immunocompromised animals. *PLoS Pathog.* 15:e1007898. doi: 10.1371/journal.ppat.1007898

Xia, Z., Dickens, M., Raingeaud, J., Davis, R. J., and Greenberg, M. E. (1995). Opposing effects of ERK and JNK-p38 MAP kinases on apoptosis. *Science* 270, 1326–1331. doi: 10.1126/science.270.5240.1326

Yang, Q., Wang, S., Dai, E., Zhou, S., Liu, D., Liu, H., et al. (2019). Pathway enrichment analysis approach based on topological structure and updated annotation of pathway. *Brief Bioinform.* 20, 168–177. doi: 10.1093/bib/bbx091

Zhang, K., and Kaufman, R. J. (2008). From endoplasmic-reticulum stress to the inflammatory response. *Nature* 454, 455–462. doi: 10.1038/nature07203

Zhao, F., Wang, Y., An, H., Hao, Y., Hu, X., and Liao, X. (2016). New Insights into the Formation of Viable but Non-culturable *Escherichia coli* O157:H7 Induced by High-Pressure CO2. *mBio* 7, e00961–16.

Zhao, S., Zhou, Y., Wang, C., Yang, Y., Wu, X., Wei, Y., et al. (2013). The N-terminal domain of EspF induces host cell apoptosis after infection with enterohaemorrhagic *Escherichia coli* O157:H7. *PLoS One* 8:e55164. doi: 10.1371/journal.pone.0055164

Conflict of Interest: HZ was employed by the Genecreate Biological Engineering Co., Ltd.

The remaining authors declare that the research was conducted in the absence of any commercial or financial relationships that could be construed as a potential conflict of interest.

Publisher's Note: All claims expressed in this article are solely those of the authors and do not necessarily represent those of their affiliated organizations, or those of the publisher, the editors and the reviewers. Any product that may be evaluated in this article, or claim that may be made by its manufacturer, is not guaranteed or endorsed by the publisher.

frontiers | Frontiers in Microbiology

TYPE Original Research
PUBLISHED 22 November 2022
DOI 10.3389/fmicb.2022.1047259

OPEN ACCESS

EDITED BY
Shihua Wang,
Fujian Agriculture and Forestry University, China

REVIEWED BY
Lauren M. Lui,
Berkeley Lab (DOE), United States
Daniel Garza,
KU Leuven, Belgium

*CORRESPONDENCE
Hao Zhang
zhanghao@wnmc.edu.cn
Mingquan Ye
ymq@wnmc.edu.cn

SPECIALTY SECTION
This article was submitted to Infectious Agents and Disease, a section of the journal Frontiers in Microbiology

RECEIVED 23 September 2022
ACCEPTED 03 November 2022
PUBLISHED 22 November 2022

CITATION
Zhang Z, Chen G, Hussain W, Qin Z, Liu J, Su Y, Zhang H and Ye M (2022) Mr.Vc v2: An updated version of database with increased data of transcriptome and experimental validated interactions.
Front. Microbiol. 13:1047259.
doi: 10.3389/fmicb.2022.1047259

Mr.Vc v2: An updated version of database with increased data of transcriptome and experimental validated interactions

Zhiyuan Zhang[1,2], Guozhong Chen[3], Wajid Hussain[4], Zixin Qin[3], Juntong Liu[1,2], Yang Su[1,2], Hao Zhang[1]*and Mingquan Ye[1,2]*

[1]School of Medical Information, Wannan Medical College, Wuhu, China, [2]Research Center of Health Big Data Mining and Applications, Wannan Medical College, Wuhu, China, [3]College of Life Sciences and Technology, Huazhong University of Science and Technology, Wuhan, China, [4]Advanced Biomaterials and Tissue Engineering Center, College of Life Sciences and Technology, Huazhong University of Science and Technology, Wuhan, China

Mr.Vc is a database of curated *Vibrio cholerae* transcriptome data and annotated information. The main objective is to facilitate the accessibility and reusability of the rapidly growing *Vibrio cholerae* omics data and relevant annotation. To achieve these goals, we performed manual curation on the transcriptome data and organized the datasets in an experiment-centric manner. We collected unknown operons annotated through text-mining analysis that would provide more clues about how *Vibrio cholerae* modulates gene regulation. Meanwhile, to understand the relationship between genes or experiments, we performed gene co-expression analysis and experiment-experiment correlation analysis. In additional, functional module named "Interactions" which dedicates to collecting experimentally validated interactions about *Vibrio cholerae* from public databases, MEDLINE documents and literature in life science journals. To date, Mr.Vc v2, which is significantly increased from the previous version, contains 107 microarray experiments, 106 RNA-seq experiments, and 3 Tn-seq projects, covering 56,839 entries of DEGs (Differentially Expressed Genes) from transcriptomes and 7,463 related genes from Tn-seq, respectively. and a total of 270,129 gene co-expression entries and 11,990 entries of experiment-experiment correlation was obtained, in total 1,316 entries of interactions were collected, including 496 protein-chemical signaling molecule interactions, 472 protein–protein interactions, 306 TF (Transcription Factor)-gene interactions and 42 *Vibrio cholerae*-virus interactions, most of which obtained from 402 literature through text-mining analysis. To make the information easier to access, Mr.Vc v2 is equipped with a search widget, enabling users to query what they are interested in. Mr.Vc v2 is freely available at http://mrvcv2.biownmc.info.

KEYWORDS

update, interactions, transcriptome, text-mining, Top 5% DEG, *Vibrio cholerae*

Introduction

Cholera is a notorious and devastating diarrheal disease, until now had caused seven epidemics in history globally and is still endemic in many parts of the world, especially developing countries like Asia, South America, and Africa (Faruque et al., 1998; Liu et al., 2008; Xia et al., 2017).

Vibrio cholerae is the causative agent of cholera resulting in 23,000 to 143,000 people dying worldwide annually (Qin et al., 2020). However, the pathogenesis of *Vibrio cholerae* is still unclear. Growing evidence suggests that *Vibrio cholerae* can rapidly modulate its gene transcriptional expression in response to the switches of different environments for better survival and infection. Therefore, studying the gene expression profile of *Vibrio cholerae* under various conditions is important to fully expose and understand the genetic mechanism of *Vibrio cholerae*.

In recent years, the transcriptional sequencing is powerful enough to study general gene expression profiles, sequencing of *Vibrio cholerae* transcriptomes rapidly increased the number and total volume of *Vibrio cholerae* transcriptome data. At present, most of the raw sequencing data has been deposited into several general-purpose databases, such as European Nucleotide Archive (ENA) (Amid et al., 2020)[1] and NCBI Sequence Read Archive (SRA) (Kodama et al., 2012).[2] In addition, several other public resources, including MicrobesOnline (Dehal et al., 2010), PubMLST (Jolley et al., 2018), BioCyc (Paley and Karp, 2017), and PATRIC (Wattam et al., 2014), collected the processed transcriptome data, microbial genome and metabolic pathway information and then organized them according to experimental conditions and organisms for the purposes to greatly promote data reuse. However, obstacles to the reusability and accessibility of the rapidly growing *Vibrio cholerae* transcriptome data remain, especially the inaccurate data sets and/or incomplete data. For example, MicrobesOnline, which integrated vast amounts of microbial genetic information, did not update transcriptome data since 2012 and only collected 42 high-throughput *Vibrio cholerae* microarray data, not collecting RNA-seq data, under different experimental conditions, deriving from seven published papers. Additionally, MicrobesOnline did not compute *p*-values in differential gene expression analysis due to lacking technical/biological replicates. PubMLST, which integrated population sequence data with provenance and phenotype information for over 100 different microbial species and genera, focus on the analysis of molecular typing and microbial genome diversity, and did not collect microbial transcriptome data, including *Vibrio cholerae*. BioCyc, a database for collection of the genome and metabolic pathways of organisms, provided annotations, essentiality and reactions of gene or protein, however, transcriptome data were not considered for collection in BioCyc.

Although identified DEGs from transcriptome data are useful to discover novel genes for phenotypes, obtaining a comprehensive regulatory network is meaningful (Saint-André, 2021). To date, several databases, including STRING (Szklarczyk et al., 2021), CollecTF (Kiliç et al., 2014), STITCH (Szklarczyk et al., 2016), and MVP (Gao et al., 2018), had provided data of protein–protein, TF (Tanscription Factor)-gene, protein-chemical signaling molecule, and *Vibrio cholerae*–virus interactions. These data will better help to understand *Vibrio cholerae* and useful for researchers to work on *Vibrio cholerae*. However, some interaction data presented in databases were obtained through prediction rather than experimental verification, which cannot ensure the data quality.

In 2019, we introduced Mr.Vc v1 as an online database of curated microarray and RNA-seq of *Vibrio cholerae* to facilitate the reusability and accessibility of the rapidly increasing *Vibrio cholerae* omics data and relevant annotation (Zhang et al., 2019). We collected data from 145 high-throughput gene expression experiments of *Vibrio cholerae* from 49 journal articles and the detailed annotation for 3,834 genes of *Vibrio cholerae* (*Vibrio cholerae O1 biovar eltor str. N16961*), we also collected relevant information including which operons they may belong to and possible interaction partners of their protein products. Mr.Vc is the first comprehensive data repository dedicated to *Vibrio cholerae* and could provide convenience for all researchers in related fields.

In current study, we are going to introduce an updated version of Mr.Vc. In this new version, we extended more annotation information, such as operon annotation through text-mining analysis, collected more transcriptome projects, samples, experiments, and performed extensive analysis, including differential gene expression analysis, operon member expression visualization, gene co-expression analysis, and experiment-experiment correlation analysis. Most importantly, we added an "Interactions" functional module in Mr.Vc v2, which listed collected experimentally validated interaction entries about *Vibrio cholerae*. We obtained them from public databases including STRING, STITCH, CollecTF, MVP, literature-describing interactions referring to *Vibrio cholerae*, and text-mining results from MEDLINE documents and literature in life science journals. Additionally, we manually categorized these interaction data into four interaction types, including protein-chemical signaling molecule interaction, protein–protein interaction, TF (Transcription Factor)-gene interaction, and *Vibrio cholerae*-virus interaction. These interaction data will provide us with more clues into the regulatory network and mechanism in *Vibrio cholerae* (Kathuria and Chattopadhyay, 2018). Mr.Vc v2 is equipped with a search widget, allowing experimental biologists and medical scientists to quick and easy finding what they are interested.

Materials and methods

Data collection and pre-processing

To give users a clear overview of the data collection, pre-processing, and integration in Mr.Vc v2, we provided the detailed workflow (Figure 1).

For data collection, as shown in Figure 1A, we searched recently updated RNA-seq projects in the NCBI BioProject

1 https://www.ebi.ac.uk/ena

2 https://www.ncbi.nlm.nih.gov/sra

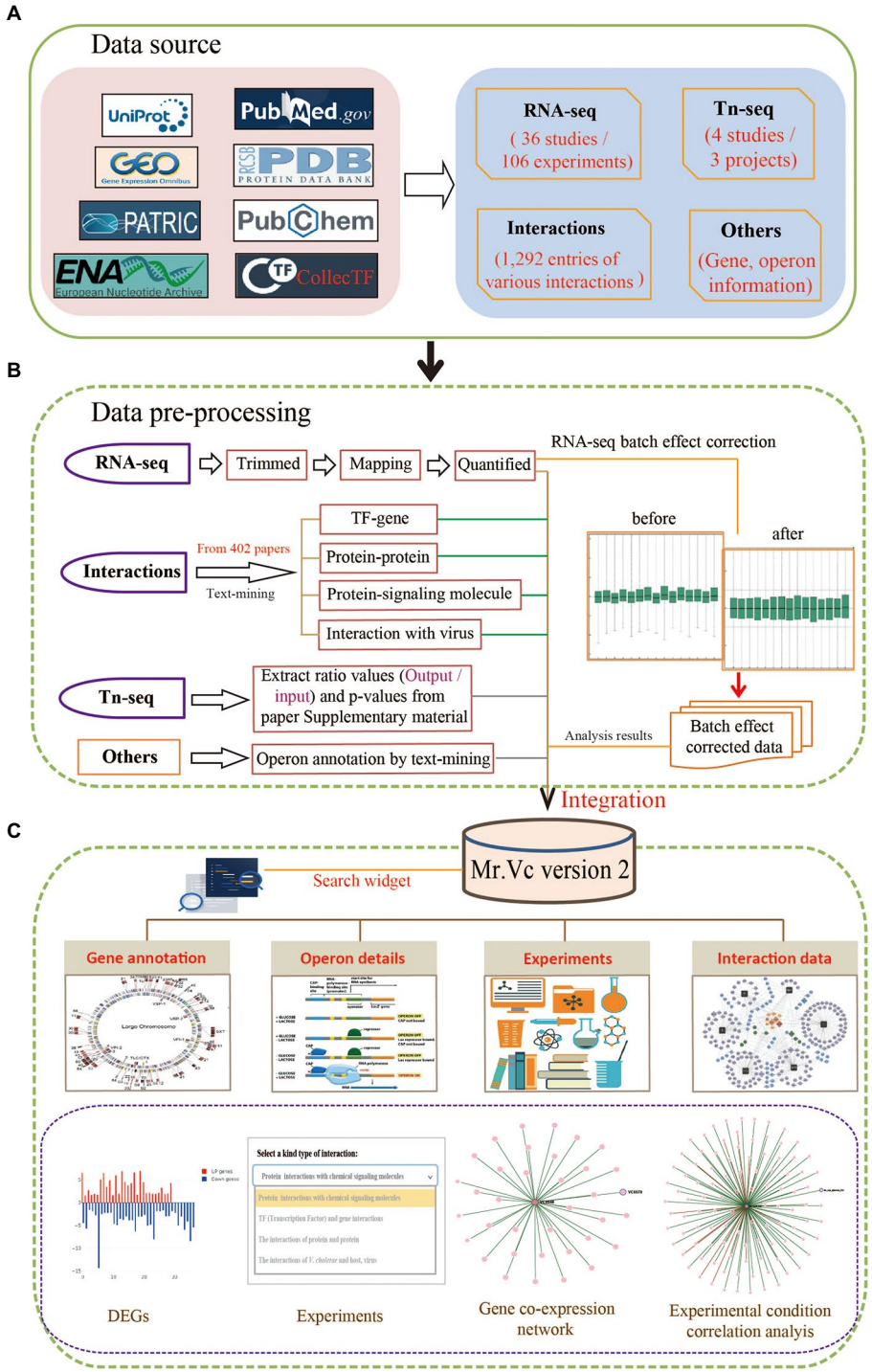

FIGURE 1
Overview of Mr.Vc v2. **(A)** The data source. All data including the raw sequencing data, information on genomic annotation, literature, Tn-seq data, and experimentally validated interactions were collected from public databases, such as NCBI GEO, ENA, PATRIC, Uniprot, collecTF, PDB, PubMed, and so on. **(B)** The data pre-processing. The RNA-seq raw data perform quality control, mapping, transcript quantification, and normalization to obtain high-quality data for further analysis. The resulting operon and interaction data were obtained from MEDLINE documents and literature in life science journals through text-mining analysis. The Tn-seq data were directly extracted from supplemental materials of literature. **(C)** The data integration. Mr.Vc v2 integrated polytype data, which was placed in the "Genes," "Operons," "Experiments," and "Interactions" pages and provided a search widget.

database[3] and publications in NCBI PubMed[4] using "*Vibrio cholerae*" as the keyword. Projects with public raw sequencing data, 106 RNA-seq datasets were collected for further analysis. The raw sequencing reads were downloaded from EBI ENA (European Nucleotide Archive,[5]) and NCBI SRA (Sequence Read Archive,[6]) using command line tools from enaBrowserTools[7] and SRA-Tools[8] facilitated by Aspera (a high-speed data transfer tool). As the related meta-data of corresponding experiments, projects and literature were obtained from NCBI PubMed and GEO databases.

For the processing of raw sequencing reads, we used FastQC[9] to evaluate the overall quality of the downloaded data, followed by the Trim_galore to remove sequencing vectors and low-quality bases (Utturkar et al., 2020). Salmon is the latest computational algorithm for transcript quantification from RNA-seq data that could make the expression data compared across experiments and projects (Patro et al., 2017). In this study, we performed transcript quantification using Salmon, which adopted TPM (Transcript Per Million) for normalization, a better unit for RNA abundance than RPKM and FPKM since it respects the invariance property and is proportional to the average relative RNA molar concentration (Zhao et al., 2020). We searched Tn-seq projects in the NCBI PubMed database and downloaded corresponding supplemental materials of literature. These data included experiment details and the ratio value of output/input.

We performed text-mining analysis for *Vibrio cholerae* operon annotation using a customized Python pipeline by searching for functional descriptions of operon member genes (e.g., gene symbol, locus ID, common name, and aliases) in the titles and abstracts of MEDILNE documents and literature in life science journals available from the NCBI PubMed database. Additionally, for each operon, we visualized the expression profile of its member genes using TPM (Transcript Per Million) values in 110 different experiments. For example, operon "OP437" is involved in the function of bacterial motility, whose member genes expression trends were intuitively observed through visualization[10] that could help us deduce a positive or negative regulatory relationship between genes.

In addition, we also had a special focus on experimentally validated interactions about *Vibrio cholerae* in this study. We retrieved related interaction entries by following steps: (1) searching for literature with the keyword: "*Vibrio cholerae*"; (2) Filtering sentence from literature, and one sentence containing two of these: *Vibrio cholerae* gene name, chemical molecule name, and virus name. (3) This sentence should also contain one of the following words/phrases: *interaction, altered, associated, caused, confer, contribute, association, downregulate, elevate, implicated, increase, induce, influence, interact, involved, lead to, link, mediate, modulate, overexpressed, reduce, regulate, related, relationship, treat, binding, environmental signals, target, pathogenic, pathogenesis, progression, and transcriptional regulation.* (4) Extracting these sentences from literature as supporting evidence and finally identified 1,316 entries of different interaction types from 402 literature shown in (Table 1), including (1) a total 472 protein–protein interactions, all of which were experimentally validated; (2) 496 protein-chemical signaling molecule interactions that included protein information extracted from Uniprot and details of chemical molecule extracted from PubChem (Kim et al., 2021) and PDB database (Burley et al., 2017); (3) 306 TF-gene interactions, most of which obtained from collecTF database; (4) 42 *Vibrio cholerae* -virus interactions, including 30 entries extracted from literature and 13 from MVP database.

Data analyses

We analyzed transcriptome data and out of a total 106 RNA-seq experiments, 318 samples, in which the expression abundances were normalized as TPM values. For RNA-seq experiments, we used a cutoff of $|\log2\ FC| > 1.5$ (FC, fold change) and p-value <0.05 to define differentially expressed genes between experiments. The 33,180 differentially expressed gene entries were extracted, representing *Vibrio cholerae* gene expression under 106 different experimental conditions. We performed gene co-expression analysis and experiment-experiment correlation analysis using an in-house Python script to calculate pearson's correlation coefficients, spearman's correlation coefficients, and p-value between genes and between experiments, separately.

TABLE 1 Data summary in Mr.Vc v2 database.

Mr.Vc	Version 1	Version 2
Genes	3,834	3,998
Well-annotated operons	415	600
Literature	49	402
Transcriptome experiment	145	213
DEGs	25,937	56,839
Tn-seq projects	0	3
Top 5% differentially expressed genes	0	161
Experimentally validated interactions	0	1,316
Gene co-expression entries	0	270,129
Entries of experiment-experiment correlation	0	11,990
Text-mining analysis	No	Yes
Data visualization	No	Yes

3 https://www.ncbi.nlm.nih.gov/bioproject
4 https://pubmed.ncbi.nlm.nih.gov/
5 https://www.ebi.ac.uk/ena
6 https://www.ncbi.nlm.nih.gov/sra
7 https://github.com/enasequence/enaBrowserTools
8 https://ncbi.github.io/sra-tools/
9 http://www.bioinformatics.babraham.ac.uk/projects/fastqc/
10 http://mrvcv2.biownmc.info/operons/OP437

Pearson's correlation coefficient have a greater statistical power than spearman's coefficients, however which requires that the statistical data should conform to normal distribution. Transcriptome data tend to conform to negative binomial distribution, causing poor reliability of pearson's correlation coefficient analysis. And if using spearman's coefficients, the statistical power is not good. So we provided both spearman's coefficients and pearson's correlation coefficients for complementation on Mr.Vc v2 database. We used a cutoff of pearson or spearman >0.8 and *p*-value <0.05 to filter data of correlation, 270,129 gene–gene correlation entries and 11,990 experiment-experiment correlation entries were obtained. In order to make more comprehensive use of these two coefficients of correlation, we calculated their average value for users' reference. In addition, we calculated the *p*-values using pearson's and spearman's coefficients, respectively, and then compared the calculated *p*-value, finally outputted the larger *p*-value (< 0.05) to page.

Propose of "Top 5% differentially expressed gene" hypothesis

During the analysis of *Vibrio cholerae* transcriptome data, we found that some genes tended to be differentially expressed in most experiments. These observations indicated multiple functions of genes. To seek out these potential genes and their biological significance, we proposed a hypothesis that 5% of genes in bacteria are active in most conditions, which defined as "Top 5% differentially expressed gene." We calculated the numbers of the experimental condition of each gene when differentially expressed in experiments, and ranked the corresponding gene by the calculated number of experimental conditions. Then, we calculated the number of "Top 5% differentially expressed gene" in *Vibrio cholerae* that used the product of 0.05 and numbers of gene except for essential genes, which is stable in gene expression and less biological significance, in total obtained 161 genes. Finally, according to the ranking result, we regarded the top 161 genes as "Top 5% differentially expressed gene." For more details of "Top 5% differentially expressed gene," please go to "Help" page.[11]

Database design and implementation

Mr.Vc v2 was designed as a relational database. All data were loaded into a MySQL database. The frontend of the website was coded using JavaScript and HTML, while the backend was coded using PHP with a Slim framework to support queries to the MySQL database and provide representational state transfer (REST) application programming interfaces (APIs) for programmable access to our data. The AngularJS framework was used to bride the front- and back-ends. Echarts.js and plotly.js used for visualizations at the front end. The website hosted on an Apache server.

Results and discussion

Overview of Mr.Vc v2

In Mr.Vc v2, we updated gene and operon annotation information, including 3,842 protein-coding genes, 98 tRNAs, 16 rRNA, 42 pseudo genes, 161 Top 5% differentially expressed genes, and 600 well-annotated operons. We also provided external links to public databases such as KEGG (Kanehisa et al., 2017), NCBI Entrez Gene,[12] OGEE (Cao et al., 2019), Uniprot (UniProt, Consortium, 2021) and MicrobesOnline to allow users to explore in more details of these genes and operons;

We analyzed 106 RNA-seq datasets and performed differentially expressed gene analysis, experiment-experiment correlation analysis, and gene co-expression analysis, in total obtaining 33,180 DEGs, 11,990 entries of experiment-experiment correlation, and 270,129 entries of gene co-expression. In addition, Mr.Vc v2 added 3 Tn-seq projects and 1,316 entries of experimentally validated interaction through public databases and text-mining analysis, including protein–protein interaction, protein-chemical signaling molecule interaction, TF-gene interaction, and *Vibrio cholerae*-virus interaction. All data shown in Table 1.

Top 5% differentially expressed genes shared by experiments

We found that experiments collected in our database shared some differentially expressed genes with other experiments, which suggested these genes might play an important role in multiple phenotypes. Therefore, the concept of "Top 5% differentially expressed gene" was proposed and according to the hypothesis, we ranked differentially expressed genes in 213 experiments based on the frequency of the gene's appearance, in total obtaining 161 Top 5% differentially expressed genes (Figure 2). For example, Top 5% differentially expressed gene VCA1028, an outer membrane protein, was differentially expressed in 67 experiments (~31% of all), including gene deletion background, stress, nutritional condition, and human infection experiment. These data indicated this gene might be involved in several signaling pathways and functions. A previous study reported that VCA1028 was associated with virulence and indirectly regulated by ToxT (Thomson et al., 2015). However, there was no research to discuss its relationship with nutrition and stress. Therefore, the appearance of a "Top 5% differentially expressed gene" could remind researchers of its multi-function.

11 http://mrvcv2.biownmc.info/help/

12 https://www.ncbi.nlm.nih.gov/gene/

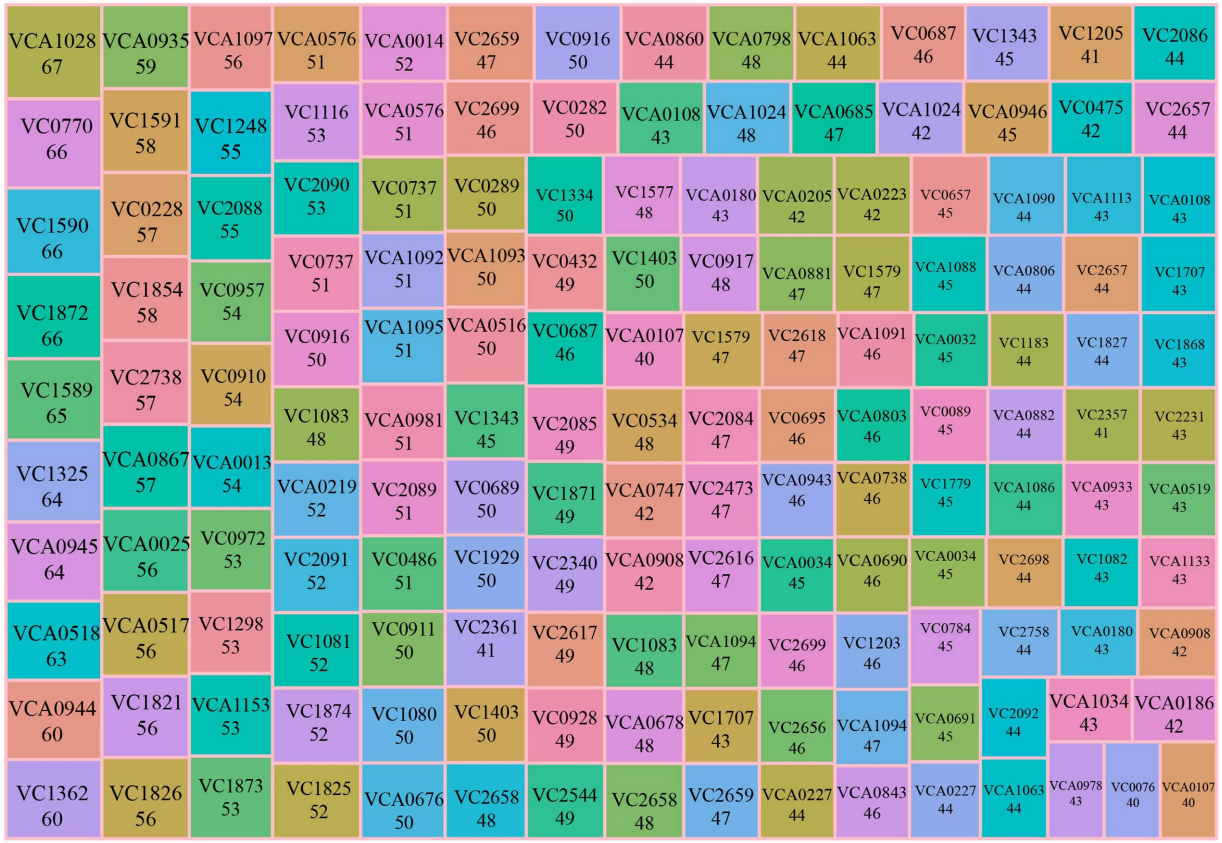

FIGURE 2
Summary of Top 5% differentially expressed genes. The treemap plot summarizes Top 5% differentially expressed genes. The number below the gene name is the number of experimental conditions that the gene was found to be differentially expressed, including up- and down-regulated. Mr.Vc v2 calculates the numbers of the experimental condition of each gene when differentially expressed in experiments, and ranks the corresponding gene by the calculated number of experimental conditions. A total of 161 Top 5% differentially expressed genes were obtained, according to ranking analysis. The Top 5% differentially expressed gene of the last rank was differentially expressed in 40 experimental conditions.

Case study

In *Vibrio cholerae*, *toxT* and *tcpN* used to refer to the same gene (VC0838). In order to make users pain-free for these synonyms, we added "Aliases" data for genes.[13] The *Vibrio cholerae toxT* gene (VC0838) was took as an example to represent how to use Mr.Vc v2 database for extraction of related information. The users have the access to five pages including "Genes," "Operons," "Experiments," "Interactions" and "Download." On the Mr.Vr v2 database functions, an additional page for instructions and a home page. On the "Genes" page, all gene records were listed, according to their gene locus. Users can find the individual gene information, including gene ID, description, gene location, gene orientation, gene length, and gene essentiality (Figure 3A). In addition, users can click the "VC0838" link to redirect to detailed gene information, which includes a list of DEGs in experimental conditions collected in the database (Figure 3C), and the gene co-expression network (Figure 3B). We found that *toxT* is differentially expressed in 28 experiments, which are mainly related to hosting infection and oxidative stress, up-regulated in 9 experiments, and down-regulated in 19 experiments. Additionally, the gene co-expression network suggested that *toxT* is involved in cholera pathogenesis. These observations were consistent with previous findings that ToxT is a transcriptional activator to regulate virulence factors (Baranova et al., 2020; Stone and Withey, 2021).

On the "Operons" page, users can directly search VC0838 to find the corresponding operon, where a table used to provide a summary report, including the Operon ID, and putative operon function. Users can expand the table by clicking the '+' sign before the "Operon ID" to view information on its member genes (Figure 3D).

The "Experiments" page summarized information on 3 Tn-seq projects and 213 transcriptome experiments, including a brief summary of experimental conditions, DEGs (Differentially Expressed Genes), and corresponding reference(s). If users want to know in which experiments VC0838 is differentially expressed, Searching on "Genes" page is a better choice, because "Experiments" page does not provide the summary report in a gene-centric manner.

13 http://mrvcv2.biownmc.info/genes/

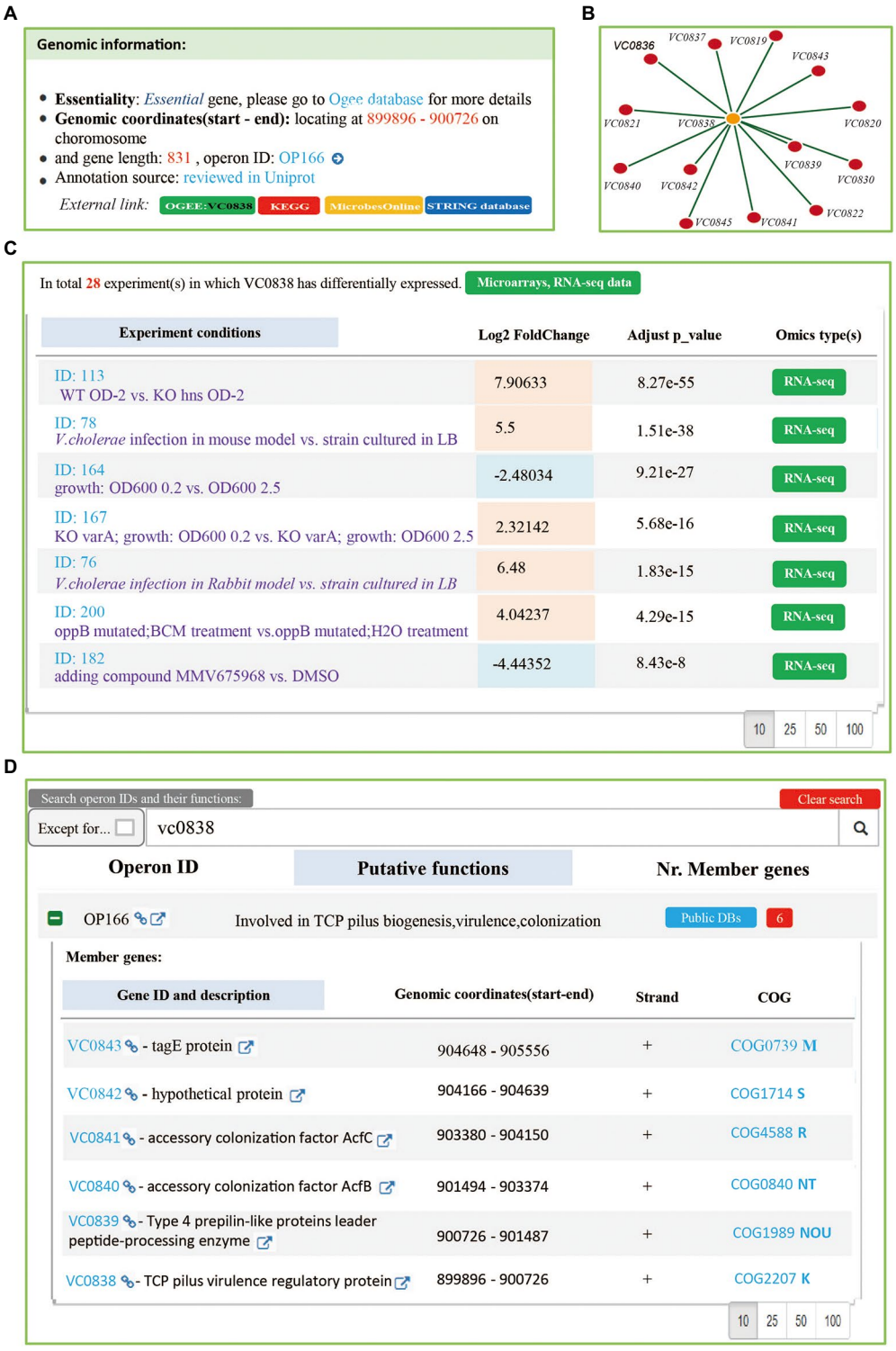

FIGURE 3
The "Genes and "Operons" page. **(A)** A summary of *Vibrio cholerae* gene VC0838. The information of gene annotation including gene ID, description, gene location, gene orientation, gene length, and gene essentiality was provided. **(B)** The gene co-expression network. Mr.Vc v2 filtered and obtained gene co-expression entries, according to the calculated pearson's correlation coefficients (>0.8), Spearman's correlation coefficients (>0.8), and *p*-value (<0.05) between genes. There are 14 genes associated with gene VC0838 in our database. **(C)** A list of experiments in which gene VC0838 is differentially expressed in. A total of 28 experiments were collected, including Microarray and RNA-seq experiments. **(D)** The operon information. Searching genes to match to corresponding operon page, which listed putative function and member genes information of operon.

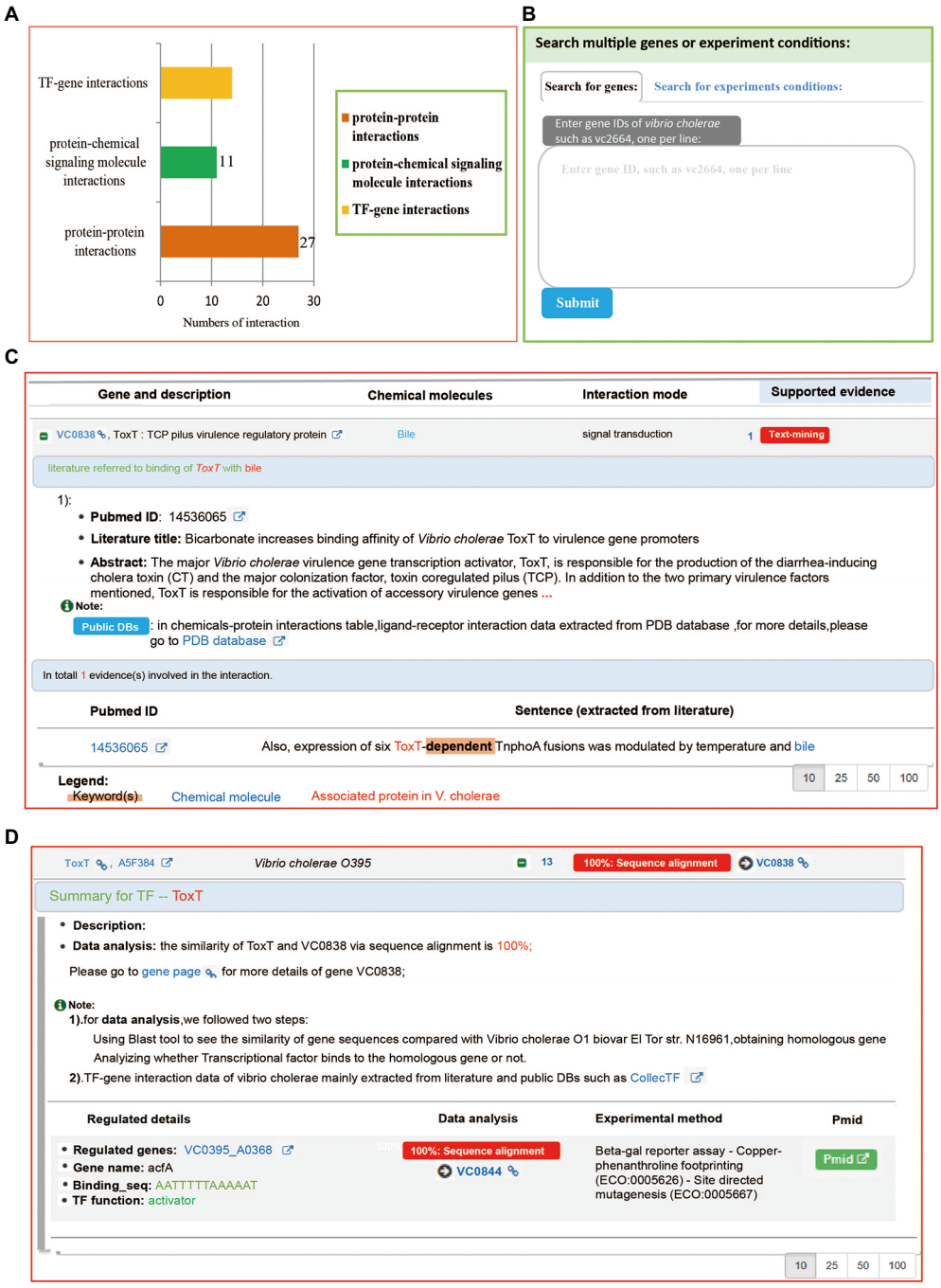

FIGURE 4
The "Experiments" page. **(A)** A barplot summarizing the interaction data associated with gene VC0803. The Y-axis represents interaction types, and the *X*-axis denotes the number of interactions. **(B)** The search function of the "Interactions" page. Two kinds of search methods: "Search by gene" and "Search by experiment conditions" were provided, allowing users to search what they are interested in. The search results are listed and visualized in an interactive network. **(C)** The protein-chemical signaling molecule interaction. The "VC0838-bile interaction" entry was supported by a sentence extracted from the literature. **(D)** The TF-gene interaction. Users can obtain regulated details they are interested in, including regulated genes, the binding site of transcription factors, and genes.

On the "Interactions" page, all interaction records categorized into four groups according to their interaction type, including protein-chemical signaling molecule interaction, protein–protein interaction, TF (Transcription Factor)-gene interaction, and *Vibrio cholerae*-virus interaction. Users can obtain data of experiment-validated interaction with VC0838. We found that a total 51 interaction records are associated with VC0838, including 27 protein–protein interactions, 11 protein-chemical signaling molecule interactions, and 13 TF-gene interactions (Figure 4A).

Regarding details of protein–protein and protein-chemical signaling molecule interactions, Mr.Vc v2 provided reference(s), sentence(s) describing interaction, and keyword(s) extracted from the sentence (Figure 4C). For TF-gene interaction details, a summary was provided that included information on transcription factor function, regulated genes, binding sequence, and experiment method (Figure 4D). Additionally, a search widget was integrated, users can search genes or experimental conditions that they are interested in (Figure 4B), to obtain gene co-expression or experiment-experiment correlation network.

In addition to the above pages, on the "Download" page, all data in Mr.Vc v2 are downloadable as excel files at the "Downloads" page. Users can click the corresponding file name to download the data tables.

Conclusion

In this study, we introduced Mr.Vc v2, an updated version of the online database of curated omics data and annotation information. Updates since the last version include increased numbers of RNA-seq experiments/samples, experimental validated interactions, and results of data analysis. So far, Mr.Vc v2 includes 3,998 genes, 2,366 operons, 213 transcriptome experiments, 3 Tn-seq projects, and 1,316 entries of experimentally validated interaction. Additionally, through data analysis, Mr.Vc v2 obtained 56,739 DEGs, 270,129 entries of gene co-expression, and 11,990 entries of experiment-experiment correlation. We believe that Mr.Vc v2 is expected to be a highly useful and important database for biologists and bioinformaticians studying *Vibrio cholerae*. In the future, we aim to update Mr.Vc v2 regularly to provide up-to-date content and include more functionalities.

Data availability statement

Publicly available datasets were analyzed in this study. This data can be found here: http://mrvcv2.biownmc.info/download/.

Author contributions

ZZ, MY, and HZ designed the study. ZZ and GC collected the data. ZZ analyzed the data prepared and the first draft. WH reviewed and edited the final draft. All authors approved the final submission.

Funding

This work was supported by the National Natural Science Foundation of China (61672386), the Academic Support Project for Top-notch Talents in Disciplines (Majors) of Universities in Anhui Province (gxbjZD2022042), and the Key Research and Development Plan of Anhui Province, China (2022a05020011).

Acknowledgments

We greatly thank Zhi Liu (Huazhong University of S&T) and Wei-hua Chen (Huazhong University of S&T) for critical review of the manuscript. We also greatly thank Mengxuan Xia (Huazhong University of S&T) for advice of database construction.

Conflict of interest

The authors declare that the research was conducted in the absence of any commercial or financial relationships that could be construed as a potential conflict of interest.

Publisher's note

References

Amid, C., Alako, B. T. F., Kadhirvelu, V. B., Burdett, T., Burgin, J., Fan, J., et al. (2020). The European nucleotide archive in 2019. *Nucleic Acids Res.* 48, D70–D76. doi: 10.1093/nar/gkz1063

Baranova, D. E., Willsey, G. G., Levinson, K. J., Smith, C., Wade, J., and Mantis, N. J. (2020). Transcriptional profiling of vibrio cholerae O1 following exposure to human anti- lipopolysaccharide monoclonal antibodies. *Pathog. Dis.* 78:ftaa 029. doi: 10.1093/femspd/ftaa029

Burley, S. K., Berman, H. M., Kleywegt, G. J., Markley, J. L., Nakamura, H., and Velankar, S. (2017). Protein data Bank (PDB): the single global macromolecular structure archive. *Methods Mol. Biol.* 1607, 627–641. doi: 10.1007/978-1-4939-7000-1_26

Cao, H., Ma, Q., Chen, X., and Xu, Y. (2019). DOOR: a prokaryotic operon database for genome analyses and functional inference. *Brief. Bioinform.* 20, 1568–1577. doi: 10.1093/bib/bbx088

Dehal, P. S., Joachimiak, M. P., Price, M. N., Bates, J. T., Baumohl, J. K., Chivian, D., et al. (2010). MicrobesOnline: an integrated portal for comparative and functional genomics. *Nucleic Acids Res.* 38, D396–D400. doi: 10.1093/nar/gkp919

Faruque, S. M., Albert, M. J., and Mekalanos, J. J. (1998). Epidemiology, genetics, and ecology of toxigenic vibrio cholerae. *Microbiol. Mol. Biol. Rev.* 62, 1301–1314. doi: 10.1128/MMBR.62.4.1301-1314.1998

Gao, N. L., Zhang, C., Zhang, Z., Hu, S., Lercher, M. J., Zhao, X.-M., et al. (2018). MVP: a microbe-phage interaction database. *Nucleic Acids Res.* 46, D700–D707. doi: 10.1093/nar/gkx1124

Jolley, K. A., Bray, J. E., and Maiden, M. C. J. (2018). Open-access bacterial population genomics: BIGSdb software, the PubMLST.org website and their applications. *Wellcome Open Res.* 3:124. doi: 10.12688/wellcomeopenres.14826.1

Kanehisa, M., Furumichi, M., Tanabe, M., Sato, Y., and Morishima, K. (2017). KEGG: new perspectives on genomes, pathways, diseases and drugs. *Nucleic Acids Res.* 45, D353–D361. doi: 10.1093/nar/gkw1092

Kathuria, R., and Chattopadhyay, K. (2018). Vibrio cholerae cytolysin: multiple facets of the membrane interaction mechanism of a β-barrel pore-forming toxin. *IUBMB Life* 70, 260–266. doi: 10.1002/iub.1725

Kiliç, S., White, E. R., Sagitova, D. M., Cornish, J. P., and Erill, I. (2014). Collec TF: a database of experimentally validated transcription factor-binding sites in bacteria. *Nucleic Acids Res.* 42, D156–D160. doi: 10.1093/nar/gkt1123

Kim, S., Chen, J., Cheng, T., Gindulyte, A., He, J., He, S., et al. (2021). PubChem in 2021: new data content and improved web interfaces. *Nucleic Acids Res.* 49, D1388–D1395. doi: 10.1093/nar/gkaa971

Kodama, Y., Shumway, M., and Leinonen, R. (2012). International nucleotide sequence database collaboration. The sequence read archive: explosive growth of sequencing data. *Nucleic Acids Res.* 40, D54–D56. doi: 10.1093/nar/gkr854

Liu, Z., Miyashiro, T., Tsou, A., Hsiao, A., Goulian, M., and Zhu, J. (2008). Mucosal penetration primes vibrio cholerae for host colonization by repressing quorum sensing. *Proc. Natl. Acad. Sci. U. S. A.* 105, 9769–9774. doi: 10.1073/pnas.0802241105

Paley, S., and Karp, P. D. (2017). Update notifications for the BioCyc collection of databases. *Database (Oxford)* 2017:bax086. doi: 10.1093/database/bax086

Patro, R., Duggal, G., Love, M. I., Irizarry, R. A., and Kingsford, C. (2017). Salmon provides fast and bias-aware quantification of transcript expression. *Nat. Methods* 14, 417–419. doi: 10.1038/nmeth.4197

Qin, Z., Yang, X., Chen, G., Park, C., and Liu, Z. (2020). Crosstalks between gut microbiota and vibrio Cholerae. *Front. Cell. Infect. Microbiol.* 10:582554. doi: 10.3389/fcimb.2020.582554

Saint-André, V. (2021). Computational biology approaches for mapping transcriptional regulatory networks. *Comput. Struct. Biotechnol. J.* 19, 4884–4895. doi: 10.1016/j.csbj.2021.08.028

Stone, J. B., and Withey, J. H. (2021). H-NS and ToxT inversely control cholera toxin production by binding to overlapping DNA sequences. *J. Bacteriol.* 203:e0018721. doi: 10.1128/JB.00187-21

Szklarczyk, D., Gable, A. L., Nastou, K. C., Gable, A. L., Nastou, K. C., Lyon, D., et al. (2021). The STRING database in 2021: customizable protein-protein networks, and functional characterization of user-uploaded gene/measurement sets. *Nucleic Acids Res.* 49, D605–D612. doi: 10.1093/nar/gkaa1074

Szklarczyk, D., Santos, A., Von Mering, C., Jensen, L. J., Bork, P., and Kuhn, M. (2016). STITCH 5: augmenting protein-chemical interaction networks with tissue and affinity data. *Nucleic Acids Res.* 44, D380–D384. doi: 10.1093/nar/gkv1277

Thomson, J. J., Plecha, S. C., and Withey, J. H. (2015). A small unstructured region in vibrio cholerae ToxT mediates the response to positive and negative effectors and ToxT proteolysis. *J. Bacteriol.* 197, 654–668. doi: 10.1128/JB.02068-14

UniProt, Consortium (2021). UniProt: the universal protein knowledgebase in 2021. *Nucleic Acids Res.* 49, D480–D489. doi: 10.1093/nar/gkaa1100

Utturkar, S., Dassanayake, A., Nagaraju, S., and Brown, S. D. (2020). Bacterial differential expression analysis methods. *Methods Mol. Biol.* 2096, 89–112. doi: 10.1007/978-1-0716-0195-2_8

Wattam, A. R., Abraham, D., Dalay, O., Disz, T. L., Driscoll, T., Gabbard, J. L., et al. (2014). PATRIC, the bacterial bioinformatics database and analysis resource. *Nucleic Acids Res.* 42, D581–D591. doi: 10.1093/nar/gkt1099

Xia, X., Larios-Valencia, J., Liu, Z., Xiang, F., Kan, B., Wang, H., et al. (2017). OxyR-activated expression of Dps is important for vibrio cholerae oxidative stress resistance and pathogenesis. *PLoS One* 12:e0171201. doi: 10.1371/journal.pone.0171201

Zhang, Z., Chen, G., Hu, J., Hussain, W., Fan, F., Yang, Y., et al. (2019). Mr.vc: a database of microarray and RNA-seq of vibrio cholerae. *Database (Oxford)* 2019:baz069. doi: 10.1093/database/baz069

Zhao, S., Ye, Z., and Stanton, R. (2020). Misuse of RPKM or TPM normalization when comparing across samples and sequencing protocols. *RNA* 26, 903–909. doi: 10.1261/rna.074922.120

frontiers | Frontiers in Microbiology

TYPE Original Research
PUBLISHED 19 January 2023
DOI 10.3389/fmicb.2023.1123524

OPEN ACCESS

EDITED BY
Xihui Shen,
Northwest A&F University, China

REVIEWED BY
Lotte Jelsbak,
Roskilde University, Denmark
Xiaohui Zhou,
Southern University of Science and Technology, China
Weili Liang,
National Institute for Communicable Disease Control and Prevention, China

*CORRESPONDENCE
Renfei Lu
✉ rainman78@163.com

†These authors have contributed equally to this work

SPECIALTY SECTION
This article was submitted to Infectious Agents and Disease, a section of the journal Frontiers in Microbiology

RECEIVED 14 December 2022
ACCEPTED 03 January 2023
PUBLISHED 19 January 2023

CITATION
Zhang Y, Xue X, Sun F, Li X, Zhang M, Wu Q, Zhang T, Luo X and Lu R (2023) Quorum sensing and QsvR tightly control the transcription of *vpa0607* encoding an active RNase II-type protein in *Vibrio parahaemolyticus*. *Front. Microbiol.* 14:1123524. doi: 10.3389/fmicb.2023.1123524

Quorum sensing and QsvR tightly control the transcription of *vpa0607* encoding an active RNase II-type protein in *Vibrio parahaemolyticus*

Yiquan Zhang[1†], Xingfan Xue[1,2†], Fengjun Sun[3], Xue Li[1], Miaomiao Zhang[1,2], Qimin Wu[1], Tingting Zhang[1], Xi Luo[1] and Renfei Lu[1*]

[1]Department of Clinical Laboratory, Affiliated Nantong Hospital 3 of Nantong University, Nantong, Jiangsu, China, [2]School of Medicine, Jiangsu University, Zhenjiang, Jiangsu, China, [3]Department of Pharmacy, The First Affiliated Hospital of Army Medical University, Chongqing, China

Vibrio parahaemolyticus, a Gram-negative, halophilic bacterium, is a leading cause of acute gastroenteritis in humans. AphA and OpaR are the master quorum sensing (QS) regulators operating at low cell density (LCD) and high cell density (HCD), respectively. QsvR is an AraC-type protein that integrates into the QS system to control gene expression by directly controlling the transcription of *aphA* and *opaR*. However, the regulation of QsvR itself remains unclear to date. In this study, we show that *vpa0607* and *qsvR* are transcribed as an operon, *vpa0607-qsvR*. AphA indirectly activates the transcription of *vpa0607* at LCD, whereas OpaR and QsvR directly repress *vpa0607* transcription at HCD, leading to the highest expression levels of *vpa0607* occurs at LCD. Moreover, VPA0607 acts as an active RNase II-type protein in *V. parahaemolyticus* and feedback inhibits the expression of QsvR at the post-transcriptional level. Taken together, this work deepens our understanding of the regulation of QsvR and enriches the integration mechanisms of QsvR with the QS system in *V. parahaemolyticus*.

KEYWORDS

***Vibrio parahaemolyticus*, quorum sensing, QsvR, VPA0607, RNase II**

Introduction

Vibrio parahaemolyticus is a Gram-negative, halophilic bacterium that often causes acute gastroenteritis in humans *via* the consumption of seafood (Chen et al., 2022a). In rare cases, *V. parahaemolyticus* is also able to cause wound infection or septicemia if it comes in contact with small open wounds or enters the blood stream (Broberg et al., 2011). Pathogenicity of *V. parahaemolyticus* depends on the production of multiple virulence factors, including thermostable direct hemolysin (TDH), TDH-related hemolysin (TRH), type III secretion systems (T3SS1 and T3SS2) and type VI secretion systems (T6SS1 and T6SS2) (Li et al., 2019). In addition, *V. parahaemolyticus* has a strong capacity to form steady biofilms on the surface, which requires the involvement of structures such as exopolysaccharide (EPS), type IV pili, and

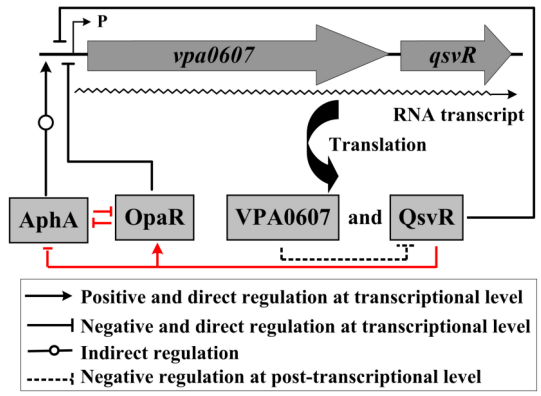

GRAPHICAL ABSTRACT
Regulatory circuit. The regulatory relationships between AphA, OpaR and QsvR are confirmed in a previous study (indicated by red lines) (Zhang et al., 2019). The letter 'P' together with the thin arrow line represents the transcription start site of the *vpa0607-qsvR* operon.

flagella, and is also a tightly regulated process (Ashrafudoulla et al., 2021; Liu et al., 2021; Ruhal and Kataria, 2021).

Quorum sensing (QS) is a sophisticated cell density-dependent communication process that involves regulating gene expression and bacterial behaviors through detection of changes in concentration of signal molecules termed autoinducers in growth environments (Lu et al., 2018). QS is known to be involved in controlling motility, biofilm development as well as virulence gene expression (Antunes et al., 2010; Rutherford et al., 2011; Lu et al., 2018; Ruhal and Kataria, 2021; Cai et al., 2022). Interference of QS function could be an alternative therapeutic approach to fight bacterial infection in clinical (Shukla et al., 2021; Rather et al., 2022). In vibrio species, QS employs the master regulators, AphA and OpaR orthologs, to regulate gene expression (Rutherford et al., 2011; Sun et al., 2012; Zhang et al., 2012; Lu et al., 2018). AphA exerts its regulatory roles at low cell density (LCD) to activate biofilm formation, motility, cyclic di-GMP synthesis, and virulence factor production, whereas OpaR or its orthologs operates at high cell density (HCD) to repress these behaviors (Rutherford et al., 2011; Sun et al., 2012, 2022; Zhang et al., 2012, 2021a; Wang et al., 2013a,b; Zhou et al., 2013; Kernell Burke et al., 2015; Lu et al., 2018, 2019, 2021; Chen et al., 2022b). However, OpaR or its orthologs also seems to have regulatory actions at LCD, as it is also expressed under LCD conditions (Rutherford et al., 2011; van Kessel et al., 2013; Wang et al., 2013b; Zhou et al., 2013; Lu et al., 2019). In addition, expression of the master QS regulators seems to be also strictly regulated by numerous regulators in vibrio species (Liu et al., 2006; Tsou et al., 2011; Williams et al., 2012; Zhang et al., 2019, 2023; Cai et al., 2022).

The AraC-family protein QsvR was originally described as a repressor of biofilm formation by *V. parahaemolyticus* (Enos-Berlage et al., 2005). A later study found that QsvR integrated into the QS regulatory cascade by directly regulating the transcription of *aphA* and *opaR* (Zhang et al., 2019). QsvR also operates at HCD to regulate the transcription of a number of genes, including *tdh2*, *toxR*, *calR*, *cpsQ-mfpABC*, *mfpABC* as well as those encoding T3SS1, T3SS2, and T6SS2 (Zhang et al., 2019, 2021b; Qiu et al., 2020). Most importantly, we recently found that QsvR worked coordinately with OpaR to negatively regulate biofilm formation by precisely controlling the transcription of multiple biofilm formation-associated genes including those involved in the biosynthesis of EPS, type IV pili and cyclic di-GMP (unpublished data). However, no potential promoters were detected within the 500 bp upstream of *qsvR* (Zhang et al., 2019), and thus the regulation of QsvR itself remains unknown to date.

The two genes, *vpa0607* and *qsvR*, are transcribed in the same direction on chromosome II and adjacent to each other with an intergenic region of only 71 bp (Makino et al., 2003), suggesting that they may be transcribed as an operon. In addition, an OpaR box-like sequence, AGCTGTTTAATTCATCAATA, was detected within the upstream DNA region of *vpa0607*, indicating that *vpa0607* transcription is likely to be directly regulated by OpaR. The *vpa0607* gene encodes a putative exoribonuclease II, but whether the VPA0607 protein possesses the enzyme activity is also still unknown.

In this study, we demonstrate that *vpa0607* and *qsvR* constitute an operon, *vpa0607-qsvR*, and are transcribed as a single primary RNA. AphA indirectly activates the transcription of *vpa0607* at LCD, whereas OpaR and QsvR directly repress *vpa0607* transcription at HCD, leading to the highest expression levels of *vpa0607* occurs at LCD. Moreover, VPA0607 works as an active RNase II-type enzyme in *V. parahaemolyticus* and feedback inhibits the expression of QsvR at the post-transcriptional level. Taken together, this work deepens our understanding of the regulation of QsvR and enriches the integration mechanisms of QsvR with the QS system in *V. parahaemolyticus*.

Materials and methods

Bacterial strains

Vibrio parahaemolyticus RIMD2210633, which was kindly provided by Dr. Dongsheng Zhou from Beijing Institute of Microbiology and Epidemiology, was used as the wild-type (WT) strain in this study (Makino et al., 2003). The *aphA*, *opaR* and *qsvR* single-gene mutants (Δ*aphA*, Δ*opaR*, and Δ*qsvR*) were constructed by our previous studies (Sun et al., 2012; Zhang et al., 2012, 2019). Δ*aphA*, Δ*opaR*, and Δ*qsvR* have been demonstrated to be non-polar (Sun et al., 2012, 2022; Zhang et al., 2012, 2019, 2021a,b; Wang et al., 2013a; Zhou et al., 2013; Qiu et al., 2020; Lu et al., 2021; Chen et al., 2022b), and thus their complementary strains were not included in this study. For over-expression of VPA0607 (Chen et al., 2022b), a polymerase chain reaction (PCR)-generated DNA fragment comprising the coding region of *vpa0607* together with an upstream synthetic Shine-Dalgarno sequence (AGGAGG) was cloned between the *Sma*I and *Sal*I sites of pBAD33containing an arabinose pBAD promoter and a chloramphenicol resistance gene. The recombinant pBAD33 plasmid (pBAD33-*vpa0607*) was introduced into the WT strain to yield the WT/pBAD33-*vpa0607* strain for over-expression of VPA0607. The empty pBAD33 vector was transferred into the WT strain to yield WT/pBAD33 for using as a control strain.

Growth conditions

Vibrio parahaemolyticus was grown as previously described (Zhang et al., 2019). Briefly, overnight cell cultures in 2.5% (w/v) Bacto Heart Infusion (HI) broth (BD Biosciences, USA) were diluted 50-fold into 15 ml of fresh HI broth and then grown at 37°C with shaking at 200 rpm to reach an optical density at 600 nm (OD_{600}) value of 1.4. The resulting bacterial cultures were diluted 1000-fold into 15 ml of HI broth for a third round of incubation and then harvested at the required cell densities. When necessary, the medium was supplemented with 50 μg/mL gentamicin, 5 μg/mL chloramphenicol, or 0.1% (w/v) arabinose.

RNA isolation and quantitative PCR (qPCR)

Total bacterial RNA was extracted using TRIzol Reagent (Invitrogen, USA). RNA quality was detected by agarose gel electrophoresis, and RNA quantity was determined by spectrophotometry. cDNA was generated from 1 μg of total RNA sample using a FastKing First Strand cDNA Synthesis Kit (Tiangen Biotech, China) according to the manufacturer's instructions. qPCR assays were performed using the Light Cycler system (Roche, Switzerland) together with FastKing One Step RT-qPCR Kit (SYBR) (TIANGEN, China) (Gao et al., 2011; Zhang et al., 2019). Relative mRNA levels of *vpa0607* were determined based on the standard curve of 16S rRNA expression for each RNA preparation. All primers used in this study are listed in **Table 1**.

Reverse transcription (RT)-PCR

Total RNA was extracted from the WT strain using TRIzol Reagent (Invitrogen, USA), and then the contaminated DNA was removed using an Ambion DNA-free kit according to the manufacturer's instructions. RT-PCR was performed similarly as the previously study (Zhang et al., 2018). Briefly, cDNAs were generated using 8 μg of total RNA and 3 μg of random hexamer primers in a 40 μl reaction mixture. A volume of 50 μl of PCR mixture contained 25 μl 2 × Taq PCR Mix (TIANGEN, China), 2 μl of cDNA sample, and 23 μl of nuclease-free water. The parameters for amplification were as follows: 95°C for 5 min; 30 cycles of 94°C for 30 s, 54°C for 50 s, and 72°C for 50 min; and a final extension step of 72°C for 5 min. The PCR products were detected by 1% agarose gel electrophoresis with ethidium bromide staining.

LacZ fusion and β-galactosidase assay

LacZ fusion assays were performed as previously described (Zhang et al., 2021b). Briefly, the regulatory DNA region of *vpa0607* was cloned into the pHRP309 vector containing a promoter-less *lacZ* gene and a gentamicin resistance gene (Parales and Harwood, 1993). Thereafter, the recombinant pHRP309 plasmid was transferred into WT and the mutant strains. The resulting transformants were cultured and then lysed to measure the β-galactosidase activity in the cellular extracts using a β-Galactosidase Enzyme Assay System (Promega, USA) according to the manufacturer's instructions. The β-galactosidase activity (represented by the Miller Units) was calculated using the formula: $10^6 \times [(OD_{420} - 1.75 \times OD_{550})/(T \times V \times OD_{600})]$ (Zhang et al., 2021b). T and V represent the reaction time (min) and volume (μL), respectively.

Primer extension

Primer extension assay was similarly performed as previously described (Zhang et al., 2021a,b). Briefly, 10 μg of total RNA were annealed with 1 pmol of 5′-^{32}P-labeled anti-sense primer to generate cDNA using a Primer Extension System (Promega, USA) according to the manufacturer's instructions. The same 5′-^{32}P-labeled primer was also used for DNA sequencing with an AccuPower and Top DNA Sequencing Kit (Bioneer, Republic of Korea) according to the manufacturer's instructions. The products of primer extension and DNA sequencing were analyzed by 8 M urea-6% polyacrylamide gel electrophoresis, and then detected by autoradiography using Fuji Medical X-ray film (Fujifilm, Japan).

Preparation of 6 × His-tagged proteins

The entire coding regions of *aphA*, *opaR*, *qsvR*, and *vpa0607* were individually cloned into the pET28a vector (Novagen, USA). Each recombinant plasmid encoding the His-tagged protein was transferred into *E. coli* BL21λDE3 for protein expression. Expression and purification of His-AphA, His-QsvR, His-OpaR, and His-VPA0607 were performed as previously described (Sun et al., 2012; Zhang et al., 2012, 2019). The purity of His-tagged proteins was confirmed by sodium dodecyl sulfate-polyacrylamide gel electrophoresis (SDS-PAGE). Purified His-tagged proteins were stored at −80°C.

Antibody preparation and western blot analysis

Specific polyclonal IgG against His-QsvR from rabbit serum was prepared in the previously study (Zhang et al., 2019). For the western blot analysis (Fang et al., 2014), cleared whole-cell lysate was prepared from harvested bacterial cells by sonication, followed by determination of protein concentrations using a Bio-Rad Protein Assay Kit (Bio-rad, USA). Equal amounts of protein from samples were separated by SDS-PAGE, immunoblotted onto polyvinylidene fluoride membranes (Immobilon P; Millipore, USA), and incubated with primary antibody, then goat anti-rabbit IRDye® 800CW secondary antibody. Signals were detected using an Odyssey Sa Infrared Imaging System (Odyssey Sa, Japan).

Electrophoretic mobility-shift assay (EMSA)

For the EMSA (Zhang et al., 2012; Kernell Burke et al., 2015), the 5′-ends of the regulatory DNA fragments of *vpa0607*

TABLE 1 Oligonucleotide primers used in this study.

Target	Primers (forward/reverse, 5′-3′)
Construction of over-expressed strain	
vpa0607	AGCGGAGCTCAGGAGGAATTCACCATGTTTCAAGATAACCCGCTA /AGCGAAGCTTTTATTCTTCACTTACAGTTTGTTC
Protein expression	
vpa0607	AGCGGGATCCATGTTTCAAGATAACCCGCTA/AGCGAAGCTTTTATTCTTCACTTACAGTTTGTTC
RT-PCR	
vpa0607	TATGCTAAAAGCGGTGAT/TGGCTGGTGGACGACTAATG
	ATGCTAAAAGCGGTGATTC/AGCCATTCTCGCCAGGTATG
	TGGGTGACACATTGGAAATCG/TGGCTGGTGGACGACTAATG
qPCR	
vpa0607	GGAAGTGGACAGCAAGAC/AAGCGAGTAAGAGATTGTTC
qsvR	TACACCGCCACCCATAACG/AGCCATTCTCGCCAGGTATG
Primer extension	
vpa0607	/TTGGATTTGCTGCTTAAGTTGG
LacZ fusion	
vpa0607	GCGCGTCGACACCCGTCTGTGCTTTACCC/GCGCGAATTCTTGGATTTGCTGCTTAAGTTGG
EMSA	
vpa0607	ACCCGTCTGTGCTTTACCC/TTGGATTTGCTGCTTAAGTTGG
DNase I footprinting	
vpa0607	GGGACGACTAAGGGAGGC/TTGGATTTGCTGCTTAAGTTGG

were labeled with [γ-^{32}P] ATP. EMSA binding was performed in a 10 μl reaction volume containing 1 mM $MgCl_2$, 0.5 mM EDTA, 0.5 mM DTT, 50 mM NaCl, 10 mM Tris–HCl/pH 7.5, 0.05 mg/ml salmon sperm DNA, 5′-^{32}P-labeled DNA probe (1000–2000 CPM/μl), and proper amount of His-tagged protein. Two controls were included in each EMSA experiment: (1) cold probe as specific DNA competitor (the unlabeled regulatory DNA fragments of *vpa0607*), and (2) negative probe as non-specific DNA competitor (the unlabeled 16S rRNA gene). Binding products were analyzed in a native 4% (w/v) polyacrylamide gel, and then detected by autoradiography after exposure to Fuji Medical X-ray film (Fujifilm, Japan).

DNase I footprinting

For DNase I footprinting (Zhang et al., 2012), the regulatory DNA fragments with a single ^{32}P-labeled end were generated by PCR, and then purified by a QiaQuick column (Qiagen, Germany). DNA binding was performed in a 10 μl reaction volume, which was the same as the EMSA, and then incubated at room temperature for 30 min. Prior to digestion, 10 μl of Ca^{2+}/Mg^{2+} solution (5 mM $CaCl_2$ and 10 mM $MgCl_2$) were added to each reaction and incubated for 1 min at room temperature. Optimized RQ1 RNase-Free DNase I (Promega, USA) was added to each reaction and then incubated at room temperature for 40–90 s. The reaction was quenched by adding 9 μl of stop solution (200 mM NaCl, 30 mM EDTA, and 1% SDS), followed by incubation for 1 min at room temperature. The partially digested DNA samples were extracted with phenol/chloroform, precipitated with ethanol, and analyzed on a 6% polyacrylamide/8 M urea gel. Protected regions were identified by comparison with the DNA sequence ladders. Radioactive species were detected by autoradiography after exposure to Fuji Medical X-ray film (Fujifilm, Japan).

Enzyme activity assay

The RNase II activity of His-VPA0607 was performed similarly as previously described (Schmier et al., 2012). Briefly, the substrate consisting of a 17-base pair duplex with a 17-nucleotide 3′ poly (A) overhang (ds17-A_{17}) was prepared by mixing the oligoribonucleotide 5′- CCCCACCACCAUCACUUAAAAAAAAAAAAAAAAA-3′ with the complementary oligoribonucleotide 5′-AAGUGAUGGUGGUGGGG-3′ in a 1:1.2 molar ratio in the presence of 10 mM Tris–HCl (pH 8.0) and 20 mM KCl, heating the mixture in a boiling water bath for 5 min, and then allowing the solution to cool slowly at room temperature. RNase II activity of His-VPA0607 was performed in 50 μl reaction mixtures containing 50 mM Tris–HCl (pH 8.0), 100 mM KCl, 10 mM $MgCl_2$, 5 mM DTT, 2 μM of substrate, and 48 μg of purified His-VPA0607. Reaction mixtures were incubated at 37°C, with 4 μl aliquots removed at the indicated time points and terminated with 2 volumes gel loading buffer containing 95% formamide, 20 mM EDTA, 0.025% bromophenol blue, and 0.025% xylene cyanol. Reaction products were analyzed by a native 12% (w/v) polyacrylamide gel, and the gel images were displayed with an ultraviolet (UV) transilluminator.

Experimental replicates and statistical methods

The qPCR and LacZ fusion assays were performed at least three times, with the values were expressed as the mean ± standard deviation (SD). A paired Student's *t*-test was used to calculate statistically differences with $P < 0.01$ considered as significant. The primer extension, western blot, EMSA, DNase I footprinting and enzyme activity assays were performed at least three independent times.

Results

vpa0607 and *qsvR* constitute an operon

We noticed that *vpa0607* and *qsvR* are placed adjacent to each other on the chromosome II, and transcribed in the same direction with a length of 71 bp intergenic DNA region (Makino et al., 2003). Therefore, we performed RT-PCR to test if *vpa0607* and *qsvR* are co-transcribed. As shown in **Figure 1**, these two genes were demonstrated to constitute an operon, *vpa0607-qsvR*, transcribed as a single primary RNA. *vpa0607* is the first gene of the *vpa0607-qsvR* operon.

Cell-density dependent transcription of *vpa0607*

Expression of QsvR manifested a cell-density dependent manner, and a high expression level was observed for QsvR at HCD (Zhang et al., 2019). The fact that *vpa0607* is co-transcribed with *qsvR* promoted us to detect the expression changes of *vpa0607* in the WT strain across growth periods. The results of qPCR showed that the mRNA levels of *vpa0607* decreased considerably with the increase of cell density from an OD_{600} value of 0.05 to 0.8 (**Figure 2A**). As further determined by primer extension (**Figure 2B**), the *vpa0607* mRNA was only capable of being detected at an OD_{600} value of 0.05 to 0.2; when the OD_{600} value was higher than 0.2, the *vpa0607* mRNA was undetectable; in addition, the nucleotide A, locating at 204 bp upstream of the first base of the start codon (+ 1), was thought to be the transcription start site of *vpa0607*. In brief, transcription of *vpa0607* was cell-density dependent, and the highest transcription levels occurred at LCD.

Regulation of *vpa0607* by the master QS regulators

The cell density-dependent transcription of *vpa0607* encouraged us to detect whether the transcription of *vpa0607* was regulated

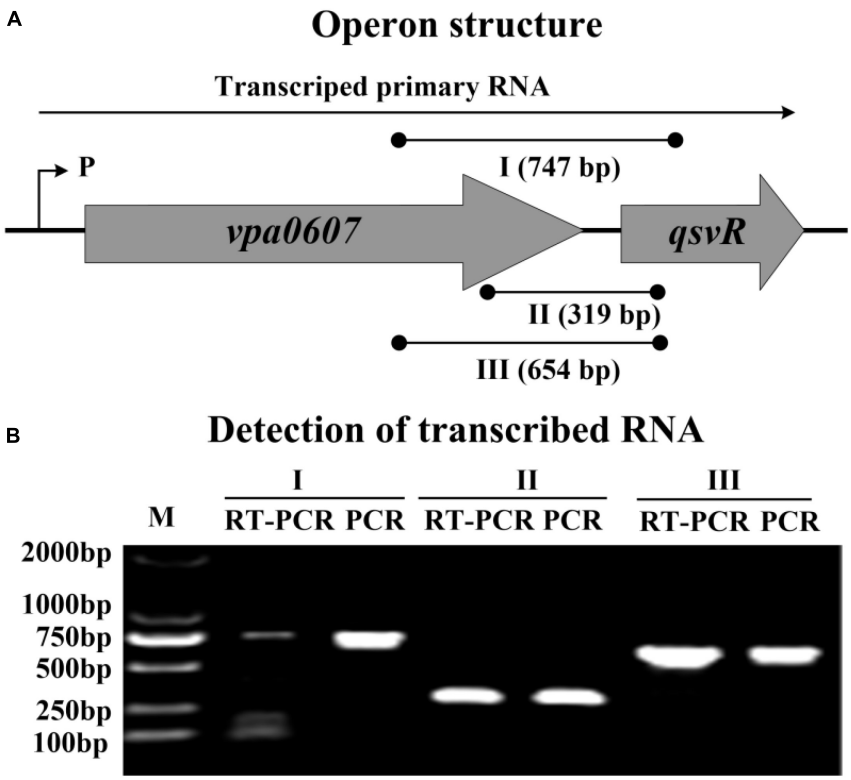

FIGURE 1
Transcriptional organization of the *vpa0607-qsvR* operon. **(A)** Operon structure. The boxed arrows represent the coding regions of corresponding genes. The broken arrow with a "P" alongside indicates the transcription start site. The long horizontal arrow depicts the putative primary RNA transcript. The lines with black dots indicate the location of primer pairs and the theoretical amplicons of PCR. I, II, and III represent different primer pairs. Numbers in parentheses indicate the theoretical length of amplicons. **(B)** Detection of transcribed RNA. cDNA samples were generated by RT from the total RNAs of WT. Genomic DNA and cDNA were used as the templates for PCR and RT-PCR, respectively. Two blank controls were included: (1) PCR reactions without template; (2) PCR reactions with the total RNA only treated by DNase I as the template. As expected, both blank controls did not provide any amplicons (data not shown).

by the master QS regulator, AphA, and OpaR. Indeed, an OpaR box-like sequence, AGCTGTTTAATTCATCAATA, was detected in the promoter DNA region of *vpa0607-0606*. Therefore, the bacterial cells were harvested at an OD_{600} value of approximately 0.15 and 0.8 to simulate LCD and HCD conditions (Sun et al., 2012; Zhang et al., 2012, 2019), respectively, to investigate AphA- and OpaR-mediated *vpa0607* transcription.

As determined by qPCR (Figures 3A, 4A), the mRNA levels of *vpa0607* were significantly decreased in Δ*aphA* but increased in Δ*opaR* relative to those in WT. The results of primer extension assay further indicated that the mRNA levels of *vpa0607* were decreased in Δ*aphA* while increased in Δ*opaR* relative to those in WT (Figures 3B, 4B). The recombinant *lacZ* fusion pHRP309 plasmid containing the promoter DNA region of *vpa0607* and a promoterless *lacZ* gene was transformed into Δ*aphA*, Δ*opaR*, and WT, respectively, to investigate whether AphA and OpaR have regulatory actions on the promoter activity of *vpa0607*. As shown in Figures 3C, 4C, the promoter activity of *vpa0607* was significantly decreased in Δ*aphA* whereas enhanced in Δ*opaR* relative to that

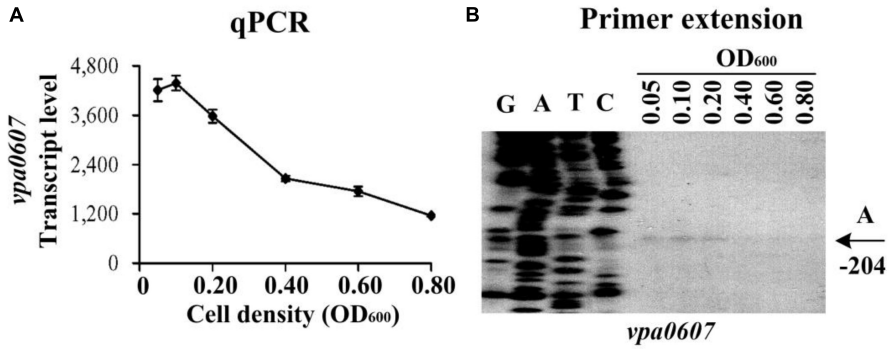

FIGURE 2
Cell density-dependent transcription of *vpa0607*. The wild-type (WT) strain was grown in HI broth at 37°C with shaking at 200 rpm, and then harvested at different cell densities. **(A)** qPCR. Relative mRNA levels of *vpa0607* were examined in the WT strain at different cell densities. **(B)** Primer extention. The products of primer extension were detected by an 8 M urea-6% acrylamide sequencing gel. Lanes G, A, T, and C represent Sanger sequencing reactions. Transcription start site of *vpa0607* is indicated by arrows with nucleotide and position. The minus number indicates the nucleotide position upstream of the first base of the start codon of *vpa0607*.

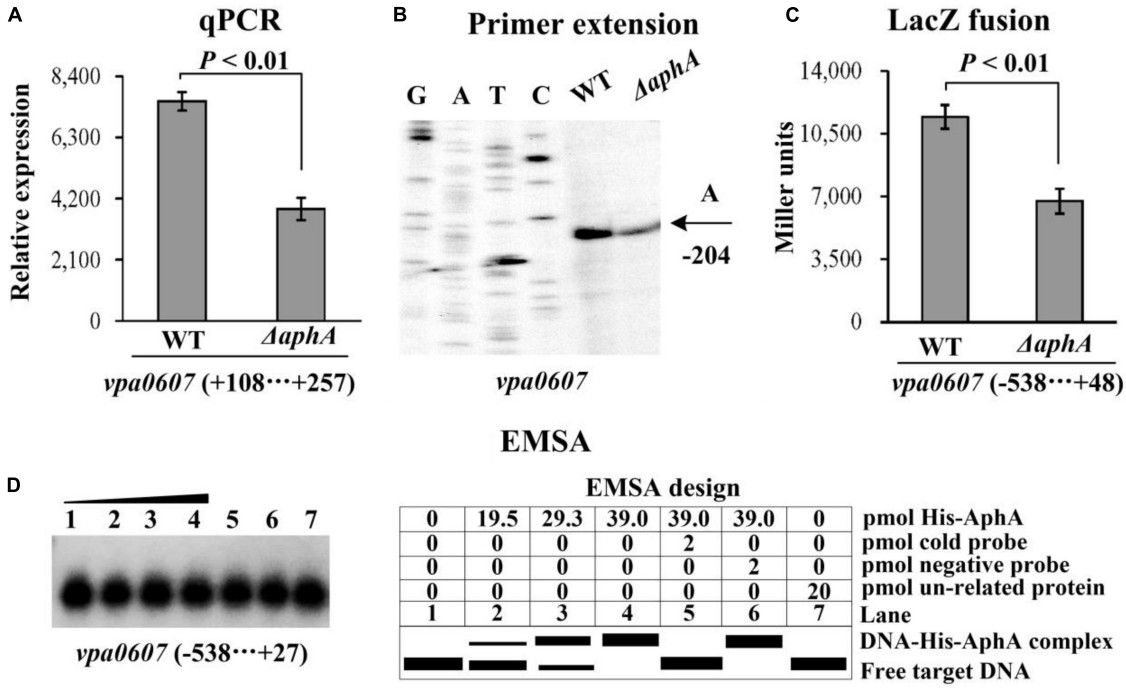

FIGURE 3
Regulation of *vpa0607* transcription by AphA. Bacterial cells were harvested at OD_{600} value of approximately 0.15 to investigate AphA-mediated *vpa0607* transcription. Negative and positive numbers indicate the nucleotide positions upstream and downstream of *vpa0607*, respectively. **(A)** qPCR. Relative mRNA levels of *vpa0607* were compared between Δ*vpa0607* and WT. Primer extension **(B)** was performed as described in Figure 2. **(C)** LacZ fusion. The regulatory DNA region of *vpa0607* was cloned into the pHRP309 vector and then, respectively, transferred into Δ*aphA* and WT to determine the promoter activity (Miller units) in the cellular extracts. **(D)** EMSA. The radioactively labeled regulatory DNA fragments of *vpa0607* were incubated with increasing amounts of purified His-AphA and then subjected to 4% (w/v) polyacrylamide gel electrophoresis. Shown on the right is the EMSA design.

in the WT strain. The results of *in vitro* EMSA showed that His-AphA did not bind to the upstream DNA fragment of *vpa0607*, while His-OpaR was able to specially and dose-dependently bind to this DNA fragment (**Figures 3D**, **4D**). However, His-AphA was capable of binding to other promoters such as its own promoter at much lower amount of protein (Sun et al., 2012). As further determined by the DNase I footprinting assay (**Figure 4E**), His-OpaR protected a single DNA region within the upstream DNA region of *vpa0607*, located 112 to 81 bp upstream of the translation start site, against DNase I digestion. Taken together, the transcription of *vpa0607* was activated indirectly by AphA at LCD, but was repressed directly by OpaR at HCD.

QsvR represses *vpa0607* transcription

QsvR integrates into the QS cascade to control gene expression in *V. parahaemolyticus*, and is highly expressed at

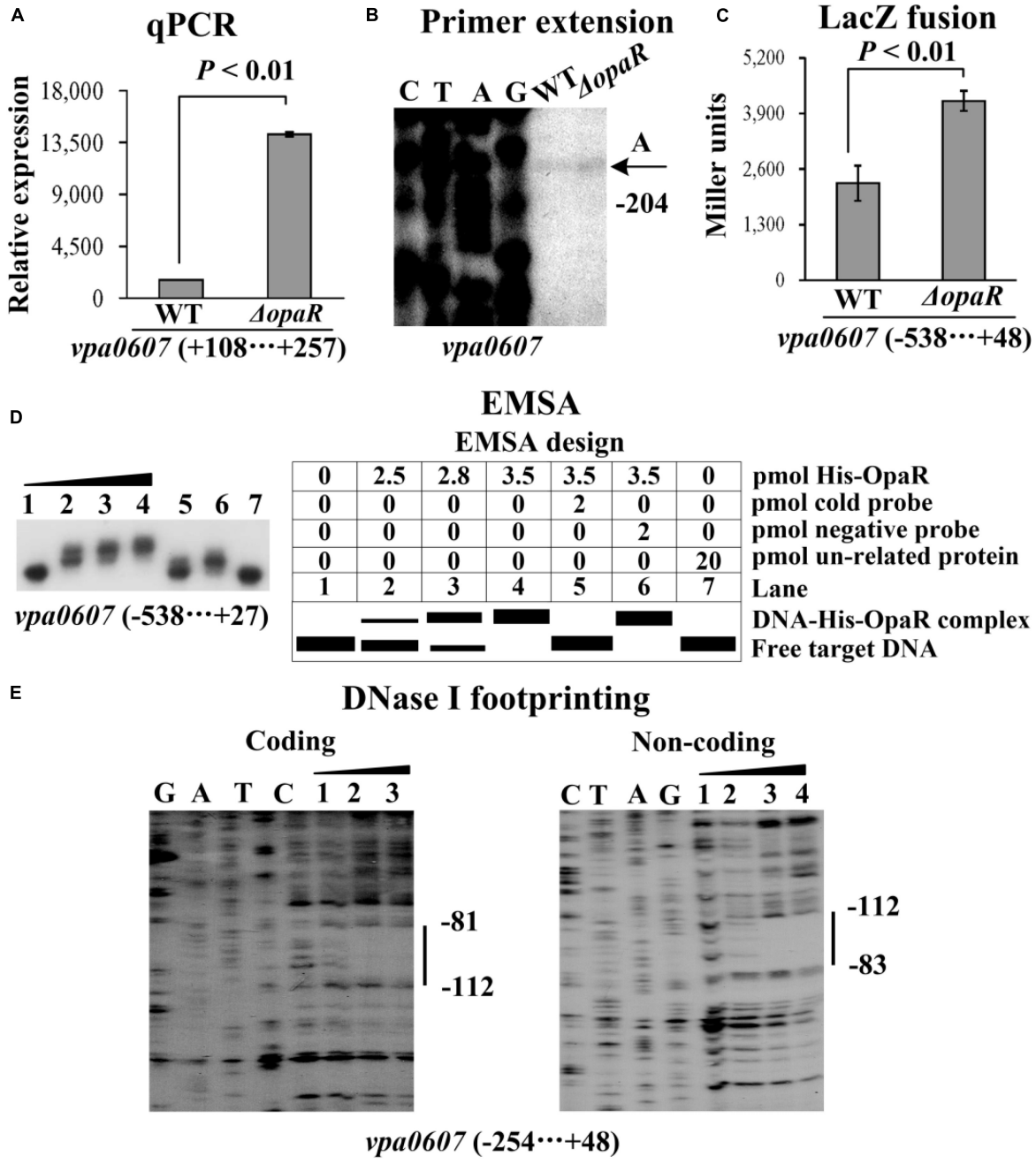

FIGURE 4
Regulation of *vpa0607* transcription by OpaR. Bacterial cells were harvested at OD_{600} value of approximately 0.8 to investigate OpaR-mediated *vpa0607* transcription. Negative and positive numbers indicate the nucleotide positions upstream and downstream of *vpa0607*, respectively. Primer extension **(B)** was performed as described in **Figure 2**. qPCR **(A)**, LacZ fusion **(C)**, and EMSA **(D)** were performed as described in **Figure 3**. **(E)** DNase I footprinting. Labeled coding or non-coding DNA probes were incubated with increasing amounts of purified His-OpaR and then subjected to DNase I footprinting. The protected regions are indicated by vertical bars, with the corresponding sequence positions also indicated. Lanes C, T, A, and G represent the Sanger sequencing reactions.

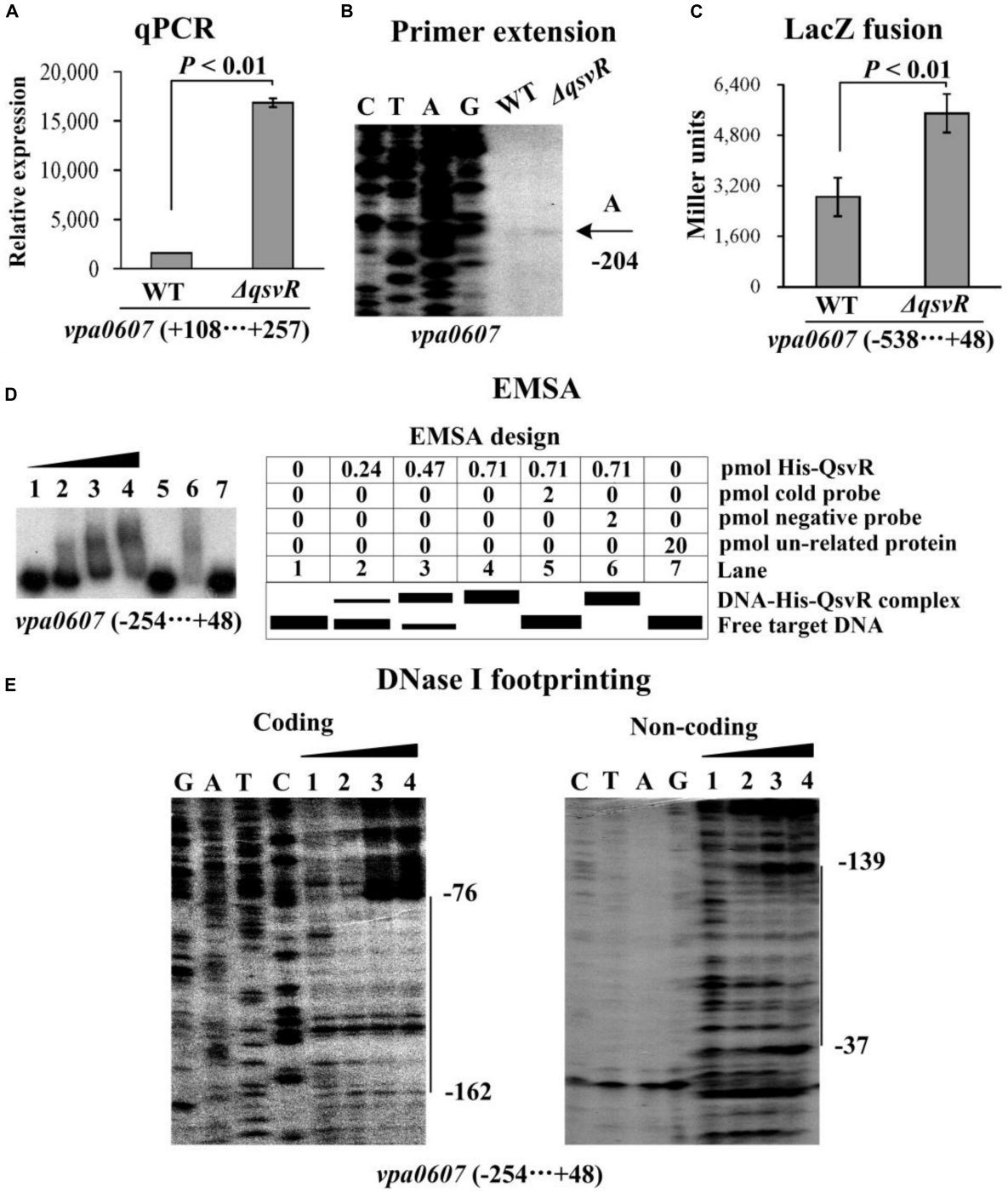

FIGURE 5
Regulation of *vpa0607* transcription by QsvR. Bacterial cells were harvested at OD_{600} value of approximately 0.8 to investigate QsvR-mediated *vpa0607* transcription. Negative and positive numbers indicate the nucleotide positions upstream and downstream of *vpa0607*, respectively. Primer extension **(B)** was performed as described in **Figure 2**. qPCR **(A)**, LacZ fusion **(C),** and EMSA **(D)** were performed as described in **Figure 3**. DNase I footprinting **(E)** was performed as described in **Figure 4**.

HCD (Zhang et al., 2019). In this study, the bacterial cells were harvested at an OD_{600} value of approximately 0.8 to investigate whether QsvR has regulatory activity on the transcription of *vpa0607* (Zhang et al., 2019). The results of qPCR and primer extension assays showed that the mRNA level of *vpa0607* was significantly enhanced in Δ*qsvR* relative to that in WT (**Figures 5A, B**). The *lacZ* fusion results demonstrated that the promoter activity of *vpa0607* in Δ*qsvR* was significantly enhanced relative to that in WT (**Figure 5C**). The EMSA results showed that His-QsvR was able to specially and dose-dependently bind to the upstream DNA fragment of *vpa0607* (**Figure 5D**). As further determined by the DNase I footprinting assay (**Figure 5E**), His-QsvR protected only one DNA region upstream of *vpa0607*, located 162 to 37 bp upstream of the translation start site, against DNase I digestion, which was considered as the QsvR site. Taken together, QsvR directly repressed the transcription of *vpa0607* at HCD.

VPA0607 acts as an active RNase II

The *vpa0607* and *qsvR* genes are transcribed as a single primary mRNA (**Figure 1**). However, the *vpa0607* mRNA was only detected at LCD (**Figure 2**), whereas QsvR was highly expressed at HCD (Zhang et al., 2019). This pt paradoxical phenomenon prompted us to look deeper into the possible mechanisms behind it. The function of VPA0607 was annotated as an exoribonuclease II, which is involved in hydrolyzing single-stranded mRNA processively in the 3′ to 5′ direction (Makino et al., 2003). We compared the amino acid sequence of VPA0607 with that of *E. coli* RNase II and found that they shared more than 50% identity in amino acid sequence, especially, the critical residue, Y253 (Barbas et al., 2008), at the active site was conserved between the two proteins (**Supplementary Figure 1**), suggesting that VPA0607 might possess a similar structure and functions with the *E. coli* RNase II. Therefore, we deduced that VPA0607 may function as an active RNase II to regulate QsvR expression at the post-transcriptional level.

We first performed western blot and qPCR to test whether over-expression of VPA0607 regulates QsvR expression. The results of western blot assays showed that the QsvR level was significantly reduced in the WT/pBAD33-*vpa0607* strain relative to that in the WT/pBAD33 strain (**Figure 6A**). As further determind by the qPCR assays (**Figure 6B**), the mRNA level of *vpa0607* in the WT/pBAD33-*vpa0607* strain was significantly higher than that in the WT/pBAD33 strain, while no significant difference was observed for the *qsvR* mRNA levels between the two strains. These results suggested that over-expression of VPA0607 negatively regulated the expression of QsvR.

RNase II is a single-stranded, sequence-independent, 3′ exoribonuclease with high hydrolytic activity toward poly (A) RNA (Andrade et al., 2009). To test whether VPA0607 is an RNase II-type enzyme, purified His-VPA0607 was incubated with the ds17-A_{17} in a 50 μl enzymatic reaction system (Schmier et al., 2012). As shown in **Figure 7**, smaller fragments were detected below the main bands and the smaller bands became brighter and brighter with the extension of incubation time. In contrast, no small bands were detected in the initial and control reactions. These results indicated that VPA0607 was able to digest the 17 nt ssRNA overhang of the substrate, and VPA0607 was likely to be an RNase II-type enzyme in *V. parahaemolyticus*.

Discussion

The data presented here shows that *vpa0607* and *qsvR* constitute an operon, *vpa0607-qsvR* (**Figure 1**). The highest transcriptional levels of *vpa0607* occurs at OD_{600} values of 0.2 to 0.4 (**Figure 2**), suggesting that the transcription of *vpa0607-qsvR* is probably regulated by QS. Indeed, the data shows that the transcription of *vpa0607-qsvR* is activated indirectly by AphA at LCD, but is repressed directly by OpaR at HCD (**Figures 3**, **4**). Moreover, QsvR is able

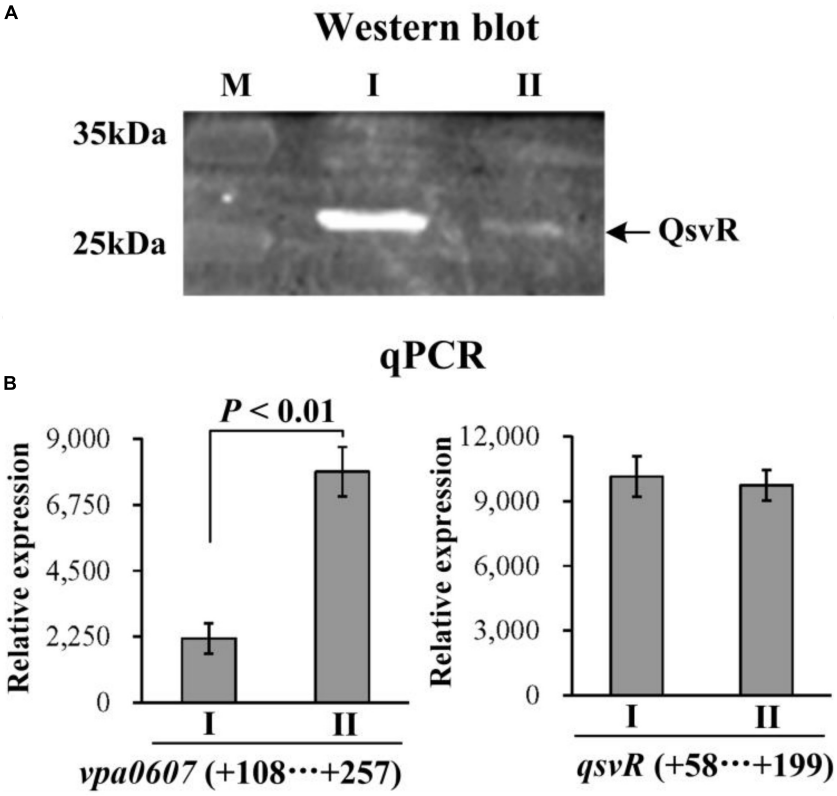

FIGURE 6
Post-transcriptional regulation of *qsvR* by VPA0607. The WT/pBAD33-*vpa0607* and WT/pBAD33 strains were grown in HI broth containing 5 μg/mL chloramphenicol and 0.1% (w/v) arabinose, and then harvested at an OD_{600} value of approximately 0.8. I and II indicate WT/pBAD33 and WT/pBAD33-*vpa0607*, respectively. **(A)** Western blot. Whole-cell proteins extracted from WT/pBAD33-*vpa0607* and WT/pBAD33 were subjected to SDS-PAGE and then incubated with anti-QsvR antibodies. Proteins were then detected using an Odyssey Sa Infrared Imaging System. **(B)** qPCR was performed as described in **Figure 3**.

to bind to the regulatory DNA region of its own operon to repress its transcription (**Figure 5**). Both the OpaR and QsvR sites for *vpa0607-qsvR* are located downstream of the transcription start site (**Figure 8**). The binding of OpaR or QsvR may block the elongation of the RNA polymerase, and thus, to repress the transcription of *vpa0607-qsvR*. Although the QsvR site entirely overlaps the OpaR site, there is very likely to be no competitive binding between the two regulators for the regulatory DNA region of *vpa0607-qsvR* according to our unpublished data. Collectively, these data demonstrate that QsvR coordinates with QS regulators, AphA, and OpaR, to precisely regulate the transcription of *vpa0607-qsvR* in *V. parahaemolyticus*, leading to the highest transcriptional levels of this operon occurs at LCD.

Some data in this study are incomprehensible to us, that is, QsvR is highly expressed at HCD (Zhang et al., 2019), while *vpa0607* is highly transcribed at LCD, but they are co-transcribed. VPA0607 shares high identity in amino acid sequence with *E. coli* RNase II (**Supplementary Figure 1**), which is an exoribonuclease that processively degrades RNA from the 3′-end (Andrade et al., 2009). Over-expressed VPA0607 represses QsvR expression at the post-transcriptional level (**Figure 6**), and the purified VPA0607 protein is able to degrade the ds17-A_{17} *in vitro* (**Figure 7**). The enzyme activity of RNase II is sequence-independent, but it prefers to degrade substrates with poly(A) tails (Cheng and Deutscher, 2002). Thus, VPA0607 probably acts as an RNase II-type enzyme in *V. parahaemolyticus*. RNase II is a component of

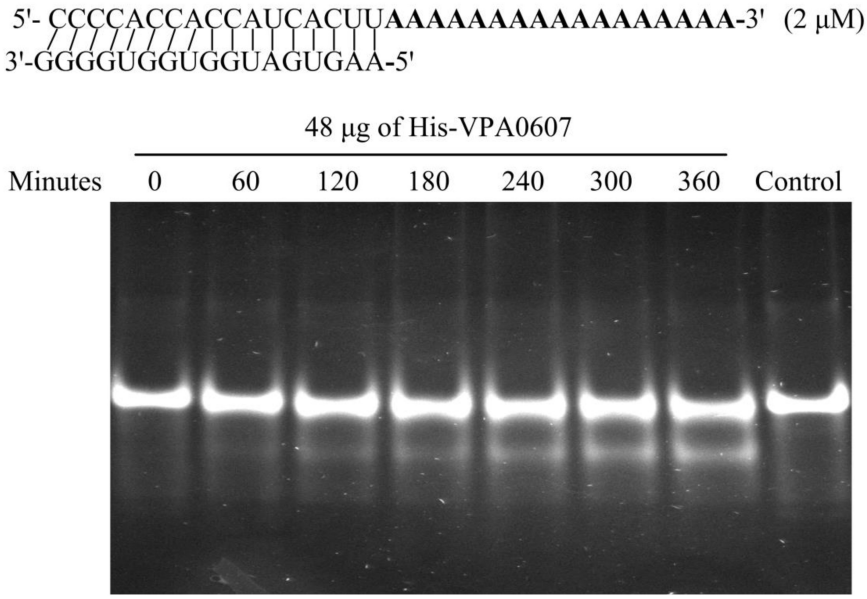

FIGURE 7
VPA0607 was an RNase II type enzyme. A total of 50 μl reactions were performed with the indicated substrate (a duplex with a 17 nt overhang) and purified His-VPA0607. A total of 4 μl aliquots were removed at the specified time points and analyzed by a native 12% (w/v) polyacrylamide gel, and the gel images were displayed with an ultraviolet (UV) transilluminator. The control was a reaction without His-VPA0607 that was incubated at 37°C for 360 min.

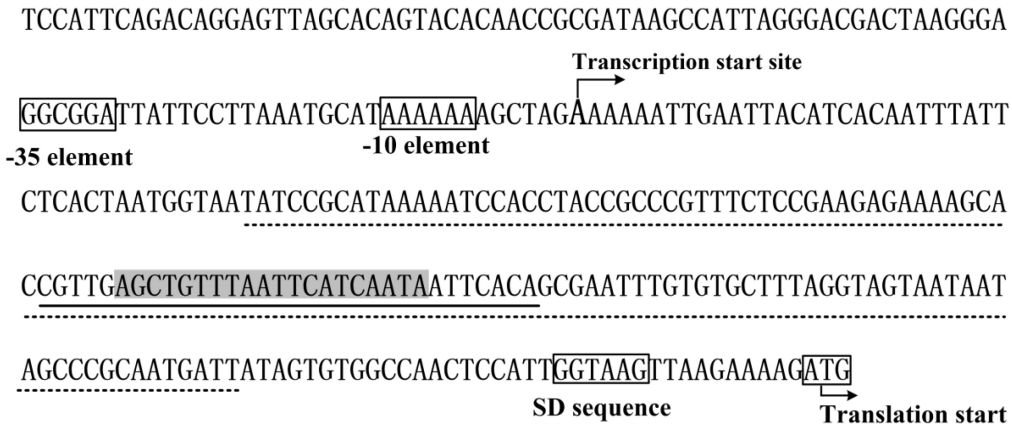

FIGURE 8
Promoter organization of *vpa0607*. The promoter-proximal DNA region of *vpa0607* were derived from the *Vibrio parahaemolyticus* strain RIMD221063. The translation and transcription start sites are indicated with bent arrows. The predicted −10 and −35 elements as well as the Shine-Dalgarno (SD) sequence are boxed. The OpaR box-like sequence is highlighted in gray. The OpaR site is underlined with solid line, while the QsvR site is underlined with dotted line.

the RNA degradosome, playing a central role in RNA processing and degradation (Lu and Taghbalout, 2014). In *E. coli*, RNase II was shown to be required for cell survival during stationary phase and upon starvation by regulating the amount and stability of RNase PH (Sulthana et al., 2017). The transcriptomic RNA-seq data showed that the deletion of RNase II significantly affected the transcription of 187 genes relative to that of the WT strain, including those involved in flagellum assembly, motility and biofilm formation (Pobre and Arraiano, 2015). Indeed, the RNase II mutant produced more biofilm than the WT strain (Pobre and Arraiano, 2015). The roles of VPA0607 are completely unknown in *V. parahaemolyticus* and worth to be investigated in the future.

Regulation of RNase II has been observed in *E. coli*, but mostly at the post-transcriptional level. For example, inactivation of RNase E and RNase III leads to altered expression levels and activity of RNase II (Zilhao et al., 1995). The Cys284Tyr mutation abolishes RNase II activity by increasing protein kinetic instability at the non-permissive temperature (Reis et al., 2019). The acetyltransferase Pka and the deacetylase CobB can determine whether the Lys501 residue in RNase II is acetylated, and thus affecting the catalytic activity of RNase II (Song et al., 2016). The putative RNase II, VPA0607, was transcriptionally regulated by QsvR and the QS system, but the post-transcriptional regulation of VPA0607, especially whether it can interact with other endonucleases, is still worthy of further in-depth study.

In conclusion, this study shows that *vpa0607* and *qsvR* are co-transcribed as an operon, and the transcription of this operon is tightly regulated by QsvR and the master QS regulators, AphA, and OpaR. In addition, VPA0607 is shown to be an active RNase II-type enzyme in *V. parahaemolyticus* and feedback inhibits QsvR expression at the post-transcriptional level. The data of this study prompts us to deduce a hypothesis as following: at LCD, the *vpa0607-qsvR* operon is highly transcribed and thus leading to a high intracellular level of VPA0607, which then negatively regulate QsvR expression at the post-transcriptional level by degrading the mRNA of *vpa0607-qsvR* from the 3′ ends; at HCD, the intracellular VPA0607 level is low due to the collective repression of QsvR and OpaR, and thus the post-transcriptional repression of QsvR by VPA0607 is abolished and the basal mRNA level of *vpa0607-qsvR* can translate QsvR. However, this hypothesis needs to be further investigated.

Data availability statement

The original contributions presented in this study are included in the article/**Supplementary material**, further inquiries can be directed to the corresponding author.

Author contributions

YZ, XX, FS, XuL, MZ, QW, TZ, and XiL performed the laboratory experiments and analyzed the results. YZ and RL designed, organized, and supervised the experiments. YZ drafted the manuscript. All authors read and approved the final manuscript.

Funding

This work was supported by the National Natural Science Foundation of China (Grant No. 82072239), the Natural Science Research Project of Nantong Science and Technology Bureau (Grant No. JC2021027), and the Research Projects of Nantong Health Commission (Grant No. QN2022044).

Conflict of interest

The authors declare that the research was conducted in the absence of any commercial or financial relationships that could be construed as a potential conflict of interest.

Publisher's note

Supplementary material

The Supplementary Material for this article can be found online at: https://www.frontiersin.org/articles/10.3389/fmicb.2023.1123524/full#supplementary-material

SUPPLEMENTARY FIGURE 1
Comparative homology of VPA0607 and *E. coli* RNase II. The amino acid sequences were derived from the *V. parahaemolyticus* strain RIMD2210633 and *E. coli* K12. Identical residues are marked with asterisks (*). The key amino acid residue (Y) is labeled in red color.

References

Barbas, A., Matos, R., Amblar, M., Lopez-Vinas, E., Gomez-Puertas, P., and Arraiano, C. (2008). New insights into the mechanism of RNA degradation by ribonuclease II: identification of the residue responsible for setting the RNase II end product. *J. Biol. Chem.* 283, 13070–13076. doi: 10.1074/jbc.M709989200

Kernell Burke, A., Guthrie, L., Modise, T., Cormier, G., Jensen, R., McCarter, L., et al. (2015). OpaR controls a network of downstream transcription factors in *Vibrio parahaemolyticus* BB22OP. *PLoS One* 10:e0121863. doi: 10.1371/journal.pone.0121863

Shukla, A., Parmar, P., Patel, B., Goswami, D., and Saraf, M. (2021). Breaking bad: Better call gingerol for improving antibiotic susceptibility of *Pseudomonas aeruginosa* by inhibiting multiple quorum sensing pathways. *Microbiol Res* 252:126863. doi: 10.1016/j.micres.2021.126863

Tsou, A., Liu, Z., Cai, T., and Zhu, J. (2011). The VarS/VarA two-component system modulates the activity of the *Vibrio cholerae* quorum-sensing transcriptional regulator HapR. *Microbiology* 157(Pt. 6), 1620–1628. doi: 10.1099/mic.0.046235-0

Schmier, B., Seetharaman, J., Deutscher, M., Hunt, J., and Malhotra, A. (2012). The structure and enzymatic properties of a novel RNase II family enzyme from *Deinococcus radiodurans*. *J. Mol. Biol.* 415, 547–559. doi: 10.1016/j.jmb.2011.11.031

Broberg, C., Calder, T., and Orth, K. (2011). *Vibrio parahaemolyticus* cell biology and pathogenicity determinants. *Microbes Infect.* 13, 992–1001. doi: 10.1016/j.micinf.2011.06.013

Zhou, D., Yan, X., Qu, F., Wang, L., Zhang, Y., Hou, J., et al. (2013). Quorum sensing modulates transcription of cpsQ-mfpABC and mfpABC in *Vibrio parahaemolyticus*. *Int. J. Food Microbiol.* 166, 458–463. doi: 10.1016/j.ijfoodmicro.2013.07.008

Lu, F., and Taghbalout, A. (2014). The *Escherichia coli* major exoribonuclease RNase II is a component of the RNA degradosome. *Biosci. Rep.* 34:e00166. doi: 10.1042/BSR20140113

Reis, F., Barria, C., Gomez-Puertas, P., Gomes, C., and Arraiano, C. (2019). Identification of temperature-sensitive mutations and characterization of thermolabile RNase II variants. *FEBS Lett.* 593, 352–360. doi: 10.1002/1873-3468.13313

Sun, F., Zhang, Y., Wang, L., Yan, X., Tan, Y., Guo, Z., et al. (2012). Molecular characterization of direct target genes and cis-acting consensus recognized by quorum-sensing regulator AphA in *Vibrio parahaemolyticus*. *PLoS One* 7:e44210. doi: 10.1371/journal.pone.0044210

Gao, H., Zhang, Y., Yang, L., Liu, X., Guo, Z., Tan, Y., et al. (2011). Regulatory effects of cAMP receptor protein (CRP) on porin genes and its own gene in Yersinia pestis. *BMC Microbiol* 11:40. doi: 10.1186/1471-2180-11-40

Andrade, J., Pobre, V., Silva, I., Domingues, S., and Arraiano, C. (2009). The role of 3′-5′ exoribonucleases in RNA degradation. *Prog. Mol. Biol. Transl. Sci.* 85, 187–229.

Cai, J., Hao, Y., Xu, R., Zhang, Y., Ma, Y., Zhang, Y., et al. (2022). Differential binding of LuxR in response to temperature gauges switches virulence gene expression in Vibrio alginolyticus. *Microbiol. Res.* 263:127114. doi: 10.1016/j.micres.2022.127114

Enos-Berlage, J., Guvener, Z., Keenan, C., and McCarter, L. (2005). Genetic determinants of biofilm development of opaque and translucent *Vibrio parahaemolyticus*. *Mol. Microbiol.* 55, 1160–1182. doi: 10.1111/j.1365-2958.2004.04453.x

Sun, J., Li, X., Qiu, Y., Xue, X., Zhang, M., Yang, W., et al. (2022). Quorum sensing regulates transcription of the pilin gene mshA1 of MSHA pilus in *Vibrio parahaemolyticus*. *Gene* 807:145961. doi: 10.1016/j.gene.2021.145961

van Kessel, J., Rutherford, S., Shao, Y., Utria, A., and Bassler, B. (2013). Individual and combined roles of the master regulators AphA and LuxR in control of the Vibrio harveyi quorum-sensing regulon. *J. Bacteriol.* 195, 436–443. doi: 10.1128/JB.01998-12

Williams, J., Ritter, A., and Stevens, A. (2012). CsrA modulates luxR transcript levels in *Vibrio fischeri*. *FEMS Microbiol. Lett.* 329, 28–35. doi: 10.1111/j.1574-6968.2012.02499.x

Makino, K., Oshima, K., Kurokawa, K., Yokoyama, K., Uda, T., Tagomori, K., et al. (2003). Genome sequence of *Vibrio parahaemolyticus*: a pathogenic mechanism distinct from that of V cholerae. *Lancet* 361, 743–749. doi: 10.1016/S0140-6736(03)12659-1

Antunes, L., Ferreira, R., Buckner, M., and Finlay, B. (2010). Quorum sensing in bacterial virulence. *Microbiology* 156(Pt. 8), 2271–2282.

Chen, L., Sun, L., Zhang, R., Liao, N., Qi, X., and Chen, J. (2022a). Surveillance for foodborne disease outbreaks in Zhejiang Province, China, 2015-2020. *BMC Public Health* 22:135. doi: 10.1186/s12889-022-12568-4

Chen, L., Zhang, M., Li, X., Wu, Q., Xue, X., Zhang, T., et al. (2022b). AphA directly activates the transcription of polysaccharide biosynthesis gene scvE in *Vibrio parahaemolyticus*. *Gene* 851:146980. doi: 10.1016/j.gene.2022.146980

Li, L., Meng, H., Gu, D., Li, Y., and Jia, M. (2019). Molecular mechanisms of *Vibrio parahaemolyticus* pathogenesis. *Microbiol. Res.* 222, 43–51.

Song, L., Wang, G., Malhotra, A., Deutscher, M., and Liang, W. (2016). Reversible acetylation on Lys501 regulates the activity of RNase II. *Nucleic Acids Res.* 44, 1979–1988. doi: 10.1093/nar/gkw053

Wang, L., Ling, Y., Jiang, H., Qiu, Y., Qiu, J., Chen, H., et al. (2013a). AphA is required for biofilm formation, motility, and virulence in pandemic *Vibrio parahaemolyticus*. *Int. J. Food Microbiol.* 160, 245–251. doi: 10.1016/j.ijfoodmicro.2012.11.004

Wang, L., Zhou, D., Mao, P., Zhang, Y., Hou, J., Hu, Y., et al. (2013b). Cell density- and quorum sensing-dependent expression of type VI secretion system 2 in *Vibrio parahaemolyticus*. *PLoS One* 8:e73363. doi: 10.1371/journal.pone.0073363

Ashrafudoulla, M., Mizan, M., Park, S., and Ha, S. (2021). Current and future perspectives for controlling Vibrio biofilms in the seafood industry: a comprehensive review. *Crit. Rev. Food Sci. Nutr.* 61, 1827–1851. doi: 10.1080/10408398.2020.1767031

Liu, M., Zhu, X., Zhang, C., and Zhao, Z. (2021). LuxQ-LuxU-LuxO pathway regulates biofilm formation by *Vibrio parahaemolyticus*. *Microbiol. Res.* 250:126791. doi: 10.1016/j.micres.2021.126791

Rather, M., Saha, D., Bhuyan, S., Jha, A., and Mandal, M. (2022). Quorum quenching: a drug discovery approach against *Pseudomonas aeruginosa*. *Microbiol. Res.* 264:127173. doi: 10.1016/j.micres.2022.127173

Fang, N., Qu, S., Yang, H., Fang, H., Liu, L., Zhang, Y., et al. (2014). HmsB enhances biofilm formation in *Yersinia pestis*. *Front. Microbiol.* 5:685. doi: 10.3389/fmicb.2014.00685

Lu, R., Osei-Adjei, G., Huang, X., and Zhang, Y. (2018). Role and regulation of the orphan AphA protein of quorum sensing in pathogenic Vibrios. *Future Microbiol.* 13, 383–391. doi: 10.2217/fmb-2017-0165

Lu, R., Tang, H., Qiu, Y., Yang, W., Yang, H., Zhou, D., et al. (2019). Quorum sensing regulates the transcription of lateral flagellar genes in *Vibrio parahaemolyticus*. *Future Microbiol.* 14, 1043–1053. doi: 10.2217/fmb-2019-0048

Lu, R., Sun, J., Qiu, Y., Zhang, M., Xue, X., Li, X., et al. (2021). The quorum sensing regulator OpaR is a repressor of polar flagellum genes in *Vibrio parahaemolyticus*. *J. Microbiol.* 59, 651–657. doi: 10.1007/s12275-021-0629-3

Parales, R., and Harwood, C. (1993). Construction and use of a new broad-host-range lacZ transcriptional fusion vector, pHRP309, for gram- bacteria. *Gene* 133, 23–30. doi: 10.1016/0378-1119(93)90220-w

Ruhal, R., and Kataria, R. (2021). Biofilm patterns in gram-positive and gram-negative bacteria. *Microbiol. Res.* 251:126829.

Zilhao, R., Regnier, P., and Arraiano, C. (1995). The role of endonucleases in the expression of ribonuclease II in *Escherichia coli*. *FEMS Microbiol. Lett.* 130, 237–244. doi: 10.1016/0378-1097(95)00212-n

Rutherford, S., van Kessel, J., Shao, Y., and Bassler, B. (2011). AphA and LuxR/HapR reciprocally control quorum sensing in vibrios. *Genes Dev.* 25, 397–408. doi: 10.1101/gad.2015011

Sulthana, S., Quesada, E., and Deutscher, M. (2017). RNase II regulates RNase PH and is essential for cell survival during starvation and stationary phase. *RNA* 23, 1456–1464. doi: 10.1261/rna.060558.116

Pobre, V., and Arraiano, C. (2015). Next generation sequencing analysis reveals that the ribonucleases RNase II, RNase R and PNPase affect bacterial motility and biofilm formation in E. coli. *BMC Genomics* 16:72. doi: 10.1186/s12864-015-1237-6

Qiu, Y., Hu, L., Yang, W., Yin, Z., Zhou, D., Yang, H., et al. (2020). The type VI secretion system 2 of *Vibrio parahaemolyticus* is regulated by QsvR. *Microb. Pathog.* 149:104579. doi: 10.1016/j.micpath.2020.104579

Zhang, Y., Qiu, Y., Tan, Y., Guo, Z., Yang, R., and Zhou, D. (2012). Transcriptional regulation of opaR, qrr2-4 and aphA by the master quorum-sensing regulator OpaR in *Vibrio parahaemolyticus*. *PLoS One* 7:e34622. doi: 10.1371/journal.pone.0034622

Zhang, Y., Qiu, Y., Gao, H., Sun, J., Li, X., Zhang, M., et al. (2021a). OpaR controls the metabolism of c-di-GMP in *Vibrio parahaemolyticus*. *Front. Microbiol.* 12:676436. doi: 10.3389/fmicb.2021.676436

Zhang, Y., Hu, L., Qiu, Y., Osei-Adjei, G., Tang, H., Zhang, Y., et al. (2019). QsvR integrates into quorum sensing circuit to control *Vibrio parahaemolyticus* virulence. *Environ. Microbiol.* 21, 1054–1067. doi: 10.1111/1462-2920.14524

Zhang, Y., Wu, X., Cai, J., Chen, M., Zhang, J., Shao, S., et al. (2023). Transposon insertion sequencing analysis unveils novel genes involved in luxR expression and quorum sensing regulation in Vibrio alginolyticus. *Microbiol. Res.* 267:127243. doi: 10.1016/j.micres.2022.127243

Zhang, Y., Qiu, Y., Xue, X., Zhang, M., Sun, J., Li, X., et al. (2021b). Transcriptional regulation of the virulence genes and the biofilm formation associated operons in *Vibrio parahaemolyticus*. *Gut Pathog.* 13:15. doi: 10.1186/s13099-021-00410-y

Zhang, Y., Hu, L., Osei-Adjei, G., Zhang, Y., Yang, W., Yin, Z., et al. (2018). Autoregulation of ToxR and its regulatory actions on major virulence gene loci in *Vibrio parahaemolyticus*. *Front. Cell Infect. Microbiol.* 8:291. doi: 10.3389/fcimb.2018.00291

Cheng, Z., and Deutscher, M. (2002). Purification and characterization of the *Escherichia coli* exoribonuclease RNase R. Comparison with RNase II. *J. Biol. Chem.* 277, 21624–21629. doi: 10.1074/jbc.M202942200

Liu, Z., Hsiao, A., Joelsson, A., and Zhu, J. (2006). The transcriptional regulator VqmA increases expression of the quorum-sensing activator HapR in *Vibrio cholerae*. *J. Bacteriol.* 188, 2446–2453. doi: 10.1128/JB.188.7.2446-2453.2006

frontiers | Frontiers in Microbiology

TYPE Original Research
PUBLISHED 01 February 2023
DOI 10.3389/fmicb.2023.1111895

OPEN ACCESS

EDITED BY
Xihui Shen,
Northwest A&F University,
China

REVIEWED BY
Masatoshi Miyakoshi,
University of Tsukuba,
Japan
Saswat S. Mohapatra,
Berhampur University,
India
Pengfei Ding,
University of Maryland,
United States

*CORRESPONDENCE
Weili Liang
✉ liangweili@icdc.cn
Biao Kan
✉ kanbiao@icdc.cn

SPECIALTY SECTION
This article was submitted to Infectious Agents and Disease, a section of the journal Frontiers in Microbiology

RECEIVED 30 November 2022
ACCEPTED 16 January 2023
PUBLISHED 01 February 2023

CITATION
Han Y, Li J, Gao H, Li X, Duan R, Cheng Q, Kan B and Liang W (2023) Serotype conversion gene *rfbT* is directly regulated by histone-like nucleoid structuring protein (H-NS) in *V. cholerae* O1.
Front. Microbiol. 14:1111895.
doi: 10.3389/fmicb.2023.1111895

Serotype conversion gene *rfbT* is directly regulated by histone-like nucleoid structuring protein (H-NS) in *V. cholerae* O1

Yu Han, Jing Li, He Gao, Xiaorui Li, Ran Duan, Qian Cheng, Biao Kan* and Weili Liang*

State Key Laboratory of Infectious Disease Prevention and Control, National Institute for Communicable Disease Control and Prevention, Chinese Center for Disease Control and Prevention, Beijing, China

Vibrio cholerae serogroup O1 (*V. cholerae* O1) is closely associated with cholera epidemics and has two main immunologically distinguishable serotypes, Ogawa and Inaba. Isolates serotype as Ogawa if the O-antigen polysaccharide (O-PS) is methylated or as Inaba if the O-PS is not methylated. This methylation is mediated by a methyltransferase encoded by the *rfbT* gene, and the mutation and low expression of *rfbT* results in serotype switch from Ogawa to Inaba. Previously, we have shown that cAMP receptor protein (CRP) activates *rfbT*. In this study, we demonstrated that histone-like nucleoid structuring protein (H-NS) is directly involved in the transcriptional repression of *rfbT*. This finding is supported by the analyses of *rfbT* mRNA level, *rfbT-lux* reporter fusions, electrophoretic mobility shift assay (EMSA), and DNase I footprinting assay. The *rfbT* mRNA abundances were significantly increased by deleting *hns* rather than *fis* which also preferentially associates with AT-rich sequences. A *single-copy chromosomal complement of hns partly restored the down-regulation of rfbT*. Analysis of *rfbT-lux* reporter fusions validated the transcriptional repression of *hns*. Subsequent EMSA and DNase I footprinting assay confirmed the direct binding of H-NS to *rfbT* promoter and mapped the exact binding site which was further verified by site-directed mutagenesis and promoter functional analysis. Furthermore, we found that in *hns* deletion mutant, CRP is no longer required for transcriptionally activating *rfbT*, suggesting that CRP functions as a dedicated transcription factor to relieve H-NS repression at *rfbT*. Together, this study expanded our understanding of the genetic regulatory mechanism of serotype conversion by global regulators in *V. cholerae* O1.

KEYWORDS

***rfbT*, H-NS, *V. cholerae*, transcriptional regulation, serotype shift**

1. Introduction

Cholera is an acute watery diarrheal disease caused by *Vibrio cholerae*, which is naturally present in the environment and autochthonous to coastal and estuarine ecosystems. People are usually infected by ingesting *V. cholerae*-contaminated water or food. Upon colonization of the host, *V. cholerae* produces cholera toxin (CT), which acts on intestinal epithelial cells, resulting in secretory diarrhea and even death within a few days if without treatment (Chiang and Mekalanos, 2000). Based on the heat-stable somatic O antigen, the species *V. cholerae* is divided into more than 200 serogroups. Among them, only two serogroups, toxigenic O1 and O139, have been demonstrated to cause epidemic and pandemic cholera. O1 serogroups have caused seven pandemics, and O139 emerged in the seventh pandemic (Longini et al., 2002). Serogroup O1 has two biotypes, El Tor and

classical. The first six pandemics are believed to be caused by the classical biotype, whereas the seventh pandemic that started in the early 1960s is caused by the El Tor biotype.

Vibrio cholerae O1 antigen consists of at least three types of antigenic factors: A, B, and C. According to the differences of the antigenic factors, each of the two biotypes can be further classified into two major cross-reacting serotypes, Ogawa and Inaba. Ogawa serotype strain expresses A and B antigens as well as a small amount of C antigens, while Inaba only expresses A and C antigens. A third serotype, Hikojima expressing both the B and C antigens, is also reported but is rare and unstable (Chatterjee and Chaudhuri, 2003). Ogawa and Inaba serotypes differ only by a single 2-*O*-methyl group that is present in the upstream (nonreducing) terminal perosamine unit of the Ogawa O-antigen polysaccharide (O-PS) but is absent in Inaba (Chatterjee and Chaudhuri, 2003). An isolate is serotyped as Ogawa if its O1 serogroup O-PS is methylated and as Inaba, if its O-PS is not methylated (Ito et al., 1993). This methylation is catalyzed by a methyltransferase encoded by the *rfbT* gene (also known as *webT* or *tsfB*; Rijpkema et al., 2004). Therefore, genetic alterations of *rfbT* resulted from various mutational events, such as specific point mutation, single nucleotide or short fragment insertion/deletion, or transposase insertion can all lead to the serotype shift from Ogawa to Inaba (Sharifnia et al., 2012; Liang et al., 2013; Karlsson et al., 2016). Once the complete *rfbT* is replenished, the Inaba type can be reverted to the Ogawa.

The serotype shifts can occur during subculture *in vitro*, passage *in vivo*, or even during pandemics (Ito et al., 1993; Liang et al., 2013; Karlsson et al., 2016). Recently, a major serotype switch (ranging from 7 to 100%) from Ogawa to Inaba was discovered after 5 years of the onset of cholera in Haiti in October, 2010 (Alam et al., 2016). Such serotransitions are nonrandom processes and thought to be related to selective pressures of serotype-specific immunity within the host population or environmental stress, the specific intrinsic drivers and regulation mechanism remain to be investigated (Longini et al., 2002; Karlsson et al., 2016). Previously, we demonstrated that a global regulator, cAMP receptor protein (CRP), positively regulates *rfbT* transcription through directly binding to a non-canonical CRP binding site (CBS) in its promoter region (Li et al., 2019).

The histone-like nucleoid structuring protein (H-NS) is a global regulator of environmentally controlled gene expression. It belongs to a small family of nucleoid-associated proteins (NAPs; Winardhi et al., 2015). This family comprises a group of basic, low molecular weight DNA binding proteins that participate in chromatin organization, restraining of DNA supercoiling, and transcription regulation. The factor for inversion stimulation (Fis), leucine-responsive protein (Lrp), heat-labile protein (HU) and integration host factor (IHF) are all members of this family. H-NS consists of a coiled-coil N-terminal domain that mediates the protein oligomerization and a C-terminal DNA-binding domain, which binds to promoters exhibiting AT-rich and highly curved regions as transcriptional inhibitors, affecting a broad spectrum of physiological processes including virulence-related genes at multiple phases of the *V. cholerae* life cycle (Winardhi et al., 2015; Ayala et al., 2017). Totally 701 genes have been identified to be regulated by H-NS in *V. cholerae* (Wang et al., 2015).

In this study, we show that H-NS negatively regulates the transcription of the serotype-switching gene *rfbT* by directly binding to its promoter region, whereas *fis* does not affect its expression. CRP likely activates transcription of *rfbT* through derepression of H-NS.

2. Materials and methods

2.1. Bacterial strains, culture conditions, and plasmids

Bacterial strains and plasmids used in this study are shown in Table 1. The *V. cholerae* O1 El Tor biotype, Ogawa serotype strain C7258 was used as wild-type (WT) precursor (Peru isolate, 1991). The mutant Δ*crp* (WL7258) was generated previously (Li et al., 2019). *E. coli* DH5α*λpir* and S17-1*λpir* were, respectively, used for cloning and conjugation purposes, ER2566 is used as host for the expression and purification of *hns* cloned into the pTXB1 vector. All strains were grown in Luria–Bertani (LB) broth (Oxoid, Basingstoke, United Kingdom) containing 1% NaCl (170 mM) at 37°C. When necessary, culture media were supplemented with ampicillin (Amp, 100 μg/ml), chloramphenicol (Cm, 10 μg/ml for *E. coli*, 2.5 μg/ml for *V. cholerae*) or polymyxin B (100 units/ml). Isopropyl-β-D-thiogalactopyranoside (IPTG) was used at a concentration of 0.5 mM for induction purposes.

2.2. Construction of mutants and complementation plasmids

Mutants Δ*hns*, Δ*fis* were constructed by homologous recombination mediated by suicide plasmid using C7258 as a precursor, while Δ*crp*Δ*hns* and Δ*crp*Δ*fis* used Δ*crp* (WL7258) as a precursor. Upstream and downstream chromosomal DNA fragments flanking the *hns* or *fis* were amplified from C7258 genomic DNA using the corresponding primers listed in Table 2. The amplicons were stitched together by overlapping PCR. Δ*hns* or Δ*fis* fragments were cloned into pWM91 and constructed in DH5α*λpir*. The resulting pWM91-Δ*hns* or pWM91-Δ*fis* was introduced into C7258 or Δ*crp* (WL7258) by conjugation from S17-1*λpir*. Exconjugants and mutants were selected as described previously (Wu et al., 2015; Li et al., 2019).

Chromosomal complementation strain Δ*hns*::*hns* was constructed using a temperature-sensitive transposable plasmid PGRG25. pGRG25 contains a Tn7 transposon that can carry the target fragment for specific recombination with the chromosome of the host bacterium, directionally inserted into the downstream of the *glms* in the chromosome (McKenzie and Craig, 2006). For this purpose, *hns* promotor region and open reading frame (ORF) was amplified and cloned into pGRG25 to generate pGRG25-*hns* which was mobilized into Δ*hns* by conjugation. The chromosomal insertion of the transposon was induced by 0.1% arabinose in LB broth at 30°C for 16 h, then screened on LB agar by a temperature at 42°C. Grown colonies were tested for Amp sensitivity, and proper insertion of *hns* downstream of *glms* was verified by PCR with primers targeting the *glms* and *hns* sequences. Primer sequences used here are shown in Table 2.

2.3. RNA extraction and quantitative reverse transcription PCR

Vibrio cholerae strains were cultured to OD_{600} 1.0. Total RNA extraction, removal of chromosomal DNA contamination and cDNA synthesis were performed as previously described (Wu et al., 2015). Equation $R = 2^{-(\Delta Cq\ rfbT - \Delta Cq\ thyA)}$ was used to calculate the relative expression values (R) of *rfbT*, where Cq is the threshold cycle fraction and *thyA* was used as an internal reference. A control reaction with total

10.3389/fmicb.2023.1111895

TABLE 1 Strains and plasmids used in this study.

Strains/plasmids	Characteristics	References/sources
E. coli		
S17-1λ*pir*	*thr thi tonA leu supE lacY recA*:: RP4-2Tc:: Mu (λ*pir*R6K)	Lab stock
DH5α*λpir*	F-D(*lacZYA-argF*)U169 *recA endA1 supE44 relA1λ*::*pir*	Lab stock
ER2566	*fhuA2 lacZ*::*T7 gene1* [*lon*] *ompT gal sulA11 R*(*mcr-73*:: *miniTn*10--Tet^S)2 [*dcm*] *R*(*zgb-210*::*Tn10*--Tet^S) *endA1* Δ(*mcrC-mrr*)*114*::*IS10*	Lab stock
V. cholerae		
C7258	Wild-type, El Tor biotype	Peru isolate, 1991
Δ*crp* (WL7258)	C7258, *crp* deletion mutant	Liang et al. (2007)
Δ*hns*	C7258, *hns* deletion mutant	This study
Δ*crp*Δ*hns*	C7258, *crp* and *hns* deletion mutant	This study
C7258Δ*hns*::*hns*	pGRG25 chromosome complementation	This study
Δ*fis*	C7258, *fis* deletion mutant	This study
Δ*crp*Δ*fis*	C7258, *crp* and *fis* deletion mutant	This study
C7258/pBBR*lux-rfbT*1	pBBR*lux-rfbT*1 in C7258	This study
Δ*hns* /pBBR*lux-rfbT*1	pBBR*lux-rfbT*1 in Δ*hns*	This study
C7258/pBBR*lux-rfbT*2	pBBR*lux-rfbT*2 in C7258	This study
Δ*hns*/pBBR*lux-rfbT*2	pBBR*lux*-p*rfbT*2 in Δ*hns*	This study
C7258/pBBR*lux-rfbT*1-M1	pBBR*lux-rfbT*1-M1 in C7258	This study
C7258/pBBR*lux-rfbT*1-M3-1	pBBR*lux-rfbT*1-M3-1 in C7258	This study
C7258/pBBR*lux-rfbT*1-M3-2	pBBR*lux-rfbT*1-M3-2 in C7258	This study
Δ*hns*/pBBR*lux-rfbT*1-M3-2	pBBR*lux-rfbT*1-M3-2 in Δ*hns*	This study
Plasmids		
pWM91	Suicide vector containing R6K ori, *sacB*, *lacZα*; Amp^R	Lab stock
pWM91-*hns*	1.6 kb *BamHI*-*SpeI* Δ*hns* fragment of C7258 in pWM91	This study
pWM91-*fis*	902 bp *BamHI*-*SpeI* Δ*fis* fragment of C7258 in pWM91	This study
pBBR*lux*	promoterless of *lux*CDABE, Cm^R	Lab stock
pBBR*lux-rfbT*1	554 bp promoter region of *rfbT* in pBBR*lux*	This study
pBBR*lux-rfbT*2	403 bp promoter region of *rfbT* without CRP binding site in pBBR*lux*	This study
pBBR*lux-rfbT*1-M1	pBBR*lux-rfbT*1 with mutations in the H-NS binding site 1	This study
pBBR*lux-rfbT*1-M3-1	pBBR*lux-rfbT*1 with mutations in the middle of the H-NS binding site 3	This study
pBBR*lux-rfbT*1-M3-2	pBBR*lux-rfbT*1 with mutations in the front part of the H-NS binding site 3	This study
pGRG25	Transposition plasmid, *oriT*, pSC101 *ori ts*, Amp^R	McKenzie and Craig (2006)
pGRG25-*hns*	*hns* promotor region and ORF of C7258 clone in pGRG25	This study
pTXB1	Expression vector for construction of in-frame	New England BioLabs
	Fusions with chitin binding domain, Amp^R	
pTXB1-*hns*	*hns* ORF in expression vector pXTB1, Amp^R	Wang H. et al. (2012)

RNA as a template was performed for each sample to exclude contamination from chromosomal DNA. Primers used were listed in Table 2.

2.4. Transcriptional reporter fusion construction and bioluminescence assay

Two different length fragments of *rfbT* promoter region were, respectively, amplified and cloned into pBBR*lux* upstream of the promoterless *luxCDABE* operon. The resultant fusion plasmids pBBRlux-*rfbT*1 and pBBRlux-*rfbT*2 were constructed in DH5α*λpir* and then mobilized into *V. cholerae* strains C7258 and Δ*hns* by conjugation from S17-1*λpir*. pBBR*lux-rfbT*1-M1, pBBR*lux-rfbT*1-M3-1, and pBBR*lux-rfbT*1-M3-2 reporter fusions containing the specific mutations in the predicted H-NS binding sites were generated by PCR-based site-directed mutagenesis with pBBRlux-*rfbT*1 as a template. Overnight cultures of *V. cholerae* strains containing *lux* reporter fusion plasmid were diluted at 1:100 in fresh LB and incubated at 37°C with shaking to grow to exponential phase. 200 μl of the broth was transferred into 96 well microtiter plates (Costar 3,917) every 1 h, and luminescence and OD_{600} were measured using a microplate reader (Infinite M200 Pro,

10.3389/fmicb.2023.1111895

TABLE 2 Primers used in this study.

Primer pairs	Oligonucleotide sequences (5′-3′)*	Purposes
hns-F1-up- *BamH*I	GCGGGATCCTTCCACAATTCATTGGCATCAC	Δ*hns* deletion strain construction
hns-F1-dn	ATCCAAATTGTGAACAGGAATTTTGCCAGA	
hns-F2-up	TGAACAGGAATTTTGCCAGAAACTAAAATG	
hns-F2-dn-*Spe*I	GGACTAGTACACCGAAGATTCCGCTAAAC	
fis-F1-up- *BamH*I	GCGGGATCCGGTGAGGCGGAATACGACAG	Δ*fis* deletion strain construction
fis-F1-dn	ACGTCGGTGAAGAATTCGGTCTAGCTCTTC	
fis-F2-up	GAAGAGCTAGACCGAATTCTTCACCGACGT	
fis-F2-dn-*Spe*I	GGACTAGTAAAGTGGGCGAGTAGGGTTTC	
hns-Tn7-*Not*I-up	GCGCGGCCGCTCAAGCGACATCATGTCAAC	C7258Δ*hns::hns* complementation strain construction and identification
hns-Tn7-*Xho*I-dn	GCTCTAGATCAGTATCCGTTCGAGTTAA	
glms-F	CGATTGCGGTAGAAGCGTC	
glms-hnsR	AGACTAAATGAGCCAAATGA	
thyA-qPCR-up	ACATGGGACGCGTGTATGG	qPCR for *thyA*
thyA-qPCR-dn	ATATGACCACCATCAGGCTTAGC	
rfbT-qPCR-up	TTCTTGAAAGCGAATTTGGATTGC	qPCR for *rfbT*
rfbT-qPCR-dn	GTGTATATGACGAGCAGCGATTC	
*rfbT*1-up-*Sac*I	CCCGAGCTCCGCAACAGAGCAAG ATGT	Construction of *rfbT-lux* reporter plasmids
*rfbT*2-up-*Sac*I	CCCGAGCTCTTAGAGCGGACGATCGAG	
rfbT-dn-*BamH*I	CGGGATCCGACTGAATAGCATCAAGC	
rfbT-hns-shift-up	CAAGGATCAGGCAGATATG (5'biotin label)	Probe-*hns*
rfbT-hns-shift-dn	CTTGCAGATGCAGGTTTGAG (5'biotin label)	
rfbT-crp-shift-up	CGTTACTTGAAGCGACTTGT(5′ biotin-labeled)	Probe-N7
rfbT-crp-shift-dn	CAAACATATCTGCCTGATCC (5′ biotin-labeled)	
rfbT-up (FAM)	CAAGGATCAGGCAGATATG	DNase I footprinting assay
rfbT-dn	CTTGCAGATGCAGGTTTGAG	
*rfbT*1-M1-R	GGGTTCGCTCTGTGTGAGGTTCAAACA	Construction of mutant *rfbT-lux* reporter plasmids
*rfbT*1-M1-F	TGTTTGAACCTCACACAGAGCGAACCC	
*rfbT*1-M3-1-R	AATGGATTTGCCATGTGTGTGACATTTAGAAG	
*rfbT*1-M3-1-F	CTTCTAAATGTCACACACATGGCAAATCCATT	
*rfbT*1-M3-2-R	GATTTGCCATTTTAGTTCCATTTAGAAG	
*rfbT*1-M3-2-F	CTTCTAAATGGAACTAAAATGGCAAATC	

*The underlined bases indicate the restriction enzyme sites.

Tecan, Austria). Luminescence activity was calculated as light unit/OD_{600} as previously described (Pan et al., 2018).

2.5. Expression and purification of H-NS protein

E. coli strain ER2566 containing the recombinant expression plasmid pXTB1-HNS (Wang H. et al., 2012) was cultured to OD_{600} of 0.5 with shaking at 37°C and then protein expression was induced with 0.4 mM IPTG for 4 h at 28°C. The cells were collected by centrifugation, resuspended in ice-cold Column buffer (20 mM Tris–HCl, pH 8.0, 0.5 M NaCl, and 1 mM EDTA), and lysed by sonication. The cell debris was removed by centrifugation, and H-NS-intein fusion protein with chitin binding domain (CBD) was purified using IMPACT™ Kit (New England Biolabs, United Kingdom) according to the manufacturer's instructions. The clarified lysate was slowly loaded onto the equilibrated chitin column, and then the chitin column was washed with 20 bed volumes of Column Buffer. Subsequently, the column was quickly washed with 5 bed volumes of the Cleavage Buffer (Column Buffer containing 80 mM DTT), and then incubated at 4°C overnight for full cleavage reaction on-column. Finally, the H-NS was eluted with Column Buffer. H-NS-containing fractions were combined and dialyzed against Column Buffer at 4°C to remove DTT. The purity of the recombinant H-NS was analyzed by SDS-PAGE (Figure 1A), and the protein concentration was determined by a Pierce BCA protein assay kit (Thermo Fisher Scientific, United States). The protein was stored in 20% glycerol at - 80°C.

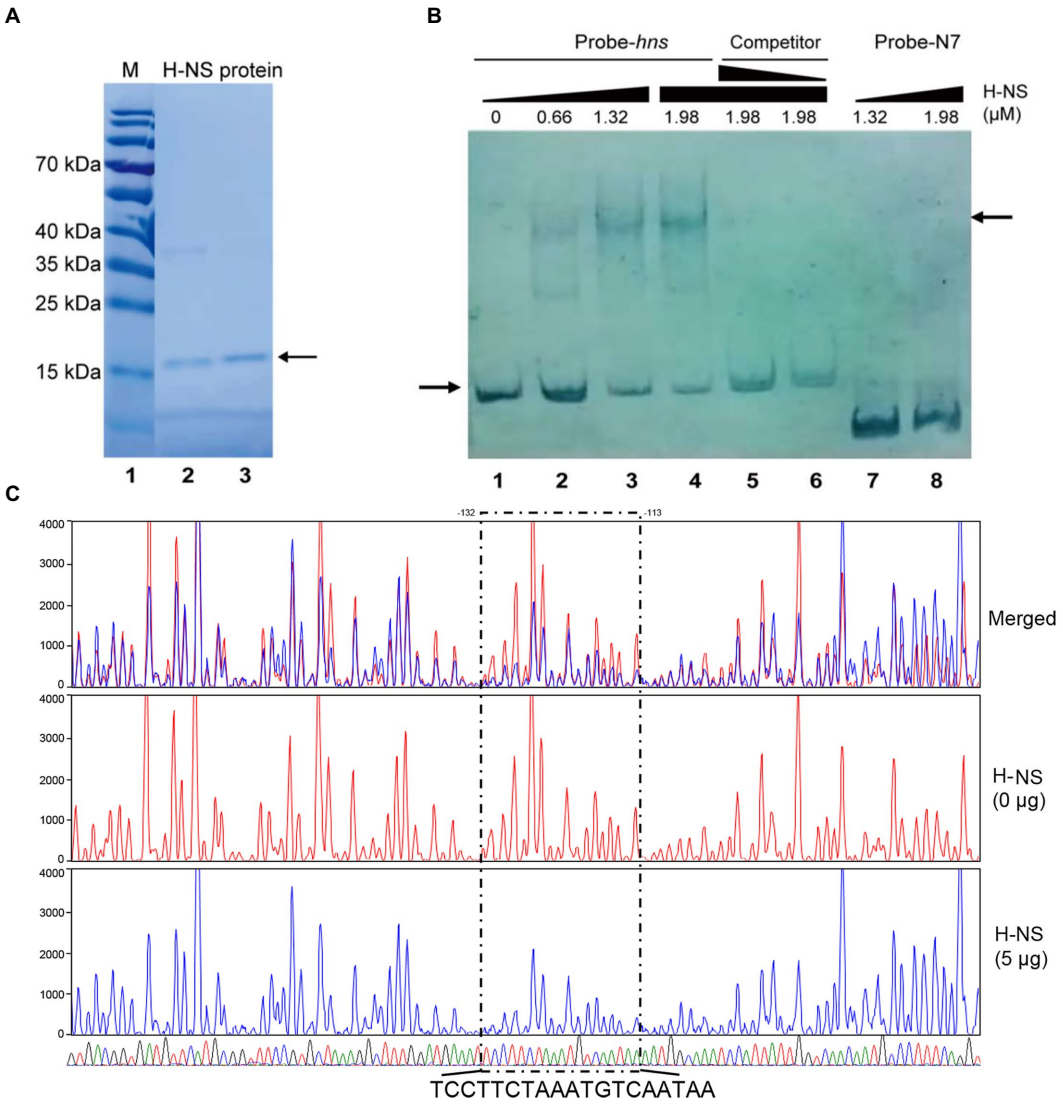

FIGURE 1
H-NS physically binds to the promoter region of *rfbT*. **(A)** H-NS protein purification. Lane 1 is protein marker, and lanes 2–3 are purified H-NS proteins. The right arrow indicates purified bands. **(B)** EMSA of H-NS bound to *rfbT* promoter regions. EMSA was described in the "Materials and Methods." Biotin-labeled 256-bp DNA probe (20ng) was incubated with increasing amounts of purified H-NS protein. For competitive analysis, the identical but unlabelled probe was added at 10 or 50-fold concentration relative to the labeled one (5–6 channels). Lanes 7 and 8 are Probe-N7 with H-NS. The left arrow indicated the free probe, whereas the right arrow referred to H-NS-*rfbT* bound one. **(C)** DNase I footprinting assay of H-NS binding to the promoter region of *rfbT*. As described in the "Materials and Methods," purified H-NS protein were incubated with FAM-labelled fragments of the *rfbT* promoter region, and then the fragments were digested with optimized DNase I. Finally, the digested fragments were analyzed, and the protected regions were boxed and marked. The colored traces representing the different concentrations of H-NS used (red, 0μg and blue, 5μg) are indicated separately and then merged, together with the DNA sequencing results (G, T, A, and C) displayed by four different colors. The region where the blue traces drop is the binding region of H-NS to the probe.

2.6. Electrophoretic mobility shift assays

Probe-*hns* was a 256 bp fragment of *rfbT* promoter region containing all of the predicted H-NS binding sequences, which was amplified with 5′ biotin-labeled primers. Competing cold probe was amplified using the same primers without a biotin label. Probe-N7 (Li et al., 2019) was a 140 bp fragment of *rfbT* promoter region containing the previously determined CRP binding site and used as a nonspecific control probe for H-NS binding (Li et al., 2019). The reaction mixture of 15 ng biotin-labeled probe with increasing amounts of purified H-NS protein in reaction buffer (10 mM Hepes, 150 mM KCl, 1 mM EDTA, 1 mM DTT, 10 mM $(NH_4)_2SO_4$, 0.2% Tween 20) together with 100 ng BSA and 100 ng *CF*-DNA in each reaction (20 μl) was incubated at 28°C for 30 min and then separated on a 6% native polyacrylamide gel. The free and H-NS-bound probes were visualized with the Chemiluminescent Nucleic Acid Detection Module (Thermo Fisher Scientific, United States) according to the manufacturer's instruction after transferring them onto nylon membranes.

2.7. DNase I footprinting assay

For preparation of fluorescent FAM-labeled probes, the promoter region was PCR amplified with 2 × HIFI DNA polymerase premix from

the plasmid pBBR*lux-rfbT*1 using primers of *rfbT*-up (FAM)and *rfbT*-dn. The FAM-labeled probes were purified by the Wizard® SV Gel and PCR Clean-Up System (Promega, United States) and were quantified with NanoDrop 2000C (Thermo, United States).

DNase I footprinting assay was performed as previously described (Wang Y. et al., 2012). For each assay, 250 ng probes were incubated with different amounts of protein in a total volume of 40 µl. After incubation for 30 min at 25°C, 10 µl solution containing about 0.015 unit DNase I (Promega, United States) and 100 nmol freshly prepared $CaCl_2$ was added and further incubation was performed at 37°C for 1 min. The reaction was stopped by adding 140 µl DNase I stop solution (200 mM unbuffered sodium acetate, 30 mM EDTA, and 0.15% SDS). Samples were first extracted with phenol/chloroform, and then precipitated with ethanol. Pellets were dissolved in 30 µl MiniQ water. The preparation of the DNA ladder, electrophoresis, and data analysis were the same as described before (Wang Y. et al., 2012), except that the GeneScan-LIZ600 size standard (Applied Biosystems) was used.

2.8. Statistical analysis

GraphPad Prism 9 software was used for statistical analysis and graphical representation of data. Statistical significance was determined by an unpaired two-tailed Student's *t*-test.

3. Results

3.1. Characterization of the promoter region of *rfbT*

Though the gene *rfbT* has been recognized as the genetic determinant of Ogawa serotype of *V. cholerae* O1 serogroup for more than 30 years (Stroeher et al., 1992) and various kinds of mutations were revealed in the *rfbT* coding sequence of isolates from different space–time sources (Sharifnia et al., 2012; Liang et al., 2013; Karlsson et al., 2016), its regulation and the molecular structural features except the transcriptional start site, putative −35 and −10 elements of the promoter-regulatory region remain unclear. Previously, we identified a *cis*-regulatory element, i.e., a non-canonical CBS in the promoter region, through which global regulator CRP exerts an activational effect (Li et al., 2019). Further sequence analysis revealed that the G+C content of promoter-intergenic region *of rfbT* (41.2%) is quite low compared with the *V. cholerae* genome in general (47.7% for chromosome I and 46.9% for chromosome II). In other words, the promoter-intergenic region of *rfbT* is AT rich and probably prone to be regulated by small nucleoid associated proteins such as H-NS and Fis which tend to bind AT rich sequences. Indeed, subsequent Virtual Footprint and PRODORIC analysis using the 10-bp H-NS consensus (Bouffartigues et al., 2007; Figure 2A) revealed 3 potential H-NS binding elements, site 1 (5'-CCTATTAAAG-3'), site 2 (5'-TATCAAACGT-3'), and site 3 (5'-TCAATAAAAT-3') in the *rfbT* promoter-intergenic region (Figure 2B). The three binding sites are, respectively, located at nucleotides −283 to −273, −250 to −240, and −120 to −110 relative to the *rfbT* start codon, and are all downstream of nonclassical CBS (Figure 2B). Of these, 8 of the 10 bp at site 3 is consistent with the consensus, followed by site 1 with 5 bp, and finally site 2 with only 4 bp (Figure 2A). It's worth noting that the site 3 overlaps the predicted −10 promoter element (Figure 2B). These findings strongly indicated the possibility that H-NS regulates serotype-shifting gene *rfbT* expression.

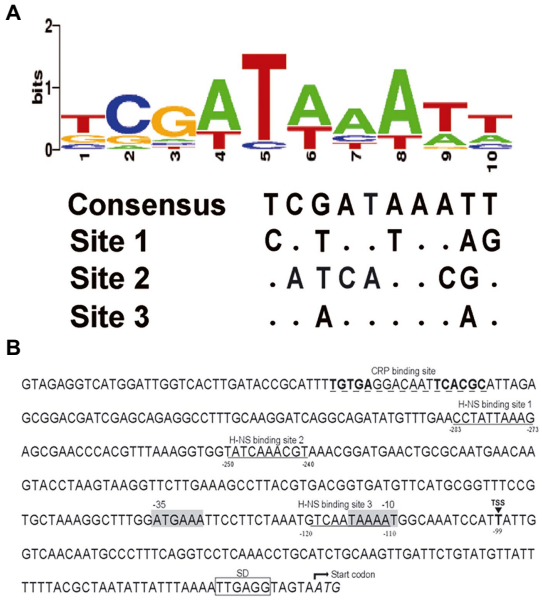

FIGURE 2
Nucleotide sequence analysis of the *rfbT* promoter region. **(A)** Conservation analysis of H-NS binding sites. Virtual Footprint was used to predict the binding sites of H-NS at the *rfbT* promoter (https://www.prodoric.de/vfp/). **(B)** Characteristics of the *rfbT* promoter region. Underlined sequences show the H-NS binding site predicted by Virtual Footprint. Dashed underlined sequences show the CRP binding sites characterized previously (Li et al., 2019). The black box marks the Shine-Dalgarno sequence (SD) (Ito et al., 1991). The triangle and the bold T represent the proved TSS of the *rfbT*, and the gray shaded sequences represent its −10 and −35 regions (Stroeher et al., 1992). The negative numbers at the bottom of sequences indicate the nucleotide positions relative to the start codon of *rfbT*.

3.2. H-NS negatively regulates *rfbT* expression

To determine whether H-NS is involved in the regulation of *rfbT*, we constructed an *hns* deletion mutant using C7258 as a precursor and detected the *rfbT* mRNA level in WT C7258, and Δ*hns* mutant. As shown in Figure 3A, compared to the C7258, Δ*hns* mutant statistically produced more *rfbT* mRNA. To further confirm the result, we constructed an *hns* complementation strain C7258Δ*hns*::*hns* where a single copy of *hns* gene with its native promoter region was integrated downstream of chromosomal *glms*. As displayed, the *rfbT* mRNA abundance was reduced in C7258Δ*hns*::*hns* compared to Δ*hns* mutant, though the expression level was not restored to the WT level (Figure 3A). Together, these results showed that H-NS negatively regulates *rfbT* expression.

In our previous study, we demonstrated that CRP could positively regulate *rfbT* transcription, and then we wondered whether H-NS regulates *rfbT* expression in a CRP-dependent manner (Li et al., 2019). For this purpose, we constructed a Δ*crp*Δ*hns* double mutant and compared its *rfbT* mRNA expression with those of Δ*hns* and Δ*crp* mutants. We found that, contrary to the Δ*crp* mutant where *rfbT* expression was obviously lower than its WT and Δ*hns*, the *rfbT* mRNA level was significantly increased in Δ*crp*Δ*hns* (Figure 3A), and

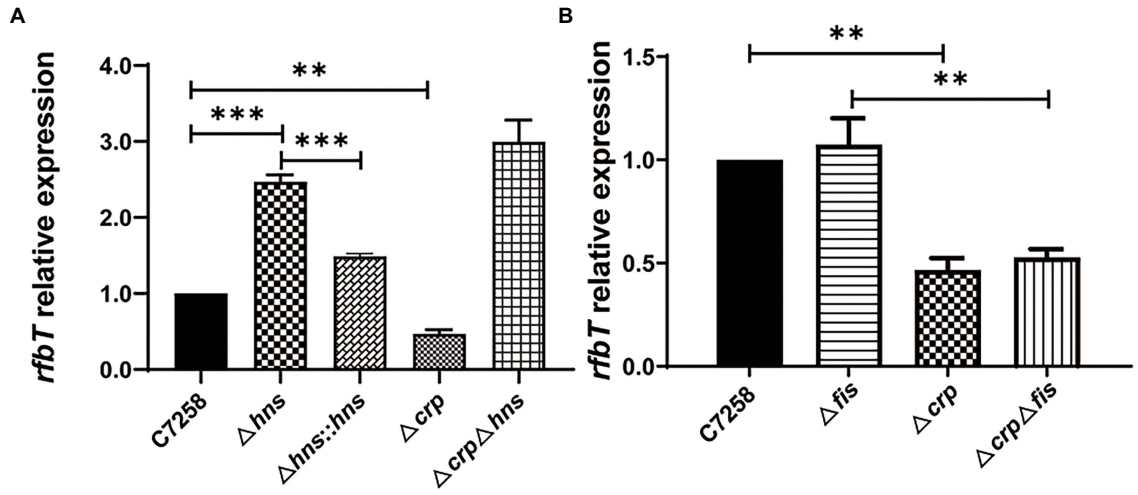

FIGURE 3
Effects of H-NS, CRP and Fis on *rfbT* expression. The mRNA abundances around OD_{600} of 1.0 were determined using qPCR. **(A)** Comparison of mRNA level of *rfbT* in *V. cholerae* strains C7258, Δ*hns*, Δ*hns::hns*, Δ*crp*, and Δ*crp*Δ*hns*. The equation $R=2^{-(\Delta Cq\ rfbT\ -\ \Delta Cq\ thyA)}$ is used to calculate the mRNA levels. **$p<0.01$, ***$p<0.001$. **(B)** The relative mRNA levels of *rfbT* in C7258, Δ*fis*, Δ*crp*, and Δ*crp*Δ*fis*. The calculation method is the same as **(A)**. **$p<0.01$.

additionally, the Δ*hns* and Δ*crp*Δ*hns* mutants displayed roughly similar *rfbT* mRNA level. These results proved that H-NS negatively regulates the expression of *rfbT* in a CRP-independent manner. From another perspective, these results also indicated that CRP is not required for *rfbT* activation in H-NS negative background.

3.3. Fis does not affect *rfbT* expression

Like H-NS, Fis belongs to the small family of nucleoid-associated proteins and is widely implicated in the control of gene expression through binding to the A−/AT-tracts-constituted binding site (Cho et al., 2008). To find out whether Fis takes part in the regulation of *rfbT*, we constructed Δ*fis* and Δ*crp*Δ*fis* deletion mutants and measured the *rfbT* mRNA levels. As displayed in Figure 3B, the *rfbT* mRNA level in Δ*fis* is similar to the WT, and deletion of *crp* significantly reduced *rfbT* expression regardless of the presence or absence of *fis*, implying that Fis is not involved in the regulation of *rfbT*.

3.4. H-NS represses the promoter activities of *rfbT*

To determine whether the H-NS-mediated repression of *rfbT* occurs at transcription level, we constructed two transcriptional reporter plasmids by fusing the different length fragments of promoter region of *rfbT* to the promoterless bioluminescence reporter genes *luxCDABE*. The 552-bp promoter fragment in pBBR*lux-rfbT*1 contains both the previously identified CBS and the predicted H-NS binding sites, while the 403-bp promoter region in pBBR*lux-rfbT*2 lacks the CBS. Consistent with the *rfbT* mRNA expression, bioluminescence activities of both pBBR*lux-rfbT*1 and pBBR*lux-rfbT*2 in Δ*hns* were significantly higher than in its WT (Figure 4). These results demonstrated that H-NS negatively regulates *rfbT* at the promoter level. H-NS represses the transcription of *rfbT* probably through binding to the predicted binding sites and therefore the direct interaction still needs to be clarified.

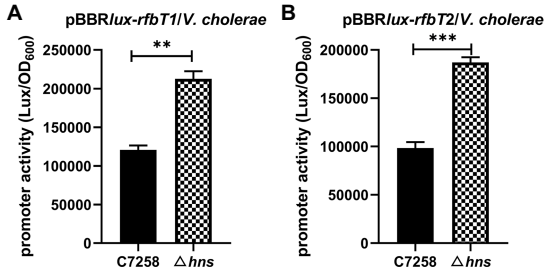

FIGURE 4
Luminescence activities of *lux* reporter fusion plasmids in *V. cholerae* C7258 and Δ*hns*. **(A)** Luminescence activities of pBBRlux-*rfbT*1 in C7258 and Δ*hns*. *rfbT*1 is a 554bp fragment of *rfbT* promoter region. **(B)** Luminescence activity of pBBRlux-*rfbT*2 in C7258 and Δ*hns*. *rfbT*2 is a 403bp fragment of the *rfbT* promoter region without CRP binding site. The luminescent activities were reported as luminescence/OD_{600} at the designated time points. ***$p<0.001$.

3.5. H-NS directly binds to the promoter of *rfbT*

To verify the direct binding of H-NS to the *rfbT* promoter region, we performed EMSA with purified H-NS protein. A 256-bp DNA fragment of *rfbT* promoter region encompassing the three predicted H-NS binding sites were labeled with biotin at 5′ end and used as specific probe. The same fragment without biotin label was employed as competing cold probe. The 135 amino acids *V. cholerae* H-NS protein was induced and purified from pTXB1-HNS recombinant plasmid (Wang H. et al., 2012) in *E. coli* host ER2566 and reached a purity of higher than 90% (Figure 1A). As displayed in Figure 1B, inclusion of H-NS (0.66 μM) generated two shifted bands with slower mobility. With the increment of H-NS (>1.32 μM), the intensity of the higher-shifted band was increased, concomitantly with the decrease of the amount of free probe. Adding the same, but unlabeled 256-bp DNA fragment greatly competed with the labeled probe in a dose-dependent manner. Both of the 10-fold and 50-fold addition of the competing cold probe

completely abolished the shifted-band, and concurrently the labeled probe was released as the free one. As expected, the amount of the released free probe is more in 50-fold cold probe reaction mixture than the 10-fold one. To further validate the specificity of H-NS binding, we adopted Probe-N7 which is a 140-bp DNA fragment of *rfbT* promoter region containing the intact CBS but without the predicted H-NS binding element (Li et al., 2019). No apparent shifted band was observed even when Probe-N7 was incubated with higher amount of H-NS (1.32 μM or 1.98 μM) under the same reaction condition, indicating that H-NS could not bind to the *rfbT* promoter fragment lack of specific binding site.

To further clarify the real H-NS binding site in the *rfbT* promoter and dissect the binding sequences, we conducted DNase I footprinting analysis. As shown in Figure 1C, the assay revealed one clearly protected region against DNase I digestion which is composed of TCCTTCTAAATGTCAATAA extending from −132 to −113 relative to the start codon of *rfbT*, i.e., this region completely overlaps the predicted binding site 3 extending from −120 to −110. Though EMSA displayed two H-NS retarded bands that seems somehow in accordance with the predicted existence of two more conserved binding sites 1 and 3, unexpectedly, the less conserved binding site 1 was not confirmed in the DNase I footprinting assay, which suggested that the more conserved site 3 is intrinsically the real binding site with high-affinity. Of course, we cannot exclude the possibility that the current assay condition did not favor binding to the low-conservation site 1.

To further validate that site 3 is the real functional H-NS binding site and the less conserved site 1 has no function, we set out to introduce mutations at sites 1 and 3 through PCR-based site-directed mutagenesis with pBBRlux-*rfbT*1 as the template (Figure 5A). We introduced 4-bp changes in the site 1 by replacing the ATT and the antepenultimate A with CAC and C, respectively, to generate a new construct pBBRlux-*rfbT*1-M1. Considering that site 3 overlaps the predicted −10 promoter element, we introduced two sets of mutations to construct pBBR*lux-rfbT*1-M3-1 and pBBR*lux-rfbT*1-M3-2. In pBBR*lux-rfbT*1-M3-1, the conserved ATA and the antepenultimate A were changed to CAC and C, where TA and A are involved in the −10 motif of *rfbT* promoter. In pBBR*lux-rfbT*1-M3-2, the TC and second A were changed to GA and C. These new constructs were mobilized into *V. cholerae* WT and Δ*hns* to measure the corresponding bioluminescence activities. As depicted in Figure 5B, pBBRlux-*rfbT*1-M1 and pBBRlux-*rfbT*1 had similar bioluminescence activities in the WT background which indicated that the mutation of sites 1 has no effect on the *rfbT* promoter, i.e., site 1 is indeed not a H-NS binding site. However, compared to the pBBRlux-*rfbT*1, pBBR*lux-rfbT*1-M3-2 displayed significantly high bioluminescence activity in WT as same as in the Δ*hns*, implying that the introduced mutation affects H-NS binding and thus relieves its repression. Not surprisingly, pBBR*lux-rfbT*1-M3-1 almost completely lost the bioluminescence signal due to the mutations that destroyed the −10 motif of *rfbT* promoter by changing TAAAAT to ACACAT. Altogether, these results further experimentally validated that site 3 partially overlaps the −10 motif of *rfbT* promoter and is the intrinsically functional H-NS binding site.

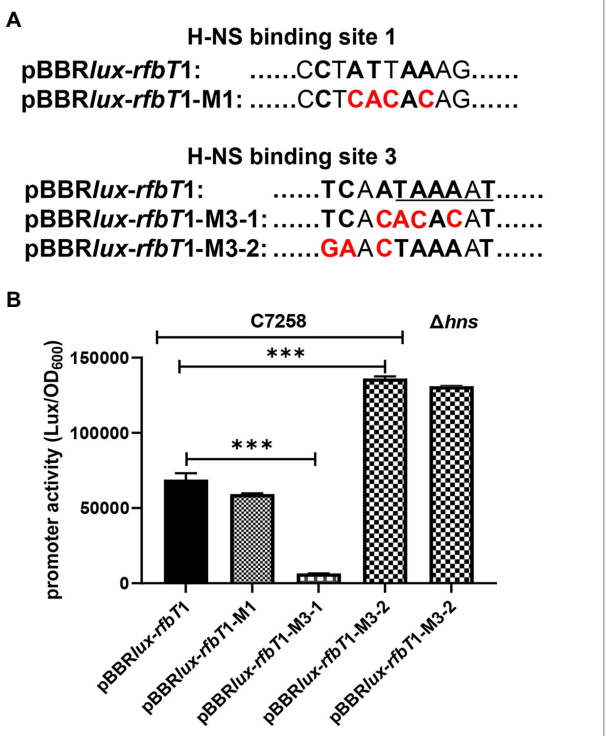

FIGURE 5
Schematics of the site-directed mutagenesis of the H-NS binding sites at *rfbT* and luminescence activities of *lux* reporter fusion plasmids containing mutations in *V. cholerae*. **(A)** The pBBR*lux-rfbT*1-M1, pBBR*lux-rfbT*1-M3-1, and pBBR*lux-rfbT*1-M3-2 were constructed by introducing specific mutations in the relevant H-NS sites at the *rfbT* promoter. The bases identical to the 10-bp H-NS binding consensus were indicated in boldface letters and the changed ones in red color. The underlined sequence is the predicted −10 motif of *rfbT* promoter. **(B)** Luminescence activities of pBBR*lux-rfbT*1, pBBR*lux-rfbT*1-M1, pBBR*lux-rfbT*1-M3-1, and pBBR*lux-rfbT*1-M3-2 in C7258 and pBBR*lux-rfbT*1-M3-2 in Δ*hns*. The luminescence activities were reported as luminescence/OD_{600} as described in the "Materials and Methods." ***$p<0.001$.

4. Discussion

rfbT (also named *webT* or *tsfB*) is a genetic determinant of Ogawa serotype of *V. cholerae* O1 by encoding an enzyme that methylates the O-PSs-terminal peraminoglycans of surface LPS. Genetic alteration of *rfbT* results in impaired function of the enzyme, causing serotype shift from Ogawa to Inaba. Various mutational events of *rfbT* leading to serotype switching have been reported under different circumstance around the world (Longini et al., 2002; Liang et al., 2013; Karlsson et al., 2016). The epidemiological significance of the two serotype variants shift, the influencing factors and regulation mechanism remain largely uninvestigated. Driven by the serotype-specific immunity acquired within the infected host population (Longini et al., 2002) is a commonly accepted speculation.

In our previous study, we reported the global regulator CRP activates the expression of *rfbT* and further revealed the underlying genetic mechanism (Li et al., 2019). In this study, we reported another global regulator H-NS which is involved in the transcriptional repression of *rfbT* by directly binding to its AT-rich promoter region (Figures 1, 3–5). Though more than one potential binding sites were predicted, binding site 3 was finally validated to be the functional H-NS binding site by DNase I footprinting assay and site-directed mutagenesis (Figures 1C, 5). This site overlaps the −10 promoter element (Figures 1C, 2B, 5), thus strongly implying that H-NS functions to block *rfbT* transcription by interfering with RNA polymerase binding and activity. In addition, we showed that though CRP activates the transcription of *rfbT* (Li et al., 2019), it loses this function in the H-NS minus background (Figures 3A, 4), indicating that CRP may act as an antisilencer by antagonizing H-NS

repression in the *rfbT* promoter. A number of virulence regulators, such as ToxT, ToxR, and IHF have been reported to act as antirepressors by displacing H-NS at specific promoters (Stonehouse et al., 2008, 2011; Kazi et al., 2016). In these cases, the H-NS binding sites generally overlap or are adjacent to the binding sites of specific activators, such as at *V. cholerae tcpA* promoter, the binding site of IHF is located between the two sites of H-NS with 6 bp intervals with the up one and overlapping the down one (Stonehouse et al., 2008). At cholera toxin *ctx* promoter, competitive binding to the overlapping H-NS/ToxT binding sites was proved in EMSA where ToxT could displace H-NS from the *ctx* promoter (Stonehouse et al., 2008). However, in our case, the detailed molecular mechanism of CRP antagonizing H-NS repression on *rfbT* remains investigated considering the CRP-specific CBS and H-NS binding site 3 are separated by 220 bp. We reasoned the alleviation of H-NS repression by CRP at *rfbT* is mechanistically distinct from *tcpA* and *ctx* and will be investigated in the future.

Selective silencing of horizontally acquired genes is a common theme in H-NS transcription regulation (Navarre et al., 2006). Horizontally acquired foreign DNA generally has a lower GC-content than its progenitor genome (Kazi et al., 2016). The G + C content of *rfbT* (31.7%) is quite low compared with the rest of the *rfb* region (39.1%) and with *V. cholerae* genome (47% in average). These observations suggest that *rfbT* is acquired as a foreign DNA and its expression is normally silenced by H-NS. This repression effect could be alleviated by other regulators such as CRP under appropriate environmental conditions. The preference for binding low GC-content DNA is also shared by IHF and Fis. Fis has been proved to be unable to affect the expression of *rfbT*, while the regulation effect of IHF remains to be determined.

The silencing function of H-NS is dependent on its oligomerization properties. It is believed that an H-NS dimer is the minimal functional binding unit (Badaut et al., 2002). Environmental stimuli such as temperature and osmolality can alter the oligomerization states of H-NS *in vivo* and hence affect its gene-silencing properties (Amit et al., 2003; Stella et al., 2006; Bouffartigues et al., 2007). At a certain osmolality, the ability of H-NS to bind DNA decreased significantly with increasing temperature (Amit et al., 2003; Bouffartigues et al., 2007). In a word, a variety of factors can affect the function of the H-NS. Whether these environmental factors affect the phenotype of Ogawa serotype strain through H-NS remains to be clarified.

In summary, we demonstrated that *V. cholerae* Ogawa serotype specific gene *rfbT* is transcriptionally repressed by the global regulator H-NS through directly binding to a specific *cis* regulatory element in the promoter region. This work expanded our knowledge of understanding the genetic determinants and complicated regulatory mechanism of *V. cholerae* O1 serotype shift.

Data availability statement

The original contributions presented in the study are included in the article/supplementary material, further inquiries can be directed to the corresponding authors.

Author contributions

WL and BK conceived and designed this study. YH, JL, HG, XL, and RD contributed to the experiment. YH and WL contributed to writing the manuscript. All authors contributed to the article and approved the submitted version.

Funding

This study is supported by the National Key R&D Program of China under grant 2021YFC2300302.

Conflict of interest

The authors declare that the research was conducted in the absence of any commercial or financial relationships that could be construed as a potential conflict of interest.

Publisher's note

References

Alam, M. T., Ray, S. S., Chun, C. N., Chowdhury, Z. G., Rashid, M. H., Madsen Beau De Rochars, V. E., et al. (2016). Major shift of toxigenic *V. cholerae* O1 from Ogawa to Inaba serotype isolated from clinical and environmental samples in Haiti. *PLoS Negl. Trop. Dis.* 10:e0005045. doi: 10.1371/journal.pntd.0005045

Amit, R., Oppenheim, A. B., and Stavans, J. (2003). Increased bending rigidity of single DNA molecules by H-NS, a temperature and osmolarity sensor. *Biophys. J.* 84, 2467–2473. doi: 10.1016/S0006-3495(03)75051-6

Ayala, J. C., Silva, A. J., and Benitez, J. A. (2017). H-NS: an overarching regulator of the *vibrio cholerae* life cycle. *Res. Microbiol.* 168, 16–25. doi: 10.1016/j.resmic.2016.07.007

Badaut, C., Williams, R., Arluison, V., Bouffartigues, E., Robert, B., Buc, H., et al. (2002). The degree of oligomerization of the H-NS nucleoid structuring protein is related to specific binding to DNA. *J. Biol. Chem.* 277, 41657–41666. doi: 10.1074/jbc.M206037200

Bouffartigues, E., Buckle, M., Badaut, C., Travers, A., and Rimsky, S. (2007). H-NS cooperative binding to high-affinity sites in a regulatory element results in transcriptional silencing. *Nat. Struct. Mol. Biol.* 14, 441–448. doi: 10.1038/nsmb1233

Chatterjee, S. N., and Chaudhuri, K. (2003). Lipopolysaccharides of *Vibrio cholerae*. I. Physical and chemical characterization. *Biochim. Biophys. Acta* 1639, 65–79. doi: 10.1016/j.bbadis.2003.08.004

Chiang, S. L., and Mekalanos, J. J. (2000). Construction of a *Vibrio cholerae* vaccine candidate using transposon delivery and FLP recombinase-mediated excision. *Infect. Immun.* 68, 6391–6397. doi: 10.1128/IAI.68.11.6391-6397.2000

Cho, B. K., Knight, E. M., Barrett, C. L., and Palsson, B. O. (2008). Genome-wide analysis of Fis binding in *Escherichia coli* indicates a causative role for A–/AT-tracts. *Genome Res.* 18, 900–910. doi: 10.1101/gr.070276.107

Ito, T., Hiramatsu, K., Ohshita, Y., and Yokota, T. (1993). Mutations in the *rfbT* gene are responsible for the Ogawa to Inaba serotype conversion in *Vibrio cholerae* O1. *Microbiol. Immunol.* 37, 281–288. doi: 10.1111/j.1348-0421.1993.tb03211.x

Ito, T., Ohshita, Y., Hiramatsu, K., and Yokota, T. (1991). Identification and nucleotide sequence determination of the gene responsible for Ogawa serotype specificity of *V. cholerae* O1. *FEBS Lett.* 286, 159–162. doi: 10.1016/0014-5793(91)80964-5

Karlsson, S. L., Thomson, N., Mutreja, A., Connor, T., Sur, D., Ali, M., et al. (2016). Retrospective analysis of serotype switching of *vibrio cholerae* O1 in a cholera endemic region shows it is a non-random process. *PLoS Negl. Trop. Dis.* 10:e0005044. doi: 10.1371/journal.pntd.0005044

Kazi, M. I., Conrado, A. R., Mey, A. R., Payne, S. M., and Davies, B. W. (2016). ToxR antagonizes H-NS regulation of horizontally acquired genes to drive host colonization. *PLoS Pathog.* 12:e1005570. doi: 10.1371/journal.ppat.1005570

Li, J., Lu, S., Kan, B., and Liang, W. (2019). Serotype-shifting gene *rfbT* is a direct transcriptional target of cAMP receptor protein (CRP) in *V. cholerae* O1. *Biochem. Biophys. Res. Commun.* 519, 874–879. doi: 10.1016/j.bbrc.2019.09.080

Liang, W., Pascual-Montano, A., Silva, A. J., and Benitez, J. A. (2007). The cyclic AMP receptor protein modulates quorum sensing, motility and multiple genes that affect intestinal colonization in Vibrio cholerae. *Microbiology (Reading)* 153, 2964–2975. doi: 10.1099/mic.0.2007/006668-0

Liang, W., Wang, L., Liang, P., Zheng, X., Zhou, H., Zhang, J., et al. (2013). Sequence polymorphisms of *rfbT* among the *Vibrio cholerae* O1 strains in the Ogawa and Inaba serotype shifts. *BMC Microbiol.* 13:173. doi: 10.1186/1471-2180-13-173

Longini, I. M., Yunus, M., Zaman, K., Siddique, A. K., Sack, R. B., and Nizam, A. (2002). Epidemic and Endemic Cholera Trends over a 33-year period in Bangladesh. *J. Infect. Dis.* 186, 246–251. doi: 10.1086/341206

McKenzie, G. J., and Craig, N. L. (2006). Fast, easy and efficient: site-specific insertion of transgenes into enterobacterial chromosomes using Tn7 without need for selection of the insertion event. *BMC Microbiol.* 6:39. doi: 10.1186/1471-2180-6-39

Navarre, W. W., Porwollik, S., Wang, Y., McClelland, M., Rosen, H., Libby, S. J., et al. (2006). Selective silencing of foreign DNA with low GC content by the H-NS protein in *salmonella*. *Science* 313, 236–238. doi: 10.1126/science.1128794

Pan, J., Zhao, M., Huang, Y., Li, J., Liu, X., Ren, Z., et al. (2018). Integration host factor modulates the expression and function of T6SS2 in *Vibrio fluvialis*. *Front. Microbiol.* 9:962. doi: 10.3389/fmicb.2018.00962

Rijpkema, S. G., Durrani, Z., Ramamurthy, T., and Balakrish Nair, G. (2004). Assessing clonality of *Vibrio cholerae* Inaba isolates by characterization of nonsense mutations in wbeT. *J. Med. Microbiol.* 53, 1105–1107. doi: 10.1099/jmm.0.45744-0

Sharifnia, A., Bakhshi, B., and Pourshafie, M. R. (2012). *wbeT* sequence typing and IS1004 profiling of *Vibrio cholerae* isolates. *Lett. Appl. Microbiol.* 54, 267–271. doi: 10.1111/j.1472-765X.2012.03204.x

Stella, S., Falconi, M., Lammi, M., Gualerzi, C. O., and Pon, C. L. (2006). Environmental control of the in *vivo* oligomerization of nucleoid protein H-NS. *J. Mol. Biol.* 355, 169–174. doi: 10.1016/j.jmb.2005.10.034

Stonehouse, E. A., Hulbert, R. R., Nye, M. B., Skorupski, K., and Taylor, R. K. (2011). H-NS binding and repression of the *ctx* promoter in *Vibrio cholerae*. *J. Bacteriol.* 193, 979–988. doi: 10.1128/JB.01343-09

Stonehouse, E., Kovacikova, G., Taylor, R. K., and Skorupski, K. (2008). Integration host factor positively regulates virulence gene expression in *Vibrio cholerae*. *J. Bacteriol.* 190, 4736–4748. doi: 10.1128/JB.00089-08

Stroeher, U. H., Karageorgos, L. E., Morona, R., and Manning, P. A. (1992). Serotype conversion in *Vibrio cholerae* O1. *Proc. Natl. Acad. Sci. U. S. A.* 89, 2566–2570. doi: 10.1073/pnas.89.7.2566

Wang, H., Ayala, J. C., Benitez, J. A., and Silva, A. J. (2012). Interaction of the histone-like nucleoid structuring protein and the general stress response regulator RpoS at *Vibrio cholerae* promoters that regulate motility and hemagglutinin/protease expression. *J. Bacteriol.* 194, 1205–1215. doi: 10.1128/JB.05900-11

Wang, H., Ayala, J. C., Benitez, J. A., and Silva, A. J. (2015). RNA-seq analysis identifies new genes regulated by the histone-like nucleoid structuring protein (H-NS) affecting *Vibrio cholerae* virulence, stress response and chemotaxis. *PLoS One* 10:e0118295. doi: 10.1371/journal.pone.0118295

Wang, Y., Cen, X. F., Zhao, G. P., and Wang, J. (2012). Characterization of a new GlnR binding box in the promoter of *amtB* in *Streptomyces coelicolor* inferred a PhoP/GlnR competitive binding mechanism for transcriptional regulation of *amtB*. *J. Bacteriol.* 194, 5237–5244. doi: 10.1128/JB.00989-12

Winardhi, R. S., Yan, J., and Kenney, L. J. (2015). H-NS regulates gene expression and compacts the nucleoid: insights from single-molecule experiments. *Biophys. J.* 109, 1321–1329. doi: 10.1016/j.bpj.2015.08.016

Wu, R., Zhao, M., Li, J., Gao, H., Kan, B., and Liang, W. (2015). Direct regulation of the natural competence regulator gene *tfoX* by cyclic AMP (cAMP) and cAMP receptor protein (CRP) in Vibrios. *Sci. Rep.* 5:14921. doi: 10.1038/srep14921

frontiers | Frontiers in Microbiology

TYPE Original Research
PUBLISHED 16 February 2023
DOI 10.3389/fmicb.2023.1063368

OPEN ACCESS

EDITED BY
Dongsheng Zhou,
Beijing Institute of Microbiology and Epidemiology, China

REVIEWED BY
Bindu Subhadra,
Long Island University, United States
Ruojun Wang,
Princeton University, United States
Ilan Rosenshine,
The Hebrew University of Jerusalem, Israel

*CORRESPONDENCE
Cristina Lara-Ochoa
✉ cristina.laraochoa@correo.buap.mx
José L. Puente
✉ jose.puente@ibt.unam.mx

SPECIALTY SECTION
This article was submitted to Infectious Agents and Disease, a section of the journal Frontiers in Microbiology

RECEIVED 07 October 2022
ACCEPTED 23 January 2023
PUBLISHED 16 February 2023

CITATION
Lara-Ochoa C, Huerta-Saquero A, Medrano-López A, Deng W, Finlay BB, Martínez-Laguna Y and Puente JL (2023) GrlR, a negative regulator in enteropathogenic *E. coli*, also represses the expression of LEE virulence genes independently of its interaction with its cognate partner GrlA. *Front. Microbiol.* 14:1063368. doi: 10.3389/fmicb.2023.1063368

GrlR, a negative regulator in enteropathogenic *E. coli*, also represses the expression of LEE virulence genes independently of its interaction with its cognate partner GrlA

Cristina Lara-Ochoa[1,2]*, Alejandro Huerta-Saquero[1,3], Abraham Medrano-López[1], Wanyin Deng[4], B. Brett Finlay[4], Ygnacio Martínez-Laguna[5] and José L. Puente[1]*

[1]Departamento de Microbiología Molecular, Instituto de Biotecnología, Universidad Nacional Autónoma de México, Cuernavaca, Mexico, [2]Centro de Detección Biomolecular, Benemérita Universidad Autónoma de Puebla, Puebla, Mexico, [3]Departamento de Bionanotecnología, Centro de Nanociencias y Nanotecnología, Universidad Nacional Autónoma de México, Ensenada, Mexico, [4]Michael Smith Laboratories, Department of Microbiology and Immunology, and Biochemistry and Molecular Biology, University of British Columbia, Vancouver, BC, Canada, [5]Vicerrectoría de Investigación y Estudios de Posgrado, Benemérita Universidad Autónoma de Puebla, Puebla, Mexico

Introduction: Enteropathogenic *Escherichia coli* (EPEC), enterohemorrhagic *E. coli* (EHEC) and *Citrobacter rodentium* (CR) belong to a group of pathogens that share the ability to form "attaching and effacing" (A/E) lesions on the intestinal epithelia. A pathogenicity island known as the locus of enterocyte effacement (LEE) contains the genes required for A/E lesion formation. The specific regulation of LEE genes relies on three LEE-encoded regulators: Ler activates the expression of the LEE operons by antagonizing the silencing effect mediated by the global regulator H-NS, GrlA activates *ler* expression and GrlR represses the expression of the LEE by interacting with GrlA. However, despite the existing knowledge of LEE regulation, the interplay between GrlR and GrlA and their independent roles in gene regulation in A/E pathogens are still not fully understood.

Methods: To further explore the role that GrlR and GrlA in the regulation of the LEE, we used different EPEC regulatory mutants and *cat* transcriptional fusions, and performed protein secretion and expression assays, western blotting and native polyacrylamide gel electrophoresis.

Results and discussion: We showed that the transcriptional activity of LEE operons increased under LEE-repressing growth conditions in the absence of GrlR. Interestingly, GrlR overexpression exerted a strong repression effect over LEE genes in wild-type EPEC and, unexpectedly, even in the absence of H-NS, suggesting that GrlR plays an alternative repressor role. Moreover, GrlR repressed the expression of LEE promoters in a non-EPEC background. Experiments with single and double mutants showed that GrlR and H-NS negatively regulate the expression of LEE operons at two cooperative yet independent levels. In addition to the notion that GrlR acts as a repressor by inactivating GrlA through protein-protein interactions, here we showed that a DNA-binding defective GrlA mutant that still interacts with

GrlR prevented GrlR-mediated repression, suggesting that GrlA has a dual role as a positive regulator by antagonizing GrlR's alternative repressor role. In line with the importance of the GrlR-GrlA complex in modulating LEE gene expression, we showed that GrlR and GrlA are expressed and interact under both inducing and repressing conditions. Further studies will be required to determine whether the GrlR alternative repressor function depends on its interaction with DNA, RNA, or another protein. These findings provide insight into an alternative regulatory pathway that GrlR employs to function as a negative regulator of LEE genes.

KEYWORDS

EPEC, type III secretion, LEE regulation, GrlR, GrlA, transcription, A/E pathogens, CAT reporter assay

Introduction

Enteropathogenic *Escherichia coli* (EPEC) is one of the main etiological agents of severe diarrhea in children under 2 years of age, predominantly in developing countries (Pearson et al., 2016). EPEC, enterohemorrhagic *E. coli* (EHEC) and *Citrobacter rodentium* belong to a group of pathogens that possess the ability to induce a unique histopathological lesion known as attaching and effacing (A/E) (Croxen and Finlay, 2010). The localized destruction of the microvilli of intestinal epithelial cells followed by rearrangements of the cytoskeleton beneath the site of bacterial adherence, leading to the formation of actin-rich cup-like structures that favor an intimate interaction between the bacterium and the host cell, are hallmarks of this lesion (Spears et al., 2006; Frankel and Phillips, 2008).

Most genes required for A/E lesion formation are located within a pathogenicity island known as the locus of enterocyte effacement (LEE) (Gaytan et al., 2016). The LEE region contains five polycistronic operons (*LEE1-LEE5*), two bicistronic operons (*espG-rorf1* and *grlRA*) and four transcriptional units (*etgA*, *cesF*, *map*, and *escD*). *LEE1* to *LEE3* encode the structural components of a type III secretion system (T3SS) responsible for translocating effector proteins into the enterocyte. The *LEE4* operon codes for translocator proteins (EspA, B, D), and *LEE5* encodes proteins involved in the intimate attachment (intimin and Tir). Genes encoding effector proteins, chaperones and transcriptional regulators are distributed within and outside the LEE (Pearson et al., 2016; Serapio-Palacios and Finlay, 2020). The cooperative action of the EPEC translocated effector proteins leads to cytoskeleton rearrangements, increased cell permeability, decreased absorption of ions and nutrients, alterations of tight junctions and modulation of the inflammatory response in the host intestinal cells and thus diarrheal disease (Guttman and Finlay, 2008; Croxen et al., 2013).

In A/E bacteria, the LEE pathogenicity island is a distinctive example of a genetic element whose expression is controlled by a complex network of global (ancestral) and horizontally acquired regulatory proteins in response to a wide variety of environmental factors (Furniss and Clements, 2018; Platenkamp and Mellies, 2018). One of the main regulatory mechanisms involved in controlling LEE gene expression is the xenogeneic silencing exerted by H-NS (Bustamante et al., 2001). As described in different enterobacteria, H-NS specifically silences gene transcription by binding to AT-rich DNA sequences of exogenous origin to maintain cell integrity but also contributes to the acquisition of beneficial sequences (Navarre, 2016). Interestingly, within the LEE, the first gene of the *LEE1* operon encodes Ler (LEE-encoded regulator), a protein belonging to the H-NS family of nucleoid-associated proteins, which is the central positive regulator controlling the expression of *LEE* genes, and genes located outside the LEE, by counteracting the silencing effect exerted by H-NS on the LEE operons (Elliott et al., 2000; Sperandio et al., 2000; Bustamante et al., 2001; Sanchez-SanMartin et al., 2001; Haack et al., 2003; Barba et al., 2005; Bingle et al., 2014). Due to its essential role, modulation of *LEE1* operon expression is key for activating or repressing all the LEE genes and non-LEE co-regulated genes; thus, its regulation is complex and multifactorial (Furniss and Clements, 2018; Platenkamp and Mellies, 2018; Turner et al., 2019).

The LEE encodes two additional regulatory proteins: GrlA (Global regulator of LEE-activator) and GrlR (Global regulator of LEE-repressor). GrlA shares homology with a small number of predicted uncharacterized proteins in different bacterial species and with CaiF, an activator of genes involved in carnitine utilization (Deng et al., 2004; Jimenez et al., 2010). A predicted helix-turn-helix (HTH) motif is found at the N-terminus of these proteins, where most of the conservation is observed. GrlA binds to the *ler* promoter to positively regulate its expression (Huang and Syu, 2008; Jimenez et al., 2010; Bustamante et al., 2011; Padavannil et al., 2013), while Ler also induces the *grlRA* operon establishing a positive regulatory loop that enhances LEE gene expression under inducing conditions (Barba et al., 2005). Point mutations at the HTH motif affect the activation function of GrlA (Jimenez et al., 2010; Islam et al., 2011; Padavannil et al., 2013). Moreover, GrlA is present in the cell in a membrane-associated inactive state that responds to mechanical stimuli (Alsharif et al., 2015; Sirisaengtaksin et al., 2020).

In contrast, GrlR acts as a repressor by forming a dimeric structure of antiparallel beta-barrel subunits with a molecular mass of 29 kDa, which exerts its function as a negative regulator through the interaction with the HTH motif of GrlA, forming a complex with a molecular mass of 47.3 kDa that prevents the activation of the *ler* promoter (Deng et al., 2004; Lio and Syu, 2004; Iyoda and Watanabe, 2005; Jobichen et al., 2007; Jimenez et al., 2010; Padavannil et al., 2013). Orthologs of GrlR are found in species of the genera *Proteus*, *Morganella*, *Serratia*, *Klebsiella* and *Salmonella*, among others, sharing between 30 to 42% identity; however, these GrlR orthologs are hypothetical proteins with no assigned function yet. The ClpXP complex, an AAA + protease, positively controls LEE gene expression in EHEC through direct regulation of GrlR levels during the stationary phase of growth (Iyoda and Watanabe, 2005). Moreover, Hfq, an RNA chaperone, together with the small

RNAs MgrR, RyhB and McaS, negatively modulate LEE gene expression in EPEC at the post-transcriptional level by destabilizing the *grlRA* mRNA and, consequently, the expression of GrlR and GrlA (Hansen and Kaper, 2009; Bhatt et al., 2017; Sudo et al., 2022). Furthermore, GrlA and GrlR also regulate the expression of genes located outside the LEE, such as the hemolysin and flagellar genes in EHEC (Iyoda et al., 2006; Saitoh et al., 2008), as well as some non-LEE encoded effector genes in EPEC (Garcia-Angulo et al., 2012), indicating that during the evolution of A/E organisms other genes were incorporated into the Ler-GrlRA regulatory network to coordinate other functions that enhanced the pathogenic capabilities of these bacteria.

Despite the current knowledge, the mechanisms underlying the interplay between GrlA and GrlR in regulating LEE and non-LEE genes under different environmental conditions are still poorly understood. In this work, we show that in addition to the notion that GrlR functions as a repressor by forming a complex with GrlA, it can also act as a repressor of LEE genes independently of this interaction, while GrlA has a dual role as a positive regulator by also antagonizing GrlR through protein-protein interactions. Our data further illustrate that LEE gene expression is negatively regulated at two levels mediated by global (H-NS) and EPEC-specific (GrlR) regulators.

Materials and methods

Bacterial strains, plasmids, and culture conditions

The bacterial strains and plasmids used in this study are listed in **Supplementary Table 1**. Bacteria were routinely cultured in Lysogeny Broth (LB) or in Dulbecco's modified Eagle's medium (DMEM) containing glucose [0.45% (wt/vol)] and L-glutamine (584 mg/l), but not sodium pyruvate (Gibco-BRL Life Technologies, Waltham, MA, USA), supplemented with 1% LB. When necessary, antibiotics were added at the following concentrations: kanamycin (Km) 30 $\mu g\ ml^{-1}$, ampicillin (Ap) 100 $\mu g\ ml^{-1}$, tetracycline (Tc) 12 $\mu g\ ml^{-1}$, streptomycin (Sm) 100 $\mu g\ ml^{-1}$ and chloramphenicol (Cm) 25 $\mu g\ ml^{-1}$. To induce the expression of the LEE virulence genes, bacteria were grown either in 50 ml DMEM under shaken or static + 5% CO_2 conditions at 37°C, while shaken LB broth was used as the non-inducing or repressing condition (Martinez-Laguna et al., 1999; Bustamante et al., 2001, 2011).

DNA manipulations

Standard genetic and molecular techniques were applied as described previously (Sambrook and Russell, 2001). Restriction enzymes were obtained from Thermo Scientific, Waltham, MA, USA and used according to the manufacturer's instructions. PCR reactions were performed in 50 µl using Platinum Taq DNA polymerase (Invitrogen, Waltham, MA, USA). The oligonucleotides used for PCR amplification were synthesized at the Oligonucleotide Synthesis Facility of the Instituto de Biotecnología/UNAM, Cuernavaca, México, and are listed in **Supplementary Table 2**.

Construction of plasmids

To construct the pT3GrlR plasmid, a DNA sequence including the RBS and the coding region of *grlR* was amplified by PCR using the GREPKE-F/GREPX-R oligonucleotide pair. The product obtained was digested with *Kpn*I-*Xho*I enzymes and ligated into vector pMPM-T3 (Mayer, 1995), digested with the same enzymes. To generate plasmids pT3GrlRA, pT3GrlRA/I44A, and pT3GrlRA/R54A fragments were amplified by PCR with the oligonucleotides XHINTERGRLAF/HIGRLAR (**Supplementary Table 2**), using plasmids pTEPGrlA1, pTEPGrlA1/I44A, and pTEPGrlA1/R54A as templates (Jimenez et al., 2010), respectively. The resulting products were digested with *Xho*I-*Hin*dIII and cloned into the pT3GrlR plasmid digested with the same enzymes.

The pDnaK-CAT plasmid was constructed by PCR amplifying a fragment comprising from position −394 to + 127 of the transcription start site of the *dnaK* gene, using the DnaKF/DnaKR oligonucleotides. The product was digested with *Bam*HI-*Hin*dIII enzymes and cloned into the pKK232-8 vector (Pharmacia Biotech) (Brosius, 1984), previously digested with the same enzymes.

Chromosomal DNA from the EPEC E2348/69 strain was used as the PCR template. All plasmids generated were verified by DNA sequencing and evaluated for their ability to complement the corresponding mutants through a profile of secreted proteins or western blotting against virulence proteins.

Construction of mutants and strains expressing FLAG-tagged proteins

The *grlR* and *grlA* mutants were produced by generating chromosomal in-frame deletions of *grlR* codons 6 to 118 or *grlA* codons 6 to 132 by the *sacB* gene-based allelic exchange method as described previously (Edwards et al., 1998). Deletion of the *grlRA* operon spans from codon 6 of *grlR* to codon 132 of *grlA*. Suicide plasmids were generated by cloning PCR-amplified fragments containing the described deletions flanked by approximately 800 to 1000 bp on each side into *Xba*I/*Sac*I-digested plasmid pRE112. The resulting suicide plasmids pRE112DgrlREP, pRE112DgrlAEP, and pRE112DgrlRAEP, respectively (**Supplementary Table 1**), were conjugated into strains WT EPEC E2348/69, Δ*hns* (JPEP36) and Δ*ler* to generate single and double mutants (**Supplementary Table 1**).

To generate the chromosomally 3xFLAG-tagged strains, a modification of the λRed recombinase system was used as described previously (Datsenko and Wanner, 2000; Uzzau et al., 2001). The PCR fragment to tag the native *grlR* gene was generated using oligonucleotides grlR-FLAGH1P1 and grlR-FLAGH2P2 and the *grlA* gene using oligonucleotides grlA-FLAGH1P1 and grlA-FLAGH2P2, and plasmid pSUB11 DNA as template. The resulting PCR products were electroporated into WT EPEC or its Δ*grlR* or Δ*grlA* mutants to generate the EPEC *grlR*:3xFLAG, *grlA*:3xFLAG, *grlR*:3xFLAG Δ*grlA* and Δ*grlR grlA*:3xFLAG (**Supplementary Table 1**).

Single and double mutants were verified by PCR amplification and DNA sequencing. The tagged strains contain the tag in their native gene chromosomal locations; thus, are expressed from the *grlRA* operon promoter.

CAT assay

Chloramphenicol acetyltransferase (CAT) activity, derived from the expression of the transcriptional fusions to the *cat* reporter gene, was determined as follows (Martinez-Laguna et al., 1999). The strains containing the transcriptional fusions were grown in 5 ml of LB supplemented with antibiotics and incubated overnight at 37°C. The next day, culture pellets were adjusted to an OD_{600} = 1.0 with 1X phosphate buffered saline (PBS) (10 mM Na2HPO4, 2 mM KH2PO4, 137 mM NaCl and 2.7 mM KCl) and used to inoculate 50 ml of LB or DMEM supplemented with antibiotics with one ml of each suspension. Cultures were incubated at 37°C under shaking or static plus 5% CO_2 growth conditions, and 1 ml samples were collected when the cultures reached an OD_{600} = 0.8 and 1.0. The cell pellet was obtained by centrifugation at 14,000 rpm for 2 minutes and washed with 1 ml of TDTT buffer (Tris-Hcl 50 mM pH 7.8 and dithiothreitol 30 μM), centrifuged again and resuspended in 0.5 ml of the same buffer. Lysis was achieved by sonication for 5 min with pulses of 10 s per minute and 5 s rest. Soluble extracts were separated from cell debris by centrifugation at 12,000 rpm for 20 min at 4°C, and 5 μl aliquots of each extract were added in duplicate to a 96-well microtiter plate followed by the addition of 200 μl of the reaction mix containing 1 mM DTNB [5,58-dithio-bis(2-nitrobenzoic acid)] (Research Organics), 0.1 mM Tris-Hcl pH 7.8, 0.1 mM acetyl-CoA (Pharmacia LKB Biotech Inc., Alameda, CA, USA), and 0.1 mM chloramphenicol (Sigma Chemical Co., Saint Louis, MO, USA). Changes in absorbance at 410 nm were recorded every 5 s for 5 min with a CERES 900C automatic microplate reader and the KC3 program set to kinetic mode. A CAT standard curve (from 0 to 2500 U/ml) was used to interpolate the activities of each sample. The protein concentration of each extract was determined by adding 10 μl of each extract in duplicate and 200 μl of the reaction mixture (25 ml of solution A + 500 μl of solution B) of the "BCA Protein Assay Kit" (Pierce) to a 96-well plate. Then incubated at 37°C for 30 min; the absorbance was read at a wavelength of 562 nm using an automatic microplate reader CERES 900 C and the KC3 program. The CAT-specific activity was determined by dividing the CAT activity by the protein concentration of each extract. The data are expressed as μmol/min/mg of protein and are the results from at least three independent assays done in duplicate. The empty vector pKK232-8 did not show measurable levels of CAT activity in any of the strains used in the study (data not shown).

Protein secretion assay

EPEC secreted proteins were analyzed as described previously (Deng et al., 2004). Briefly, bacterial cultures in LB and DMEM were incubated at 37°C under shaking or static conditions. Triplicate 1.5 ml samples were collected per culture when the cultures reached an OD_{600} of 1.0 and were subjected to centrifugation at 17,900 x *g* for 5 min in Eppendorf tubes. Bacterial pellets were saved when convenient, and 1.3 ml of each supernatant was separated into fresh tubes and 160 μl of 100% trichloroacetic acid (TCA) was added per tube. Proteins were allowed to precipitate at 4°C overnight. Subsequently, the proteins were concentrated by centrifugation at 20,000 × *g* for 30 min and resuspended in 10 μl of 1× Laemmli loading buffer and the triplicate samples were mixed in the same tube, boiled for 5 min and resolved by 12% SDS-polyacrylamide gel electrophoresis (PAGE).

Western blotting

Bacteria were grown in DMEM or LB under shaking or static conditions until they reached an OD_{600} of 1. Total extracts were obtained from 3 ml samples of the bacterial cultures. Cells were resuspended in 500 μl of urea solution (8 M) and lysed by sonication. Aliquots of total extracts were mixed with Laemmli buffer, boiled for 5 min and analyzed by SDS-PAGE (12% acrylamide) and, subsequently, transferred to 0.45-μm-pores-size PVDF membrane (Millipore) using a semi-dry transfer chamber (BioRad, Hercules, CA, USA).

The membrane was blocked in 10% non-fat milk and incubated with one of the following primary antibodies: a 1:10,000 dilution of monoclonal anti-Tir, a 1:7,500 dilution of polyclonal anti-intimin (kindly provided by J.A. Giron), a 1:20,000 dilution of polyclonal anti-EspA (kindly provided by J. Kaper), a 1:10,000 dilution of polyclonal anti-EscJ (kindly provided by Dr. Bertha González-Pedrajo), a 1:5,000 dilution of monoclonal anti-FLAG M2 (Sigma-Aldrich, Saint Louis, MO, USA), a 1:15,000 dilution of polyclonal anti-maltose binding protein (MBP) (New England Biolabs, Ipswich, MA, USA), a 1:10,000 dilution of polyclonal anti-DnaK (Invitrogen, Waltham, MA, USA) and a 1:50,000 dilution of monoclonal anti-GroEL (Sigma-Aldrich, Saint Louis, MO, USA). The membrane was washed with 1x phosphate buffer saline (PBS) containing 0.05% Tween 20 and incubated with a 1:10,000 dilution of secondary anti-rabbit or anti-mouse antibodies coupled to horseradish peroxidase (Thermo Scientific, Waltham, MA, USA). The membrane was developed with the commercial kit "Western Lightning Chemiluminescence Reagent Plus" (Perkin Elmer, Waltham, MA, USA) according to the manufacturer's instructions.

Native gel electrophoresis

EPEC E2348/69 *grlR*:3xFLAG, *grlA*:3xFLAG, Δ*grlR grlA*:3xFLAG, and *grlR*:3xFLAG Δ*grlA* strains were transformed with pT3GrlA1/I44A or pT3GrlA1/R54A and grown overnight in 5 ml of LB medium supplemented with antibiotics. The next day, 0.5 ml of these cultures were inoculated into 20 ml DMEM or LB medium supplemented with antibiotics and allowed to grow at 37°C with shaking. When the cultures reached an OD_{600} of 1.0, 5 ml samples were taken and the cells were concentrated by centrifugation at 18,000 x*g* at 4°C, resuspended in 500 μl PBS and lysed by sonication. Samples were taken at an OD_{600} of 0.3, 0.6, 0.8, and 1.0 from 50 ml cultures when needed.

Total extracts were resuspended in a non-denaturing buffer (50% glycerol, 25 mM Tris-Hcl pH 6.8 and 0.05% bromophenol Blue) and separated by 12% native PAGE at 4°C. The gel was transferred to a 0.45-μm-pore-size PVDF membrane (Millipore) and processed for western blotting.

Simultaneously, aliquots obtained from the same assays were processed for 12% SDS-PAGE and western blotting.

Statistical analysis

Data analyses were performed by two-way ANOVA followed by Tukey's multiple comparisons posttest using GraphPad Prism version 8.4.3 (471) for Mac OS. *P*-values < 0.05 were considered statistically significant.

Results

GrlR negatively regulates LEE gene expression under repression conditions

GrlR represses LEE gene expression mainly under non-permissive conditions such as growth in LB (Deng et al., 2004; Lio and Syu, 2004; Iyoda and Watanabe, 2005). To further explore this feature, we evaluated the expression of the *LEE1*, *LEE2*, *LEE4*, *LEE5*, and *dnaK* promoters fused to the *cat* reporter gene in WT EPEC E2348/69 and its Δ*grlR* non-polar deletion mutant cultured under LEE inducing (DMEM/37°C) and repressing (LB/37°C) growth conditions. Under inducing conditions, the CAT reporter activity of all LEE fusions increased between 1.5- to 4-fold in EPEC Δ*grlR* compared to the WT strain (**Figure 1A**); however, under repression conditions, the fold increase was higher, between 5 and 13.5 (**Figure 1A**). In contrast, *dnaK-cat* expression, used as a LEE unrelated control, was similar in both strains and growth conditions (**Figure 1A**).

The analysis of the T3SS-dependent protein secretion profile of WT, Δ*grlR* and Δ*ler* EPEC strains showed that, under repressing conditions (LB), the Δ*grlR* mutant abundantly secreted proteins into the medium, while the WT strain did not secrete detectable levels of LEE-encoded proteins (**Figure 1B**). This phenotype reversed by complementing the mutant strain with a plasmid containing the *grlR* gene (pT3GrlR) (**Figure 1B**). Growth under inducing conditions (DMEM) allowed secretion of LEE-encoded proteins by the WT strain and higher secretion levels by the Δ*grlR* strain. Moreover, complementing the Δ*grlR* mutant with the pT3GrlR plasmid suppressed protein secretion, even under inducing conditions (DMEM), indicating that GrlR overexpression can override the presence of GrlA under T3S permissive conditions (**Figure 1B**). As expected, the Δ*ler* mutant did not secrete under both growth conditions.

These results highlight the negative regulatory effect that GrlR exerts on the *LEE* genes in agreement with previous reports (Deng et al., 2004; Lio and Syu, 2004; Iyoda and Watanabe, 2005).

GrlR represses the expression of LEE operons in the absence of H-NS

H-NS globally represses LEE-gene expression, while Ler acts as an antagonist to overcome this repression; thus, in the absence of H-NS, the role of Ler is dispensable (Friedberg et al., 1999; Leh et al., 2017; Shin, 2017). Moreover, GrlR expression from a plasmid strongly represses the expression of the LEE genes in WT EPEC even under conditions permissive to LEE expression (Deng et al., 2004; Lio and Syu, 2004; Jobichen et al., 2007). Evidence showing that GrlR and GrlA establish protein-protein interactions led to propose that GrlR negatively regulates LEE gene expression by preventing GrlA from binding to and activating the *ler* promoter (Creasey et al., 2003; Jobichen et al., 2007; Jimenez et al., 2010; Padavannil et al., 2013).

Based on such evidence, we hypothesized that overexpression of GrlR in EPEC lacking H-NS, which expresses LEE genes constitutively even under non-permissive growth conditions in a Ler- and GrlA-independent manner, would not affect LEE gene expression. Therefore, we analyzed the transcriptional activity of the *LEE1-*, *LEE2-*, *LEE4-*, and *LEE5-cat* fusions and the expression of LEE-encoded proteins in WT and Δ*hns* EPEC strains carrying or not plasmid pT3GrlR (**Supplementary Table 1**). Consistent with previous reports for other A/E pathogens, overexpression of GrlR in WT EPEC repressed the transcriptional activity of all LEE fusions tested (**Figure 2A**), as well as the expression of Tir, intimin and EspA, as shown by western blot (**Figure 2B**), and of EspC (**Supplementary Figure 1A**), an autotransporter encoded outside the LEE and whose expression is also regulated by Ler (Elliott et al., 2000; Li et al., 2004; Vidal and Navarro-Garcia, 2008). Unexpectedly, GrlR also significantly repressed the transcriptional activity of the LEE promoters in the EPEC Δ*hns* mutant (**Figures 2A, B**). Under these conditions, all strains similarly expressed proteins DnaK and MBP,

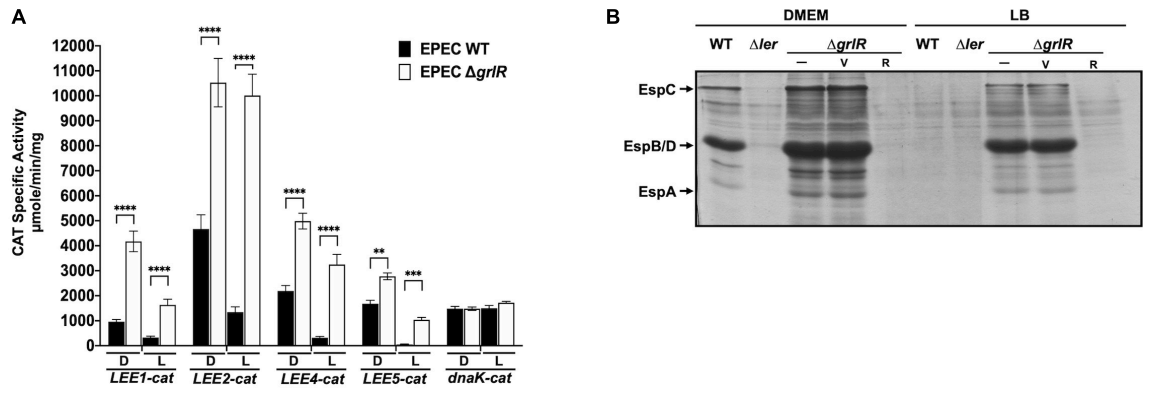

FIGURE 1
The absence of GrlR derepresses the expression of locus of enterocyte effacement (LEE) operons under repressing conditions. **(A)** The transcriptional activity of the *LEE1-cat*, *LEE2-cat*, *LEE4-cat*, *LEE5-cat*, and *dnaK-cat* fusions was analyzed in WT EPEC (black bars) and its Δ*grlR* isogenic mutant (white bars), grown in 50 ml DMEM (D) or LB medium (L) with shaking at 37°C. Specific chloramphenicol acetyltransferase (CAT) activity was determined from samples collected at an OD_{600} of 1. Values are an average of three independent experiments performed in duplicate. Error bars indicate standard deviations. Statistically different values are indicated (**p-value < 0.01; ***p-value < 0.001; ****p-value < 0.0001). **(B)** Profile of secreted proteins of EPEC WT, Δ*ler* and Δ*grlR* (carrying the empty vector pMPM-T3 or its derivative pT3GrlR) grown under the same conditions as in panel **(A)**. Secreted proteins were concentrated from culture supernatants by precipitation with trichloroacetic acid (TCA) and separated by 12% SDS-PAGE. V: pMPM-T3, R: pT3GrlR.

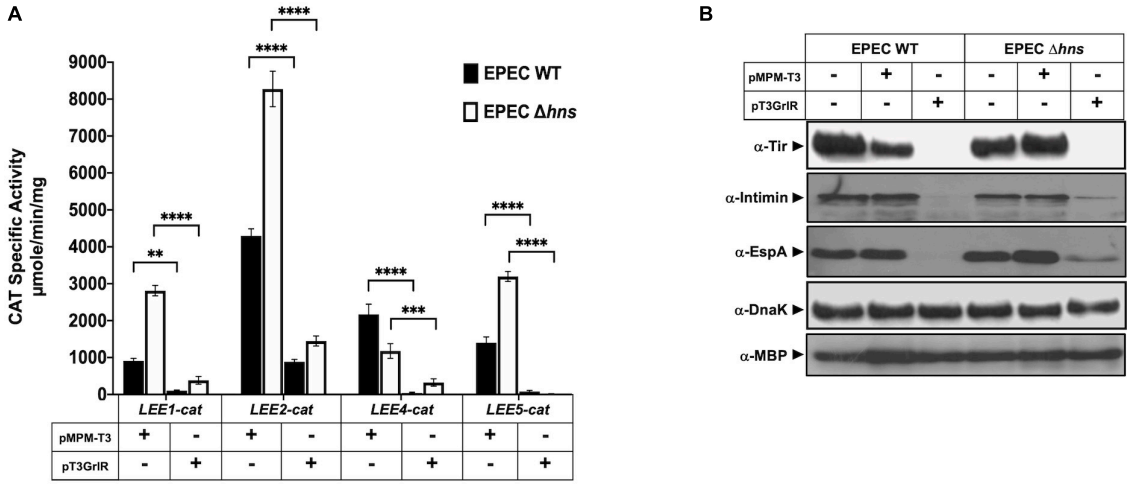

FIGURE 2
GrlR represses the expression of locus of enterocyte effacement (LEE) genes in the absence of H-NS. **(A)** Expression of the *LEE1-cat*, *LEE2-cat*, *LEE4-cat*, and *LEE5-cat* fusions was analyzed in WT enteropathogenic *Escherichia coli* (EPEC) (black bars) and its Δ*hns* isogenic mutant (white bars) carrying the empty vector pMPM-T3 (V) or its derivative pT3GrlR (R), grown in DMEM with shaking at 37°C. Specific chloramphenicol acetyltransferase (CAT) activity was determined using samples collected from cultures grown in 50 ml Dulbecco's modified Eagle's medium (DMEM) or Lysogeny Broth (LB) at an OD_{600} of 1. Values are an average of three independent experiments performed in duplicate. Error bars indicate standard deviations. Statistically different values are indicated (**p-value < 0.01; ***p-value < 0.001; ****p-value < 0.0001). **(B)** Total extracts were prepared from the same culture samples and separated by 12% SDS-PAGE. The expression of Tir, intimin and EspA was analyzed by western blotting using polyclonal anti-intimin and anti-EspA and monoclonal anti-Tir antibodies. As controls for protein loading, maltose binding protein (MBP) and DnaK were also detected using monoclonal anti-DnaK and polyclonal anti-MBP antibodies.

used as loading controls, indicating that repression did not result from an unspecific pleiotropic effect in EPEC physiology due to GrlR overexpression.

To address this concept, we evaluated the effect of GrlR expressed from a plasmid under growth conditions where GrlA is not the primary activator of Ler expression. When EPEC grows in static DMEM cultures under 5% CO_2 atmosphere at 37°C, the EAF plasmid-encoded regulator PerC is the main activator of *LEE1* promoter expression and therefore of *ler* (Bustamante et al., 2011). Thus, we analyzed the secreted protein profile and intimin and EspA expression in WT EPEC and the Δ*hns* mutant harboring plasmid pT3GrlR or the empty vector pMPM-T3, grown in shaken and static + 5% CO_2 DMEM. As shown, GrlR expressed from pT3GrlR repressed protein secretion (**Supplementary Figure 1A**) and expression of EspA and Intimin in both strains and conditions, but not that of DnaK (**Supplementary Figure 1B**), confirming the results shown in **Figure 1B**.

These data suggested that GrlR can repress LEE gene expression through an alternative pathway, probably independent of its interaction with GrlA.

The global regulator H-NS and the EPEC specific regulator GrlR act cooperatively, but at different levels, to repress the expression of LEE genes

Ler and GrlA establish a positive regulatory feedback loop that counteracts the repression exerted by H-NS (Barba et al., 2005; Jimenez et al., 2010). According to the results described above, GrlR and H-NS act cooperatively to repress the expression of LEE genes. To further explore this observation, we evaluated the expression of the *LEE1-cat*, *LEE2-cat*, and *LEE5-cat* transcriptional fusions in EPEC WT and Δ*hns* grown under inducing and repressing conditions and also analyzed the secretion profile of these strains from samples of their culture supernatants. Under inducing conditions, the activity of the *LEE2-cat* and *LEE5-cat* fusions increased about 2-fold in the absence of either of the two repressors, whereas that of the *LEE1-cat* fusion was 4.7-fold and 3.7-fold in the Δ*grlR* and Δ*hns* mutants, respectively (**Figure 3A**). Under repressing conditions, the derepression observed for the *LEE1*, *LEE2*, and *LEE5* promoters operons was about 13-, 7-, and 14-fold, respectively, in the absence of GrlR; whereas in the Δ*hns* mutant it was 2-, 3-, and 5-fold, respectively, relative to the activity displayed in the WT strain (**Figure 3A**). In agreement with these results, while the WT strain poorly secreted LEE-encoded proteins under repressing conditions (LB), the Δ*grlR* and Δ*hns* mutants showed a clear increase in protein secretion (**Figure 3B**).

To delve deeper into the role of both H-NS and GrlR in the negative regulation of the LEE genes, we analyzed the transcriptional activity of the *LEE2-cat* fusion and the protein secretion profile in WT EPEC and its Δ*ler*, Δ*hns*, Δ*grlR*, Δ*grlA*, Δ*grlRA*, Δ*ler*Δ*grlR*, and Δ*grlR*Δ*hns* isogenic mutants grown under inducing and repressing conditions (**Figure 4**). As expected, compared to the WT strain, the Δ*ler* and Δ*grlA* strains significantly downregulated *LEE2-cat* fusion expression and protein secretion, while the Δ*grlR* mutant expressed higher levels of *LEE2-cat* activity (**Figures 4A, B**). Interestingly, the Δ*grlRA* double mutant displayed a phenotype similar to the Δ*grlA* single mutant, confirming the important role of GrlA in *ler* activation and, indirectly, in derepression of Ler-dependent promoters that in the absence of GrlR remained repressed by H-NS (**Figures 4A, B**). In the Δ*grlR*Δ*hns* double mutant, the transcriptional activity of the *LEE2-cat* fusion showed expression levels similar to those observed in the Δ*grlR* and Δ*hns* single mutants under inducing conditions, while under repressing conditions, its expression was closer to the activity

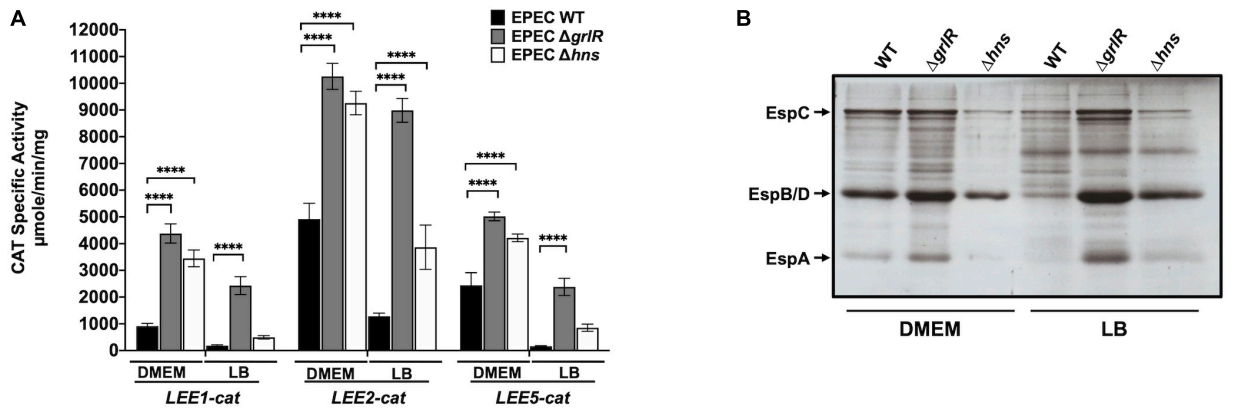

FIGURE 3
GrlR is the main repressor of locus of enterocyte effacement (LEE) gene expression under repressing conditions. **(A)** Expression of the *LEE1-cat*, *LEE2-cat* and *LEE5-cat* fusions was analyzed in WT EPEC (black bars) and its Δ*grlR* (gray bars) and Δ*hns* (white bars) isogenic mutants, grown in 50 ml of Dulbecco's modified Eagle's medium (DMEM) or Lysogeny Broth (LB) with shaking at 37°C. Specific chloramphenicol acetyltransferase (CAT) activity was determined from samples collected from cultures at an OD_{600} of 1. Values are an average of three independent experiments performed in duplicate. Error bars indicate standard deviations. Statistically different values are indicated (****p-value < 0.0001). **(B)** Secreted proteins of the same cultures were concentrated from supernatants by precipitation with trichloroacetic acid (TCA), separated by 12% SDS-PAGE and stained with Coomassie brilliant blue.

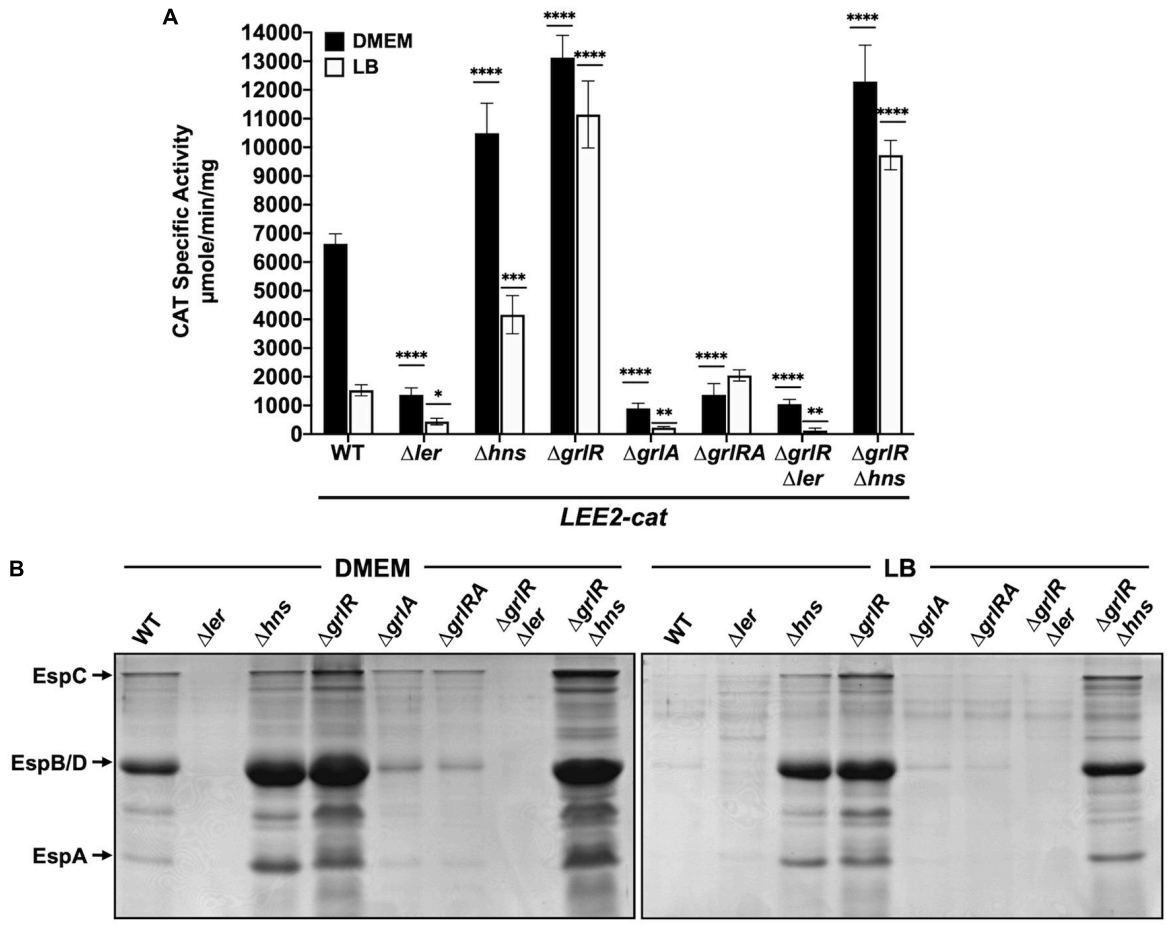

FIGURE 4
GrlR and H-NS repress locus of enterocyte effacement (LEE) gene expression by an indirect cooperative mechanism. **(A)** chloramphenicol acetyltransferase (CAT) activity of the *LEE2-cat* fusion was determined in WT enteropathogenic *Escherichia coli* (EPEC) and its Δ*ler*, Δ*hns*, Δ*grlR*, Δ*grlA*, Δ*grlRA*, Δ*grlR*Δ*ler*, and Δ*grlR*Δ*hns* derivative mutants grown in 50 ml of Dulbecco's modified Eagle's medium (DMEM) (black bars) or Lysogeny Broth (LB) (white bars) with shaking at 37°C. Specific CAT activity was determined from samples collected at an OD_{600} of 1. Values are an average of three independent experiments performed in duplicate. Error bars indicate standard deviations. Statistically different values are indicated (*p-value < 0.1; **p-value < 0.01; ***p-value < 0.001; ****p-value < 0.0001). **(B)** Secreted proteins of the same cultures were concentrated from supernatants by precipitation with TCA, separated by 12% SDS-PAGE and stained with Coomassie brilliant blue.

observed in the Δ*grlR* strain (Figure 4A). These results coincided with the secreted protein profile since, in DMEM and LB, the Δ*grlR* and Δ*hns* single mutants and the double Δ*grlR*Δ*hns* mutant showed increased secretion in contrast to the WT strain (Figure 4B). Finally, the phenotype of the Δ*grlR*Δ*ler* mutant confirmed that Ler is essential to antagonizing the repression exerted by H-NS regardless of the growth condition (Figures 4A, B).

The inclusion of the Δ*ler*Δ*hns* double and the Δ*ler*Δ*hns*Δ*grlRA* quadruple mutant in this assay was cumbersome due to the poor growth shown by these strains. To overcome this limitation, we expressed ectopically H-NS^{G113D}, a dominant negative version of H-NS that carries a mutation affecting its DNA binding capacity without altering the oligomerization domain (Ueguchi et al., 1996), to inhibit H-NS activity. WT EPEC and its mutant derivatives Δ*ler*, Δ*hns*, Δ*grlR*, Δ*grlA*, Δ*grlRA*, Δ*ler*Δ*grlR*, Δ*ler*Δ*grlA*, Δ*ler*Δ*grlRA* and Δ*escN* carrying plasmid pT6-HNS/G113D, expressing H-NS^{G113D} under the control of an arabinose inducible promoter (Bustamante et al., 2008; Jimenez et al., 2010), were grown under repressing conditions with and without arabinose. We collected samples from these cultures to analyze the secreted proteins by PAGE and the expression of Tir and EscJ in total cell extracts by western blotting. In the absence of arabinose, we did not observed T3S of EspA, EspB and EspD nor Tir and EscJ expression in the WT or any strain carrying the Δ*ler* or Δ*grlA* deletions (Figures 5A, B). In contrast, upon induction of H-NS^{G113D}, de-repression of T3S was evident even in the absence of Ler and/or GrlA, while the Δ*grlR* mutant showed protein secretion and Tir and EscJ expression both without or with H-NS^{G113D} induction (Figures 5A, B). The Δ*escN* strain, a mutant defective in T3S, was used as a control that did not secrete virulence proteins even upon H-NS^{G113D} induction, except for EspC, a non-T3 secreted protein, whose gene is also repressed by H-NS and derepressed by Ler (Figure 5A). In contrast, Tir and EscJ were observed in total cell extracts of this strain when H-NS^{G113D} was induced (Figure 5B).

Taken together, these results indicate that GrlR and H-NS negatively regulate the expression of LEE operons at two independent levels that are indirectly cooperative (see Section "Discussion").

GrlA counteracts the repressor effect of GrlR through protein-protein interactions

We previously observed that under inducing conditions, the negative effect of GrlR is counteracted when co-expressed with GrlA in *C. rodentium* (Deng et al., 2004). A possible explanation of this phenotype is that the co-expression of both proteins prevents the titration effect that overexpressing only GrlR from a plasmid has on the native levels of GrlA. However, there is also the possibility that under these conditions, the interaction between GrlR and GrlA also plays a role in preventing the GrlR-mediated independent repression described above (Figure 2 and Supplementary Figure 1).

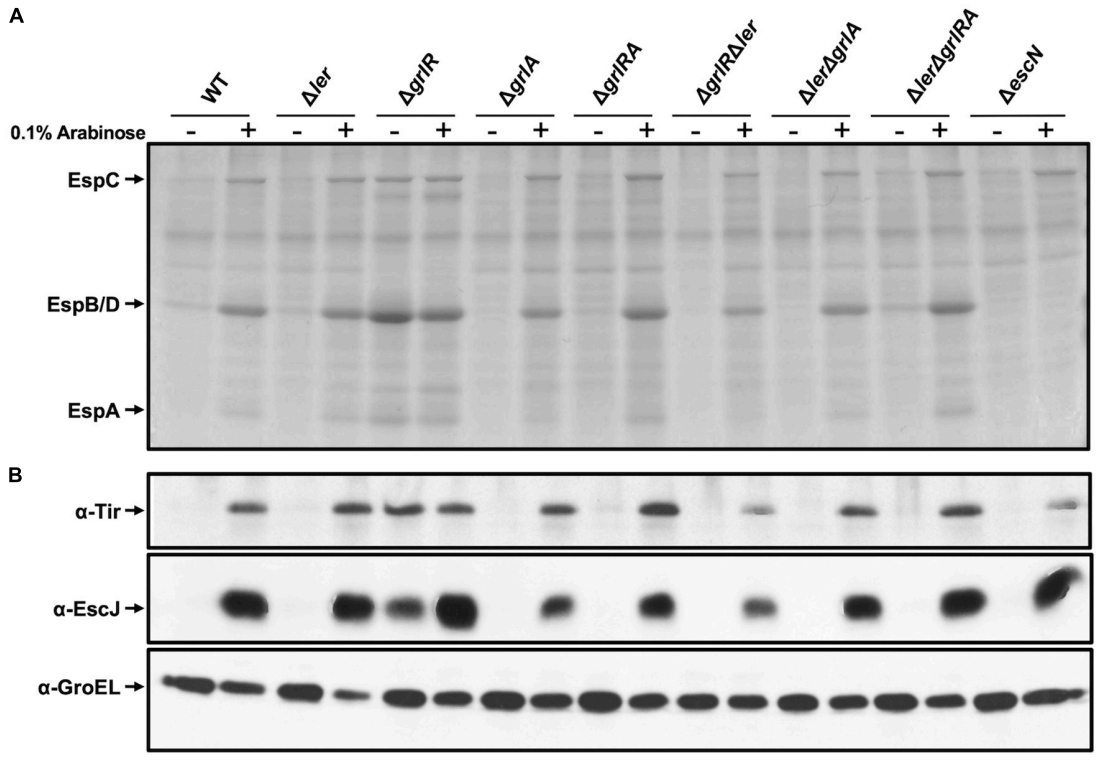

FIGURE 5
Protein secretion profile in the presence of a dominant negative H-NS mutant. **(A)** Secreted proteins from WT enteropathogenic *Escherichia coli* (EPEC) and its Δ*ler*, Δ*grlR*, Δ*hns*, Δ*grlA*, Δ*grlRA*, Δ*grlR*Δ*ler*, Δ*ler*Δ*grlA*, Δ*ler*Δ*grlRA*, and Δ*escN* derivative mutants, carrying plasmid pT6-HNS/G113D expressing H-NS^{G113D}, grown in 50 ml Lysogeny Broth (LB) with (+) and without (–) 0.1% arabinose at 37°C with shaking, were concentrated from culture supernatants by precipitation with trichloroacetic acid (TCA), separated by 12% SDS-PAGE and stained with Coomassie brilliant blue. **(B)** Total extracts were prepared from the corresponding bacterial pellets and separated by 12% SDS-PAGE. Tir and EscJ expression was analyzed by western blotting using an anti-Tir monoclonal antibody and anti-EscJ polyclonal antibodies. As a control for protein loading, GroEL expression was also analyzed using an anti-GroEL monoclonal antibody.

To evaluate this possibility, we transformed plasmids pT3GrlRA, pT3GrlR, pTEPGrlA1 and the empty vector pMPM-T3 (**Supplementary Table 1**) into WT EPEC and grew the resulting strains under inducing and repressing conditions to analyze the secretion profile. As shown in **Figure 2**, GrlR overexpression repressed the LEE genes and inhibited T3S even under inducing conditions, while overexpression of GrlA overcame the repressing effect of growth in LB (**Figure 6A**). In turn, as observed in *C. rodentium* (Deng et al., 2004), GrlR-GrlA co-expression prevented the negative effect of GrlR, even under repressing conditions, but to a lesser extent (**Figure 6A**).

To further explore this notion, we took advantage of the phenotype of two GrlA mutants, GrlA/I44A and GrlA/R54A, that cannot activate the *LEE1* operon because they no longer bind to the *ler* regulatory region due to a single amino acid change in the HTH domain. Additionally, the GrlA/I44A mutant cannot interact with GrlR (Jimenez et al., 2010; Padavannil et al., 2013). The genes encoding these mutants were cloned into pT3GrlR to co-express them with WT *grlR*. WT EPEC containing the resulting plasmids pT3GrlRA/I44A or pT3GrlRA/R54A were then grown under inducing and repressing conditions to examine their T3S profile. Under inducing conditions, T3S in the presence of pT3GrlRA/I44A was similar to the secretion profile seen with pT3GrlR, as in both cases protein secretion was significantly reduced (**Figure 6A**). In contrast, in the presence of GrlR-GrlA/R54A, T3S was unaltered (**Figure 6A**), suggesting that GrlA/R54A probably prevented GrlR-mediated repression by interacting with it and not because it was over inducing Ler expression. Moreover, in LB medium, where the WT strain does not secrete T3S substrates, we observed a clear de-repression of virulence protein secretion in the presence of GrlR-GrlA/R54A, but not with GrlR-GrlA/I44A, suggesting that GrlA/R54A titrated away both the endogenous GrlR expressed from the chromosomal gene and that expressed from the plasmid (**Figure 6A**). To confirm the above observations, we performed a similar experiment with the EPEC Δ*grlR* strain but grown under repressing conditions (LB medium). Co-expression of GrlR with GrlA/I44A did not prevent GrlR from complementing the repression phenotype and the effect was similar to that observed for the strain with pT3GrlR (**Figure 6B**); however, this was not the case when GrlR was co-expressed with GrlA/R54A, as protein secretion was still observed (**Figure 6B**). Western blotting to detect intimin, Tir and EspA in total cell extracts of the same strains, showed similar results (**Figure 6C**).

These results are consistent with the notion that GrlA, in addition to its activating effect on the *ler* promoter as a DNA binding protein, could also counteract the alternative GrlR repression effect by interacting with it.

GrlR and GrlA are expressed and interact under inducing and repressing conditions

The results described above further indicated that GrlR has a critical role as a repressor under non-permissive growth conditions for LEE expression, thus implying that EPEC expresses it in both LB and DMEM. To analyze GrlR and GrlA expression and

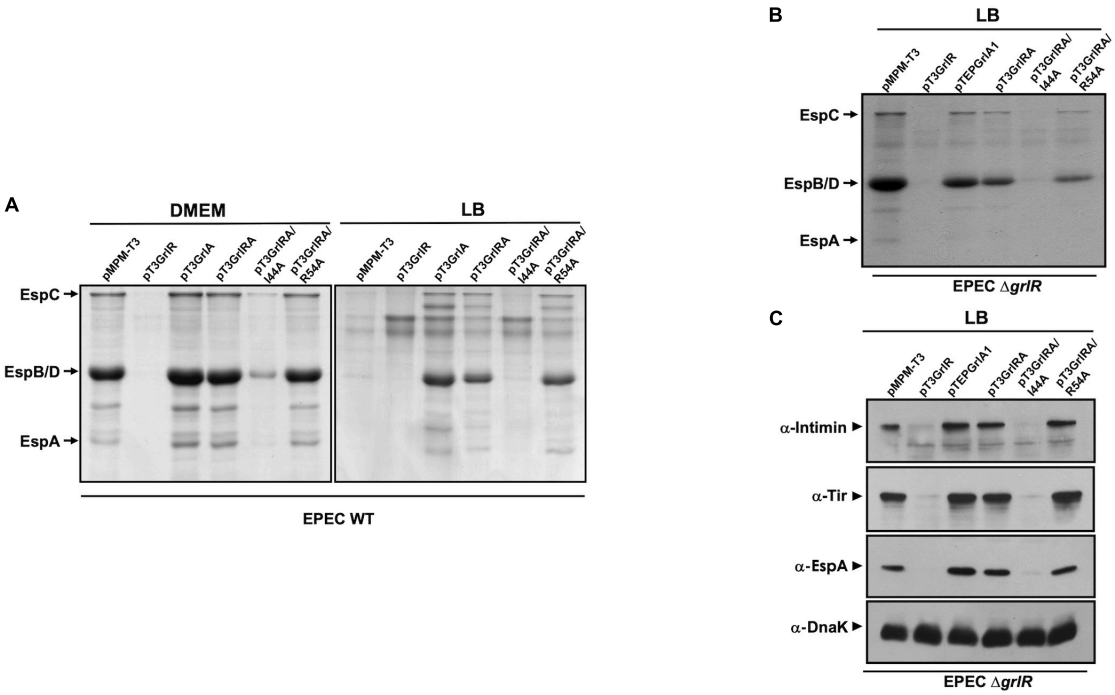

FIGURE 6
GrlA antagonizes GrlR-mediated repression. **(A)** Profile of secreted proteins from WT enteropathogenic *Escherichia coli* (EPEC) carrying the empty vector pMPM-T3 or its derivatives pT3GrlR, pTEPGrlA1, and pT3GrlRA, pT3GrlRA/I44A and pT3GrlRA/R54A grown in 50 ml Dulbecco's modified Eagle's medium (DMEM) or Lysogeny Broth (LB) to an OD_{600} of 1. Secreted proteins were concentrated from culture supernatants by precipitation with trichloroacetic acid (TCA), separated by 12% SDS-PAGE and stained with Coomassie brilliant blue. **(B)** Secreted proteins from EPEC Δ*grlR* carrying the same plasmids as in panel **(A)** grown in 50 ml of LB with shaking at 37°C. **(C)** Total extracts were prepared from bacterial samples of the same cultures described in panel **(B)**. Proteins were separated by 12% SDS-PAGE and expression of intimin, Tir and EspA was analyzed by western blotting using anti-intimin, anti-Tir and anti-EspA antibodies. As a control for protein loading, DnaK expression was also analyzed using anti-DnaK antibodies.

their interaction in more detail, we grew the EPEC *grlR*:3xFLAG, *grlA*:3xFLAG, Δ*grlA-grlR*:3xFLAG and Δ*grlR-grlA*:3xFLAG strains, as well as the Δ*grlA-grlR*:3xFLAG strain carrying the plasmids encoding the GrlA/I44A and GrlA/R54A mutants (**Supplementary Table 1**), under inducing and repressing conditions and analyzed total cell extracts by native PAGE and western blotting from samples taken from each culture. As shown in **Figure 7**, the formation of the GrlR-GrlA complex occurred under both growth conditions (**Figure 7A**, lanes 1, 2, 7, and 8, upper band). The EPEC *grlR*:3xFLAG strain also showed the GrlR dimer and monomer (**Figure 7A**, lanes 1 and 7), while the banding pattern of the Δ*grlA-grlR*:3xFLAG strain, where the upper band is not present due to the absence of GrlA (**Figure 7A**, lanes 3 and 9), confirmed the nature of the second and third bands. The EPEC *grlA*:3xFLAG strain only showed a band corresponding to the GrlR-GrlA complex (**Figure 7A**, lanes 2 and 8), while in the absence of GrlR, GrlA-3xFLAG did not enter the gel (**Figure 7A**, lanes 4 and 10), likely due to its isoelectric point (theoretical pI: 9.71), which changes when in complex with GrlR. Moreover, the expression of the plasmid-encoded GrlA/I44A and GrlA/R54A mutants in the Δ*grlA-grlR*:3xFLAG strain further confirmed these observations as the GrlA/I44A mutant, which does not interact with GrlR, did not form the $GrlR_2$-GrlA complex (**Figure 7A**, lanes 5 and 11) seen with the GrlA/R54A mutant (**Figure 7A**, lanes 6 and 12). Interestingly, the GrlA/R54A mutant drove GrlR to mainly form the complex with GrlA since the dimeric and monomeric forms were not visible. In part, this may be why overexpression of GrlA in the EPEC WT strain overrode the repression in LB (**Figure 6A**). SDS-PAGE and anti-FLAG western blot with the same cell extracts showed the presence of the tagged proteins (**Figure 7B**).

Native PAGE analysis also suggested, based on the banding pattern shown by GrlR and GrlA (as discussed above), that GrlR and GrlA are expressed and interact, although not to the same extent, independently of the growth conditions. To analyze this observation in more detail, we took samples from LB and DMEM cultures of the EPEC *grlR*:3xFLAG and *grlA*:3xFLAG strains at different growth stages and analyzed them by SDS-PAGE and native PAGE followed by western blot. The qualitative analysis showed that GrlR and GrlA were expressed at moderately higher levels in DMEM than in LB; however, although enriched in DMEM, heterotrimers formed under both growth conditions independently of the expression levels of these proteins (**Figures 8A, B**, upper panels).

These data allowed us to hypothesize that heterotrimer formation plays a bidirectional role, on the one hand, preventing the activation of *ler* by reducing the levels of free GrlA and, on the other, antagonizing the independent repressor function of GrlR. A future more quantitative analysis of the relative concentrations of GrlA under both growth conditions, as well as the effect of these conditions on the ability of GrlA to activate the *ler* promoter and on the kinetics of GrlR-GrlA interaction, will allow a better understanding of the mechanism that regulates the expression of LEE genes in response to environmental cues.

Together, these results further supported the notion that GrlA counteracts the repressor effect of GrlR by interacting with it and showed that the $GrlR_2$-GrlA heterotrimeric complex, the GrlR-GrlR dimer and the GrlR monomer are present in EPEC under both growth conditions.

GrlR represses the expression of LEE promoters in a non-EPEC background

To further explore the notion that GrlR can repress the constitutive expression of LEE promoters independently of its interaction with GrlA, we assessed the activity of the *LEE1* and *LEE2* promoters in a background lacking not only H-NS, but also GrlA and Ler. We then transformed the empty vector pMPM-T3 or plasmids pT3GrlR, pTEPGrlA1 o pT3GrlRA into the Δ*hns* mutant of the LEE-negative lab strain *E. coli* MC4100 (JPMC1) containing the *LEE1-cat*

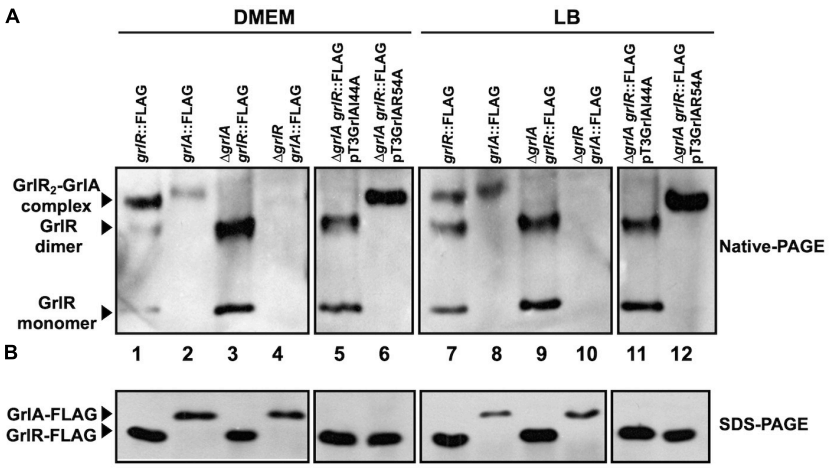

FIGURE 7
Analysis of $GrlR_2$-GrlA complex formation by native gel electrophoresis. **(A)** $GrlR_2$-GrlA protein complex formation in the enteropathogenic *Escherichia coli* (EPEC) strains *grlR*:3xFLAG, *grlA*:3xFLAG, Δ*grlR_grlA*:3xFLAG, *grlR*:3xFLAG_Δ*grlA,* as well as in the *grlR*:3xFLAG_Δ*grlA* strain carrying plasmids pTEPGrlA1/I44A or pTEPGrlA1/R54A, was analyzed from samples taken from cultures grown in Dulbecco's modified Eagle's medium (DMEM) or Lysogeny Broth (LB) at an OD_{600} of 1. Total extracts were obtained from bacterial pellets and separated by 12% native PAGE. The $GrlR_2$-GrlA and GrlR-GrlR complexes and the GrlR monomer (indicated by arrows) were identified by western blotting using anti-FLAG monoclonal antibodies. **(B)** The same cell extracts were also separated by 12% SDS-PAGE and transferred to a PVDF membrane for western blotting to confirm GrlR-3xFLAG and GrlA-3xFLAG expression in the different strains using anti-FLAG antibodies.

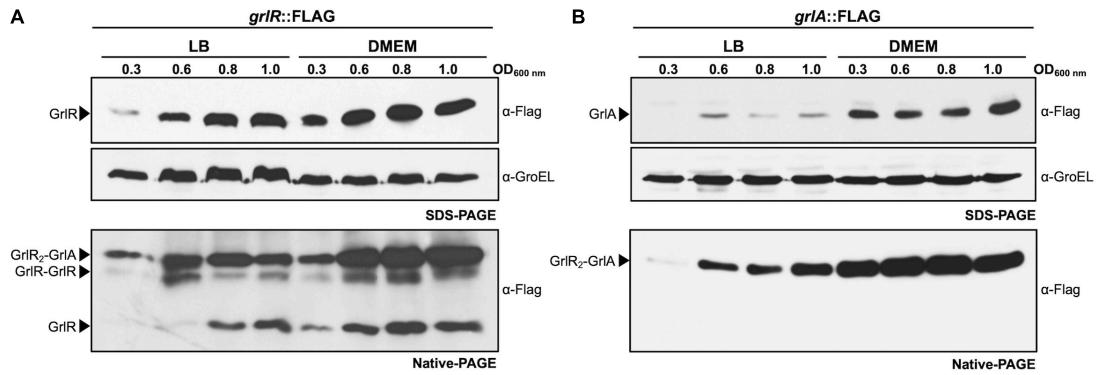

FIGURE 8
GrlR and GrlA are expressed under both repressing and inducing conditions and interact to form the $GrlR_2$-GrlA heterotrimer. The enteropathogenic *Escherichia coli* (EPEC) *grlR*:3xFLAG **(A)** and *grlA*:3xFLAG **(B)** strains were grown in 50 ml of Dulbecco's modified Eagle's medium (DMEM) or Lysogeny Broth (LB) with shaking at 37°C. Total cell extracts were collected at OD_{600} of 0.3, 0.6, 0.8, and 1.0 and separated by 12% native PAGE. $GrlR_2$-GrlA and GrlR-GrlR complexes and GrlR monomer are indicated by arrows and were identified by western blotting using anti-FLAG monoclonal antibodies. The same cell extracts were also separated by 12% SDS-PAGE to evaluate the expression of GrlR-FLAG and GrlA-FLAG by western blotting using anti-FLAG antibodies. As a control for protein loading, GroEL expression was also analyzed using anti-GroEL antibodies.

or *LEE2-cat* fusion. The WT strain was the control, where the *LEE1-cat* fusion, but not the *LEE2-cat* fusion, was active in the presence of pTEPGrlA1 (**Figure 9A**), as previously shown (Bustamante et al., 2011). Interestingly, GrlR also repressed the constitutive expression of the *LEE1-cat* and *LEE2-cat* fusions in the Δ*hns* background but not when co-expressed with GrlA (**Figure 9B**). This result supported the proposal that GrlR also negatively regulates LEE gene expression independently of its interaction with GrlA. Also, GrlA had a dual role as a positive regulator by, in addition to its function as a *ler* activator, preventing GrlR's negative effect, most likely by trapping it in the heterotrimer. Defining the underlying mechanism by which GrlR represses the constitutive expression of the LEE promoters will require further investigation.

Discussion

In this study, we further investigated the role of GrlR as a repressor and the function of its interaction with GrlA in modulating LEE gene expression. Our results revealed a novel feature of its mechanism of action as GrlR also seems to act as a repressor independently of its interaction with GrlA; however, it remains to be seen if GrlR exerts this function by directly interacting with Ler-dependent promoters or with Ler-derived transcripts recognizing a common motif or indirectly by interacting with or modulating the function of a conserved element that is also present in *E. coli* K12.

A summary of the events leading to the control of LEE gene expression in response to the growth conditions is shown in **Figure 10** and described below. GrlR and H-NS act independently to negatively regulate the LEE at two different levels, establishing an indirect cooperative repressive effect on the expression of LEE operons when EPEC is grown under repressing conditions (**Figures 10A, F**, red dotted lines). In the WT strain, H-NS silences Ler-dependent promoters (**Figure 10A**), while GrlR inactivates GrlA by forming $GrlR_2$-GrlA heterotrimers previously shown to prevent GrlA binding to the *ler* promoter (Jimenez et al., 2010; Padavannil et al., 2013; **Figure 10F**). When GrlR is not present, free GrlA efficiently activates *ler* expression (**Figure 10C**), leading to Ler-dependent elimination of H-NS-mediated repression of LEE promoters (**Figure 10B**), thus resembling the phenotype shown by the double Δ*grlR*Δ*hns* mutant; however, mutants lacking *grlR* but also *ler* or *grlA*, cannot activate LEE gene expression because H-NS is still present and there is no Ler to overcome this repression.

In addition to identifying the role of GrlR as a negative regulator independent of its interaction with GrlA, our findings show that GrlA plays a dual role in the positive regulation of LEE genes by binding to the *ler* regulatory region and activating its expression (Jimenez et al., 2010; Islam et al., 2011), and antagonizing the independent repressor activity of GrlR through the formation of the $GrlR_2$-GrlA heterotrimer (**Figures 10C, D**, respectively); thus establishing an indirect coherent-positive feedforward loop (Shoval and Alon, 2010).

How the growth conditions determine whether EPEC induces or represses the LEE genes when both proteins are present and interact needs to be clearly understood; however, current knowledge and the results described here open up interesting possibilities for future investigation. For example, GrlR, in addition to reciprocally antagonizing GrlA through their interaction, may also interact with other proteins to modulate the transcriptional activity of LEE genes or directly with DNA promoter regions or the RNA transcripts derived from Ler-regulated genes. Along with our results, reports showing that GrlA activity in EHEC is mechanoresponsive and modulated by its membrane-bound state (Sirisaengtaksin et al., 2020), that Hfq differentially regulates GrlR and GrlA synthesis (Hansen and Kaper, 2009; Bhatt et al., 2017; Sudo et al., 2022) and that ClpXP posttranslationally regulates GrlR at the stationary phase (Iyoda and Watanabe, 2005), illustrate that there is more to learn about the mechanism of action of the GrlR and GrlA duet. How the growth conditions impact the GrlR and GrlA ratio in the cell, which seems to have a profound effect on the function and interaction between GrlR and GrlA, and thus in LEE gene expression, warrants future investigation.

The presence of the $GrlR_2$-GrlA complex, GrlR dimer and its monomer under both growth conditions, which is consistent with previous observations indicating that the basal activity of the *grlRA* promoter is higher than most of the LEE promoters under non-inducing conditions (Yerushalmi et al., 2014), indicate that certain levels of free GrlA are also present at any given moment during growth. Thus, the growth conditions must also play a role

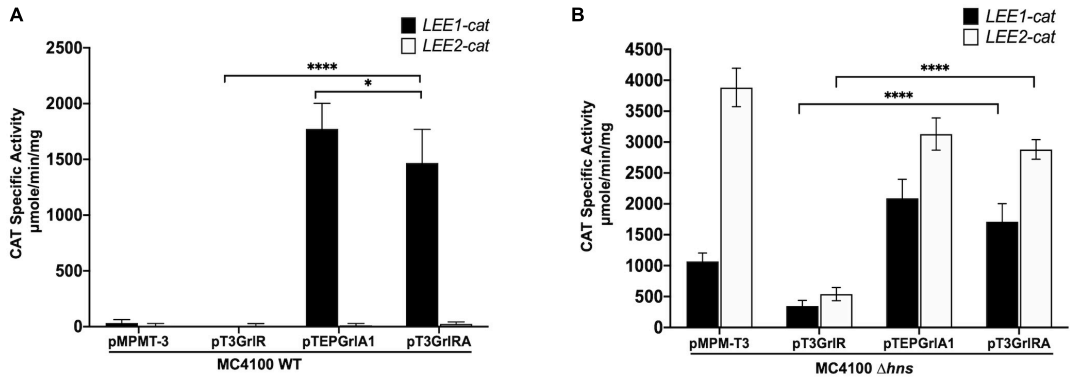

FIGURE 9
GrlR represses the expression of *LEE1* and *LEE2* operons in the absence of H-NS, GrlA and Ler. Expression of *LEE1-cat* (black bars) and *LEE2-cat* (white bars) fusions was analyzed in panel **(A)** WT *Escherichia coli* MC4100 and **(B)** MC4100 Δ*hns* (JPMC1) strains, carrying the empty vector pMPMT-3 or its derivatives pT3GrlR, pTEPGrlA1 and pT3GrlRA grown in 50 ml of Dulbecco's modified Eagle's medium (DMEM) with shaking at 37°C. Specific chloramphenicol acetyltransferase (CAT) activity was determined from samples collected from cultures grown in DMEM at an OD_{600} of 1. Values are an average of 3 independent experiments performed in duplicate. Error bars indicate standard deviations. Statistically different values are indicated (*p-value < 0.1; ****p-value < 0.0001).

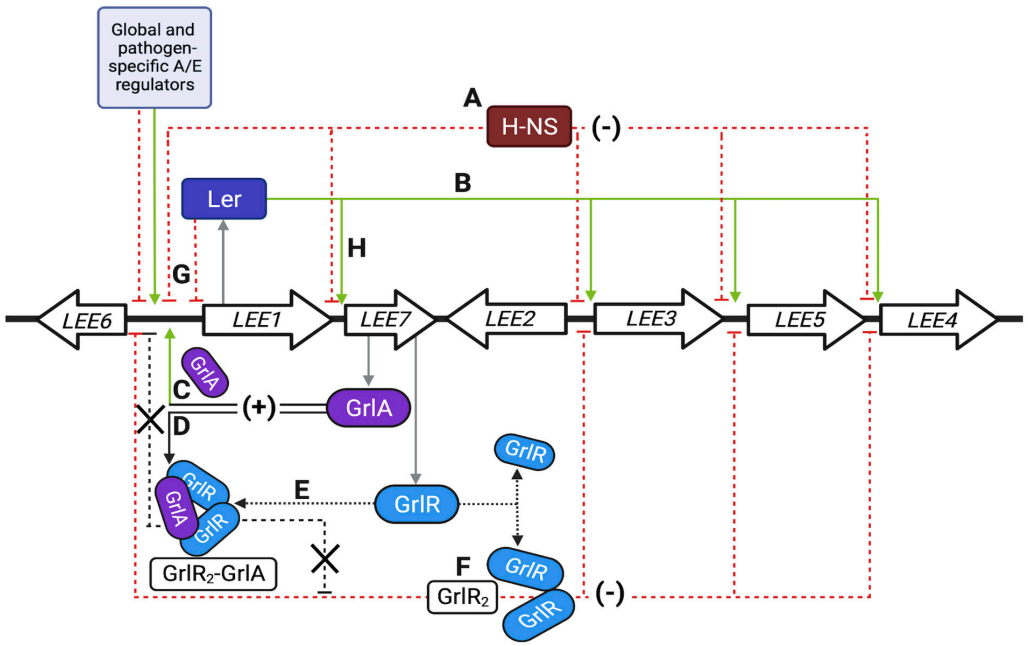

FIGURE 10
Schematic representation of the locus of enterocyte effacement (LEE) regulatory network. **(A–H)** Represent the primary regulatory circuits controlling LEE gene expression, as described in detail in the discussion. Green and red dashed lines indicate positive and negative regulatory pathways; black arrows indicate protein interactions. Thick arrows show a simplified representation of the seven operons previously reviewed in detail (Gaytan et al., 2016). Single genes are not illustrated. The first gene of the polycistronic *LEE1* operon encodes Ler, while the bicistronic *LEE7* operon codes for GrlR and GrlA. The light blue box represents several other global, ancestral and pathotype-specific regulators that modulate LEE gene expression, mainly by acting, but not exclusively, on Ler expression. Other colleagues have extensively and elegantly reviewed the regulatory elements known to modulate the regulation of the LEE (Furniss and Clements, 2018; Platenkamp and Mellies, 2018; Turner et al., 2019; Serapio-Palacios and Finlay, 2020). Created with BioRender.com.

in determining GrlR and GrlA competency to repress or activate, respectively, when the complex is disrupted, either due to its natural dissociation or by the influence of additional environmental factors. GrlR can displace GrlA from the *ler* promoter (Padavannil et al., 2013) and here we showed that overexpression of GrlR or GrlA drives the other protein to predominantly form the $GrlR_2$-GrlA complex (**Figures 10D, E**). In this complex, they reciprocally antagonize each other and, consequently, free GrlR or GrlA would act without competition with the other protein to either strongly repress (**Figure 10F**) or activate (**Figure 10C**) LEE gene expression, respectively. Thus, this dynamic behavior is likely modulating the activation or repression state of the LEE, whose expression has, unsurprisingly, been shown to be bimodal and render a fitness advantage to the cell (Leh et al., 2017; Ronin et al., 2017).

The acquisition of a pathogenicity island imposes on bacteria the need to adopt and adapt pre-existent and horizontally acquired regulatory mechanisms to prevent the deleterious expression of recently incorporated genes (Navarre, 2016). Although LEE gene

expression is modulated by a complex assortment of global regulatory proteins, its specific activation relies on the LEE-encoded regulators Ler and GrlA. In contrast, its negative control is mediated at two levels by a global regulator (H-NS) and an EPEC-specific regulator (GrlR). In this context, self-regulation of gene expression mediated by GrlR and GrlA may have provided a fitness advantage during the acquisition of the LEE, where GrlR down-regulated its uncontrolled expression preventing detrimental effects on bacterial fitness, while GrlA counteracted this self-encoded sentinel function. It is tempting to speculate that the incorporation of pre-existing or ancestral regulatory mechanisms, such as the repression exerted by H-NS to finetune LEE gene expression further, led to the incorporation of additional regulatory proteins, such as Ler, as well as other regulators that are known to modulate Ler expression in response to various environmental, stress or metabolic signals (Furniss and Clements, 2018; Platenkamp and Mellies, 2018; Turner et al., 2019).

In line with the diversification and opposing effects of GrlR and GrlA functions, a Δ*grlR* mutant showed reduced levels of flagellin (FliC) expression and motility, while overexpression of GrlA had the opposite effect suggesting that GrlA may be acting directly as a repressor on flagellar genes (Iyoda et al., 2006; Kitagawa et al., 2011). Iyoda's work also indicated that GrlA represses the expression of *flhD*, which encodes a master regulator of flagellar gene expression; consistently, GrlA binds to the *flhDC* regulatory region, while GrlR outcompetes this interaction (Padavannil et al., 2013), further supporting the notion that GrlA can also act as a repressor. Although details of the underlying mechanism remain undescribed, in the context of our work, the previously cited papers support the notion that the $GrlR_2$:GrlA interaction plays a reciprocal modulatory role in GrlR and GrlA activities.

Overall, LEE regulation is a fine example of the integration of ancestral and horizontally acquired regulators that now comprise a complex and coordinated set of network motifs (Shoval and Alon, 2010), orchestrating a consensus response to a myriad of signals concurring to regulate the expression of the LEE genes. For example, Ler negatively regulates its own expression, establishing a checkpoint that prevents the overexpression of the LEE (**Figure 10G**; Berdichevsky et al., 2005), while Ler and GrlA represent a positive feedback loop (**Figures 10C, H**; Barba et al., 2005); however, depending on the growth conditions, activation of the *grlRA* operon by Ler may also lead to an indirect coherent-negative feedforward loop where GrlR inactivates GrlA through the formation of heterotrimers and independently represses the *ler* and other LEE promoters (**Figures 10E, F**; Jimenez et al., 2010; Padavannil et al., 2013). In contrast, GrlA controls an indirect coherent-positive feedforward loop by activating *ler* expression and antagonizing GrlR (**Figures 10C, D**; Jimenez et al., 2010; Islam et al., 2011; Padavannil et al., 2013; this work). Deciphering the unknown nuances of this intertwined regulatory network and the implications for virulence gene regulation during the transit of the pathogen from the environment to the host or within the host during the colonization process is an exciting challenge for future research.

Data availability statement

The original contributions presented in this study are included in this article/**Supplementary material**, further inquiries can be directed to the corresponding authors.

Author contributions

CL-O and JP conceived the project, designed the experiments, and wrote the original draft of the manuscript with input and edits from all authors. CL-O, AH-S, WD, and AM-L performed the experiments. CL-O, AH-S, AM-L, WD, BF, YM-L, and JP performed data analysis. BF, YM-L, and JP provided funding. All authors approved the submitted version.

Funding

This work was supported by Consejo Nacional de Ciencia y Tecnología (60796, 239659, and FC-2015-2/950) and Dirección General de Personal Académico (PAPIIT IN224107 and IN218322) to JP and Programa institucional del fortalecimiento a grupos de investigación de la VIEP/BUAP and a CIHR Foundation grant to BF.

Acknowledgments

We are particularly thankful to A. Vázquez for mutant construction, B. González-Pedrajo for the generous donation of anti-Tir, -EspA and -Intimin antibodies, F. Santana for technical assistance, R. Jiménez for sharing constructs and J. A. Ibarra for valuable comments on the manuscript. We also thank the Oligonucleotide Synthesis Facility of the Instituto de Biotecnología. CL-O and AM-L were supported by fellowships from CONACyT (165332 and 173678, respectively).

Conflict of interest

The authors declare that the research was conducted in the absence of any commercial or financial relationships that could be construed as a potential conflict of interest.

Publisher's note

Supplementary material

The Supplementary Material for this article can be found online at: https://www.frontiersin.org/articles/10.3389/fmicb.2023.1063368/full#supplementary-material

References

Alsharif, G., Ahmad, S., Islam, M. S., Shah, R., Busby, S. J., and Krachler, A. M. (2015). Host attachment and fluid shear are integrated into a mechanical signal regulating virulence in *Escherichia coli* O157:H7. *Proc. Natl. Acad. Sci. U.S.A.* 112, 5503–5508. doi: 10.1073/pnas.1422986112

Barba, J., Bustamante, V. H., Flores-Valdez, M. A., Deng, W., Finlay, B. B., and Puente, J. L. (2005). A positive regulatory loop controls expression of the locus of enterocyte effacement-encoded regulators Ler and GrlA. *J. Bacteriol.* 187, 7918–7930.

Berdichevsky, T., Friedberg, D., Nadler, C., Rokney, A., Oppenheim, A., and Rosenshine, I. (2005). Ler is a negative autoregulator of the LEE1 operon in enteropathogenic *Escherichia coli*. *J. Bacteriol.* 187, 349–357. doi: 10.1128/JB.187.1.349-357.2005

Bhatt, S., Egan, M., Ramirez, J., Xander, C., Jenkins, V., Muche, S., et al. (2017). Hfq and three Hfq-dependent small regulatory RNAs-MgrR, RyhB and McaS-coregulate the locus of enterocyte effacement in enteropathogenic *Escherichia coli*. *Pathog Dis.* 75:ftw113. doi: 10.1093/femspd/ftw113

Bingle, L. E., Constantinidou, C., Shaw, R. K., Islam, M. S., Patel, M., Snyder, L. A., et al. (2014). Microarray analysis of the Ler regulon in enteropathogenic and enterohaemorrhagic *Escherichia coli* strains. *PLoS One* 9:e80160. doi: 10.1371/journal.pone.0080160

Brosius, J. (1984). Plasmid vectors for the selection of promoters. *Gene* 27, 151–160.

Bustamante, V. H., Martinez, L. C., Santana, F. J., Knodler, L. A., Steele-Mortimer, O., and Puente, J. L. (2008). HilD-mediated transcriptional cross-talk between SPI-1 and SPI-2. *Proc. Natl. Acad. Sci. U.S.A.* 105, 14591–14596. doi: 10.1073/pnas.0801205105

Bustamante, V. H., Santana, F. J., Calva, E., and Puente, J. L. (2001). Transcriptional regulation of type III secretion genes in enteropathogenic *Escherichia coli*: Ler antagonizes H-NS-dependent repression. *Mol. Microbiol.* 39, 664–678. doi: 10.1046/j.1365-2958.2001.02209.x

Bustamante, V. H., Villalba, M. I., Garcia-Angulo, V. A., Vazquez, A., Martinez, L. C., Jimenez, R., et al. (2011). PerC and GrlA independently regulate Ler expression in enteropathogenic *Escherichia coli*. *Mol. Microbiol.* 82, 398–415. doi: 10.1111/j.1365-2958.2011.07819.x

Creasey, E. A., Delahay, R. M., Daniell, S. J., and Frankel, G. (2003). Yeast two-hybrid system survey of interactions between LEE-encoded proteins of enteropathogenic *Escherichia coli*. *Microbiology* 149(Pt 8), 2093–2106. doi: 10.1099/mic.0.26355-0

Croxen, M. A., and Finlay, B. B. (2010). Molecular mechanisms of *Escherichia coli* pathogenicity. *Nat. Rev. Microbiol.* 8, 26–38.

Croxen, M. A., Law, R. J., Scholz, R., Keeney, K. M., Wlodarska, M., and Finlay, B. B. (2013). Recent advances in understanding enteric pathogenic *Escherichia coli*. *Clin. Microbiol. Rev.* 26, 822–880. doi: 10.1128/CMR.00022-13

Datsenko, K. A., and Wanner, B. L. (2000). One-step inactivation of chromosomal genes in *Escherichia coli* K-12 using PCR products. *Proc. Natl. Acad. Sci. U.S.A.* 97, 6640–6645. doi: 10.1073/pnas.120163297

Deng, W., Puente, J. L., Gruenheid, S., Li, Y., Vallance, B. A., Vazquez, A., et al. (2004). Dissecting virulence: Systematic and functional analyses of a pathogenicity island. *Proc. Natl. Acad. Sci. U.S.A.* 101, 3597–3602.

Edwards, R. A., Keller, L. H., and Schifferli, D. M. (1998). Improved allelic exchange vectors and their use to analyze 987P fimbria gene expression. *Gene* 207, 149–157. doi: 10.1016/s0378-1119(97)00619-7

Elliott, S. J., Sperandio, V., Giron, J. A., Shin, S., Mellies, J. L., Wainwright, L., et al. (2000). The locus of enterocyte effacement (LEE)-encoded regulator controls expression of both LEE- and non-LEE-encoded virulence factors in enteropathogenic and enterohemorrhagic *Escherichia coli*. *Infect. Immun.* 68, 6115–6126. doi: 10.1128/IAI.68.11.6115-6126.2000

Frankel, G., and Phillips, A. D. (2008). Attaching effacing *Escherichia coli* and paradigms of Tir-triggered actin polymerization: Getting off the pedestal. *Cell Microbiol.* 10, 549–556. doi: 10.1111/j.1462-5822.2007.01103.x

Friedberg, D., Umanski, T., Fang, Y., and Rosenshine, I. (1999). Hierarchy in the expression of the locus of enterocyte effacement genes of enteropathogenic *Escherichia coli*. *Mol. Microbiol.* 34, 941–952. doi: 10.1046/j.1365-2958.1999.01655.x

Furniss, R. C. D., and Clements, A. (2018). Regulation of the locus of enterocyte effacement in attaching and effacing pathogens. *J. Bacteriol.* 200:e00336-17. doi: 10.1128/JB.00336-17

Garcia-Angulo, V. A., Martinez-Santos, V. I., Villasenor, T., Santana, F. J., Huerta-Saquero, A., Martinez, L. C., et al. (2012). A distinct regulatory sequence is essential for the expression of a subset of nle genes in attaching and effacing *Escherichia coli*. *J. Bacteriol.* 194, 5589–5603. doi: 10.1128/JB.00190-12

Gaytan, M. O., Martinez-Santos, V. I., Soto, E., and Gonzalez-Pedrajo, B. (2016). Type three secretion system in attaching and effacing pathogens. *Front. Cell Infect. Microbiol.* 6:129. doi: 10.3389/fcimb.2016.00129

Guttman, J. A., and Finlay, B. B. (2008). Subcellular alterations that lead to diarrhea during bacterial pathogenesis. *Trends Microbiol.* 16, 535–542. doi: 10.1016/j.tim.2008.08.004

Haack, K. R., Robinson, C. L., Miller, K. J., Fowlkes, J. W., and Mellies, J. L. (2003). Interaction of Ler at the LEE5 (tir) operon of enteropathogenic *Escherichia coli*. *Infect. Immun.* 71, 384–392. doi: 10.1128/IAI.71.1.384-392.2003

Hansen, A. M., and Kaper, J. B. (2009). Hfq affects the expression of the LEE pathogenicity island in enterohaemorrhagic *Escherichia coli*. *Mol. Microbiol.* 73, 446–465. doi: 10.1111/j.1365-2958.2009.06781.x

Huang, L. H., and Syu, W. J. (2008). GrlA of enterohemorrhagic *Escherichia coli* O157:H7 activates LEE1 by binding to the promoter region. *J. Microbiol. Immunol. Infect.* 41, 9–16.

Islam, M. S., Bingle, L. E., Pallen, M. J., and Busby, S. J. (2011). Organization of the LEE1 operon regulatory region of enterohaemorrhagic *Escherichia coli* O157:H7 and activation by GrlA. *Mol. Microbiol.* 79, 468–483. doi: 10.1111/j.1365-2958.2010.07460.x

Iyoda, S., and Watanabe, H. (2005). ClpXP protease controls expression of the type III protein secretion system through regulation of RpoS and GrlR levels in enterohemorrhagic *Escherichia coli*. *J. Bacteriol.* 187, 4086–4094. doi: 10.1128/JB.187.12.4086-4094.2005

Iyoda, S., Koizumi, N., Satou, H., Lu, Y., Saitoh, T., Ohnishi, M., et al. (2006). The GrlR-GrlA regulatory system coordinately controls the expression of flagellar and LEE-encoded type III protein secretion systems in enterohemorrhagic *Escherichia coli*. *J. Bacteriol.* 188, 5682–5692. doi: 10.1128/JB.00352-06

Jimenez, R., Cruz-Migoni, S. B., Huerta-Saquero, A., Bustamante, V. H., and Puente, J. L. (2010). Molecular characterization of GrlA, a specific positive regulator of ler expression in enteropathogenic *Escherichia coli*. *J. Bacteriol.* 192, 4627–4642. doi: 10.1128/JB.00307-10

Jobichen, C., Li, M., Yerushalmi, G., Tan, Y. W., Mok, Y. K., Rosenshine, I., et al. (2007). Structure of GrlR and the implication of its EDED motif in mediating the regulation of type III secretion system in EHEC. *PLoS Pathog.* 3:e69. doi: 10.1371/journal.ppat.0030069

Kitagawa, R., Takaya, A., and Yamamoto, T. (2011). Dual regulatory pathways of flagellar gene expression by ClpXP protease in enterohaemorrhagic *Escherichia coli*. *Microbiology* 157(Pt 11), 3094–3103. doi: 10.1099/mic.0.051151-0

Leh, H., Khodr, A., Bouger, M. C., Sclavi, B., Rimsky, S., and Bury-Mone, S. (2017). Bacterial-chromatin structural proteins regulate the bimodal expression of the locus of enterocyte effacement (LEE) pathogenicity island in enteropathogenic *Escherichia coli*. *mBio* 8:e00773-17. doi: 10.1128/mBio.00773-17

Li, M., Rosenshine, I., Tung, S. L., Wang, X. H., Friedberg, D., Hew, C. L., et al. (2004). Comparative proteomic analysis of extracellular proteins of enterohemorrhagic and enteropathogenic *Escherichia coli* strains and their ihf and ler mutants. *Appl. Environ. Microbiol.* 70, 5274–5282. doi: 10.1128/AEM.70.9.5274-5282.2004

Lio, J. C., and Syu, W. J. (2004). Identification of a negative regulator for the pathogenicity island of enterohemorrhagic *Escherichia coli* O157:H7. *J. Biomed. Sci.* 11, 855–863. doi: 10.1007/BF02254371

Martinez-Laguna, Y., Calva, E., and Puente, J. L. (1999). Autoactivation and environmental regulation of bfpT expression, the gene coding for the transcriptional activator of bfpA in enteropathogenic *Escherichia coli*. *Mol. Microbiol.* 33, 153–166. doi: 10.1046/j.1365-2958.1999.01460.x

Mayer, M. P. (1995). A new set of useful cloning and expression vectors derived from pBlueScript. *Gene* 163, 41–46. doi: 10.1016/0378-1119(95)00389-n

Navarre, W. W. (2016). The impact of gene silencing on horizontal gene transfer and bacterial evolution. *Adv. Microb. Physiol.* 69, 157–186. doi: 10.1016/bs.ampbs.2016.07.004

Padavannil, A., Jobichen, C., Mills, E., Velazquez-Campoy, A., Li, M., Leung, K. Y., et al. (2013). Structure of GrlR-GrlA complex that prevents GrlA activation of virulence genes. *Nat. Commun.* 4:2546. doi: 10.1038/ncomms3546

Pearson, J. S., Giogha, C., Wong Fok Lung, T., and Hartland, E. L. (2016). The genetics of enteropathogenic *Escherichia coli* virulence. *Annu. Rev. Genet.* 50, 493–513. doi: 10.1146/annurev-genet-120215-035138

Platenkamp, A., and Mellies, J. L. (2018). Environment controls LEE regulation in enteropathogenic *Escherichia coli*. *Front. Microbiol.* 9:1694. doi: 10.3389/fmicb.2018.01694

Ronin, I., Katsowich, N., Rosenshine, I., and Balaban, N. Q. (2017). A long-term epigenetic memory switch controls bacterial virulence bimodality. *Elife* 6:e19599. doi: 10.7554/eLife.19599

Saitoh, T., Iyoda, S., Yamamoto, S., Lu, Y., Shimuta, K., Ohnishi, M., et al. (2008). Transcription of the ehx enterohemolysin gene is positively regulated by GrlA, a global regulator encoded within the locus of enterocyte effacement in enterohemorrhagic *Escherichia coli*. *J. Bacteriol.* 190, 4822–4830. doi: 10.1128/JB.00231-08

Sambrook, J., and Russell, D. W. (2001). *Molecular Cloning: A Laboratory Manual*, 3rd Edn. Cold Spring Harbor, NY: Cold Spring Harbor Laboratory Press.

Sanchez-SanMartin, C., Bustamante, V. H., Calva, E., and Puente, J. L. (2001). Transcriptional regulation of the orf19 gene and the tir-cesT-eae operon of enteropathogenic *Escherichia coli*. *J. Bacteriol.* 183, 2823–2833. doi: 10.1128/JB.183.9.2823-2833.2001

Serapio-Palacios, A., and Finlay, B. B. (2020). Dynamics of expression, secretion and translocation of type III effectors during enteropathogenic *Escherichia coli* infection. *Curr. Opin. Microbiol.* 54, 67–76. doi: 10.1016/j.mib.2019.12.001

Shin, M. (2017). The mechanism underlying Ler-mediated alleviation of gene repression by H-NS. *Biochem. Biophys. Res. Commun.* 483, 392–396. doi: 10.1016/j.bbrc.2016.12.132

Shoval, O., and Alon, U. (2010). SnapShot: Network motifs. *Cell* 143, 326–e321. doi: 10.1016/j.cell.2010.09.050

Sirisaengtaksin, N., Odem, M. A., Bosserman, R. E., Flores, E. M., and Krachler, A. M. (2020). The *E. coli* transcription factor GrlA is regulated by subcellular compartmentalization and activated in response to mechanical stimuli. *Proc. Natl. Acad. Sci. U.S.A.* 117, 9519–9528. doi: 10.1073/pnas.1917500117

Spears, K. J., Roe, A. J., and Gally, D. L. (2006). A comparison of enteropathogenic and enterohaemorrhagic *Escherichia coli* pathogenesis. *FEMS Microbiol. Lett.* 255, 187–202. doi: 10.1111/j.1574-6968.2006.00119.x

Sperandio, V., Mellies, J. L., Delahay, R. M., Frankel, G., Crawford, J. A., Nguyen, W., et al. (2000). Activation of enteropathogenic *Escherichia coli* (EPEC) LEE2 and LEE3 operons by Ler. *Mol. Microbiol.* 38, 781–793. doi: 10.1046/j.1365-2958.2000.02168.x

Sudo, N., Lee, K., Sekine, Y., Ohnishi, M., and Iyoda, S. (2022). RNA-binding protein Hfq downregulates locus of enterocyte effacement-encoded regulators independent of small regulatory RNA in enterohemorrhagic *Escherichia coli*. *Mol. Microbiol.* 117, 86–101. doi: 10.1111/mmi.14799

Turner, N. C. A., Connolly, J. P. R., and Roe, A. J. (2019). Control freaks-signals and cues governing the regulation of virulence in attaching and effacing pathogens. *Biochem. Soc. Trans.* 47, 229–238. doi: 10.1042/BST20180546

Ueguchi, C., Suzuki, T., Yoshida, T., Tanaka, K., and Mizuno, T. (1996). Systematic mutational analysis revealing the functional domain organization of *Escherichia coli* nucleoid protein H-NS. *J. Mol. Biol.* 263, 149–162. doi: 10.1006/jmbi.1996.0566

Uzzau, S., Figueroa-Bossi, N., Rubino, S., and Bossi, L. (2001). Epitope tagging of chromosomal genes in *Salmonella*. *Proc. Natl. Acad. Sci. U.S.A.* 98, 15264–15269.

Vidal, J. E., and Navarro-Garcia, F. (2008). EspC translocation into epithelial cells by enteropathogenic *Escherichia coli* requires a concerted participation of type V and III secretion systems. *Cell Microbiol.* 10, 1975–1986. doi: 10.1111/j.1462-5822.2008.01181.x

Yerushalmi, G., Litvak, Y., Gur-Arie, L., and Rosenshine, I. (2014). Dynamics of expression and maturation of the type III secretion system of enteropathogenic *Escherichia coli*. *J. Bacteriol.* 196, 2798–2806. doi: 10.1128/JB.00069-14

Frontiers in Microbiology

Explores the habitable world and the potential of microbial life

The largest and most cited microbiology journal which advances our understanding of the role microbes play in addressing global challenges such as healthcare, food security, and climate change.

Discover the latest Research Topics

See more →

Frontiers

Avenue du Tribunal-Fédéral 34
1005 Lausanne, Switzerland
frontiersin.org

Contact us

+41 (0)21 510 17 00
frontiersin.org/about/contact